UNIVERSIDAD CARLOS III DE MADRID

TESIS DOCTORAL

Diseño y Procesado de Aleaciones de Titanio mediante Técnicas Pulvimetalúrgicas Avanzadas

Autor:
Leandro Bolzoni

Directoras:
Elena Gordo Odériz
Elisa M. Ruiz-Navas

DEPARTAMENTO DE CIENCIA E INGENIERÍA DE MATERIALES E INGENIERÍA QUÍMICA

Leganés, 2011

TESIS DOCTORAL

DISEÑO Y PROCESADO DE ALEACIONES DE TITANIO MEDIANTE TÉCNICAS PULVIMETALÚRGICAS AVANZADAS

Autor: Leandro Bolzoni

Directoras: Elena Gordo Odériz, Elisa M. Ruiz-Navas

Firma del Tribunal Calificador:

Firma

Presidente:

Vocal:

Vocal:

Vocal:

Secretario:

Calificación:

Leganés, de de 2011

AGRADECIMIENTOS

En primer lugar me gustaría dar las gracias a todos los miembros del departamento de Ciencia e Ingeniería de Materiales e Ingeniería Química (profesores, técnicos y secretarias) ya que cada uno, con su particular actitud, me ha motivado para afrontar y terminar el reto de la tesis doctoral.

Además, querría agradecer el esfuerzo de todos los miembros del grupo de tecnología de polvos (GTP), que ha sido mi familia de adopción durante los últimos cinco años, por hacer posible que todo funcione correctamente. Gracias a José Manuel para los regalitos de diferentes partes del mundo y por su entusiasmo hacía la ingeniería de materiales.

Quiero agradecer el apoyo de Beatriz Gómez, sin el cual no habría llegado a esta meta ya que gracias a su entusiasmo y pasión para la investigación y los materiales nunca me habría embargado en la experiencia del doctorado.

Gracias a Maria Luisa Delgado por su naturaleza extrovertida porque me ayudó y animó para poder afrontar las primeras prácticas de laboratorio.

Doy las gracias a todos mis compañeros de despacho y a mi más cercanos, los que ya han terminado (Diego, Sagrario, Chema, Pablo, Pepe y Luz), los que me han acompañado a los largos de todos estos años (Luz, Paula, María, Raquel, Sophia, Elena, Javi, Diógenes, y Eloy) y los que acaban de empezar (Nerea, Carol y Roberto). Tampoco quiero olvidarme de todos los que han pasado por el departamento (proyectos fin de carrera, técnicos del LACTE, etc.) y todos los amigos y conocidos, si bien resulta imposible nombrarlos todos, que esta experiencia en España me ha dado la posibilidad de encontrar.

Un gracias particular y especial para el "despacho de las chicas", es decir Beatriz, Gema, Elena A., Patricia, Mariu, Elena R. y, por supuesto, Mariola por hacer el comienzo y el recorrido de este desafío mucho más placentero.

I would like to thank the "Powder Technology Centre" of the Austrian Research Centre (nowadays, AIT – Austrian Institute of Technology) and, especially Erich Neubauer, for the help and the possibility provided me during my stays in Vienna. Moreover, I want to thank to people I met over there and, particularly, Souzan, Monica and Luis for making my stay more enjoyable.

En particular, agradezco inmensamente la amistad, apoyo y ayuda de Isa, y por supuesto Manu, sin la cual mi estancia en Viena no habría sido ni mucho menos aprovechada, entretenida y divertida tal y como lo ha sido.

I also would like to thank the people of the "Waikato Centre for Advanced Materials" of the University of Waikato for assisting me during my stay and a special thank to Deliang Zhang to welcome me as one of his PhD student in the labs of the Waikato Centre, give me the possibility to visit New Zealand and the nice farewell. Thanks to Aamir to help me in finding a place where to stay and the good talks we had. Thanks to everyone from Brookfield, the staff and the people I met in there (especially Razia), for sharing with me pleasant hours.

Un grazie di cuore a "Little Italy" a.k.a (Antonio, Chiara, Patrizia e Viola) per il tempo passato insieme ovvero convivenza con cene varie, feste, escursioni, film e discussioni che hanno fatto del mio periodo trascorso in Nuova Zelanda assolutamente indimenticabile.

I am really grateful to the people from the Fraunhofer Institute IFAM of Dresden, just to name a few Bernd, Thomas Weissgaerber, Vicente, Thomas Hutsch, Conrad, Lars and Sabine, for the help provided me during my stay in Dresden.

No puedo concluir sin agradecer el esfuerzo y el empeño de mis dos directoras de tesis, Elena y Elisa, que me han guiado, apoyado, animado y cuidado a lo largo de todo el desarrollo de esta tesis doctoral ayudándome a entender mejor "la realidad".

Tampoco puedo olvidarme de mis compañeros de pisos o más bien de mis dos grandes amigos Mohamed y Rachid por ser como son. Ha sido verdaderamente un placer y un honor compartir estos años juntos.

Finalmente, vorrei ringraziare la mia famiglia per tutto ció che hanno fatto, per l'appoggio incondizionale e per credere in me; questa tesi di dottorato di ricerca é, praticamente, vostra.

Спасибо Светлана.

Alla mia famiglia:

quella che ricordo, quella che ho, e quella che verrá

ÍNDICE DE CONTENIDOS

ÍNDICE DE CONTENIDOS I
RESUMEN 1
ABSTRACT 3
MOTIVACIÓN Y OBJETIVOS 5
CAPÍTULO 1: Marco Teórico 9
CAPÍTULO 2: Procedimiento Experimental 81
CHAPTER 3: Powder Production and Characterisation 119
CHAPTER 4: Study of the Sintering Tray 149
CHAPTER 5: Preliminary Sinterability Study 159
CHAPTER 6: Results and Discussion 177
CHAPTER 7: General Conclusions 379
CHAPTER 8: Suggestions for Further Work 383

1 – Marco Teórico 9

1.1 – Introducción 9

1.2 – El Titanio y sus Aleaciones 13

1.2.1 – Métodos de Obtención del Titanio 13

1.2.2 – Propiedades Características del Titanio 17

1.2.3 – Efecto de los Elementos de Aleación 24

1.2.4 – Clasificación de las Aleaciones de Titanio 25

1.2.5 – Transformaciones de Fases 30

1.2.6 – Aleación Ti–3Al–2,5V 34

1.2.7 – Aleación Ti–6Al–4V 35

1.2.8 – Aleación Ti–6Al–7Nb 37

1.2.9 – Aplicaciones del Titanio y de sus Aleaciones 39

1.3 – Tecnología Pulvimetalúrgica 47

1.3.1 – Prealeado y Mezcla Elemental 48

1.3.2 – Compactación en Frío y Sinterización 49

1.3.3 – Compactación en Caliente 50

1.4 – Titanio Pulvimetalúrgico 52

1.4.1 – Prensado y Sinterización 52

1.4.2 – Compactación Isostática en Caliente 55

1.4.3 – Compactación Uniaxial en Caliente 58

1.4.4 – Otras Técnicas 62

1.4.5 – Conclusiones 65

1.5 – Referencias 66

2 – Procedimiento Experimental 81

2.1 – Composiciones a Estudiar 81

2.2 – Materias Primas y Producción de Polvos 85

2.3 – Caracterización de Polvos 89

2.3.1 – Análisis del Tamaño de Partícula 90

2.3.2 – Análisis Químico 90

2.3.3 – Densidad, Velocidad de Flujo y Microdureza 91

2.3.4 – Morfología y Microestructura de los Polvos 92

2.3.5 – Compresibilidad y Resistencia en Verde 93

2.3.6 – Análisis Dilatométrico 93

2.3.7 – Análisis Térmico Diferencial 93

2.4 – Selección del Soporte de Sinterización 95

2.5 – Conformado mediante Técnicas P/M 97

2.5.1 – Compactación Uniaxial en Frío y Sinterización 98

2.5.2 – Compactación Isostática en Frío y Sinterización 99

2.5.3 – Compactación Isostática en Caliente 99

2.5.4 – Compactación Uniaxial en Caliente 101

2.6 – Caracterización de los Materiales Sinterizados 106

2.6.1 – Variación Dimensional 106

2.6.2 – Densidad y Porosidad 107

2.6.3 – Dureza 107

2.6.4 – Ensayo de Flexión en Tres Puntos 108

2.6.5 – Ensayo de Tracción 108

2.6.6 – Módulo de Elasticidad Dinámico 109

2.6.7 – Difracción de rayos X 109

2.6.8 – Conductividad Térmica 110

2.6.9 – Resistividad Eléctrica 112

2.6.10 – Análisis Químico y Estudio Microestructural 112

2.7 – Correlación entre Propiedades 113

2.8 – Referencias 114

3 – Powder Production and Characterisation 119

3.1 – Preparation of Master Alloys 120

3.1.1 – Aluminium:Vanadium Master Alloy 120

3.1.2 – Aluminium:Niobium Master Alloy 122

3.1.3 – Alloys Fabrication 124

3.2 – Powder Characterisation 125

3.2.1 – Particle Size Distribution 125

3.2.2 – Chemical Analysis, Density, Flow Rate and Microhardness 127

3.2.3 – Powder Morphology 130

3.2.4 – Powder Microstructure 132

3.2.5 – Compressibility Test 134

3.2.6 – Green Strength 135

3.2.7 – Dilatometric Analysis 137

3.2.8 – Differential Thermal Analysis (DTA) 140

3.2.9 – Summary 145

3.2.10 – Partial Conclusions 147

3.3 – References 148

4 – Study of the Sintering Tray 149

4.1 – Partial Conclusions 157

4.2 – References 158

5 – Preliminary Sinterability Study 159

5.1 – Partial Conclusions 175

5.2 – References 176

6 – Results and Discussion 177

6.1– Elemental Titanium 179

6.1.1 – Uniaxial Pressing and Sintering (P&S) 179

6.1.1.1 – Relative Density 179

6.1.1.2 – Chemical Analysis 180

6.1.1.3 – Hardness 182

6.1.1.4 – Properties from Bending Test 183

6.1.1.5 – Properties from Tensile Test 187

6.1.1.6 – Microstructural Analysis 188

6.1.1.7 – Thermal Conductivity 191

6.1.1.8 – Electrical Resistivity 193

6.1.2 – Hot Isostatic Pressing (HIP) 195

6.1.2.1 – Relative Density 196

6.1.2.2 – Chemical Analysis 196

6.1.2.3 – Hardness 198

6.1.2.4 – Properties from Bending Test 199

6.1.2.5 – Properties from Tensile Test 201

6.1.2.6 – Microstructural Analysis 203

6.1.3 – Conventional Hot–pressing (HP) 205

6.1.3.1 – Relative Density 206

6.1.3.2 – Chemical Analysis 207

6.1.3.3 – Hardness 212

6.1.3.4 – Properties from Bending Test 212

6.1.3.5 – Microstructural Analysis 215

6.1.4 – Inductive Hot–pressing (IHP) 218

6.1.4.1 – Relative Density 219

6.1.4.2 – Chemical Analysis 220

6.1.4.3 – Hardness 220

6.1.4.4 – Microstructural Analysis 221

6.1.5 – P/M Techniques Comparison 222

6.1.6 – Partial Conclusions 225

6.2 – Ti–3Al–2.5V Alloy 227
6.2.1 – Uniaxial Pressing and Sintering (P&S) 227
6.2.1.1 – Relative Density 227
6.2.1.2 – Chemical Analysis 229
6.2.1.3 – Hardness 231
6.2.1.4 – Properties from Bending Test 234
6.2.1.5 – Properties from Tensile Test 239
6.2.1.6 – Microstructural Analysis 241
6.2.1.7 – Thermal Conductivity 244
6.2.1.8 – Electrical Resistivity 247
6.2.2 – Hot Isostatic Pressing (HIP) 250
6.2.2.1 – Relative Density 250
6.2.2.2 – Chemical Analysis 251
6.2.2.3 – Hardness 252
6.2.2.4 – Properties from Bending Test 254
6.2.2.5 – Properties from Tensile Test 256
6.2.2.6 – Microstructural Analysis 258
6.2.3 – Conventional Hot–pressing (HP) 260
6.2.3.1 – Relative Density 261
6.2.3.2 – Chemical Analysis 261
6.2.3.3 – Hardness 263
6.2.3.4 – Properties from Bending Test 264
6.2.3.5 – Microstructural Analysis 268
6.2.4 – Inductive Hot–pressing (IHP) 270
6.2.4.1 – Relative Density 271
6.2.4.2 – Chemical Analysis 272
6.2.4.3 – Hardness 273
6.2.4.4 – Microstructural Analysis 274
6.2.5 – P/M Techniques Comparison 275
6.2.6 – Partial Conclusions 279

6.3 – Ti–6Al–4V Alloy 281
6.3.1 – Uniaxial Pressing and Sintering (P&S) 281
6.3.1.1 – Relative Density 281
6.3.1.2 – Chemical Analysis 283
6.3.1.3 – Hardness 285
6.3.1.4 – Properties from Bending Test 288
6.3.1.5 – Properties from Tensile Test 293
6.3.1.6 – Microstructural Analysis 294
6.3.1.7 – Thermal Conductivity 298
6.3.1.8 – Electrical Resistivity 301
6.3.2 – Hot Isostatic Pressing (HIP) 303
6.3.2.1 – Relative Density 303
6.3.2.2 – Chemical Analysis 304
6.3.2.3 – Hardness 305
6.3.2.4 – Properties from Bending Test 307
6.3.2.5 – Properties from Tensile Test 310
6.3.2.6 – Microstructural Analysis 312
6.3.3 – Conventional Hot–pressing (HP) 314
6.3.3.1 – Relative Density 315
6.3.3.2 – Chemical Analysis 315
6.3.3.3 – Hardness 317
6.3.3.4 – Properties from Bending Test 318
6.3.3.5 – Microstructural Analysis 322
6.3.4 – Inductive Hot–pressing (IHP) 324
6.3.4.1 – Relative Density 324
6.3.4.2 – Chemical Analysis 325
6.3.4.3 – Hardness 326
6.3.4.4 – Microstructural Analysis 327
6.3.5 – P/M Techniques Comparison 328
6.3.6 – Partial Conclusions 332

6.4 – Ti–6Al–7Nb Alloy 335
6.4.1 – Uniaxial Pressing and Sintering (P&S) 335
6.4.1.1 – Relative Density 335
6.4.1.2 – Chemical Analysis 336
6.4.1.3 – Hardness 337
6.4.1.4 – Properties from Bending Test 338
6.4.1.5 – Properties from Tensile Test 341
6.4.1.6 – Microstructural Analysis 343
6.4.1.7 – Thermal Conductivity 344
6.4.1.8 – Electrical Resistivity 347
6.4.2 – Hot Isostatic Pressing (HIP) 349
6.4.2.1 – Relative Density 349
6.4.2.2 – Chemical Analysis 350
6.4.2.3 – Hardness 352
6.4.2.4 – Properties from Bending Test 353
6.4.2.5 – Properties from Tensile Test 355
6.4.2.6 – Microstructural Analysis 356
6.4.3 – Conventional Hot–pressing (HP) 358
6.4.3.1 – Relative Density 358
6.4.3.2 – Chemical Analysis 359
6.4.3.3 – Hardness 360
6.4.3.4 – Properties from Bending Test 361
6.4.3.5 – Microstructural Analysis 363
6.4.4 – Inductive Hot–pressing (IHP) 364
6.4.4.1 – Relative Density 365
6.4.4.2 – Chemical Analysis 366
6.4.4.3 – Hardness 367
6.4.4.4 – Microstructural Analysis 367
6.4.5 – P/M Techniques Comparison 368
6.4.6 – Partial Conclusions 371
6.5 – References 373

7 – General Conclusions 379

8 – Suggestions for Further Work 383

RESUMEN

En esta tesis doctoral se plantea el diseño de aleaciones base titanio y su procesado mediante técnicas pulvimetalúrgicas tanto convencionales como avanzadas con el objetivo de obtener materiales con propiedades comparables a las aleaciones fabricadas por técnicas convencionales.

Las aleaciones elegidas para el estudio han sido la Ti–6Al–4V, típica de la industria aeronáutica, la Ti–6Al–7Nb, característica de las aplicaciones biomédicas, la Ti–3Al–2,5V, normalmente empleada en los dos sectores anteriores, y se ha procesado también titanio elemental como referencia.

El primer paso ha sido establecer la forma de obtener las composiciones deseadas puesto que exclusivamente la aleación más conocida, es decir la Ti–6Al–4V, está disponible en forma de polvos prealeados; por lo tanto, ha sido necesario diseñar la forma de añadir los aleantes y comprobar su viabilidad estudiando la mezcla elemental de polvos y el empleo de aleaciones maestras.

En segundo lugar se realizó la búsqueda de las materias primas adecuadas, tendiendo en cuenta el contenido de elementos intersticiales, el coste y las características físico–químicas de los polvos y, a continuación, se realizó la caracterización de los polvos, tanto prealeados como los producidos por mezcla elemental o molienda de alta energía, como etapa previa a su procesado.

El procesado se ha llevado a cabo utilizando distintas técnicas: (1) compactación uniaxial en frío y sinterización (P&S), (2) compactación isostática en caliente (HIP) y (3) compactación uniaxial en caliente tanto convencional (HP) como inductiva (IHP). La descripción de todos estos pasos se encuentra en el capitulo de procedimiento experimental (Capitulo 2).

Para el estudio de la ruta 1 (P&S), se ha realizado un estudio preliminar de sinterabilidad, variando la temperatura de sinterización en el intervalo 900–1400ºC y manteniendo el tiempo de sinterización en 120 minutos, considerando compactos de geometría rectangular para determinar las propiedades de flexión, cuyos resultados se detallan en el capitulo 5. Previamente, se ha estudiado la selección del soporte de sinterización adecuado para evitar o minimizar la interacción con los componentes de titanio (Capitulo 4).

A partir del estudio preliminar, se ha realizado un estudio más detallado limitando el intervalo de temperatura de sinterización a 1250–1350ºC pero considerando el efecto del tiempo de meseta a la máxima temperatura (Capitulo 6).

En los materiales procesados se determinaron propiedades físicas, químicas, mecánicas, microestructurales, eléctricas y térmicas que se emplean como referencia para la comparación con los resultados obtenidos cuando se procesan las aleaciones mediante técnicas pulvimetalúrgicas avanzadas.

En general, la ruta P&S permite obtener aleaciones de titanio con elevada densidad relativa y propiedades de tracción equiparables a las de las respectivas aleaciones obtenidas por metalurgia convencional.

La ruta 2 (HIP) se ha empleado como etapa de postprocesado con el objetivo de reducir la porosidad residual de los materiales obtenidos mediante la vía 1 (P&S). La selección de los parámetros de procesado influye notablemente en el comportamiento mecánico debido a los cambios microestructurales asociados a las diferentes condiciones (Capitulo 6).

En el caso de la ruta 3 (HP o IHP), el parámetro que se ha modificado es la temperatura de conformado y el objetivo que se persigue es obtener piezas completamente densas a temperaturas menores y tratando de limitar el tamaño de grano de la microestructura (Capitulo 6).

Mediante el desarrollo de esta tesis se ha demostrado que el método de aleación maestra permite obtener propiedades equiparables a las de los polvos prealeados, que suelen ser más costosos, y se propone como técnica para poder diseñar aleaciones a medida y fabricar materiales cuya composición no está disponible actualmente en el mercado.

Además, el conformado de los polvos mediante las diferentes técnicas pulvimetalúrgicas permite obtener un gran abanico de propiedades mecánicas comparables o superiores a las de las respectivas aleaciones fabricadas por metalurgia convencional ajustables para aplicaciones específicas.

ABSTRACT

This PhD thesis deals with the design of titanium based alloys and their fabrication by means of conventional and advanced powder metallurgy techniques with the aims of producing materials with final properties comparable to those of the respective alloys fabricated by ingot metallurgy.

More in detail, the materials studied includes the Ti–6Al–4V alloy, which is normally employed in the aerospace industry, the Ti–6Al–7Nb alloy, which was developed for the production of biomedical devices, the Ti–3Al–2.5V conventionally used on both the previous mention industries, as well as elemental titanium manufactured as reference material.

First at all it was decided the way to obtain the desired compositions since exclusively the well–known Ti–6Al–4V alloy is available as prealloyed powder; therefore, the way to add the alloying elements had to be planned and checked considering the blending elemental as well as the master alloy addition approaches.

Secondly, the search of the right alloying elements on the base of the interstitials content, of the costs and of the powder features followed by the characterisation of the purchased (prealloyed) as well as produced (blended elemental or high–energy milled) powders was done before proceeding with the shaping of the powders.

The manufacturing of the components was done by means of different powder metallurgy techniques: (1) cold uniaxial pressing and sintering (P&S), (2) hot isostatic pressing (HIP) and (3) uniaxial hot–pressing either conventional (HP) or inductive (IHP). The description of the production, characterisation and shaping of the powder can be found in the experimental procedure chapter (Chapter 2).

For the study of the route number 1 (P&S), a preliminary sinterability study was carried out ranging the sintering temperature in the 900–1400ºC range, keeping the sintering time constant at 120 minutes and considering rectangular shaped specimens to perform three–point bending tests and measure the bending properties, whose results can be found in Chapter 5. Previously, the selection of the appropriate sintering tray to avoid or, at least, minimize the interaction with the titanium components was done (see Chapter 4).

On the base of the preliminary sinterability study, a more detailed sinterability study limiting the sintering temperature range (1250–1350ºC) but considering the influence of the dwell time at temperature was carried out (see Chapter 6).

Physical, chemical, mechanical and microstructural analyses as well as thermal and electrical properties were measured on the specimens sintered under diverse conditions and the results are kept as reference for the comparison with the properties obtained when processing the materials with advanced powder metallurgy techniques.

Generally, the P&S route allows to obtain titanium alloys with high level of relative density and mechanical properties similar to those of the respective alloys obtained by ingot metallurgy.

The route number 2 (HIP) was employed as secondary process with the aim of reducing the residual porosity of the specimens attained by means of the P&S technique. The selection of the processing parameters, namely the temperature, the time and the pressure influences significantly the mechanical behaviour due to the microstructural changes that they induce (Chapter 6).

On the case of the uniaxial hot–pressing (both HP and IHP) the sintering temperature was changed in order to manufacture fully dense materials at lower temperatures compared to other processes trying to limit the mean grain size of the microstructural features (Chapter 6).

By means of the development of this doctoral thesis it could be demonstrated that the master alloy addition approach permits to obtain materials with mechanical properties comparables to those of the prealloyed powders, which are normally more expensive, and it is proposed as production method to design alloy with the desired composition or as manufacturing method of conventional alloys not commercially available.

Moreover, the processing of the titanium powders by means of different powder metallurgy techniques permits to obtain a great range of mechanical properties comparable o higher than the respective alloys fabricated by ingot metallurgy and tailorable for specific applications.

MOTIVACIÓN Y OBJETIVOS

El titanio es un material relativamente nuevo en el campo de la ingeniería en comparación a otros metales como el cobre, el acero o el aluminio. Este retraso en la aplicación del titanio y en el desarrollo de sus aleaciones, que se concentró en los años 50 del siglo XX, se debe principalmente a la alta afinidad del titanio con elementos atmosféricos, en particular con el oxígeno, que disminuyen las propiedades de ductilidad y tenacidad además de afectar los métodos de procesado.

La reactividad del titanio, que le permite formar compuestos, intermetálicos, etc. con la mayoría de los elementos de la tabla periódica, aumenta al incrementar la temperatura de procesado, por lo tanto, es muy difícil encontrar un material que no interaccione con el titanio cuando este se encuentra en estado liquido, es decir durante su procesado por fundición.

La consideración de las técnicas pulvimetalúrgicas (P/M) para la fabricación de componentes de titanio, que conllevan la ventaja intrínseca de ser procesos en estado sólido limitando, por lo tanto, los fenómenos de interacción del titanio, se remontan a principios de 1970 cuando se llevó a cabo una intensa investigación tanto a nivel académico como en distintos sectores de la industria.

Cabe destacar que en esos años la utilización de polvos para los procesos P/M se limitaba a polvo tipo esponja procedente del procesado Kroll y de la ruta convencional para la obtención de lingotes.

La morfología de estos polvos, esponjosa, permitía alcanzar buenos niveles de densidad en verde tras el conformado uniaxial en frío, niveles de densidad relativa tras la sinterización aceptables y propiedades mecánicas estáticas comparables a las obtenidas mediante enfoques más convencionales.

Sin embargo, las propiedades de fatiga de las piezas obtenidas por mezcla elemental eran, normalmente, inferiores a las de las aleaciones convencionales. Esto se debe a la presencia de cloruros, como por ejemplo NaCl o $MgCl_2$, que permanecen después del proceso de extracción y que durante la etapa de sinterización generan porosidad residual que contiene gas y que, por lo tanto, es muy difícil de eliminar.

Esta porosidad residual se comporta como defectos microestructurales y actúa como concentrador de tensiones disminuyendo las propiedades de fatiga y la tenacidad del material. Además, estos gases hacen el material prácticamente insoldable a causa de las violentas reacciones que se pueden generar durante la soldadura.

A lo largo de los años se han ido desarrollando nuevos procesos de obtención de polvos, como por ejemplo el proceso de hidruración–dehidruración (HDH), que aprovecha la afinidad del titanio con el hidrógeno a altas temperaturas para fragilizarlo y molerlo, lo que permite obtener polvo con morfología irregular/angular apto, por lo tanto, para el proceso P/M convencional de compactación y sinterización (P&S).

Por otro lado, procesos de atomización tanto en gas como en plasma han permitido obtener polvos con un mayor grado de pureza. Además, cabe destacar que estos últimos se suelen emplear para fabricar polvos prealeados, es decir polvos que ya tienen la composición final de la aleación deseada.

No obstante, los polvos prealeados pueden también ser producidos mediante el proceso HDH, si bien, normalmente, con este método se procesan materiales elementales que se utilizan en el enfoque de mezcla elemental, tanto añadiendo elementos de aleación elementales como en forma de aleaciones maestras.

Normalmente, los polvos de morfología irregular se procesan mediante la ruta P/M convencional mientras que los polvos atomizados, de morfología más esférica, se conforman mediante técnicas avanzadas como la compactación isostática en caliente (HIP) o el moldeo por inyección de polvos metálicos (MIM). Estos polvos, que son más puros y por lo tanto más costosos, proporcionan propiedades dinámicas (fatiga) equivalentes a las de los productos obtenidos por metalurgia convencional, si bien hay que prestar mucha atención en la obtención de la microestructura más apropiada y evitar la presencia de inclusiones muy dañinas para la fatiga.

En base a lo descrito anteriormente y a los desarrollos técnicos e industriales, en esta tesis doctoral se considera el procesado de polvos de titanio elemental y de algunas de sus aleaciones a partir de polvos HDH para evitar el problema relacionado con los cloruros.

Además, se contempla el procesado de los polvos mediante diferentes técnicas P/M, que incluyen la ruta convencional (prensado uniaxial en frío y sinterización), el HIP como procesado secundario y el prensado en caliente como método para obtener productos de alta densidad y que han sido poco explorados hasta el momento para las aleaciones de titanio.

Los materiales investigados abarcan la mayoría de las tipologías de aleaciones de titanio y de sus fases y microestructuras:

- ✓ Titanio no aleado: titanio elemental
- ✓ Aleación "casi–alfa": Ti–3Al–2,5V
- ✓ Aleaciones alfa–beta: Ti–6Al–4V y Ti–6Al–7Nb

El objetivo principal del trabajo de investigación ha sido **obtener mediante pulvimetalurgia piezas de elevada densidad relativa y propiedades comparables a las obtenidas por metalurgia convencional** ya que el empleo de técnicas pulvimetalúrgicas permitiría disminuir el coste final de los componentes.

El objetivo principal se puede subdividir en objetivos parciales:

- ✓ Elegir las materias primas y los métodos de obtención de las aleaciones considerando dos enfoques: mezcla elemental y prealeado;
- ✓ Caracterizar de los polvos de partida para la fabricación de las aleaciones y de los polvos finales producidos;
- ✓ Seleccionar el soporte de sinterización para evitar y/o limitar el efecto de la reactividad del titanio a altas temperaturas con los óxidos cerámicos, como por ejemplo Al_2O_3 y ZrO_2;

- ✓ Investigar la influencia de la temperatura y del tiempo de sinterización en las propiedades físicas, químicas y mecánicas (flexión y tracción) de los materiales sinterizados;
- ✓ Evaluar la influencia de los parámetros del post–procesado mediante HIP en la propiedades físicas, químicas y mecánicas de las aleaciones de titanio;
- ✓ Estudiar el efecto de los parámetros de procesado de compactación en caliente tanto convencional (HP) como inductiva (IHP) para el titanio elemental y sus aleaciones;
- ✓ Relacionar la microestructura con las propiedades obtenidas y los parámetros de procesado empleados;
- ✓ Llevar a cabo la comparación de todas las propiedades consideradas obtenidas mediante diferentes técnicas de conformado por vía P/M.

CAPÍTULO 1

MARCO TEÓRICO

1.1 – INTRODUCCIÓN

El término metales ligeros se refiere a aquellos metales que por tener una densidad menor que el acero, normalmente, se emplean para disminuir el peso de un componente o de la estructura a la que pertenecen.

Si bien existen diferentes metales ligeros, solo cuatro de ellos han sido utilizados y siguen siendo empleados con el propósito de aprovechar sus propiedades estructurales en diferentes sectores de la ingeniería. Estos cuatro metales son: el aluminio (ρ_{Al} 2,70 = g/cm^3), el magnesio (ρ_{Mg} = 1,75 g/cm^3), el titanio (ρ_{Ti} = 4,51 g/cm^3) y el berilio (ρ_{Be} = 1,85 g/cm^3), cuya estructura cristalina a temperatura ambiente es hexagonal compacta (H.C.) a excepción del aluminio que es cúbica centrada en las caras (F.C.C).

El empleo de los metales ligeros y el desarrollo de sus respectivas aleaciones han estado principalmente asociados al sector aerospacial, lo que ha limitado la percepción de estos materiales como metales para aplicaciones más comunes.

Además del hecho de ser ligeros y, por lo tanto, disminuir el peso de los componentes con las consiguientes ventajas que esto conlleva, no hay que olvidarse de que estos metales tienen otras propiedades de notable importancia tecnológica, como por ejemplo la buena resistencia a la corrosión junto con la alta conductividad eléctrica y térmica del aluminio, el buen comportamiento frente al mecanizado del magnesio o la excelente resistencia frente a los diversos tipos de corrosión del titanio.

Este último se encuentra ampliamente distribuido en el universo, tanto que ha sido encontrado en las estrellas, en los meteoritos y en la superficie de la tierra, y su distribución lo hace el noveno elemento más abundante en la corteza terrestre (aproximadamente 0,86% en peso)[1-4] y el cuarto en cuanto a metales estructurales después de aluminio, hierro y magnesio. Además, el titanio es 20 veces más abundante que el cromo, 30 más que el níquel, 60 más que el cobre, 100 más que el wolframio y 600 más que el molibdeno. Sin embargo, su abundancia es algo ilusoria ya que normalmente no se encuentra en concentraciones extraíbles económicamente.

Fuentes concentradas de este metal son sus minerales, es decir, la ilmenita ($FeO{\bullet}TiO_2$), la titanomagnetita ($Fe_{2/3}{\bullet}Ti_{1/3}{\bullet}O_4$), el rutilo, la anatasa y la brookita; estos últimos tres minerales se identifican con la formula química TiO_2. La Figura 1.1 muestra unos ejemplos de cristales de óxidos de titanio. De todos ellos, los dos minerales de titanio más importantes desde el punto de vista comercial son la ilmenita y el rutilo debido a su relativa facilidad de procesado en comparación a los demás[2].

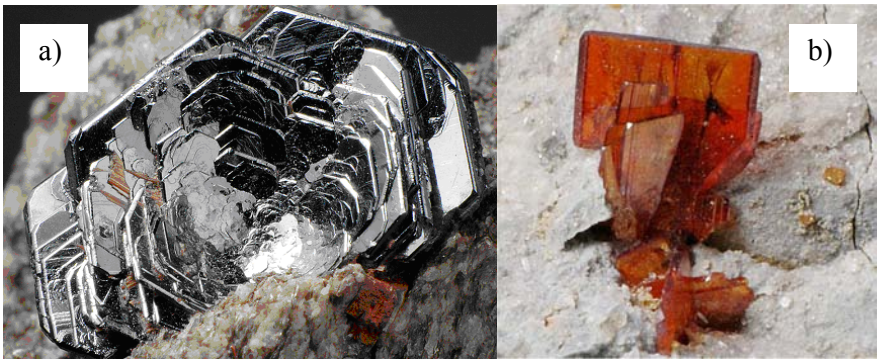

Figura 1.1 – Ejemplos de cristales de óxidos de titanio: a) rutilo y b) brookita[5].

Como se ha mencionado anteriormente, el estimulo para el empleo y el desarrollo del titanio se debe principalmente a la industria aeronáutica donde su relativa baja densidad junto con su elevado punto de fusión (1667°C) lo indicaban como candidato ideal para la sustitución del aluminio en estructuras de aviones de alta velocidad sometidos al calentamiento debido a elevadas cargas aerodinámicas en motores de jet y en aviones militares.

Sin embargo, la extensiva investigación llevada a cabo en los años 50 del siglo XX, acerca de aproximadamente 3000 aleaciones, reveló que el titanio y sus aleaciones son relativamente poco resistentes a fenómenos de fluencia en caliente (creep) con respecto a su alto punto de fusión.

Este descubrimiento, junto con el cambio de perspectiva en el sector aeronáutico, indujo a una disminución en el interés acerca del titanio en el campo de la ingeniería, relegándolo a aplicaciones donde se especifican combinaciones de propiedades únicas. De hecho, las aplicaciones para el sector aerospacial suponían aproximadamente el 75% de la producción de titanio, aunque actualmente este porcentaje ha bajado alrededor del 40%.

A lo largo de los años se ha aumentado el empleo del titanio en aplicaciones para la industria química y petroquímica en intercambiadores de calor y para la generación de energía, donde es crucial su excelente resistencia a la corrosión.

Otra de las aplicaciones que ha ido tomando más importancia es la fabricación de implantes y prótesis para el sector biomédico, debido a la elevada biocompatibilidad del titanio proporcionada por la capa de óxido exterior muy estable que se forma espontáneamente cuando el titanio es expuesto al aire.

Sin embargo, uno de los sectores que se muestra reticente al empleo del titanio de forma masiva es la industria de la automoción, si bien en los últimos años se pueden destacar algunas aplicaciones del titanio, de sus aleaciones o de compuestos de base Ti para componentes específicos[6, 7].

Si bien caracterizado por sus excelentes propiedades, a causa de su elevado coste, el empleo del titanio a nivel industrial siempre ha sido dependiente de la industria aeronáutica y sometido a las fluctuaciones que esta generaba en la demanda de este metal[8, 9].

La producción de titanio a nivel mundial debería haberse incrementado en un 20% durante el año 2010 alcanzando las 150000 toneladas volviendo a la tendencia creciente, después de la drástica bajada dictada por la crisis financiera de finales del 2008, que caracterizó los años 2005–2008 cuando la producción de titanio esponja había subido de 104000 toneladas a 176000 toneladas y que se reflejó en una disminución continua del precio del titanio esponja a partir del año 2006[10].

En el año 2009 la producción del titanio esponja ha sido confinada principalmente en seis naciones, que en orden de producción son: China, Japón, Rusia, Kazajistán, Estados Unidos y Ucrania. La Figura 1.2 muestra los porcentajes relativos de los diferentes países basado en los datos disponibles para el año 2009 y la previsión para el año 2010[11].

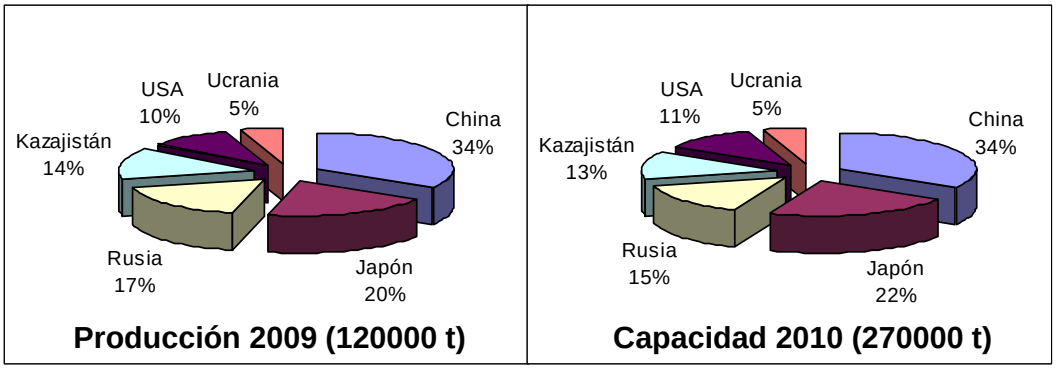

Figura 1.2 – División de la producción (2009) y capacidad productiva (2010) de titanio esponja para diferentes países[11].

Actualmente existen 18 empresas que se dedican a la producción de titanio esponja, nueve de las cuales se sitúan en China, y muchas de ellas han presentado planes para una ulterior expansión, lo que supondría alcanzar las 400000 toneladas por año en el 2015[10]. Sin embargo, el alto coste de extracción y fabricación sigue siendo la mayor barrera para expandir posteriormente el empleo del titanio en la industria[9].

Además, según los datos del 2004, de las 50000–60000 toneladas de componentes de titanio producidas, el 40% fue demandado por el sector aeronáutico y el 16% por el sector militar[12], industrias reticentes a la aplicación de nuevas tecnologías de fabricación y que siguen determinando las fluctuaciones del mercado del titanio.

Esta situación no parece haber cambiado demasiado ya que, según los datos disponibles relativos al año 2009, el sector aeronáutico detiene todavía el 39% de los productos de titanio, las aplicaciones industriales tuvieron un 48% y los productos consumibles un 13%.

Cabe destacar que hay diferencias significativas entre los diversos países ya que en Estados Unidos es el sector aeronáutico el que predomina, llegando a demandar más del 50% del consumo de titanio, mientras que en China, Japón y otros mercados asiáticos son las aplicaciones industriales, especialmente el sector químico, las preponderantes[13].

1.2 – EL TITANIO Y SUS ALEACIONES

1.2.1 – Métodos de Obtención del Titanio

El titanio fue inicialmente descubierto a finales del siglo XVIII en la ilmenita ($FeO•TiO_2$) y en forma de óxido rutilo (TiO_2); fue Gregor quién aisló un oxido metálico de la que fue llamada manaccanita en 1791 y Klaproth encontró en 1795 un nuevo metal en las rocas de Boinik que llamó titanio. Sin embargo, no fue hasta 1910 cuando Hunter preparó una pequeña cantidad de titanio de alta pureza (98-99%) mediante la reducción con sodio[2] y después en el año 1937 cuando el científico Kroll desarrolló un proceso que permitió la explotación industrial del titanio[3]. Por lo tanto, el empleo del titanio a nivel industrial es relativamente reciente, ya que empezó a finales de los años 40 del siglo XX.

Este retraso en el empleo del titanio es debido principalmente a su elevada afinidad con elementos como el oxigeno, el nitrógeno, el hidrogeno y el carbono y, por lo tanto, a la complejidad del proceso de purificación de los óxidos de partida.

La energía necesaria para obtener titanio metálico elemental, normalmente en forma de esponja, es significativamente superior a la utilizada para producir otros metales, aproximadamente 14 veces la empleada para fabricar la misma cantidad de acero. Por esta razón, el titanio es mucho más costoso de lo que se podría suponer considerando su abundancia. La elevada energía de extracción junto con la necesidad de limitar el contenido de elementos contaminantes, que incluso en pequeñas cantidades afectan notablemente la ductilidad y la resiliencia, justifica el alto coste de este metal.

El proceso de reducción del rutilo (TiO_2) a titanio elemental fue estudiado exhaustivamente pero fue solo al final de los años 30 del siglo XX cuando Wilhelm Kroll, un filólogo alemán, consiguió desarrollar un proceso de extracción para cantidades significativas que luego fue nombrado, en honor a su descubridor, proceso KROLL[14-16], y que sigue siendo utilizado a nivel industrial[17].

La obtención de titanio elemental a partir de sus óxidos resulta ser complicada a causa de la alta energía libre negativa de formación del TiO_2[18] y de la capacidad del titanio de disolver una cantidad significativa de oxígeno en forma de solución sólida[19]. Por lo tanto, cada candidato a la reducción del oxido de titanio no solo tiene que enfrentarse a la barrera impuesta por la elevada energía libre sino que debe poder sobrepasar la gran afinidad del titanio por el oxígeno, ya que esta aumenta al disminuir el porcentaje relativo de este elemento[20].

El método desarrollado por Kroll, cuyo esquema se muestra en la Figura 1.3, es un proceso discontinuo de reducción metalotérmica que incluye la carbocloración del rutilo en un lecho fluido a aproximadamente 1000°C mediante la reacción $TiO_2 + 2Cl_2 + C \rightarrow TiCl_4 + CO_2$ para poder obtener tetracloruro de titanio ($TiCl_4$) libre de oxígeno. Sucesivamente, se lleva a cabo una destilación fraccionada con el fin de eliminar la mayoría de las impurezas que quedan antes de introducir lentamente el $TiCl_4$ en un recipiente que contiene magnesio líquido a una temperatura comprendida entre 800ºC y 900°C.

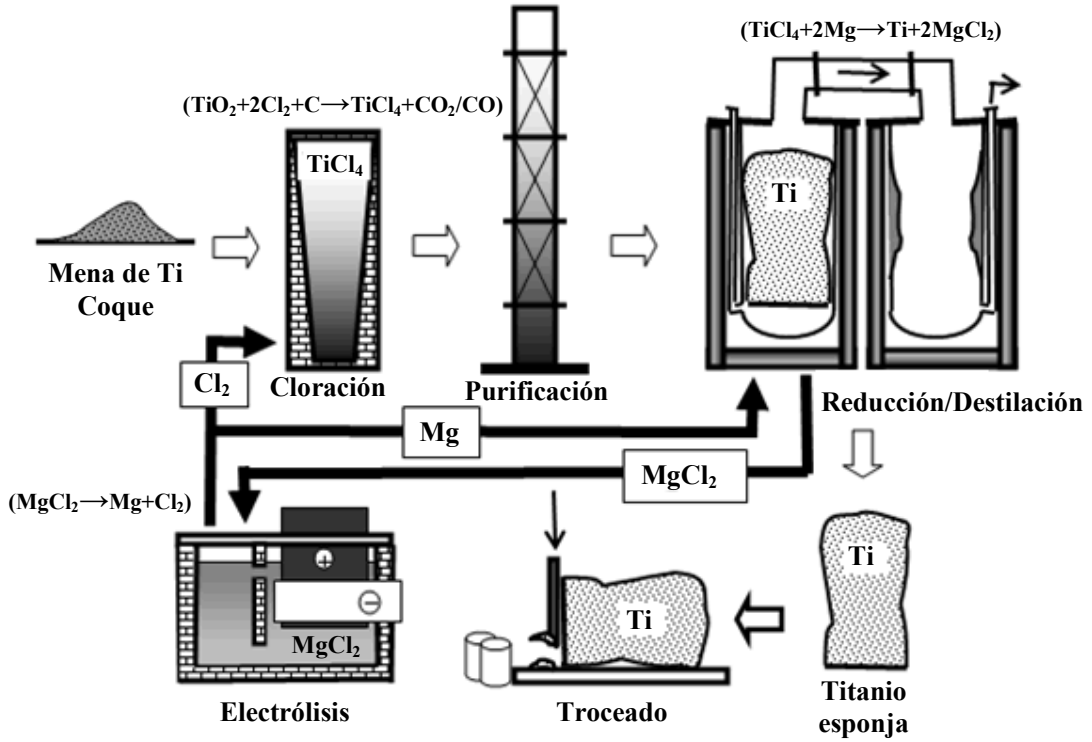

Figura 1.3 – Esquema del proceso Kroll para la obtención de titanio en forma metálica[21].

En presencia de exceso de magnesio se obtiene titanio elemental en forma de esponja mediante la reacción $TiCl_4 + Mg \rightarrow Ti + 2MgCl_2$ evitando la formación de dicloruro de titanio ($TiCl_2$). El tiempo de reducción es muy largo debido a la elevada cantidad de calor generado por la reacción exotérmica que gobierna esta etapa del proceso.

Una vez obtenido, el titanio esponja se somete a molienda, aleación y consolidación, utilizando el proceso de fusión por arco en vacío (Vacuum Arc Remelting)[22] o en un horno de fusión mediante haz de electrones (Electron Beam Cold Hearth Melting)[23] en función del producto final deseado.

A lo largo de los años se han llevado a cabo mejoras del proceso Kroll, como por ejemplo emplear $TiCl_4$ como materia prima en lugar del TiO_2, siendo esto más costoso, pero estas han sido solo evoluciones del proceso original siendo necesaria una nueva técnica de extracción metalúrgica para poder disminuir significativamente el coste del titanio elemental[24].

Una variante del proceso Kroll es el proceso Hunter donde en lugar de magnesio se emplea sodio para reducir el TiO_2 a titanio elemental[25, 26]; todavía este proceso no se utiliza para la producción de titanio a nivel industrial, ya que resulta ser ligeramente más costoso[2, 14, 16].

En la última década se han ido desarrollado nuevos procesos de reducción para la obtención de titanio metálico en forma de polvo[27] entre los cuales destacan el proceso ITP/Armstrong[15, 16, 28, 29] y el proceso Cambridge/FFC (Fray-Farthing-Chen)[30, 31] que se describen brevemente a continuación. Una comparación de los polvos actualmente disponibles se puede encontrar en diferentes artículos[32-35].

El ITP/Armstrong es un método continuo de bajo coste para la obtención de titanio elemental o aleaciones de titanio, ambos con un elevado grado de pureza, en una sola etapa que, en combinación con las técnicas pulvimetalúrgicas actualmente disponibles debería aportar una reducción de los costes finales de fabricación de los componentes hasta un 50%[15].

Esta técnica se basa en las mismas reacciones químicas empleadas en el proceso Hunter, pero se utiliza tetracloruro de titanio en fase gaseosa que viene inyectado en un circuito cerrado de sodio líquido permitiendo la finalización de la reacción a baja temperatura y obteniendo partículas muy finas de titanio elemental y cloruro de sodio.

El flujo continuo de sodio líquido retira las partículas de la zona de reacción limitando el atrapamiento de elementos no reaccionados y de co-productos de la reacción y, por lo tanto, aumenta la pureza del producto final y la eficiencia del proceso. Controlando la geometría de la zona de reacción y las velocidades relativas de los flujos es posible variar la morfología y la distribución del tamaño de partículas.

El polvo de titanio obtenido es sometido a un proceso de lavado antes de ser comercializado ya que cumple las especificaciones de los estándares en cuanto a composición química. Además, unos primeros experimentos han demostrado que es posible inyectar como reactivos cloruros de metales diferentes de forma simultanea en el reactor para poder obtener directamente la aleación deseada[15].

Sin embargo, algunos de los cloruros empleados son muy corrosivos, como por ejemplo el cloruro de aluminio ($AlCl_3$), y el control de la distribución del tamaño de partícula mediante la boquilla del inyector es crítica porque el polvo de titanio producido tiene que ser lo suficientemente grande para evitar la contaminación por parte del oxígeno cuando es expuesto al aire[14].

La Figura 1.4 muestra un esquema del diagrama de flujo del proceso ITP/Armstrong para obtener titanio elemental o la aleación Ti–6Al–4V donde se destaca la morfología dendrítica tipo coral del polvo obtenido[15].

La novedad del proceso electrolítico Cambridge/FFC[30] está en el enfoque empleado para la extracción del titanio, donde en lugar de intentar disolver el TiO_2 en una sal fundida[36], como en todos los intentos precedentes, se sujetan pellets de rutilo mediante un hilo Kanthal (Ni–Cr) y se sumergen en un baño fundido de $CaCl_2$.

A una temperatura suficientemente alta, aproximadamente 900°C, y aplicando una corriente eléctrica el TiO_2, notoriamente aislante, el rutilo se transforma en TiO_x ($x < 2$) que es conductor. Mediante esta configuración el oxígeno de los pellets se disuelve en la sal fundida y migra hacía el ánodo obteniéndose como resultado titanio metálico que se acumula en el cátodo.

La gran ventaja de este proceso es que no es necesario emplear rutilo puro, mucho más costoso, sino óxidos de metales mixtos[30] u otros precursores más económicos como residuos ricos en titanio[37].

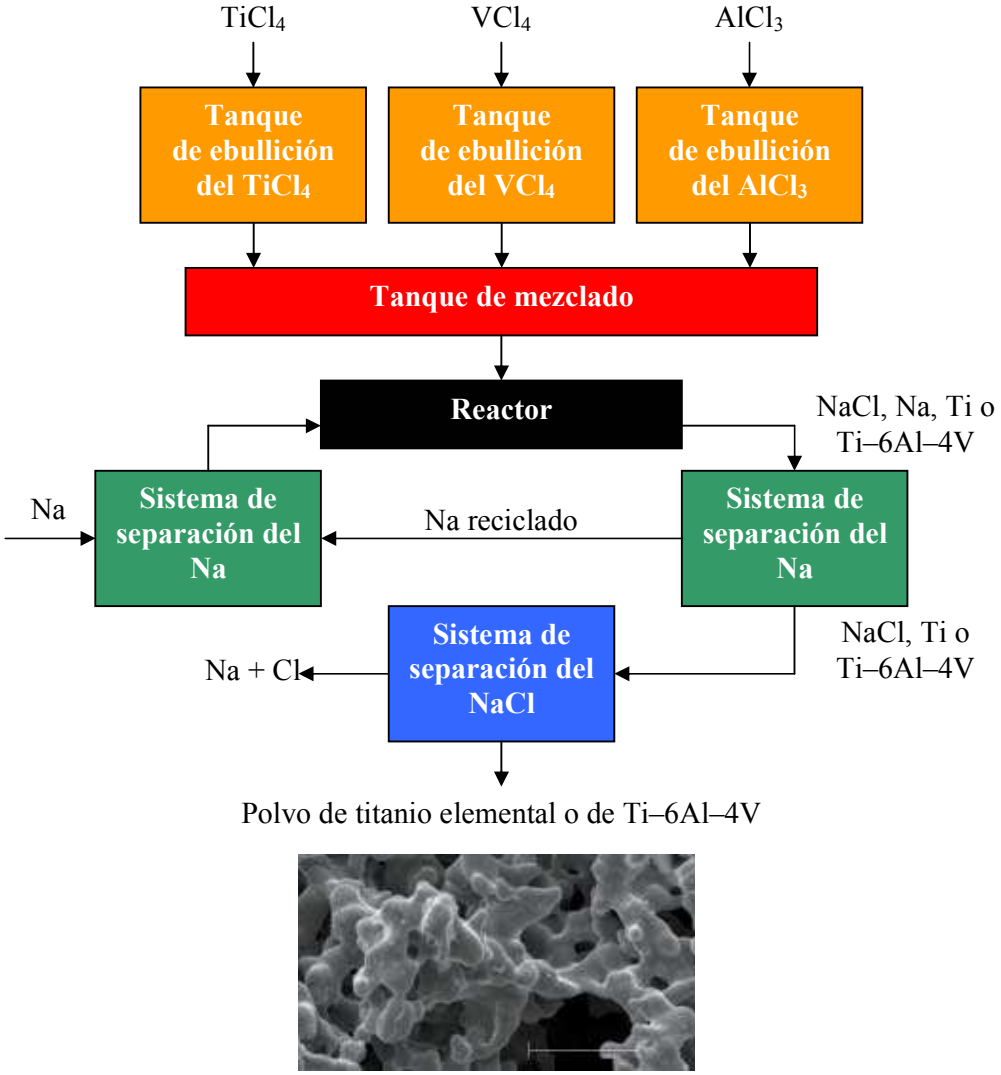

Figura 1.4 – Diagrama de flujo del proceso ITP/Armstrong para la obtención de titanio elemental o directamente la aleación Ti–6Al–4V[15].

Como en el caso del proceso Kroll, el proceso Cambridge produce titanio esponja, que no es nada más que una mezcla de titanio elemental y sales de elementos alcalinos o álcalis que es necesario moler y destilar con el fin de eliminar los sales.

El método FFC debería disminuir significativamente el coste del titanio hasta un tercio del valor actual[3], ya que puede producir titanio con un contenido de oxígeno alrededor de 60 ppm[14, 16, 38] y aleaciones de titanio convencionales[14] y novedosas[39].

La Figura 1.5 muestra un esquema del proceso electrolítico Cambridge/FFC[40] y una micrográfica del polvo de titanio elemental con morfología tipo esponja[37].

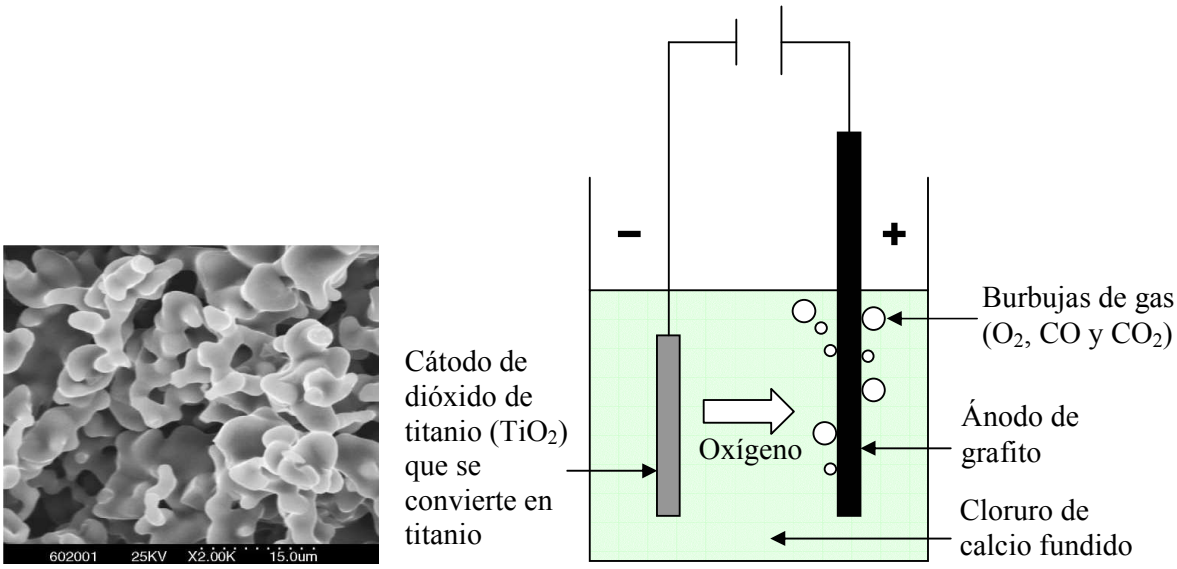

Figura 1.5 – Esquema del proceso electrolítico Cambridge/FFC[37, 40].

1.2.2 – Propiedades Características del Titanio

Independientemente de su forma de obtención, el titanio elemental es un metal dúctil y amagnético de color blanco plata caracterizado por una estructura cristalina de tipo Mg, hexagonal compacta a temperatura ambiente, si bien ligeramente comprimida a lo largo del eje "c" (c/a = 1,585), y con un radio atómico de 0,145 nm, que corresponde a un número de coordinación de 6[41].

Al aumentar el contenido de oxigeno, nitrógeno, hidrógeno y carbono, elementos intersticiales, aumenta ligeramente la longitud del parámetro "a" y, significativamente, la del parámetro "c" donde el carbono tiene el efecto más marcado y el hidrogeno el menos perceptible[2, 42].

Siendo el vigésimo segundo elemento de la tabla periódica, el titanio forma parte de los elementos del grupo IV y, por lo tanto, es un metal reactivo y electropositivo si bien, al contrario de la mayoría de los elementos vecinos, como las tierras raras y los elementos alcalinos, se pasiva, es decir, forma una capa superficial de óxido altamente resistente a la difusión que lo protege tanto de la corrosión en ambiente acuoso como de la oxidación a altas temperaturas, hasta aproximadamente 500ºC, porque a partir de esta temperatura la ganancia de peso debida a la oxidación aumenta notablemente[2].

Como los otros metales del cuarto grupo, el zirconio (Zr) y el hafnio (Hf), el titanio está caracterizado por una baja conductividad eléctrica y térmica, lo que se debe a la estructura electrónica y, principalmente, a la interacción de los electrones más cercanos al núcleo con los electrones exteriores de conducción.

Por lo tanto, el titanio se caracteriza por una particular combinación de propiedades físicas que se muestran y comparan con las de aluminio y las del hierro en la Figura 1.6

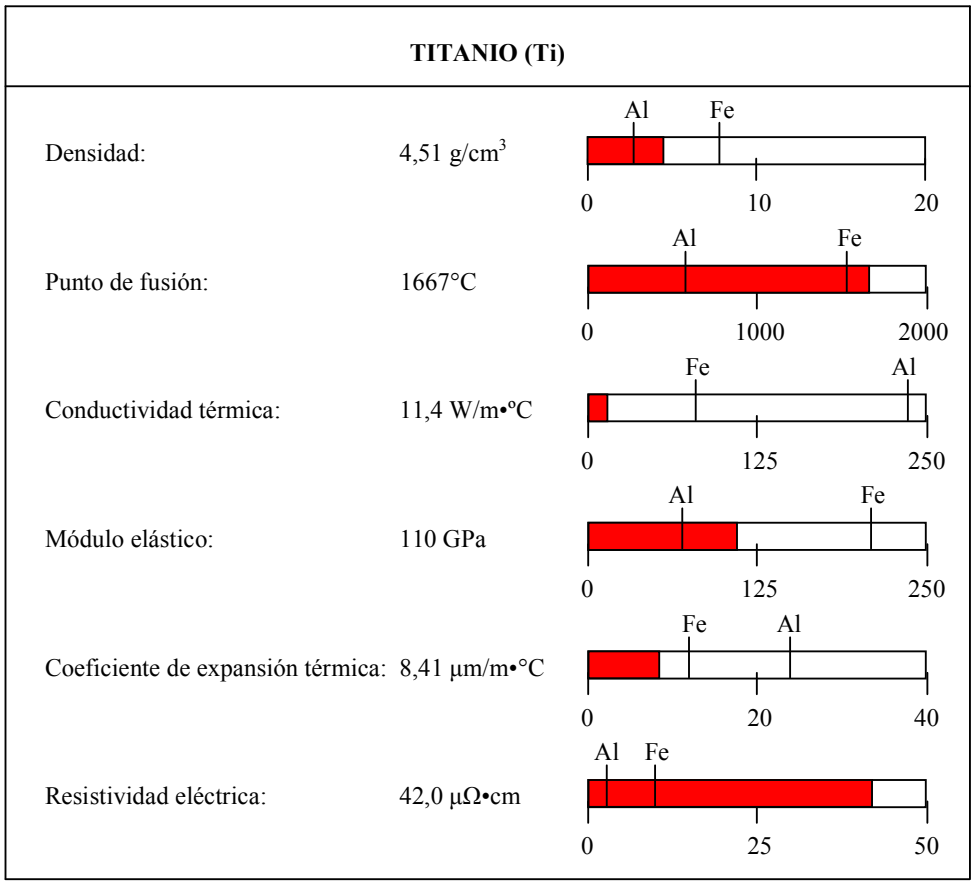

Figura 1.6 – Valores medios de las propiedades físicas del titanio en comparación a las de aluminio y hierro[3].

Las propiedades del titanio elemental indicadas en la Figura 1.6 se refieren a valores medios y a temperatura ambiente ya que muchas de las propiedades del titanio varían en función de la presencia de impurezas y de los tratamientos térmicos y mecánicos aplicados.

Come es sabido, los defectos de la estructura cristalina cambian las propiedades eléctricas, térmicas y el comportamiento plástico; por ejemplo el trabajo en frío aumenta la dureza y la resistencia y reduce tanto la conductividad eléctrica como la conductividad térmica. Sin embargo, la aplicación de un tratamiento térmico de recocido (300–500°C) o de recristalización (500–800°C) permite obtener nuevamente las propiedades de partida.

La combinación de propiedades del titanio lo convierte en uno de los materiales más atractivos para una amplia gama de aplicaciones. En comparación con el aluminio, el titanio ofrece una mayor resistencia especifica y la posibilidad de trabajar a temperaturas relativamente altas, hasta aproximadamente los 600°C[40]. Con respecto al acero, el titanio permite reducir el peso de los componentes hasta un 45% (Figura 1.6) además de proporcionar unas propiedades mecánicas mayores que muchos aceros actualmente empleados en el campo de la ingeniería.

Asimismo, el titanio se caracteriza por su excelente resistencia a la corrosión y es inerte en el cuerpo humano, lo que permite su aplicación en la fabricación de prótesis biocompatibles.

La Tabla 1.1 muestra algún ejemplo de propiedades importantes, desde el punto de vista industrial, del aluminio, del acero y del acero inoxidable con respecto al titanio. Cabe destacar que estas propiedades varían en función de la composición final de la aleación y del tipo de tratamiento térmico llevado a cabo. Además, hay que añadir que el ratio entre la resistencia y el peso es un parámetro significativo durante el diseño de un componente y que, a la vista de esta igualdad de peso, el titanio es tres veces más resistente que un acero.

Tabla 1.1 – Propiedades de algunos de los metales más importantes a nivel industrial[15].

Metal	Peso	Resistencia	Resistencia/ peso	Índice de corrosión	Vida estimada*
Titanio	1,00	1,00	1,00	1,00	Ilimitada
Aluminio	0,57	0,29	0,51	0,36	2 años
Acero	1,67	0,59	0,35	0,06	1 año
Acero inox	1,67	0,59	0,35	0,31	200 años

*Tiempo para que la corrosión penetre en un laminado de aproximadamente 1,5 mm de espesor (16-gauge) expuesto a agua marina por un lado

Sin embargo, el titanio es mucho menos empleado a nivel industrial con respecto al aluminio y al acero a causa de su alto coste de extracción a partir de los minerales, 15 veces el del acero y 3 veces el del aluminio, así como su alto coste de fabricación, aproximadamente 30, 6 y 4 veces respectivamente para la fabricación de un componente a partir de un lingote[43]. Por lo tanto, este metal no se emplea a menos que no pueda garantizar un mejor rendimiento, una mayor vida útil o una reducción de los costes de mantenimiento[44].

El titanio y sus aleaciones tienen una resistencia comparable a la de los aceros más resistentes pero su módulo de elasticidad es solo aproximadamente la mitad, es decir 110 GPa frente a 207 GPa, lo que confiere un mayor grado de flexibilidad a las estructuras fabricadas empleando este metal.

La alta resistencia frente a su relativo bajo módulo de Young confiere también al titanio un excepcional módulo de resiliencia permitiendo el almacenamiento de una cantidad de energía elástica significativamente mayor con respecto a materiales con mayor módulo de elasticidad, como el acero[3]. Esto hace posible la aplicación del titanio y de sus aleaciones en el campo deportivo, como por ejemplo en la cabeza de los palos de golf o las raquetas de tenis, ya que la energía almacenada que se libera al golpear la pelota permite imprimir un mayor impulso a esta.

Sin embargo, un alto módulo de resiliencia conlleva también un significativo efecto de recuperación elástica durante el conformado en frío porque el metal recupera la parte elástica de la deformación cuando se retira la carga. Por lo tanto, los moldes para conformar el titanio son, normalmente, sobredimensionados con el fin de compensar este efecto. Por otro lado, el empleo de un procesado en caliente permite reducir el efecto de recuperación elástica y conlleva un alivio de las tensiones almacenadas en el metal.

El titanio se caracteriza también por un pronunciado efecto Bauschinger, un fenómeno de endurecimiento por deformación que puede provocar una disminución drástica de la resistencia a compresión, hasta un 50%, cuando se aplica previamente una carga de tracción que induce una deformación entre el 1% y el 5%[3].

El titanio elemental de elevada pureza (high–purity Ti), con un contenido de oxígeno inferior al 0,05% en peso, presenta un límite elástico de 140 MPa, una resistencia a fractura de 235 MPa y una deformación que alcanza el 50%. Sin embargo, tal como se aprecia en la Figura 1.7, al aumentar el contenido de impurezas intersticiales, como el oxigeno, la resistencia aumenta significativamente.

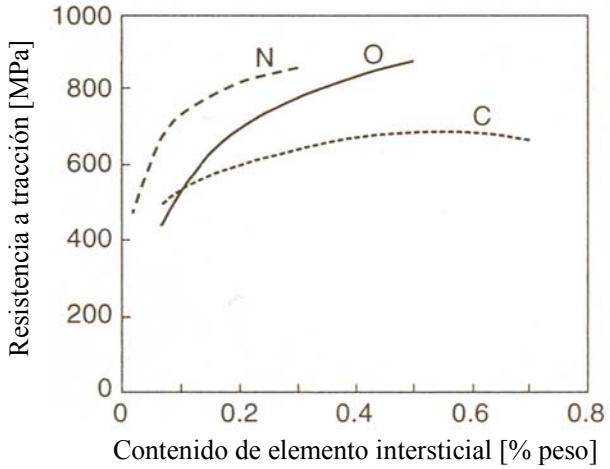

Figura 1.7 – Efecto de los elementos intersticiales en la resistencia a tracción del titanio[45].

El titanio elemental, comercialmente conocido con la sigla CP (Commercially Pure), supone una porción importante del porcentaje total de titanio fabricado anualmente ya que su resistencia a corrosión en ambientes acuosos es mayor que la de sus aleaciones. Esto permite el uso del titanio comercialmente puro en componentes como intercambiadores de calor, tanques o recipientes de reacción.

El titanio comercialmente puro siempre contiene trazas de otros elementos contaminantes debido a su gran afinidad por los gases atmosféricos. Como se puede apreciar en la Tabla 1.2, actualmente existen diferentes grados de titanio elemental, caracterizados por un contenido de oxigeno variable entre 0,18% y 0,40% (en peso) y un porcentaje de hierro de 0,20–0,50% (en peso), comúnmente empleados a nivel industrial en función de las propiedades requeridas para una particular aplicación.

Tabla 1.2 – Composición química, propiedades físicas y propiedades mecánicas de los grados de titanio elemental clasificados como comercialmente puros[46, 47].

Propiedad		**Ti Elemental**			
Grado ASTM		*CP 1*	*CP 2*	*CP 3*	*CP 4*
Análisis químico	O [% peso]	0,18	0,25	0,35	0,40
	N [% peso]	0,03		0,05	
	C [% peso]	0,08			
	H [% peso]	0,15			
	Fe [% peso]	0,20	0,30	0,30	0,50
Propiedades físicas	T_β [ºC]	890	915	920	950
	ρ [g/cm^3]	4,51			
Propiedades eléctricas	σ [S/cm]	18,5E+3	17,9E+3		16,7E+3
	ρ (RT) [$\mu\Omega$·cm]	54	56		60
Propiedades térmicas	k [W/m·ºC]	20,8		19,7	17,3
	α (RT) [10^{-6}/ºC]	8,6			
Propiedades mecánicas	E [GPa]	103			105
	σ_y [MPa]	170	275	380	480
	σ_f [MPa]	240	345	445	550
	ε [%]	24	20	18	15
	HV (HRB)	127 (70)	162 (82)	192 (90)	253 (100)
	σ_{10^7} [MPa]*	–	–	280	350

*R = –1

Convencionalmente, tal y como muestra la Figura 1.7, a mayor porcentaje de impurezas corresponde una mayor resistencia y un menor coste, pero también una menor ductilidad, resiliencia y resistencia a la corrosión. Cabe destacar que de todos los contaminantes, exclusivamente el oxigeno se añade con el fin de aumentar la resistencia a fractura mientras que los otros son impurezas que derivan del proceso de producción.

El titanio elemental denominado CP–Ti grado 1 es el más dúctil, lo que proporciona excelente conformabilidad en frío. Normalmente se procesa por embutición y suele ser empleado donde se precisa buena resistencia a corrosión y relativamente alta resistencia, como los recubrimientos de recipientes de reacción de acero.

El CP–Ti grado 2 es el más ampliamente utilizado a nivel industrial, gracias a su buena conformabilidad en frío, especialmente para fabricar componentes capaces de soportar cargas estáticas hasta temperaturas modestas, aproximadamente 250°C.

Las propiedades del CP–Ti grado 3 permiten producir contenedores a presión con espesor reducido en comparación al CP–Ti grado 1 o grado 2, siendo esta su aplicación principal, mientas que el CP–Ti grado 4 se emplea para la construcción de componentes de aviones gracias tanto a su resistencia frente a la corrosión (conductos y tuberías hidráulicas) como por su mayor resistencia (sistemas de cierres).

El titanio elemental, que está constituido exclusivamente por granos de la fase α, puede ser endurecido por diferentes vías: por solución sólida tanto intersticial (O, C y N) como de sustitución (Al, Sn y Zr), por disminución del tamaño de grano, por formación de textura o deformación plástica y por precipitación de la fase α_2. Esto último consiste en la formación del intermetálico Ti_3Al, equivalente a la estructura cristalina ordenada (DO_{19}), y solo se puede formar cuando el contenido mínimo de aluminio equivalente (Al_{eq}) es superior al 5,5 %[48].

El endurecimiento por disminución del tamaño de grano es uno de los métodos más efectivos para obtener diferentes niveles de resistencia en el titanio elemental, por ejemplo, se obtiene un aumento de la resistencia de aproximadamente 50 MPa por un aumento de 5 puntos de $d^{-1/2}$ ($mm^{-1/2}$) en la relación de Hall–Petch[49].

Finalmente, la resistencia a corrosión del titanio elemental, especialmente la resistencia a corrosión bajo tensión, puede ser incrementada mediante el empleo de un pequeño porcentaje, normalmente entre el 0,05% y el 0,20% en peso, de elementos del grupo del platino (Pt) y, en particular, el paladio (Pd) y el rutenio (Ru)[50]. Esto ha dado origen a diferentes grados ASTM comerciales, como por ejemplo el grado 7 (Ti–0,2Pd), el grado 16 (Ti–0,05Pd) y el grado 26 (Ti–0,1Ru), hasta un total de diez materiales con varios niveles de resistencia a la corrosión y a distintos tipos de corrosión.

La mejora de la resistencia a corrosión se debe al hecho de que la presencia del Pd disminuye el tamaño de grano en la superficie oxidada favoreciendo la adherencia de la capa de óxido e inhibe la estratificación y el desprendimiento de la misma.

A pesar de todo, la mayor contribución se obtiene mediante la formación tanto de precipitados de Ti_2Pd como de una fase de titanio β rica en Ru dispersa que actúan como pequeños sitios catódicos de despolarización en la superficie del metal. Este fenómeno induce un desplazamiento del potencial de corrosión hacia la parte más positiva o más noble, aumentando la cinética de reducción de los iones H^+ suprimiendo su evolución[3].

Como se ha mencionado anteriormente, el titanio puede ser clasificado como metal ligero pero se diferencia con respecto a los demás en cuatro aspectos fundamentales que transforman su metalurgia física al mismo tiempo en compleja e interesante:

- ✓ **El titanio presenta dos estructuras cristalinas**: hexagonal compacta (α) estable a bajas temperaturas y cúbica centrada en el cuerpo (β) a partir de 882°C hasta el punto de fusión (Figura 1.8). En principio, la presencia de esta transición alotrópica ofrece la posibilidad de obtener aleaciones compuestas por una microestructura solo de α, solo de β o mixta de α + β y, por lo tanto, la posibilidad de aprovechar diferentes tipos de tratamientos térmicos para modificar los constituyentes microestructurales y, consecuentemente, las propiedades proporcionadas. A nivel general, la fase α resiste principalmente a la deformación plástica, es menos dúctil y es más resistente a la fluencia en caliente, si bien las propiedades físicas y mecánicas son más anisótropas. Además, las velocidades de difusión de los diferentes elementos en la fase α son dos órdenes de magnitud inferiores a las de los mismos elementos en la fase β. Cabe destacar que a elevadas presiones el titanio puede formar una tercera fase con estructura hexagonal denominada ω muy frágil que puede causar problemas durante los tratamientos térmicos[3]. Sin embargo, el control apropiado de la composición y la aplicación de tratamientos de recocido suprimen la formación de esta fase no deseada;

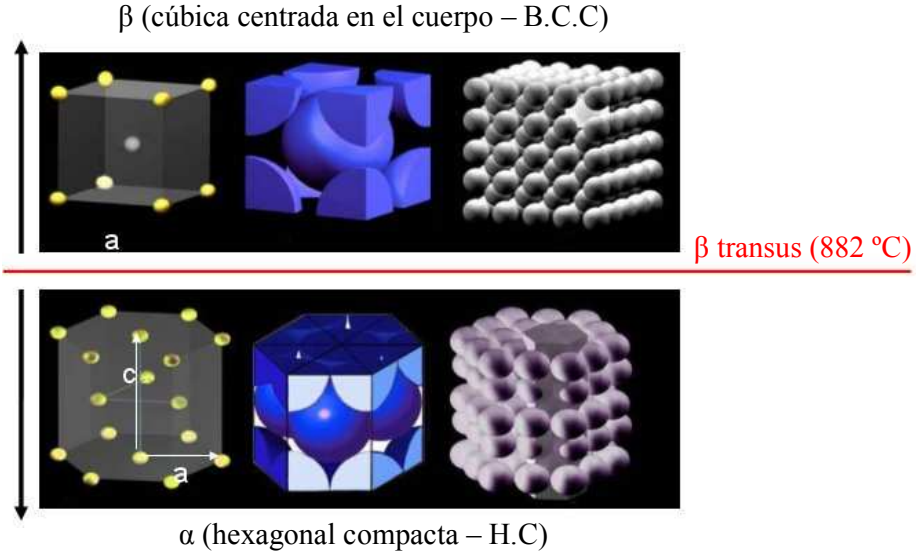

Figura 1.8 – Poliformismo del titanio: alfa (H.C.) y beta (B.C.C.).

- ✓ **El titanio es un metal de transición**: su particular posición en la tabla periódica le confiere una estructura electrónica capaz de formar soluciones sólidas con la mayoría de los elementos sustitucionales que tienen un factor de tamaño de ± 20%[51];

- ✓ **El titanio y sus aleaciones reaccionan con diferentes elementos intersticiales**: debido a su particular estructura electrónica el titanio se caracteriza también por una elevada afinidad por elementos como el oxígeno y el nitrógeno con un límite de solubilidad del 14,5% y del 20% en peso respectivamente. Estos valores resultan ser extremadamente altos si se comparan con los del acero para estos elementos intersticiales, que son del orden de partes por millón (ppm). Los elementos intersticiales más importantes y deletéreos para la ductilidad y la resiliencia son el oxígeno, el nitrógeno y el carbono. El aspecto más importante es que las reacciones con los elementos intersticiales pueden ocurrir a temperatura netamente inferiores a la de los respectivos puntos de fusión. En particular, cuando el titanio se encuentra en presencia de oxigeno a altas temperaturas no solo se pasiva sino que se forma una capa superficial endurecida comúnmente denominada "alpha–case" que suele ser eliminada mediante mecanizado o ataque químico;

- ✓ **El titanio puede formar soluciones sólidas y compuestos con otros elementos** mediante los tres tipos de enlaces primarios, es decir, metálico, covalente o iónico.

1.2.3 – Efecto de los Elementos de Aleación

El propósito principal de añadir elementos de aleación al titanio es mejorar sus propiedades mecánicas[2] si bien pueden también conllevar otros efectos, como por ejemplo favorecer la resistencia a la corrosión.

Los elementos aleantes se suelen clasificar en función de la capacidad de estabilizar la fase α o la fase β y esto está relacionado con la estructura electrónica; elementos con un ratio de electrones/átomo inferior a 4, como el aluminio, estabilizan la fase α, elementos con ratio igual a 4 son neutros y, finalmente, elementos con ratio superior a 4 como el vanadio son betágenos o estabilizadores de la fase beta[52].

Por otro lado, los elementos de la tabla periódica pueden ser divididos en cuatro grupos en función de la interacción que inducen en el titanio[53]:

- **Elementos con solubilidad total en estado sólido con titanio α o bien titanio β**: circonio y hafnio tienen la misma configuración electrónica exterior del titanio y, por lo tanto, su estructura es isomorfa a la del titanio y proporciona un diagrama de fases con solubilidad completa en el estado sólido tanto con la fase hexagonal como con la fase cúbica centrada en el cuerpo. Otros elementos como vanadio, niobio, tantalio y molibdeno son isomorfos con respecto a la fase beta y forman una solución sólida con la forma alotrópica β, pero tienen una solubilidad muy limitada en la fase alfa;

- **Elementos con solubilidad parcial en estado sólido con titanio α o titanio β**: cromo, manganeso, hierro, cobalto, níquel y cobre inducen una transformación eutectoide y disminuyen la temperatura de beta transus donde, al aumentar el número del grupo en la tabla periódica, disminuye la solubilidad máxima y aumenta la temperatura de transformación eutectoide. Aluminio, galio e indio presentan una transformación peritectoide con el titanio e inducen un aumento de la temperatura beta transus. Cabe destacar que estos últimos elementos se caracterizan por una solubilidad en la fase alfa superior en comparación a la de los elementos isomorfos;

- **Elementos que forman compuestos iónicos o covalentes con el titanio**: flúor, cloro, bromo, yodo, azufre, selenio, telurio y fósforo forman compuestos químicos pero no tienen solubilidad en el estado sólido en el titanio;

- **Elementos inertes con el titanio**: ninguno de los metales alcalinos y alcalino–térreos interacciona con el titanio a excepción del berilio que tiene una solubilidad limitada con el titanio beta.

Los elementos como oxigeno, nitrógeno, carbono, boro y hidrogeno forman soluciones sólidas intersticiales debido a la gran diferencia en su radio atómico y su solubilidad varia significativamente entre la fase alfa y la fase beta, en la que el hidrógeno es el único que presenta una mayor solubilidad en la fase β además de inducir una reacción eutectoide.

La Figura 1.9 muestra una descripción gráfica del efecto de los diferentes elementos de aleación en el diagrama de fases del titanio.

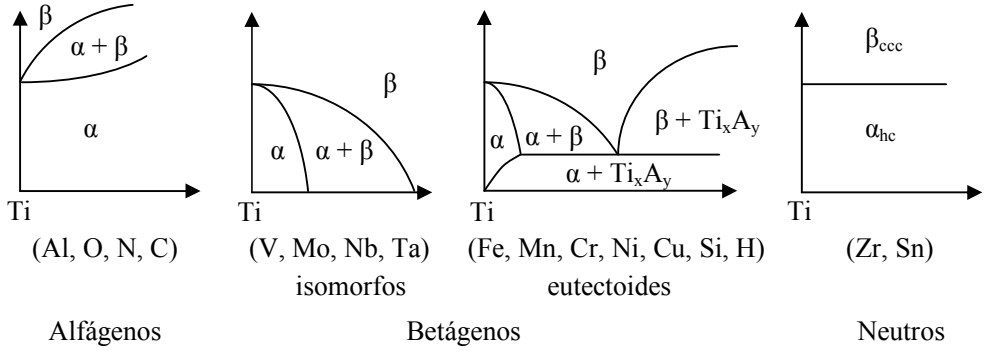

Figura 1.9 – Efecto de los elementos de aleación clasificados en función del efecto estabilizador[46, 54].

1.2.4 – Clasificación de las Aleaciones de Titanio

Las aleaciones de titanio suelen ser clasificadas como alfa, alfa + beta y beta, en función de las fases presentes a temperatura ambiente después de un tratamiento de recocido[2] tal como se representa en la Figura 1.10.

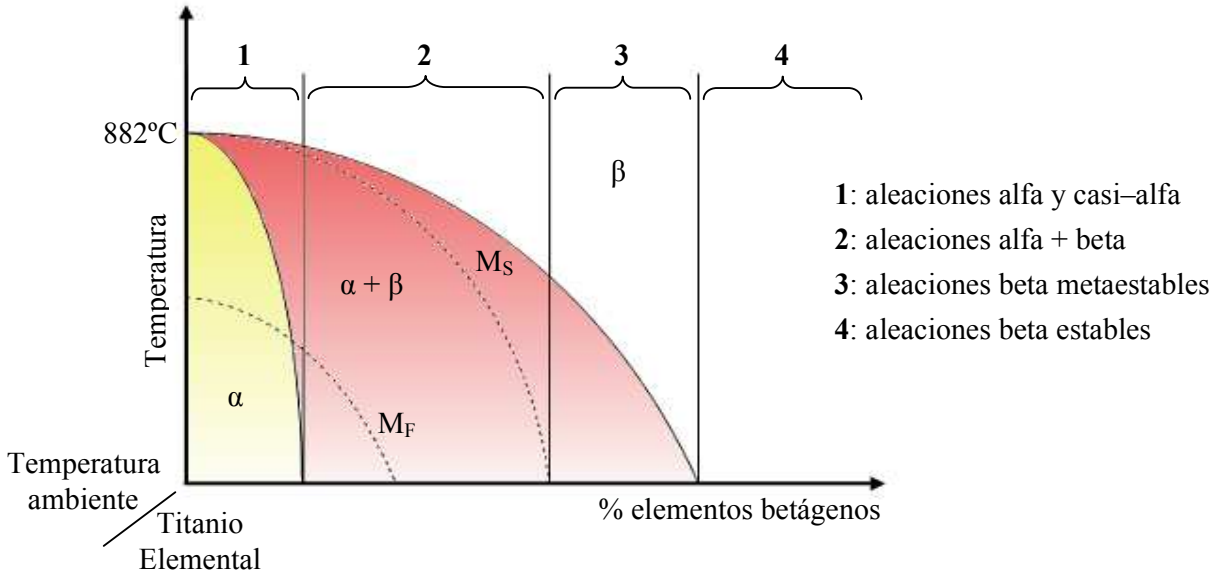

Figura 1.10 – Clasificación de las aleaciones de titanio mediante diagrama de fases pseudo–binario[45, 46].

De manera genérica, la densidad de las aleaciones α y α + β comerciales varía entre 4,37 g/cm^3 y 4,56 g/cm^3 mientras que para la aleaciones β se alcanzan valores máximos de 4,94 g/cm^3.

El módulo elástico aumenta con el contenido de elementos intersticiales y de aluminio. Además, el módulo de Young se puede modificar mediante el tratamiento de recocido siendo menor al disminuir la temperatura de recocido[55].

Añadiendo metales nobles o elementos como el molibdeno, el zirconio, el hafnio, el níquel, el tantalio o el niobio aumenta la resistencia a corrosión de las aleaciones de titanio, mientras que al aumentar el porcentaje de metales como hierro, cromo y aluminio, o impurezas intersticiales como el oxígeno, el nitrógeno y el hidrógeno, se obtiene el efecto contrario[2].

A continuación se describen más en detalle las principales características de cada grupo de aleaciones.

Aleaciones de titanio α: los elementos que estabilizan la fase α, es decir el aluminio, el indio y el galio, que forman estructuras cristalinas mixtas por substitución, y el oxigeno, el nitrógeno y el carbono, elementos intersticiales normalmente presentes como impurezas, desplazan la temperatura de transición beta hacia temperaturas más altas y aumentan la resistencia del titanio gracias a fenómenos de endurecimiento por precipitación. Además, los elementos alfágenos inhiben la formación de la fase β durante la etapa de calentamiento en procesos como la deformación en caliente y, por lo tanto, las aleaciones de titanio alfa son aleaciones monofase.

En particular, el empleo del aluminio, el único elemento alfágeno de importancia comercial, resulta ser deseable ya que este metal es barato, disminuye la densidad de la aleación, permite mantener una mejor ductilidad en comparación a otros elementos alfágenos y aumenta la resistencia a la oxidación a temperaturas elevadas. Sin embargo, no se utilizan porcentajes superiores al 6–8% en peso, tanto de aluminio elemental como de aluminio equivalente (según la relación de Rosenberg $Al_{eq} = Al + Sn/3 + Zr/6 + 10 \cdot (O + C + N)$[48]) para evitar la formación de la fase intermetálica α_2 (Ti_3Al) que disminuye significativamente la ductilidad del titanio.

Las aleaciones de titanio α, cuya resistencia a tracción varía entre 830–1030 MPa[2], muestran mejor resistencia a la fluencia en caliente que las aleaciones de titanio compuestas entera o parcialmente por fase β debido a la menor velocidad de difusión en la estructura hexagonal compacta (α) y a la limitada presencia de bordes de grano. Gracias a su excelente resistencia a la corrosión, las aleaciones de titanio alfa suelen ser empleadas para productos dedicados a la industria química y a la de ingeniería de procesos.

La aleación alfa más empleada es la Ti–5Al–2,5Sn, la cual queda completamente formada por titanio alfa hasta los 950°C y puede ser endurecida notablemente mediante temple y envejecimiento. Igualmente, posee una excelente soldabilidad y buena resiliencia en aplicaciones criogénicas a la vez de ser conocida por ser una aleación difícil de procesar[46].

Algunas aleaciones α contienen un pequeño porcentaje de elementos betágenos, como por ejemplo 1–2% en peso de V, Nb o Mo, que permite la formación de una pequeña cantidad de fase β durante el enfriamiento o llevando a cabo un tratamiento de solubilización y maduración. Estas aleaciones se denominan casi–alfa (near–α o super–α) y, estando compuestas casi exclusivamente por alfa, presentan buena soldabilidad y resiliencia pero con una resistencia a fractura ligeramente superior. Además, la combinación de propiedades que proporcionan hace de estas aleaciones materiales ideales para aplicaciones de altas temperaturas.

Una de las aleaciones casi–α más avanzadas es la aleación conocida como IMI834 (Ti–5,5Al–4Zr–4Sn–1Nb–0,6C–0,5Mo–0,35Si) que puede ser empleada hasta una temperatura de 550°C gracias a su buena combinación de resistencia a fatiga y resistencia a la fluencia en caliente[51].

Aleaciones de titanio α + β: estas aleaciones de titanio son las más comúnmente utilizadas ya que conteniendo tanto elementos alfágenos como betágenos, normalmente entre 4% y 6% en peso, su microestructura está compuesta por una mezcla de alfa y beta que les confiere excelente resistencia a fractura, resiliencia y resistencia a corrosión.

Al aumentar la cantidad de elementos betágenos se obtiene un aumento de la densidad de la aleación, una mejor respuesta a los tratamientos térmicos, un aumento de la procesabilidad y mayor sensibilidad a la velocidad de deformación, pero disminuye la resistencia a la fluencia en caliente y la soldabilidad. Una aleación de titanio α + β está caracterizada por una microestructura que varía en función del tratamiento termo–mecánico[56-60].

Se puede encontrar una estructura completamente laminar, totalmente equiaxial o una combinación de las dos anteriores denominada bimodal o "duplex", compuesta por granos primarios de α englobados en una matriz de láminas de α + β. La Figure 1.11 muestra un ejemplo de microestructura bimodal y de microestructura en "cesta" (basketweave).

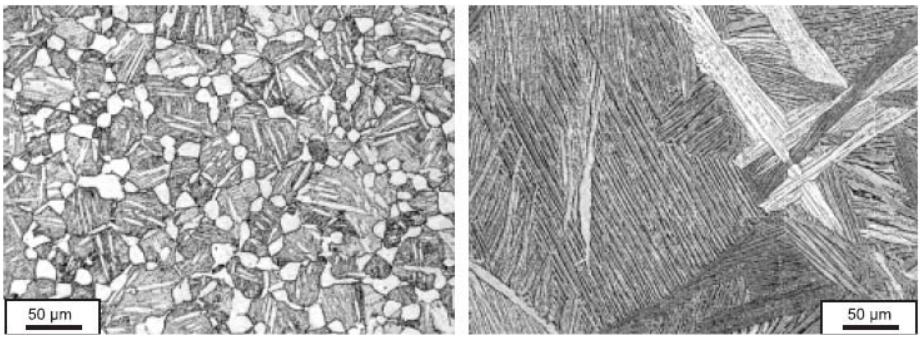

Figura 1.11 – Ejemplo de microestructura bimodal (izquierda) y de microestructura en "cesta" (derecha)[51].

Un tratamiento de solubilización y maduración puede aumentar la resistencia de una aleación de titanio α + β entre un 30% y un 50% con respecto a la misma aleación con una microestructura recocida. Sin embargo, la composición de la aleación, la temperatura de solubilización y la temperatura de maduración tienen que ser elegidas muy cuidadosamente para poder obtener un determinado nivel de propiedades mecánicas o una combinación de ellas.

La aleación α + β más conocida es la Ti–6Al–4V ya que ha dominado el mercado de la metalurgia del titanio durante décadas llegando a suponer hasta el 45% del total de los componentes obtenidos por laminación. Su resistencia a rotura es de 900 MPa después de un tratamiento de recocido y puede ser incrementada en aproximadamente 200 MPa mediante temple[2].

Aleaciones de titanio β: contrariamente a los alfágenos, los elementos betágenos, como el vanadio, el molibdeno, el cromo, el cobre o bien el hidrógeno, disminuyen la temperatura de beta transus y, cuando su porcentaje es suficientemente alto, se puede obtener una microestructura metaestable compuesta prioritariamente por titanio beta mediante enfriamiento en aire o mediante temple en función del espesor del componente.

Las aleaciones de titanio beta pueden ser subdivididas en metaestables y estables en función del porcentaje de elementos betágenos; un porcentaje del 10–15% genera una fase beta metaestable y porcentajes superiores al 30% permiten la retención de la fase beta de forma estable a temperatura ambiente.

Las aleaciones estables se parecen a los metales refractarios debido a su alta densidad y baja ductilidad[51]. Las aleaciones metaestables de titanio beta son caracterizadas por una estructura cristalina cúbica centrada en el cuerpo que les confiere una excelente conformabilidad a temperatura ambiente aunque sus resistencias son relativamente bajas.

Estas aleaciones pueden ser endurecidas tanto a través de una importante deformación en frío a temperatura ambiente como por calentamiento a una temperatura moderadamente elevada, normalmente variable entre 450ºC y 650°C, gracias a la precipitación de partículas de fase α finamente dispersas en la matriz de titanio beta.

Ejemplos de aleaciones β son la Ti–15V–3Cr–3Sn–3Al, la Ti–3Al–8V–6Cr–4Zr–4Mo y la Ti–15Mo–3Nb–3Al–Si que, con una resistencia variable entre 1000 MPa y 1200 MPa, se emplean principalmente para la fabricación de láminas para el sector aerospacial[2]. Asimismo, existen aleaciones de titanio β especiales, como la Ti–8V–5Fe–1Al que llegan a proporcionar una resistencia muy elevada después de envejecimiento, σ_y = 1500 MPa y σ_f = 1700 MPa, si bien su empleo está limitado a aplicaciones especificas ya que requieren un procesado de fundición particular, son poco dúctiles y no son soldables.

Como se puede deducir, el amplio intervalo de composiciones disponibles equivale a una impresionante gama de microestructuras y, por lo tanto, combinaciones de propiedades mecánicas como se índica en el gráfico de la Figura 1.12 donde se representa el limite elástico ($\sigma_{0.2}$) frente a la tenacidad a fractura K_{IC} de diferentes aleaciones de base titanio.

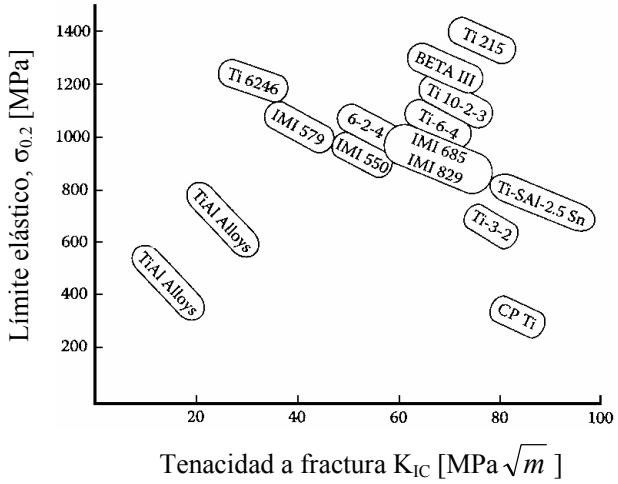

Figura 1.12 – Ejemplo del amplio intervalo de propiedades mecánicas de las aleaciones de titanio[51].

De todas las aleaciones de titanio desarrolladas, este trabajo de tesis se centra en tres de ellas, cuya propiedades principales se exponen a partir del apartado 1.2.6. Más en detalle, las aleaciones consideradas son la Ti–3Al–2,5V, la Ti–6Al–4V y la Ti–6Al–7Nb que, junto, con el titanio elemental, permiten abarcar la mayoría de las tipologías de aleaciones de titanio, es decir aleaciones de titanio alfa, las aleaciones casi–alfa o las aleaciones alfa + beta.

1.2.5 – Transformaciones de Fases

Los elementos de aleación que se añaden al titanio suele ser clasificados en función del efecto estabilizador que tiene con respecto a una u otra fase, es decir, alfágenos, betágenos o neutros, tal como se ha explicado en el apartado 1.2.3.

El contenido de aluminio, que resulta ser el más importante de los elementos de aleación alfágenos, suele estar limitado a un 6% en peso con el fin de evitar la formación de cantidades significativas de precipitados Ti_3Al en la fase α.

En el caso del vanadio y del niobio, que están caracterizados por un diagrama de fases binario con el titanio cuantitativamente muy parecido[19], el porcentaje máximo suele estar limitado aproximadamente a un 15% en peso, obteniendo una disminución de la temperatura de beta transus de 150–180ºC.

Sin embargo, las aleaciones de titanio comerciales son multicomponentes, es decir llevan más de un elemento de aleación, y por lo tanto hay que referirse a diagramas de fases ternarios ó cuaternarios.

En la Figura 1.13 se muestran ejemplos del diagrama ternario Ti–Al–V en diferentes secciones isotérmicas para el ángulo más rico en titanio donde se puede identificar la aleación Ti–6Al–4V (•).

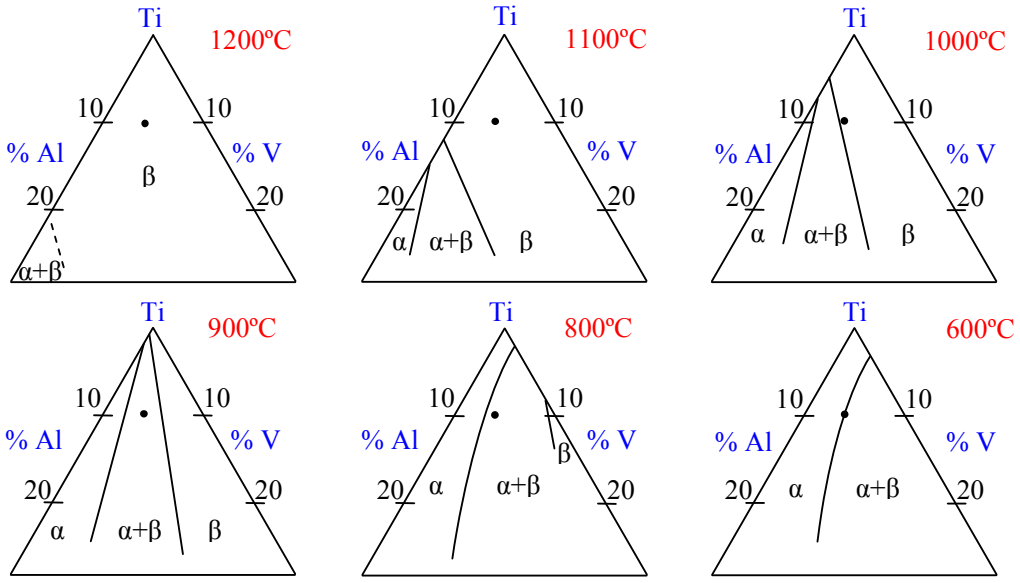

Figura 1.13 – Secciones isotérmicas del diagrama de fases ternario Ti–Al–V donde se especifica la aleación Ti–6Al–4V (•)[61].

La transformación de fase que se genera al enfriar el titanio elemental o una de sus aleaciones, es decir de una estructura cúbica centrada en el cuerpo (fase β) a una estructura hexagonal compacta (fase α), puede ocurrir mediante dos procesos particulares en función de la velocidad de enfriamiento empleada y de la composición de la aleación:

- ✓ **Nucleación y crecimiento gobernado por la difusión**: si la velocidad es lo suficientemente baja, durante el enfriamiento la fase α empieza a nuclear preferentemente en los bordes de grano de la fase β en forma de agujas o láminas y crece en el interior de los granos de β hasta que se encuentran unas con otras. Al final las láminas de fase α quedan separadas en el interior de las colonias por la fase β retenida originando una microestructura denominada laminar[62];

- ✓ **Transformación adifusional ("martensítica")**: en el caso de una velocidad de enfriamiento superior a la critica, que conlleva cruzar la temperatura de inicio de la transformación adifusional M_s (Figura 1.10), los átomos no tienen el tiempo suficiente para difundir y, por lo tanto, se origina un movimiento cooperativo de estos átomos que pasan de una estructura cristalina cúbica centrada en el cuerpo a una hexagonal denominada martensita (α') que se caracteriza por poseer la misma orientación que tiene α con respecto a β, por lo que en ocasiones es difícil de distinguir de la fase acicular. A su vez, esta martensita hexagonal puede tener dos tipos de morfologías[46] designadas como masiva, que se encuentra exclusivamente en el titanio puro y está compuesta por zonas irregulares relativamente grandes (50–100 μm) que contienen agrupaciones de pequeñas láminas de fase α con un espesor variable entre 0,5 y 1 μm, y acicular. Esta última se encuentra en aleaciones con elevado contenido de elementos betágenos, equivalente a una baja temperatura de transformación adifusional, y se compone de láminas de α con diferentes orientaciones. Con el aumento del porcentaje de los elementos de aleación, la estructura hexagonal se distorsiona y denomina martensita ortorrómbica (α'').

Finalmente, si bien no tiene ninguna aplicación comercial en las aleaciones de titanio, es importante remarcar que, aquellas donde la transformación martesítica está inhibida, la fase β se descompone atérmicamente tras el temple, formándose la fase ω aterma, es decir una dispersión uniforme de partículas extremadamente finas (2–4 nm).

La fase α puede ser endurecida por solución sólida intersticial, principalmente aumentando el contenido de oxigeno, o bien por solución sólida de sustitución mediante pequeños porcentajes de aluminio, estaño y circonio. Además, puede obtenerse el endurecimiento por precipitación de la fase coherente Ti_3Al siempre y cuando el contenido de aluminio sea superior al 5% en peso. Sin embargo, las aleaciones de titanio alfa no pueden ser tratadas térmicamente con el fin de aumentar la resistencia porque son aleaciones compuestas por una sola fase.

Por otro lado, cuando una aleación alfa + beta es calentada hasta campo de la fase β y sucesivamente enfriada lentamente, parte de los granos de beta se transforman en alfa formando una microestructura Widmanstätten de α + β en equilibrio donde la fase alfa nuclea a lo largo de los bordes de grano de la fase beta como se muestra en la Figura 1.14.

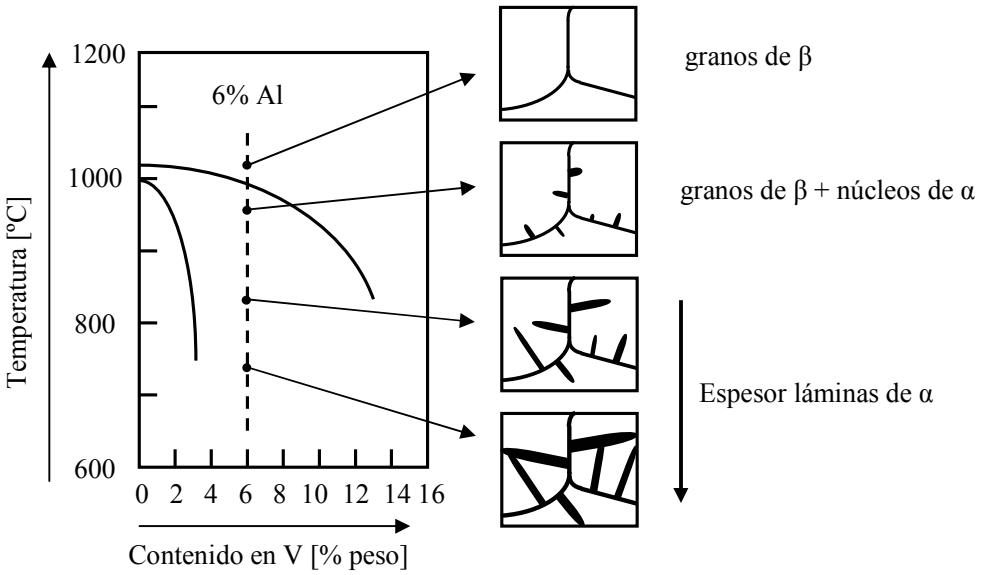

Figura 1.14 – Esquema de la formación de la microestructura Widmanstätten en la aleación Ti–6Al–4V[45].

La morfología de la fase Widmanstätten α puede variar entre una colonia de láminas de α alineadas y de forma similares hasta una microestructura en "cesta" al aumentar la velocidad de enfriamiento y el contenido de elementos de aleación[51].

Cuando se somete una de estas aleaciones al tratamiento de temple en agua, gran parte de la fase beta se transforma martensíticamente en la fase metaestable α', que está caracterizada por una estructura cristalina hexagonal, o en la fase metaestable α'' (ortorrómbica) donde α'' prevalece sobre α' al aumentar el contenido de elementos betágenos.

Estas fases martensíticas no son tan duras como en el caso de los aceros ya que las impurezas intersticiales son más solubles en la fase hexagonal compacta de baja temperatura con respecto a la fase cúbica centrada en el cuerpo (B.C.C.) de alta temperatura. Consecuentemente, la deformación del retículo cristalino inducida por los elementos intersticiales que quedan atrapados no endurecen el titanio; por lo contrario, las fases α' o α'' aumentan la resistencia a fractura del titanio debido al menor tamaño de grano que la caracteriza y a la elevada densidad de dislocaciones que se genera.

No obstante, estas aleaciones de titanio pueden ser endurecidas mediante maduración ya que la fase metaestable resulta ser sobresaturada de elementos betágenos que precipitan formando una fase sub-micrométrica de titanio beta en el interior de las agujas de martensita.

Las microestructuras que se obtienen mediante el tratamiento de solubilización en el campo de la fase beta, es decir a una temperatura superior a la beta transus, o mediante la transformación de la fase beta metaestable suelen ser denominadas estructura beta–transformada o beta–tratada térmicamente independientemente de los detalles de la microestructura misma[51].

La Figura 1.15 muestra un resumen de las diferentes fases que se pueden obtener en función del tipo de enfriamiento adoptado.

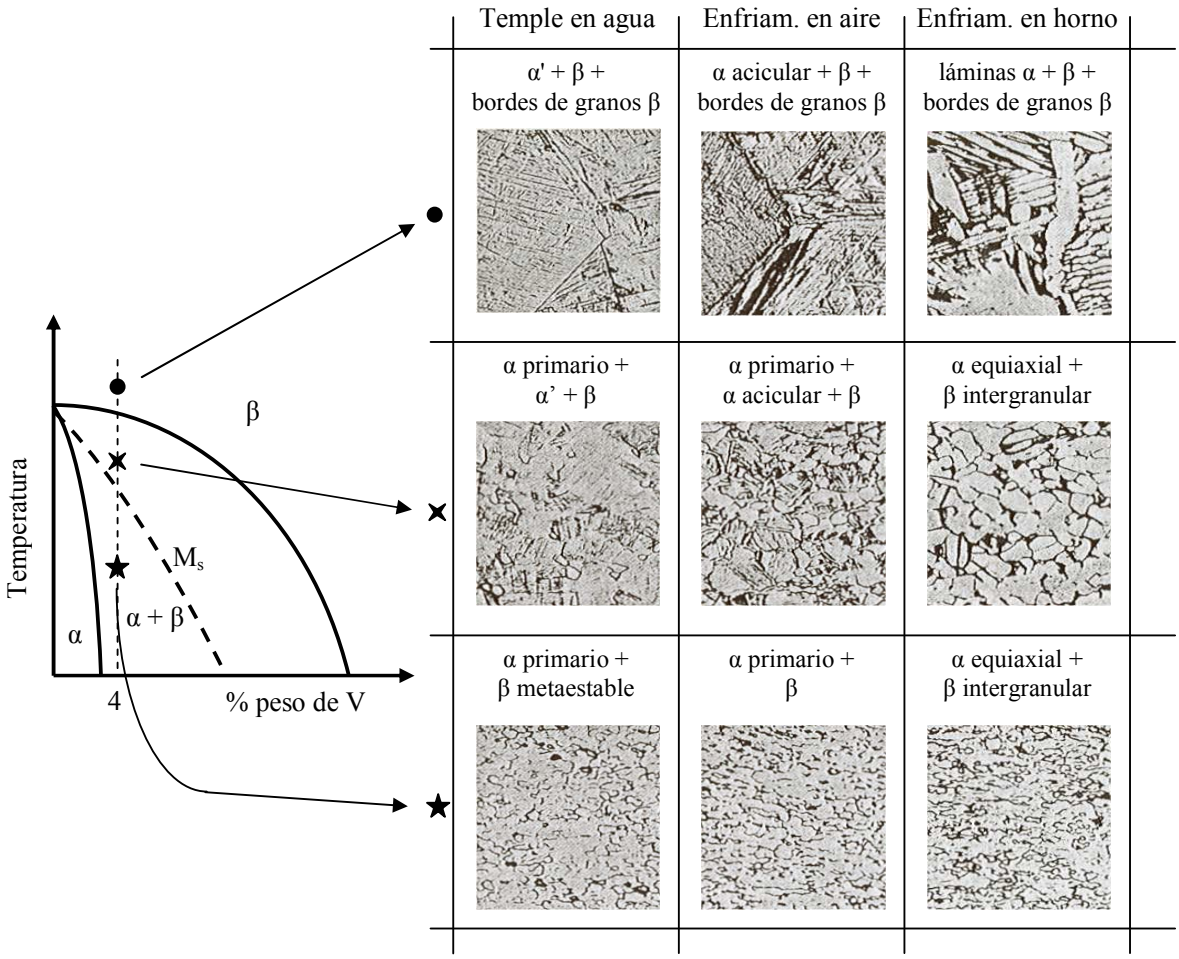

Figura 1.15 – Resumen de las fases obtenibles tras distintos tratamientos térmicos de las aleaciones de titanio[45].

Por lo tanto, existe una variada combinación de tratamientos térmicos que se pueden aplicar a las aleaciones de titanio con el fin de optimizar propiedades específicas en función de la aplicación planeada.

Sin embargo, no todas las aleaciones se someten a tratamientos térmicos porque su respuesta depende de la composición final y de las fases presentes y, por lo tanto, los cambios inducidos por un tratamiento para una aleación y aplicación específica podrían ser perjudiciales para otra. Por ejemplo, la aleación Ti–5Al–2,5Sn ha sido diseñada para proporcionar buena soldabilidad y difícilmente se somete a tratamientos térmicos.

Por otro lado, hay que tener en cuenta que cuando se plantean tratamientos térmicos de las aleaciones de titanio a una temperatura superior a los 427ºC hay que llevarlo a cabo en un atmósfera inerte para evitar la reacción con el nitrógeno o el oxígeno y la formación del "alpha–case"[63].

1.2.6 – Aleación Ti–3Al–2,5V

La aleación Ti–3Al–2,5V, también conocida como ASTM grado 9 o "half Ti–6–4", se suele clasificar como aleación casi–α y tiene la ventaja de poder ser procesada mediante extrusión o bien en un laminador Pilger para producir tuberías sin soldaduras.

La resistencia a corrosión de esta aleación no es tan buena como la del titanio elemental pero su superior resistencia mecánica combinada con la procesabilidad la hacen el material ideal para aplicaciones hidráulicas y para estructuras que trabajan bajo presión donde el peso es un factor crítico desde el punto de vista del transporte.

Efectivamente, la aleación Ti–3Al–2,5V fue inicialmente pensada para producir tuberías de sistemas hidráulicos y de suministro de carburante para aviones y ha sido empleada tanto en aviones militares como en aviones comerciales gracias a sus excelentes prestaciones. Además, esta aleación se utiliza en otras aplicaciones no aerospaciales como por ejemplo la obtención de equipos para el deporte, como palos de golf, raquetas de tenis y chasis de bicicletas, implantes médicos y dentales o para bolígrafos de alta gama.

Como en el caso del titanio elemental, a partir de ella se han desarrollado aleaciones con resistencia frente a la corrosión mejorada añadiendo pequeños porcentajes de paladio o rutenio. La Tabla 1.3 muestra la composición y algunas propiedades físicas y mecánicas de la aleación Ti–3Al–2,5V y de sus variantes.

Siendo una aleación cuya microestructura está constituida principalmente por granos de fase α, con pequeñas cantidades de fase β dispersas en la matriz y en los bordes de grano, los aspectos más importantes de su microestructura son la morfología y la textura de la fase α.

Durante el enfriamiento de esta aleación por debajo de la temperatura de inicio de la transformación adifusional (M_S), aproximadamente 790ºC, gran parte de la fase β se transforma en la fase martensítica hexagonal sobresaturada α''.

Entre M_S y M_F (temperatura a la cual termina la transformación adifusional), aproximadamente 740ºC y en condiciones isotérmicas, la fase β residual se puede transformar en fase α. Por debajo de 750ºC, la fase α'' se descompone discontinuamente en una microestructura bifásica α + β y una fase β metaestable enriquecida de elementos betágenos.

Si durante un enfriamiento continuo se emplea una velocidad de enfriamiento superior a los 22ºC/s se obtiene una estructura martensítica hexagonal mientras que si la velocidad es inferior la microestructura está compuesta por granos de alfa y granos de beta metaestable.

Empleando velocidades de enfriamiento menores de 5ºC/h por debajo de los 500ºC se forma un precipitado con forma de agujas a partir de la fase beta metaestable mientras que para velocidades mayores de 50ºC/h a los 900ºC las plaquetas típicas de la microestructura Widmanstätten empiezan a formarse en los bordes de granos o a partir de los núcleos entre los granos.

Tabla 1.3 – Composición química, propiedades físicas y propiedades mecánicas de la aleación Ti–3Al–2,5V[47, 64].

Propiedad		**Ti–3Al–2,5V**	**Ti–3Al–2,5V–0,05Pd**	**Ti–3Al–2,5V–0,1Ru**
Grado ASTM		*9*	*18*	*28*
Análisis químico	O [% peso]	0,15		
	N [% peso]	0,03		
	C [% peso]	0,08		
	H [% peso]	0,015		
	Fe [% peso]	0,25		
Propiedades físicas	T_β [ºC]	935		
	ρ [g/cm^3]	4,48		
Propiedades eléctricas	σ [S/cm]	7,9E+3		
	ρ (RT) [μΩ·cm]	126		
Propiedades térmicas	k [W/m·ºC]	8,3		
	α (RT) [10^{-6}/ºC]	9,6		
Propiedades mecánicas	E [GPa]	107		
	σ_y [MPa]	485		
	σ_f [MPa]	620		
	ε [%]	15		
	HV (HRC)	267 (25)		
	σ_{10^7} [MPa]*	320	–	–

*R = –1, f = 30 Hz[61]

1.2.7 – Aleación Ti–6Al–4V

La aleación Ti–6Al–4V es la aleación de titanio α + β más estudiada y más comúnmente empleada ya que fue desarrollada con el propósito especifico de ser utilizada para la construcción de estructuras tanto móviles como estáticas de aviones; su uso todavía representa el 40% de total del titanio en las diferentes industrias.

Esta aleación suele ser suministrada a nivel comercial en el estado recocido denominado "mill–annealed". En la Tabla 1.4 se muestra la composición química y algunas propiedades físicas y mecánicas de esta aleación.

Tabla 1.4 – Composición química, propiedades físicas y propiedades mecánicas de la aleación Ti–6Al–4V[47].

Propiedad		**Ti–6Al–4V**	**Ti–6Al–4V (ELI)**	**Ti–6Al–4V–0,1Ru**
Grado ASTM		*5*	*23*	*29*
Análisis químico	O [% peso]	0,20	0,13	
	N [% peso]	0,05	0,03	
	C [% peso]	0,08		
	H [% peso]	0,010	0,012	0,015
	Fe [% peso]	0,25		
Propiedades físicas	T_β [ºC]	996	982	
	ρ [g/cm^3]	4,43		
Propiedades eléctricas	σ [S/cm]	5,8E+3	6,1E+3	
	ρ (RT) [μΩ·cm]	171	165	
Propiedades térmicas	k [W/m·ºC]	6,6	7,3	
	α (RT) [10^{-6}/ºC]	9,0	9,2	
Propiedades mecánicas	E [GPa]	114		
	σ_y [MPa]	827	793	759
	σ_f [MPa]	896	862	827
	ε [%]	10	10	10
	HV (HRC)	321 (33)	316 (32)	
	σ_{10^7} [MPa]*	500	–	–

*R = –1, microestructura equiaxial gruesa (12 μm)[61]

Enfriando la aleación Ti–6Al–4V a partir del intervalo de temperatura de estabilidad de las fases α + β se puede alterar la microestructura final porque sigue estando presente parte de alfa primaria; por lo tanto, el enfriamiento en aire convierte la fase beta presente en beta transformada, principalmente formada por agujas de alfa (acicular), mientras que la fase α primaria queda inalterada.

En general, cuanto menor la temperatura de enfriamiento en el interior del campo donde coexisten α y β tanto menor es la longitud de las agujas de alfa que se genera ya que menor es el tamaño de grano de la fase beta a esa misma temperatura.

En el caso de un enfriamiento rápido mediante agua en lugar de aire a partir del campo α + β, la fase alfa primaria sigue quedando invariada pero la fase beta se transforma en la fase martensítica hexagonal α'.

Cuando se lleva a cabo un temple en agua a partir de una temperatura menor de M_s (850°C), la fase beta presente queda estabilizada a lo largo del tratamiento originando una microestructura compuesta por alfa primaria y beta no transformada. Esto se debe a que a un menor porcentaje de fase beta corresponde un mayor porcentaje de vanadio disuelto que garantiza la estabilización durante el temple. La fase beta no transformada que se forma mediante este temple es metaestable y puede quedar indefinidamente a temperatura ambiente, pero se transforma martensiticamente si es sometida a deformación.

Como se puede intuir, existe una amplia variedad de microestructuras que se pueden obtener, lo que debería corresponder a una variación significativa de las propiedades mecánicas en función de la temperatura de tratamiento. Sin embargo, el límite elástico de la aleación Ti–6Al–4V varía de entre 830 MPa y 930 MPa después de un recocido, hasta 1100 MPa después de temple y envejecimiento, y la ductilidad disminuye del 15% al 10%.

La aleación Ti–6Al–4V proporciona unas buenas propiedades mecánicas hasta temperaturas relativamente altas, aproximadamente 400ºC, además de una excelente resistencia a la corrosión. Esta combinación de propiedades ha permitido su empleo en sectores de muy alto nivel tecnológico como el aeronáutico, para la producción de paletas de turbinas, componentes para motores (discos y ruedas) y componentes estructurales.

Además, esta aleación se emplea extensivamente en el sector biomédico para la obtención tanto de implantes como de tornillos para los huesos gracias a su incomparable biocompatibilidad. En el sector marítimo, la aleación Ti–6Al–4V ha sido utilizada para la obtención de equipos sonar, armamentos o válvulas para submarinos nucleares.

Uno de los sectores que todavía se resisten a la utilización del titanio a gran escala es el automovilístico si bien la aleación Ti–6Al–4V ha sido empleada en coches de carreras para producir partes rotativas, válvulas, muelles y ejes. Finalmente, esta aleación ha sido estudiada y procesada mediante técnicas pulvimetalúrgicas a partir de polvos elementales si bien no se obtienen componentes completamente densos y, por lo tanto, presenta menor ductilidad, tenacidad y resistencia a la fatiga.

El empleo de polvos prealeados y, consecuentemente, más caros, ha sido el enfoque utilizado para la obtención de componentes críticos pero su aplicaciones se limitan a un pequeño nicho a causa del alto coste final del componente.

1.2.8 – Aleación Ti–6Al–7Nb

La aleación de titanio Ti–6Al–7Nb fue desarrollada en los años 80 del siglo XX con el fin específico de poder producir componentes para prótesis de cadera debido a su alta resistencia, buena ductilidad y tenacidad y excelente biocompatibilidad.

Esta aleación fue diseñada para remplazar la aleación Ti–6Al–4V durante la búsqueda de aleaciones libres de vanadio[65-67] con mejores propiedades frente al desgaste[68] y mejor comportamiento durante los procesados de fundición. La Tabla 1.5 muestra algunas propiedades de esta aleación de titanio.

Tabla 1.5 – Composición química, propiedades físicas y propiedades mecánicas de la aleación biomédica Ti–6Al–7Nb[47].

Propiedad		**Ti–6Al–7Nb**
Grado ASTM		*F1295*
Análisis químico	O [% peso]	0,20
	N [% peso]	0,05
	C [% peso]	0,08
	H [% peso]	0,01
	Fe [% peso]	0,25
Propiedades físicas	T_β [ºC]	1010
	ρ [g/cm^3]	4,52
Propiedades eléctricas	σ [S/cm]	6,3E+3
	ρ (RT) [$\mu\Omega$·cm]	158
Propiedades térmicas	k [W/m·ºC]	7,0
	α (RT) [10^{-6}/ºC]	8-9,8
Propiedades mecánicas	E [GPa]	105
	σ_y [MPa]	800
	σ_f [MPa]	900
	ε [%]	10
	HV	290[69] – 350[67]
	σ_{10^7} [MPa]*	500

*Flexión rotativa[61]

Como se ha especificado anteriormente, la aleación Ti–6Al–7Nb ha sido desarrollada explícitamente para el sector biomédico y aplicaciones típicas son las prótesis del fémur, placas para la fijación de fracturas, componentes para la espina dorsal, grapas, barras, hilos y clavos.

La resistencia frente a la corrosión de la aleación Ti–6Al–7Nb en cloruro de sodio resulta ser equivalente a la del titanio elemental y la de la aleación Ti–6Al–4V debido a la formación de una capa pasivante altamente estable y densa[70, 71].

El grado de biocompatibilidad de la aleación Ti–6Al–7Nb en vivo[66] así como las propiedades de tracción y resistencia a la fatiga en ambiente corrosivo[72] han sido estudiadas exhaustivamente.

1.2.9 – Aplicaciones del Titanio y de sus Aleaciones

La industria aeronáutica, y en particular la militar, ha sido siempre uno de los sectores que más ha empleado el titanio ya que sus excelentes prestaciones justifican el alto coste del producto final[73]. Tanto en aviones militares como comerciales, el titanio se utiliza en motores de turbinas de gas, para la fabricación de los álabes de los compresores ya que se precisan un ratio entre resistencia y densidad elevado, una buena ductilidad y una buena resistencia a corrosión. El empleo del titanio para la fabricación de aviones garantiza una reducción del peso total de aproximadamente el 17% donde esta reducción se hace más efectiva al aumentar la velocidad de crucero.

En el sector químico y petroquímico el titanio y sus aleaciones, especialmente las que contienen paladio, se emplean para la producción de tuberías, contenedores de reacción, intercambiadores de calor, filtros y válvulas gracias a su excelente resistencia a corrosión [4] ya que permiten aumentar la vida útil, reducir el mantenimiento y disminuir la contaminación por parte del hierro que es el material que se empleaba anteriormente[2].

Además, el titanio se emplea para la fabricación de utensilios para la industria alimenticia, como mezcladoras y contenedores debido a su excelente resistencia frente a diferentes ácidos orgánicos. Asimismo, el titanio ha aportado mejoras en la industria del papel y de la celulosa, la industria textil y la industria de la perforación tanto en alta mar como cerca de la costa.

En cuanto al sector biomédico, el titanio se utiliza para obtener prótesis artificiales para las articulaciones, implantes dentales, "stents" cardiovasculares, válvulas cardíacas, gafas y sillas de ruedas.

Las aplicaciones para el sector náutico incluyen cascos tanto para embarcaciones como para submarinos, hélices y sistemas para el suministro de agua.

Además, el titanio es utilizado para la producción de artículos deportivos como palos de golf, bicicletas, esquís, cilindros para almacenar gases para las inmersiones y palos de lacrosse.

El titanio ha sido también limitadamente empleado en industrias altamente sensibles al coste como por ejemplo la arquitectura o el sector automovilístico para fabricar respectivamente recubrimientos de fachadas y válvulas y componentes de motores de altas prestaciones.

Finalmente, el titanio suele ser también utilizado como elemento de aleación para otros metales, como en los aceros inoxidables, ya que minimiza la corrosión intergranular de los mismos.

A continuación se describen algunas aplicaciones particulares del titanio y sus aleaciones:

Aplicaciones relacionadas con la industria aeronáutica: la aleación Ti–6Al–4V en el estado de recocido ha sido la aleación de titanio predominante en el sector de la aeronáutica para la fabricación de estructuras y motores de aviones. Sin embargo, a lo largo de los años, diferentes aleaciones de alta resistencia y tratables térmicamente han sido aplicadas extensivamente, como por ejemplo Ti–10V–2Fe–3Al o Ti–35V–15Cr (Alloy C)[74]. La Figura 1.16 muestra ejemplos de componentes de reactores de turbinas para aplicaciones aeronáuticas normalmente obtenidos a partir de titanio.

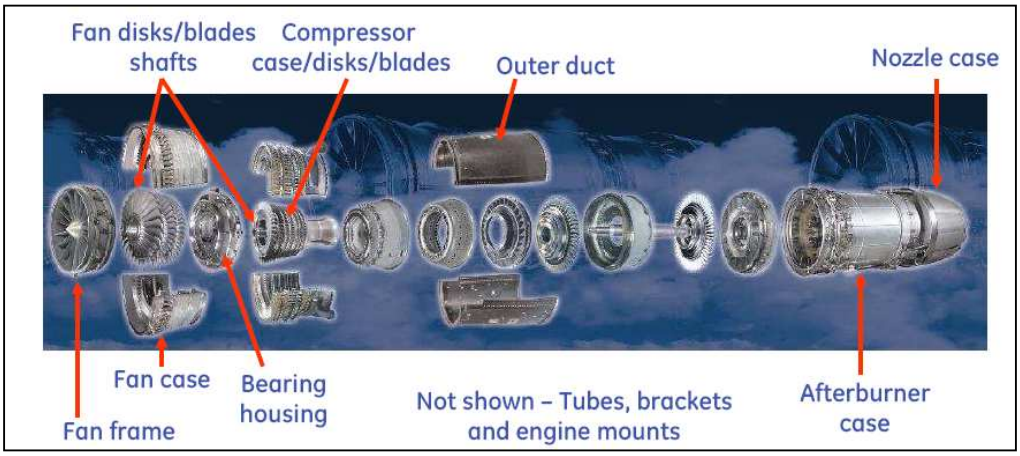

Figura 1.16 – Componentes de reactores para aplicaciones aeronáutica producidos empleando titanio y sus aleaciones[75].

A continuación se propone un pequeño resumen de las aplicaciones aeronáuticas del titanio y de sus aleaciones divididas en función del tipo de aleación[76]:

- aleaciones α: el titanio elemental se emplea en estado recocido por su conformabilidad y resistencia a la corrosión en aplicaciones como las tuberías de los servicios o los conductos del sistema de control ambiental y anticongelante (ECS). La aleación Ti–3Al–2,5 se emplea exclusivamente para la fabricación de tuberías hidráulicas y la aleación Ti–5Al–2,5Sn recocida para aplicaciones criogénicas como los inyectores para motores turbo[77]. Otros componentes muy importantes son los dispositivos móviles de motores de turbinas de gas como las paletas, los discos o los rotores que trabajan hasta una temperatura máxima de 540°C. Estos tienen que caracterizarse por una alta resistencia a la fluencia en caliente y, por lo tanto, se emplean aleaciones como la Ti–6Al–2Sn–4Zr–2Mo–0,1Si y la Ti–5,5Al–3,5Sn–3Zr–1Nb–0,25Mo–0,3Si (IMI 829)[46]. Para poder alcanzar temperaturas ligeramente más elevadas han sido desarrolladas otras aleaciones como la Ti–5,8Al–4Sn–3,5Zr–0,7Nb–0,5Mo–0,35Si–0,06C (IMI 834)[46] y la Ti–6Al–2,8Sr–4Zr–0,4Mo–0,4Si (Timetal–1100)[78, 79];

- aleaciones α + β: la aleación Ti–6Al–4V es la más empleada y sus propiedades pueden ser optimizadas mediante tratamientos térmicos como se ha indicado anteriormente. Las aplicaciones varían entre los componentes estructurales como el fuselaje, las alas o el tren de aterrizaje hasta los componentes estáticos (conductos de escape, marcos de ventanillas o uniones críticas de aletas verticales al fuselaje) y los componentes móviles como discos y paletas de compresores de baja presión. Otra aleación α + β utilizada extensivamente para la fabricación de estructuras de soporte del tren de aterrizaje es la Ti–6Al–6V–2Sn ya que permite una reducción de peso con respecto a la Ti–6Al–4V. Las aleaciones Ti–6Al–2Sn–2Zr–2Mo–2Cr, Ti–6Al–2Sn–4Zr–6Mo y Ti–5Al–2Zr–2Sn–4Mo–4Cr han sido desarrollada para remplazar la Ti–6Al–4V donde se precisa una mayor resistencia a temperaturas moderadas;

- aleaciones β: la primera aleación beta importante desde el punto de vista comercial ha sido la Ti–13V–11Cr–3Al y ha sido utilizada por su buena estabilidad térmica aunque actualmente se emplea exclusivamente para fabricar muelles. La aleación Ti–15V–3Cr–3Al–3Sn ha sido usada debido a su buena conformabilidad en frío para obtener láminas o piezas de forma rectangular, redonda u oval para ECS, extintores, clips y corchetes para las estructuras de soporte del suelo. Otra aleación ampliamente utilizada en el tren de aterrizaje es la Ti–10V–2Fe–3Al ya que permite una ulterior reducción de peso y elimina completamente la eventual formación de grietas por corrosión bajo tensión si bien suele ser utilizada también para la fabricación de puertas de aviones de carga, el "sistema Nacelle" que protege la turbina y la cola (empenaje) compuesta por el estabilizador horizontal, estabilizador vertical, timón de dirección y timón de profundidad. Finalmente, esta aleación ha encontrado muchas aplicaciones en la fabricación de helicópteros gracias a la combinación de una muy buena vida a fatiga, alta resistencia a fractura y baja rigidez. Para aplicación a elevadas temperaturas, en el intervalo 480–565°C, se utiliza la aleación Ti–15Mo–2,7Nb–3Al–0,2Si (BETA 21S) aunque la mayor ventaja de esta aleación es la inmunidad frente a los efectos del ácido orgánico-fosfórico generado por el fluido hidráulico caliente empleado en aviones comerciales.

Aplicaciones relacionadas con la industria química y ambientes corrosivos: cuando el titanio es expuesto al aire se pasiva (potencial estándar de electrodo –1,75 V para la reacción $Ti \leftrightarrow Ti^{2+} + 2e^-$) formando una capa de óxido de unos pocos nanómetros de espesor que protege el metal frente a sucesivos fenómenos de corrosión. En el caso de que se fracture, la capa de óxido se forma nuevamente necesitando exclusivamente un muy pequeño porcentaje de oxígeno o agua.

Esta capa de óxido es muy adherente al substrato metálico y muy estable a lo largo de un amplio intervalo de concentraciones pH para soluciones corrosivas siempre y cuando esté presente una pequeña cantidad de H_2O u oxígeno para mantener la capa de óxido o no se trate de condiciones altamente reductoras, ambientes extremadamente oxidantes o haya iones de fluoruro (F^{-1}) ya que estos son los únicas que pueden atacar el titanio y sus aleaciones.

Cuando el titanio es expuesto al aire a elevadas temperaturas, los fenómenos de difusión entre titanio y oxigeno inducen un crecimiento gradual de la capa de oxidación pasando de los pocos nanometros de la capa original a unas cuantas micras para una exposición de 30 minutos en aire a 700°C y unas centenas de micras cuando se incrementa la temperatura hasta los 1050°C[3]. El crecimiento de la capa de óxido es proporcional a la fragilización de la superficie por lo que debe evitarse ya que no es tolerable para muchas aplicaciones porque provocaría el fallo del componente en servicio.

La utilización de las aleaciones de titanio en el sector de la generación de energía y, en particular, para la fabricación de álabes de turbinas de vapor ha sido evaluada para poder incrementar la eficiencia mediante un aumento de la longitud de los álabes. En particular, ha sido empleada la aleación Ti–6Al–4V y han sido desarrolladas otras nuevas aleaciones beta[80], como la Ti–15Mo–5Zr, la Ti–10V–2Fe–3Al y la Ti–5Al–2Zr–2Sn–4Mo–4Cr, conocida como Ti–17[47].

Otra aplicación muy prometedora del titanio es el sector del trasporte naval donde las aleaciones Ti–6Al–4V y la Ti–3Al–8V–6Cr–4Mo–4Zr, comercialmente llamada Ti Beta C[47], han sido utilizadas con éxito[80].

La Figura 1.17 muestra unos componentes obtenidos a partir de titanio o aleaciones de titanio para aplicaciones en la industria química y en ambientes corrosivos.

Figura 1.17 – Componentes para la industria química y para ambientes corrosivos producidos con el titanio y sus aleaciones[81].

Aplicaciones relacionadas con la industria biomédicas: las aleaciones de titanio resultan ser muy atractivas para aplicaciones como implantes biomédicos, tanto dentales[82, 83] como ortopédicos[84, 85], gracias a la combinación de propiedades que proporcionan[86]: resistencia a la corrosión, propiedades mecánicas (resistencia a fatiga), bajo módulo elástico que tiene que ser lo más parecido al del hueso (variable entre 10 y 30 GPa)[87], baja densidad, biocompatibilidad y buena osteointegración, es decir, buena capacidad de unirse a los huesos y a los otros tejidos humanos[88].

Existen tres grupos de aleaciones de titanio utilizadas a nivel industrial: titanio elemental, aleaciones α + β y aleaciones β. El titanio elemental y la aleación Ti–6Al–4V fueron los primeros en ser utilizados y lo siguen siendo pero debido a los supuestos efectos citotóxicos a largo plazo del vanadio en el cuerpo humano, fueron desarrolladas otras aleaciones α + β como la Ti–5Al–2,5Fe[89] y la Ti–6Al–7Nb[90]. Una mejora de la biocompatibilidad y una disminución del módulo de elasticidad se ha alcanzado con la segunda generación de aleaciones, es decir: Ti–12Mo–6Zr–2Fe[91], Ti–15Mo–5Zr–3Al, Ti–15Mo–3Nb–3O, Ti–15Zr–4Nb–2Ta–0,2Pd, Ti–15Sn–4Nb–2Ta–0,2Pd[92] y la aleación "completamente biocompatible" Ti–13Nb–13Zr[93]. Finalmente, aleaciones beta con módulo de Young similar al de los huesos han sido obtenidas mediante la aleaciones denominadas "TNZT" basadas en el sistema Ti–Nb–Zr–Ta[94].

Las técnicas pulvimetalúrgicas pueden ser empleadas en el ámbito biomédico para producir componentes con superficies caracterizadas por una estructura de poro controlada[95] con el fin de favorecer la estabilización e integración de los implantes médicos[84, 96]. Para favorecer la formación de un nuevo hueso alrededor del implante se precisa una porosidad con un tamaño variable entre 50 y 400μm[97] así como un porcentaje relativo de porosidad del 30–40%[98].

Un ejemplo de aleación con biocompatibilidad mejorada y muy bajo módulo de elasticidad, alrededor de 55 GPa, es la aleación Ti–35Nb–7Zr–5Ta obtenida mediante técnicas pulvimetalúrgicas, estudiada por Taddei et al.[88].

La Figura 1.18 muestra unos ejemplos de implantes biomédicos producidos convencionalmente empleando tanto titanio elemental como sus aleaciones.

Figura 1.18 – Implantes biomédicos obtenidos a partir de titanio elemental o aleaciones de titanio: a) implante para la sustitución del fémur y b) implante para los huesos del cráneo[99].

Aplicaciones relacionadas con la industria automovilísticas: si bien las posibles aplicaciones del titanio y de sus aleaciones en el sector del automóvil podrían ser muchas, como por ejemplo sistemas de escape (titanio elemental), ejes (Ti–6Al–4V), muelles de suspensión (aleaciones beta) y válvulas o rotores de turbocompresores (intermetálicos de base titanio), su aplicación a nivel de producción industrial no se ha producido todavía a causa del alto precio de obtención y fabricación del mismo titanio[6, 7, 43, 100-106].

La Figura 1.19 muestra algunas de las potenciales aplicaciones del titanio en el ámbito automovilístico y algunos ejemplos de productos ya empleados y producidos mediante técnicas pulvimetalúrgicas.

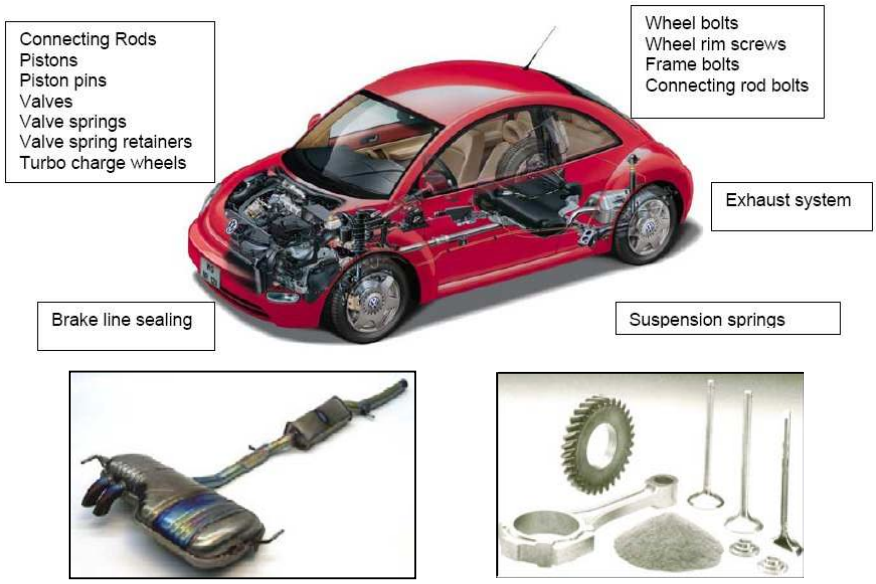

Figura 1.19 – Aplicaciones del titanio en ámbito automovilístico: potenciales aplicaciones (arriba) y componentes empleados en coches actuales (abajo)[6, 100].

Aplicaciones relacionadas con el deporte: el alto ratio entre la resistencia y la densidad, que permite la obtención de equipos más ligeros, así como un bajo módulo de Young y la resistencia a la corrosión propician la utilización del titanio y de sus aleaciones en aplicaciones para el deporte. Los mismos productos nombrados durante la breve descripción de las aplicaciones en campo automovilístico se pueden trasladar a coches o motos de carreras. Además, bicicletas o diferentes componentes de ellas, palos de golf, etc. suelen ser obtenidos a partir de aleaciones de titanio[107]. En particular, las aleaciones más utilizadas son la Ti–6Al–4V y la Ti–15V–3Cr–3Sn–3Al[80]. La Figura 1.20 muestras unos ejemplos de productos relacionados con el deporte.

a) b) c)

Figura 1.20 – Ejemplos de empleo del titanio para la producción de artículos relacionados con el deporte: a) palo de golf, b) bastidor trasero monoplaza para motocicletas y c) tapa de protección piñón[108].

Aplicaciones relacionadas con la apariencia: en este grupo de aplicaciones se puede distinguir dos diferentes categorías: aquella donde se explota la apariencia de naturaleza brillante propia del titanio y aquella donde este color natural se cambia de forma artificial mediante anodizado.

Por su apariencia, el titanio se emplea en arquitectura para la fabricación de la cobertura del exterior de los edificios (Museo Guggenheim – España), en la construcción, en joyería, relojería y otros artículos como monturas de gafas o plumas[109]. La Figura 1.21 muestras unos ejemplos de aplicaciones del titanio relacionadas con su apariencia.

a) b) c)

Figura 1.21 – Ejemplos de empleo del titanio por su apariencia: a) Museo Guggenheim de Bilbao, b) plato "ride" para batería y c) reloj.

Aleaciones con propiedades especificas mejoradas: acerca del desarrollo de nuevas aleaciones estas pueden ser clasificadas en función de la propiedad deseada[80]. A continuación se muestran algunos ejemplos:

- Resistencia a la corrosión: se trata de titanio elemental o aleaciones comerciales a las cuales se les añade un pequeño porcentaje de Pd con Mo (SMI–ACE), Ru con Ni (TICOREX) o, alternativamente, una mezcla de una pequeña cantidad de todos estos elementos (AKOT);
- Conformabilidad en frío: son aleaciones beta diseñadas para disminuir la resistencia a la deformación como por ejemplo las aleaciones Ti–22V–4Al (DAT–51), Ti–20V–4Al–1Sn (SAT–2041CF) o Ti–16V–4Sn–3Nb–3Al;
- Alta resistencia a la fractura: se han estudiado aleaciones de titanio beta, como la Ti–0,5Fe–0,1N (TIX–80), o alfa–beta, como la Ti–4,5Al–3V–2Mo–2Fe (SP–700), con muy alta resistencia y apropiado nivel de ductilidad y deformabilidad;
- Aleaciones avanzadas: estas aleaciones han sido desarrolladas para hacer frente a funciones específicas como por ejemplo la aleación Ti–3Al–2V–0,1S que está caracterizada por un buen comportamiento frente al mecanizado;
- Superconductividad: descubierta por Onnes se manifiesta en materiales metálicos cuando son expuestos a muy baja temperatura donde la resistividad eléctrica disminuye significativamente hasta anularse a una temperatura específica T_C. En particular, uno de los superconductores de baja temperatura y alta corriente se fabrica empleando la aleación Nb–47Ti[46];

- Aleaciones con memoria de forma: como su propio nombre indica, la peculiaridad de estas aleaciones es su capacidad de recuperar la forma geométrica inicial, después de haber sufrido una deformación plástica, mediante el calentamiento a una temperatura de unos pocos centenares de grados centígrados. En la actualidad, las aleaciones del sistema TiNi son unas de las más empleadas para diferentes aplicaciones, que pueden ser divididas en cuatro grupos: recuperación libre de la forma, recuperación forzada de la forma, actuadores y dispositivos superplásticos[46]. La Figura 1.22 muestra una aplicación de las aleaciones con memoria de forma, un "stent" cardiovascular autoexpandible.

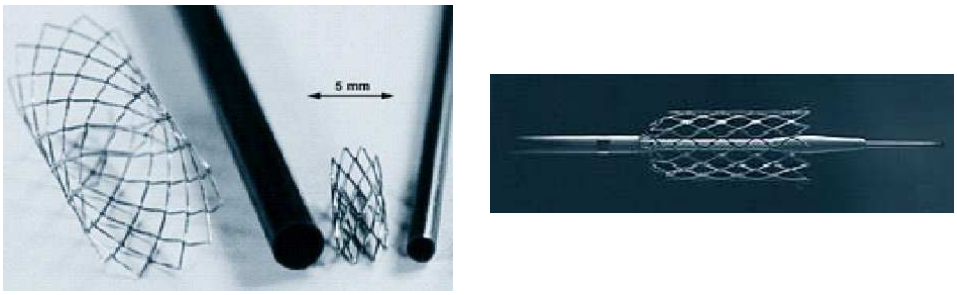

Figura 1.22 – "Stent" cardiovascular autoexpandible producido con la aleación con memoria de forma TiNi[110].

Aleaciones de titanio de bajo coste: a lo largo de los años se ha intentado desarrollar aleaciones de bajo coste como alternativa a la aleación Ti–6Al–4V donde el hierro ha sido considerado como elemento viable y económico, siendo estudiado su efecto en diferentes trabajos[111-115].

Las aleaciones de bajo coste que se emplean actualmente tienen un contenido máximo del 5,5% en peso de hierro para evitar la posible formación de intermetálicos de TiFe que fragilizan la microestructura. Por otro lado, la introducción de Fe dificulta el procesado convencional de las aleaciones al producirse segregación de los metales durante la fusión mientras que el procesado pulvimetalúrgico elimina estos problemas[116].

Por ello, en los últimos años se ha evaluado el desarrollo de aleaciones de titanio de bajo coste con un contenido de hierro superior al contenido máximo convencional a partir del enfoque de mezcla de polvos elementales como mediante aleaciones maestras[117-120]. Las nuevas aleaciones han sido caracterizadas tanto en términos de comportamiento frente al prensado y sinterización como sus propiedades mecánicas finales[121, 122].

1.3 – TECNOLOGÍA PULVIMETALÚRGICA

La pulvimetalurgia (P/M) puede ser definida como el estudio del procesado de polvo, tanto metálico como cerámico, empezando por la producción del polvo mismo, pasando a su caracterización para llegar a la obtención de un producto macizo con una forma específica. El proceso de producción de un polvo determina la morfología, las propiedades y la estructura del polvo que a su vez influye en todas las etapas del proceso P/M.

Independientemente de la técnica considerada, hay dos etapas básicas en el proceso pulvimetalúrgico: el conformado del polvo en una preforma con forma muy parecida a la final del producto que se quiere obtener y la sinterización, es decir, el tratamiento térmico a una temperatura inferior a la de fusión del elemento mayoritario constituyente del material considerado para inducir fenómenos de difusión que generan enlaces químicos entre las partículas del polvo. Sin embargo, en algunos casos estas dos etapas se llevan a cabo simultáneamente, como en las técnicas de conformado en caliente, con el fin de alcanzar mejores propiedades tanto físicas como mecánicas.

Con respecto a los métodos de procesado más convencionales, la pulvimetalurgia está caracterizada por algunas ventajas intrínsecas como la fabricación de piezas con la geometría final deseada o muy parecida, por eso se definen como técnicas "net–shape" o "near–net–shape"[123], limitando significativamente o eliminado completamente la necesidad de operaciones de mecanizado.

Además, la P/M permite un mejor control de la microestructura, una mayor homogeneidad en los componentes, menores costes en las producciones de gran escala y ofrece la posibilidad de conformar materiales difíciles de procesar, por ejemplo a causa de la elevada diferencia entre las temperaturas de fusión de sus constituyentes, materiales compuestos[104, 124-127], materiales porosos[87] o nuevas composiciones con propiedades especificas[128-130].

Como todos los métodos de procesado, la P/M está caracterizada por algunas desventajas y, en particular, estas se refieren al alto coste de las materias primas, ya que tienen que ser convertidas en forma de polvo, al coste de producción y mantenimiento de las matrices y las herramientas, así como en la relativamente limitada complejidad de las piezas.

La obtención de buenas propiedades mecánicas en productos P/M está directamente relacionada con alcanzar elevados niveles de densidad relativa, equivalente a pequeños porcentajes de porosidad residual, ya que esta afecta la mayoría de las características de un componente.

1.3.1 – Prealeado y Mezcla Elemental

Como indica su propio nombre, las técnicas pulvimetalúrgicas se basan en materiales en forma de polvo como materia prima. Actualmente existen diferentes enfoques para la obtención de polvos con la composición final deseada que se emplean en función del método utilizado en la etapa de consolidación y del tamaño de partícula de los constituyentes.

En lo que concierne a la fabricación de aleaciones de titanio, estas pueden ser producidas principalmente mediante dos rutas[131]: a partir de polvo con la composición final deseada, comúnmente denominados polvos prealeados (prealloyed – PA), o a partir de la mezcla de polvos elementales (blending elemental – BE). En este último caso los elementos aleantes pueden ser añadidos tanto en forma de polvos elementales como en forma de aleaciones maestras (master alloy – MA), como ocurre por ejemplo con el empleo de la aleación maestra Al:V 60:40 para la obtención de la aleación Ti–6Al–4V[132].

Si bien las aleaciones obtenidas mediante estos dos enfoques presentan la misma composición final después de la etapa de sinterización, se comportan de forma diversa tanto durante las etapas previas, es decir almacenamiento, compactación, etc., como durante la misma etapa de sinterización. Esto se debe a que cada partícula de un polvo prealeado tiene la composición final mientras que la mezcla de polvos elementales está constituida por partículas de composición diferente entre ellas.

Es importante además destacar que los polvos prealeados son más duros y conllevan un desgaste más importante de las matrices, ya que los elementos de aleación están disueltos dentro de la matriz base endureciéndola, mientras que los polvos de mezcla elemental requieren más tiempo o mayor temperatura durante la sinterización para poder alcanzar la homogeneidad microestructural por fenómenos de difusión.

Normalmente, la producción de componentes a partir de polvos de mezcla elemental resulta ser la vía más económica[133, 134] si bien estos llegan a proporcionar propiedades dinámicas, como la vida a fatiga, ligeramente inferiores con respecto a productos fabricados empleando polvos prealeados, especialmente los obtenidos mediante atomización[135].

Tanto los polvos de mezcla elemental como los prealeados pueden ser consolidados mediante prensado uniaxial en frío y sinterización, es decir la técnica pulvimetalúrgica más económica, a excepción de cuando están caracterizados por una morfología esférica, típica del proceso de atomización tanto en gas como en plasma.

Convencionalmente, en el procesado del titanio y de sus aleaciones mediante técnicas P/M, los polvos BE suelen ser conformados mediante el método más convencional, es decir, compactación uniaxial y sinterización[136, 137] resultando ser la vía más económica para fabricar componentes no críticos de titanio[133, 134] ya que se pueden evitar post–procesados como la compactación isostática en caliente[132].

Por otro lado, los polvos prealeados, generalmente de morfología esférica, se procesan mediante técnicas P/M avanzadas como la compactación isostática en caliente o el moldeo por inyección de polvo (MIM)[138, 139].

1.3.2 –Compactación en Frío y Sinterización

Entre los diferentes métodos de compactación en frío se encuentran la forja de polvos (powder forging), la compactación isostática en frío, la compactación de polvos precalentados (warm compaction), la laminación de polvos (powder rolling) y el prensado uniaxial.

En este apartado se procederá a la descripción de la técnica de compactación en frío más sencilla, es decir el prensado uniaxial seguido de la etapa de sinterización (P&S).

La compactación uniaxial en frío más sencilla se lleva a cabo aplicando una presión mediante un pistón y empleando matrices con la forma deseada. Este procedimiento lleva el nombre de compactación por simple efecto. Cuando la presión se aplica empleando también un pistón inferior, la compactación se denomina de doble efecto. Por otro lado, se puede emplear una prensa de simple efecto pero utilizando una matriz flotante para garantizar una mejor distribución de la densidad.

La etapa de sinterización conlleva la formación de enlaces químicos entre las partículas inducidos mediante un tratamiento térmico a relativamente alta temperatura gracias a fenómenos de transporte de masa en el estado sólido.

En el caso del titanio y de sus aleaciones la sinterización se lleva a cabo en hornos de alto vacío, con el fin de evitar la contaminación de material, en el intervalo de temperatura entre los 1100ºC y los 1315ºC[45]. En todos los casos, la sinterización de las aleaciones de titanio se lleva a cabo a una temperatura superior a la beta transus. Detalles acerca la compactación en frío y la sinterización del titanio y de sus aleaciones se puede encontrar en la revisión redactada por Qian[140].

Para poder alcanzar el nivel de propiedades mecánicas, es decir resistencia a fractura, ductilidad y resistencia a fatiga, igual a las de componentes obtenidos mediante técnicas convencionales, un componente obtenido mediante técnicas pulvimetalúrgicas convencionales debe presentar una buena homogeneidad en cuanto a composición química y microestructural. Sin embargo esto no es suficiente ya que se precisa conseguir una densidad relativa superior al 98% con respecto al valor teórico[141, 142].

En el caso del titanio y de sus aleaciones, la densidad relativa alcanzable a partir de un polvo de mezcla elemental normalmente no supera el 95%[143]. Por lo tanto, para poder mejorar la densidad final, el componente sinterizado puede ser sometido a un proceso secundario de deformación en caliente, como por ejemplo la compactación isostática en caliente (HIP)[135].

1.3.3 – Compactación en Caliente

La compactación y los procesos de deformación en caliente implican la aplicación simultánea de presión y temperatura al polvo, el cual puede estar en un contenedor cerrado o en una matriz. La ventaja de estos procesos es que permiten alcanzar valores de densidad mayores respecto a los obtenibles mediante pulvimetalurgia convencional llegando incluso a obtener piezas completamente densas. Cabe recordar que, en general, a una mayor densidad corresponden mejores propiedades.

A continuación se presenta una breve descripción de las técnicas de consolidación en caliente utilizadas en el desarrollo de esta tesis:

Compactación isostática en caliente: la compactación isostática en caliente puede ser utilizada tanto para compactar polvo como para cerrar la porosidad residual de muestras previamente compactadas y sinterizadas.

La compactación en caliente a partir de polvo se aplica para consolidar materiales de altas prestaciones, como los empleados en el sector aeronáutico (superaleaciones de níquel, titanio y aluminio), materiales compuestos o aceros rápidos.

Las propiedades de los polvos que afectan a las propiedades finales incluyen la morfología, el tamaño de partícula y su distribución, la composición y el nivel de contaminantes.

En el caso de piezas previamente sinterizadas existen dos posibilidades: una comporta la encapsulación de la muestra en un molde antes de someterla al procesado y la otra no precisa esta etapa previa.

Para este último caso se recomienda que la densidad relativa de los sinterizados no sea inferior al 92% del valor teórico ya que este valor corresponde a la formación de una estructura porosa compuesta exclusivamente por porosidad cerrada[144], la única que puede ser eliminada mediante el procesado de HIP sin encapsulación. Por lo tanto, el porcentaje de porosidad residual que se puede cerrar mediante HIP varía entre 0,1 y 8% aproximadamente en función de la tipología de porosidad[136].

Durante el HIP, la densificación de los polvos y/o la reducción de la porosidad residual se obtiene gracias a un gas a alta presión, como el argón o el nitrógeno, que es utilizado para transferir el calor y la presión. Los principales parámetros a controlar durante el procesado son la presión, que equivale a la tensión aplicada a las piezas, la temperatura y el tiempo.

En general, todos los polvos metálicos pueden ser densificados a 100 MPa con una meseta que varía entre 2 y 4 horas mientras que la temperatura varía significativamente en función del material.

En el caso del titanio y sus aleaciones se aconseja que sea entre 800ºC y 960ºC[145] y, por lo tanto, suelen ser consolidadas a una temperatura inferior a la transición beta; condiciones típicas para la aleación Ti–6Al–4V son 950ºC a 100 MPa durante 4 horas.

Compactación uniaxial en caliente: la forma más simple de prensado en caliente implica verter el polvo con la composición deseada en un molde, generalmente de grafito[45, 54, 144, 146], que suele ser recubierto de un folio de material de baja reactividad con el fin de limitar la reacción entre el molde y el polvo.

Además, se emplean sprays de materiales cerámicos de alta temperatura, como el nitruro de boro (BN) o la zirconia (ZrO_2), para reducir los fenómenos de reacción y para favorecer la separación y la extracción de las piezas finales[146, 147].

La atmósfera más comúnmente usada durante el proceso de prensado en caliente es gas inerte, como argón o nitrógeno, o vacío. La utilización de moldes y elementos de calentamiento de grafito genera una atmósfera rica en carbono en el interior de la cámara de compactación, que puede dificultar la compactación de polvos que tengan una fuerte tendencia a reaccionar con el carbono.

Aunque el prensado en caliente se aplica mayoritariamente a polvos elementales o mezclas de polvos, en las aplicaciones mas avanzadas esta técnica puede ser empleada para la fabricación de materiales compuestos.

Finalmente, cabe destacar que no hay constancia de la aplicación del procesado de compactación en caliente del titanio a nivel industrial.

1.4 – TITANIO PULVIMETALÚRGICO

Además de la reducción de los costes de extracción, la investigación acerca del titanio se ha centrado en el desarrollo y aplicación de técnicas que permiten obtener componentes con la forma final deseada o muy parecida a ella con el fin de limitar los procesos de mecanizado. Entre estos métodos se encuentran la fundición (como la fundición a la cera perdida o en molde permanente), el conformado superplástico (SPF), la forja y la pulvimetalurgia ya que permiten minimizar los desechos de material[102, 107, 148-153].

La investigación y la producción de componentes de titanio mediante técnicas pulvimetalúrgicas han sido exhaustivamente llevadas a cabo durante los años 70 y 80 del siglo XX[137], tanto con polvos prealeados como con polvos de mezclas elementales especialmente centrados en la aleación Ti–6Al–4V[136, 154].

Sin embargo, debido al alto coste y a la baja calidad de los polvos empleados esta técnica no ha sido explotada eficientemente como para garantizar su aplicación a nivel industrial de forma económica y eficaz[40].

Además, la mayoría de los estudios llevados a cabo en esos años se basaban en polvo de titanio esponja, es decir producido tanto mediante el proceso Kroll como el Hunter. El problema de estos polvos es que las sales residuales que se quedan después del refinado impiden la completa densificación de las piezas a causa de los gases que forman durante el calentamiento y que se quedan atrapados en los poros.

1.4.1 – Prensado y Sinterización

Los primeros estudios acerca del procesado de titanio y de sus aleaciones mediante técnicas pulvimetalúrgicas se centraron en la compactación en frío y sinterización con el fin de reducir el coste final de los componentes al mismo tiempo que se obtiene un mejor ratio de utilización de la materia prima[155-159].

Por otro lado, polvos prealeados obtenidos mediante el proceso de plasma por electrodo rotatorio (PREP o REP) fueron conformados mediante compactación isostática en caliente exhibiendo propiedades comparables a las de productos fabricados a partir de lingotes[160-166].

La Tabla 1.6 muestra un resumen de los trabajos llevados a cabo por diferentes autores mediante el método de prensado y sinterización del titanio. En particular, junto con los autores se especifican los tipos de aleaciones estudiadas, las propiedades de los polvos de partida, las condiciones de procesado y los resultados más relevantes.

Tabla 1.6 – Resumen de los principales trabajos llevados a cabo considerando el prensado uniaxial en frío y la sinterización con polvos de titanio elemental y de sus aleaciones.

Autores	Aleación/es estudiadas	Método de producción	Propiedades del polvo	Condiciones de procesado	Propiedades tras conformado (P&S)
Smugeresky y Dawson[167]	Ti–6Al–4V Ti–6Al–4V–0,5Fe Ti–6Al–4V–0,5Ni Ti–6Al–6V–6Mo Ti–10V–2Fe–3Al	Polvo esponja de titanio elemental y aleaciones maestras	Morfología irregular y tamaño de partícula menor de 150 µm	Compactación isostática en frío (densidad en verde aproximadamente de 84%) y sinterización a 1238ºC durante 4	Densidades relativas del 94%, resistencia a tracción entre 800 MPa y 966 MPa y deformaciones entre 3% y 6% Tratamiento secundario de HIP a 900ºC, 100 MPa durante 2 horas. Densidad relativa mínima del 98%, resistencia a tracción entre 920 – 1090 MPa y deformaciones de 5–9 %
Fujita et al[168].	Ti–6Al–4V Ti–4,5Al–3V–2Fe–2Mo (SP–700)	Mezcla elemental empleando polvo de titanio HDH y aleaciones maestras	Morfología irregular y tamaño de partícula menor de 150 µm	Compactación uniaxial en frío y sinterización a 1260ºC durante 4 horas	Densidades relativas alrededor de 99%, resistencia a tracción entre 900 MPa y 1000 MPa y deformaciones en el intervalo 8–20%
Ivasishin et al. [150-153]	Ti–6Al–4V	Titanio elemental electrolítico, esponja y TiH_2 mezclado tanto con polvos elementales (Al y V) o aleación maestra	Morfología irregular y tamaño de partícula entre 75 µm y 150 µm	Compactación uniaxial en frío entre 300 MPa y 1000 MPa (densidad en verde entre 63% y 93%) más sinterización durante 4 horas (950–1350ºC)	Densidades relativas variable entre 84% y 99%, resistencia a tracción 880–1020 MPa y deformación máxima del 3%

Autores	Aleación/es estudiadas	Método de producción	Propiedades del polvo	Condiciones de procesado	Propiedades tras conformado (P&S)
Froes y Eylon (revisión) [156, 158, 159, 169-173]	Ti–6Al–4V Ti–6Al–6V–2Sn Ti–6Al–2Sn–4Zr–2Mo Ti–6Al–2Sn–4Zr–6Mo Ti–10V–2Fe–3Al	Mezcla elemental de polvos esponjas	Morfología irregular y tamaño de partícula menor de 150 µm	Compactación uniaxial en frío (densidad en verde variable entre 85% y 90%) y sinterización a 1260ºC	Densidad relativa entre 95% y 99,5% mejorable mediante HIP, propiedades mecánicas comparables a las obtenidas con el proceso convencional con la excepción de la resistencia a fatiga por la presencia de porosidad como consecuencia de los cloruros
	Ti–6Al–4V Ti–6Al–6V–2Sn Ti–6Al–2Sn–4Zr–2Mo Ti–5Al–5Mo–1,5Cr Ti–10V–2Fe–3Al Ti–6Al–5Zr–0,5Mo–0,25Si	Polvos prealeados obtenidos tanto mediante el proceso HDH o fusión y atomización	–	HIP, compactación en molde fluido (Fluid Die Compaction – FDC) y compactación en caliente bajo vacío (Vacuum Hot Pressing – VHC)	Materiales completamente densos con propiedades mecánicas similares a los productos obtenidos por metalurgia convencional y ligeramente superiores a las alcanzadas a partir de un polvo esponja, especialmente en términos de resistencia a fatiga
	Ti–6Al–4V Ti–Mo–Al	Polvos de solidificación rápida	Morfología esférica	HIP de alta presión y baja temperatura (High pressure low temperature – HPLT), compactación omnidireccional rápida (Rapid omnidictional compaction – ROC), compactación por explosión	–

Como se pude apreciar en el resumen presentado en la Tabla 1.6, son diferentes las aleaciones de titanio producidas mediante la ruta convencional pulvimetalúrgica, si bien la mayoría de los trabajos consideran la aleación Ti–6Al–4V. Sin embargo, no ha sido posible encontrar investigaciones acerca de las aleaciones de titanio Ti–3Al–2,5V y Ti–6Al–7Nb.

Además, en ningún caso los autores mencionan haber tenido problemas de interacción entre las muestras a sinterizar y el soporte de sinterización, nuevamente, tampoco se especifica la naturaleza de estos sustratos.

1.4.2 – Compactación Isostática en Caliente

A lo largo de los años la tecnología HIP ha sido empleada para mejorar las propiedades mecánicas de las aleaciones de titanio. La mayoría de las investigaciones llevadas a cabo se realizaron en los años 80 del vigésimo siglo.

El procesado por HIP puede también ser empleado como procesado secundario con el fin de cerrar la porosidad residual de piezas obtenidas sea por procesos convencionales (fundición) sea por procesos pulvimetalúrgicos donde la única porosidad que puede quedar es la porosidad superficial a menos que se proceda a la utilización de un molde.

El procesado por HIP de la aleación Ti–6Al–4V, tanto de productos obtenidos por fundición como a partir de polvo esférico prealeado, suele llevarse a cabo en el intervalo 890-960°C aplicando una presión entre 100 y 200 MPa durante 2-4 horas[174]. Estos parámetros son muy parecidos para todas las aleaciones de titanio, especialmente cuando se trata de aleaciones $\alpha + \beta$, como la Ti–6Al–6V–2Sn[175].

La Tabla 1.7 muestra un resumen de los trabajos más relevantes referentes tanto al procesado por HIP a partir de polvos como al post–procesado por HIP de componentes en estado sólido, normalmente obtenidos por pulvimetalurgia convencional.

Tabla 1.7 – Resumen de los principales trabajos llevados a cabo considerando la compactación isostática en caliente con polvos de titanio elemental y de sus aleaciones.

Autores	Aleación/es estudiadas	Método de producción	Propiedades del polvo	Condiciones de procesado	Propiedades tras conformado (HIP)
Friedman y Regn[176]	Titanio elemental y Ti–6Al–4V	Polvo esponja de titanio elemental y aleaciones maestras Al:V (60:40)	Morfología irregular y tamaño de partícula menor de 150 µm	Compactación isostática en frío y sinterización en vacío entre 1100ºC y 1300ºC durante 4 h. Las muestras sinterizadas con un 95% de densidad relativa fueron sometidas a HIP empleando una temperatura de 930°C durante 2 h	Densidad relativa después del post–procesado alrededor del 99%. Resistencia a tracción y alargamiento del Ti: 498–664 MPa y 19,8–20,9%. Resistencia a tracción y alargamiento de la aleación Ti–6Al–4V: 881–1050 MPa y 5,3–13,2%
Mohs y Sibum[166]	Ti–6Al–4V	Proceso de atomización por rotación continua (KRZ – krupp forschungs institut)	Morfología esférica con un tamaño de partícula en el intervalo comprendido entre 250 y 355 µm	Encapsulado del polvo, desgasificación a 450°C, temperatura de procesado de 920°C aplicando una presión de 150 MPa y una meseta de 3 horas	Componentes completamente densos con resistencia a tracción de 970 ± 10 MPa y alargamiento de 15 ± 3%
Broomfield et al.[177]	Ti–6Al–4V	Polvo prealeado (REP)	Morfología esférica con un tamaño de partícula inferior a 500 µm	Molde de acero inoxidable recubierto de esteadita ($MgO{\cdot}SiO_2$) o zirconia ($ZrO_2{\cdot}SiO_2$) rellenado y desgasificado a 800°C. Procesado por HIP a 950°C o 1050ºC, utilizando una presión de 100MPa con una meseta de 3 horas	Piezas completamente densas con resistencia a tracción de 940 MPa y deformación del 15%. Cabe destacar que la aleación reaccionó con el molde cerámico induciendo la difusión del oxígeno hacia el interior generando una capa de material endurecido extremadamente frágil (alpha-case)
		Mezcla de titanio elemental (esponja) y aleación maestra Al:V (60:40)	Polvos con morfología irregular con tamaño de partícula: Ti: < 100 µm Al:V: < 75 µm		

Autores	Aleación/es estudiadas	Método de producción	Propiedades del polvo	Condiciones de procesado	Propiedades tras onformado (HIP)
Herteman et al.[178]	Ti–6Al–4V	Polvo prealeado (PREP) y polvo PSV (Pulverisátion, Sous Vide – fusión por haz de electrones bajo vacío)	Polvos con morfología esférica y tamaño de partícula: PREP: < 35 µm PSV: 630–100 µm	Procesado por HIP empleando, respectivamente, 925°C/1050MPa/5h y 950°C/1000MPa/5h	No se especifica el nivel de densidad relativa alcanzado. Resistencia a tracción de 937 MPa y 17% para el polvo PREP y 1095 MPa y 9% para el polvo PSV aunque este último fue sometido a un tratamiento térmico de solubilización en campo beta y sobre envejecimiento (975°C/1h/temple en agua + 700°C/2h/enfriamiento en aire) antes de ser ensayado
Eylon et al.[179]	Ti–6Al–4V	Polvos de titanio esponja y aleación maestra	Polvo de morfología irregular pero no se especifica el tamaño de partícula	Compactación isostática en frío (CIP) a 420 MPa y sinterización a 1260°C en vacío y posteriormente densificada hasta un 99,9% de densidad relativa mediante HIP (denominada CHIP) sin especificar las condiciones de procesado	Algunas muestras fueron sometidas a tratamiento térmico (1025°C/20min/temple en agua + 815°C/24h/enfriamiento en aire) o termoquímico a 1025°C/20min/temple en agua, hidrurado a 0,8% en peso de hidrogeno a aproximadamente 600°C y dehidrurado a 760°C. La resistencia a fractura y deformación obtenida después de HIP, tratamiento térmico o termoquímico fueron de 986 MPa y 11%, 1034 MPa y 7% y 938 MPa y 13%, respectivamente

Además, Minabe y Endoh[180] llevaron a cabo un estudio de sinterizado y HIP, denominado Sinter-HIP, sobre las aleaciones Ti–6Al–4V y Ti–6Al–6V–2Sn producidas mediante mezcla elemental de polvo esponja de titanio con tamaño de partícula menor de 150 μm (-100 mesh), aleaciones maestras de Al:V 60:40 y 50:50 con tamaño inferior a 61 μm (-230 mesh) y estaño de 74 μm (-200 mesh).

Las piezas fueron prensadas en frío a 490 MPa y sinterizadas en vacío a 1250°C durante 90 minutos (densidad relativa aproximadamente 96%) y alternativamente sinterizadas a 1250°C durante 90 minutos y, manteniendo la temperatura estable, sometida a una presión de 98 MPa mediante argón alcanzando una densidad relativa final de 99%.

Las propiedades mecánicas de resistencia a tracción y deformación para la aleación Ti–6Al–4V sinterizada (823 MPa y 5,7%) y Sinter-HIP (911 MPa y 9,2%) y la aleación Ti–6Al–6V–2Sn sinterizada (941 MPa y 4,1%) y Sinter-HIP (1029 MPa y 6,8%) indican una mejora de aproximadamente un 10% en resistencia y 1,6% en deformación al aplicar el procesado Sinter-HIP.

En la actualidad el procesado de HIP sigue siendo investigado y aplicado para la producción de componentes de titanio o de sus aleaciones mayoritariamente a partir de polvos esféricos prealeados, tanto PREP como atomizados en gas, como el trabajo de Wang et al. demuestra[181].

Como se puede apreciar en el resumen mostrado en este apartado, la investigación sobre el empleo del procesado por HIP tanto a partir de polvos como su utilización como post–procesado para disminuir la porosidad residual de componentes obtenidos por la ruta pulvimetalúrgica convencional se ha centrado, principalmente, en el estudio del titanio elemental y de la aleación Ti–6Al–4V.

Cabe destacar, que la mayoría de las investigaciones fueron llevadas a cabo con polvos de tipo esponja con los relativos problemas inducidos por la presencia de cloruros o polvo obtenidos con procesos no actualmente comerciales como el proceso de atomización por rotación continua (KRZ) o la fusión por haz de electrones bajo vacío (PSV).

Además, durante la revisión bibliográfica no se han encontrado trabajos que tratan el procesado de las aleaciones Ti–3Al–2,5V y Ti–6Al–7Nb a partir de un enfoque pulvimetalúrgico.

1.4.3 – Compactación Uniaxial en Caliente

Las primeras investigaciones acerca de la compactación en caliente del titanio y de sus aleaciones aparecen en los primeros años de 1970 cuando Goetzel y de Marchi investigaron la aplicación de la compactación en caliente activada eléctricamente, conocida como “spark sintering”, a polvos de titanio elemental[182, 183] y a polvos de la aleación Ti–6Al–4V[184].

La Tabla 1.8 muestra un resumen de los principales trabajos llevados a cabo a lo largo de los años acerca de la compactación uniaxial en caliente considerando tanto polvos de titanio elemental como de sus aleaciones.

Tabla 1.8 – Resumen de los principales trabajos llevados a cabo considerando la compactación uniaxial en caliente con polvos de titanio elemental y de sus aleaciones.

Autores	Aleación/es estudiadas	Método de producción	Propiedades del polvo	Condiciones de procesado	Propiedades tras Conformado (HP)
Goetzel y de Marchi[182-184]	Titanio elemental	Polvo esponja con diferentes grados de pureza y polvo obtenido por métodos electrolíticos	Morfología irregular y tamaño de partícula menor de 150 µm	"Spark sintering": molde de grafito empleando una temperatura de 1150ºC, una presión de 14 MPa y una corriente de 230A/cm^2 tanto en aire como en atmósfera protectora (Ar)	Densidades relativas mayores de 98% y propiedades mecánicas, resistencia a tracción y deformación, satisfactorias pero altamente variables debido a la contaminación por oxigeno y nitrógeno
	Ti–6Al–4V	Polvo hidrurado–dehidrurado (HDH) y polvo obtenido por REP	Polvo HDH con morfología irregular y tamaño de partícula menor de 350 µm o polvo esférico REP (500–125 µm)		Densidades relativas del 99%. Propiedades mecánicas comparables a las obtenidas con el proceso convencional pero con alta variabilidad debido a una significativa contaminación por oxígeno y del nitrógeno
					Las muestras fueron también sometidas a un tratamiento térmico de solubilización a 950ºC durante 1 hora, temple en agua, maduración a 540ºC durante 4 horas y enfriamiento en horno. El tratamiento térmico propuesto aumenta la cantidad de fase beta retenida e induce un crecimiento de la fase alfa que se traduce en un aumento de la resistencia a tracción y del límite elástico pero en una disminución de la ductilidad

Autores	Aleación/es estudiadas	Método de producción	Propiedades del polvo	Condiciones de procesado	Propiedades tras Conformado (HP)
Malik[185, 186]	Ti–6Al–4V	Polvo prealeado hidrurado–dehidrurado (HDH) y polvo prealeado REP	Polvo HDH con morfología irregular y tamaño de partícula menor de 425 µm y polvo esférico REP con tamaño de partícula menor de 45 µm	Compactación uniaxial en caliente inductiva con una presión aplicada de 100 toneladas	Densidades relativas superiores al 99%, propiedades mecánicas y microestructurales similares a las obtenidas con el proceso convencional con ligera contaminación en términos de oxígeno, nitrógeno y carbono
Kao[187]	Ti–6Al–4V	Polvo prealeado REP y polvo prealeado hidrurado denominado (HYD)	Morfología esférica (REP) o irregular (HYD) con tamaño de partícula entre 100 µm y 500 µm	Compactación uniaxial en caliente inductiva evaluando el efecto de la presión (34–102 MPa) y de la temperatura de procesado (760–953ºC)	Piezas completamente densas pero sin especificar propiedades mecánicas
Liu y Kao[188]	Titanio elemental	Polvo irregular comercial	Polvos irregulares con diferente tamaño de partículas, menor de 75 µm y 45 µm	"Resistance sintering": molde de acero inoxidable 304, presión aplicada de 200 MPa, tiempo de procesado 2 s, y energía especifica suministrada entre 2 kJ/g y 3 kJ/g	Densidades relativas mayores de 96%, resistencia a tracción entre 500 MPa y 600 MPa y alargamientos de 2–18%

Autores	Aleación/es estudiadas	Método de producción	Propiedades del polvo	Condiciones de procesado	Propiedades tras Conformado (HP)
Henriques et al. [192-196]	Ti–6Al–7Nb	Polvos elementales de titanio y niobio (HDH) y polvo elemental de aluminio (atomizado en gas)	Polvos irregulares: Ti (< 10 μm), Nb: < 9 μm Polvo esférico: Al (< 33 μm)	Compactación en caliente en molde de grafito, nivel de vacío de 10^{-2} Torr, variando la temperatura en el intervalo 700–1500ºC, presión entre 5 y 25 MPa, velocidad de calentamiento entre 10ºC/min y 30ºC/min y tiempo a temperatura máxima de 15–60 minutos	Densidad relativa variable entre 93% y 99,8% de la teórica. Análisis de la evolución microestructural obteniendo una microestructura completamente homogénea a partir de 1300ºC. Se destaca un significativo aumento del contenido de carbono, la formación de TiB_2 en la superficie de las muestras cuando el molde de grafito se recubre de BN y la presencia de las fases intermétalicas TiAl y Ti_3Al en las muestras sinterizadas entre 700ºC y 1000ºC. La única propiedad mecánica mencionada es la dureza que varía entre 370 y 400 HV
Varios autores: primeros años del 2000	La investigación se diversificó en aspectos diferentes como la búsqueda de modelos constitutivos para la simulación del procesado de compactación en caliente[147, 189], en la comparación con otras técnicas, por ejemplo el SPS[190] y en el procesado de titanio elemental y la aleación Ti–6Al–4V a partir de polvo de última generación, como el obtenido mediante el proceso Armstrong[191]				

Como se puede apreciar en el resumen mostrado en la Tabla 1.8, la mayoría de las investigaciones disponibles se centran en el titanio elemental y la aleación Ti–6Al–4V, que fueron llevadas a cabo durante los años 70–80 del siglo XX y, por lo tanto, directamente a partir de polvo tipo esponja o sometiendo el mismo polvo esponja a un proceso de hidrurado–dehidrurado. Además, en el caso de la aleación de titanio Ti–6Al–4V se trata de polvos prealeados, independientemente del proceso de fabricación empleado.

La única excepción es el trabajo desarrollado por Henriques et al., ya en los primeros años de siglo XXI, que considera la aleación Ti–6Al–7Nb, si bien no investiga ninguna propiedad mecánica a excepción de la dureza.

1.4.4 – Otras Técnicas

En este apartado se proponen algunos ejemplos de investigaciones llevadas a cabo a lo largo de los años empleando técnicas no–convencionales para conformar polvo de titanio.

Mahajan et al.[197] estudiaron la modificación de la microestructura de la aleación de titanio Ti–6Al–4V obtenida por pulvimetalurgia. En particular, se consideró el proceso "Strain Energizing process – SEP" donde la deformación del polvo por laminado induce una recristalización de la fase alfa que disminuye el ratio de aspecto que resulta en mayores propiedades de fatiga.

Weiss et al.[198] estudiaron el efecto de un procesado de forja isotérmico en la microestructura y en las propiedades a fatiga de la aleación Ti–6Al–4V obtenida por mezcla elemental, compactación isostática en frío y sinterización a 1260ºC obteniendo un sustancial incremento de la densidad relativa final y de las propiedades tanto estáticas como dinámicas.

Técnicas de prototipado rápido, como la sinterización por láser (Selective Laser Sintering – SLS) o fusión por haz de electrones (Electron Beam Melting)[199], fueron evaluadas para la fabricación de componentes de titanio. En particular, el SLS fue utilizado para producir piezas con una capa exterior con densidad relativa superior al 98% e interior con densidad relativa superior al 80%. Esta "preforma" fue posteriormente sometida a un ciclo de HIP a 925ºC durante 4 horas empleando una presión de 93 MPa para obtener piezas completamente densas[200].

En otro trabajo, Froes describe la producción de componentes de titanio y de sus aleaciones (Ti–6Al–4V, Ti–5Al–2,5Sn, Ti–6Al–2Sn–4Zr–2Mo–0,1Si y Ti–6Al–2Sn–2Zr–2Cr–2Mo–0,25Si) empleando la técnica de prototipado rápido de "Laser Forming" a partir de diferentes precursores. Las propiedades de fatiga investigadas para la aleación Ti–6Al–4V se sitúan en los valores más altos del intervalo de propiedades obtenidas en piezas fabricadas por fundición y en los valores más bajos si se comparan con las de componentes producidos a partir de lingotes debido a la microestructura generada por el proceso láser[201, 202].

Las espumas metálicas están caracterizadas por una muy baja densidad y una combinación única de propiedades mecánicas, térmicas, eléctricas y acústicas y pueden ser empleadas para la fabricación de implantes biocompatibles porque la estructura celular abierta que las caracterizas permite el crecimiento del hueso en su interior además del paso de fluidos corporales[203, 204]. El procesado de espumas metálicas a base de titanio fue estudiado por Wen et al. que obtuvieron una estructura celular abierta con un 78% de porosidad, un tamaño de poros variable entre 200 μm y 500 μm, una resistencia a compresión de 35 MPa y módulo de Young de 5,3 GPa[205].

Eriksson et al.[206] consideraron la compactación a alta velocidad (High Velocity Compaction) de polvo de titanio donde al aumentar el número de impactos de uno a dos se obtiene un aumento significativo de la densidad en verde de los componentes pero un ulterior aumento del número de impactos no supone un mejora significativa de la misma.

El empleo de compactación a presiones muy altas (Ultra–high Pressure Warm Compaction) donde el polvo de partida es calentado hasta los 150ºC antes de ser sometido a un conformado uniaxial fue estudiado por Takamiya et al.[207]. Según los autores esta técnica conlleva alcanzar mayores densidades y mejores propiedades dinámicas limitando significativamente la contracción durante la sinterización (menor del 1%) y, por lo tanto, puede ser empleada para fabricar componentes para el sector automovilístico.

La investigación se ha centrado también en el desarrollo de técnicas de fabricación por spray ya que ofrece la posibilidad de obtener componentes de forma rápida y minimizar los desperdicios. En el trabajo de Blose et al.[208] el proceso de "Cold spray" fue evaluado para el recubrimiento de piezas a partir de polvo de la aleación Ti–6Al–4V con diferente morfología, esférica e irregular, alcanzando porosidades mínimas residuales del 18%. Las piezas recubiertas fueron posteriormente o bien sometidas a tratamientos térmicos, lo que no obtuvo ningún efecto sobre la porosidad, o bien procesadas por HIP produciendo recubrimientos completamente densos independientemente del nivel de porosidad inicial.

La idea de activar o favorecer la etapa de sinterización mediante la aplicación de un tratamiento físico, como la aplicación de una tensión eléctrica que incremente la cinética de la sinterización se remonta a los primeros años 30 del siglo XX y fue nombrada como "electrical resistance sintering under pressure"[209]. Esta técnica permite alcanzar mayores densidades a menores temperaturas o mayores grados de densificación a la misma temperatura pero empleando tiempos más cortos además de proporcionar mejores propiedades mecánicas debido al reducido incremento del tamaño de grano. Por lo tanto, este resulta ser un método atractivo para fabricar materiales difíciles de procesar[210-212] garantizando ventajas económicas y tecnológicas[213].

En los últimos años se han desarrollado numerosos procesos que emplean una corriente pulsada para favorecer el conformado de polvos[210, 213] denominadas "field assisted sintering technique – FAST"[214]. Entre estas técnicas se encuentra la sinterización asistida por plasma (spark plasma sintering – SPS) que implica la aplicación simultanea de presión y de descargas eléctricas pulsadas que permiten trabajar con velocidades de calentamiento de hasta 200ºC/min.

La influencia de los parámetros de procesado más importantes como la temperatura, la velocidad de calentamiento, la presión y la secuencia de impulsos eléctricos en las propiedades físicas y mecánicas fueron investigadas para el titanio elemental[190, 215], para la aleación Ti–6Al–4V[216] y para la aleación Ti–6Al–4V reforzada con SiC o TiB_2[217]. Fueron obtenidos componentes completamente densos empleando una temperatura superior a 850ºC alcanzando una resistencia a tracción alrededor de 550 MPa y 950 MPa y deformaciones de aproximadamente 15% y 10% para el titanio elemental (grado 3) y la aleación Ti–6Al–4V, respectivamente.

Cabe destacar que en el caso del titanio elemental la geometría típica de los granos de la fase alfa que constituyen la microestructura (equiaxial), empieza a distorsionarse generando una microestructura heterogénea con muchos granos alargados e irregulares cuando se emplea una temperatura de procesado superior a los 950ºC[215].

En el caso de los materiales compuestos, destacan un aumento de la resistencia a tracción junto a una disminución de la ductilidad debido a la interacción de la aleación Ti–6Al–4V con el refuerzo además de un aumento significativo de la dureza del material.

Una técnica muy estudiada durante los últimos años es el moldeo por inyección de polvos, también conocida como PIM (Powder Injection Moulding), variante del moldeo por inyección de polímeros, de la que hereda parte de su metodología y equipamiento[218, 219]. Normalmente, cuando se utiliza esta técnica y se trabaja con polvos de metales, el método es llamado MIM (Metal Injection Moulding)[220]. Este proceso es adecuado para fabricar piezas de tamaño medio/pequeño y de forma ya definida y muy compleja sin la necesidad o, reduciendo mucho, las operaciones secundarias, como el mecanizado. Además, el moldeo por inyección de metales permite reducir drásticamente los costes de fabricación cuando se realiza producción a gran escala.

El moldeo por inyección comprende cuatro operaciones básicas: mezcla del polvo de metales con un medio orgánico (binder) para obtener el denominado "feedstock", inyección de la mezcla en el molde, eliminación del ligante (debinding) con diferentes técnicas (tratamiento térmico, inmersión en disolvente, descomposición catalítica, secado o evaporación), y sinterización o densificación[221, 222].

Esta técnica genera mucho interés a nivel industrial especialmente para la fabricación de componentes para aplicaciones biomédicas[223] pero, tratándose de titanio, el impedimento mayor resulta ser respetar las especificaciones del contenido de elementos contaminantes, en particular de carbono y oxígeno[224-226]. Por lo tanto, la investigación se ha centrado tanto en el estudio de ligantes convencionales, de base polietileno[227, 228], como en el desarrollo de nuevos sistemas ligantes que no induzcan un significativo aumento de estos elementos.

Ejemplo de estudios son la utilización de ligantes de base polimetilmetacrilato[229, 230], de base acuosa[231-233], de base naftaleno[234-236], de base poliacrilonitrilo (PAN)[237] y a base de cera de carnauba[229, 238].

Algunos autores prefieren no desvelar el ligante empleado o centrarse en las propiedades obtenibles en titanio[239, 240], a partir de TiH_2[241], en aleaciones de titanio[240, 242-247], en materiales compuestos[237, 248-250], en TiNi[251] y en TiAl[252].

1.4.5 – Conclusiones

Como se deduce de la revisión bibliográfica presentada en el capitulo 1.4, la investigación acerca del procesado del titanio mediante técnicas pulvimetalúrgicas tanto convencionales como más avanzadas o especificas se ha extendido a lo largo de los últimos 50 años.

Sin embargo, muchas de los estudios fueron llevados a cabo a partir de polvo tipo esponja, con los problemas que conlleva la presencia de cloruros, o mediante el procesado de hidrurado–dehidrurado de los mismos polvos esponja. Además, la gran mayoría de los trabajos se limitan al estudio de la aleación de titanio más conocida, es decir la aleación Ti–6Al–4V.

1.5 – REFERENCIAS

[1] I. J. Polmear, *Light Alloys. Metallurgy of the Light Metals*, 2nd ed, Edward Arnold, pp. 211-273, 1989

[2] H. Sibum, et al., *Titanium, Titanium Alloys, and Titanium Compounds*, 2002

[3] A. M. Russell and K. L. Lee, *Structure-property Relations in Nonferrous Metals*, Wiley-Interscience, pp. 179-197, 2005

[4] I. J. Polmear, *Light Alloys. From Traditional Alloys to Nanocrystals*, 4th ed, Butterworth-Heinemann, UK, pp. 299-365, 2006

[5] Minerali e Pietre, "Gli Ossidi del Titanio", *available at: http://www.mineraliepietre.com/storeimgs/Gli%20ossidi%20del%20titanio%20parte%201.pdf*, 2006

[6] F. H. Froes, et al., "Titanium in the Family Automobile: The Cost Challenge", *JOM,* vol. 56, pp. 40-44, Feb 2004

[7] Y. Kosaka, et al., "Newly Developed Titanium Alloy Sheets for the Exhaust Systems of Motorcycles and Automobiles", *JOM,* vol. 56, pp. 32-34, 2004

[8] P. Allen, "Titanium Alloy Development", *Advanced Materials & Processes,* vol. 150, pp. 35-37, 1996

[9] F. H. Froes, "Titanium - Is the Time Now?", *JOM,* vol. 56, pp. 30-30, 2004

[10] Roskill Information Services, "Global Supply of Titanium is Forecast to Increase", *available at: http://www.prnewswire.com/news-releases/roskill-information-services-global-supply-of-titanium-is-forecast-to-increase-105243193.html,* 2010

[11] P. Dewhurst, "Titanium Sponge Supply - Past, Present and Future", *available at: http://www.roskill.com/reports/minor-and-light-metals/news/titanium-2010-the-annual-meeting-of-the-international-titanium-association/?searchterm=titanium*, 2010

[12] F. Froes, "Tenth World Titanium Conference", *Materials Technology & Advanced Performance Materials,* pp. 109-114, 2004

[13] Roskill Information Services, "Titanium Metal: Market Outlook to 2015", *available at: http://www.roskill.com/reports/minor-and-light-metals/titanium-metal*, 2010

[14] M. Jackson and K. Dring, "Materials Perspective - A Review of Advances in Processing and Metallurgy of Titanium Alloys", *Materials Science and Technology,* vol. 22, pp. 881-887, 2006

[15] G. Crowley, "How to Extract Low-cost Titanium", *Advanced Materials & Processes,* vol. 161, pp. 25-27, 2003

[16] S. J. Gerdemann, "Titanium Process Technologies", *Advanced Materials & Processes,* vol. 159, pp. 41-43, 2001

[17] W. J. Kroll, "The Production of Ductile Titanium", *Transaction of the American Electrochemical Society,* vol. 78, pp. 35-47, 1940

[18] I. Barin, *Thermochemical Data of Pure Substances*. Weinheim, Germany, VCH Verlags Gesellschaft, pp. 1-1739, 1993

[19] J. L. Murray, *Phase Diagrams of Binary Titanium Alloys*, 1st ed, ASM International, pp. 1-345, 1987

[20] W.-E. Wang and Y. S. Kim, "A Thermodynamic Evaluation of the Titanium-oxygen System from O/Ti = 0 to 3/2", *Journal of Nuclear Materials,* vol. 270, pp. 242-247, 1999

[21] Toho Titanium Co, avalilable at: http://www.titaniumexposed.com/titanium-industries.html
[22] K. Rüdinger, et al., "Investigation of Heat-exchange in the Electrode Tip of the Non-consumable Electrode Vacuum Arc Furnace for Melting Titanium" in *Titanium '92: Science and Technology*, San Diego, California, pp. 1355-2362, 1992
[23] C. H. Entrekin and H. R. Harker, "State of the Art in Electron Beam Melting of Titanium" in *Titanium '92: Science and Technology*, San Diego, California, pp. 2339-2346, 1992
[24] F. H. Froes, "The Production of Low-cost Titanium Powders", *JOM,* vol. 50, pp. 41-43, 1998
[25] M. A. Hunter, "Metallic Titanium", *Journal of the American Chemical Society,* vol. 32, pp. 330–336, 1910
[26] A. D. Hartman, et al., "Producing Lower-cost Titanium for Automotive Applications", *JOM,* vol. 50, pp. 16-19, 1998
[27] V. G. Gopienko and O. D. Neikov, *Production of Titanium and Titanium Alloy Powders in Handbook of Non-Ferrous Metal Powders* Elsevier, pp. 314-323, 2008
[28] W. H. Peter, et al., "Non-melting Processing of "Low-cost" Armstrong Titanium and Titanium Alloy Powders" in *Proceedings of the Light Metals Technology Conference 2007*, Saint-Sauveur, Québec, Canada, 2007
[29] C. A. Lavender and K. S. Weil, "Low-cost Titanium Powder for Feedstock", available at: http://www1.eere.energy.gov/vehiclesandfuels/pdfs/lm_07/4_automotive_metals-titanium.pdf 2007
[30] G. Z. Chen, et al., "Direct Electrochemical Reduction of Titanium Dioxide to Titanium in Molten Calcium Chloride", *Nature,* vol. 407, pp. 361-364, 2000
[31] "Metalysis Leads Charge for Change in Titanium Production", *Metal Powder Report,* vol. 64, pp. 6-11, 2009
[32] F. H. Froes, "Lightweight Heavyweight", *Metal Powders Report,* vol. 57, pp. 14-19, 2002
[33] F. H. Froes, et al., "Cost Affordable Titanium - An Update", *Materials Technology: Advanced Performance Materials,* vol. 21, pp. 206-209, 2006
[34] F. H. Froes, et al., "Cost-affordable Titanium: The Component Fabrication Perspective", *JOM,* vol. 59, pp. 28-31, 2007
[35] C. G. McCracken, et al., "Review of Titanium-powder-production Methods", *International Journal of Powder Metallurgy,* vol. 46, pp. 19-26, 2010
[36] J. M. Capus, "More Roads Point to Cheaper Titanium Powder", *Metal Powder Report,* vol. 60, pp. 22-23, 2005
[37] M. Ma, et al., "Extraction of Titanium from Different Titania Precursors by the FFC Cambridge Process", *Journal of Alloys and Compounds,* vol. 420, pp. 37-45, 2006
[38] R. O. Suzuki and S. Inoue, "Calciothermic Reduction of Titanium Oxide in Molten CaCl2", *Metallurgical and Materials Transactions B,* vol. 34, pp. 277-285, 2003
[39] K. Dring, et al., "Direct Electrochemical Production of Ti-10W Alloys from Mixed Oxide Preform Precursors", *Journal of Alloys and Compounds,* vol. 419, pp. 103-109, 2006
[40] C. M. Ward-Close, et al., "Titanium Made the EDO Way Should See Prices Drop", *Metal Powder Report,* vol. 60, pp. 20-25, 2005

[41] Z. G. Hägg, *Phys. Chem. Abt. B,* vol. 11, pp. 433-454, 1931
[42] R. I. Jaffee, "The Physical Metallurgy of Titanium Alloys", *Progress in Metal Physics,* vol. 7, pp. 65-163, 1958
[43] K. Faller and F. S. Froes, "The Use of Titanium in Family Automobiles: Current Trends", *JOM,* vol. 53, pp. 27-28, 2001
[44] T. E. Norgate and G. Wellwood, "The Potential Applications for Titanium Metal Powder and their Life Cycle Impacts", *JOM,* vol. 58, pp. 58-63, 2006
[45] M. J. Donachie, *Titanium. A Technical Guide*, 2nd Edition ed. Ohio, USA, ASM International, pp. 1-137, 2000
[46] G. Lütjering and J. C. Williams, *Titanium: Engineering Materials and Processes*, 1st ed. Manchester, UK, Springer, pp. 1-356, 2003
[47] RMI, "Titanium Company: Titanium Alloy Guide", *available at: http://rtiintl.s3.amazonaws.com/RTI-Reports/tiguideWeb.pdf,* 2000
[48] H. W. Rosenberg, "Titanium Alloying in Theory, Practice" in *Proceeding of the Science, Technology and Application of Titanium Conference*, pp. 851-859, 1970
[49] R. L. Jones and H. Conrad, *Transactions of the Metallurgical Society of AIME,* vol. 245, p. 779, 1969
[50] J. A. Picas, et al., "Optimization of the Ti-0.2Pd Alloy Properties through Heat Treatments", *Journal of Light Metals,* vol. 2, pp. 57-64, 2002
[51] V. A. Joshi, *Titanium Alloys: An Atlas of Structures and Fracture Features*, Taylor & Francis, pp. 1-15, 2006
[52] R. I. Jaffee and H. M. Burte, "Metallurgical Synthesis" in *Proceedings of the Titanium Science and Technology Conference*, pp. 1665-1693, 1973
[53] I. I. Kornilov, "Interaction of Titanium with Elements of the Periodic System" in *Proceedings of the Science, Technology and Application of Titanium Conference*, pp. 407-421, 1970
[54] C. Leyens and M. Peters, *Titanium and Titanium Alloys. Fundamentals and Applications.* Köln, Germany, Wiley-VCH, pp. 1-497, 2003
[55] W. H. Graft, et al., "The Influence of Alloying on the Elastic Modulus of Titanium Alloys", *Transactions of the American Society for Metals (ASM),* vol. 49, pp. 263-279, 1957
[56] S. L. Semiatin, et al., "The Thermomechanical Processing of Alpha/Beta Titanium Alloys", *Journal of the Minerals, Metals and Materials Society,* vol. 49, pp. 33-39, 1997
[57] F. H. Froes and B. Trindade, "The Mechanochemical Processing of Aerospace Metals", *Journal of Materials Processing Technology,* vol. 153-154, pp. 472-475, 2004
[58] M. Zitnanský and L. Caplovic, "Effect of the Thermomechanical Treatment on the Structure of Titanium Alloy Ti6Al4V", *Journal of Materials Processing Technology,* vol. 157-158, pp. 643-649, 2004
[59] I. Weiss and S. L. Semiatin, "Thermomechanical Processing of Beta Titanium Alloys - An Overview", *Materials Science and Engineering A,* vol. 243, pp. 46-65, 1998
[60] I. Weiss and S. L. Semiatin, "Thermomechanical Processing of Alpha Titanium Alloys - An Overview", *Materials Science and Engineering A,* vol. 263, pp. 243-256, 1999

[61] R. Boyer, et al., "Materials Properties Handbook: Titanium Alloys", 2nd ed, ASM-International, Ed. Ohio, USA, 1998
[62] P. Beiss, et al., *International Atlas of Powder Metallurgical Microstructures*. Princeton, New Jersey, U.S.A., ASM International, pp. 134-135, 2002
[63] D. N. Williams and R. A. Wood, "Effects of Surface Condition on the Mechanical Properties of Titanium and its Alloys", Battelle Columbus Labs Ohio Metals and Ceramics Information Center 1971
[64] P. A. Russo and R. S. Seagle, "Properties of Titanium for Industrial Applications with Emphasis on Ti-3Al-2.5V" in *Industrial Applications of titanium and Zirconium: 3rd Conference*, pp. 99-112, 1984
[65] M. Semlitsch, et al., "Titanium-aluminium-niobium Alloy Development for Biocompatible, High Strength Surgical Implants", *Biomedizinische Technik/Biomedical Engineering,* vol. 30, pp. 334–339, 1985
[66] S. M. Perren, et al., "Quantitative Evaluation of Biocompatibility of Vanadium Free Titanium Alloys" in *Biological and Biomechanical Performance of Biomaterials* Paris, France, Elsevier, pp. 397-402, 1986
[67] M. Semlitsch, et al., "Fifteen Years Experience with Ti-6AI-7Nb Alloy for Joint Replacements" in *Titanium '95: Science and Technology*, Birmingham - UK, pp. 1742-1759, 1995
[68] R. M. Streicher, et al., "New Surface Modification for Ti-6Al-7Nb Alloy: Oxygen Diffusion Hardening (ODH)", *Biomaterials,* vol. 12, pp. 125-129, 1991
[69] ASM International, *Materials and Coatings for Medical Devices: Cardiovascular*. Ohio, USA, ASM International, pp. 151-186, 2009
[70] Y. Oshida, *Bioscience and Bioengineering of Titanium Materials*. Oxford, UK, Elsevier, pp. 11-24, 2007
[71] C. Sittig, et al., "Surface Characterization of Implant Materials CP Ti, Ti-6Al-7Nb and Ti-6Al-4V with Different Pretreatments", *Journal of Materials Science: Materials in Medicine,* vol. 10, pp. 35-46, 1999
[72] M. Semlitsch, et al., "Development of a Vital, High-Strength Titanium-aluminium-niobium Alloy for Surgical Implants" in *Biological and Biomechanical Performance of Biomaterials* Paris, France, Elsevier, pp. 69-74, 1986
[73] K. Roncone, et al., "A Conversation with Titanium Suppliers and End Users", *JOM,* vol. 57, pp. 11-13, 2005
[74] S. R. Seagle, "The State of the USA Titanium Industry in 1995", *Materials Science and Engineering: A,* vol. 213, pp. 1-7, 1996
[75] J. Rigney, "GE Aviation's Perspective on Titanium Availability" in *Proceedings of DoD/DLA, Titanium Symposium. 2008*, Las Vegas, Nevada USA 2008
[76] R. R. Boyer, "An Overview on the Use of Titanium in the Aerospace Industry", *Materials Science and Engineering: A,* vol. 213, pp. 103-114, 1996
[77] R. H. Van Stone, et al., "Influence of Composition, Annealing Treatment, and Texture on the Fracture Toughness of Ti-5Al-2.5Sn Plate at Cryogenic Temperatures" in *Toughness and Fracture Behavior of Titanium*, pp. 154-179, 1978
[78] P. J. Bania, "Ti-1100: A new High Temperature Titanium Alloy" in *Sixth World Conference on Titanium*, France, pp. 825-830, 1989

[79] M. Hagiwara and S. Emura, "Blended Elemental P/M Synthesis and Property Evaluation of Ti-1100 Alloy", *Materials Science and Engineering A,* vol. 352, pp. 85-92, 2003

[80] M. Yamada, "An Overview on the Development of Titanium Alloys for Non-aerospace Application in Japan", *Materials Science and Engineering: A,* vol. 213, pp. 8-15, 1996

[81] American Society for Metals - ASM, *ASM Handbook* vol. 2, Properties and Selection: Nonferrous Alloys and Special-purpose Materials. Ohio, USA, 1990

[82] B. J. Story, et al., "In Vivo Performance of a Modified CSTi Dental Implant Coating", *The International Journal of Oral & Maxillofacial Implants,* vol. 13, pp. 749-756, 1998

[83] D. A. Deporter, et al., "Use of a Tapered, Porous-surfaced Dental Implant in Combination with Osteotomes to Restore Edentulism in the Difficult Maxilla", *Implant Dentistry,* vol. 8, pp. 233-240, 1999

[84] R. M. Pilliar, "Powder Metal-made Orthopaedic Implants with Porous Surface for Fixation by Tissue Ingrowth", *Clinical Orthopaedics and Related Research,* vol. 176, pp. 42-51, 1983

[85] R. M. Pilliar, "Porous-surfaced Metallic Implants for Orthopaedic Applications", *Journal of Biomedical Materials Research,,* vol. 21, p. 1, 1987

[86] T. Ebel, "Titanium and Titanium Alloys for Medical applications: Opportunities and Challenges", *PIM International,* vol. 2, pp. 21-30, 2008

[87] I.-H. Oh, et al., "Mechanical Properties of Porous Titanium Compacts Prepared by Powder Sintering", *Scripta Materialia,* vol. 49, pp. 1197-1202, 2003

[88] E. B. Taddei, et al., "Production of New Titanium Alloy for Orthopedic Implants", *Materials Science and Engineering: C,* vol. 24, pp. 683-687, 2004

[89] K.-H. Borowy and K.-H. Kramer, "On the Properties of a New Titanium Alloy (TiAl5Fe2.5) as Implant Material" in *Titanium'84 Science and Technology, vol. 2.* Munich, Deutsche Gesellschaft Für Metallkunde EV, pp. 1381-1386, 1995

[90] K. Wang, "The Use of Titanium for Medical Applications in the USA", *Materials Science and Engineering: A,* vol. 213, pp. 134-137, 1996

[91] K. Wang, et al., "The Characterization of Ti–12Mo–6Zr–2Fe. A New Biocompatible Titanium Alloy Developed for Surgical Implants" in *Beta Titanium in the 1990's* Warrendale, The Minerals, Metals & Materials Society, pp. 49-60, 1993

[92] Y. Okazaki, et al., "Effect of Alloying Elements on Mechanical Properties of Titanium Alloys for Medical Implants", *The Japan Institute of Metals,* vol. 57, pp. 332-337, 1993

[93] A. K. Mishra, et al., "Ti–13Nb–13Zr: A New Low Modulus, High Strength, Corrosion Resistant Near-beta Alloy for Orthopaedic Implants" in *Beta Titanium in the 1990's* Warrendale, The Minerals, Metals & Materials Society, pp. 61-72, 1993

[94] T. Ahmed, et al., "A new Low Modulus, Biocompatible Titanium Alloy" in *8th World Titanium Conference.*, Birmingham, UK, pp. 1760-1767, 1995

[95] M. V. Oliveira, et al., "Porous Structure Characterization in Titanium Coating for Surgical Implants". vol. 5, scielo, pp. 269-273, 2002

[96] R. M. Pilliar, in *Metal and Ceramic Biomaterial*, pp. 80-105, 1994

[97] J. D. Bobyn, et al., "The Optimum Pore Size for the Fixation of Porous Surfaced Metal Implants by the Ingrowth of Bone", *Clinical Orthopaedics and Related Research,* vol. 150, pp. 263-270, 1980
[98] R. J. Haddad, et al., "Biological Fixation of Porous-coated Implants", *The Journal of Bone and Joint Surgery,* vol. 69, pp. 1459-1466, American volume 1987
[99] Arcam, *available at:* http://www.arcam.com/industry-segments/medical-implants.aspx,
[100] F. H. Froes, et al., "Titanium Powder Metallurgy - Automotive and More" in *International Conference on Powder Metallurgy & Particulate Materials* Chicago, pp. 178-187, 2004
[101] D. Helm and O. Roder, "Recent Titanium Research and Development in Germany" in *The 11th World Conference on Titanium (JIMIC5) - Ti-2007*, Kyoto - Japan, pp. 25-32, 2007
[102] O. M. Ivasishin, et al., "Titanium Powder Metallurgy for Automotive Components", *Materials Technology,* vol. 17, pp. 20-25, 2002
[103] A. M. Sherman, et al., "The Use of Titanium in Production Automobiles: Potential and Challanges", *JOM,* vol. 49, pp. 38-41, 1997
[104] T. Saito, "The Automotive Application of Discontinuosly Reinforced TiB-Ti Composites", *JOM,* vol. 56, pp. 33-36, 2004
[105] R. German, "Production of Heavy Vehicle Components from Low-cost Titanium Powder, Contractor: Pacific Northwest national laboratory", available at: http://www1.eere.energy.gov/vehiclesandfuels/pdfs/lm_09/cover_toc.pdf 2007
[106] H. Fukii, et al., "Application of Titanium and its Alloys for Automobile Parts", Nippon Steel Technical Report Nº 88 2003
[107] F. H. Froes, "Cost Effective Synthesis, Processing and Applications of Light-weight Metallic Materials", *Materials Technology,* vol. 21, pp. 94-101, 2006
[108] Ducati, "Ducati Performance: 999/749 Accessories and Kit Catalogue", 2002
[109] F. H. Froes, "How to Market Titanium: Lower the Cost", *JOM,* vol. 56, pp. 39-39, 2004
[110] E. Verné, "Leghe a Memoria di Forma, Personal Communication" Politecnico di Torino, Torino (Italia), 2007
[111] K. Majima, et al., "Microstructures and Tensile Properties of Hot Isostatically Pressed Ti-Fe Alloys", *Journal of the Japan Institute of Metals,* vol. 52, pp. 1113-1120, 1988
[112] W. Wei, et al., "Effect of Fe Addition on Sintering Behaviour of Titanium Powder", *Powder Metallurgy,* vol. 46, pp. 246-250, 2003
[113] D. Kuroda, et al., "Development of New Ti-Fe-Ta and Ti-Fe-Ta-Zr System Alloys for Biomedical Applications", *Materials Transactions,* vol. 46, pp. 1532-1539, 2005
[114] Y. Liu, et al., "Design of Powder Metallurgy Titanium Alloys and Composites", *Materials Science and Engineering: A,* vol. 418, pp. 25-35, 2006
[115] H. Hotta, et al., "Synthesis of Ti-Fe Alloys by Mechanical Alloying", *Journal of Alloys and Compounds,* vol. 439, pp. 221-226, 2007
[116] P. G. Esteban, "Diseño y Procesado por vía Pulvimetalúrgica Convencional de Aleaciones de Ti de Bajo Coste" in *Tesis Doctoral*, Universidad Carlos III de Madrid, 2009

[117] P. G. Esteban, et al., "P/M Develpment of Low-cost Titanium Alloys by Means of Iron Additions", *Proceedings Euro PM2007 - Lightweight & Porous Materials,* vol. 2, pp. 353-358, 15-17 October 2007
[118] P. G. Esteban, et al., "Study of Sintering Aspects for the Manufacturing of Low-cost Titanium Alloys" in *PM 2008 - Advances in Powder Metallurgy & Particulate Materials - 2008*. vol. 5 Washington, D.C. - U.S.A., MPIF, pp. 161-175, 2008
[119] P. G. Esteban, et al., "Sinterización y Caracterización de Aleaciones de Titanio de Bajo Coste" in *II Congreso Nacional de Pulvimetalurgia* San Sebastián - Spain, 2008
[120] P. G. Esteban, et al., "Low-cost Titanium Alloys? Iron May Hold the Answers", *Metal Powder Report,* vol. 63, pp. 24-27, 2008
[121] P. G. Esteban, et al., "Ensayos de Tracción en Aleaciones de Titanio Pulvimetalúrgicas de Bajo Coste" in *XXV Encuentro del Grupo Español de Fractura*. vol. 1 5-7 de Marzo de 2008, Sigüenza, Grupo Español de Fractura, pp. 181-186, 2008
[122] P. G. Esteban, et al., "Propiedades Mecánicas de Aleaciones de Ti Pulvimetalúrgicas de Bajo Coste" in *X Congreso Nacional de Materiales*. vol. 1 Donostia - San Sebastián - Spain, pp. 151-154, 2008
[123] R. M. German, *Powder Metallurgy of Iron and Steel*, John Wiley & Sons, Inc., 1998
[124] T. Saito, "A Cost-effective P/M Titanium Matrix Composite for Automobile Use", *Advanced Performance Materials,* vol. 2, pp. 121-144, 1995
[125] T. Saito, et al., "Thermomechanical Properties of P/M [Beta] Titanium Metal Matrix Composite", *Materials Science and Engineering A,* vol. 243, pp. 273-278, 1998
[126] M. Frary, et al., "Microstructure and Mechanical Properties of Ti/W and Ti-6Al-4V/W Composites Fabricated by Powder-metallurgy", *Materials Science and Engineering A,* vol. 344, pp. 103-112, 2003
[127] H. Choe, et al., "Effect of Tungsten Additions on the Mechanical Properties of Ti-6Al-4V", *Materials Science and Engineering A,* vol. 396, pp. 99-106, 2005
[128] O. N. Senkov and F. H. Froes, "Thermohydrogen Processing of Titanium Alloys", *International Journal of Hydrogen Energy,* vol. 24, pp. 565-576, 1999
[129] M. Chandrasekaran, et al., "Development of a New PM Titanium Alloy for Improved Processability", *Materials Science and Technology,* vol. 21, pp. 185-190, 2005
[130] M. Chandrasekaran and Z. S. Xia, "Effect of Alloying Time and Composition on the Mechanical Properties of Ti Alloy", *Materials Science and Engineering A,* vol. 394, pp. 220-228, 2005
[131] L. Parsons, et al., "Titanium P/M Comes of Age", *Metal Progress,* vol. 126, pp. 83-94, 1984
[132] F. H. Froes, "The Manufacturing of Titanium P/M" in *The Symposium on High Performance P/M Components* Coimbra, Portugal, pp. 1-16, 2002
[133] B. E. Hurless and F. H. Froes, "Lowering the Cost of Titanium", *The AMPTIAC Quaterly,* vol. 6, pp. 3-10,
[134] V. A. Druz, et al., "Blending an Elemental Approach to Volume Titanium Manufacture", *Metal Powder Report,* vol. 61, pp. 16-21, 2006

[135] F. H. Froes, et al., "The Technologies of Titanium Powder Metallurgy", *JOM,* vol. 56, pp. 46-48, 2004
[136] American Society for Metals - ASM, *Powder Shaping and Consolidation Techniques* vol. 7, ASM Metals Handbook Ninth Edition - 3rd Printing, Powder Metallurgy. Ohio, USA, 1988
[137] W. Schatt and K.-P. Wieters, *Powder Metallurgy. Processing and Materials*. Shrewsbury, UK, EPMA - European Powder Metallurgy Association, pp. 1-476, 1997
[138] F. H. Froes, "Developments in Titanium P/M", *available at: http://www.webs1.uidaho.edu/imap/MPR%20Paper.pdf,*
[139] J. Li, et al., "New Cost Effective Titanium Powders", *Materials Technology,* vol. 17, pp. 143-147, 2002
[140] M. Qian, "Cold Compacting and Sintering of Titanium and its Alloys for Near-Net-Shape or Preform Fabrication", *International Journal of Powder Metallurgy,* vol. 46, pp. 29-44, 2010
[141] V. S. Moxson, et al., "Ti-6Al-4V Properties Achieved via Extra Low Chlorine Titanium Powder", *Advances in Powder Metallurgy and Particulate Materials,* vol. 6, pp. 125-140, 1992
[142] V. Moxson, et al., "Production, Characterization and Applications of Low Cost Titanium Powder Products", *Non-aerospace Applications of Titanium,* pp. 127-134, 1998
[143] S. Abkowitz and D. Rowell, "Superior Fatigue Properties for Blended Elemental P/M Ti-6Al-4V", *Journal of Metals,* pp. 36-39, 1986
[144] R. M. German, *Powder Metallurgy Science*, 2nd Edition ed. Princeton, USA, MPIF - Metal Powder Industries Federation, pp. 191-340, 1994
[145] M. H. Bocanegra-Bernal, "Review Hot Isostatic Pressing (HIP) Technology and its Applications to Metals and Ceramics", *Journal of Materials Science,* vol. 39, pp. 6399-6420, 2004
[146] A. Bose and W. B. Eisen, *Hot Consolidation of Powders & Particulates*. Princeton, USA, Metal Powder Industries Federation, pp. 1-88, 2003
[147] K. T. Kim and H. C. Yang, "Densification Behavior of Titanium Alloy Powder during Hot Pressing", *Materials Science and Engineering A,* vol. 313, pp. 46-52, 2001
[148] B. E. Hurless and F. S. Froes, "Cutting the Cost of Titanium", *Advanced Materials & Processes,* vol. 160, pp. 37-40, 2002
[149] O. M. Ivasishin, "Cost-effective Manufacturing of Titanium Parts with Powder Metallurgy Approach", *Materials Forum* vol. 29, pp. 1-8, 2005
[150] O. M. Ivasishin, et al., "High Integrity, Low Cost Titanium Powder Metallurgy Components", *High-performance Metallic Materials for Cost Sensitive Applications, Proceedings,* pp. 117-128, 2002
[151] O. M. Ivasishin, et al., "Synthesis of Alloy Ti-6Al-4V with Low Residual Porosity by a Powder Metallurgy Method", *Powder Metallurgy and Metal Ceramics,* vol. 41, pp. 382-390, 2002
[152] O. M. Ivasishin, et al., "Cost-effective Blended Elemental Powder Metallurgy of Titanium Alloys for Transportation Application", in *Development in Light Metals*, vol. 188, pp. 55-62, 2000

[153] F. H. Froes, et al., "Cost–effective Synthesis of Ti–6Al–4V Alloy Components via the Blended Elemental P/M Approach" in *Symposium on TMS Symposium on High Performance Metallic Materials for Cost Sensitive Applications*, Seattle, WA, 2002
[154] G. Friedman, "Titanium Powder Metallurgy", *International Journal of Powder Metallurgy,* vol. 6, pp. 43-55, 1970
[155] F. H. Froes and J. E. Smugeresky, *Powder Metallurgy of Titanium Alloys*, The Metallurgical Society of AIME, 1980
[156] G. Welsch, et al., "Deformation Behaviour of Blended Elemental Ti-6Al-4V Compacts", *Metallurgical and Materials Transactions A,* vol. 14, pp. 761-769, 1983
[157] G. Welsch, et al., "Characterization of Fracture Surface, Pores and Inclusions in Sintered Ti-6Al-4V", *Powder Metallurgy International,* vol. 14, pp. 190-194, 1984
[158] F. H. Froes and D. Eylon, "Powder Metallurgy of Titanium Alloys - A Review", *Powder Metallurgy International,* vol. 17, pp. 163-167, 1985
[159] F. H. Froes and D. Eylon, "Powder Metallurgy of Titanium Alloys - A Review", *Powder Metallurgy International,* vol. 17, pp. 235-238, 1985
[160] G. Friedman, *Air Force Materials Laboratory,* vol. Report No. AFML-TR-75-9, 1975
[161] P. W. Sutcliffe, "Review of Advanced Powder Metallurgical Fabrication Tehcniques in European Nato Countries", *AGARD report no. 641,* 1976
[162] R. F. Vaughan, et al., *AGARD Conf. Proc. Nº 200, Paper P.,* p. 11, 1976
[163] W. Keinath, *AGARD Conf. Proc. Nº 200, Paper SC.,* p. 8, 1976
[164] J. H. Schwertz, et al., *Air Force Materials Laboratory,* vol. Report No. AFML-TR-78-41, 1978
[165] D. B. Dawson and M. G. Ulitchney, "Characterisation of the Tensile Properties of Hot Isostatically Pressed Ti-6Al-6V-2Sn", *Powder Metallurgy of Titanium Alloys,* pp. 115-126, 1980
[166] R. Mohs and H. Sibum, "Powder Metallurgical Production of Titanium Alloy Ti6Al4V Parts", *Powder Metallurgy International,* vol. 16, pp. 163-166, 1984
[167] J. E. Smugeresky and D. B. Dawson, "New Titanium Alloys for Blended Elemental Powder Processing", *Powder Technology,* vol. 30, pp. 87-94, 1981
[168] T. Fujita, et al., "Microstructure and Properties of Titanium Alloy Produced in the Newly Developed Blended Elemental Powder Metallurgy Process", *Materials Science and Engineering: A,* vol. 213, pp. 148-153, 1996
[169] F. H. Froes and D. Eylon, "Titanium Powder Metallurgy - A Review" in *PM Aerospace Materials*, Bern - Switzerland, pp. 1-19, 1984
[170] F. H. Froes and D. Eylon, "Powder Metallurgy of Titanium Alloys" in *Titanium: Science and Technology*, Munich - Germany, pp. 267-286, 1985
[171] F. H. Froes, et al., "Developments in Titanium Powder Metallurgy", *Journal of Metals,* vol. 32, pp. 47-54, 1980
[172] S. Krishnamurthy, et al., "Developments in Titanium Powder Metallurgy" in *Progress in Powder Metallurgy 1983*, New Orleans - U.S.A, pp. 603-623, 1984
[173] J. Park, et al., "Forming of Near Net Shapes of Titanium Alloys by Blended Elemental Powder Metallurgy", *Industrial Heating,* pp. 32-35, 1984
[174] D. Eylon, et al., "Developments in Titanium-alloy Casting Technology", *Journal of Metals,* vol. 35, pp. 35-47, 1983

[175] C. H. Smith, "Consolidation of a Rapidly Solidified Titanium Alloys by Hot Isostatic Pressing", *Materials Science and Engineering,* vol. 89, pp. 103-117, 1987
[176] G. Friedman and R. Regn, "Titanium PM Gyro Components", *Metal Powders Report,* pp. 273-281, 1984
[177] R. W. Broomfield, et al., "Application of Advanced Powder Process Technology to Titanium Aeroengine Components", *Powder Metallurgy,* vol. 28, pp. 27-34, 1985
[178] J. P. Herteman, et al., "Mechanical-properties of Advanced Titanium Powder-metallurgy Compacts", *Powder Metallurgy International,* vol. 17, pp. 116-119, 1985
[179] D. Eylon, et al., "Property Improvement of Low Chlorine Titanium Alloy Blended Elemental Powder Compacts by Microstructure Modification", *Progress in Powder Metallurgy,* vol. 42, pp. 625-634, 1986
[180] M. Minabe and H. Endoh, "Development of High Density Sintered Titanium Alloys using a Sinter-HIP Process", *Metal Powders Report,* pp. 673-682, 1990
[181] L. Wang, et al., "Properties and Forming Process of Prealloyed Powder Metallurgy Ti-6Al-4V Alloy", *Trans. Non Ferrous Met. Soc. China,* vol. 17, pp. s639-s643, 2007
[182] C. G. Goetzel and V. S. de Marchi, "Electrically Activated Pressure Sintering (Spark Sintering) of Titanium Powders", *Modern Developments in Powder Metallurgy,* vol. 3, pp. 80-87, 1971
[183] C. G. Goetzel and V. S. de Marchi, "Electrically Activated Pressure Sintering (Spark Sintering) of Titanium Powders", *Modern Developments in Powder Metallurgy,* vol. 3, pp. 134-136, 1971
[184] C. G. Goetzel and V. S. de Marchi, "Electrically Activated Pressure Sintering (Spark Sintering) of Titanium-aluminium-vanadium Alloy Powders", *Modern Developments in Powder Metallurgy,* vol. 4, pp. 127-150, 1971
[185] R. K. Malik, "Hot Pressing of Titanium Aerospace Components", *The International Journal of Powder Metallurgy & Powder Technology,* vol. 10, pp. 115-129, 1974
[186] R. K. Malik, "Vacuum Hot Pressing of Titanium Alloy Powders", *Progress in Powder Metallurgy,* vol. 31, pp. 277-288, 1975
[187] W. H. Kao and L. M. Orsborn, "Consolidation Characteristics of Rotating Electrode and Hydride Titanium Powders", *Powder Metallurgy of Titanium Alloys,* pp. 163-173, 1980
[188] C. H. Liu and P. W. kao, "Microstructure and Mechanical Properties of Resistance Sintered Titanium", *Scripta Metallurgica et Materialia,* vol. 24, pp. 2279-2284 1990
[189] B. Ye, et al., "Enhanced Densification of Ti-6Al-4V Powders by Transformation-mismatch Plasticity", *Acta Materialia,* vol. 58, pp. 3851-3859, 2010
[190] M. Eriksson, et al., "Fast Densification and Deformation of Titanium Powder", *Powder Metallurgy,* vol. 48, pp. 231-236, 2005
[191] J. D. K. Rivard, et al., "The Thermomechanical Processing of Titanium and Ti-6Al-4V Thin Gage Sheet and Plate", *JOM,* vol. 57, pp. 58-61, 2005
[192] V. A. R. Henriques, et al., "Production of Ti-6%Al-7%Nb Alloy by Powder Metallurgy (P/M)", *Journal of Materials Processing Technology,* vol. 118, pp. 212-215, 2001

[193] V. A. R. Henriques, et al., "Production of Titanium Alloys for Medical Implants by Powder Metallurgy", *Key Engineering Materials* vol. Advanced Powder Technology II pp. 443-448, 2001
[194] V. A. R. Henriques, et al., "Microstructural Evolution during Hot Pressing of the Blended Elemental Ti-6%Al-7%Nb Alloy", *Materials Science and Engineering A,* vol. 347, pp. 315-324, 2003
[195] V. A. R. Henriques, et al., "Use of Titanium Powders obtained by Sponge Screening and for the HDH Process in Titanium Alloy Production for Powder Metallurgy (P/M) ", *Materials Science Forum,* vol. Advanced Powder Technology III, pp. 23-28, 2003
[196] V. A. R. Henriques, et al., "Dissolution of Niobium Particles during Ti-6Al-7Nb Sintering", *Materials Science Forum,* vol. Advanced Powder Technology III, pp. 275-262, 2003
[197] Y. R. Mahajan, et al., "Modification of Titanium Powder-metallurgy Alloy Microstructures by Strain Energizing and Rapid Omni-directional Compaction", *Powder Metallurgy International,* vol. 17, pp. 75-78, 1985
[198] I. Weiss, et al., "Effect of Isothermal Forging on Microstructure and Fatigue Behavior of Blended Elemental Ti-6Al-4V Powder Compacts", *Metallurgical and Materials Transactions A,* vol. 17, pp. 549-559, 1986
[199] L. Facchini, et al., "Microstructure and Mechanical Properties of Ti-6Al-4V Produced by Electron Beam Melting of Pre-alloyed Powders", *Rapid Prototyping Journal,* vol. 15, pp. 171-178, 2009
[200] S. Das, et al., "Direct Laser Freeform Fabrication of High Performance Metal Components", *Rapid Prototyping Journal,* vol. 4, pp. 112-117, 1998
[201] F. H. Froes, "Laser Forming Titanium Components from Powder", *Materials Technology: Advanced Performance Materials,* vol. 15, pp. 8-12, 2000
[202] F. G. Arcella and F. H. Froes, "Producing Titanium Aerospace Components from Powder using Laser Forming", *JOM,* vol. 52, pp. 28-30, 2000
[203] A. J. T. Clemow, et al., "Interface Mechanics of Porous Titanium Implants", *Journal of Biomedical Materials Research,* vol. 15, pp. 73-82, 1981
[204] L. D. Zardiackas, et al., "Structure, Metallurgy and Mechanical Properties of a Porous Tantalum Foam", *Journal of Biomedical Materials Research Part B: Applied Biomaterials,* vol. 58, pp. 180-187, 2001
[205] C. E. Wen, et al., "Processing of Biocompatible Porous Ti and Mg", *Scripta Materialia,* vol. 45, pp. 1147-1153, 2001
[206] M. Eriksson, et al., "High Velocity Compaction of Titanium Powder" in *EUROPM 2003*, Valencia - Spain, pp. 301-304, 2003
[207] H. Takamiya, et al., "Ultra–high Pressure Warm Compaction for P/M Titanium Components" in *Cost-affordable Titanium Symposium*, pp. 185-192, 2004
[208] R. E. Blose, et al., "New Opportunities to Use Cold Spray Process for Applying Additive Features to Titanium Alloys", *Metal Powder Report,* vol. 61, pp. 30-37, 2006
[209] G. F. Taylor, "Apparatus for Making Hard Metal Compositions". vol. United States Patent 1896854, 1933
[210] J. R. Groza and A. Zavaliangos, "Sintering Activation by External Electrical Field", *Materials Science and Engineering A,* vol. 287, pp. 171-177, 2000

[211] X. Wu and J. Guo, "Effect of Liquid Phase on Densification in Electric-discharge Compaction", *Journal of Materials Science,* vol. 42, pp. 7787-7793, 2007
[212] W. Knoess, "Shockwave - new Powder Metallurgy Process", *Materials World,* vol. 11, pp. 12-14, 2003
[213] R. Orrù, et al., "Consolidation/Synthesis of Materials by Electric Current Activated/Assisted Sintering", *Materials Science and Engineering R: Reports,* vol. 63, pp. 127-287, 2009
[214] Z. A. Munir, et al., "The Effect of Electric Field and Pressure on the Synthesis and Consolidation of Materials: A Review of the Spark Plasma Sintering Method", *Journal of Material Science,* vol. 41, pp. 763-777, 2006
[215] M. Zadra, et al., "Microstructure and Mechanical Properties of CP-titanium Produced by Spark Plasma Sintering", *Powder Metallurgy,* vol. 51, pp. 59-65, 2008
[216] A. Molinari and M. Zadra, "Influence of the Sintering Temperature on Microstructure and Tensile Properties of Ti6Al4V Produced by Spark Plasma Sintering" in *EUROPM 2009*, Copenhagen - Denmark, pp. 267-272, 2009
[217] M. Zadra, et al., "Ti6Al4V-based MMC Obtained by Means of Spark Plasma Sintering" in *World Congress on Powder Metallurgy & Particulate Materials 2008*, Washington, D.C. - U.S.A., pp. 60-66, 2008
[218] R. M. German, *Powder Injection Molding*, MPIF, 1990
[219] O. Gulsoy, et al., "A New Technology in Production of Aerospace Components: Powder Injection Molding (PIM)", *Rast 2003: Recent Advances in Space Technologies, Proceedings,* pp. 575-578, 2003
[220] R. M. German and A. Bose, *Injection Molding of Metals and Ceramics*, MPIF, 1997
[221] F. H. Froes and R. M. German, "Cost Reductions Prime Ti PIM for Growth", *Metal Powder Report,* vol. 55, pp. 26-28, 2000
[222] F. H. Froes, et al., "Titanium Powder Injection Molding - A Cost Effective Alternative", in *High-performance Metallic Materials for Cost Sensitive Applications, Proceedings* Warrendale: Minerals, Metals & Materials Soc, pp. 129-136, 2002
[223] D. Whittaker, "Developments in the Powder Injection Moulding of Titanium at EuroPM2006", *PIM International,* vol. 1, pp. 27-32, 2007
[224] W. Limberg, et al., "Doctor's Orders? Less Oxygen = More Life for Titanium MIM", *Metal Powder Report,* vol. 60, pp. 22-27, 2005
[225] F. H. S. Froes, "Advances in Titanium Metal Injection Molding", *Innovations in Titanium Technology,* pp. 157-166, 2007
[226] F. H. Froes, "Advances in Titanium Metal Injection Molding", *Powder Metallurgy and Metal Ceramics,* vol. 46, pp. 303-310, 2007
[227] E. Baril, et al., "Development of a Composite Porous/Dense Titanium Dental Implant using a MIM Preform" in *EUROPM2007*, Toulouse - France, pp. 117-122, 2007
[228] E. Baril, et al., "Foam-coated MIM Gives New Edge to Titanium Implants", *Metal Powder Report,* vol. 63, pp. 46-50, 52, 54-55, 2008
[229] H.-D. Kunze, et al., "Investigation of Binders for MIM of Titanium", *Powder Metallurgy World Congress* vol. 2, pp. 1185-1188, 1994
[230] Y. X. Wu, et al., "Injection Molding of HDH Titanium Powder", *International Journal of Powder Metallurgy,* vol. 42, pp. 59-66, 2006

[231] J. C. LaSalle, "Aqueous Binder Allows Economic Net Shape Processing of Larger MIM Parts", *Metal Powder Report,* vol. 55, pp. 32-32, 2000
[232] J. A. Grohowski, et al., "Processing of Titanium by Metal Injection Molding" in *Advances in Powder Metallurgy & Particulate Materials*, Las Vegas - U.S.A., pp. 273-281, 2003
[233] A.A, "Combining the Best that PIM has to Offer to Put the Bite on a New Approach", *Metal Powder Report,* vol. 61, pp. 22-27, 2006
[234] K. S. Scott, et al., "Use of a Naphthalene-based Binder in Injection Molding Net-shape Titanium Components of Controlled Porosity", *Materials Transactions,* vol. 46, pp. 1525-1531, 2005
[235] E. Nyberg, et al., "Microstructure and Mechanical Properties of Titanium Components Fabricated by a New Powder Injection Molding Technique", *Materials Science and Engineering: C,* vol. 25, pp. 336-342, 2005
[236] K. Scott Weil, et al., "A New Binder for Powder Injection Molding Titanium and other Reactive Metals", *Journal of Materials Processing Technology,* vol. 176, pp. 205-209, 2006
[237] E. S. Thian, et al., "Effects of Debinding Parameters on Powder Injection Molded Ti-6Al-4V/HA Composite Parts", *Advanced Powder Technology,* vol. 12, pp. 361-370, 2001
[238] R. Vargas Cortes, et al., "Titanium Parts Obtained by MIM using HDH Powder", *58th Annual Congress of ABM - International, Rio de Janeiro - Julio 21-24,* pp. 1835-1841, 2003
[239] T. Deguchi, et al., "Trial Production of Titanium Orthodontic Brackets Fabricated by Metal Injection Molding (MIM) with Sintering", *Journal of Dental Research,* vol. 75, pp. 1491-1496, 1996
[240] TiJet Medizintechnik GmbH, "Innovative Injection Moulding of Titanium", *available at: www.tijet.de/en/?download=TiJet_MIMofTitanium_english.pdf*, 2006
[241] A. F. Galio and L. Schaeffer, "Characteristics of Titanium Parts Produced by Powder Injection Moulding", *Proceedings of the Institution of Mechanical Engineers Part B - Journal of Engineering Manufacture,* vol. 220, pp. 783-786, 2006
[242] G. Shi-bo, et al., "Influence of Sintering Temperature on Mechanical Properties of Ti-6A-4V Compacts by Metal Injection Molding", *Materials Science Forum,* vol. 475-479, pp. 2639-2642, 2005
[243] G. Shibo, et al., "Powder Injection Molding of Ti-6Al-4V Alloy", *Journal of Materials Processing Technology,* vol. 173, pp. 310-314, 2006
[244] Y. Itoh, et al., "Fabrication of Ti-6Al-7Nb Alloys by Metal Injection Molding", *Materials Science Forum,* vol. Progress in Powder Metallurgy, Pts 1 and 2, pp. 357-360, 2007
[245] Y. Itoh, et al., "Improvement of the Properties of Ti-6Al-7Nb Alloy by Metal Injection Molding" in *Advances in Powder Metallurgy & Particulate Materials*, pp. Part 4, 81-86, 2007
[246] G. Shi-bo, et al., "Effect of Annealing Processing on Microstructure and Properties of Ti-6Al-4V Alloy by Powder Injection Molding", *Transactions of Nonferrous Metals Society of China,* vol. 16, pp. s701-s704, 2006
[247] K. Songsiri, et al., "Effects of Sintering Temperature and Sintering Time on Mechanical and Impact Properties of Injection Moulded Ti-6Al-4V Employing

Prealloyed and Mixed Powders" in *Advances in Powder Metallurgy & Particulate Materials*, Washington, D.C. - U.S.A., pp. 175-182, 2008

[248] E. S. Thian, et al., "Ti-6Al-4V/HA Composite Feedstock for Injection Molding", *Materials Letters,* vol. 56, pp. 522-532, 2002

[249] E. S. Thian, et al., "Microstructures and Mechanical Properties of Powder Injection Molded Ti-6Al-4V/HA Powder", *Biomaterials,* vol. 23, pp. 2927-2938, 2002

[250] P. Divya, et al., "Injection Moulding of Titanium Metal and AW-PMMA Composite Powders", *Trends Biomater. Artif. Organs,* vol. 18, pp. 247-253, 2005

[251] E. Schüller, et al., "Metal Injection Molding of Shape Memory Alloys Using Prealloyed NiTi Powders", *Journal of Materials Science,* vol. 40, pp. 4231-4238, 2005

[252] Y. C. Kim, et al., "Application of Metal Injection Molding Process to Fabrication of Bulk Parts of TiAl Intermetallics", *Journal of Materials Science,* vol. 42, pp. 2048-2053, 2007

CAPÍTULO 2

PROCEDIMIENTO EXPERIMENTAL

2.1 – COMPOSICIONES A ESTUDIAR

En esta tesis se plantea el estudio y la obtención de materiales base titanio, tanto elemental como aleado, mediante técnicas pulvimetalúrgicas convencionales y avanzadas con el fin de obtener componentes de altas prestaciones mecánicas que, en el caso de la pulvimetalúrgia, se refleja en alcanzar elevadas densidades relativas tras el proceso de producción junto con una microestructura fina y homogénea.

En este capitulo se describe la metodología de la investigación seguida y se detallan las características de los equipos utilizados y las normas de referencia consideradas.

La primera etapa del trabajo ha consistido en una amplia búsqueda bibliográfica acerca de los procesos de obtención de polvos de titanio y de sus aleaciones para poder identificar las características propias de cada proceso de producción y seleccionar el proceso de conformado más idóneo para cada polvo.

Además, la búsqueda se ha centrado en la recopilación de los diferentes productores y proveedores de polvos así como de los diversos tipos de productos disponibles a nivel comercial tanto para el titanio elemental como para sus aleaciones.

La Tabla 2.1 y la Tabla 2.2 recogen un resumen de los tipos de polvos disponibles según algunos autores.

Tabla 2.1 – Polvos de titanio disponibles en 2002 según Froes[1].

Organization	Type	Size [μm]	Price [$/lb]	Market activity
PYROGENISIS (PA)	Various	– 45 < 45	~ 180 35 – 75	Powder available
STARMET (PREP/REP)	Various	Average 150	50 – 100 ~ 200 (PIM)	Powder available level about 1 ton/year but potential to increase
CRUCIBLE RESEARCH (GA)	Various	– 500 + 45 – 45	~ 45 (CP/6–4) ~ 50 (TiAl) 134 – 155	2–3 Tons/year market growing slowly
SUMITOMO SITIX (ingot drip/GA)	CP 6–4 TiAl	– 45 – 150 – 250 – 250	40 – 50 (MIM) 20 – 30	1–3 Tons/year Unstable market Powder available
MER (plasma discharge)	CP Alloys	1 to 15	60	R & D Stage
AFFINITY (GA)	CP 6–4	Various size fractions from – 230 + 43	20 – 48	Powder available with O_2, Fe lower than ASTM B–265 requirement
AFFINITY (HDH)	CP	Various size fractions from – 140 + 25	8 – 12	R & D Stage
METAMORPHIC METALS Ltd. (HDH)	CP 3–2 6–4	– 250 for Plasma – 149 for Press/Sinter – 74 and – 44 for PIM	20 – 25	Capacity @ 2 ton/year Custom lots/blends and low O_2 powders available
HYPER INDUSTRIES (Hydride)	6–4	– 200	20 – 25	Powder available
ADMA Chips (HDH)	CP 6–4	– 45	10	Samples available
ADMA Fines	CP	– 45	20	Powder available
READING ALLOYS (HDH)	CP 6–4	– 300 + 50	20 – 50	Powder available
FRAY (Reverse Electrolytic)	Various	To be defined	To be defined	Research base

Tabla 2.2 – Polvos de titanio disponibles en 2006 según Titanium Information Group (TIG)[2].

Company	Country	Powder type	Approximate cost/kg
AP&C	Canada	Plasma	500–1000 €
Bogen/Affinity	China/USA	GA	150–200 €
Bogen/Affinity	China/USA	HDH	25–150 €
Crucible	USA	GA	150–200 €
International Titanium Powder	USA	Direct Reduction	–
Pioneer Metals & Technology	USA	PREP	500–1000 €
Pyrogenesis	Greece/Canada	Plasma	500–1000 €
Reading Alloys	USA	HDH	25–150 €
Se-Jong	Korea	HDH	25–150 €
Starmet	USA	PREP	500–1000 €
Sumitomo	Japan	GA	150–200 €
TLS	Germany	GA	150–200 €
TLS	Germany	HDH	25–150 €
ToHo	Japan	HDH	25–150 €
Zunyi Titanium	China	HDH	25–150 €

En una etapa previa se hizo una búsqueda de las aleaciones de titanio actualmente más utilizadas con el fin de identificar los elementos más significativos para poder diseñar nuevas aleaciones o mejorar algunas propiedades de las existentes.

En particular se identificaron aleaciones con propiedades interesantes, fundamentalmente desde el punto de vista de las propiedades mecánicas, pero sin descuidar el aspecto de biocompatibilidad, y cuyos costes de procesado por métodos convencionales puedan ser disminuidos por vía P/M.

Finalmente, se decidió centrar el trabajo en los aspectos relativos al procesado de aleaciones actualmente disponibles a nivel comercial en forma de lingotes, fundiciones o laminados, y en la selección de la adición de los elementos de aleación o las técnicas de conformado, en lugar de en el diseño de nuevas composiciones. En base a esto se consideraron los siguientes materiales:

- ✓ **Titanio elemental (α)**: material de referencia durante el desarrollo del proyecto. Además fue empleado para el estudio de la influencia del tamaño de partícula del polvo y de su distribución, así como del proceso de obtención; para investigar la variabilidad de las propiedades de los polvos procedentes de diferentes lotes de producción y como materia prima para la preparación de las aleaciones;
- ✓ **Aleación Ti–3Al–2,5V (casi α)**: esta aleación fue considerada porque no suele ser procesada mediante técnicas pulvimetalúrgicas y debido a su facilidad de producción. En particular se han considerado dos vías para añadir los elementos aleantes: a partir de una aleación maestras de Al:V y de la mezcla de los polvos de titanio elemental y de Ti–6Al–4V. Esto permite identificar cual de las dos vías es la más eficiente para añadir elementos de aleación al titanio elemental.

- ✓ **Aleación Ti–6Al–4V (α + β)**: esta aleación esta muy bien estudiada y caracterizada cuando es obtenida por metalurgia convencional. En esta tesis se ha considerado su fabricación tanto a partir de polvo prealeado (PA) como de mezcla convencional utilizando una aleación maestra (MA) como medio para introducir los elementos de aleación. Esto permite la comparación de los dos enfoques clásicos de la pulvimetalúrgia del titanio empleados para la obtención de sus aleaciones.
- ✓ **Aleación Ti–6Al–7Nb (α + β)**: esta aleación es relativamente novedosa y fue desarrollada exclusivamente para implantes biomédicos y raramente se procesa por P/M. Esto permite estudiar la viabilidad de las técnicas pulvimetalúrgicas para la producción de componentes biomédicos.

2.2 – MATERIAS PRIMAS Y PRODUCCIÓN DE POLVOS

Una vez identificadas las aleaciones, la investigación se centró en el diseño de la etapa de aleación evaluando pros y contras tanto del enfoque de prealeado como de la mezcla elemental a partir de polvos elementales y aleaciones maestras. Finalmente, se eligió llevar a cabo una comparación entre ambas. Sin embargo, se han encontrado dificultades para llevar a cabo la comparación propuesta, ya que, desafortunadamente, muchos de los fabricantes mostrados en las Tablas 2.1 y 2.2 no suministran polvos con las características requeridas para el desarrollo de esta tesis, o no proporcionan los polvos en pequeñas cantidades normalmente utilizadas a nivel de investigación. Además, hay una falta de productores de polvos prealeados de aleaciones de titanio, ya que normalmente se comercializa exclusivamente la aleación Ti–6Al–4V, o aleaciones maestras.

La búsqueda bibliográfica acerca de los procesos de obtención de titanio en forma metálica y de los métodos de producción de polvos permitió identificar el proceso de hidrurado–dehidrurado (HDH) como idóneo para el desarrollo de este estudio. Entre las diferentes técnicas disponibles, el proceso HDH constituye la mejor solución al compromiso de obtener polvo de titanio y sus aleaciones apto para ser procesados mediante técnicas P/M convencionales (morfología irregular), con buena calidad (relativamente bajo nivel de impurezas) y al menor precio.

El proceso HDH utiliza como materia prima polvo esponja, virutas de mecanizados o lingotes previamente seleccionados, limpiados y secados. La materia prima es hidrurada en un horno a una temperatura comprendida entre 400°C y 700°C gracias a la reacción exotérmica entre el titanio y un flujo de hidrógeno de alta pureza. Una vez terminada la hidruración, se muele el polvo bajo una atmósfera de argón para evitar la oxidación antes de ser sometido al proceso de deshidruración en vacío a una temperatura comprendida entre 600°C y 700°C.

Las partículas de polvo de titanio obtenidas mediante el proceso HDH se caracterizan por una morfología angular y, normalmente, no contienen cloruros aunque depende del origen de la materia prima empleada. Como se ha mencionado anteriormente, mediante el proceso HDH es posible obtener también polvos prealeados de aleaciones de titanio, lo que debería disminuir ulteriormente el coste, aunque el empleo de estos polvos, que son más duros, conlleva un mayor desgaste de las matrices utilizadas en la etapa de consolidación.

En función de los condicionantes mencionados anteriormente, finalmente se optó por la adquisición de los siguientes polvos:

- ✓ polvo de titanio elemental (HDH) con diferentes tamaños de partícula suministrados por la empresa GfE – Metalle und Materialen GmbH;
- ✓ polvo prealeado de la aleación Ti–6Al–4V (HDH) del fabricante coreano "SE–JONG Materials CO., Ltd.";
- ✓ aleación maestras de Al:V (35:65 porcentaje en peso) suministrados por la empresa GfE – Metalle und Materialen GmbH;

- ✓ aleación maestra de Nb:Al:Ti (60:35:5 porcentaje en peso) suministrados por la empresa GfE – Metalle und Materialen GmbH.

Las características principales del polvo de titanio elemental y de las aleaciones maestras proporcionadas por el fabricante se detallan en el apartado 3.1 (Tabla 3.1 y Tabla 3.4) donde se describe el proceso de obtención de las aleaciones estudiadas en esta tesis.

Cabe destacar que fueron adquiridos cinco polvos de titanio elemental con diferentes características con el fin de identificar el mejor para su posterior utilización tanto como material de referencia como base para la producción de las aleaciones propuestas. La caracterización de estos polvos de titanio elemental se describe en el apartado 3.2.

Seguidamente se llevó a cabo la caracterización de las materias primas a través de su análisis morfológico y microestructural mediante microscopia electrónica de barrido (MEB), análisis del tamaño de partículas por difracción láser, determinación de densidad mediante picnometría de helio, análisis químico para determinar el contenido de O, N y C (LECO) y medida de la densidad aparente y de la velocidad de flujo.

Simultáneamente se abordó la producción de las aleaciones a partir de las aleaciones maestras para poder determinar las propiedades finales de las mismas tal como se indica en el esquema de la Figura 2.1. El equipamiento utilizado para esta fase de producción y caracterización de los polvos de partida se detalla en el apartado 2.3.

El proceso de molienda de alta energía (MAE) se aplicó a las aleaciones maestras con el fin de reducir el tamaño de partícula y alcanzar el ratio correcto entre los elementos de aleación deseados. Se espera a partir de ello una mejora en la sinterabilidad del material así como en las propiedades mecánicas generales del material sinterizado, debido a la reducción del tamaño de partícula e introducción de defectos como la reducción del tamaño de grano que favorezca la difusión de los elementos de aleación y, por lo tanto, la homogenización de la microestructura[3]. Por otro lado, la mezcla convencional se realizó con el fin de conseguir una mezcla homogénea entre el polvo de titanio elemental y la aleación maestra.

De los diferentes tipos de molinos que se pueden emplear para la molienda mecánica, en este trabajo se ha utilizado el molino planetario, que debe su nombre al movimiento de las vasijas análogo al de los planetas. Las vasijas están colocadas sobre un disco de soporte y un mecanismo de rotación especial que permite que estas den vueltas alrededor de su propio eje. La fuerza centrífuga producida por esta rotación junto con la fuerza centrífuga generada por la rotación del disco de soporte, en sentido contrario a la primera, produce un movimiento de las bolas empleadas como medio de molienda hacia la parte inferior de las paredes de la vasija a lo largo de la pared de la misma. Este movimiento crea un efecto de impacto y de fricción entre las partículas de polvo, las partículas y las bolas y las partículas y la pared permitiendo la reducción del tamaño de partícula típico de la molienda así como la homogenización de las materias primas[4]. La Figura 2.2 muestra un esquema de los movimientos involucrados durante la etapa de molienda mediante un molino planetario.

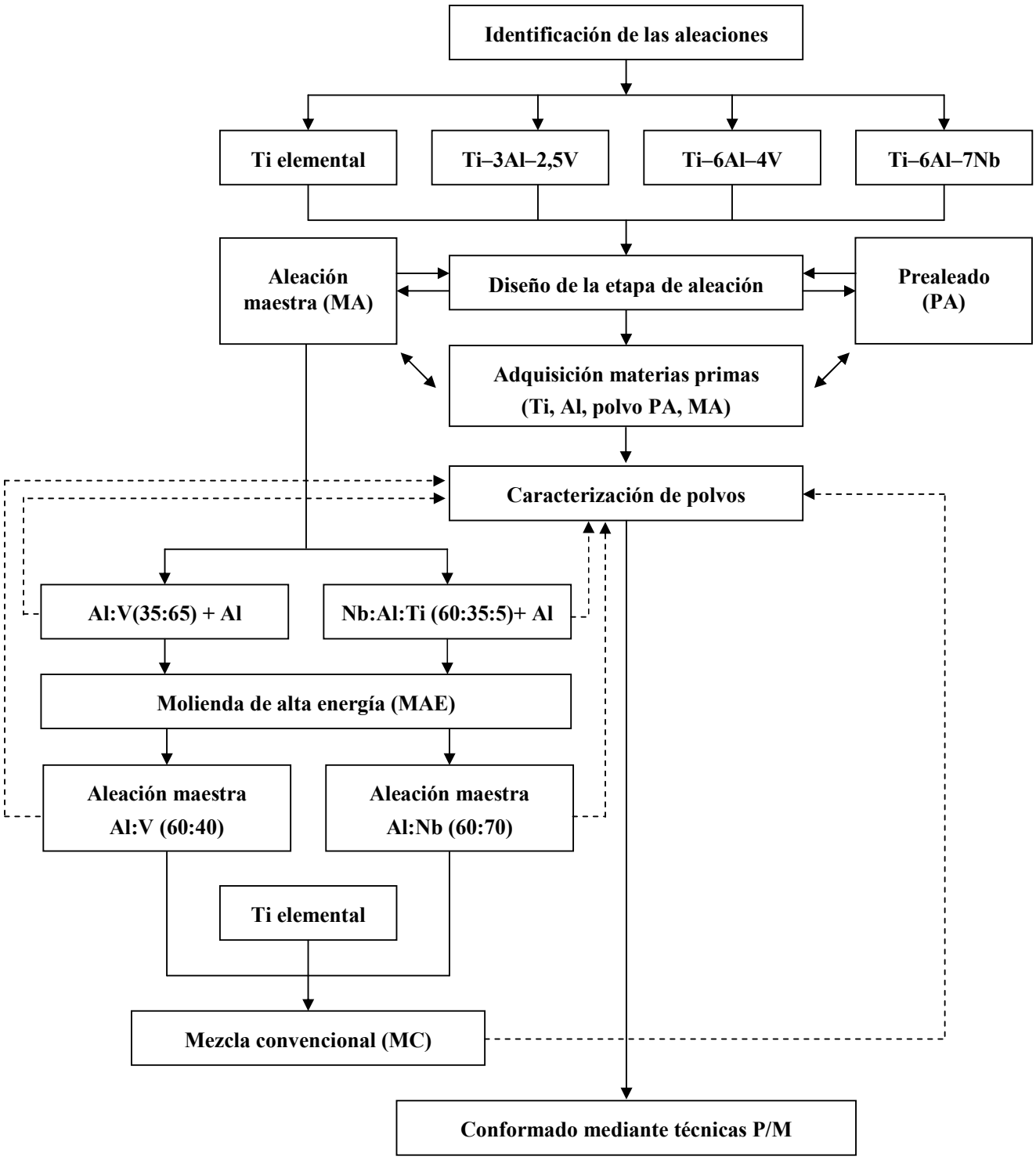

Figura 2.1 – Esquema de las etapas iniciales de la investigación donde se refleja la identificación de las aleaciones a estudiar, la adquisición de las materias primas, la producción y la caracterización de las aleaciones.

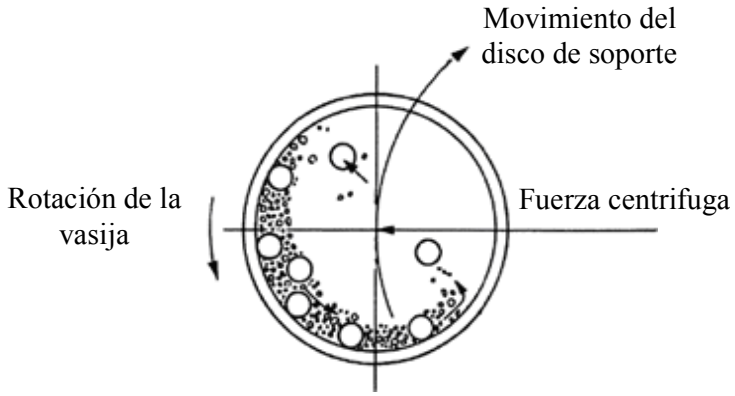

Figura 2.2 – Vista en planta del movimiento de la vasija de molienda en un molino planetario[4].

Las condiciones de molienda empleadas para la reducción del tamaño de partícula de las aleaciones maestras fueron:

- Molino planetario Fritsch Pulverisette 6;
- Vasija y medio de molienda de WC-Co;
- Relación bolas/carga: 5 (en peso);
- Velocidad de giro: 400 rpm;
- Agente de control del proceso (PCA): adición de un 1% en peso de cera Microwax para evitar la adhesión del polvo a la vasija y reducir el tiempo de molienda;
- Atmósfera protectora de argón;
- Tiempo máximo de molienda: 90 minutos.

Durante el estudio de optimización de la etapa de molienda de alta energía, se extrajeron muestras cada 15 minutos para realizar su caracterización mediante análisis granulométrico con un analizador láser.

En función de dichos resultados se seleccionó un tiempo de molienda de 1 hora para la aleación maestra Al:V, que garantiza la obtención de un polvo homogéneo y permite alcanzar un tamaño de partícula menor de 63 μm. En el caso de la aleación maestra Nb:Al:Ti se identificó como tiempo óptimo 30 minutos para producir un polvo con tamaño de partícula menor de 63 μm. El criterio para seleccionar el tiempo de molienda óptimo fue el tamaño de partícula, de manera que fuese el menor posible manteniendo un tamaño similar al polvo de titanio elemental.

Terminada la etapa de optimización de las aleaciones maestras, estas fueron mezcladas con el porcentaje apropiado de titanio elemental en una mezcladora "WAB – TURBULA tipo T2F" durante 30 minutos obteniendo un polvo con la composición porcentual requerida en cada caso considerado adecuado para la posterior etapa de prensado en frío.

2.3 – CARACTERIZACIÓN DE POLVOS

En este apartado se describen las diferentes técnicas y equipos empleados para la completa caracterización de las materias primas adquiridas, de los polvos obtenidos tras la etapa de molienda de alta energía y de los polvos de las aleaciones una vez fabricadas.

La Tabla 2.3 muestra los materiales finales con los cuales se decidió llevar a cabo la investigación y algunos detalles acerca del método y de las condiciones de fabricación empleados.

Tabla 2.3 – Materiales estudiados durante el desarrollo de la tesis y detalles del método de obtención.

Material	Método de producción	Enfoque P/M	Denominación	Comentario
Titanio elemental	Hidrurado dehidrurado (HDH)	–	Ti HDH	Polvo de morfología irregular/angular con diferente distribución de tamaños de partícula
Ti–6Al–4V	Hidrurado dehidrurado (HDH)	Prealeado	Ti64–PA	Polvo de morfología irregular/angular
	–	Aleación Maestra	Ti64–MA	Fabricado mediante la mezcla de titanio elemental HDH y aleación maestra Al:V (60:40)
Ti–3Al–2,5V	–	Mezcla Elemental	Ti32–PA	Fabricado mediante la mezcla de titanio elemental HDH y polvo de Ti–6Al–4V prealeado
	–	Aleación Maestra	Ti32–MA	Fabricado mediante la mezcla de titanio elemental HDH y aleación maestra Al:V (60:40)
Ti–6Al–7Nb	–	Aleación Maestra	Ti67–MA	Fabricado mediante la mezcla de titanio elemental HDH y aleación maestra Al:Nb (60:70)

2.3.1 – Análisis del Tamaño de Partícula

Entre las diferentes tipologías de análisis del tamaño de partícula, es decir microscopía, análisis de imagen, tamizado, sedimentación y difracción láser, se decidió utilizar esta última basada en la teoría de difracción postulada por Joseph Von Fraunhofer según la cual las partículas dispersan luz en todas las direcciones con un patrón de intensidad que es dependiente del tamaño de partícula.

El equipo utilizado fue un Mastersizer 2000 de Malvern Instrument con una unidad de dispersión Hydro 2000SM ya que la medida se realizó dispersando el polvo en agua o un disolvente como se especifica en la norma ASTM B822[5]. En particular, se empleó alcohol en el caso de las aleaciones maestras molidas debido a la presencia de cera que invalidaba las medidas llevadas a cabo en agua produciendo burbujas.

La determinación de los datos de las medidas así como su representación en forma de gráfico se realizó mediante el programa de análisis proporcionado por la misma empresa.

2.3.2 – Análisis Químico

El análisis químico elemental se centró en la determinación del contenido de oxígeno (ASTM B1409)[6], nitrógeno (ASTM B1937)[7] y carbono (ASTM B1941)[8] tanto en las materias primas como en las muestras conformadas ya que estos elementos intersticiales influyen significativamente en las propiedades mecánicas del titanio y de sus aleaciones.

En el caso del oxígeno y del nitrógeno estos fueron determinados mediante un equipo LECO TC–500, cuyo funcionamiento se basa en la fusión de las muestras y arrastre de los gases producidos mediante un gas inerte, concretamente helio.

La medida se realiza pesando una cantidad especifica de muestra, tanto en forma de polvo como maciza, si bien en el caso de los polvos se precisa el uso de un papel de estaño para contenerlos. A continuación se coloca la muestra en una cestita de níquel que tiene la función de favorecer la fusión del titanio disminuyendo su punto de fusión.

La medida se lleva a cabo en un crisol de grafito situado en el interior de un horno de inducción que funde la muestra, liberando el oxígeno y el nitrógeno disueltos en la matriz de titanio. El oxígeno se combina en forma de CO o CO_2 y llega a un detector de infrarrojos gracias al flujo de helio mientras que el nitrógeno en estado molecular se detecta mediante una célula termo-conductora[9].

La metodología y el procedimiento empleados para la determinación de O y N está especificada por LECO[10, 11] y los patrones de calibración utilizados fueron:

- ✓ 501-653: 0,047% O ± 0,003, 0,008% N ± 0,002
- ✓ 501-664: 0,139% O ± 0,008, 0,009% N ± 0,002
- ✓ 502-201: 0,304% O ± 0,005, 0,002% N ± 0,001

Para obtener el porcentaje de carbono se utilizó un analizador LECO CS–200 basado en la fusión en oxígeno de las muestras y determinación del contenido por radiofrecuencia.

Para poder llevar a cabo el ensayo se pesa la muestra y se coloca en un crisol cerámico de alúmina que se introduce en un horno de inducción al que se aplica un voltaje en radiofrecuencia para producir la combustión de la muestra.

Dado que el ensayo se lleva a cabo bajo un flujo de oxígeno, el carbono liberado por la matriz reacciona formando monóxido de carbono que es transportado a varias trampas y catalizadores para su transformación y medida mediante detectores de infrarrojos[12]. Para garantizar la fusión completa y rápida de la muestra se añade una pequeña cantidad de acelerador de la combustión denominado LECOCEL II.

Nuevamente el método y los parámetros de análisis están detallados por LECO[13, 14] y los patrones empleados fueron:

- ✓ 501-501: 0,0345% C ± 0,0011
- ✓ 501-664: 0,0430% C ± 0,0020
- ✓ 502-201: 0,181% C ± 0,0020

2.3.3 – Densidad, Velocidad de Flujo y Microdureza

Las medidas de la **densidad** de los polvos tanto de partida como los obtenidos en la etapa de molienda se realizaron mediante picnometría de helio que se basa en el principio de desplazamiento de fluido de Arquímedes y en la ley de Boyle para determinar el volumen y la densidad del material[15]. El picnómetro empleado es el modelo Accupyc 1330 de Micromeritics.

Los valores obtenidos durante esta etapa han sido mantenidos como valores de densidad teórica para los materiales conformados, ya que se ha comprobado por microscopia que las partículas de los polvos son totalmente densas, siendo:

- ✓ Titanio elemental: 4,5028 ± 0,0055 g/cm^3
- ✓ Ti–6Al–4V: 4,4146 ± 0,0037 g/cm^3 (polvo Ti64-PA)
- ✓ Ti–3Al–2,5V: 4,4561 ± 0,0037 g/cm^3 (polvo Ti32-PA)
- ✓ Ti–6Al–7Nb: 4,52 g/cm^3 (teórica)[16]

Cabe especificar que en el caso de los polvos obtenidos a partir de aleaciones maestras los valores de densidad proporcionados por la picnometría de helio resultaban ser menores tanto con respecto a los teóricos disponibles en la literatura, como los experimentales determinados en los polvos prealeados, debida a la presencia de la cera empleada como agente de control durante la etapa de molienda de alta energía.

Por lo tanto, en el caso de las aleaciones Ti–6Al–4V y Ti–3Al–2,5V se decidió mantener los valores determinados para los polvos prealeados, muy similares a los disponibles en la literatura, mientras que para la aleación Ti–6Al–7Nb se eligió el valor facilitado por RMI–Titanium[17].

La picnometría de helio fue también empleada para medir la densidad de piezas sinterizadas durante la etapa de optimización del estudio de sinterabilidad, para poder discernir los porcentajes relativos de porosidad cerrada y porosidad abierta.

La **densidad aparente** de los polvos fue determinada tanto empleando un flujómetro de Hall como el de Carney, haciendo referencia a las normas MIPF 04[18] y MPIF 28[19], o equivalentes ASTM B212[20] y ASTM B417[21], para polvos que fluyen libremente y para los que no fluyen, respectivamente.

Además de la medida de densidad aparente se llevó a cabo la determinación de la **velocidad de flujo** aplicando la norma MPIF 03[22] o ASTM B213[23] si bien esta solo puede ser realizada con polvos que fluyen.

Para la determinación de la **microdureza**, que fue llevada a cabo utilizando un medidor TIME Technology Europe, modelo HVS–1000 y aplicando una carga de 10 g ($HV_{0.01}$), se embutió el polvo en resina y se pulió con gel de sílice para poder obtener unas superficies especulares. Los ensayos fueron realizados según la norma ASTM B 933[24].

2.3.4 – Morfología y Microestructura de los Polvos

El estudio de la morfología y de la microestructura de los polvos se llevó a cabo mediante un microscopio electrónico de barrido (SEM) Philips XL–30, con emisión termoiónica gracias a un filamento de wolframio, utilizando un potencial acelerador de 20 kV. Este equipo está también provisto de un analizador EDAX DX–4 de espectroscopia de energía de rayos X dispersados (EDS) que permite el análisis semi–cuantitativo de la composición química. Además, el análisis microestructural fue también realizado mediante un microscopio óptico Olympus GX71.

Tanto la microscopia electrónica de barrido como la óptica se utilizaron a lo largo del desarrollo de la tesis tanto para el estudio de la microestructura de las muestras conformadas como para el estudio de la superficie de fractura.

En todos casos, la preparación de muestras pulidas para determinar los microconstituyentes se ha llevado a cabo siguiendo la ruta metalográfica convencional para el titanio[25], es decir corte de una sección representativa, embutido en resina, desbaste con lijas de carburo de silicio de granulometría decreciente (180, 300, 400, 600, 1000) y pulido con gel de sílice. Donde se precisó, los componentes microestructurales fueron resaltados mediante el ataque Kroll (1–3 ml HF, 2–6 ml HNO_3 y 100 ml agua)[26].

2.3.5 – Compresibilidad y Resistencia en Verde

El ensayo de compresibilidad fue llevado a cabo según la norma MPIF 45[27], equivalente a la norma ASMT B331[28], donde se procede al conformado del polvo en muestra de geometría rectangular y mediante la medida de las dimensiones y del peso se determina la densidad en verde en función de la presión de compactación. En este caso se empleó una prensa uniaxial de simple efecto, una matriz flotante con paredes lubricadas con estearato de zinc y se varió la presión entre 300 MPa y 700 MPa.

Se determinó igualmente la resistencia en verde, según la norma MPIF 15[29] o equivalente ASTM B312[30]. La resistencia en verde de los materiales se calcula en función de las dimensiones de las probetas a las cuales se aplica una carga uniaxial en un equipo de flexión en tres puntos. Nuevamente, se representa la resistencia del material en función de la presión de conformado, que en este caso especifico varía entre 300 MPa y 700 MPa.

2.3.6 – Análisis Dilatométrico

El análisis dilatométrico se llevo a cabo para investigar la variación de las dimensiones que experimentan los compactos en verde durante la etapa de sinterización. Para ello se compactaron muestras con geometría paralelepípeda (aproximadamente 5 x 5 x 12 mm^3) utilizando las respectivas presiones óptimas determinadas a partir de los resultados obtenidos en los ensayos de compresibilidad y resistencia en verde.

Durante el estudio se empleó una ciclo térmico compuesto de una rampa de calentamiento (velocidad 10°C/min) hasta los 1400ºC, una meseta de 15 minutos y posterior enfriamiento a 10°C/min hasta temperatura ambiente.

Los ensayos, realizados en un dilatómetro Netzsch Dil 402 E, han sido llevados a cabo bajo un flujo constante de argón de 90 l/h después de 5 ciclos de purgado, es decir bajo vacío mediante bomba rotatoria y rellenado con argón.

El análisis dilatométrico se realizó durante una estancia en el instituto IFAM (Fraunhofer-Instituts für Fertigungstechnik und Angewandte Materialforschung) de Dresde en Alemania.

2.3.7 – Análisis Térmico Diferencial

Con el fin de estudiar el comportamiento de las diferentes aleaciones e identificar eventuales fenómenos de transformación y/o reacción, se llevó a cabo un análisis térmico diferencial mediante un equipo Netzsch STA 449 C Jupiter.

Las muestras en forma de polvo fueron calentadas empleando un ciclo térmico compuesto por una rampa de calentamiento hasta los 1400ºC con una velocidad de 10ºC/min, meseta de 15 minutos y posterior enfriamiento hasta temperatura ambiente (10ºC/min).

De esta forma se abarca todo el intervalo de temperaturas convencionalmente empleado para procesar el titanio y sus aleaciones y los datos obtenidos pueden ser analizados conjuntamente con los obtenidos del análisis dilatométrico.

El análisis térmico diferencial se realizó durante una estancia en el instituto IFAM (Fraunhofer-Instituts für Fertigungstechnik und Angewandte Materialforschung) de Dresde en Alemania.

2.4 – SELECCIÓN DEL SOPORTE DE SINTERIZACIÓN

El titanio es un metal altamente reactivo, lo que ha dado lugar a que se le denomine el disolvente universal, y su reactividad aumenta al aumentar la temperatura, por lo que es muy difícil de procesar por colada ya que cuando se encuentra en el estado líquido reacciona con los moldes cerámicos formando una capa de interacción muy frágil.

Los moldes que se suelen utilizar son materiales refractarios con baja energía libre de Gibbs, como los óxidos: alúmina (Al_2O_3), magnesia (MgO_2) o circona (ZrO_2)[31], para intentar limitar la interacción con el titanio.

Si bien se han llevado a cabo muchas investigaciones en universidades, laboratorios y empresas con el fin de encontrar un material adecuado para la colada del titanio, no ha sido desarrollado todavía un molde cerámico que sea completamente resistente a la interacción con este material.

Las investigaciones realizadas se han centrado en diferentes tópicos, como por ejemplo:

- ✓ Variación del material que constituye el molde o de la composición de la barbotina utilizada para preparar el molde: los primeros estudios acerca de la reactividad del titanio surgen en los años 1950 y entre estos cabe destacar el trabajo de Chapin y Friske que estudiaron varios óxidos (Al_2O_3, BeO, ZrO_2, ThO_2 y Gd_2O_3)[32], carbono, grafito y carburos (TiC, ZrC, VC, NbC, TaC y WC)[33], boruros (TiB_2, ZrB_2 y CrB_2) y sulfuros (CeS)[34], no encontrando un material completamente inerte al titanio. En los mismos años otros autores probaron los mismos materiales y también otros como TmO_2, Cr_3C_2, MoB_2, TaB_2, $MoSi_2$, Zr_3Si, Mo_2Zr, Mo_3Al, Ti_2O_3, $TiO_{0,42}$, $TiO_{0,26}$, ZrO_2 estabilizada con MgO y ZrO_2–Ti y nuevamente no descubrieron un material que no reaccionara si bien de manera limitada[35]. A lo largo de los años otros autores[36-46] han intentado igualmente desarrollar un molde completamente inerte frente al titanio fundido;
- ✓ Disminución de la temperatura del molde que recoge el titanio fundido[31] y efecto de la diferencia de presión de las dos cámaras del equipo de moldeo[47];
- ✓ Estudios teóricos mediante las ecuaciones de termodinámica de las posibles reacciones con el fin de elegir el material más apropiado para el molde[48-50].

Uno de los pocos trabajos relativos a la interacción del titanio con materiales cerámicos en el campo de la pulvimetalúrgia donde estos materiales (óxidos, carburos y nitruros) son utilizados como soporte para la sinterización es el de Gauthier y Baril[51] que destacan que el soporte de sinterización ideal para el titanio debería de presentar un punto de fusión muy alto, una solubilidad limitada con el titanio y no formar fases intermedias tanto con el titanio como con los elementos de aleación presentes.

En la investigación mencionada se consideraron tres soportes diferentes (ZrO_2, BN y TiC) empleando dos temperaturas de sinterización, 1300–1500ºC (nivel de vacío aproximadamente de $5 \cdot 10^{-5}$ torr) obteniendo en todos los casos un cierto grado de interacción con el soporte cerámico.

Durante el desarrollo de esta tesis se consideraron diferentes materiales como soporte de sinterización, en particular, barquillas de alúmina (Al_2O_3) tanto porosa (Lite–Cell 170-D2) como completamente densa (Kerasetter KVS 174/1000) suministradas por Interbil–España, barquillas de carbono de alta estabilidad (H–board proporcionada por Kureha Corporation, Japón) y gránulos densos de circona (ZrO_2) ZIRMIL de diámetro variable entre 1,9 y 2,5 mm comercializados por Saint-Gobain – Francia.

Sin embargo, en función de los resultados preliminares, el estudio de optimización se centró en la utilización de barquillas de alúmina densa y en las bolitas de circona considerando exclusivamente el titanio elemental.

Más en detalle, se llevó a cabo un estudio de sinterabilidad en el intervalo de tiempo y temperaturas convencionalmente empleadas para la sinterización del titanio, concretamente considerando tres temperaturas: 1250ºC, 1300ºC y 1350ºC y dos tiempos de sinterización, es decir 2 horas y 4 horas.

Todos los tratamientos de sinterización de las diferentas aleaciones considerando las diversas condiciones estudiadas fueron llevados a cabo en un horno tubular de alto vacío Carbolite HVT 15/50/450.

2.5 – CONFORMADO MEDIANTE TÉCNICAS P/M

Tras la fabricación y la caracterización de las aleaciones, se llevó a cabo la etapa de conformado de los polvos y, en particular, se platearon las técnicas mostradas en la Figura 2.3 cuyas condiciones de procesado se detallan en los siguientes apartados:

- compactación uniaxial en frío y sinterización (P&S);
- compactación isostática en frío (CIP) y sinterización;
- compactación isostática en caliente (HIP) de polvos y como post–procesado de muestras previamente sinterizadas para disminuir la porosidad residual;
- compactación uniaxial en caliente convencional (HP);
- compactación uniaxial en caliente inductiva (IHP).

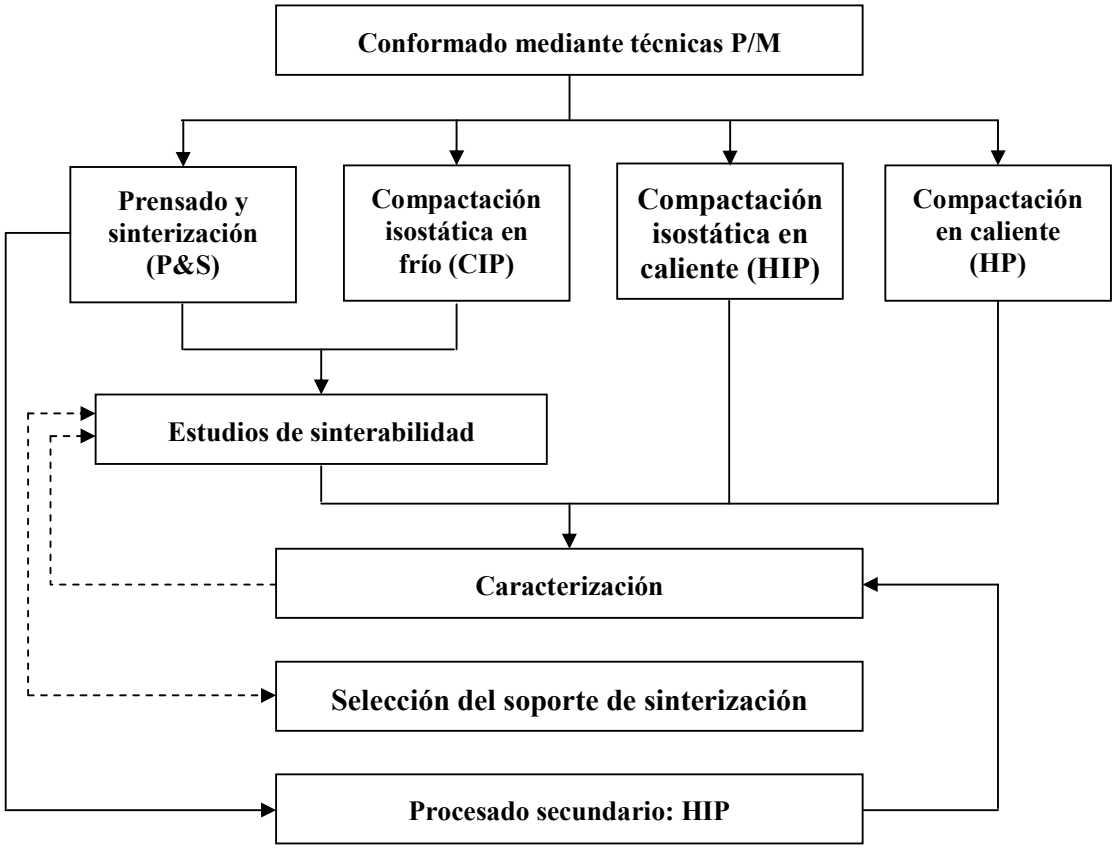

Figura 2.3 – Esquema de las etapas de conformado por técnicas P/M y caracterización.

2.5.1 – Compactación Uniaxial en Frío y Sinterización

La compactación de las muestras se llevó a cabo mediante prensado uniaxial empleando una matriz flotante cuyas paredes fueron lubricadas con estearato de zinc. La presión de compactación fue determinada para cada material y en función de la geometría de las muestras en un estudio previo (apartado 3.2.10).

En primer lugar se llevó a cabo un estudio de sinterabilidad preliminar, en el que se estudió la variación de la densidad relativa modificando exclusivamente la **temperatura de sinterización** entre 900ºC y 1400ºC y manteniendo las demás condiciones estables.

En particular, el tiempo de sinterización se fijó en 2 horas, la velocidad de calentamiento y de enfriamiento en 5ºC/min, el nivel de vacío mínimo de 10^{-5} mbar y las probetas fueron sinterizadas utilizando como soporte bolitas de circona.

En el caso de los polvos producidos a partir de aleación maestra se añadió una meseta previa de 30 minutos a la temperatura de 330ºC para eliminar la cera utilizada como agente de control durante la etapa de molienda de alta energía. Los parámetros de la meseta empleada para la eliminación de la cera fueron determinados en un trabajo previo[52] y mediante DTA. La Figura 2.4 muestra un esquema del ciclo térmico utilizado durante esta fase del estudio.

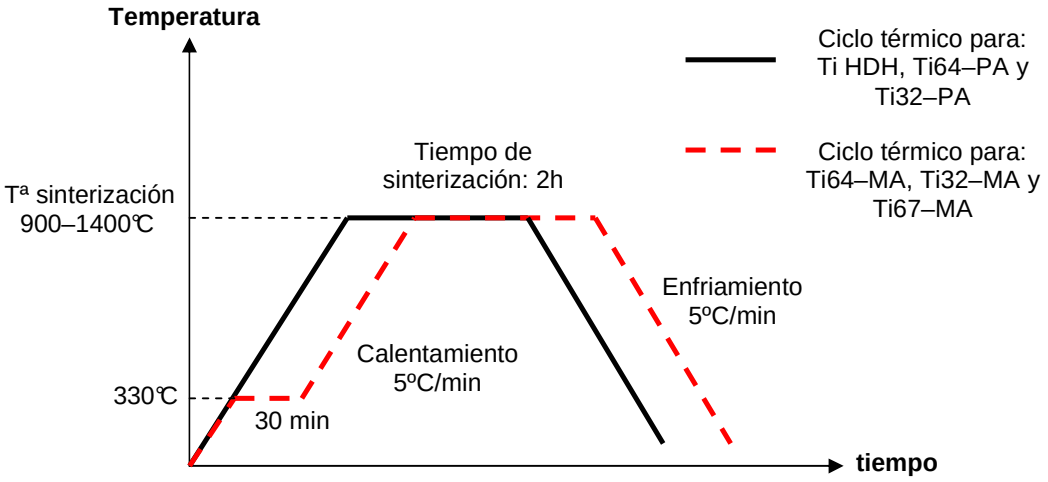

Figura 2.4 – Esquema de los ciclos térmicos empleados durante el estudio de sinterabilidad preliminar donde se distinguen el polvo elemental (HDH) o los prealeados (PA) de los polvos producidos a partir de aleación maestra (MA).

A partir de los resultados del estudio de sinterabilidad preliminar y del análisis térmico diferencial (DTA), se eligió proseguir con el estudio de las aleaciones durante la etapa de sinterización limitando el intervalo de temperatura e introduciendo otra variable critica de la etapa de sinterización, es decir el **tiempo**.

En particular, y como se ha mencionado en el capitulo de la selección del soporte de sinterización (apartado 2.4), los parámetros de fabricación empleados fueron tres temperaturas (1250ºC, 1300ºC y 1350ºC) y dos tiempos de sinterización (2h y 4h) obteniendo un total de seis diferentes condiciones de procesado.

En cuanto a las demás variables, es decir velocidad de calentamiento y enfriamiento, nivel de vacío, soporte de sinterización, meseta de 30 minutos a 330ºC para las aleaciones obtenidas a partir de aleación maestra, fueron mantenidas constantes.

Cabe destacar que este estudio se realizó utilizando muestras de geometría rectangular para ensayo de flexión y, posteriormente, el mismo estudio se llevó a cabo con probetas de tracción pero evaluando únicamente la temperatura y fijando el tiempo de sinterización en 2 horas.

2.5.2 – Compactación Isostática en Frío y Sinterización

De la misma forma tanto el titanio elemental como la aleación Ti–6Al–4V prealeada fueron procesadas mediante compactación isostática en frío empleando moldes de silicona para obtener muestras cilíndricas.

Durante el conformado se utilizó la presión máxima aportada por el equipo (EPSI: Engineering Pressure Systems Internacional – Bélgica), es decir 3000 bar, equivalente a 300 MPa, y se evaluaron dos tiempos de compactación, específicamente 5 minutos y 10 minutos.

A partir de los resultados de densidad en verde se eligió conformar las muestras para el estudio de sinterabilidad solo a 5 minutos ya que no se destacaron diferencias significativas al variar el tiempo de meseta a la presión máxima.

Para estudiar la influencia de los parámetros de procesado se varió la temperatura y el tiempo de sinterización como en los estudios previos, es decir 1250ºC, 1300ºC y 1350ºC durante 2 horas o 4 horas.

No obteniéndose diferencias destacables con respecto al procesado P&S, se eligió este último para el desarrollo del proceso experimental de la tesis debido a su mayor simplicidad en términos de preparación de las probetas.

2.5.3 – Compactación Isostática en Caliente

El estudio acerca de la compactación isostática en caliente, tanto a partir de polvos enlatados como de muestras previamente sinterizadas, fue llevado a cabo durante una estancia en el "Waikato Centre for Advanced Materials" de la universidad "The university of Waikato" de Hamilton, Nueva Zelanda.

Inicialmente, el estudio se centró en el procesado secundario de muestras sinterizadas con geometría rectangular estándar para el ensayo de flexión en tres puntos con el fin de disminuir el porcentaje de porosidad residual.

Para ello se evaluaron las propiedades obtenidas tras sinterización, identificando la condición de 1250ºC–2h como la que proporcionaba el mayor porcentaje de porosidad cerrada y, por lo tanto, las características más favorables para el HIP.

Para el procesado por HIP, se eligieron cuatro diferentes condiciones; una vez fijada la primera, denominada HIP–1, se consideró la variación del tiempo (HIP–2), la disminución de la temperatura (HIP–3) y el aumento de la presión (HIP–4) para poder identificar y relacionar el efecto de todas las variables de fabricación en las propiedades finales de las aleaciones de titanio.

Concretamente, las condiciones empleadas fueron:

- ✓ **HIP–1**: T = 1000ºC, P = 100 MPa, t = 20 min
- ✓ **HIP–2**: T = 1000ºC, P = 100 MPa, t = 2 h
- ✓ **HIP–3**: T = 850ºC, P = 100 MPa, t = 20 min
- ✓ **HIP–4**: T = 850ºC, P = 200 MPa, t = 20 min

En todos los casos las muestras fueron colocadas en un crisol de alúmina en el interior de la cámara del equipo, una prensa de compactación isostática en caliente AIP6–30H de la empresa americana AIP–American Isostatic Presses, Incorporated, y desgasificadas tres veces antes de proceder con el ensayo.

El primer paso fue aumentar la temperatura hasta 300ºC en 50 minutos, tal como especifica el fabricante para evitar que las resistencias del equipo se estropeen; a continuación se procedió con el calentamiento, a una velocidad de 10ºC/min hasta la temperatura final.

Por otro lado, la presión fue incrementada utilizando argón hasta aproximadamente 15 MPa que se incrementó hasta un 90% del valor final deseado gracias al aumento de temperatura y, finalmente, se aumentó para alcanzar la presión máxima de procesado simultáneamente a la temperatura prevista para la meseta.

El enfriamiento hasta los 300ºC fue llevado a cabo a una velocidad de 10ºC/min bajo presión, que fue disminuyendo aproximadamente hasta los 60 MPa. Alcanzados los 300ºC, se disminuyó la presión mediante una válvula hasta alcanzar la presión atmosférica, lo que provocó la disminución de la temperatura hasta, aproximadamente, temperatura ambiente.

La Figura 2.5 representa un esquema del ciclo térmico considerado durante la investigación.

Esta etapa del estudio ha permitido identificar las mejores condiciones en términos de densidad relativa y propiedades mecánicas para las probetas de flexión. Las mismas condiciones fueron aplicadas para el procesado de muestras de tracción de los distintos materiales previamente sinterizadas a 1250ºC durante 2 horas.

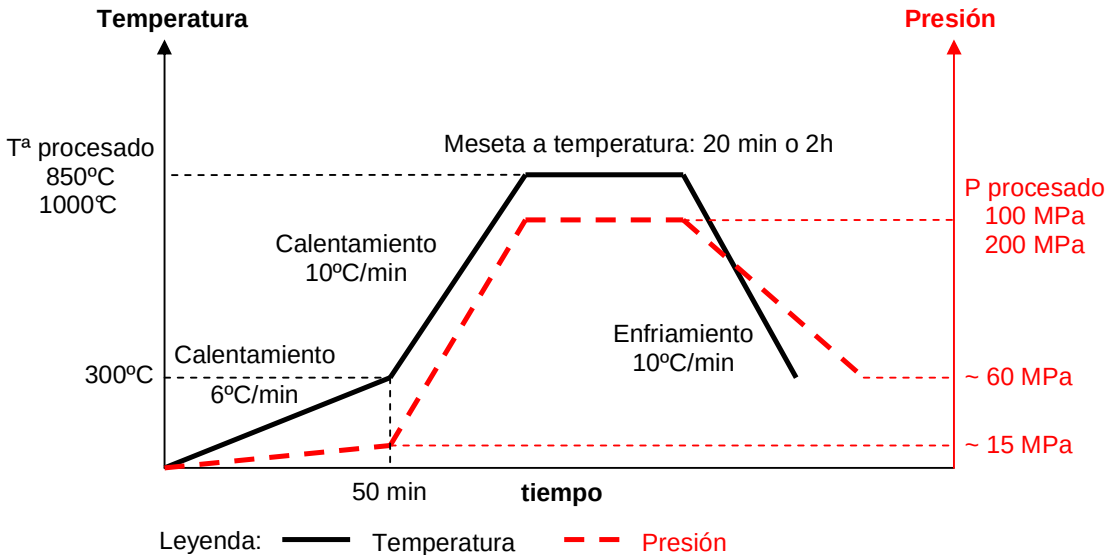

Figure 2.5 – Esquema del ciclo térmico y de la variación de presión durante la etapa de compactación isostática en caliente.

De igual forma, estos mismos parámetros de fabricación fueron utilizados para conformar muestras de las aleaciones a partir de polvo encapsulado en latas de acero inoxidable con geometría cilíndrica de diámetro aproximado de 34 mm y altura 41 mm. Después de algunas pruebas preliminares, se optó por desgasificar las latas a una temperatura máxima de 400ºC durante 2 horas antes de proceder a su cierre.

Debido a problemas prácticos a la hora de llevar a cabo la compactación de los polvos enlatados no fue posible aplicar las condiciones deseadas, en particular la presión; por lo tanto, se han obtenido valores de densidad relativa inferiores a los esperados y, consecuentemente, esta etapa de caracterización no se comenta en el apartado de los resultados (capitulo 6).

2.5.4 – Compactación Uniaxial en Caliente

El estudio del conformado en caliente fue llevado a cabo durante una estancia en el centro de investigación "Austrian Institute of Technology GMBH – AIT, Seibersdorf – Austria", concretamente en el departamento de "Advanced Materials and Aerospace Technologies" del "Powder Technology Center – PTC".

Durante esta etapa se consideró la compactación de todos los polvos con morfología irregular, tanto prealeados como obtenidos por aleación maestra, mediante dos técnicas de compactación en caliente que difieren por el sistema de calentamiento y que se denominan "**compactación en caliente convencional**" y "**compactación en caliente inductiva**".

Los parámetros de procesado de las dos técnicas son ligeramente diferentes, especialmente por cuanto concierne a la velocidad de calentamiento y enfriamiento, como se resume a continuación:

Compactación en caliente convencional: la prensa utilizada es una prensa HPW 315/400–2200–1000–PS de la empresa "FCT Anlagenbau GMBH – Alemania" donde el calentamiento se obtiene mediante resistencias eléctricas.

La primera etapa del procesado consiste en la preparación de la matriz, que incluye el recubrimiento de la misma con un folio de grafito de espesor de 0,75 mm para evitar que el polvo esté directamente en contacto con la matriz.

Posteriormente se sitúa un disco de grafito en su parte inferior y, antes de verter el polvo, se coloca un folio de grafito recubierto de nitruro de boro (BN) en la cara que estará en contacto con el polvo con el fin de reducir los fenómenos de reacción y favorecer la separación y la extracción de las piezas finales.

Otro disco con una cara recubierta de BN y un disco de grafito se colocan nuevamente después de verter el polvo tal como se indica en la Figura 2.6, que muestra un esquema de la fase de preparación de la matriz y una foto de la prensa utilizada.

Figure 2.6 – Esquema de la preparación de la matriz para el procesado por compactación en caliente (izquierda) y foto de la prensa de compactación en caliente convencional (derecha).

Durante el estudio se han utilizado 75 gramos de cada polvo, lo que permite obtener discos de 65 mm de diámetro con un espesor final de aproximadamente 5 mm. Ya que la misma matriz fue rellenada con 6 polvos distintos, cada polvo ha sido compactado en frío a 18 MPa mediante una prensa hidráulica uniaxial antes de proceder a verter el siguiente polvo.

Durante el estudio se han considerado tres temperaturas diferentes, 900ºC, 1100ºC y 1300ºC, intentando mantener constante el tiempo a la temperatura de procesado en 30 minutos. Sin embargo, en el caso de 900ºC y 1100ºC ha sido necesario programar una meseta de una hora debido a la inercia del sistema, para permitir que las muestras alcanzasen la temperatura deseada.

La presión aplicada ha sido en todos los casos 30 MPa, la velocidad de calentamiento igual a 10ºC/min y el nivel de vacío de 10^{-1} mbar. El enfriamiento de las muestras se ha llevado a cabo apagando el horno y dejándolas enfriar al mismo tiempo que se disminuía la presión.

La Figura 2.7 muestra un esquema del ciclo de prensado en caliente donde se destacan la temperatura, la presión y el tiempo de procesado.

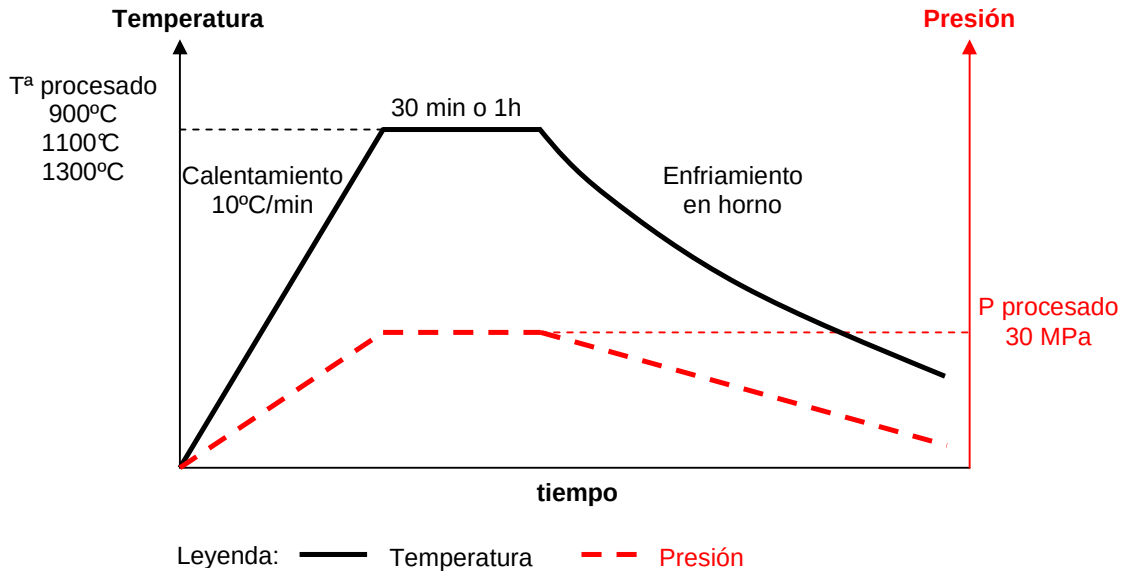

Figure 2.7 – Esquema del ciclo de compactación en caliente convencional donde se muestra el enfriamiento lento llevado a cabo en horno.

Como se ha mencionado anteriormente, tras la etapa de conformado en caliente se han obtenido discos de 65 mm que han sido sometidos a limpieza con chorro de arena para eliminar posibles residuos debidos a los discos de grafito o al recubrimiento de BN.

Posteriormente, los discos han sido cortados para fabricar probetas de geometría rectangular para poder determinar la resistencia a flexión. Cabe especificar que se decidió mecanizar la superficie con el fin de evaluar la influencia de la capa superficial y descubrir posibles fenómenos de contaminación por parte del recubrimiento de nitruro de boro.

Compactación en caliente inductiva: en este tipo de procesado el calentamiento de las muestras se obtiene por inducción, lo que permite utilizar velocidades de calentamiento mayores y, por lo tanto, tiempos de procesado notablemente inferiores.

Durante el desarrollo de este trabajo se compactaron muestras cilíndricas de 12 mm de diámetro a partir de aproximadamente 1,5 gramos de polvo, del cual se han obtenido probetas de 3,5 mm de espesor.

La Figura 2.8 muestra un esquema de la etapa de preparación de la matriz para poder llevar a cabo el conformado y una foto de la cámara de la prensa de compactación en caliente inductiva.

Figure 2.8 – Esquema de la preparación de la matriz para la compactación en caliente inductiva y foto del equipo de compactación en caliente inductivo.

La cámara principal, que está construida en acero inoxidable, está provista de refrigeración gracias a un sistema de circulación forzosa de agua y puede operar bajo alto vacío, hasta niveles de 10^{-6} mbar, o con incrementos de la presión parcial de gas, específicamente N_2, H_2, O_2, hasta presión ambiente.

La carga máxima aplicable mediante esta prensa es de 70 MPa con una frecuencia máxima de 70 Hz y señales con diferentes formas. Además, durante el conformado, la medida de la variación de la altura de las piezas, es decir la contracción debida a la sinterización, se puede realizar tanto con un extensómetro como mediante un sistema de medida sin contacto.

Los diferentes polvos han sido compactados en una prensa uniaxial manual antes del prensado en caliente, en el que se utilizó una presión constante de 50 MPa. A lo largo del estudio mediante prensado en caliente inductivo se han mantenido constantes la rampa de calentamiento de 50°C/min, el nivel de vacío de 10^{-3} mbar y el tiempo de procesado de 15 min, mientras que se ha variado la temperatura utilizándose 1100°C y 1300°C. El enfriamiento de las muestras se realizó apagando el horno de inducción y resulta ser muy rápido debido a las reducidas dimensiones de las probetas.

La prensa empleada es un equipo construido ad hoc que cuenta con un sistema de calentamiento de inducción con una potencia máxima de 30 kW capaz de llevar a cabo de forma automática el ajuste y la optimización de la frecuencia, la cual puede variar entre 20 y 150 KHz, permitiendo alcanzar temperaturas de aproximadamente 2500ºC y velocidades de calentamiento hasta los 50ºC/s dependiendo del material considerado.

La Figura 2.9 muestra un esquema de ciclo térmico normalmente utilizado durante la sinterización de las aleaciones de titanio, donde cabe destacar que el tiempo máximo de procesado es alrededor de 40 minutos, notablemente inferior a las seis o más horas requeridas en un procesado por compactación en caliente convencional.

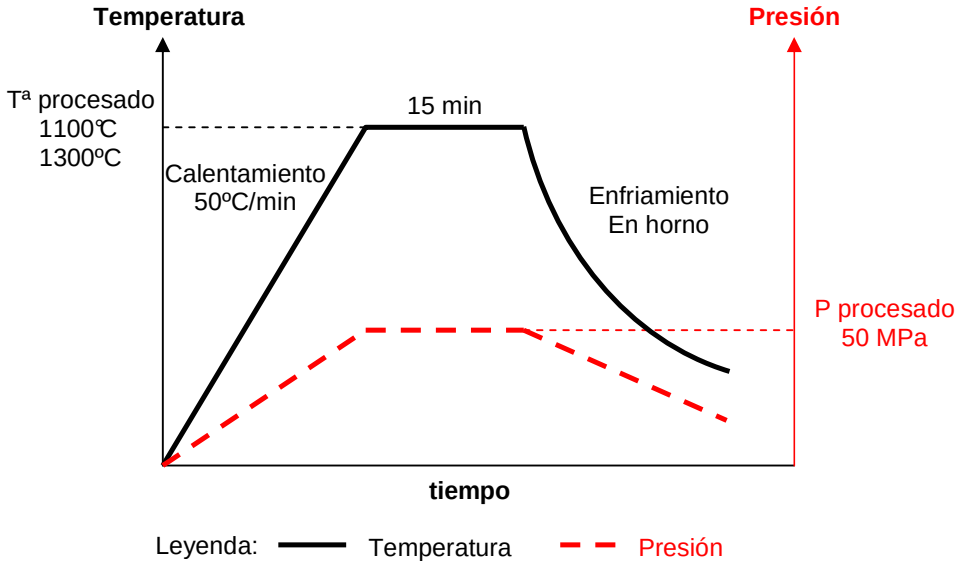

Figura 2.9 – Esquema del ciclo de compactación en caliente inductiva donde se aprecia la elevada velocidad de enfriamiento y el reducido tiempo de procesado.

Como en el caso de la compactación en caliente convencional, las muestras fueron limpiadas con chorro de arena pero, debido a sus reducidas dimensiones, no fue posible realizar ensayos mecánicos de flexión o tracción sino exclusivamente dureza, además del estudio microestructural.

2.6 – CARACTERIZACIÓN DE LOS MATERIALES SINTERIZADOS

En este apartado se describen las técnicas de caracterización de los materiales sinterizados empleadas y los parámetros considerados más significativos para correlacionar los diferentes aspectos inherentes a la etapa de conformado con las propiedades mecánicas, la microestructura, el análisis químico y las propiedades físicas.

2.6.1 – Variación Dimensional

La variación de las dimensiones de los compactos en verde, es decir longitud, ancho, espesor y, consecuentemente, volumen así como peso, fueron evaluadas exclusivamente durante la etapa de sinterización tras compactación uniaxial en frío, ya que se supuso que el HIP secundario afecta únicamente la microestructura y el porcentaje de porosidad residual.

La determinación de la variación de cada una de las magnitudes mencionadas anteriormente se llevó a cabo según la norma MPIF 44[53] o equivalente ASTM B 610[54] empleando la formula general:

$$Variación\ porcentual = \frac{Valor\ final - Valor\ inicial}{Valor\ inicial} * 100\ [\%] \qquad \text{(Ec. 1)}$$

Otro parámetro que se suele considerar para cuantificar el efecto de los fenómenos que gobiernan la sinterización es la densificación (Ψ [%]), la cual proporciona una idea acerca del grado de contracción o hinchamiento de las muestras, y que se define como:

$$\psi = \frac{\rho_S - \rho_V}{\rho_T - \rho_V} * 100\ [\%] \qquad \text{(Ec. 2)}$$

donde:

ρ_S: densidad tras la sinterización [g/cm^3];

ρ_V: densidad en verde [g/cm^3];

ρ_T: densidad teórica del material [g/cm^3].

En este caso, los valores de densidad teórica utilizados son los valores de densidad de los polvos determinados mediante picnometría de helio tal como se ha explicado en el apartado 2.3.3.

Para que estos valores se puedan considerar teóricos, las partículas de polvo deben estar libres de porosidad residual, lo cual se comprobó mediante SEM como se ha indicado en el párrafo 2.3.4.

Las medidas de las dimensiones fueron realizadas mediante un calibre centesimal (longitud y ancho) y un micrómetro (espesor), mientras que el peso se midió mediante una balanza de precisión de cuatro dígitos.

2.6.2 – Densidad y Porosidad

La determinación de la densidad (ρ) de los materiales sinterizados fue llevada a cabo aplicando el principio de Arquímedes como se indica en la Norma MPIF 42[55] o ASTM B 962[56] utilizando la siguiente ecuación:

$$\rho = \frac{Masa\ en\ aire\ (g)}{\left(\frac{Masa\ con\ laca\ en\ aire\ (g) - Masa\ con\ laca\ en\ agua\ (g)}{Densidad\ agua\ (g/cm^3)}\right) - \left(\frac{Masa\ con\ laca\ en\ aire\ (g) - Masa\ en\ aire\ (g)}{Densidad\ laca\ (g/cm^3)}\right)}\ [g/cm^3] \quad \text{(Ec. 3)}$$

Cabe especificar que el valor de la densidad del agua a 20ºC es de 0,977 g/cm^3 y la densidad de la laca transparente empleada para recubrir las muestras es igual a 1,2 g/cm^3.

La densidad relativa (ρ_r) se obtiene dividendo la densidad obtenida mediante la ecuación 3 por la densidad teórica ya mencionada, según la ecuación 4:

$$\rho_r = \frac{\rho}{\rho_{teórica}} \cdot 100\ [\%] \quad \text{(Ec. 4)}$$

Los porcentajes relativos de porosidad residual total (P_T), porosidad cerrada (P_C) y porosidad abierta (P_A) se calculan, respectivamente, empleando las ecuaciones 5, 6 y 7 en función de la densidad de las muestras sinterizadas medida mediante el método de Arquímedes ($\rho_{Arq.}$) y mediante picnometría de helio ($\rho_{Pic.}$):

$$P_T = 100 - \left(\frac{\rho_{Arq.}}{\rho_{teórica}} \cdot 100\right)\ [\%] \quad \text{(Ec. 5)}$$

$$P_C = 100 - \left(\frac{\rho_{Pic.}}{\rho_{teórica}} \cdot 100\right)[\%] \quad \text{(Ec. 6)}$$

$$P_A = P_T - P_C\ [\%] \quad \text{(Ec. 7)}$$

2.6.3 – Dureza

A lo largo del desarrollo de esta tesis se decidió emplear como escala de dureza la Vickers, concretamente la HV30 donde se aplican 30 Kg de carga, y las medidas se llevaron a cabo mediante un equipo universal Wilson Wolpert Universal Hardness DIGI–TESTOR 930 siguiendo la norma MPIF 43[57].

2.6.4 – Ensayo de Flexión en Tres Puntos

En la mayoría de los casos, la resistencia de los materiales sinterizados o fabricados mediante técnicas pulvimetalúrgicas se evalúa mediante el ensayo de flexión en tres puntos debido a la menor tenacidad de estos materiales causada por la presencia de porosidad residual.

En este caso, el ensayo fue llevado a cabo según la norma MIPF 41[58] o equivalente ASTM B 528[59] utilizando muestras con geometría rectangular y empleando una maquina de ensayos MicroTest.

Mediante el programa de gestión de los ensayos se obtienen la flecha [mm], la deformación máxima [%] y la fuerza máxima (F [N]), la cual se emplea para calcular la tensión, tanto máxima como de rotura, (σ [MPa]) en función de la distancia de los soportes (L [mm]), el ancho (w [mm]) y el espesor (t [mm]) de la muestra empleando la siguiente relación:

$$\sigma = \frac{3 \cdot F \cdot L}{2 \cdot w \cdot t^2} \text{ [MPa]} \qquad \text{(Ec. 8)}$$

La deformación (ε_f) se calcula considerando el espesor del componente (t), su deformación (D [mm]) en la parte central y la distancia entre los soportes (L) mediante la siguiente ecuación:

$$\varepsilon_f = \frac{6 \cdot D \cdot t}{L^2} \text{ [\%]} \qquad \text{(Ec. 9)}$$

Mediante los parámetros del ensayo, es decir la distancia entre los soportes y las dimensiones de la muestra, el valor de la pendiente (m) medida en la parte lineal de la curva fuerza frente a desplazamiento y la fórmula matemática que se muestra a continuación se puede obtener el modulo de Young en flexión (E_B):

$$E_B = \frac{L^3 \cdot m}{4 \cdot w \cdot t^3} \text{ [GPa]} \qquad \text{(Ec. 10)}$$

2.6.5 – Ensayo de Tracción

Los ensayos de tracción de las muestras conformadas mediante prensado uniaxial y sinterización, así como las muestras sometidas a procesado secundario de compactación isostática en caliente fueron llevados a cabo mediante un maquina universal MicroTest con una célula de carga de 50 kN y un extensómetro Hottinger Baldwin Messtechnik, tipo DD1.

La geometría de las probetas, que se denomina “muestra de tracción plana y no mecanizada”, se especifica en las normas MPIF 10[60] o ASTM B 925[61] y se muestra en la Figura 2.10.

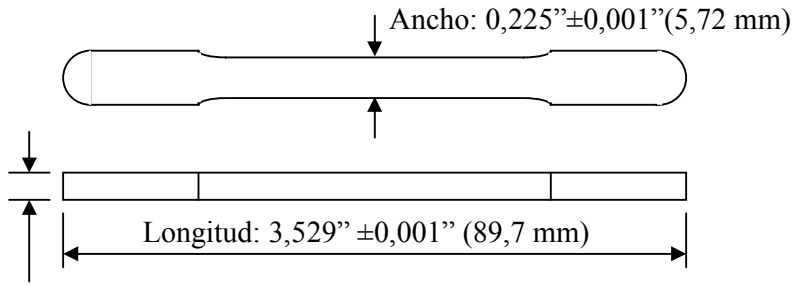

Figure 2.10 – Esquema de las probetas para la determinación de la resistencia a tracción en materiales pulvimetalúrgicos.

Los ensayos fueron realizados basándose en las condiciones especificadas por la norma UNE–EN 10002–1 utilizando una velocidad de aplicación de la carga de 1 mm/min para determinar los parámetros típicos de este ensayo, es decir tensión a rotura [MPa] y deformación a rotura [%] en condiciones casi–estáticas.

2.6.6 – Módulo de Elasticidad Dinámico

El módulo de Young (E) de un material se puede evaluar a partir de la pendiente de la parte lineal de la curva tensión–deformación (σ–ε) y suele ser determinado mediante el análisis de los resultados obtenidos durante pruebas estáticas o casi–estáticas, como el ensayo de tracción a baja velocidad.

Alternativamente, el módulo de elasticidad se puede determinar mediante medidas de la velocidad del sonido (v) en el material estudiado y la densidad (ρ) empleando la formula $v = \sqrt{E/\rho}$ de manera que este módulo se define módulo de elasticidad dinámico.

Las medidas del módulo de elasticidad dinámico han sido llevadas a cabo en muestras rectangulares extraídas de probetas de tracción con las siguientes dimensiones: 1,4 x 1,4 x 45 mm^3.

Las medidas se han realizado en el Departamento de Materiales de la ETSI Caminos, Canales y Puertos de la Universidad Politécnica de Madrid empleando un transductor piezoeléctrico proporcionado por la empresa Grindosonic cuyo intervalo de frecuencia varía entre 20 Hz y 100 KHz y con una precisión mejor del 0,005% en contacto directo con la pieza.

El valor del módulo ha sido calculado mediante el software suministrado por la misma empresa.

2.6.7 – Difracción de rayos X

La difracción de rayos X se ha empleado para analizar las muestras consolidadas y sinterizadas en diferentes condiciones, si bien se ha llevado a cabo también un ensayo en los polvos para poder analizar las fases presentes.

En particular, la técnica se ha utilizado durante el estudio de sinterabilidad preliminar, donde las aleaciones han sido compactadas a las presiones óptimas y sinterizadas durante dos horas variando la temperatura entre 900°C y 1400°C con intervalos de 100°C como se ha explicado en el apartado 2.5.1.

Además, se han llevado a cabo análisis de la superficie de las muestras consolidadas mediante compactación en caliente convencional (párrafo 2.5.4) para estudiar la composición y determinar la capa de reacción de los polvos con el recubrimiento de BN empleado con el fin de reducir los fenómenos de reacción y favorecer la extracción de los componentes.

Todos los ensayos de difracción de rayos X se han llevado a cabo a temperatura ambiente empleando los mismos parámetros, es decir, variando el ángulo 2θ entre 20° y 120° con un paso de goniómetro de 0,02° y un tiempo de permanencia de 2 segundos.

El equipo utilizado es un Bruker AXS D8–Advance con una fuente de rayos X de Cu y monocromador de focalización Vario1 Johansson para garantir la utilización únicamente $K\alpha_1$ durante experimentos de reflexión, de transmisión de lámina o capilar.

El análisis de los difractogramas para la identificación de las fases constituyentes se ha llevado a cabo mediante el programa EVA proporcionados por la misma empresa.

La caracterización de las muestras mediante la técnica de difracción de rayos X se ha llevado a cabo durante una estancia en el instituto de investigación IFAM (Fraunhofer-Instituts für Fertigungstechnik und Angewandte Materialforschung) de Dresde en Alemania.

2.6.8 – Conductividad Térmica

La conductividad térmica (k) a temperatura ambiente de las aleaciones ha sido determinada mediante un equipo Netzsch LFA 447 Nanoflash durante una estanca en Alemania en el instituto IFAM (Fraunhofer-Instituts für Fertigungstechnik und Angewandte Materialforschung) de Dresde.

Durante la medida una lámpara de Flash Xenón 10 J/impulso emite un haz de luz infrarroja que, después de cruzar el espesor de la muestra, es recolectado y medido. La variación de la intensidad de esta radiación transmitida ha sido analizada mediante el software Proteus y ajustada al modelo de Cape-Lehmann para poder determinar la **difusividad térmica** (**α** en m^2/s) del material, es decir la rapidez con la que varía la temperatura del material ante una solicitud térmica.

La Figura 2.11 muestra en ejemplo de grafico obtenido durante la determinación de la conductividad térmica donde se aprecia el flash de luz inicial y el ajuste al modelo de Cape-Lehmann.

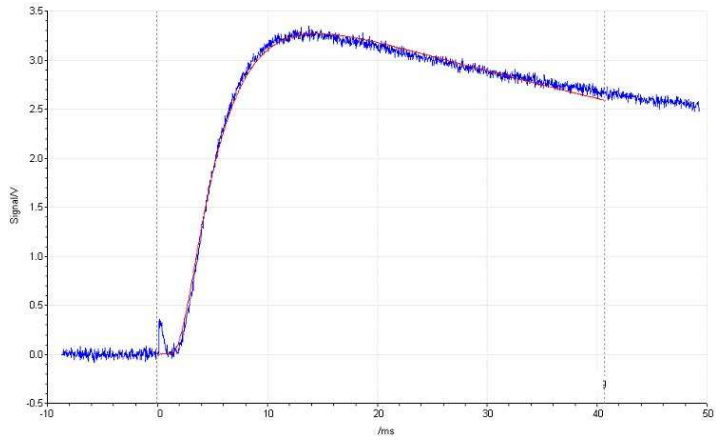

Figure 2.11 – Ejemplo de grafico de variación de la difusividad térmica empleado para determinar la conductividad térmica de las aleaciones de titanio.

La conductividad térmica se calcula considerando la densidad (ρ en kg/m^3) y el calor especifico a presión constante (C_p en J/Kg·K) mediante la formula:

$$K = \alpha \cdot \rho \cdot C_p \ [W/m \cdot ºC] \qquad \text{(Ec. 11)}$$

Además de la conductividad a temperatura ambiente, se ha llevado a cabo el estudio de la variación de la conductividad con la temperatura, tanto del titanio como de sus aleaciones producidas mediante técnicas pulvimetalúrgicas. Más en detalle, las muestras sinterizadas a 1250ºC durante 2 horas han sido calentadas hasta los 300ºC midiendo la conductividad cada 50ºC.

Los valores determinados mediante estas medidas, que se denominan "**conductividad térmica medida**", no consideran la variación con la temperatura del calor específico a presión constante (C_p); parámetro que afecta directamente la conductividad térmica como especificado en la ecuación 11.

Por lo tanto, se ha procedido a determinar la variación del calor especifico C_p empleando la ecuación propuesta para el titanio alfa[16] expresando la temperatura en Kelvin:

$$C_p = 669{,}0 - (0{,}037188 \cdot T) - (1{,}080 \cdot 10^7 \cdot T^{-2}) \ [J/Kg \cdot ºC] \qquad \text{(Ec. 12)}$$

Los datos de C_p en función de la temperatura han sido utilizados para determinar lo que se denomina "**conductividad térmica calculada**", la cual ha sido empleada junto con los datos encontrados en la "**literatura**"[62] para evaluar y destacar eventuales diferencias significativas del comportamiento de conductividad térmica del titanio pulvimetalúrgico y de sus aleaciones.

2.6.9 – Resistividad Eléctrica

La resistividad eléctrica (ρ) o su inversa, la conductividad eléctrica (σ = 1/ ρ), de un material conductor se puede determinar de diferentes formas como son el método básico, el método de dos puntas, el método de cuatro puntas o el método de Van der Pauw, siempre que se cumplan algunos requisitos específicos para cada método.

En el caso de la técnica de Van der Pauw, empleada para la caracterización de las aleaciones de titanio consideradas en esta tesis, la medida se lleva cabo en muestras planas de forma arbitraria (aunque homogénea en composición) cumpliendo los siguientes requerimientos: los contactos están en la periferia de la muestra, los contactos son suficientemente pequeños, la muestra tiene un espesor (t) homogéneo y la superficie de la muestra está conectada singularmente, es decir, la muestra no debe tener huecos[63, 64].

Empleando los cuatro contactos sucesivos A, B, C y D, entre dos de ellos se aplica una corriente (I) y entre los dos restantes se mide la tensión (V), se determina la resistencia y, posteriormente, la resistividad del material.

Por ejemplo, si se mide la tensión entre C y D (V_{CD}) haciendo pasar una corriente entre A y B (I_{AB}) y, después, se mide la tensión entre A y D (V_{AD}) haciendo pasar una corriente entre C y B (I_{CB}), de acuerdo con el método de van der Pauw la resistividad se calcula como:

$$\rho = \frac{\pi \cdot t}{\ln 2} \cdot \frac{\left(R_{AB,\,DC} + R_{BC,\,AD}\right)}{2} \,[\mu\Omega\cdot\text{cm}] \qquad \text{(Ec. 13)}$$

donde t es el espesor de la muestra y R la resistencia entre los contactos calculada en función de los valores de tensión y corriente.

Los ensayos de conductividad eléctrica mediante la técnica de van der Pauw han sido realizados en el instituto de investigación IFAM (Fraunhofer-Instituts für Fertigungstechnik und Angewandte Materialforschung) en Dresde (Alemania).

2.6.10 – Análisis Químico y Estudio Microestructural

Además de las caracterizaciones detalladas a lo largo de este capitulo, en las muestras conformadas se determinó el porcentaje de oxígeno, nitrógeno y carbono según el procedimiento especificado en el apartado "2.3.2 – Análisis Químico" y se llevó a cabo el estudio microestructural para identificar las fases constituyentes adoptando la metodología descrita en el apartado "2.3.4 – Morfología y Microestructura de los Polvos".

2.7 – CORRELACIÓN ENTRE PROPIEDADES

Con el fin de entender mejor la variación del comportamiento mecánico del titanio y de sus aleaciones obtenidos mediante técnicas pulvimetalúrgicas, y sabiendo que estas propiedades se ven afectadas significativamente por el contenido de elementos intersticiales[65-67], se ha considerado el parámetro de contenido equivalente de oxígeno (O_{Eq}).

En la literatura existen diferentes modelos y formulas que consideran el efecto conjunto del contenido de oxígeno (O), nitrógeno (N) y carbono (C) en función de cada propiedad especifica[68].

En esta tesis se han considerado cuatro diferentes ecuaciones para calcular el contenido de oxígeno equivalente, según se fuera a relacionar con las siguientes propiedades:

- ✓ dureza: la relación empleada en el caso de la dureza Vickers es la propuesta por Okazaki y Conrad[69]:

$$O_{Eq} = O + 1{,}96 * N + 0{,}52 * C \text{ [at.\%]} \quad \text{(Ec. 14)}$$

- ✓ resistencia a fractura: en el caso de la resistencia a flexión en tres puntos se eligió emplear la formula destacada por Wood, si bien esta se propone para la resistencia máxima a tracción (UTS)[70]:

$$O_{Eq} = O + 2{,}29 * N + 0{,}76 * C \text{ [at.\%]} \quad \text{(Ec. 15)}$$

- ✓ deformación: el mismo Wood[70] presenta también una formula para la variación de la reducción de área de las muestras sometidas a ensayo de tracción que se eligió para determinar el contenido de oxígeno equivalente para estudiar su influencia en la deformación:

$$O_{Eq} = O + 2{,}29* N + 0{,}59 * C \text{ [at.\%]} \quad \text{(Ec. 16)}$$

- ✓ conductividad térmica y conductividad eléctrica: en este caso no existe una relación especifica, por lo tanto, se decidió emplear la ecuación propuesta por Conrad en su trabajo acerca de los mecanismos que controlan la "cedencia" (yielding) y el flujo de un material por debajo del 40% de su temperatura de fusión[71] ya que esta se refiere a cambios microestructural los cuales están más relacionados con las propiedades a estudiar:

$$O_{Eq} = O + 2{,}00 * N + 0{,}75 * C \text{ [at.\%]} \quad \text{(Ec. 17)}$$

Estas mismas ecuaciones han sido empleadas para determinar el contenido de oxígeno equivalente de muestras obtenidas por distintas técnicas de conformado con el fin de poder comparar las propiedades mecánicas alcanzadas.

2.8 – REFERENCIAS

[1] V. S. Moxson and F. H. Froes, "Fabricating Sports Equipment Components via Powder Metallurgy", *JOM,* vol. 53, pp. 39-41, 2001

[2] Titanium Information Group (TIG), "Data Sheet 16: Titanium Powder Suppliers & Processors", *Available at: http://www.titaniuminfogroup.co.uk/tech-data-links.php,* 2006

[3] O. M. Ivasishin, et al., "Diffusion during Powder Metallurgy Synthesis of Titanium Alloys", *Defect and Diffusion Forum,* vol. Diffusion and Diffusional Phase Transformations in Alloys, pp. 177-185, 2008

[4] C. Suryanarayana, "Mechanical Alloying and Milling", *Progress in Materials Science,* vol. 46, pp. 1-184, 2001

[5] ASTM B 822, "Standard Test Method for Particle Size Distribution of Metal Powders and Related Compounds by Light Scattering", 2002

[6] ASTM E 1409, "Standard Test Method for Determination of Oxygen in Titanium and Titanium Alloys by the Inert Gas Fusion Technique", 1997

[7] ASTM E 1937, "Standard Test Method for Determination of Nitrogen in Titanium and Titanium Alloys by the Inert Gas Fusion Technique", 1997

[8] ASTM E 1941, "Standard Test Method for Determination of Carbon in Refractory and Reactive Metals and their Alloys", 2004

[9] LECO Corporation, "LECO TC-500 Nitrogen/Oxygen Determination Instruction Manual", 2001

[10] LECO Corporation, "Oxygen and Nitrogen Determination - Inert Gas Fusion Instruments", 2007

[11] LECO Corporation, "Determination of Oxygen and Nitrogen in Reactive/Refractory Metals and their Alloys - Inorganic Application Note", 2007

[12] LECO Corporation, "LECO CS-200 Carbon and Sulfur Analyser Instruction Manual", 2000

[13] LECO Corporation, "Carbon and Sulfur Determination - LECO Induction Furnace Instruments", 2007

[14] LECO Corporation, "Carbon in Refractory and Reactive Metals and their Alloys - Inorganic Application Note", 2007

[15] ASTM B 923, "Standard Test Method for Metal Powder Skeletal Density by Helium or Nitrogen Pycnometry", 2002

[16] R. Boyer, et al., "Materials Properties Handbook: Titanium Alloys", 2nd ed, ASM-International, Ed. Ohio, USA, 1998

[17] RMI, "Titanium Company: Titanium Alloy Guide", *available at: http://rtiintl.s3.amazonaws.com/RTI-Reports/tiguideWeb.pdf,* 2000

[18] MPIF, "Standard 04, Method for Determination of Apparent Density of Free-flowing Metal Powders using the Hall Apparatus", Metal Powder Industries Federation, 1985

[19] MPIF, "Standard 28, Determination of Apparent Density of Non-free-flowing Metal Powders using the Carney Apparatus", Metal Powder Industries Federation, 1985

[20] ASTM B 212, "Standard Test Method for Apparent Density of Free-flowing Metal Powders using the Hall Flowmeter Funnel", 1999

[21] ASTM B 417, "Standard Test Method for Apparent Density of Non-free-flowing Metal Powders using the Carney Funnel", 2000
[22] MPIF, "Standard 03, Method for Determination of Flow Rate of Free-flowing Metal Powders using the Hall Apparatus", Metal Powder Industries Federation, 1985
[23] ASTM B 213, "Standard Test Method for Flow Rate of Metal Powders", 2003
[24] ASTM B 933, "Standard Test Method for Microindentation Hardness of Powder Metallurgy (P/M) Materials", 2009
[25] Struers Application Notes, "Metallographic Preparation of Titanium", 2002
[26] ASTM E 407, "Standard Test Method for Microetching Metals and Alloys", 1999
[27] MPIF, "Standard 45, Method for Determination of Compactability (Compressibility) of Metal Powders", Metal Powder Industries Federation, 1988
[28] ASTM B 331, "Standard Test Method for Compressibility of Metal Powders in Uniaxial Compaction", 2002
[29] MPIF, "Standard 15, Method for Determination of Green Strength of Compacted Metal Powder Specimens", Metal Powder Industries Federation, 1990
[30] ASTM B 312, "Standard Test Method for Green Strength for Compacted Metal Powder Specimens", 2002
[31] H. Kikuchi, et al., "Titanium Casting: the Surface Reaction Layer of Castings obtained using Ultra-low-temperature Molds", *Journal of Oral Science,* vol. 43, pp. 27-33, 2001
[32] E. J. Chapin and W. H. Friske, "A Metallurgical Evaluation of Refractory Compounds for Containing Molten Titanium. Part I - Oxides", *Naval Research Lab. Washington DC,* pp. 1-42, 1954
[33] E. J. Chapin and W. H. Friske, "A Metallurgical Evaluation of Refractory Compounds for Containing Molten Titanium. Part II - Carbon, Graphite and Carbides", *Naval Research Lab. Washington DC,* pp. 1-30, 1954
[34] E. J. Chapin and W. H. Friske, "A Metallurgical Evaluation of Refractory Compounds for Containing Molten Titanium. Part III - Borides and Sulfides", *Naval Research Lab. Washington DC,* pp. 1-38, 1955
[35] C. Frueh, et al., "Attempts to Develop a Ceramic Mould for Titanium Casting - A Review", *International Journal of Cast Metals Research* vol. 9, pp. 233-240, 1996
[36] V. S. Pugin and M. S. Maurakh, "Interaction between the Metal and the Mold during the Casting of Titanium", *Foreign Technology Div. Wright-Patterson AFB Ohio,* pp. 1-22, 1968
[37] L. Wictorin, et al., "Metallographic Studies of Cast Titanium – An Experimental Study of Metal/Mould Reaction", *Cast Metals,* vol. 4, pp. 182-187, 1992
[38] T. Sato, et al., "A New Process of Producing Titanium Alloys Castings" in *6th World Conference on Titanium*, Cannes - France, 1988
[39] G. W. Sales and K. Kendall, "A Study of Interactions between Titanium 6:4 and Selected Ceramic Materials", *Journal of Materials Science Letters* vol. 19, pp. 1877-1878, 2000
[40] S. Veeck, et al., "Titanium Investment Castings", *Advanced Materials & Processes,* vol. 160, pp. 59-63, 2002
[41] C.-C. Hung, et al., "Pure Titanium Casting into Zirconia-modified Magnesia-based Investment Molds", *Dental Materials,* vol. 20, pp. 846-851, 2004

[42] R. V. B. Cruz, et al., "Effect of the Ceramic Mould Composition on the Surface Quality of As-cast Titanium Alloy", *Journal of Materials Science,* vol. 40, pp. 6041-6043, 2005

[43] H. C. Hsu, et al., "Evaluation of Different Bonded Investments for Dental Titanium Casting", *Journal of Materials Science: Materials in Medicine* vol. 16, pp. 821-825, 2005

[44] C. C. Hung, et al., "Pure Titanium Casting into Titanium-modified Calcia-based and Magnesia-based Investment Molds", *Materials Science and Engineering: A,* vol. 454-455, pp. 178-182, 2007

[45] Y. Guilin, et al., "The Effects of Different Types of Investments on the Alpha-case Layer of Titanium Castings", *The Journal of Prosthetic Dentistry,* vol. 97, pp. 157-164, 2007

[46] A. Liu, et al., "Study of Interfacial Reaction between TiAl Alloys and Four Ceramic Molds", *Rare Metal Materials and Engineering,* vol. 37, pp. 956-959, 2008

[47] I. Watanable, et al., "Effect of Pressure Difference on the Quality of Titanium Casting", *Journal of Dental Research,* vol. 76, pp. 773–779, 1997

[48] J. Jia, et al., "Thermodynamic Calculation of Interface Rreactions between Titanium Melt and Special Mold Materials", *Transactions of Nonferrous Metals Society of China* vol. 9, pp. 218-222, 1999

[49] A. Kostov and B. Friedrich, "Selection of Crucible Oxides in Molten Titanium and Titanium Auminium Alloys by Thermo-chemistry Calculations", *Journal of Mining and Metallurgy,* vol. 41 B, pp. 113-125, 2005

[50] A. Kostov and B. Friedrich, "Predicting Thermodynamic Stability of Crucible Oxides in Molten Titanium and Titanium Alloys", *Computational Materials Science,* vol. 38, pp. 374-385, 2006

[51] M. Gauthier and E. Baril, "High–temperature Interaction of Titanium with Ceramic Materials" in *Proceedings of the 2005 International Conference on Powder Metallurgy & Particulate Materials*, Montréal, Canada, pp. 127-140, 2005

[52] M. L. Delgado Tienda, "Sinterización con Fase Líquida de Aleaciones de Aluminio de la Serie 2xxxx. Estudio de su Aleación Mecánica, Adición de Estaño y Refuerzo con TiCN" in *Tesis Doctoral*, Universidad Carlos III de Madrid, 2008

[53] MPIF, "Standard 44, Method for Determination of Dimensional Changes from Die Size of Sintered Metal Powder Specimens", Metal Powder Industries Federation, 1986

[54] ASTM B 610, "Standard Test Method for Measuring Dimensional Change of Metal Powder Specimens Due to Sintering", 2000

[55] MPIF, "Standard 42, Method for Determination of Density of Compacted or Sintered Metal Powder Products", Metal Powder Industries Federation, 1986

[56] ASTM B 962, "Standard Test Methods for Density of Compacted or Sintered Powder Metallurgy (PM) Products Using Archimedes' Principle", 2008

[57] MPIF, "Standard 43, Determination of Hardness of Powder Metallurgy Materials", Metal Powder Industries Federation, 1991

[58] MPIF, "Standard 41, Determination of Transverse Rupture Strength of Powder Metallurgy Materials", Metal Powder Industries Federation, 1991

[59] ASTM B 528, "Standard Test Method for Transverse Rupture Strength of Metal Powders Specimens", 1999

[60] MPIF, "Standard 10, Method for Tension Test Specimens for Pressed and Sintered Metal Powder", Metal Powder Industries Federation, 1963
[61] ASTM B 925, "Standard Practise for Production and Preparation of Powder Metallurgy (P/M) Test Specimens", 2003
[62] R. W. Powell and R. P. Tye, "The Thermal and Electrical Conductivity of Titanium and its Alloys", *Journal of the Less Common Metals,* vol. 3, pp. 226-233, 1961
[63] L. J. van der Pauw, "A Method of Measuring Specific Resistivity and Hall Effect of Discs of Arbitrary Shape", *Philips Research Reports,* vol. 13, pp. 1-9, 1958
[64] L. J. van der Pauw, "A Method of Measuring Specific Resistivity and Hall Effect on Lamellae of Arbitrary Shape", *Philips Technical Review,* vol. 20, pp. 220-224, 1958
[65] R. I. Jaffee and I. E. Campbell, "The Effect of Oxygen, Nitrogen and Hydrogen on Iodide Refined Titanium", *Transactions of the American Institute of Mining and Metallurgical Engineers,* vol. 185, pp. 646-654, 1949
[66] R. I. Jaffee, et al., "Alloys of Titanium with Carbon, Oxygen and Nitrogen", *Transactions of the American Institute of Mining and Metallurgical Engineers,* vol. 188, pp. 1261-1266, 1950
[67] W. L. Finlay and J. A. Snyder, "Effects of Three Interstitial Solutes (Nitrogen, Oxygen and Carbon) on the Mechanical Properties of High-purity Alpha Titanium", *Journal of Metals* vol. 188, pp. 277-286, 1950
[68] H. Conrad, "Effect of Interstitial Solutes on the Strength and Ductility of Titanium", *Progress in Materials Science,* vol. 26, pp. 123-404, 1981
[69] K. Okazaki and H. Conrad, *Trans. TIM,* vol. 14, pp. 364-367, 1973
[70] R. A. Wood, "The Effect of Interstitials on the Mechanical Properties of Titanium and its Alloys" in *Titanium Metallurgy Course* New York University, 1965
[71] H. Conrad, "The Rate Controlling Mechanism during Yielding and Flow of α-titanium at Temperatures below 0.4 TM", *Acta Metallurgica,* vol. 14, pp. 1631-1633, 1966

CHAPTER 3

POWDER PRODUCTION AND CHARACTERISATION

This chapter describes the production of powders from the master alloys and the results of their characterisation. After the optimisation of the milling step, the powders with the right ratio of alloying elements were used to produce the titanium alloys considered during the development of this thesis.

Moreover, the characterisation of the starting powders was carried out to identify the best elemental titanium powder to be used during the blending elemental step and to study the behaviour of the alloys produced.

Parameters such as the particle size distribution, flow and packing properties, microstructure and morphology analysis as well as thermal behaviour (dilatometry and DTA), compressibility and green strength were determined.

3.1 – PREPARATION OF MASTER ALLOYS

Master alloy (MA) addition is a lower cost way to obtain titanium alloys than the use of prealloyed powders (PA) and it is expected to perform better during the compaction step.

In this thesis, the master alloy addition approach was considered to produce the Ti–6Al–4V, Ti–3Al–2.5V and Ti–6Al–7Nb alloys and, for that purpose, two master alloys composed by Al:V and Al:Nb were purchased.

After an extensive research about the master alloy suppliers and the respective compositions available, best compromise between price and powder features was chosen. In particular, a master alloy of Al:V (35:65 weight percentage) and a master alloy of Nb:Al:Ti (60:35:5 weight percentage) were bought from GfE – Metalle und Materialen GmbH (Germany).

3.1.1 – Aluminium:Vanadium Master Alloy

Regarding the aluminium:vanadium master alloy, the powder purchased has a 35:65 (Al:V) weight ratio, is irregular in shape and particle size in the range between 0.25 mm and 6.3 mm (+60 mesh -1/4 inch). Since this master alloys neither does have the right alloying elements proportion nor the particle size desired to produce the Ti–6Al–4V alloy, it was decided the use of high–energy ball milling to reduce or adjust the particle size[1, 2].

In particular, during the milling process optimisation, the right ratio of Al:V master alloy, elemental aluminium spherical powder (< 150 μm), a small amount of elemental HDH titanium powder (< 75 μm) and the grinding media (tungsten carbide balls) were loaded into a tungsten carbide container. Aluminium powder was purchased to Sulzer Metco Ltd.

Table 3.1 shows physical properties and chemical analysis for elemental powders and master alloy used during this step.

Table 3.1 – Chemical analysis and physical properties of the powders employed to obtain the Al:V (60:40) master alloy (suppliers' specifications).

Material	Element [wt.%]								Shape	Size
	Ti	Al	V	O	N	H	C	Fe		
Elemental Ti (HDH)	99.6	–	–	0.31	0.008	0.005	0.007	0.027	Irregular	< 75 μm
Al:V (35:65)	–	35^{+}	65^{+}	0.3*	0.05*	0.02*	0.05*	0.5*	Irregular	< 6.3 mm
Elemental Al (Atomised)	–	99	–	–	–	–	–	–	Spherical	< 150 μm

$^{+}$Mean value; *Maximum values

Milling was carried out in a Fritsch Pulverisette mill under inert gas atmosphere (Ar) to avoid or at least minimise oxidation and nitridation during milling, and a ball–to–powder weight ratio of 5:1 and 400 revolutions per minute (rpm) were used.

In order to prevent adhesion of the powder to the vessel or to the grinding media, a small amount of wax, approximately 1% of the total weight, was added as process control agent (PCA). During this part of the study, powder samples were collected every 15 minutes during 90 minutes and their particle size distribution, whose results are displayed in Table 3.2, was analysed by a Mastersizer 2000 particle size analyser.

Table 3.2 – Particle size distribution results for the Al:V (60:40) master alloy as a function of the milling time.

Time [min]	D_{10} [μm]	D_{50} [μm]	D_{90} [μm]
15	4.47	30.94	124.86
30	3.10	17.24	71.13
45	4.66	30.12	97.38
60	**2.46**	**12.61**	**55.81**
75	2.40	13.18	45.63
90	2.91	16.28	76.34

Based on the particle size analysis results, the optimum milling time was set in 60 minutes since this time leads to homogenous master alloy powder with the proper ratio of Al:V (60:40) and a particle size lower than 56 μm with relatively short milling time. Longer times do not provide significant particle size reduction.

The morphology of the selected milled powder was analysed by SEM and it is shown in Figure 3.1; the percentage of the interstitial elements of the milled powder was determined by LECO and the results are reported in Table 3.3.

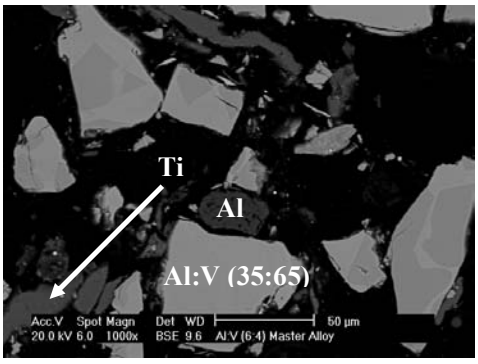

Figure 3.1 – SEM image (BSE mode) of the morphology of the powder of the Al:V (60:40) master alloy milled during 60 minutes.

Table 3.3 – Percentage of the interstitial elements determined on the Al:V (60:40) powder milled during 60 minutes.

Element	Al:V (60:40) – 60'
O [wt.%]	1.160
N [wt.%]	0.0384
C [wt.%]	0.792

As it can be seen in Table 3.3, oxygen and carbon contents of the master alloy milled during 1 hour are significantly higher compared to the value of the starting powders where oxygen is most probably due from the contamination from the atmosphere whilst the carbon is due to the wax (PCA).

3.1.2 – Aluminium:Niobium Master Alloy

The purchased aluminium:niobium master alloy has a weight ratio percentage of 60:35:5 (Nb:Al:Ti) with particle size lower than 0.8 mm (- 20 mesh) whose characteristics are shown in Table 3.4.

Table 3.4 – Chemical analysis and physical properties of the powders employed to obtain the Al:Nb (60:70) master alloy (suppliers' specifications).

Material	Element [wt.%]								Shape	Size
	Ti	Al	V	O	N	H	C	Fe		
Elemental Ti (HDH)	99.6	–	–	0.31	0.008	0.005	0.007	0.027	Irregular	< 75 μm
Nb:Al:Ti (60:35:5)	5^{+}	35^{+}	60^{+}	0.15*	0.05*	–	0.05*	0.2*	Irregular	< 0.8 mm
Elemental Al (Atomised)	–	99	–	–	–	–	–	–	Spherical	< 150 μm

$^{+}$Mean value; *Maximum values

Once more, the Nb:Al:Ti master alloy does not have either the correct proportion of alloying elements or the appropriate particle size, thus a high–energy ball milling step was planned. As for the Ti–6Al–4V alloy, the Nb:Al:Ti master alloy, the aluminium powder and a small percentage of elemental titanium were milled using the same processing parameters, the same atmosphere and the same process control agent described for the Al:V master alloy.

Once again, milled powders samples were drawn out of the container every 15 minutes during 90 minutes and characterised in terms of particle size distribution. The results of this characterisation are shown in Table 3.5.

Table 3.5 – Particle size distribution results for the Al:Nb (60:70) master alloy as a function of the milling time.

Time [min]	D_{10} [µm]	D_{50} [µm]	D_{90} [µm]
15	5.83	24,55	1087,97
30	**4.94**	**17.84**	**54.34**
45	2.47	20.08	98.15
60	2.23	17.90	79.76
75	4.36	12.59	45.18
90	1.99	12.31	49.89

The optimum and shortest milling time was found to be 30 minutes which guarantees adjusting the alloying elements ratio and a particle size lower than 55 µm. Morphology analysis and the chemical analysis of this powder were carried out and the results are shown in Figure 3.2 and Table 3.6, respectively.

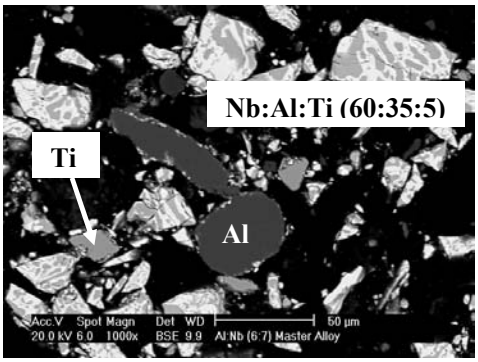

Figure 3.2 – SEM image (BSE mode) of the morphology of the powder of the Al:Nb (60:70) master alloy milled during 30 minutes.

Table 3.6 – Percentage of the interstitial elements determined on the Al:Nb (60:70) powder milled during 30 minutes.

Element	Al:Nb (60:70) – 30’
O [wt.%]	1.130
N [wt.%]	0.0879
C [wt.%]	0.634

As it was found for the Al:V master alloy, the chemical analysis of the Al:Nb milled powder (Table 3.6) shows an important oxygen pick–up from the atmosphere and a high carbon content, due to the wax (PCA), with respect to the starting powder, although the values obtained are comparable with that of the Al:V master alloy.

3.1.3 – Alloys Fabrication

The Al:V (60:40) master alloy powder obtained after 60 minutes milling was mixed during 30 minutes with elemental HDH titanium powder in a Turbula mixer for the production of the Ti–6Al–4V alloy (Ti64–MA).

On the other side, the Al:Nb (60:70) master alloy milled during 30 minutes was used to produce the Ti–6Al–7Nb alloy (Ti67–MA) by mixing with the proper ratio of elemental titanium during 30 minutes.

Regarding the Ti–3Al–2.5V alloy, it was produced either mixing the Ti–6Al–4V prealloyed (Ti64–PA) powder or the Al:V (60:40) master alloy with elemental titanium in a turbula mixer during 30 minutes. Therefore, two different Ti–3Al–2.5V powders named Ti–3Al–2.5V prealloyed (Ti32–PA) and Ti–3Al–2.5V master alloy (Ti32–MA), respectively, were considered.

These steps are shown and explained in the scheme of Figure 2.1 (Section 2.2). It is worth mentioning that during the titanium alloy production step an elemental titanium powder with particle size lower than 75 μm, termed as 3rd batch in Section 3.2, was used since this powder showed the best compressibility behaviour.

3.2 – POWDER CHARACTERISATION

In this chapter the results of the characterisation of both purchased and prepared powders are described. The details of the characterisation carried out and the equipment employed for this purpose were explained in Section 2.3.

It is worth mentioning that, as shown in Section 2.2, five different elemental titanium powders were analysed in order to identify the best one to be used to produce the titanium alloys studied in this thesis.

A resume of the different powders characterised is described hereafter:

- ✓ Elemental titanium: three batches with particle size lower than 75 µm purchased at the same supplier but in different period of time. A powder with particle size lower than 125 µm and a powder with particle size in the range 200–350 µm;
- ✓ Ti–6Al–4V alloy: Ti64–PA and Ti64–MA;
- ✓ Ti–3Al–2.5V alloy: Ti32–PA and Ti32–MA;
- ✓ Ti–6Al–7Nb alloy: Ti67–MA.

3.2.1 – Particle Size Distribution

The results of the particle size distribution analysis, displayed as frequency curve and cumulative undersize percentage curve, are shown for elemental titanium (Figure 3.3, Figure 3.4 and Table 3.7) and titanium alloy powders (Figure 3.5, Figure 3.6 and Table 3.8), respectively.

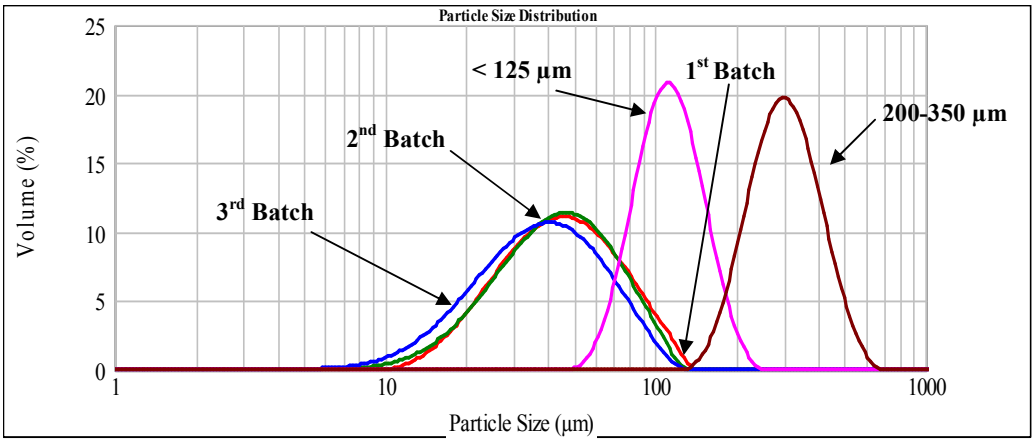

Figure 3.3 – Particle size distribution results: frequency curve for elemental titanium powders.

Particle size distribution results of the three batches of elemental titanium lower than 75 µm (Figure 3.3, Figure 3.4 and Table 3.7) reveal that the 1st and 2nd batch are similar but the 3rd batch has a slightly lower particle size and it is the only one which fulfils completely the specification (< 75 µm).

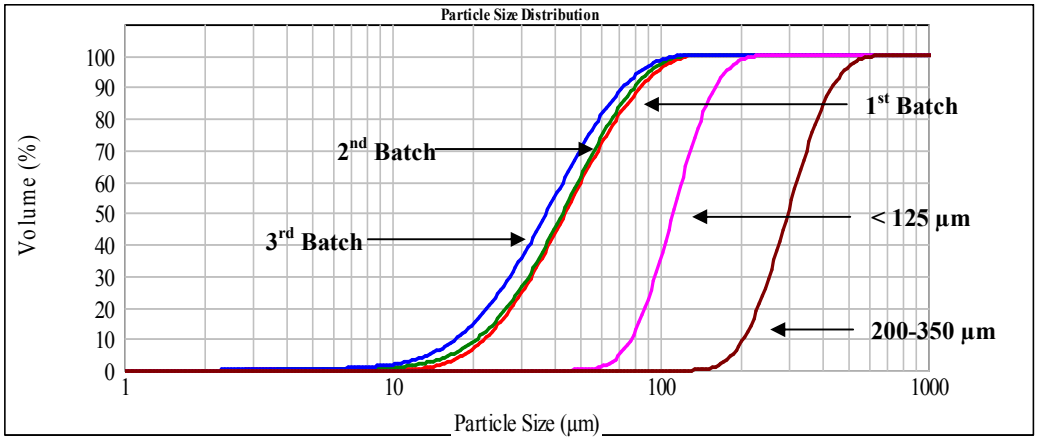

Figure 3.4 – Particle size distribution results: cumulative undersize percentage curve for elemental titanium powders.

Table 3.7 – Particle size distribution results for elemental titanium powders.

Elemental Ti		1st Batch	2nd Batch	3rd Batch	125 µm	200-350 µm
Production method		HDH				
Morphology		Irregular				
Particle size analysis	**D_{max} [µm]**	< 75*	< 75*	< 75*	< 125*	200-350*
	D_{10} [µm]	22.16	20.74	17.31	77.70	204.51
	D_{50} [µm]	44.25	43.22	37.59	111.66	299.11
	D_{90} [µm]	84.32	79.78	72.59	160.43	438.21

*Supplier specification

Titanium < 125 µm analysis shows that this powder is not smaller than 125 µm but it has a particle size distribution which ranges approximately from 53 µm to 180 µm. Finally, titanium powder 200–350 µm has a larger distribution than the theoretical one, since it ranges roughly from 125 µm to 500 µm.

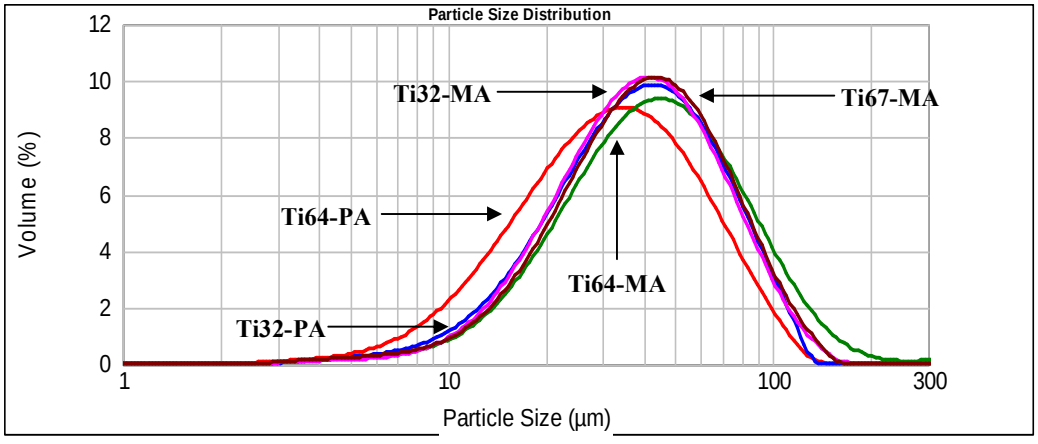

Figure 3.5 – Particle size distribution results: frequency curve for titanium alloys powders.

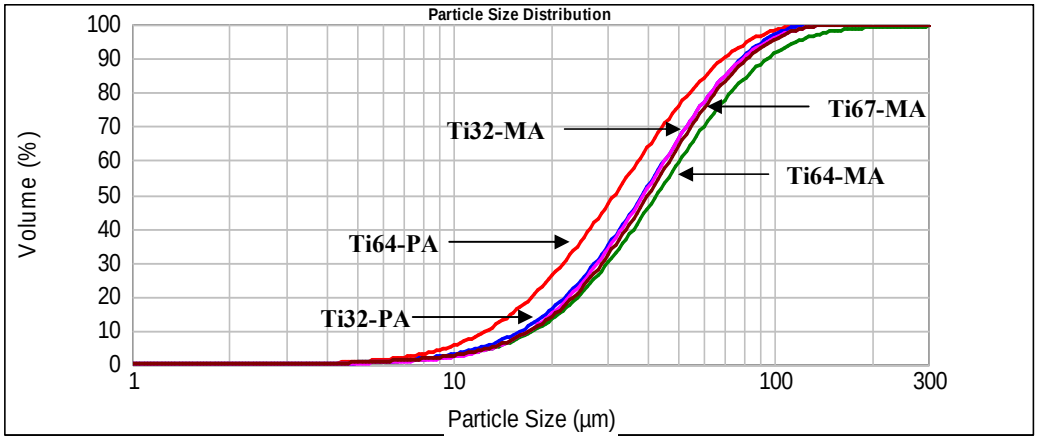

Figure 3.6 – Particle size distribution results: cumulative undersize percentage curve for titanium alloys powders.

Table 3.8 – Particle size distribution results for titanium alloys powders.

Ti Alloys		Ti64–PA[1]	Ti64–MA[2]	Ti32–PA[1]	Ti32–MA[2]	Ti67–MA[2]
Production method		HDH	–	–	–	–
Morphology		Irregular				
Particle size analysis	**D_{max} [µm]**	< 75*	< 106	< 75	< 90	< 90
	D_{10} [µm]	12.67	17.85	16.25	17.22	17.40
	D_{50} [µm]	31.78	42.94	38.79	39.00	40.39
	D_{90} [µm]	69.44	95.17	74.63	79.65	81.94

[1]Prealloyed; [2]Master alloyed; *Supplier specification

Analysing particle size distribution results for titanium alloys (Figure 3.5, Figure 3.6 and Table 3.8), it can be seen that the prealloyed titanium alloy powder Ti64–PA has the smaller particle size and it is lower than 75 µm as supplier's specifications affirms.

Except for Ti64–MA powder, which has slightly bigger particle size, the other titanium alloy powders have more or less the same particle size distribution since the diverse curves overlap even if the parameters D_{10}, D_{50} and D_{90} are a bit different. By the way, all of them can be considered suitable for the pressing and sintering P/M route.

3.2.2 – Chemical Analysis, Density, Flow rate and Microhardness

Chemical analysis results for elemental titanium powder, shown in Table 3.9, indicate that all the titanium powders, independently from the particle size, can be classified as "grade 4"[3, 4] with the exception of the 3rd batch HDH powder that fits to the specification for "grade 3"[3, 4].

Table 3.9 – Chemical, physical and mechanical properties of elemental titanium powders.

Elemental Ti		1st Batch	2nd Batch	3rd Batch	125 μm	200-350 μm
Chemical analysis	O [wt.%]	0.357	0.336	0.272	0.244	0.279
	N [wt.%]	0.0067	0.1027	0.0159	0.0754	0.0507
	C [wt.%]	0.0081	0.0103	0.0202	0.0038	0.0100
ρ_{th} He [g/cm^3]		4.5028	4.5217	4.5189	4.5171	4.5057
Hall [g/cm^3]		–	1.64±0.004	–	1.79±0.003	1.95±0.003
Flow rate [s/50g]		–	56	–	41	9
Carney [g/cm^3]		1.36±0.005	1.65±0.001	1.61±0.005	1.79±0.003	1.94±0.005
$HV_{0.01}$		120.6±29.8	130.4±23.2	106.1±12.8	138.6±9.2	193.2±10.4

As it can be seen in Table 3.9, some of the elemental titanium powders do not flow in the Hall apparatus and, thus, the flow rate could not be determined; for the others, the bigger the particle size the higher the apparent density and the lower the flow rate, as it could be expected.

The values of bulk density and flow rate shown in Table 3.9 are comparable to that found in elemental HDH titanium powder with particle size of 38 μm subjected to shape modification (spheroidisation) by a particles composite system which uses high speed mixer blending and impacting[5].

Powders density values obtained by He picnometry are very similar, varying between 4.502 and 4.521 g/cm^3, and near the theoretical value of wrought titanium, which is considered to be 4.51 g/cm^3[3].

From hardness measurements, it seems that this property increases with particle size for HDH powders, and for the powders with the same particle size, the hardness is greatly influenced by nitrogen, then by oxygen and least by carbon content [6-8]. The 2nd batch, which has the highest N percentage, is the hardest powder followed by the 1st batch which has higher oxygen content than the 3rd batch.

The chemical analysis, density, apparent density, flow rate and microhardness results for the different titanium alloys considered are reported in Table 3.10.

As it can be seen in Table 3.10, oxygen content is approximately constant at 0.40 wt.% for each titanium alloy with the exclusion of the Ti32–MA which has a lower oxygen percentage most probably due to the influence of the HDH powder used to fabricate it.

Nitrogen content is approximately 0.01 wt.% for all the alloys, which is very similar to the HDH titanium powder (< 75 μm) content used for their fabrication, with exclusion of the Ti64–PA that has slightly lower value, approximately 0.007 wt.%.

Table 3.10 – Chemical, physical and mechanical properties of titanium alloy powders.

Ti Alloys		Ti64–PA	Ti64–MA	Ti32–PA	Ti32–MA	Ti67–MA
Chemical analysis	**O [wt.%]**	0.418	0.428	0.402	0.337	0.393
	N [wt.%]	0.0072	0.0121	0.0101	0.0118	0.0173
	C [wt.%]	0.0124	0.1050	0.0120	0.0666	0.0706
ρ_{th} He [g/cm^3]		4.4146	4.3702	4.4560	4.4410	4.4748
Hall [g/cm^3]		–	–	–	–	–
Flow rate [s/50g]		–	–	–	–	–
Carney [g/cm^3]		1.47±0.008	1.84±0.006	1.48±0.006	1.91±0.006	2.04±0.011
$HV_{0.01}$		142.8±20.0	–	–	–	–

Carbon content is low for Ti64–PA and Ti32–PA powders and relatively much higher for the alloys produced with master alloy addition. This is surely due to the wax used as control agent during milling step and it is confirmed by the fact that Ti32–MA, which has half of the amount of master alloy respect to Ti64–MA, has approximately half of C content.

The densities of the prealloyed powders measured by helium picnometry (Table 3.10), which were kept as reference for the calculation of the relative density, are very similar to the wrought products, that is 4.43 g/cm^3 and 4.48 g/cm^3[3], for Ti–6Al–4V and for Ti–3Al–2.5V, respectively.

Compared to prealloyed powders, master alloy powder densities are somewhat lower due to the obtaining process, where a master alloy and a small amount of wax were used during milling. Ti–6Al–7Nb has a wrought density of 4.52 g/cm^3[3] whereas the value obtained is 4.4748 g/cm^3, which is lower again due to addition of wax in the fabrication step.

Finally, measurements of the apparent densities and flow rates by means of the Hall apparatus failed due to the morphology of the powder. The apparent densities were therefore measured by Carney apparatus with the help of a wire to agitate the powder to promote its flow[9]. The values obtained are very similar for the two PA powders and they result to be lower than those for the MA powders.

This observation can be explained based on the particle size distribution of the milled master alloy and the elemental titanium starting powder shown in Table 3.7 (elemental titanium), Table 3.2 (Al:V master alloy) and Table 3.5 (Al:Nb master alloy). Because the master alloy has a slightly lower particle size than HDH Ti, its particles fit in between the bigger ones, leading to a better packing and, therefore, higher apparent densities.

As it can be seen in Table 3.10, the microhardness was determined exclusively for the Ti64–PA, whose value can be compared to that of elemental titanium, since the others are composed by diverse elements.

3.2.3 – Powder Morphology

The morphology of the powders studied by scanning electron microscopy is shown in Figure 3.7 and Figure 3.8 for elemental titanium and titanium alloys, respectively, where the inlet in the left up/corner of each picture is a magnification of a single powder particle.

During this characterisation step every picture of the morphology was taken at the same magnification, with the exception of the bigger HDH powder (200-350 μm), in order to allow the comparison of the particle size.

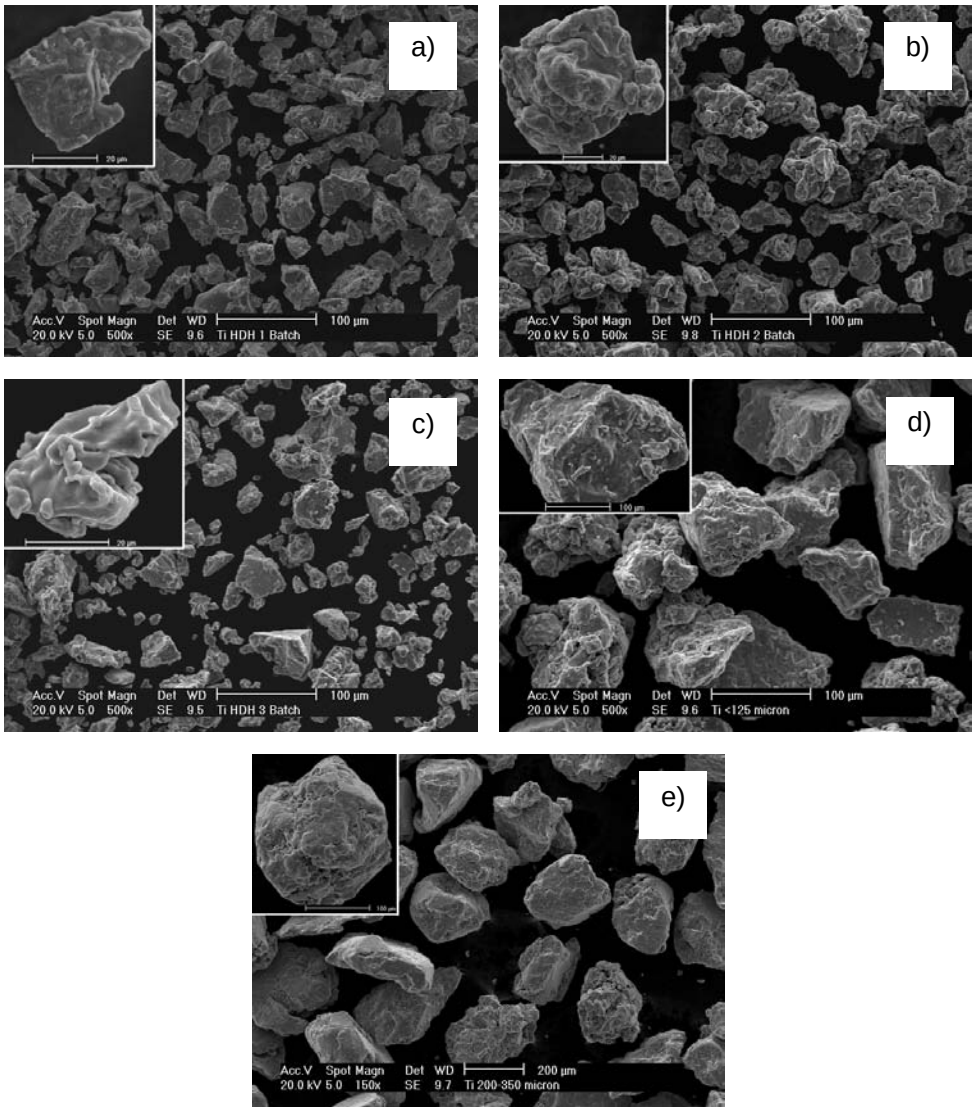

Figure 3.7 – SEM images (SE mode) of the morphology of the elemental titanium powders: a) 1st batch < 75 μm, b) 2nd batch < 75 μm, c) 3rd batch < 75 μm, d) < 125 μm and e) 200–350 μm.

Among the three batches of Ti HDH < 75 μm (Figure 3.7 a, b and c) there is a great difference in morphology even if they were produced with the same method. More in detail, the 1st batch has angular shape, the 2nd batch is irregular with rounded edges and the 3rd batch shows an intermediate morphology between the previous two.

These data clarify why the 2nd batch flows through the Hall flowmeter meanwhile the other two batches did not flow. The titanium powders with bigger particle size (Figure 3.7 d and e) have rounded morphology and flow freely because of their bigger size.

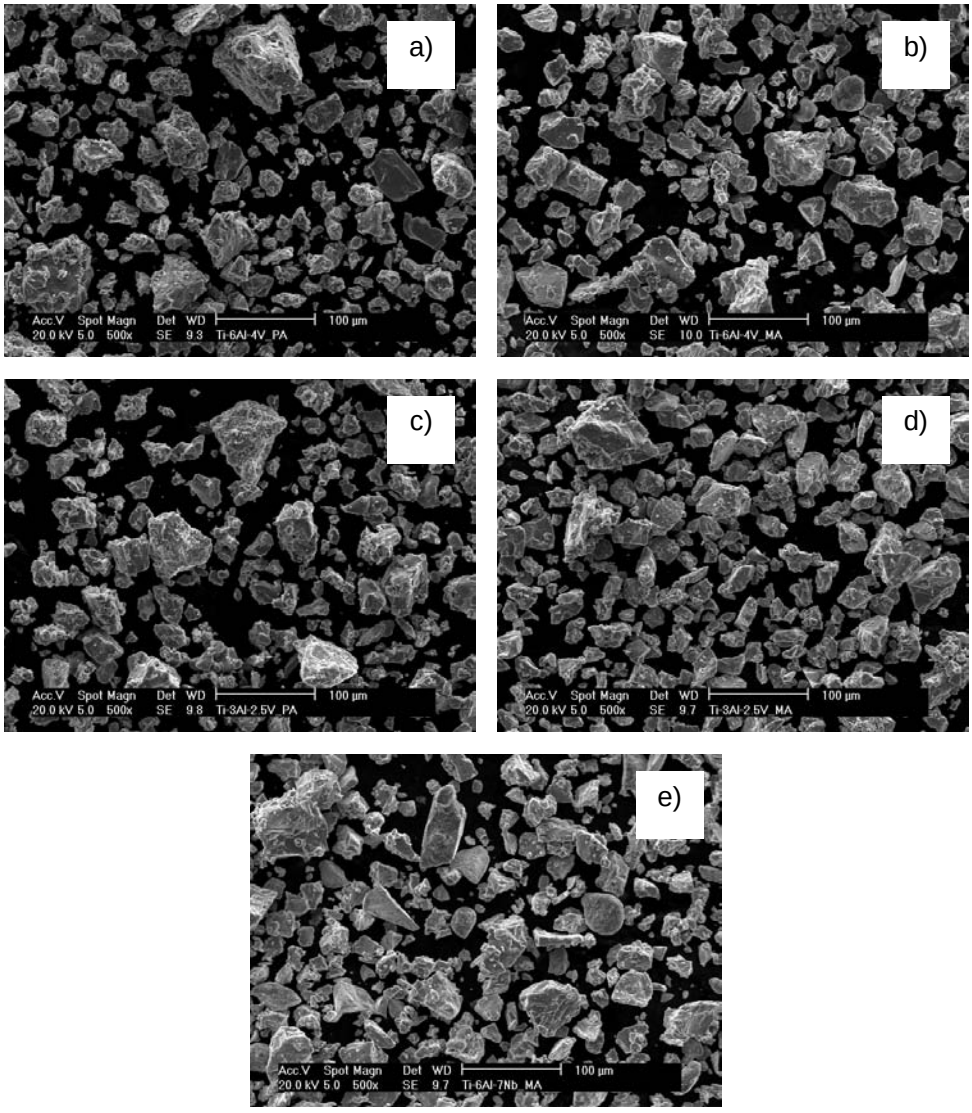

Figure 3.8 – SEM images (SE mode) of the morphology of the titanium alloys powders: a) Ti64–PA, b) Ti64–MA, c) Ti32–PA, d) Ti32–MA and e) Ti67–MA.

Both the prealloyed and master alloyed titanium powders, which were obtained by the hydride–dehydride method, have angular or even irregular in shape (Figure 3.8 a, b, c, d and e), what could explain why they do not flow in the Hall apparatus.

3.2.4 – Powder Microstructure

Figure 3.9 and Figure 3.10 show, respectively, SEM images (BSE mode) of the microstructure of the elemental titanium and titanium alloys powders obtained on samples which have been previously mounted, polished and etched.

The magnification used to characterise the microstructure of the powders was optimised as a function of the particle size to clearly identify the microstructural elements; thus, the diverse pictures are not directly comparable. The different elements composing an alloy, namely elemental titanium, elemental aluminium and master alloys, were identified by means of EDS technique.

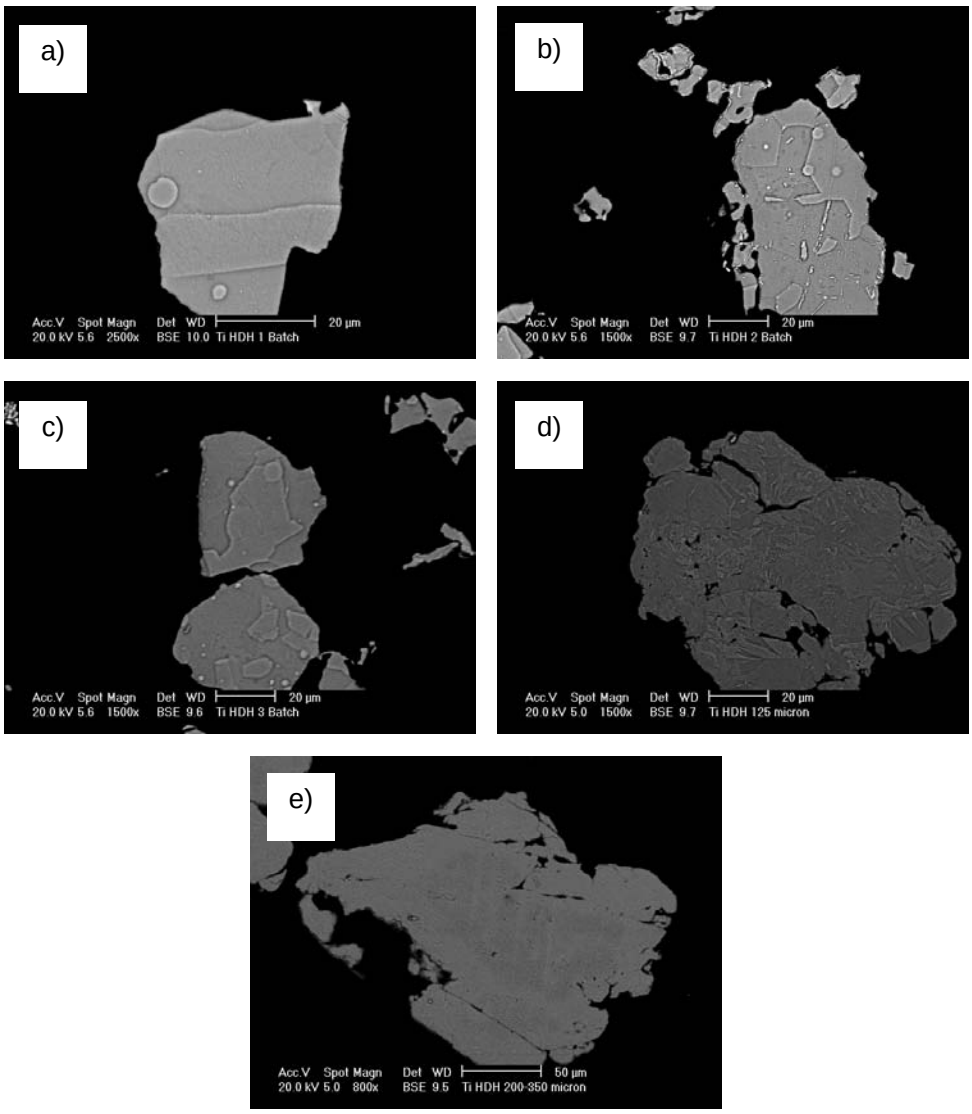

Figure 3.9 – SEM images (BSE mode) of the metallographic cross section of the elemental titanium powders: a) 1st batch < 75 µm, b) 2nd batch < 75 µm, c) 3rd batch < 75 µm, d) < 125 µm and e) 200–350 µm.

Regardless of the particle size, the microstructure of elemental titanium HDH powders (Figure 3.9 a, b, c, d, and e) is composed by equiaxial α grains of different size generated by the hydride–dehydride process where the titanium particles are hydrogenated to make them brittle in order to mill them. Furthermore, elemental titanium HDH powders with big particle size, namely < 125 μm and 200–350 μm (Figure 3.9 d, and e), show internal porosity and cracks again due to the comminution process.

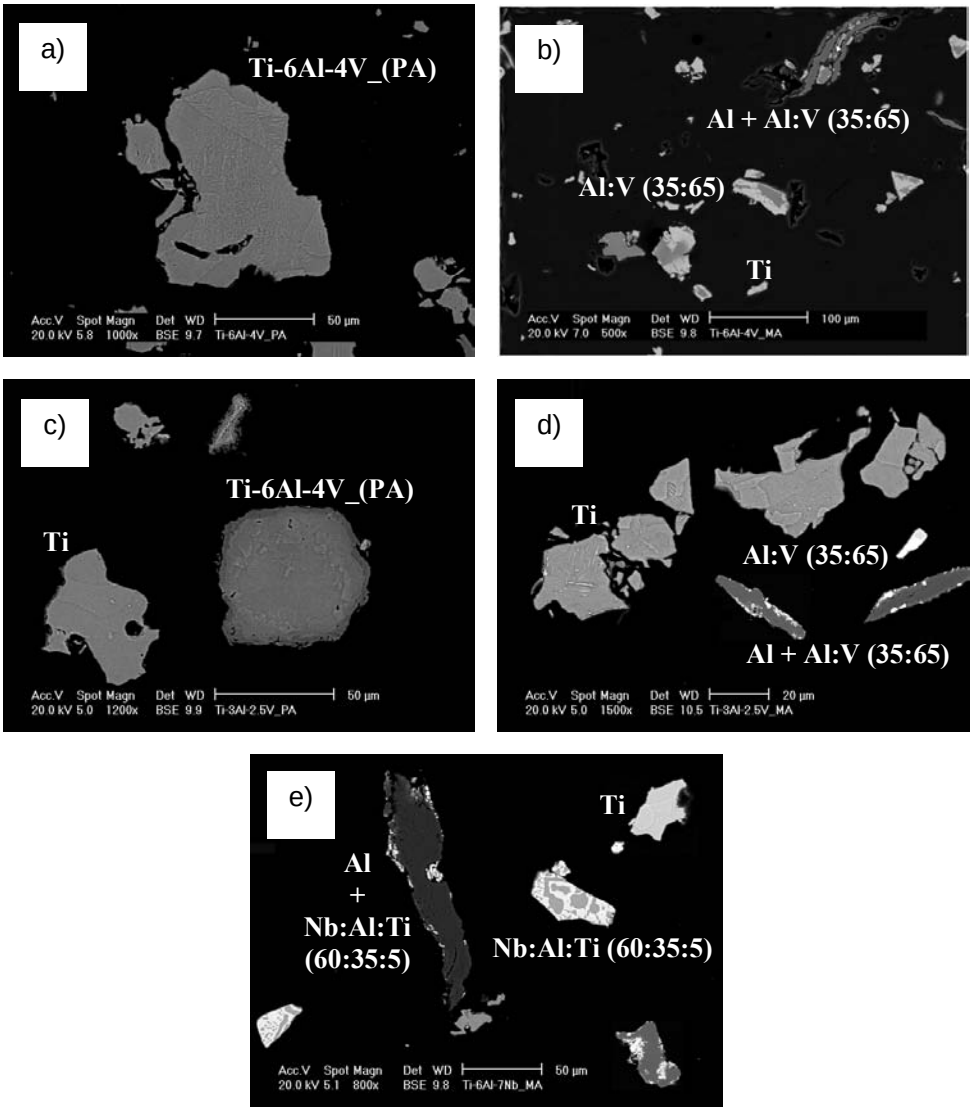

Figure 3.10 – SEM images (BSE mode) of the metallographic cross section of the titanium alloys powders: a) Ti64–PA, b) Ti64–MA, c) Ti32–PA, d) Ti32–MA and e) Ti67–MA.

The microstructure of the Ti64–PA (Figure 3.10 a) consist of equiaxial α grains and α + β grains, as expected from the composition. The Ti32–PA alloy was obtained by mixing Ti64–PA powder with elemental Ti powder, as shown in Figure 3.10 c), where the two types of particles with slightly different contrast can be distinguished.

In the image corresponding to the Ti64–MA or the Ti32–MA alloy (Figure 3.10 b and d), the powders that composed the alloy can be seen. The brightest particles with dark shadows correspond to the Al:V (35:65) master alloy, the darkest particles correspond to elemental Al or Al mixed with the Al:V master alloy and the grey particles correspond to elemental titanium.

The individual elements are still distinguishable because the Ti64–MA and Ti32–MA alloys were produced by conventional blending, and the milling was carried out only to reduce its particle size and to adjust the final composition, and not to produce a prealloyed powder.

Figure 3.10 e) shows the components of the Ti–6Al–7Nb master alloy titanium powder where it can be distinguished elemental titanium particles (grey), Nb:Al:Ti master alloy particles (bright with grey areas) and elemental aluminium with embedded some master alloy (dark particles with bright outer zones).

3.2.5 – Compressibility Test

A good compressibility is one of the most important factors for powders to be used in conventional P/M routes because the higher the green density, the lower the shrinkage of the part during sintering, which results in a smaller dimensional change in the final shape of a component.

Therefore, compressibility test for elemental titanium and for titanium alloy powders were done and the results are displayed in Figure 3.11 (left) and Figure 3.11 (right), respectively, where, normally, green density increases when raising the consolidation pressure up.

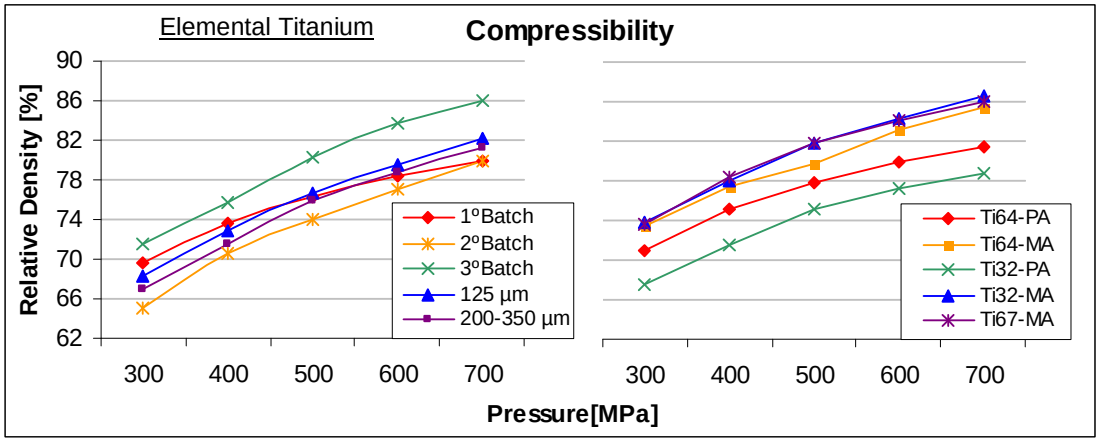

Figure 3.11 – Relative density as a function of the compaction pressure (compressibility): elemental titanium (left) and titanium alloys (right).

Analysing Figure 3.11 (left) it can be seen that the 2nd batch has the lowest compressibility while the 3rd batch presented the highest one, reaching values of relative density as high as 86% at 700 MPa.

Similar results were obtained by Wei et al.[10] using a HDH powder with a mean particle size of 56 μm (purity > 99.2%) and uniaxial die pressing even if the authors do not specify the pressure employed whereas El Kadiri et al.[11] obtained a green density of 72% compacting an HDH elemental titanium powder with particle size lower than 45 μm. This could indicate that lowering to much the particle size of the HDH powder leads to a lost of compressibility.

The behaviour of the other elemental titanium powders shown in Figure 3.11 lays in between the 2nd and the 3rd batch and titanium powder < 125 μm always presented higher relative density than 200–350 μm powder. Furthermore, the 1st batch has higher density at low pressure but lower at higher pressure with respect to the two bigger powders.

The great difference found in the compressibility behaviour of the three HDH batches with particle size lower than 75 μm is primarily due to their morphology and interparticle friction as well as to their interstitial elements content. The 2nd batch, which has the highest nitrogen content and high oxygen content, has the lowest compressibility since these elements harden titanium[6-8], whereas the 3rd batch, with the lowest oxygen and low nitrogen content, has the highest compressibility.

Regarding titanium alloy powders (Figure 3.11–right), as expected, prealloyed powders have lower compressibility since they are harder and less deformable because already have the alloying elements dissolved. However, it is interesting to note that Ti32–PA, which has been fabricated by blending elemental HDH titanium powder and Ti–6Al–4V prealloyed powder, has lower compressibility than Ti64–PA which is completely prealloyed. This lower compressibility is due to the small mismatch in particle size distribution between the raw powders and the slightly lower nitrogen content of the Ti64–PA powder compared to the elemental Ti powder.

The Ti32–MA and the Ti–6Al–7Nb powders have a better behaviour under pressure than the Ti64–MA powder, which can be related to the better apparent density or the lower oxygen content of these powders. In this case, the carbon content does not affect the compressibility and mechanical properties of the powders because it is not dissolved in the material.

3.2.6 – Green Strength

The results of the green strength as a function of the compacting pressure for elemental titanium powders and for titanium alloy powders are presented in Figure 3.12.

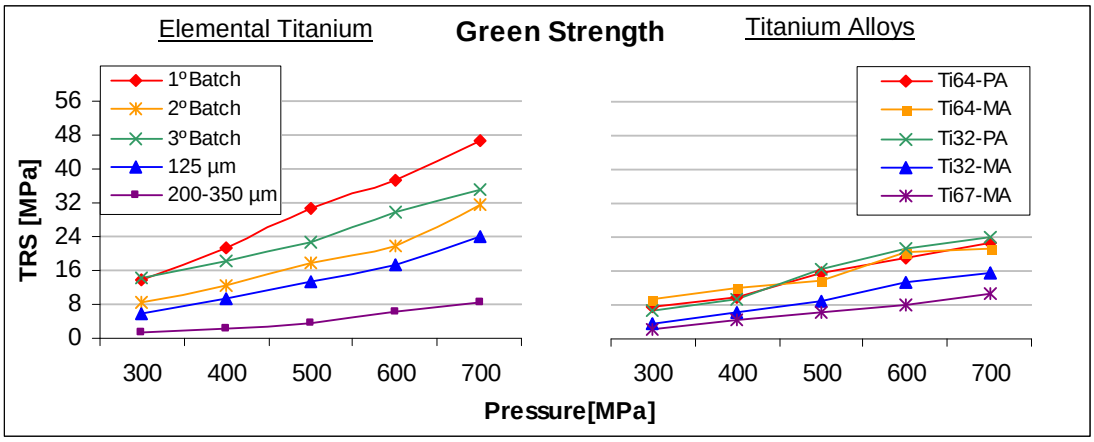

Figure 3.12 – Green strength (MPa) as a function of the compaction pressure: elemental titanium (left) and titanium alloys (right).

Figure 3.12 (left) shows the results of the green strength as a function of the compaction pressure for all the HDH titanium powders, where it can be seen that the green strength increases with the compacting pressure for each powder even if there are great differences between the powders analysed.

It seems that the higher the particle size, the lower the green strength. However, among the three batches with 75 µm, the 1st batch attained the highest green strength, the 2nd batch presented the lowest and the 3rd batch lies in between. Since the particle size distributions are quite similar, this behaviour could be attributed to the different morphologies of the powders, which guarantees more or less efficient particle rearrangement, elastic and plastic deformation of contact areas and the relative work hardening associated with plastic deformation at increasing the compacting pressure.

Even if mechanical interlocking makes the major contribution to green strength[12], this property is also dependent on the chemical analysis and, especially, on the interstitial elements content because they harden titanium. In particular, the higher the N content, the lower the ductility of the powder, which justify the low green strength of the 2nd batch which had the highest nitrogen percentage.

When nitrogen amount is relatively low, it is oxygen content which influences greatly the mechanical properties, as it can be verified in Figure 3.12 (left) where the 1st batch has higher strength compared to the 3rd batch.

For titanium alloy powders (Figure 3.12–right), even if there is not a clear difference between them, it seems that prealloyed powders have a bit higher green strength with the increasing of the pressure compare to the master alloy titanium powders.

More in detail, the prealloyed powders (Ti64–PA and Ti32–PA) reaches the higher strength of all the titanium alloy studied, especially starting from 500 MPa, where the Ti32–PA has a slight better performance.

The Ti64–MA powder has approximately the same green strength behaviour with the compaction pressure of the prealloyed powder reaching similar but somewhat lower values. Ti32–MA has intermediate green strength between the previous described powders and Ti67–MA, which has the lowest resistance.

It is interesting to notice that the relative position of the titanium alloy powders found by analysing the green strength data is the opposite of that found for the compressibility (Figure 3.11–right). Precisely, Ti32–PA has the lowest compressibility but the highest green strength; subsequently, Ti64–PA has better compressibility than Ti32–PA but slightly lower green strength and so on. This unexpected behaviour seems to indicate that a higher compressibility of the powder leads to more rigid compacts which, therefore, fails before when tested by a bending load.

On the other side, the compressibility of the master alloy addition powders could be affected by the little mismatch in terms of particle size and morphology between elemental titanium and the master alloys as well as the presence of the was (PCA) which makes less effective the mechanical interparticle bonding.

Concluding, the green strength of titanium alloy powders increases with the compaction pressure and independently of the values itself, the strength obtained guarantees the handling of the components even at 300 MPa.

3.2.7 – Dilatometric Analysis

The dilatometric analysis was carried out at the IFAM Fraunhofer Institute for Manufacturing and Advanced Materials of Dresden using a NETZSCH DIL 402 E dilatometer. The thermal cycle analysed is composed of a heating step (10°C/min) from room temperature up to 1400°C, a dwell of 15 minutes at temperature and cooling (10°C/min) down to room temperature under a constant flow of argon (90 l/h). The results of the dilatometric study are presented in Figure 3.13 where the variation of the length of the specimen is represented as a function of the temperature.

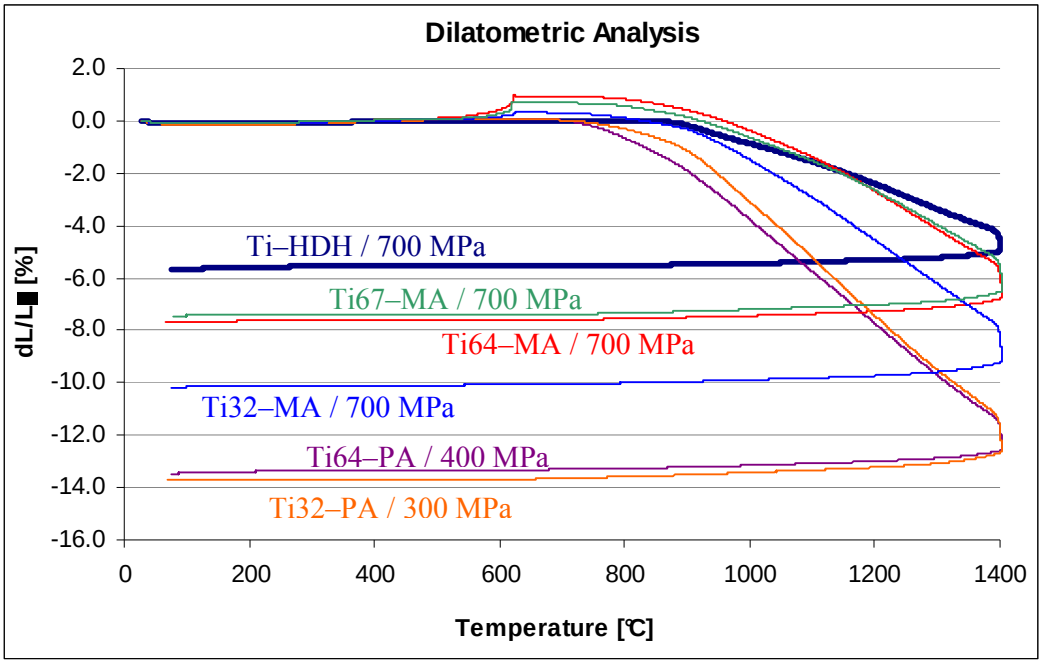

Figure 3.13 – Length variation as a function of the temperature (dilatometric analysis) for elemental titanium and titanium alloys.

As it can be seen in Figure 3.13, all the materials analysed shrink uniformly during the three steps of the thermal cycles even if, obviously, the most significant amount of contraction of the length of the specimens takes place during the heating. Moreover, it can be stated that the compaction pressure plays an important role since the shrinkage is higher for the alloy compacted at lower pressure such as the Ti64–PA and Ti32–PA alloys.

The details of the results of the dilatometric, namely maximum length variation and onset temperature for each material are reported in Table 3.11.

Table 3.11 – Maximum shrinkage and onset temperature determined by the dilatometric analysis of titanium alloys.

Material	Compaction pressure [MPa]	Maximum shrinkage [%]	Onset temperature [°C]	Nominal beta transus [ºC]
Ti–HDH	700	–5.70	870.7	882±2
Ti64–PA	400	–13.47	723.3	996±15
Ti64–MA	700	–7.69	819.2	
Ti32–PA	300	–13.72	810.8	935±15
Ti32–MA	700	–10.18	816.4	
Ti67–MA	700	–7.44	812.4	1010±15

Analysing the data shown in Table 3.11, it can be noticed that elemental titanium, which was compacted at the highest pressure (700 MPa) and does not have any alloying elements has the lowest length shrinkage.

Regarding the Ti–6Al–4V and the Ti–3Al–2.5V and, therefore, comparing the powder production method, which in this case allows estimating the influence of the compaction pressure, it can be confirmed that, as expected, the lower the compaction pressure the higher the variation of the final dimensions during sintering.

On the other side, comparing the master alloy addition powders, Ti64–MA, Ti67–MA and Ti32–MA, it can be seen that the lower the amount of the alloying elements that have to diffuse to reach a homogeneous microstructure the higher the shrinkage obtained. This could indicate that a great among of the thermal energy available in the system is invested in diffusion processes instead of in the densification of the green compact.

Looking at the onset temperature determined during the experiments, it seems that the elemental titanium P/M components start to sinter in correspondence with the allotropic transformation for the H.C.P. (α) to the B.C.C. (β) phase whilst the titanium alloys start to shrink at a temperature lower than the respective beta transus.

Moreover, the titanium alloys where the alloying elements have to diffuse seem to have quite the same onset temperature of approximately 815°C with the exception of the fully prealloyed powder (Ti64–PA) where no alloying elements have to diffuse which has a lower onset temperature of about 100ºC.

Another remarkable difference between the elemental or prealloyed powders and the master alloy addition ones is the swelling of the samples, between 0.4% and 1% depending on the alloy considered, which starts at 500°C and culminates at approximately 620°C as it can be seen in Figure 3.14 which displays the dilatometric behaviour of the powder between 500°C and 900°C.

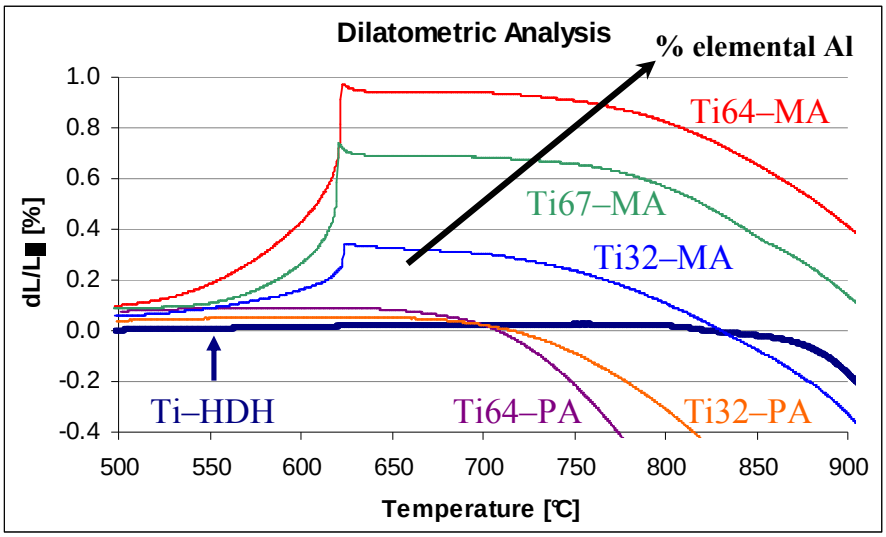

Figure 3.14 – Details of the 500–900°C temperature range of the results of the dilatometric study.

As it can be seen in Figure 3.14, starting form 500ºC, the dL/L_0 parameter of the alloys obtained by master alloy addition increases exponentially until 620ºC and, then, it starts to decrease.

This effect is due to the melting of the elemental aluminium added during the preparation of the titanium alloys which reacts with elemental titanium and induces a small swelling of the P/M component before it starts to sinter.

It is worth mentioning that the height of the peaks shown in Figure 3.14 is proportional to the percentage of elemental aluminium added to adjust the final composition where the greater the amount of elemental Al, the higher the swelling of the samples.

3.2.8 – Differential Thermal Analysis (DTA)

As it has been explained in Section 2.3.7, DTA analysis of every powder was carried out under inert gas (Ar) increasing the temperature up to 1400ºC with a heating rate of 10ºC/min, a dwell step of 15 minutes and cooling at 10ºC/min.

DTA results were subdivided as a function of the P/M approach, therefore, from one side elemental titanium and PA powders and from the other MA powders.

The results for the elemental titanium powder and the prealloyed titanium alloys powders were analysed together and presented in Figure 3.15.

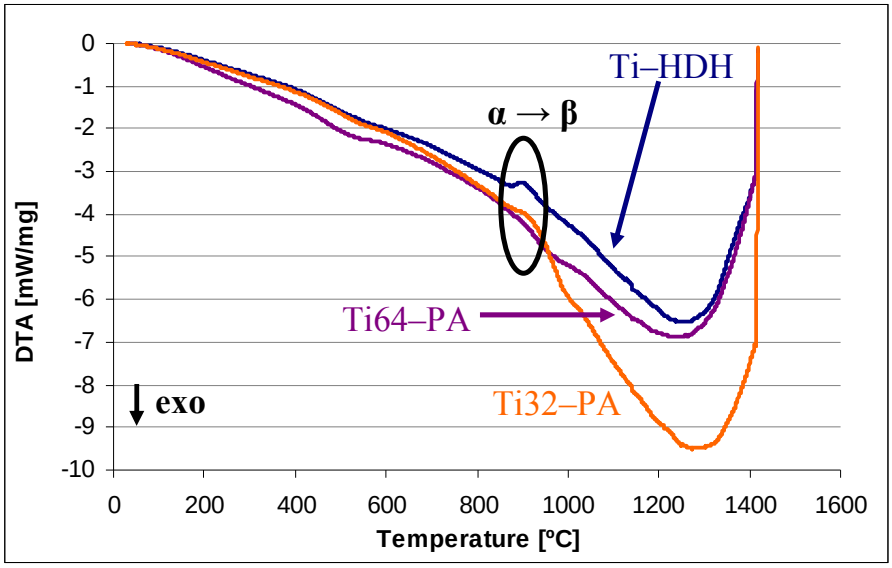

Figure 3.15 – DTA signal as a function of the temperature for elemental titanium (HDH) and PA powders (Ti64–PA and Ti32–PA).

As it can be seen in Figure 3.15, the behaviour of the elemental and prealloyed titanium powders with the temperature is very similar and the only remarkable event is the endothermic peak in the proximity of 900ºC which coincides with the allotropic transformation of titanium.

More in detail, the endothermic peak of elemental titanium is well distinguishable whilst that of Ti64–PA is almost unappreciable, as shown in Figure 3.16, most probably due to the prealloyed nature of the powder which is already composed by the alpha and beta phases.

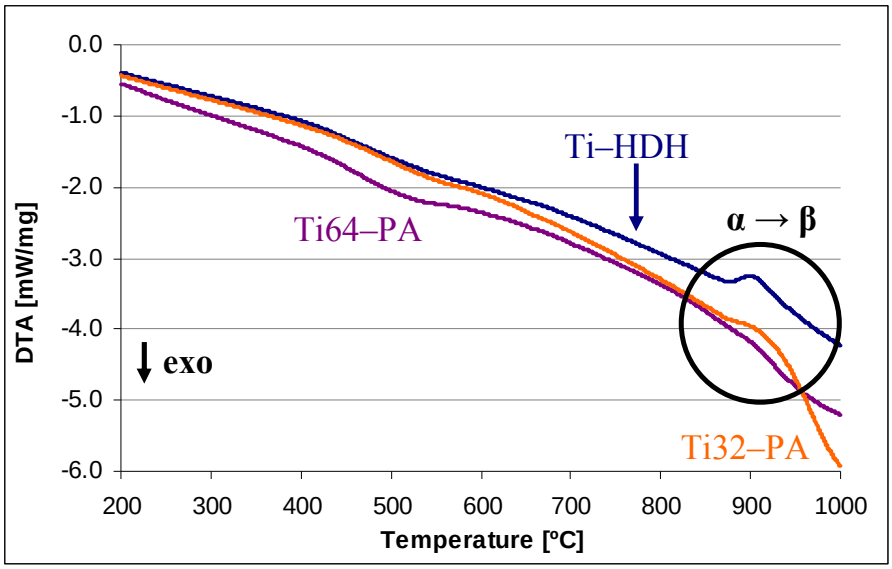

Figure 3.16 – Details of the allotropic transformation (endothermic peak) for elemental titanium (HDH) and PA powders (Ti64–PA and Ti32–PA).

The behaviour of the Ti32–PA powder (Figure 3.16) is something in between the previous two and, thus, the phase transition is visible but not well defined due to the fact that the Ti32–PA powder was obtained by blending, almost in equal parts, the HDH elemental titanium powder and the Ti64–PA powder. The data relative to the endothermic peak calculated on the DTA graphs are reported in Table 3.12.

Table 3.12 – Onset temperature, temperature of the top of the peak and nature of the reaction for elemental titanium (HDH) and PA powders (Ti64–PA and Ti32–PA).

Material	Onset temperature [°C]	Top of the peak [°C]	Reaction	Nominal beta transus [ºC]
Ti–HDH	875.51	904.71	α → β	882±2
Ti64–PA	906.47	959.89		996±15
Ti32–PA	887.26	928.00		935±15

Analysing the data shown in Table 3.12, it can be seen that onset temperature for the endothermic transformation found in elemental titanium corresponds to the nominal alpha to beta phase transformation but the top of the peak, which correspond to the end of the transformation, is placed at 905ºC because of the continuous heating conditions.

In the case of Ti64–PA, the phase transformation starts at 900ºC and its top is at 960ºC, temperature which results to be lower than the nominal beta transus most probably due to the presence of some elemental titanium even if the powder should be completely prealloyed.

For the Ti32–PA powder, the presence of Ti64–PA switches the onset temperature of 10ºC reaching its top at 928ºC very similar to its nominal beta transus.

It is worth mentioning that the DTA curve of the Ti64–PA powder seems to have a broad exothermic peak at approximately 500ºC which could be due either to some oxidation of the powder or to the decomposition of some aluminium/vanadium compound used by the supplier during the production of the powder in order to adjust the final composition.

The DTA results for the MA powders, precisely the Ti64–MA, Ti32–MA and Ti67–MA alloys, are displayed in Figure 3.17.

As for the prealloyed powders, the differential thermal analysis of the master alloys (Figure 3.17) indicates that the behaviour of these powders is very similar among them since two endothermic and one exothermic peaks are visible.

More in detail, the first endothermic peak at approximately 330ºC corresponds to the elimination of the wax used as PCA during milling while the second one at 900ºC is the alpha to beta transformation. This temperature results to be lower than the nominal beta transus of the titanium alloys considered and it is due to the powder production method where the alloying elements are added either as elemental powder or as master alloy and have to diffuse inside the titanium matrix.

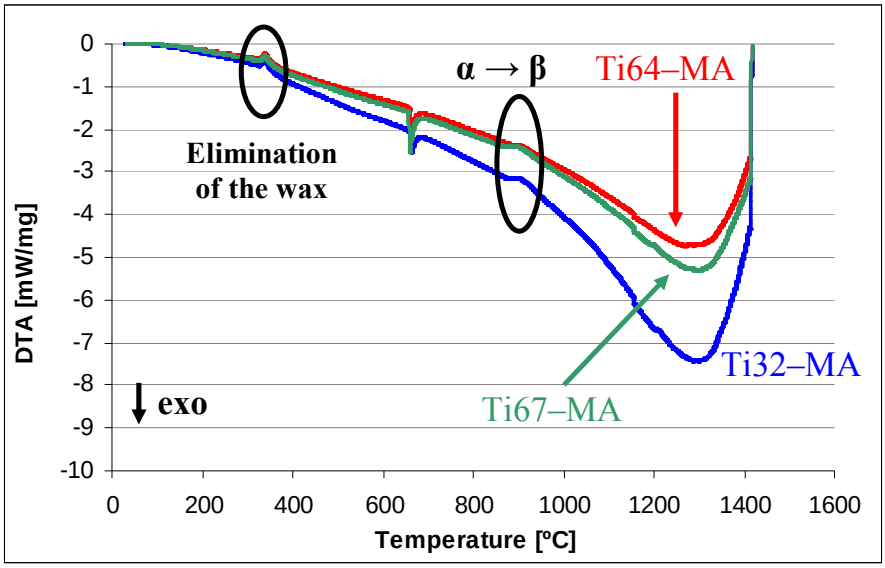

Figure 3.17 – DTA signal as a function of the temperature for the MA powders (Ti64–MA, Ti32–MA and Ti67–MA).

Therefore, the endothermic peak detected should correspond to that of elemental titanium. This is, actually, confirmed comparing the shape and position (temperature) of the endothermic peak of elemental titanium (Figure 3.16) and the shapes and positions of the peaks of titanium alloys shown Figure 3.18.

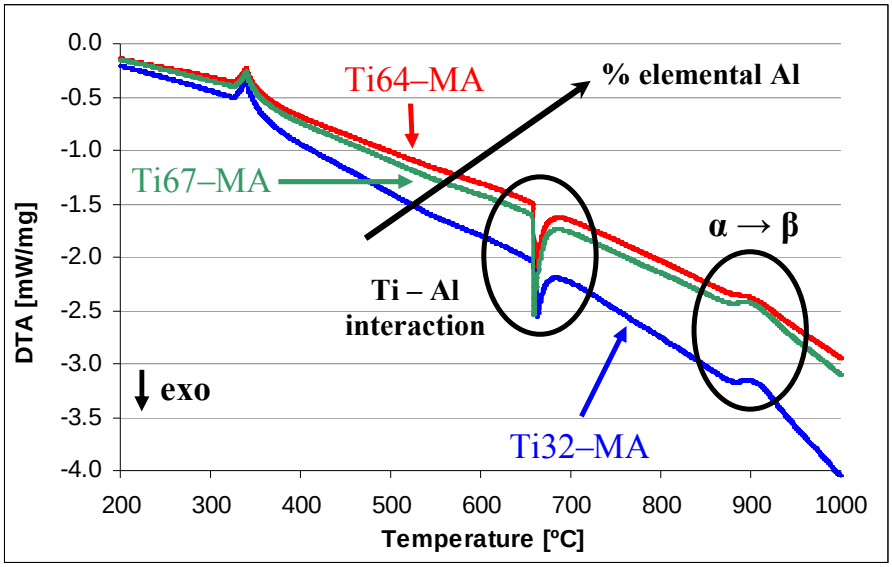

Figure 3.18 – Details of the endothermic and exothermic transformations for MA powders (Ti64–MA, Ti32–MA and Ti67–MA).

The exothermic peak found at 660ºC in the three master alloy addition powders (Figure 3.18) is due to some kind of interaction between elemental titanium and the elemental aluminium added to the powders in order to reach the desired composition which, accordingly to the dilatometric results shown in Figure 3.14 should already be in the melted state. Besides, the onset and the maximum temperature of the reaction remain constant whereas the intensity and the area seem to increases with the amount of elemental aluminium.

Based on the Ti–Al phase diagram, which is displayed in Figure 3.19, and supposing that locally an elemental titanium particle is in contact with an elemental aluminium particle which melts and diffuses, different titanium aluminates compound such as Ti_3Al, TiAl and $TiAl_3$, could be formed at 660ºC where the intermetallic $TiAl_3$ seems to be the most probable[13, 14].

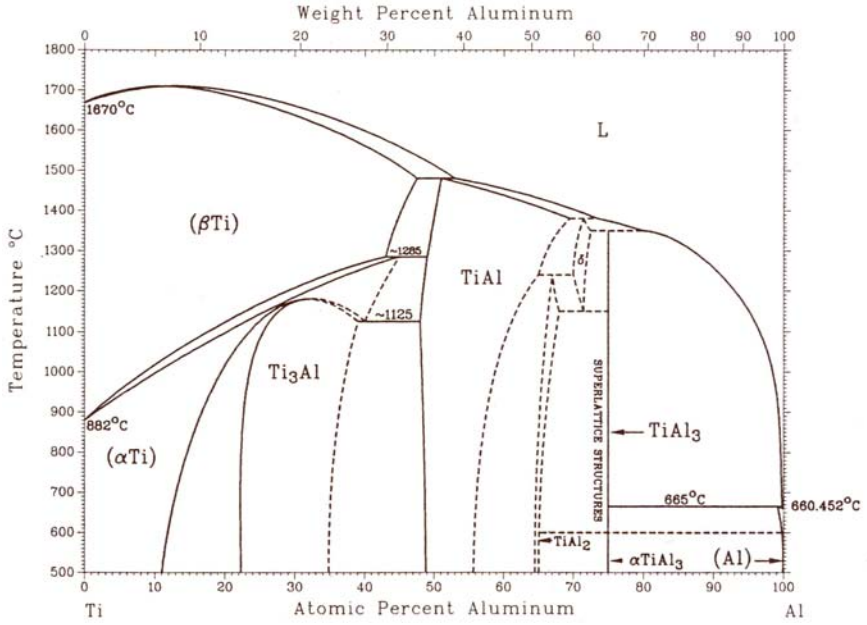

Figure 3.19 – Ti–Al phase diagram[15].

The values of onset temperature and temperature of the top of the peak for the exothermic and endothermic reactions found in the master alloy addition titanium alloys are shown in Table 3.13.

From the data reported in Table 3.13, it can be seen that the elimination of the wax is independent from the nature of the alloying elements since it always starts at 325ºC and the top of the peak is at 339ºC.

Also the reaction that takes place between elemental titanium and elemental aluminium is independent of the nature and amount of the master alloy added since its starts at approximately 656ºC having its top at 660ºC which due to its exothermic nature corresponds to the formation of the $TiAl_3$ compound as other authors suggest, as the phase diagram of Figure 3.19 indicates, when elemental aluminium reacts with elemental titanium[16, 17].

Table 3.13 – Onset temperature, temperature of the top of the peak and nature of the reaction for master alloy addition powders (Ti64–MA, Ti32–MA and Ti67–MA).

Material	Onset temperature [°C]	Top of the peak [°C]	Reaction	Nominal beta transus [ºC]
Ti64–MA	325.63	339.65	Wax elimination	996±15
	657.79	660.65	Ti–Al reaction	
	881.45	901.23	$\alpha \rightarrow \beta$	
Ti32–MA	325.36	339.29	Wax elimination	935±15
	656.82	662.97	Ti–Al reaction	
	880.76	907.88	$\alpha \rightarrow \beta$	
Ti67–PA	325.75	339.60	Wax elimination	1010±15
	654.56	659.25	Ti–Al reaction	
	876.06	901.62	$\alpha \rightarrow \beta$	

Finally, from the data shown in Table 3.13 it is clear that the alpha to beta phase transformation detected in the master alloy addition powders during DTA analysis corresponds to that of elemental titanium used to fabricate them and not that of the respective beta transus of the titanium alloys because the alloying elements are not completely diffused yet.

3.2.9 – Summary

Particle size analysis of elemental titanium reveals that the particle size and its distribution are normally slightly bigger with respect to the specification of the supplier, which could be due to the characterisation technique employed in order to determine these parameters. Moreover, particle size distribution of three batches with the same supplier specifications bought in different periods is somewhat dissimilar, which indicates that, conversely to iron powder producer, titanium powder suppliers should optimise their processes in order to guarantee a more reliable production.

Chemical analysis confirms that there is a great variation in interstitial elements content between different kinds of powders, which is comprehensible because they were fabricated under different conditions, but also between powders with the same theoretical characteristics. This chemical analysis variability between powders that should be equal proves that better process consistency and repeatability should be achieved.

Powders morphology and microstructure analyses show that hydride–dehydride powders are composed by broken equiaxial α grains and have angular or even irregular with rounded edges morphology. This slight difference in morphology has a great effect on technological properties such as the flow rate as the results of its analysis demonstrate.

Ti–6Al–4V prealloyed powder has angular morphology and microstructure composed by α + β grains, while titanium alloys powders produced by master alloy approach have morphology and microstructure as well as technological and mechanical properties that depend on the characteristics of the powders used to obtain them.

Compressibility test demonstrated that green density increases with consolidation pressure for irregular shaped powders. Among them, the bigger the particle size, the lower the green density values, even if between the three batches with the same particle size it seems that the chemical composition, especially nitrogen and oxygen content, influences significantly the compressibility. This is due to the fact the nitrogen, oxygen and carbon harden and brittle titanium where nitrogen has the highest effect, followed by oxygen and then by carbon. This justify why the 2nd batch of HDH elemental titanium powder with particle size lower than 75 μm has the lowest compressibility and the lowest green strength with respect to the 1st and the 3rd batch.

Resuming, the elemental titanium powder with the higher nitrogen content is the hardest and, on the other hand, the higher the oxygen content, the higher the green strength. Moreover, for elemental titanium powders, the higher the particle size, the lower the green strength, which is most probably due to the fact that the utilisation of bigger particle powder generates less contact areas and interlocking between the particles.

Regarding titanium alloy powders, alloys produced by blending elemental approach, using the master alloy addition, demonstrated to have better compressibility since prealloyed powders are harder and more brittle as they have the alloying elements dissolved in the titanium matrix. Green strength of titanium alloy powders increases with the compaction pressure and the slight differences found are mainly due to the morphology and hardness of the different powders. Anyway, the values obtained permit the handling of the compacts without any problem.

Dilatometric analysis indicates that the green samples shrink when subjected to a sintering cycle and that the compaction pressure has a significant influence on the final maximum shrinkage where the higher the compaction pressure the lower the shrinkage. Moreover, it can be stated that the lower the amount of the alloying elements that have to diffuse inside the titanium matrix the higher the shrinkage, revealing that an important amount of the thermal energy available in the system is spent for diffusion phenomena instead of in the densification of the material.

In the master alloy addition powders a slight swelling of the samples, variable between 0.4% and 1%, was detected in the proximity of the melting of elemental aluminium. Nevertheless, this does not seem to have any significant effect on the sintering and shrinkage of the components.

Finally, DTA analysis permits to detect the allotropic transformation from the alpha to the beta phase (at approximately 900ºC) in all the powders considered with the exception of the Ti–6Al–4V prealloyed powder most probably due to the fact that the microstructure of this powder is already characterised by some stable beta phase.

When considering the master alloy addition powders, an endothermic peak was detected at 330ºC, which corresponds to the elimination of the wax, and an exothermic peak at 660ºC is clearly remarkable due to the interaction of elemental titanium and elemental aluminium in the melted state.

3.2.10 – Partial Conclusions

Based on the characterisation presented and, especially, on compressibility and green strength results, it was chosen to follow with the study just considering one elemental titanium HDH powder, specifically the 3rd batch with particle size lower than 75 μm.

The results of the compressibility tests and green strength permitted to select the appropriate compacting pressures to produce the samples used. The highest pressure compatible with the avoiding of delamination phenomena or breaking of the edges of the samples was chosen and it is reported in Table 3.14.

Table 3.14 – Compacting pressure as a function of the materials and the geometry of the specimens.

Material	**Compaction pressure [MPa]**	
	Bending specimens	**Tensile specimens**
Ti–HDH	700	700
Ti64–PA	400	700
Ti64–MA	700	700
Ti32–PA	300	700
Ti32–MA	700	700
Ti67–MA	700	700

As it can be seen in Table 3.14, elemental titanium and master alloy addition powders do not show any problem during the pressing step whilst in the case of the prealloyed powder or the powder prepared by mixing this powder, the compacting pressure has to be limited. This is mainly due to the fact that, as said before, the prealloyed powder is much harder and, therefore, difficult to press due to the alloying elements dissolved inside the titanium matrix.

3.3 – REFERENCES

[1] C. Suryanarayana, "Mechanical Alloying and Milling", *Progress in Materials Science,* vol. 46, pp. 1-184, 2001

[2] C. Suryanarayana, et al., "The Science and Technology of Mechanical Alloying", *Materials Science and Engineering A,* vol. 304-306, pp. 151-158, 2001

[3] RMI, "Titanium Company: Titanium Alloy Guide", *available at: http://rtiintl.s3.amazonaws.com/RTI-Reports/tiguideWeb.pdf,* 2000

[4] M. J. Donachie, *Titanium. A Technical Guide*, 2nd Edition ed. Ohio, USA, ASM International, pp. 1-137, 2000

[5] G. Gai, et al., "Particle Shape Modification and Related Property Improvements", *Powder Technology,* vol. 183, pp. 115-121, 2008

[6] R. I. Jaffee and I. E. Campbell, "The Effect of Oxygen, Nitrogen and Hydrogen on Iodide Refined Titanium", *Transactions of the American Institute of Mining and Metallurgical Engineers,* vol. 185, pp. 646-654, 1949

[7] R. I. Jaffee, et al., "Alloys of Titanium with Carbon, Oxygen and Nitrogen", *Transactions of the American Institute of Mining and Metallurgical Engineers,* vol. 188, pp. 1261-1266, 1950

[8] W. L. Finlay and J. A. Snyder, "Effects of Three Interstitial Solutes (Nitrogen, Oxygen and Carbon) on the Mechanical Properties of High-purity Alpha Titanium", *Journal of Metals* vol. 188, pp. 277-286, 1950

[9] MPIF, "Standard 28, Determination of Apparent Density of Non-free-flowing Metal Powders using the Carney Apparatus", Metal Powder Industries Federation, 1985

[10] W. Wei, et al., "Effect of Fe Addition on Sintering Behaviour of Titanium Powder", *Powder Metallurgy,* vol. 46, pp. 246-250, 2003

[11] H. El Kadiri, et al., "Development of a Ti-based Alloy: Design and Experiment", *JOM,* vol. 61, pp. 60-66, 2009

[12] R. M. German, *Powder Metallurgy Science*, 2nd Edition ed. Princeton, USA, MPIF - Metal Powder Industries Federation, pp. 191-340, 1994

[13] F. J. J. van Loo and G. D. Rieck, "Diffusion in the Titanium-aluminium System - I. Interdiffusion between Solid Al and Ti or Ti-Al alloys", *Acta Metallurgica,* vol. 21, pp. 61-71, 1973

[14] F. J. J. van Loo and G. D. Rieck, "Diffusion in the Titanium-aluminium System - II. Interdiffusion in the Composition Range between 25 and 100 at.% Ti", *Acta Metallurgica,* vol. 21, pp. 73-84, 1973

[15] J. L. Murray, *Phase Diagrams of Binary Titanium Alloys*, 1st ed, ASM International, pp. 1-345, 1987

[16] O. M. Ivasishin, et al., "Cost-effective Blended Elemental Powder Metallurgy of Titanium Alloys for Transportation Application", in *Development in Light Metals*, vol. 188, pp. 55-62, 2000

[17] O. M. Ivasishin, "Cost-effective Manufacturing of Titanium Parts with Powder Metallurgy Approach", *Materials Forum* vol. 29, pp. 1-8, 2005

CHAPTER 4

STUDY OF THE SINTERING TRAY

Titanium is a highly reactive metal and for that it is called the universal solvent. As it was described in Section 2.4, many researches were carried out and are still done to find an inert material to use when casting titanium. In the case of P/M processing, titanium does not reach the melt state but, anyway, it reacts with the sintering support, which is normally made out of ceramic materials.

During the development of this thesis, four sintering trays were considered (see Section 2.4); however, based on thermodynamic study[1] and some preliminary results, the study of the influence of the sintering tray on the physical and mechanical properties of titanium parts was limited to two ceramic oxides: alumina (Al_2O_3) and zirconia (ZrO_2). In particular, fully dense alumina plates (Kerasetter KSV 174/1000) and zirconia beads ZIRMILL with a diameter variable between 1.9 and 2.5 mm were used. Moreover, exclusively elemental titanium powder with particle size lower than 75 μm was used to obtain the specimens studied in this research.

Three–point bending test samples were obtained by uniaxial pressing at 700 MPa using a floating die and vacuum sintered (approximately 10^{-5} mbar) for 2 and 4 hours at 1250°C, 1300ºC and 1350°C (heating rate: 5°C/min). The specimens prepared were characterised in terms of shrinkage (volume variation) [2, 3], weight change, relative density as well as maximum bending strength, flexural strain, HV30 and $HV_{0.1}$ microhardness.

The volume change was measured as explained in Section 2.6.1 and the dimensions of the samples were measured by means of a digital calliper and a micrometer. For weight change, the mass of the specimens was obtained by a 4–place electronic balance. Figure 4.1 and Figure 4.2 show the shrinkage and the weight change as a function of the sintering conditions employed, respectively.

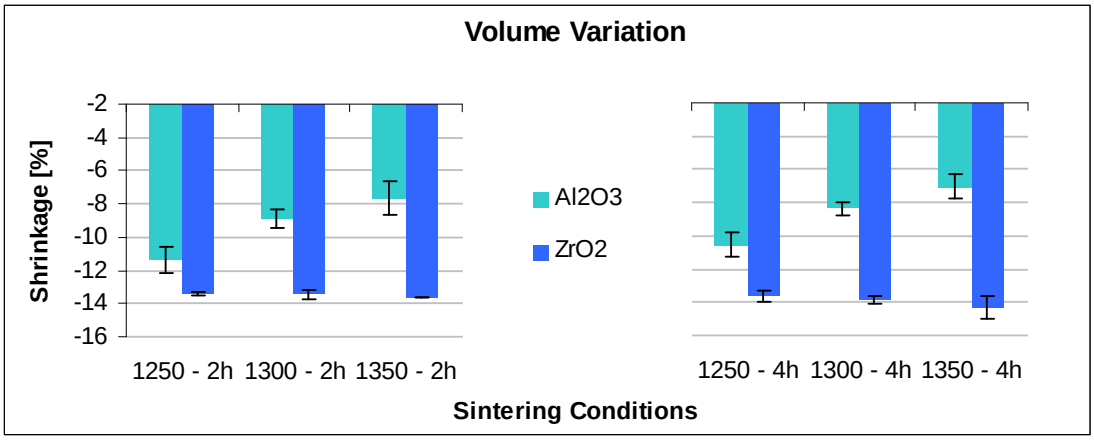

Figure 4.1 – Shrinkage of the elemental titanium specimens sintered on alumina plate and zirconia beads as a function of the sintering conditions.

As it can be seen from the data shown in Figure 4.1, volume changes are all negative which means that the samples shrink during sintering. Generally, the shrinkage of the specimens sintered on Al_2O_3 plate decreases with the increasing of the temperature whereas for the samples sintered on ZrO_2 beads the shrinkage slightly increases with the temperature.

Nonetheless, the most important point is that the shrinkage of the samples sintered on alumina plate is much lower with greater standard deviation which could indicate that there was some sort of interaction between the titanium samples and the Al_2O_3 plate which could limit the shrinkage and that this interaction is getting more significant as the processing temperature increases.

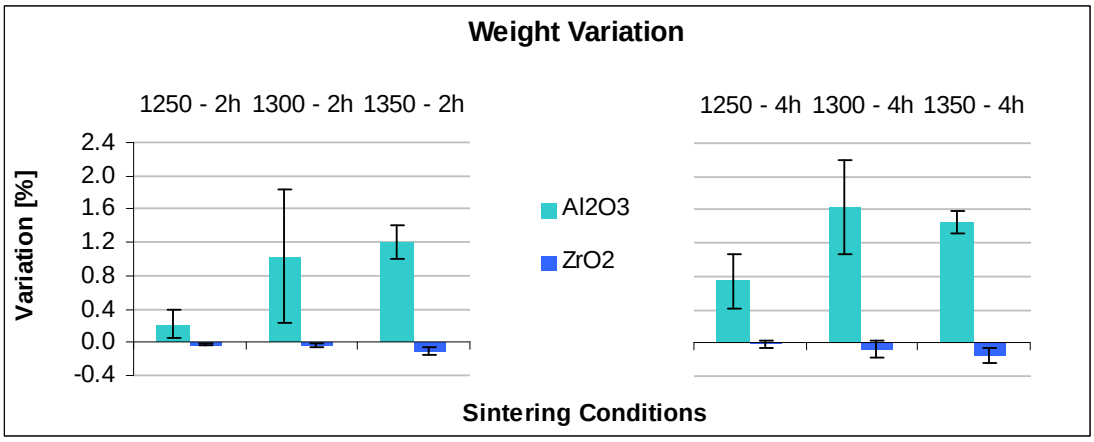

Figure 4.2 – Specimens weight change of the elemental titanium specimens sintered on alumina plate and zirconia beads as a function of the sintering conditions.

The weight change data presented in Figure 4.2 indicate that there is almost no weight variation for the specimens sintered on the zirconia beads, just a little weight lost, whereas there is a significant weight gain of at least 0.8% for the samples laid on alumina plate, where the smallest weight change corresponds to the lowest temperature in combination with the shortest time. This clearly confirms that there has been some kind of interaction that leads to an increment of the mass of the specimens.

A piece of alumina plate with a specimen which was sintered on it as well as some zirconia beads with a sample processed on it are shown in Figure 4.3.

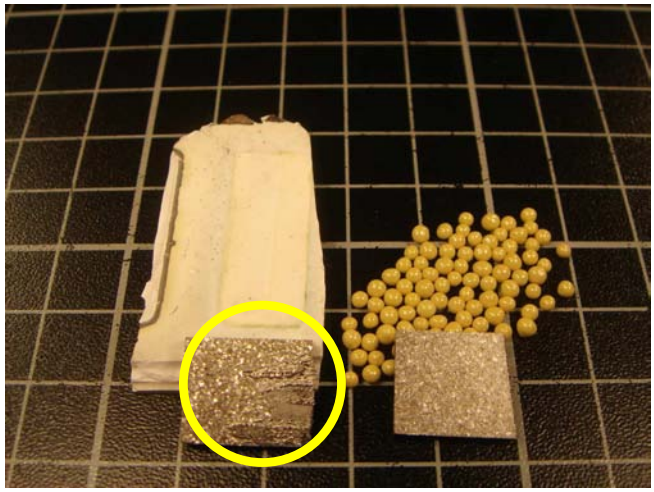

Figure 4.3 – Alumina plate and zirconia beads with an example of specimen sintered on them.

As it can be seen in Figure 4.3, the specimen sintered on Al_2O_3 plate shows a strong reaction zone on the surface which was in contact with the support whereas there are not visible defects on the surface of the sample sintered on ZrO_2.

To study the nature of this reacted area, the samples were analysed by means of scanning electron microscope using backscattered electron and a comparison of the border of a specimen sintered at 1350ºC during 2 hours on Al_2O_3 tray or ZrO_2 beads is shown on Figure 4.4.

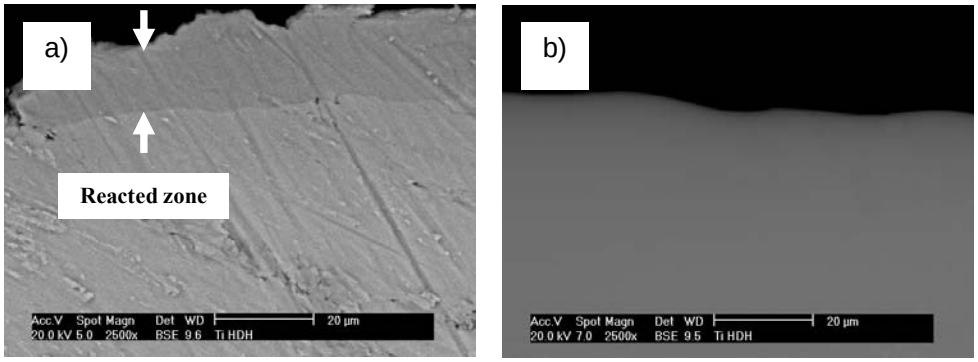

Figure 4.4 – Cross–section of a specimen sintered at 1350°C – 2h on Al_2O_3 plate (a) or ZrO_2 beads (b).

Analysing the backscattering SEM image reported in Figure 4.4 it can be clearly distinguished an interaction zone of approximately 15 µm at the surface of the specimen that was in contact with the Al_2O_3 sintering plate. The surface of the specimens was not characterised by a uniform and well defined layer but by some reacted zones, characterised a darker grey colour, such as the one shown in Figure 4.4 a). Such kind of interaction could not be found when analysing the specimens sintered on zirconia beads (Figure 4.4 b).

EDS characterization, whose results are reported in Figure 4.5, indicates that the reacted zone is characterised by a significant amount of aluminium whose percentage diminishes when moving from the surface towards the centre of the samples.

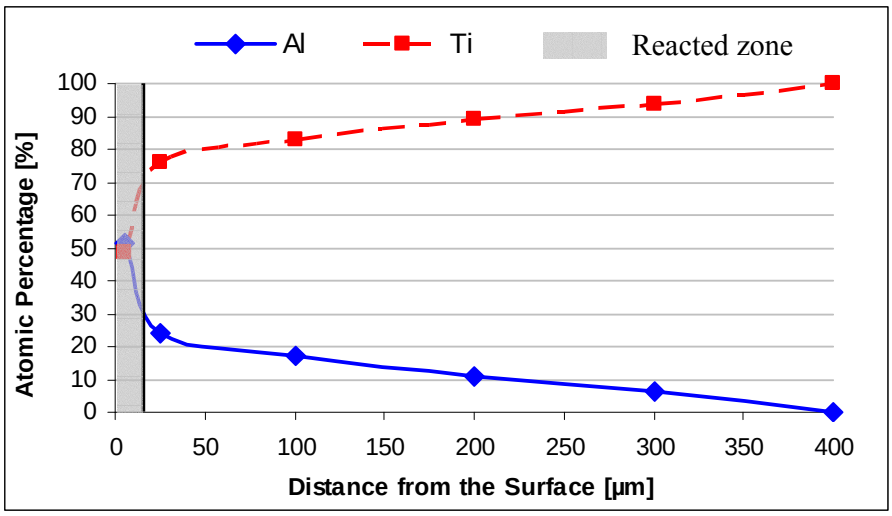

Figure 4.5 – Distribution of the elements as a function of the distance from the surface in contact with the Al_2O_3 plate.

Analysing the data shown in Figure 4.5, it can be seen that the atomic percentage of Al in the reacted zone (labelled by a line) is somewhat higher than 50% and then it halves at already 25 µm from the surface going down to zero at approximately 400 µm.

Bearing in mind that the percentage of aluminium needed to form TiAl intermetallic varies approximately between 49 at.% and 68 at.% at 1350ºC[4], it can be supposed that the diffusion processes that take place can lead to the formation of some intermetallic phases, where a spontaneous reaction that could govern the process is the decomposition of the Al_2O_3 to form more stable compounds[1]:

$$Al_2O_3 + 5Ti \rightarrow 2TiAl + 3TiO \ (G = -126.6 \text{ kJ} < 0)$$

Figure 4.6 shows the results of the relative density for the elemental HDH titanium specimens as a function of the sintering temperature and subdivided, as previously done, between 2 and 4 hour of dwell time.

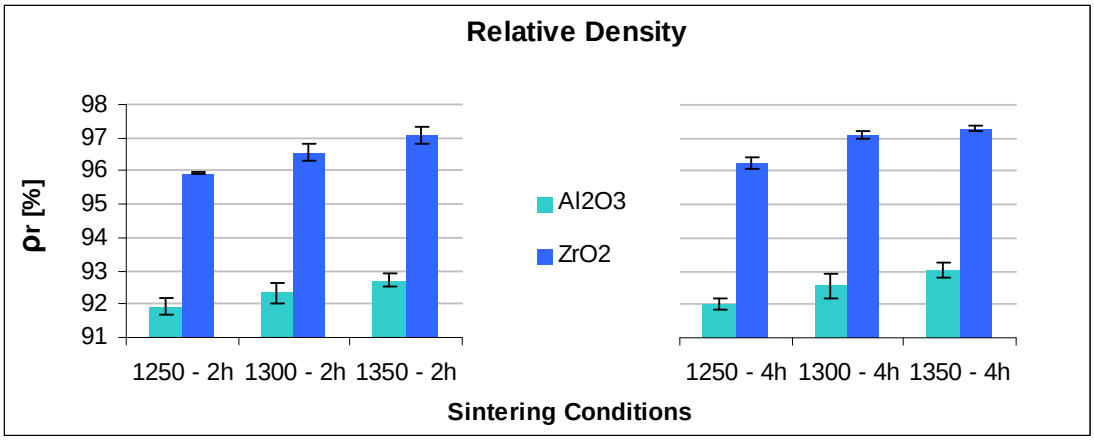

Figure 4.6 – Relative density of the elemental titanium specimens sintered on alumina plate and zirconia beads as a function of the sintering conditions.

Comparing the relative density results obtained (Figure 4.6) it can be noticed that specimens sintered on ZrO_2 have always higher density, approximately 4%, than those sintered on alumina plate, which is in agreement with the shrinkage data.

In both cases, independently of the sintering support and as expected, the density increases with the temperature. From these results it can be seen that the processing time has a much lower influence on the final density than the temperature. Moreover, it should be noted that with the proper sintering tray it is possible to reach relative density values as high as 97% just employing the most conventional P/M process.

Figure 4.7 and Figure 4.8 report the results of the three–point bending tests expressed as maximum bending strength and flexural strain.

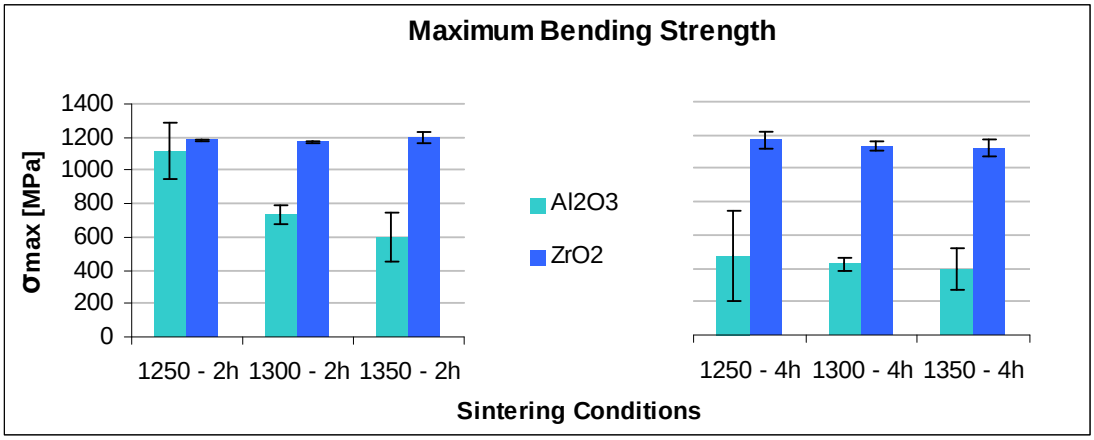

Figure 4.7 – Maximum bending strength of the elemental titanium specimens sintered on alumina plate and zirconia beads as a function of the sintering conditions.

The maximum bending strength (Figure 4.7) of the samples sintered on alumina plate decreases considerably with the temperature, especially for 2 hours of dwell time, and it is significantly lower compared to the resistance of the specimens sintered on ZrO_2 and showing also a larger deviation. Once more, the data shown point out that the interaction that takes place between elemental titanium and the sintering support brittle markedly the material.

Concerning the samples sintered on zirconia, they have almost constant or slight decreasing values of maximum bending strength with the temperature for 2 and 4 hour, respectively, where the maximum bending strength is approximately 1200 MPa. This slight decrease in strength can be most probably attributed to the grain growth induced by the increment of the processing temperature.

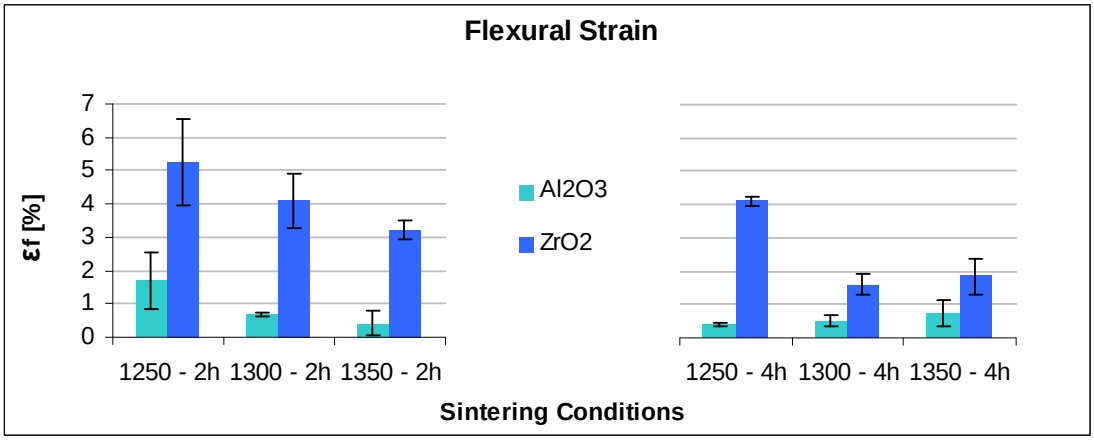

Figure 4.8 – Flexural strain of the elemental titanium specimens sintered on alumina plate and zirconia beads as a function of the sintering conditions.

Flexural strain (Figure 4.8) of elemental titanium samples has a quite curious behaviour since it decreases for 2 hours and increases for 4 hours with the sintering temperature for samples sintered on Al_2O_3 plate and decreases almost continuously for zirconia specimens. However, even if in most of the cases the standard deviation is rather big, samples processed on ZrO_2 always present higher deformation capability, as minimum as double than the strain of the materials sintered on alumina plate, reaching values of 5%.

Figure 4.9 displays the HV30 hardness test result obtained along the cross–section of the specimens sintered under different conditions.

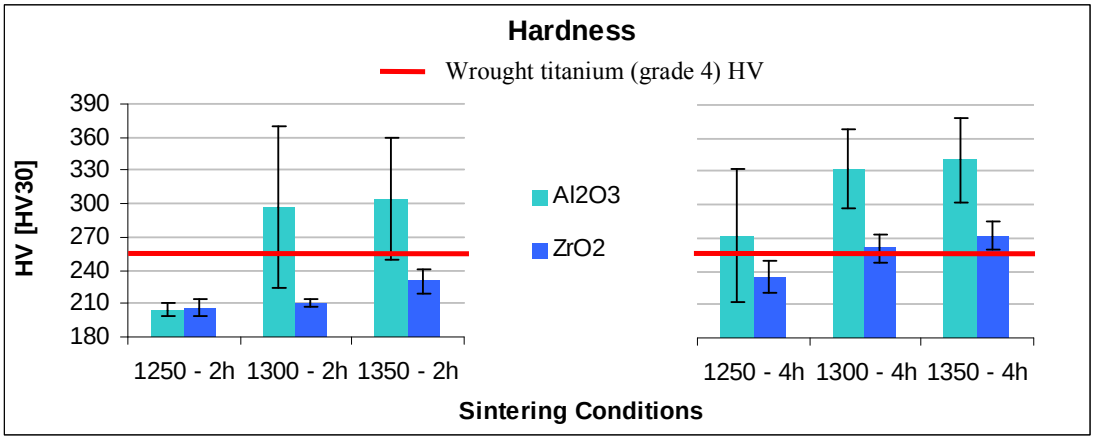

Figure 4.9 – Hardness of the elemental titanium specimens sintered on alumina plate and zirconia beads as a function of the sintering conditions.

Analysing the hardness data (Figure 4.9), it can be seen that the specimens sintered on alumina plate are much harder and their variability is also much bigger. This confirms that the interaction with the Al_2O_3 plate greatly affects the mechanical properties of titanium. However, regardless of the sintering support, the hardness of titanium increases with the processing temperature exactly like the relative density, which is the common behaviour of P/M components. This increment is surely due to the reduction of the residual porosity but could also be due to some oxygen pick–up.

Actually, comparing the hardness of the specimens sintered on zirconia beads, where, theoretically, there was no interaction with the sintering tray, with that of wrought titanium (grade 4), it can be seen that the hardness of the specimens sintered at 1350ºC–4h is somewhat higher, despite of the residual porosity, indicating some contamination.

As it has been said, microhardness $HV_{0.1}$ measurements were taken along the cross–section of the samples in diagonal direction (Figure 4.10–left), thus, performing one measurement on each surface and one on the centre. An example of the typical and representative behaviour found is shown in Figure 4.10, in particular for the specimens sintered at 1250ºC during 4 hours.

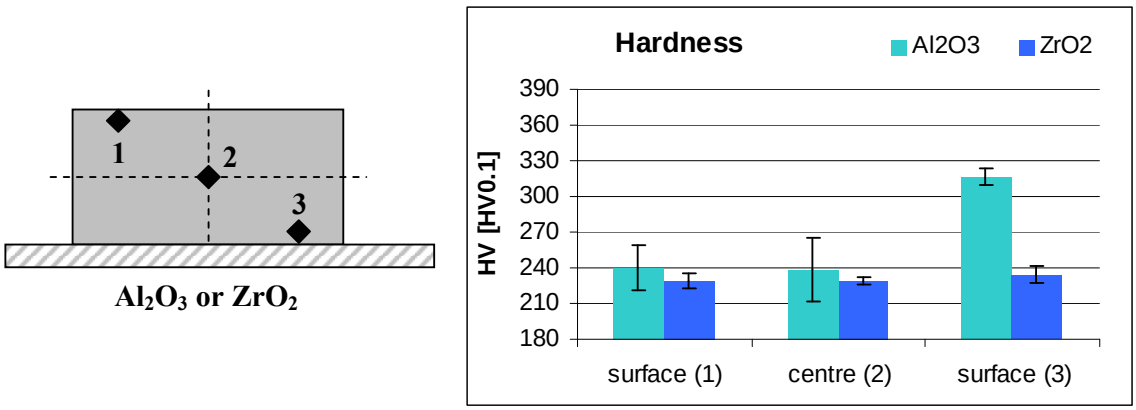

Figure 4.10 – Microhardness of the elemental titanium specimens sintered at 1250ºC–4h on alumina plate and zirconia beads.

As it can be seen in Figure 4.10, the microhardness remains practically constant for the specimens sintered on ZrO_2 beads whereas for specimens sintered on Al_2O_3 plate the microhardness increases significantly on the surface that was in contact with the sintering tray. Moreover, it should be noted that, in general, the specimens sintered on alumina plate have a somewhat higher hardness than those sintered on ZrO_2 beads most probably due to higher amount of oxygen dissolved inside the matrix.

4.1 – PARTIAL CONCLUSIONS

Based on the results obtained it can be stated that the ZrO_2 beads is a good sintering support for powder metallurgy titanium components since it does not react. Conversely, Al_2O_3 plate does not seem to be suitable as sintering support for titanium since it reacts with it forming reacted zones that could easily be TiAl intermetallics.

Furthermore, the results show that using an appropriate sintering support the volume shrinkage is higher as well as almost independent of the sintering conditions, temperature and time, and there is not weight gain as when using a refractory that interacts with the metal.

The final relative density of the specimens is higher, with smaller variability, and the mechanical properties better. With a proper tray, relative density as high as 97%, strength of 1200 MPa, strain of 5% and hardness directly comparable to that of wrought titanium, were obtained in titanium products processed by the simplest P/M technique, pressing and sintering.

Based on the results of this study, the ZrO_2 beads were selected as tray for the sintering step since they do not react with titanium and do not alter the surface of the components.

4.2 – REFERENCES

[1] P. G. Esteban, "Diseño y Procesado por vía Pulvimetalúrgica Convencional de Aleaciones de Ti de Bajo Coste" in *Tesis Doctoral*, Universidad Carlos III de Madrid, 2009

[2] MPIF, "Standard 44, Method for Determination of Dimensional Changes from Die Size of Sintered Metal Powder Specimens", Metal Powder Industries Federation, 1986

[3] ASTM B 610, "Standard Test Method for Measuring Dimensional Change of Metal Powder Specimens Due to Sintering", 2000

[4] J. L. Murray, *Phase Diagrams of Binary Titanium Alloys*, 1st ed, ASM International, pp. 1-345, 1987

CHAPTER 5

PRELIMINARY SINTERABILITY STUDY

A preliminary sinterability study was done in order to analyse the influence of the sintering temperature on the mechanical properties of titanium and titanium alloys. The temperature range selected for this study was chosen on the bases of the dilatometric and thermal analyses described in Chapter 3. Rectangular shaped specimens were prepared by uniaxial pressing using a floating die and zinc stearate as die wall lubricant.

The substrate used to sinter the samples was ZrO_2 beads, as explained in the chapter of the selection of the sintering tray (Chapter 4), and sintering was carried out in a tubular furnace under a vacuum level of approximately 10^{-5} mbar. Heating and cooling rates as well as dwell time during sintering were kept constant at 5°C/min and 2 hours, respectively, and the temperature was ranged between 900°C and 1400°C, every 100ºC.

The specimens were characterised in terms of relative density, dimensional change[1] and microstructure analysis by means of optical and electron microscopy. Moreover, three–point bending tests[2] were performed to determine the maximum bending strength and flexural strain and Vickers hardness was also measured.

Figure 5.1 shows the variation of the volume of the specimens made out from elemental titanium and titanium alloy powders versus the sintering temperature.

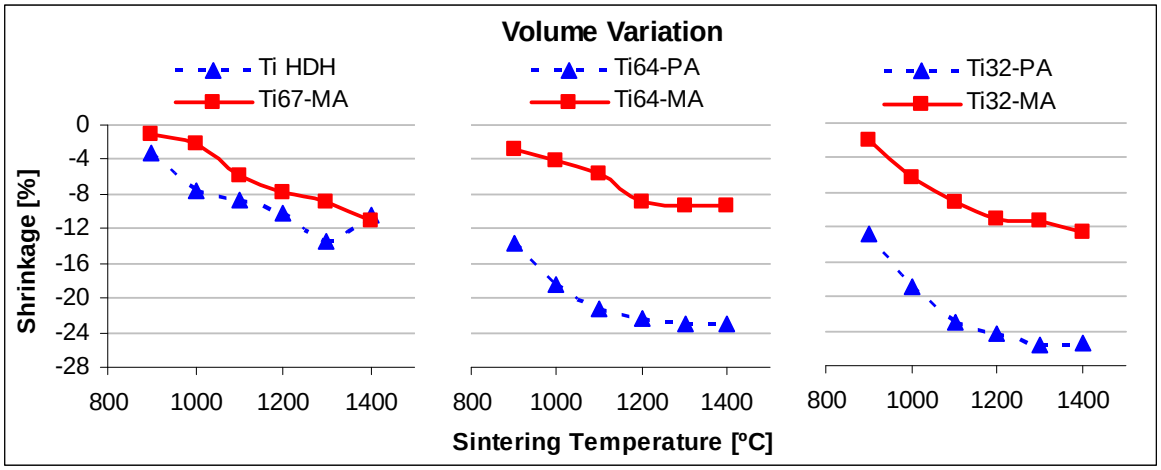

Figure 5.1 – Volume variation as a function of the sintering temperature for elemental titanium and titanium alloys.

The shrinkage of elemental titanium and titanium alloys (Figure 5.1) increases with the sintering temperature but there is a less significant increment when raising the temperature from 1200ºC up to 1400ºC, which could indicate that overcoming this temperature part of the thermodynamic energy supplied is spent to promote grain growth instead of densification.

Moreover, it is interesting to notice that the PA materials show much higher volume shrinkage, as high as 25%, than MA and it is slightly higher for Ti32–PA than for Ti64–PA. This is in complete agreement with the behaviour expected since a lower compaction pressure was used for these alloys and, therefore, a lower green density value corresponds to a higher shrinkage when the material reach the same final relative density. This is owed to the high level of energy available in the system in terms of surface of the powders whose reduction is the driving force of sintering.

One of the most important parameters for P/M products is the relative density obtained after sintering, which, in this case, is plotted versus the temperature for every processed material in Figure 5.2.

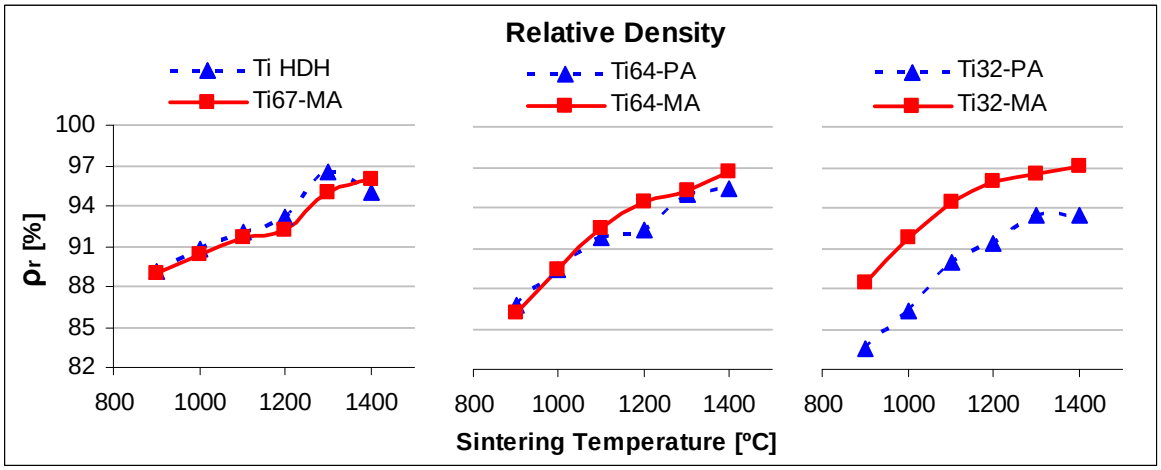

Figure 5.2 – Relative density as a function of the sintering temperature for elemental titanium and titanium alloys.

As expected, the relative density (Figure 5.2) increases with the sintering temperature, reaching the maximum value at the highest temperature. Furthermore, the typical relative density of 95% for Ti P/M samples processed by conventional techniques[3, 4] is reached with each one of the materials processed.

Only for elemental titanium HDH powder, a slightly higher relative density, 96.5% vs 95%, is obtain at 1300°C instead of at 1400°C which could be due to the growth of residual porosity induced by the higher temperature or to some interaction with the sintering tray at 1400ºC.

Usually, titanium alloys produced from master alloys reach higher density compared to those obtained from prealloyed powders. These results are surely affected by the compacting pressure, which was lower for the prealloyed powders, but they agree with the dilatometric study.

Along with the relative density, the hardness of sintered components is another important measurement since it is used as checking parameter due to its non–destructive nature. Figure 5.3 shows the hardness values for each material versus the sintering temperature.

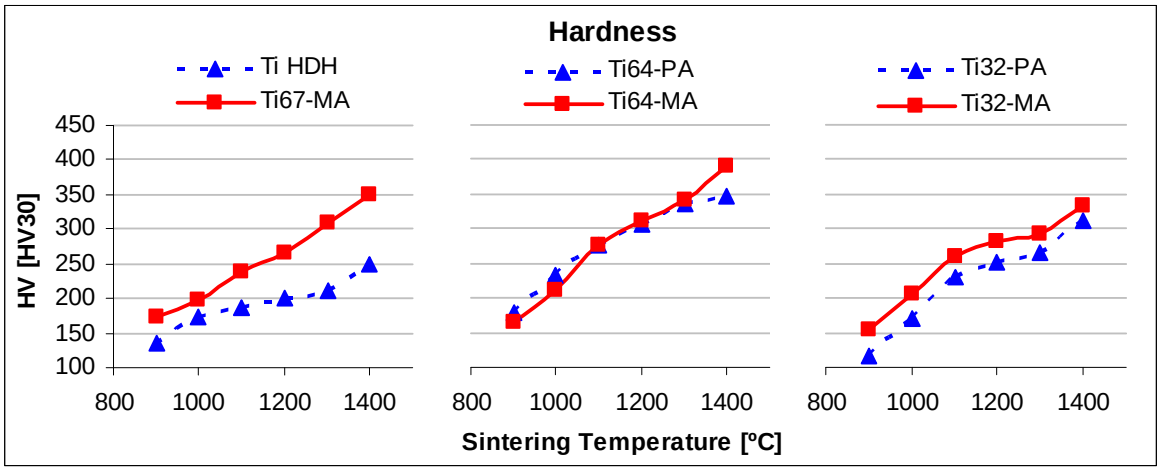

Figure 5.3 – Hardness as a function of the sintering temperature for elemental titanium and titanium alloys.

The hardness (Figure 5.3) increases with the sintering temperature in the same way that the relative density, which is common for components obtained by the P/M route. Moreover, it can be noticed that, as well as for the density, the alloys produced by master alloy reach higher hardness values than prealloyed powders, confirming that this approach is an economical and viable way to obtain cheaper titanium products.

More in detail, elemental titanium reaches the same hardness than wrought titanium grade 3 at a sintering temperature of 1300ºC since the chemical composition is quite similar.

In the case of the Ti–6Al–4V alloy, a hardness similar to that of the wrought alloys (321 HV) is obtained at 1200ºC for both PA and MA powders and then it increases due to the reduction of the residual porosity and to the higher oxygen content of the starting powders, which is approximately the double of the conventional value.

For Ti–3Al–2.5V, a minimum temperature of 1300ºC should be reached to equalize the hardness of wrought materials (267 HV) but at 1400ºC is higher again due to the oxygen percentage.

Ti–6Al–7Nb hardness follows the same trend as the other alloys and it is directly comparable to that of the other α + β alloy (Ti–6Al–4V) but to obtain the typical value of 350 HV found in the literature[5] it is necessary to sinter the powder at 1400ºC.

Figure 5.4 reports the maximum bending strength obtained by the three–point bending test as a function of the sintering temperature for elemental titanium and titanium alloys.

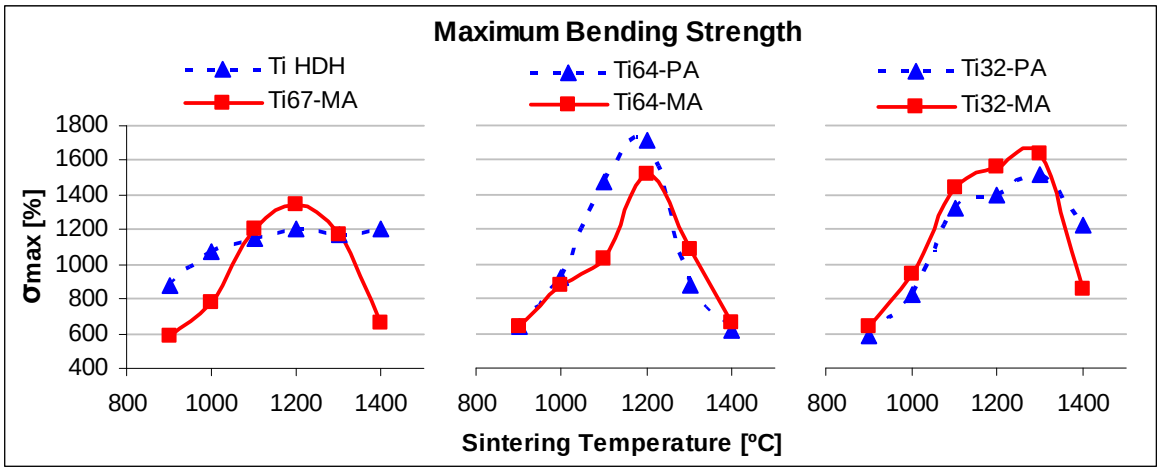

Figure 5.4 – Maximum bending strength as a function of the sintering temperature for elemental titanium and titanium alloys.

Conversely to relative density and hardness, the strength of the sintered materials, which is shown in Figure 5.4, increases with the processing temperature but, overtaking 1200°C for Ti–6Al–4V and Ti–6Al–7Nb or 1300°C for Ti–3Al–2.5V alloys, there is a quite important fall. This is most probably due to the grain growth provoked by the increment of the temperature and the contamination of the specimens.

Once more, elemental titanium powder behaves differently from the alloys since the maximum bending strength increases up to 1200 MPa at 1200°C and, afterwards, it stabilises instead of decreasing, indicating that, most probably, the decrement of the residual porosity is counterbalanced by the grain growth induced by the higher sintering temperature employed.

When comparing the production route, it can be seen that Ti–6Al–4V prealloyed powder show higher maximum bending strength but, on the other hand, Ti32–MA reaches higher resistance than Ti32–PA. This can be explained considering the amount of interstitial elements[6-8] of the starting powder, where Ti64–PA powder has lower oxygen content that Ti64–MA and Ti32–PA has higher percentage of oxygen than Ti32–MA.

From the same three–point bending test, the flexural strain or deformation of the rectangular samples was determined and it is shown in Figure 5.5 as a function of the sintering temperature.

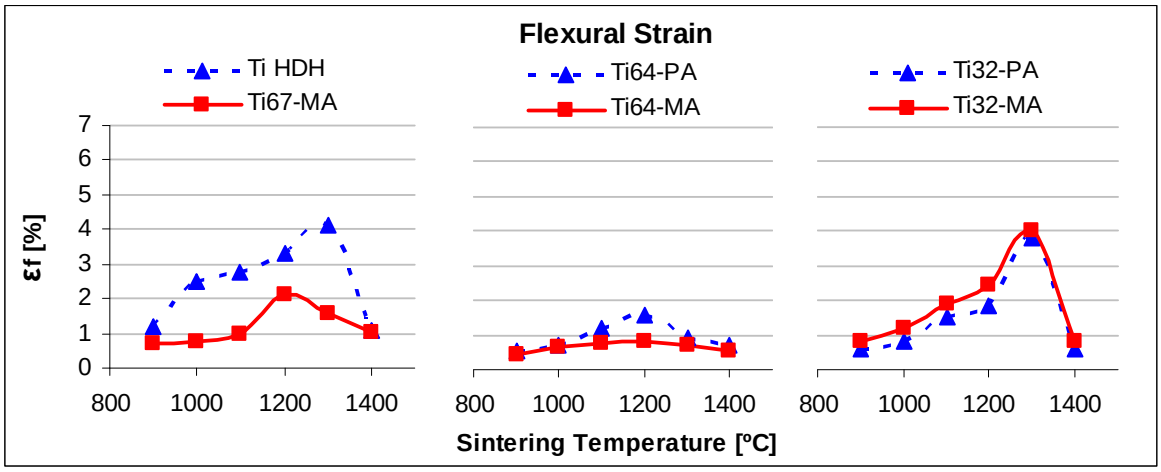

Figure 5.5 – Flexural strain as a function of the sintering temperature for elemental titanium and titanium alloys.

Analysing Figure 5.5 it can be seen that the deformation behaviour of the titanium alloys studied follows the same trend of the maximum bending strength, precisely, it increases with the sintering temperature up to 1200°C for Ti–6Al–4V and Ti–6Al–7Nb alloys and to 1300°C for Ti–3Al–2.5V alloys and then it drops. However, it is interesting to note that the Ti–3Al–2.5V alloy reaches a value of deformation as high as 4% independently of the powder production route.

Concerning elemental titanium, on the contrary to maximum bending strength, the flexural strain increases up to approximately 4% at 1300°C and then it falls significantly instead of stabilising.

As for maximum bending strength, the strain is influenced significantly by the chemical composition where, the lower the oxygen the higher the ductility.

Some representative examples of the microstructure features, in particular the evolution of the residual porosity with the sintering temperature for the Ti64–PA alloy, evaluated by scanning electron microscopy (SEM) in secondary electrons (SE) mode, and microstructure development for the Ti67–MA alloy by SEM in backscattered electrons (BSE) mode are presented in Figure 5.6 and Figure 5.8, respectively.

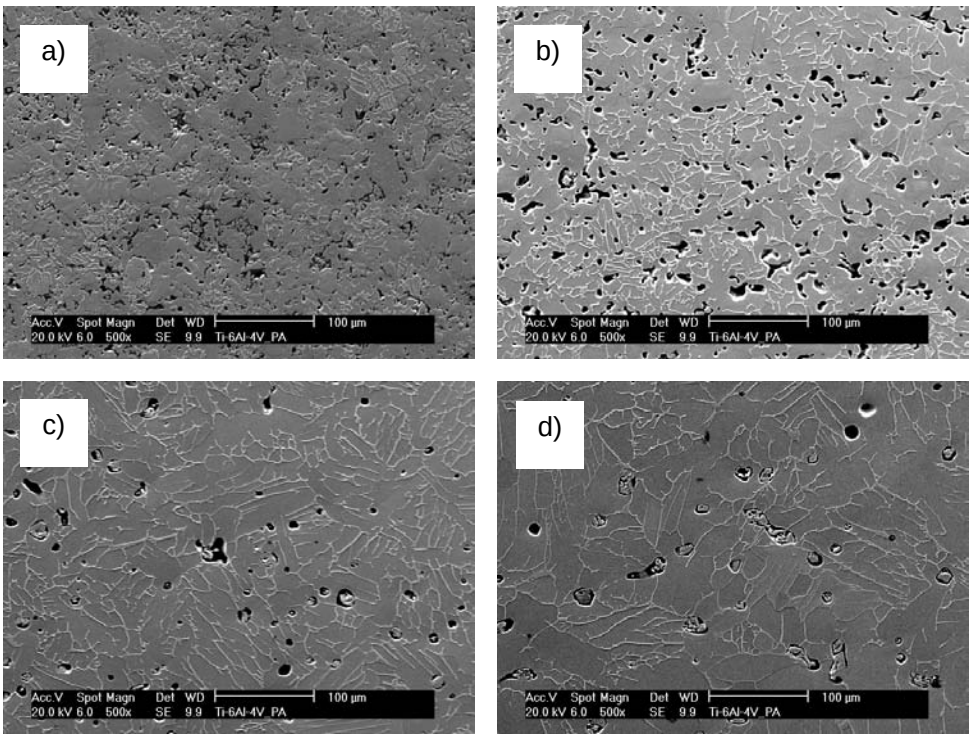

Figure 5.6 – SEM images (SE mode) showing the residual porosity of the samples for the Ti64–PA alloy: a) 900°C, b) 1000°C, c) 1200°C and d) 1400°C.

As it can be seen in Figure 5.6, at 900°C (Figure 5.6 a) the formation of the sintering necks is still under development, the boundaries between different particles are still visible and the porosity is interconnected.

Increasing the temperature up to 1000°C (Figure 5.6 b) the interparticle boundaries are not distinguishable anymore but the residual porosity is mainly still interconnected and mostly irregular in shape.

At 1200ºC (Figure 5.6 c) the microstructure is completely formed, the residual porosity is much lower in percentage, which is in agreement with the relative density measurement, and it is primarily round shaped even if there are some large irregular pores. However, it is worth mentioning that already at 1100ºC the pores are practically isolated.

At 1400°C (Figure 5.6 d) the microstructure is fully developed and the porosity is lower in amount but somehow bigger in size and predominantly spherical in shape and isolated.

The evolution of the microstructure described for Ti64–PA is representative for all the other materials even if it should be noted that for the master alloy addition materials, precisely Ti64–MA, Ti32–MA and Ti67–MA alloys, the interparticle boundaries already disappeared at 1000ºC instead of 1100ºC, as the example for the Ti–3Al–2.5V alloy shown in Figure 5.7 confirms but the composition is not completely homogeneous until 1200ºC.

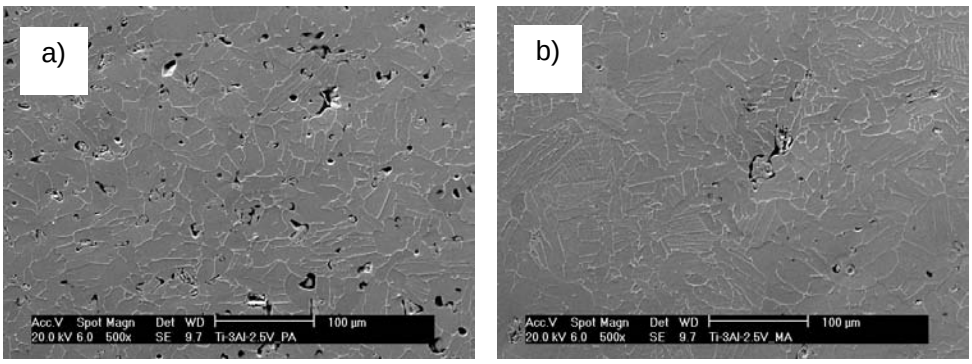

Figure 5.7 – SEM images (SE mode) showing the comparison of the residual porosity between Ti32–PA a) and Ti32–MA b) sintered at 1100°C.

The delay found in the prealloyed powder is most probably due to the lower compacting pressure even thought of the more important percentage of the thermal energy quite surely invested in the diffusion of the alloying elements in the MA powders.

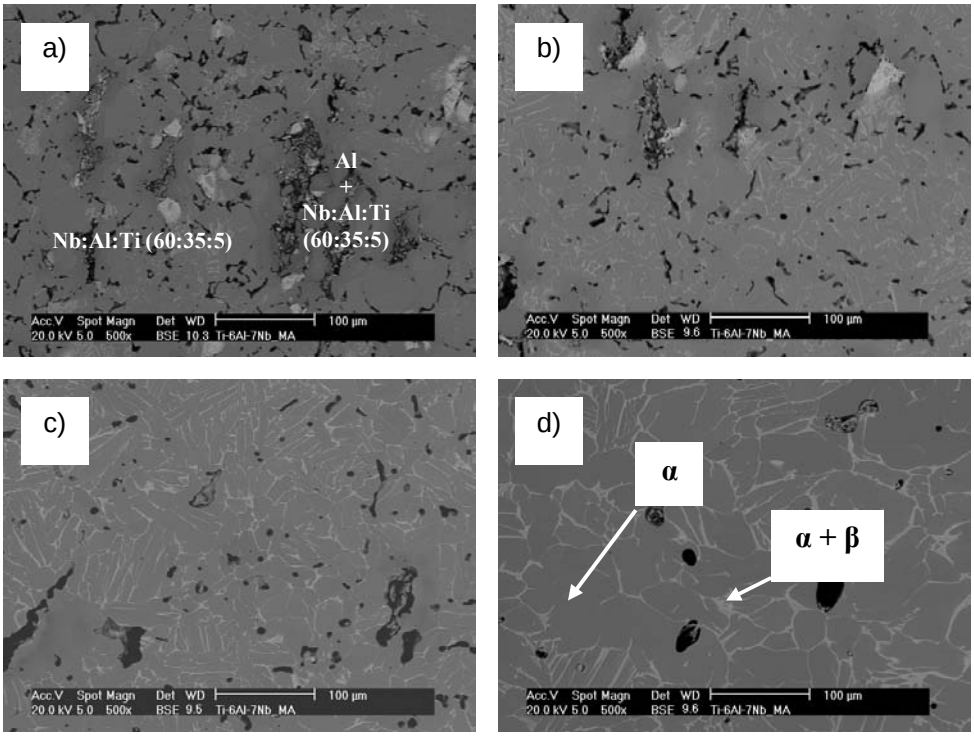

Figure 5.8 – SEM images (BES mode) of the microstructure at different sintering temperatures for the Ti–6Al–7Nb alloy: a) 900°C, b) 1000°C, b) 1100°C and c) 1400°C.

Figure 5.8 a) shows the microstructure of a specimen of the Ti67–MA alloy sintered at 900°C during 2 hours where it can be clearly distinguished the diverse components employed to prepare this alloy: aluminium (dark grey), titanium (grey) and Al:Nb master alloy (bright).

The presence of undissolved elements is due to the temperature and the dwell time that are not high or long enough in order to allow the diffusion phenomena to take place completely. However, there are already some very small islands of α + β lamellae embedded in the alpha matrix even if the beta transus should be approximately 1010°C[6].

Once overtaken 1100°C (Figure 5.8 c), the microstructure seems to be fully developed and composed by α grains and α + β needles even though α grain size at 1400°C is, obviously, bigger since the higher the temperature the higher the energy available for grain growth.

The same behaviour is worth for the other titanium alloys where EDS analysis indicates that for MA powders it is necessary to reach 1200ºC to allow to the diffusion phenomena to take place completely whereas for PA powders, at 1100ºC the microstructure is wholly homogenous.

To better understand the behaviour of the powders considered during the sintering step and to confirm the microstructural analysis results, the specimens were analysed by means of XRD and the results are presented as patterns in Figure 5.9 to Figure 5.14.

As it can be seen in Figure 5.9, the only phase that was found either in the elemental powder or in the sintered samples is the alpha phase as expected since this material does not have any alloying element that stabilises the beta phase at room temperature and the contaminants, precisely oxygen, nitrogen and carbon, are alpha stabilisers.

The main phase found during the XRD analysis of the Ti64–PA alloy (Figure 5.10) is the alpha phase even thought some beta phase and some aluminium/vanadium phase, precisely Al_2V_3, were detected in the prealloyed powder and in the components sintered at 900°C. This last compound is most probably due to the preparation of the powder by the HDH process and could have been added by the supplier to adjust the final composition. Moreover, the presence of the beta peak already in the powder or the specimens sintered at 900°C, temperature below the beta transus for this alloy, indicates that, actually, the alloying elements are already partially dissolved into the titanium matrix.

Regarding the Ti64–MA alloy (Figure 5.11), in the powder it could be identified all the elements used to prepare it. More in detail, titanium alpha phase, due to the elemental HDH titanium powder, elemental aluminium, and aluminium/vanadium phases labelled as Al_2V_3 due to the master alloy employed during the production of the powder are found. It is worth mentioning that the main peak of aluminium coincides with the second most intense peak of the alpha phase (002 at 38.4º). This is the reason why the relative intensity of the main peak of α phase (101 at 40.1º) is not the highest as for the sintered specimens. At 900°C the elemental aluminium peaks disappear but some Al_2V_3 is still detectable, confirming that this temperature is not high enough in order to promote the complete diffusion of the alloying elements. It is interesting to notice that not any titanium aluminates (Ti_3Al, TiAl or $TiAl_3$) was detected at any of the sintering temperature studied even if titanium reacts with elemental aluminium at 660ºC as found during DTA analysis (Figure 3.18).

As it can be seen in Figure 5.12, the Ti–3Al–2.5V alloy produced by mixing elemental titanium and Ti–6Al–4V prealloyed powder is composed by the same phases found in the Ti64–PA, precisely α and β titanium and some Al_2V_3 compound. Once again, when the Ti32–PA powder is sintered at 900ºC, the Al_2V_3 could be detected but then disappears when increasing the sintering temperature.

The XRD analysis of the Ti32–MA powder (Figure 5.13) identifies the elements that composed the powder itself; alpha titanium, due to the elemental HDH titanium powder, elemental aluminium, which was added to obtain the desired composition, and a Al_2V_3 phase due to the master alloy employed and no titanium aluminates were found.

As for the other master alloy addition powders, in the XRD pattern of the Ti67–MA powder (Figure 5.14) it is possible to identify the components employed during its preparation and precisely they are elemental titanium (alpha), elemental aluminium and a Al:Nb master alloy identified as $AlNb_2$ phase. The XRD pattern of the Ti–6Al–7Nb alloy sintered at 900ºC confirms that this temperature does not guarantee a complete diffusion of the alloying elements since the relative peak of the alloying elements are still detectable by X–rays. As already found in the other master alloy addition powders, even if DTA analysis reveals that elemental titanium reacts exothermically with the melted aluminium at a temperature of 660ºC no titanium aluminates were found during the XRD analysis.

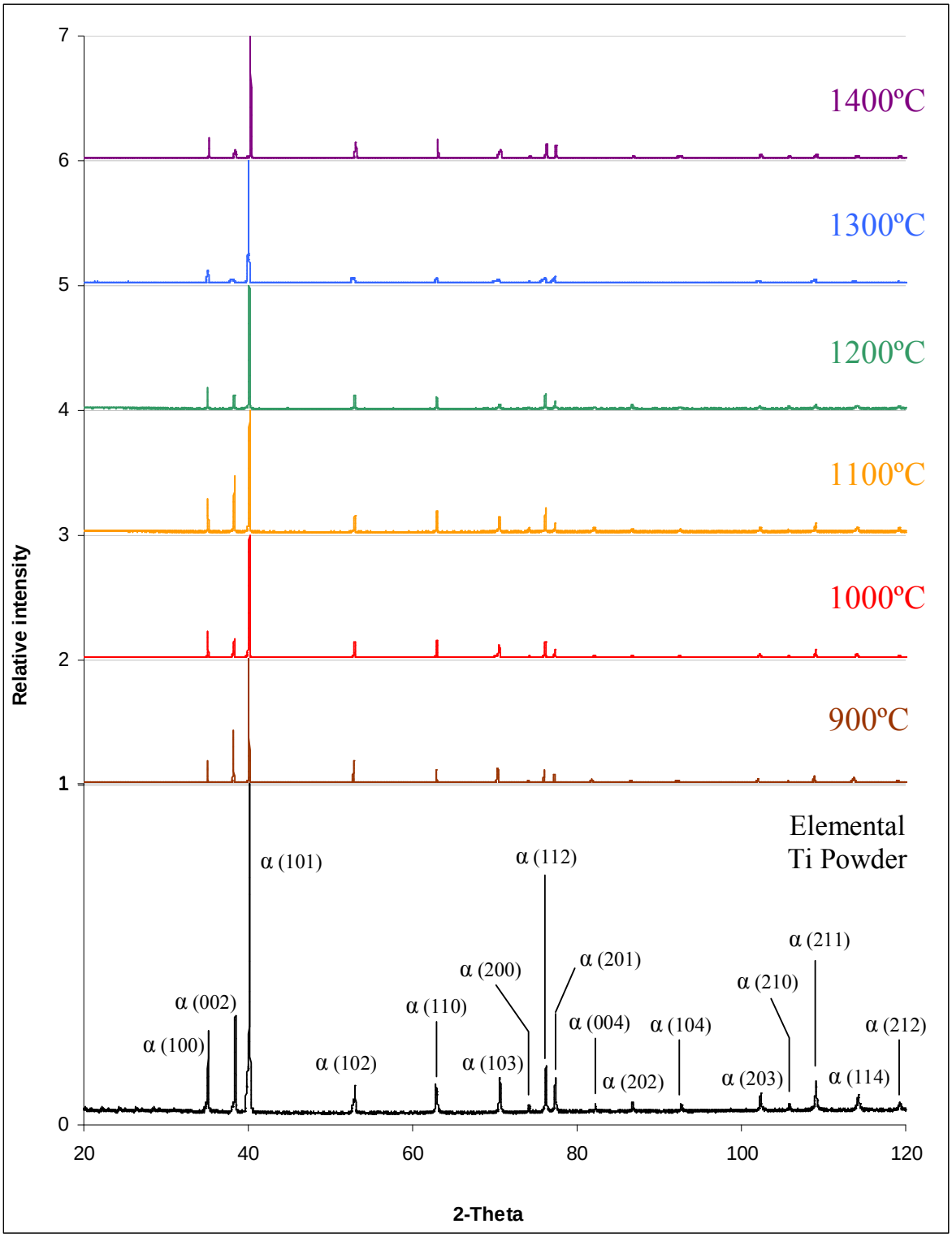

Figure 5.9 – XRD patterns for elemental titanium powder and specimens sintered at different temperatures.

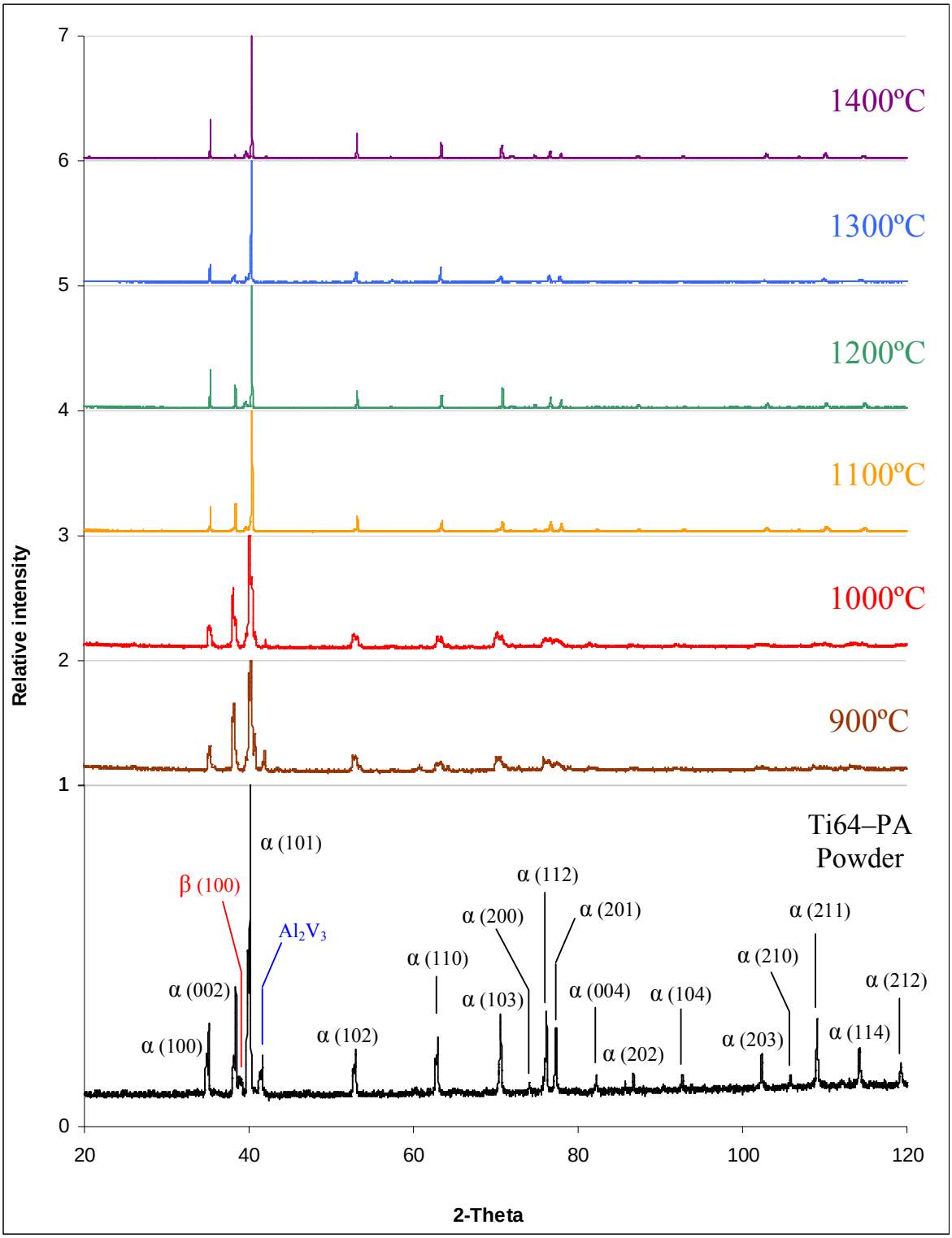

Figure 5.10 – XRD patterns for the Ti64–PA powder and specimens sintered at different temperatures.

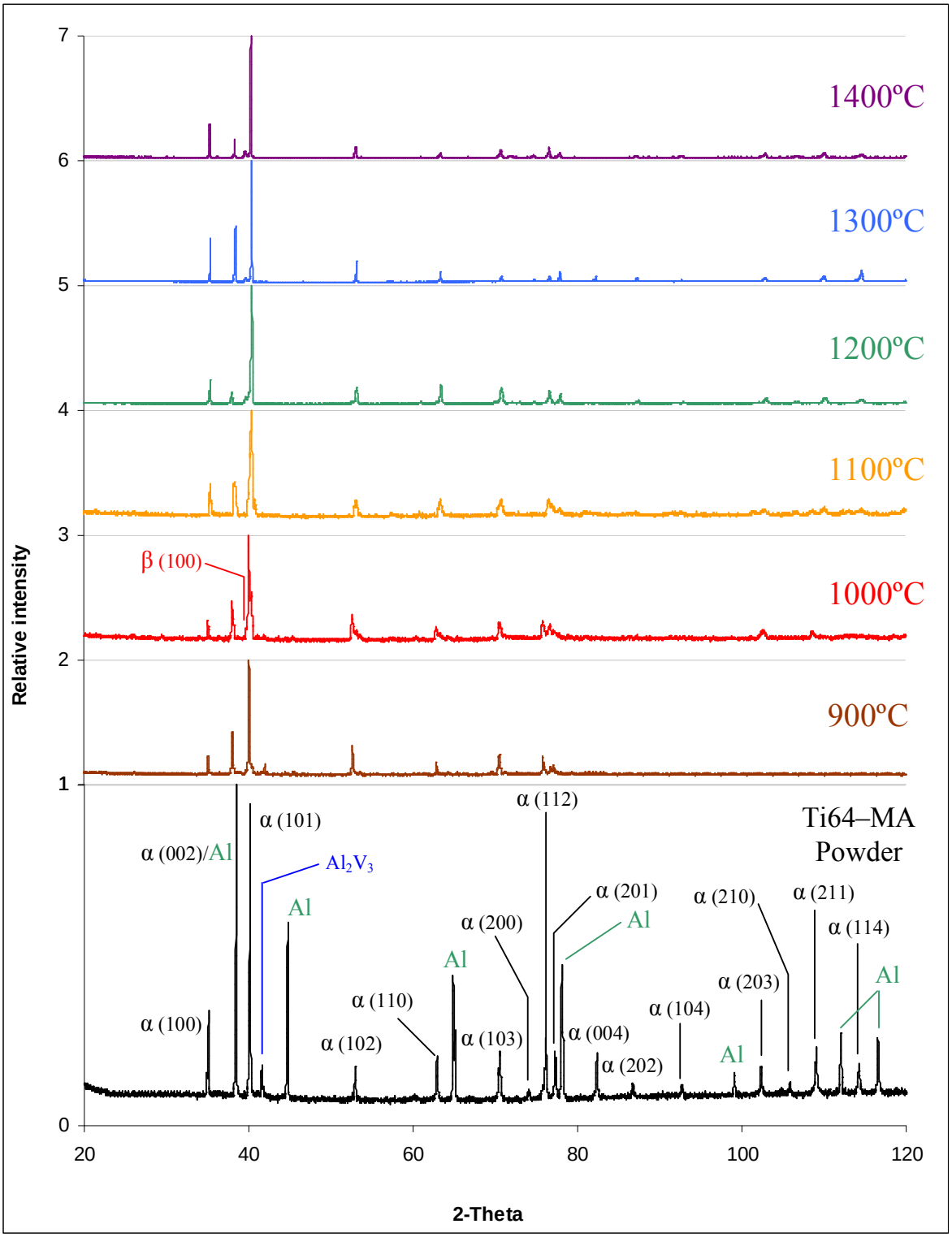

Figure 5.11 – XRD patterns for the Ti64–MA powder and specimens sintered at different temperatures.

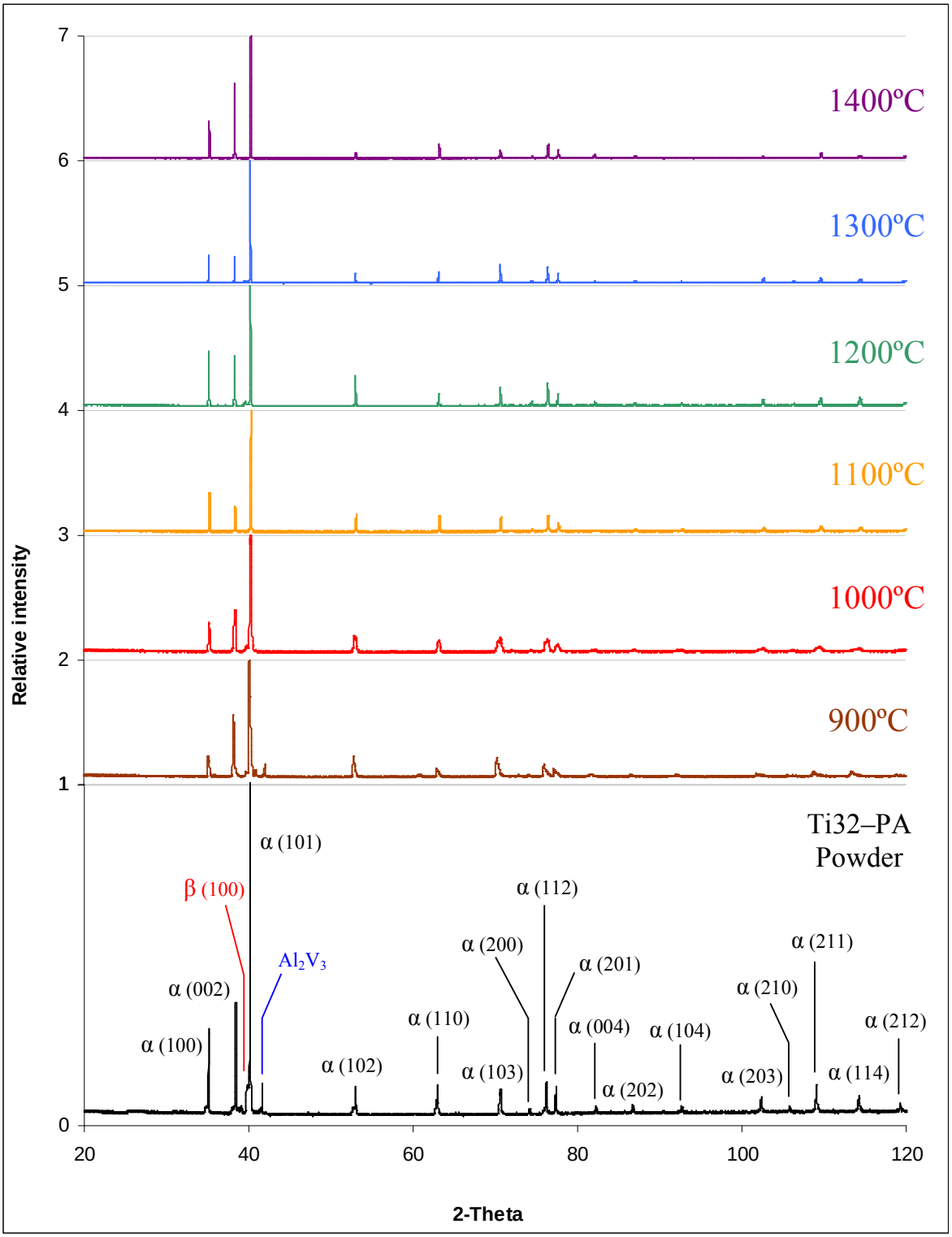

Figure 5.12 – XRD patterns for the Ti32–PA powder and specimens sintered at different temperatures.

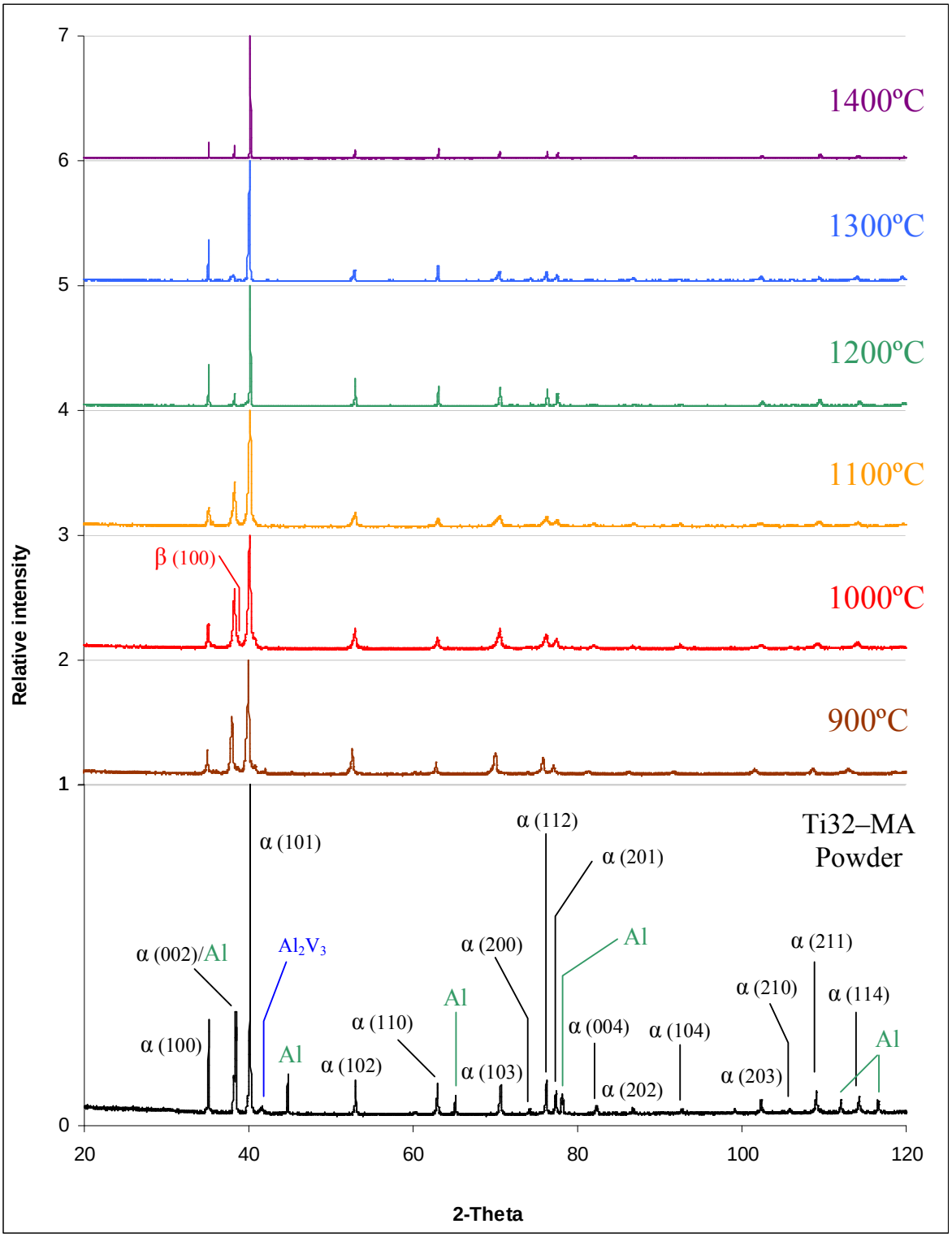

Figure 5.13 – XRD patterns for the Ti32–MA powder and specimens sintered at different temperatures.

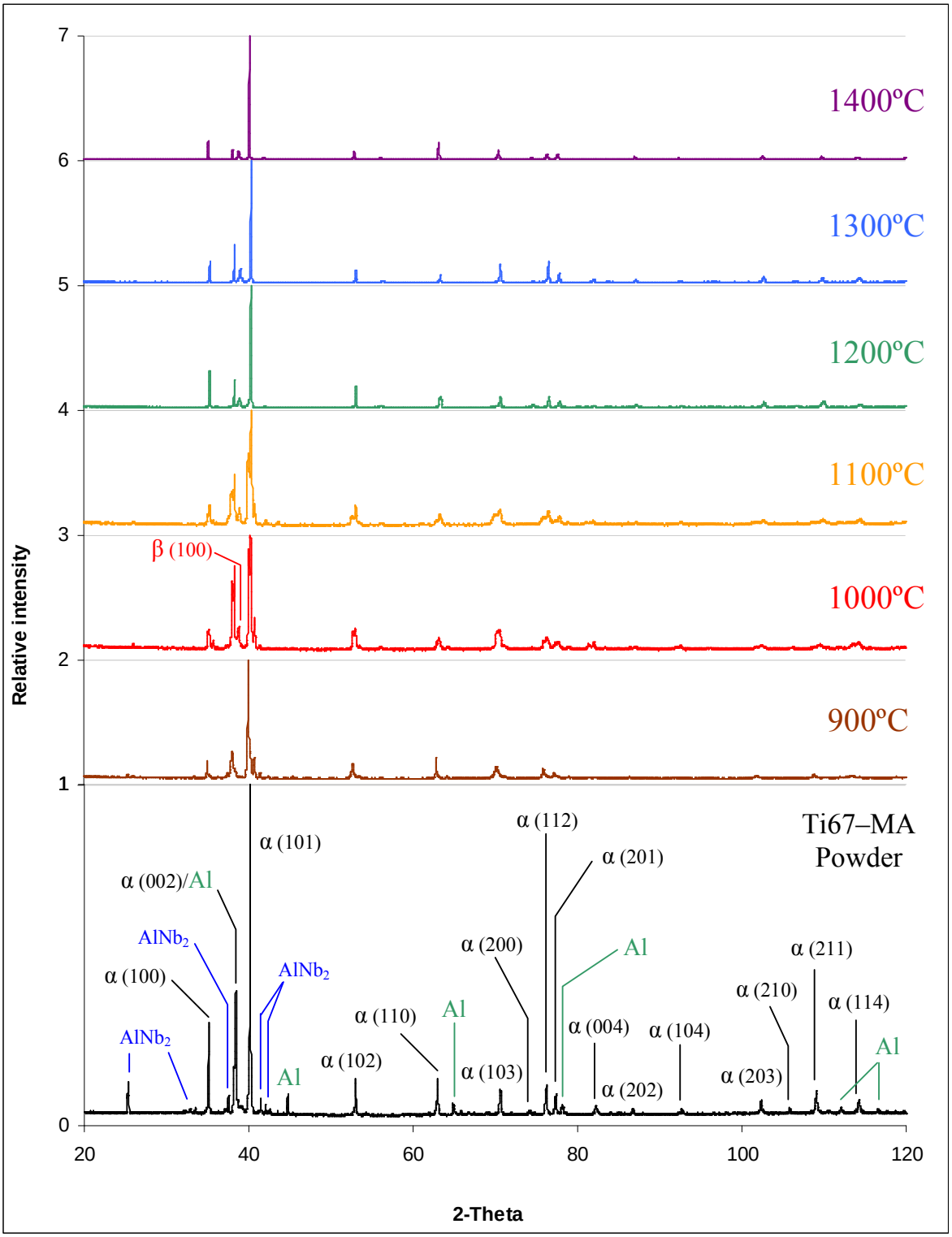

Figure 5.14 – XRD patterns for the Ti67–MA powder and specimens sintered at different temperatures.

5.1 – PARTIAL CONCLUSIONS

The results obtained in this study indicate that the employment of the simple pressing and sintering P/M route is a viable way to produce titanium and titanium alloy components with good properties.

Moreover, the utilization of the cheaper master alloy addition approach allows to attain slightly higher relative density and, therefore, higher hardness values compared to the prealloyed powders.

Concerning the mechanical properties studied, the maximum bending strength and the flexural strain, it was found that these characteristics increase with the sintering temperature up to a specific temperature for each material but then they drop. This is most probably due to a combined effect of the grain growth induced by the raising of the sintering temperature and the increment of interstitial elements like oxygen and nitrogen.

The residual porosity and microstructure analysis carried out by SEM reveals that a minimum temperature of 1100ºC or higher, even if this varies for each titanium alloy powder, is needed in order to obtain a fully developed microstructure and to allow the diffusion phenomena to take place completely. This statement is further confirmed by the XRD analysis which identifies the phases which correspond to the master alloys employed below this specific temperature.

Based on the results of this preliminary sinterability study, the sintering temperature range was narrowed around the sintering temperature of 1300ºC, which permits to obtain relative density of approximately 94%, the highest maximum bending strength and flexural strain as well as a homogenous microstructure, to study the influence of the sintering time whose results are discussed in Chapter 6.

5.2 – REFERENCES

[1] MPIF, "Standard 44, Method for Determination of Dimensional Changes from Die Size of Sintered Metal Powder Specimens", Metal Powder Industries Federation, 1986

[2] MPIF, "Standard 41, Determination of Transverse Rupture Strength of Powder Metallurgy Materials", Metal Powder Industries Federation, 1991

[3] S. Abkowitz and D. Rowell, "Superior Fatigue Properties for Blended Elemental P/M Ti-6Al-4V", *Journal of Metals,* pp. 36-39, 1986

[4] F. H. Froes, et al., "Cost–effective Synthesis of Ti–6Al–4V Alloy Components via the Blended Elemental P/M Approach" in *Symposium on TMS Symposium on High Performance Metallic Materials for Cost Sensitive Applications*, Seattle, WA, 2002

[5] M. Semlitsch, et al., "Fifteen Years Experience with Ti-6AI-7Nb Alloy for Joint Replacements" in *Titanium '95: Science and Technology*, Birmingham - UK, pp. 1742-1759, 1995

[6] RMI, "Titanium Company: Titanium Alloy Guide", *available at: http://rtiintl.s3.amazonaws.com/RTI-Reports/tiguideWeb.pdf,* 2000

CHAPTER 6

RESULTS AND DISCUSSION

In this chapter the main results obtained through the development of this thesis are reported and discussed. The results are presented as a function of the materials studied and the processing methods employed as sketched in Figure 6.1.

As it can be seen in Figure 6.1, each material was processed by means of four P/M techniques: uniaxial pressing and sintering (P&S), conventional hot–pressing (HP) and inductive hot–pressing (IHP) for shaping of powders and hot isostatic pressing (HIP) as post–processing method of sintered components.

The P&S route was designed based on the results of the preliminary sinterability study described in Chapter 5. The sintering temperature is narrowed to the 1250–1350ºC temperature range to study the influence of the sintering time (2 and 4 hours).

Rectangular samples with normalised dimensions for the three–point bending test were produced by uniaxial pressing at the respective optimum pressing pressure (Chapter 3) and vacuum sintered in the conditions mentioned above. This type of samples is preferred to the tensile test specimen due to the lower quantity of powder used.

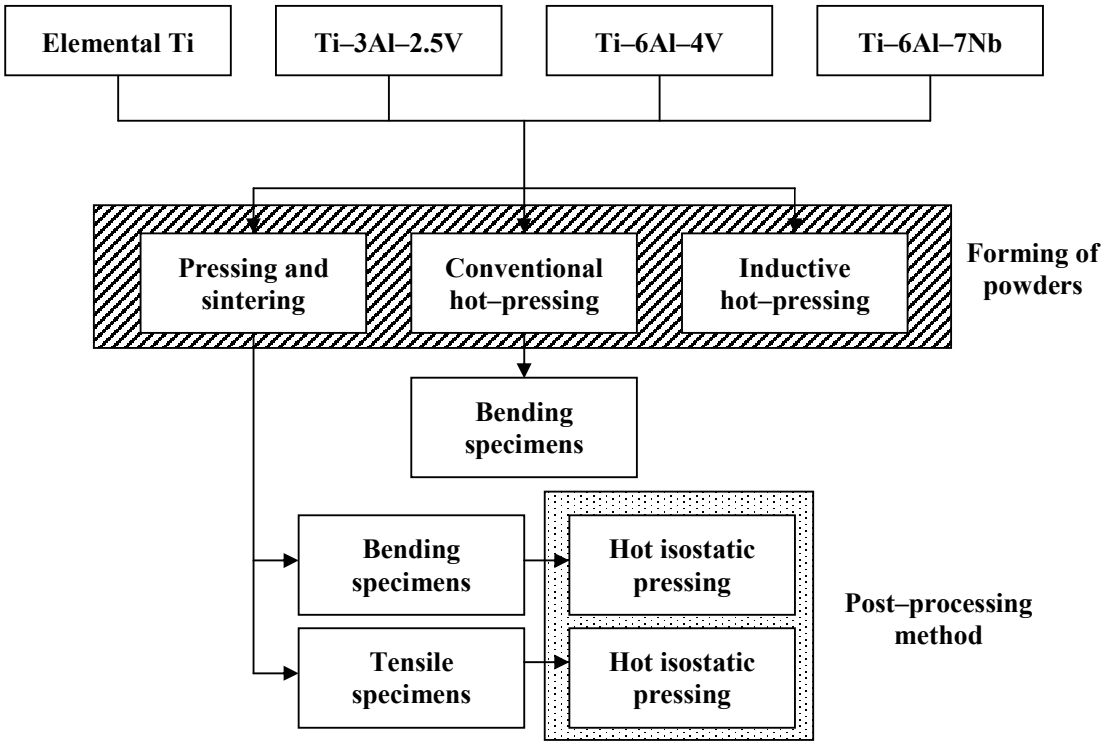

Figure 6.1 – Scheme showing the titanium alloys studied and the powder metallurgy techniques considered for their consolidation.

After the characterisation of the samples, the best conditions of sintering were identified and used to produce tensile test specimens, whose results (tensile strength and strain) are much more important for industries and could be compared to those of the respective wrought materials.

Both bending and tensile test samples were post–processed by HIP with the aim to reduce the residual porosity as well as study the influence of temperature, time and pressure on the final properties of the materials.

The other processing routes are HP and IHP (Figure 6.1), where temperature and pressure are applied simultaneously using a direct high–temperature resistance heating system or an inductive heating system. Due to the respective dimensions of the specimens obtained, just in the case of conventional hot–pressing, three–point bending test samples could be manufactured and the relative mechanical properties measured.

6.1 – ELEMENTAL TITANIUM

In this section the results concerning elemental titanium (powder produced by the HDH method) are reviewed and they will be kept as a reference for the titanium alloys developed starting from this elemental powder.

Where possible, the results obtained will be compared to those of other authors that work with elemental HDH titanium powder and P/M processes or, alternatively, to those of wrought titanium. Nonetheless, it is worth mentioning that the majority of the researches available were carried out in the 80s of the XX century using elemental titanium sponge powders to produce the Ti–6Al–4V alloy but without studying the properties of elemental titanium, as explained in Section 1.4.

6.1.1 – Uniaxial Pressing and Sintering (P&S)

6.1.1.1 – Relative Density

The density of sintered specimens, expressed as relative density, measured in three–point bending test samples or in tensile test specimens are displayed in Figure 6.2.

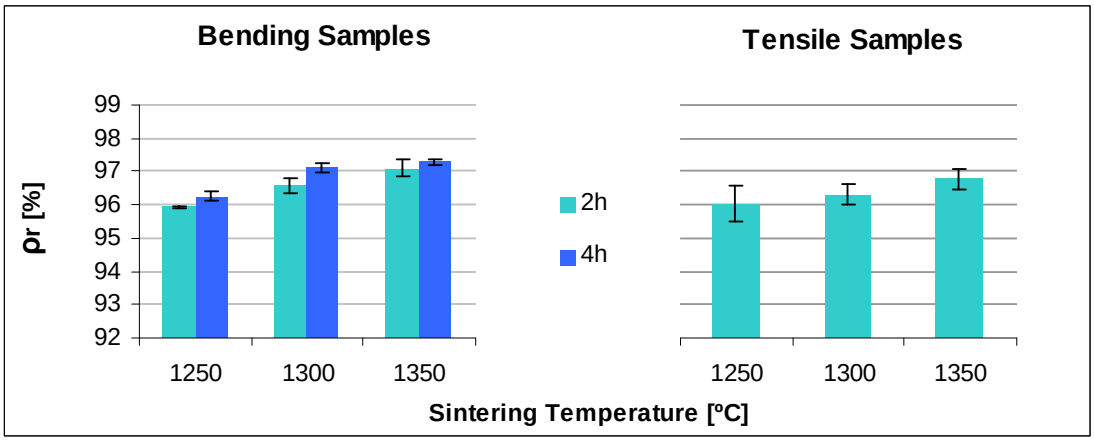

Figure 6.2 – Relative density as a function of the sintering temperature and time for elemental titanium specimens: bending (left) and tensile (right).

Generally speaking, the relative density of three–point bending test samples (Figure 6.2–left) increases with the sintering temperature and it is higher for longer dwell time. The maximum values obtained are the typical for conventional P/M processes (cold uniaxial pressing and sintering), approximately 95% for titanium alloys[1], and there is a stronger effect of the processing temperature on final density compared to the time.

The results shown in Figure 6.2 agrees with that found during the study of the influence of the sintering temperature (see Figure 5.2) and reveals that doubling the sintering time from 2 hours to 4 hours does not increase the relative density that much to justify the higher production cost which results from a prolonged processing time. That is why tensile test samples were sintered considering exclusively 2 hours of dwell time at maximum temperature.

Comparing the relative density value of tensile test specimens (Figure 6.2–right) with the bending ones (Figure 6.2–left), it can be noticed that they are similar, which was expected since the same powder was compacted at the same pressure (Table 3.14) and sintered under the same conditions, or a little bit lower indicating a possible effect of the geometry and size of the components to be produced. Since the green density of tensile specimens (84.77% ± 0.83%) is a little bit higher with respect to that of rectangular samples (83.16% ± 0.33%), it can be stated that "dogbone" specimens experience slightly lower densification.

A relative density of 95.5 % was obtained by Wei et al.[2] using an elemental HDH titanium powder (mean size 56 μm) sintered at 1250ºC during 3 hours in high vacuum, and by Friedman[3] using a sponge fines powder sintered in the range 1200–1260ºC (2–4 hours).

El Kadiri et al.[4] obtained a relative density of 91.8% when sintering HDH elemental titanium powder at 1275ºC during 60 minutes. Considering that they used a powder with lower particle size (45 μm) which, theoretically, should favour the sintering step due to the greater surface area but reached lower relative density, it seems that 2 hours of soaking time is a good compromise between the final relative density and the production costs.

6.1.1.2 – Chemical Analysis

It is well known that the mechanical properties of titanium are highly influenced by the percentage of interstitial elements and, in particular, oxygen, nitrogen and carbon harden, strengthen and brittle titanium[5-7].

In this case, the oxygen and nitrogen content were considered, since no significant differences in terms of carbon content were found, and the results are shown in Figure 6.3 and Figure 6.4 for bending and tensile specimens, respectively.

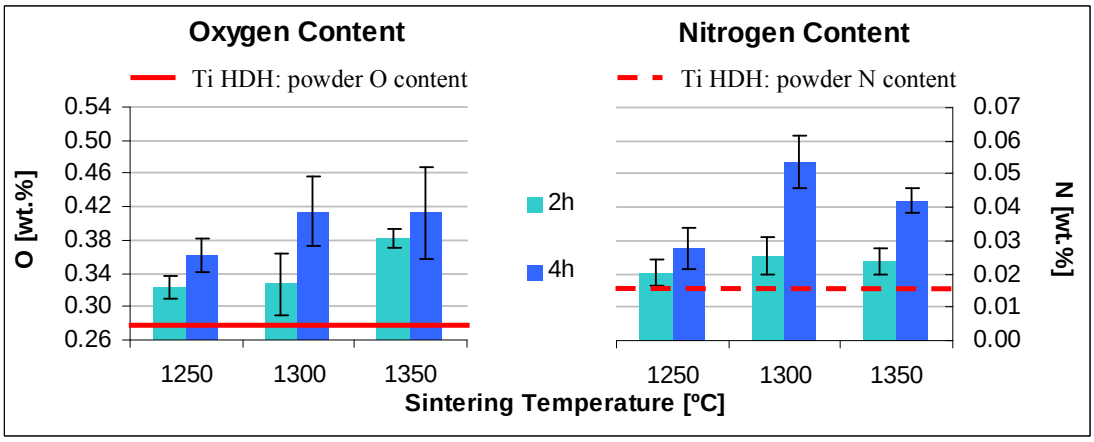

Figure 6.3 – Chemical analysis as a function of the sintering temperature and time for elemental titanium bending specimens: oxygen (left) and nitrogen (right).

As it can be seen in Figure 6.3, there is some contamination with oxygen as well as nitrogen with respect to the initial powder content which can be attributed both to the handling of the powder and the air trapped into the green samples. Moreover, both oxygen and nitrogen percentage increases with the sintering temperature or time revealing that this step greatly influences the final composition either because it allows the contaminants adsorbed on the surface to diffuse inside the material or because it promotes contaminants pick–up from the walls of the furnace.

However, for many of the processing conditions studied, the final composition of the samples fits the oxygen and nitrogen limit specified for wrought titanium grade 4[8].

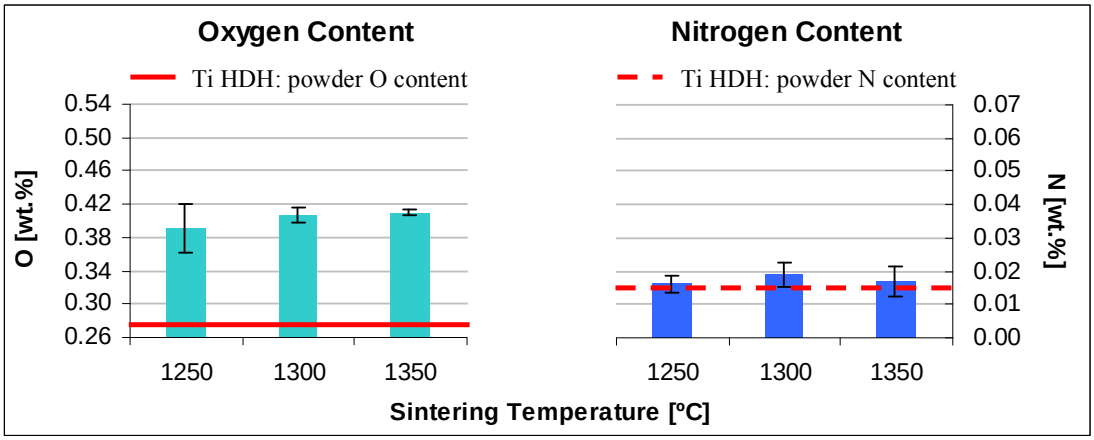

Figure 6.4 – Chemical analysis as a function of the sintering temperature and time for elemental titanium tensile specimens: oxygen (left) and nitrogen (right).

Analysing the data shown in Figure 6.4, it can be seen that there is a significant oxygen pick–up compared to the initial amount of the powder and almost no variation in terms of nitrogen content.

When compared to bending samples (Figure 6.3), oxygen content shown in Figure 6.4 is somewhat higher and nitrogen slightly lower. Given that a greater amount of powder is used to produced tensile specimens, this could be due to the oxygen adsorbed onto the powder particles coupled with the greater affinity of titanium for oxygen than for nitrogen and the slower diffusion rate of nitrogen in elemental titanium than oxygen[5].

Since oxygen content is approximately 0.40 wt.% and nitrogen lower than 0.05 wt.%, the tensile elemental titanium sample can be classified as elemental titanium grade 4[9] and, therefore, the mechanical properties obtained will be compared with that of wrought grade 4.

6.1.1.3 – Hardness

The results of the HV30 hardness measurements carried out are shown in Figure 6.5 for both bending and tensile specimens.

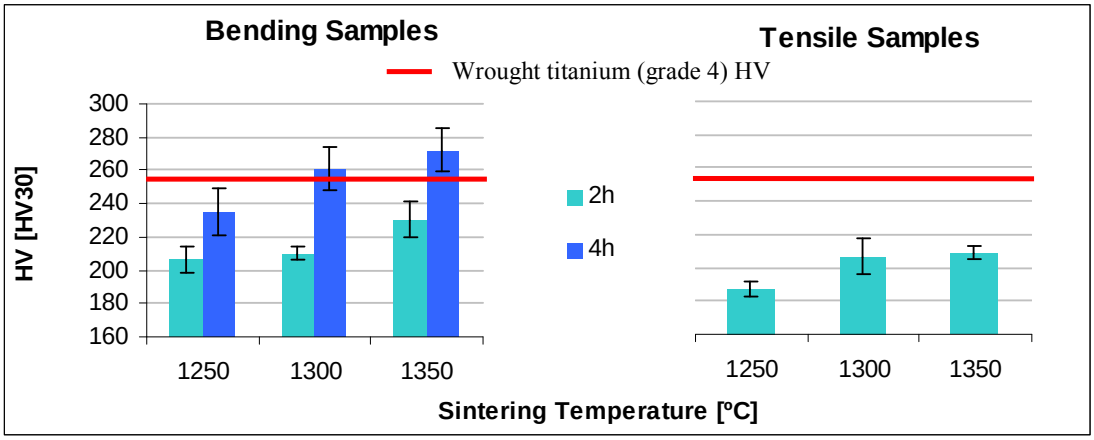

Figure 6.5 – Hardness as a function of the sintering temperature and time for elemental titanium specimens: bending (left) and tensile (right).

As for the relative density, the hardness of P/M elemental titanium (Figure 6.5) increases either with the sintering temperature and time but, conversely to relative density, for hardness results is the dwell time that seems to influence more the final hardness.

Comparing hardness values for tensile and bending samples, the former are somewhat lower most probably due to the slightly difference in terms of relative density and level of contamination found, especially nitrogen which has a stronger hardening effect than oxygen[5-7].

It should also be pointed out that, in most of the cases, the hardness values obtained are to some extent lower compared to the hardness of wrought titanium grade 4 on annealed state (253 HV)[10] and only in the case of sintering at 1300ºC or 1350ºC during four hours they are equal.

As the mechanical properties of titanium highly depend on the percentage of interstitial elements, the equivalent oxygen content was calculated employing the equation proposed by Okazaki and Conrad[11], which was discussed in the Section 2.7 (see Eq. 14). The hardness versus the equivalent oxygen content is presented in Figure 6.6 for bending samples.

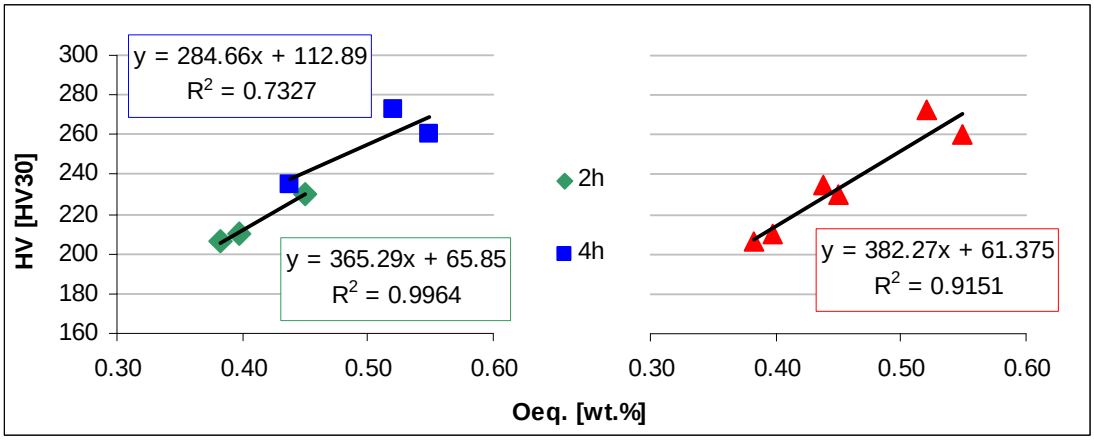

Figure 6.6 – Hardness as a function of equivalent oxygen content for elemental titanium bending specimens: for diverse sintering times (left) and general trend (right).

The hardness of elemental titanium produced using a HDH powder processed by pressing and sintering increases with the equivalent oxygen content for both the processing times analysed (Figure 6.6–left) and it can be described by a linear correlation where this last is much more suitable for 2 hours of dwell time being the coefficient of determination R^2 almost 1.

The discrepancy from the linear behaviour of the 4 hours dwell time specimens could be primarily due to three factors: level of contamination, mean alpha grain size and porosity (size and percentage). In particular, the increment of the sintering temperature and time, generally, induces an increment of the mean alpha grain size as well as the coarsening of the pores as explained later on (see Section 6.1.1.6).

Regarding the general trend of the hardness with the total amount of interstitials (Figure 6.6–right), where the data available are considered independently of the sintering parameters, it can be seen that there is a very good linear correlation between the hardness and the interstitials content, with a coefficient of determination R^2 higher than 0.9.

6.1.1.4 – Properties from Bending Test

The typical bending stress–strain behaviour of elemental titanium samples sintered under diverse conditions and tested by the three–point bending test is represented in Figure 6.7 in terms of bending stress versus flexural strain.

Normally, the results of the three–point bending test are represented as load versus deflection; however, in this case, it has been chosen to consider the stress–strain behaviour to allow the direct comparison between different processing conditions.

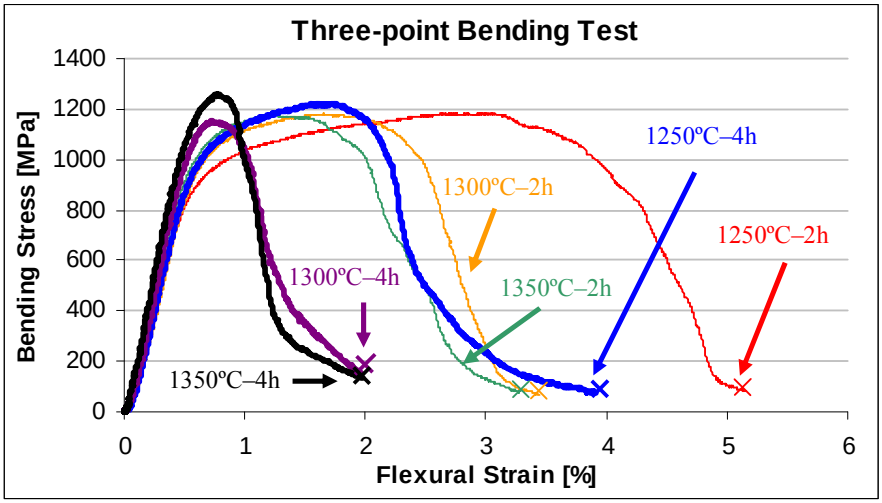

Figure 6.7 – Representative bending stress–strain curves for elemental titanium specimens.

As it can be seen in Figure 6.7, the maximum stress of the samples is almost the same for all the conditions studied and there is a great decrease in strain and in deformation energy stored and, therefore, in toughness of the materials with the increment of the sintering temperature or time. In particular, all the curves show a linear elastic deformation followed by plastic yielding and strain hardening up to a peak stress and then the stress drops indicating that no catastrophic fracture occurs.

The flexural modulus for each specimen has been calculated using the equation reported by the ASTM E 855 standard[12] obtaining a slight increment either when raising the temperature or doubling the time resulting in a mean value of 97 GPa with a standard deviation of 7 GPa. This value results to lay in between the flexural modulus found by other authors, precisely 66 GPa obtained by Plotino et al.[13] for elemental titanium or Walker et al.[14] for a beta titanium alloy using the same formula specified in the previous mentioned ASTM standard, and 126 GPa of Xu et al. obtained applying the method of Oliver and Pharr for elemental titanium data obtained by an Isotron TriboIndenter[15].

Anyway, the absolute value of the flexural modulus determined on P&S elemental titanium is not an intrinsic property of the material since greatly depends on the ratio between the span length (L) and the diameter of the specimen (D) as demonstrated by various authors[16-18] where the increment of the L/D ratio leads to an increase of the flexural modulus.

Figure 6.8 displays the results of three–point bending tests represented in terms of maximum bending strength and flexural strain as a function of the sintering temperature and time.

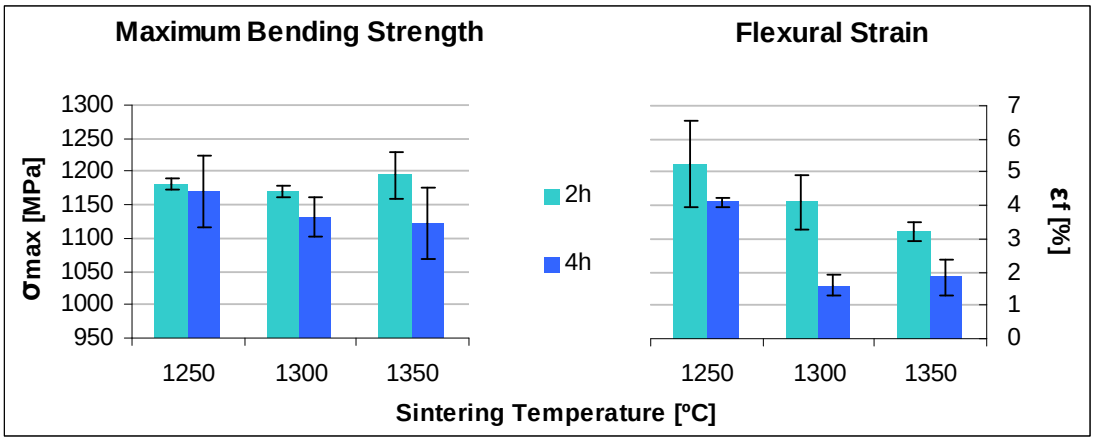

Figure 6.8 – Mechanical properties as a function of the sintering temperature and time for elemental titanium specimens: maximum bending strength (left) and flexural strain (right).

Analysing the results shown in Figure 6.8–left, two different behaviours can be seen depending on the sintering time: for 2 hours, the maximum bending strength remains almost constant around 1180 MPa, whereas for 4 hours it decreases when the sintering temperature increases. Furthermore, for a given sintering temperature, the longer the processing time, the lower the maximum bending strength. This tendency contrasts with the expected on the bases of the reduction of the residual porosity. Thus, it can be most probably due to the grain growth induced by a longer time at high temperature.

No terms of comparison could be found in the literature for the maximum bending strength of elemental titanium produced by powder metallurgy techniques. Nonetheless, the values shown in Figure 6.8 seems to be lower with respect to the value found by other authors, such as Plotino et al.[13] which got a flexural strength of 1281 MPa.

However, it should be mentioned that they studied wrought elemental titanium cylindrical endodontic posts whose chemical analysis is not specified. Therefore, the higher strength could be due to the absence of porosity, to a lower interstitial content as well as to a smaller mean grain size.

On the other side, the flexural strain always diminishes with the increment of the temperature for the two processing times, where these two parameters seem to have the same effect, causing an average drop of approximately 1% in strain either increasing 50ºC or doubling the time from 2 hours to 4 hours. Exceptions are the specimens sintered at 1300ºC for 4 hours which has the lowest flexural strain due to the higher contamination, especially from nitrogen (see Figure 6.3), in comparison to the other conditions.

It is interesting to find out the relationship between the mechanical properties with the interstitials to evaluate their influence. The maximum bending strength is correlated with the equivalent oxygen content obtained by the equation proposed by Wood[19] (see Eq. 15 in Section 2.7) and the results are shown in Figure 6.9.

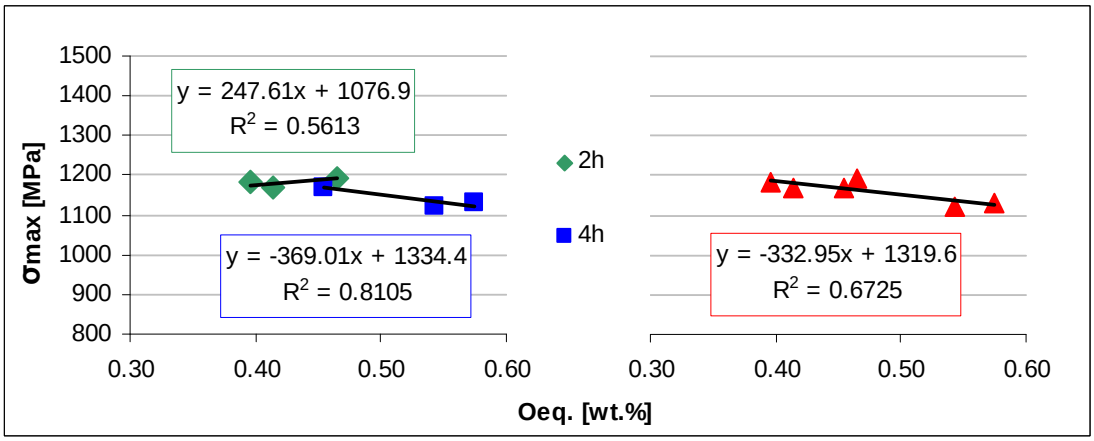

Figure 6.9 – Maximum bending strength as a function of the equivalent oxygen content for elemental titanium bending specimens: for diverse sintering times (left) and general trend (right).

Analysing the behaviour of the maximum bending strength with the equivalent oxygen content divided as a function of the sintering time (Figure 6.9–left), it can be noticed that there are two opposite trends when increasing the amount of interstitial elements: the maximum bending strength slightly increases with $O_{Eq.}$ for 2 hours, which is the behaviour expected since oxygen and nitrogen strengthen titanium[5, 6], whilst the strength decreases for 4 hours.

Considering all the data (Figure 6.9–right), it can be seen that the general trend shows the decreasing of the maximum bending strength when the equivalent oxygen content increases. This trend is not expected and the reason could be found in the microstructure, due to the grain growth with the temperature and the time. The microstructural analysis is explained in Section 6.1.1.6.

The trend of the flexural strain with the amount of interstitials dissolved inside the matrix, calculated by the formula indicated by Wood[19] (see Eq. 16 in Section 2.7) is presented in Figure 6.10.

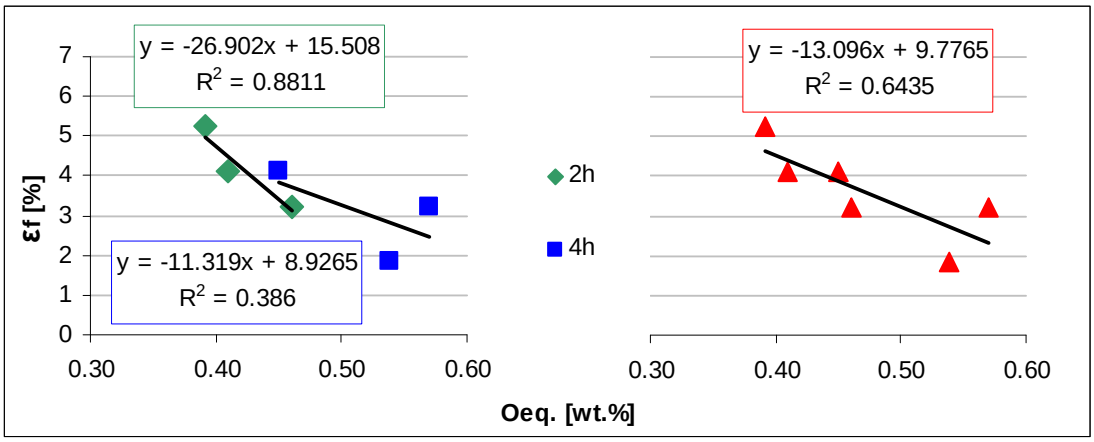

Figure 6.10 – Flexural strain as a function of the equivalent oxygen content for elemental titanium bending specimens: for diverse sintering times (left) and general trend (right).

In the case of the flexural strain, either the trends for different processing times (Figure 6.10–left) or the general tendency (Figure 6.10–right) indicate that this property decreases with the increment of the equivalent oxygen content.

However, it is worth mentioning that the linear regression for 4 hours is much less appropriate than for 2 hours which is, once again, most probably due to the influence of the microstructural changes which is not considered in the formula used to describe the variation of the flexural strain.

6.1.1.5 – Properties from Tensile Test

Figure 6.11 reports a representative example of tensile stress–strain curves obtained for elemental HDH titanium. In particular, it is represented one curve for every sintering temperature studied to show the similar shape in all the cases that indicates similar behaviour.

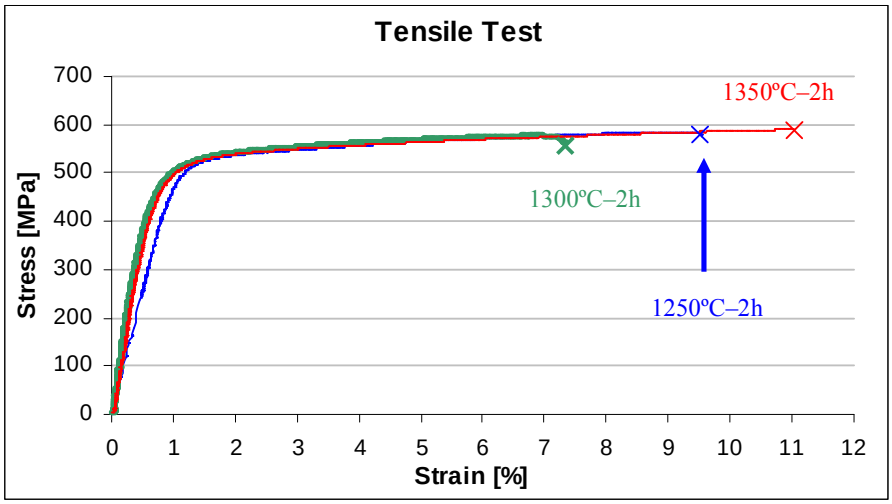

Figure 6.11 – Representative tensile stress–strain curves for elemental titanium specimens.

Dynamic elastic modulus measurements, carried out as specified in Section 2.6.6, results to be quite similar for the three sintering temperatures, since the individual values obtained are in the order of 100 MPa giving a mean value of 104 ± 9 GPa which is very similar to the typical value of 105 GPa of wrought titanium grade 4[9].

Ultimate tensile strength and strain mean values versus the sintering temperature for elemental titanium are presented in Figure 6.12.

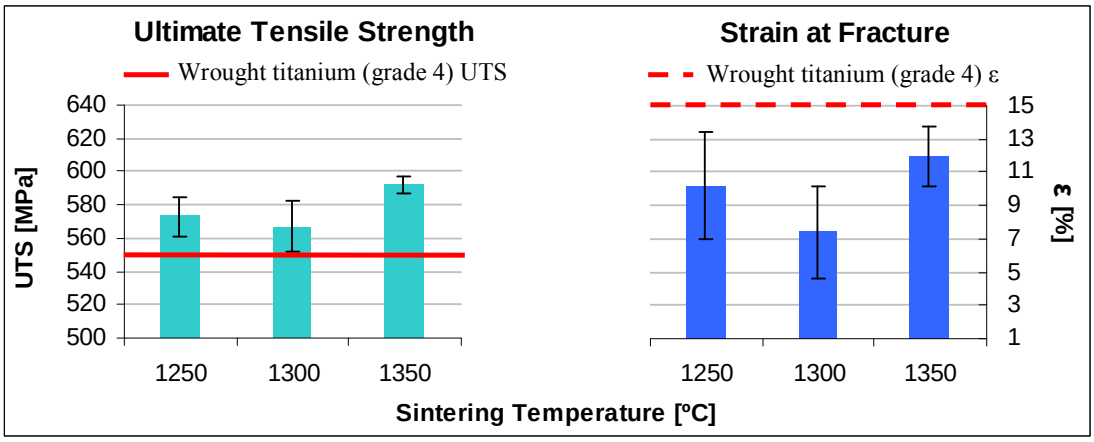

Figure 6.12 – Mechanical properties as a function of the sintering temperature and time for elemental titanium specimens: ultimate tensile strength (left) and strain (right).

As it can be seen in Figure 6.12, ultimate tensile strength remains approximately constant for 1250ºC and 1300ºC and then increases slightly at 1350ºC. This small variation of the UTS with the sintering temperature could be due to the balance of three factors: the lower porosity, the higher oxygen and nitrogen content that would increase the UTS, and the grain growth, that would decrease the maximum strength.

However, the values found are comparable or higher than the tensile properties indicated for wrought titanium grade 4, where the specified UTS is 550 MPa[8] or that found by Ivasishin et al.[20] using an electrolytic titanium powder (550–570 MPa).

On the other hand, strain values are somewhat lower than the required strain of 15%[9], which is the normal behaviour of P/M materials due to the presence of the residual porosity. Moreover, the value of strain for 1300ºC is lower than the expected from the trend and it is, once again, determined by the influence of the three factors mentioned.

Compared to the mechanical properties obtained by other authors such as the work of El Kadiri et al.[4], who tested elemental titanium samples with a relative density of 91.8% whose chemical analysis is not specified, the strain shown in Figure 6.12 is, at least, 2.5 times higher.

6.1.1.6 – Microstructural Analysis

The evolution of the microstructure and porosity with the sintering parameters, temperature and time was studied either by optical microscopy (LOM) or by SEM using secondary electron. LOM images of etched samples of every sintering condition are displayed in Figure 6.13 whereas SEM micrographs are not reported.

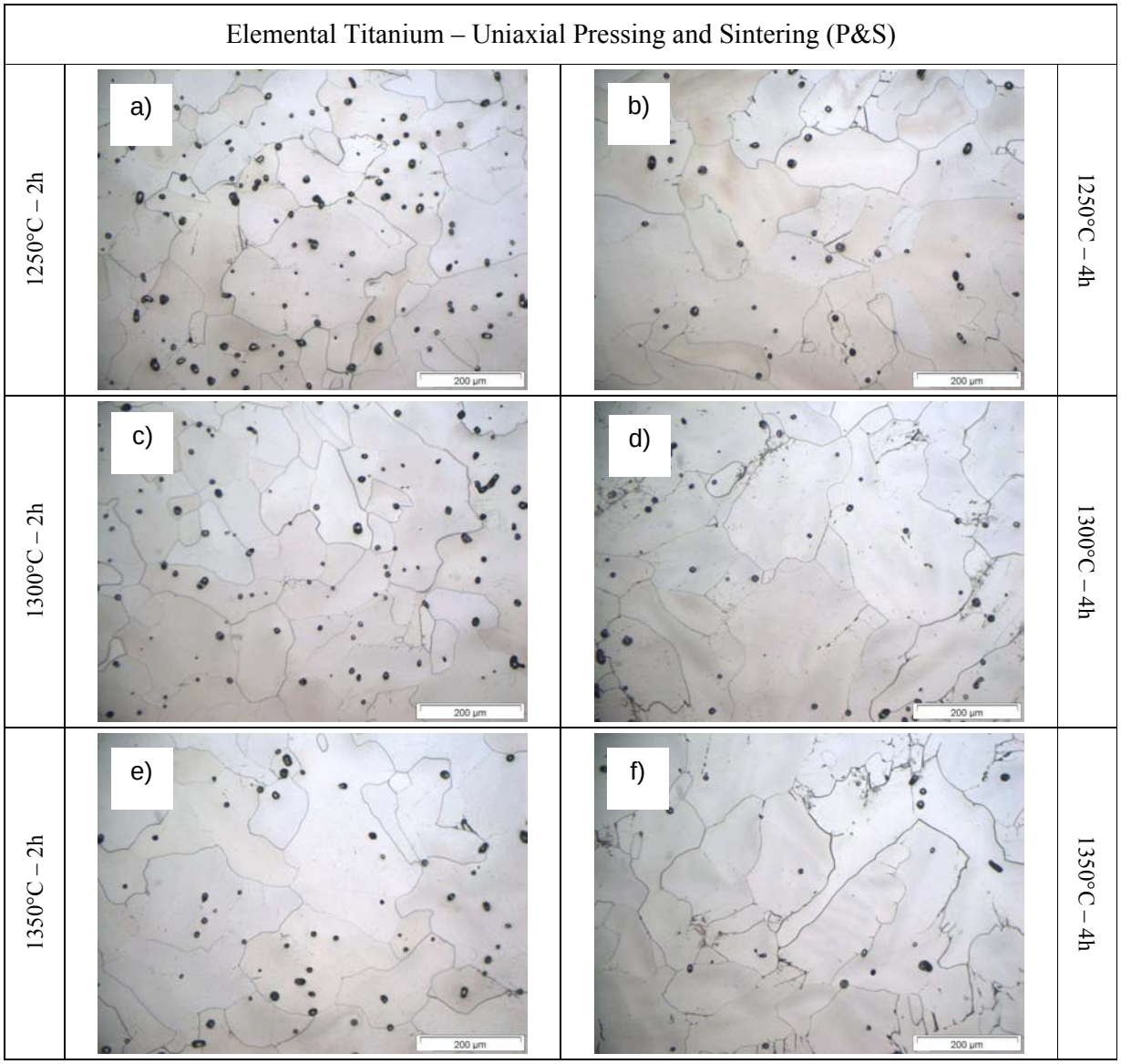

Figure 6.13 – Optical microscopy images for elemental titanium sintered at: a) 1250°C–2h, b) 1250°C–4h, c) 1300°C–2h d) 1300°C–4h, e) 1350°C–2h and f) 1350°C–4h.

Microstructural analysis by optical microscopy (Figure 6.13), which is representative for both bending and tensile specimens, reveals that the microstructure is composed by alpha grains of different shape, size and orientation[21, 22] and it seems that the mean size gets bigger either when increasing the sintering temperature and time.

Regarding the residual porosity, at the conditions considered, it is generally round shaped, decreases in percentage and grows in size with both the increment of the sintering temperature or time.

These features explains that the decreasing of the residual porosity and increment in contaminants content is balanced by the grain growth for 2 hours of sintering, and that is why the maximum bending strength or the UTS remain almost constant while for 4 hours of sintering the grain growth is greater and the maximum bending strength decreases.

During SEM and LOM analyses not significant differences could be found between the tensile test samples and the three–point bending test specimens, since the microstructure is composed by alpha grains and residual porosity, and no other phases were detected. Therefore, the low strain obtained with specimens sintered at 1300ºC during two hours could be an error introduced by the clamps of the tensile testing machine.

SEM was also employed to carry out the fractographic study of the fracture surface of tensile specimens and the results are shown in Figure 6.14.

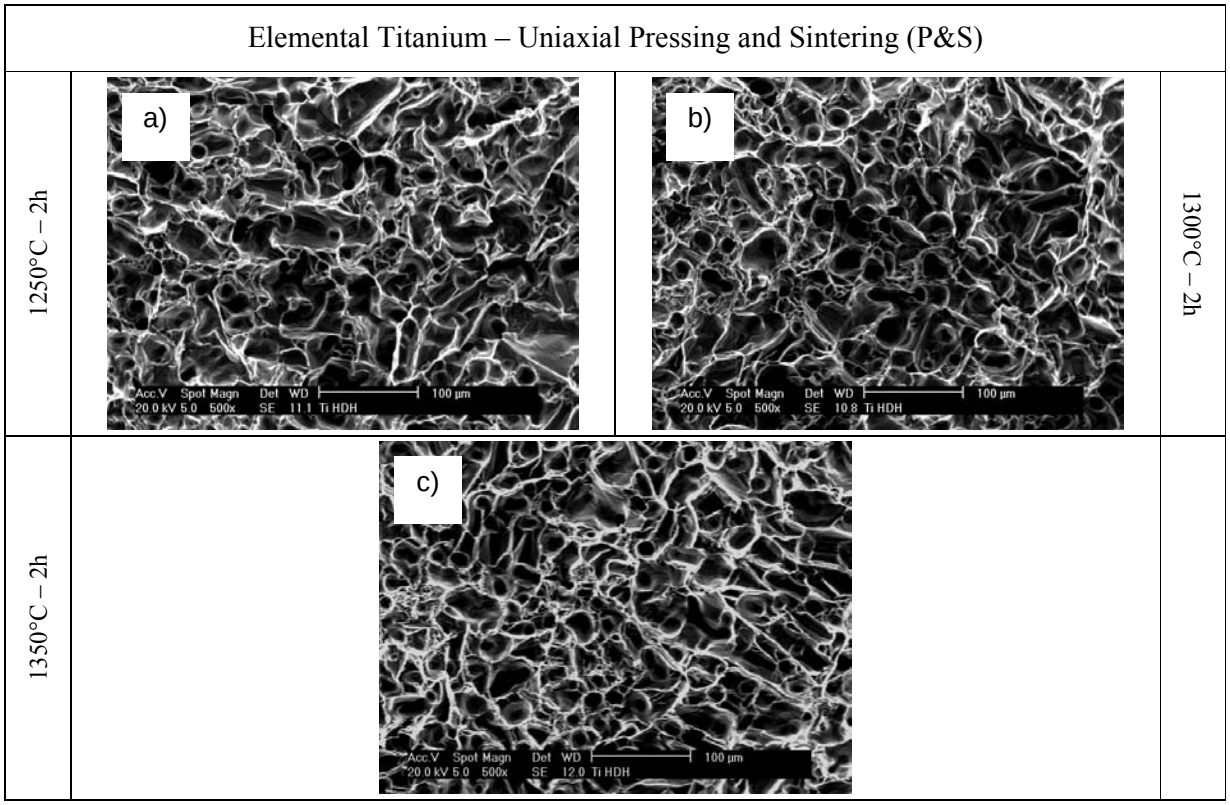

Figure 6.14 – Fracture surface from tensile test specimens for elemental titanium sintered for 2 hours at: a) 1250ºC, b) 1300ºC and c) 1350ºC.

Fractography indicates that the fracture surface is composed by equiaxed and well distributed dimples with some small isolated areas that could either be conical dimples or cleavage zones and, thus, the specimens broke in a ductile way by microvoid coalescence known as dimple rupture which most probably starts from the residual porosity.

6.1.1.7 – Thermal Conductivity

As it has been explained in the experimental procedure (Chapter 2), the influence of the processing parameters on the thermal conductivity of elemental titanium obtained by P/M techniques was also studied.

The results of this characterisation is presented displaying the property of interest as a function of the relative density and the equivalent oxygen percentage (see Eq. 17[23] in Section 2.7) for 2 and 4 hours of sintering due to the great influence of this parameter on microstructural features. The data obtained from the measurement of the thermal conductivity at room temperature are shown in Figure 6.15.

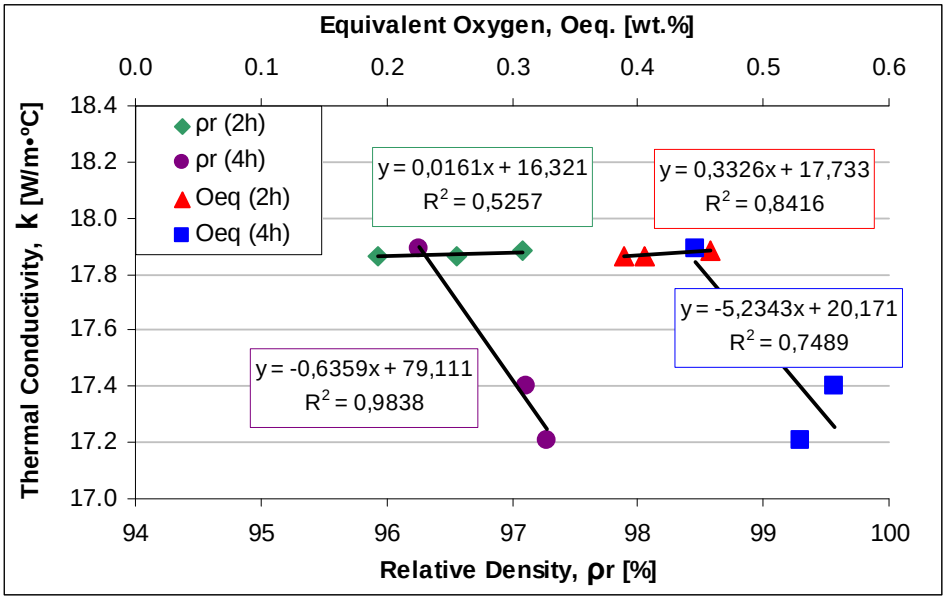

Figure 6.15 – Thermal conductivity at room temperature as a function of the relative density and equivalent oxygen content for elemental titanium specimens.

The thermal conductivity at room temperature of elemental titanium sintered under the different temperatures and times (Figure 6.15) has two different trends depending on the processing time considered. Precisely, when elemental titanium is sintered during 2 hours, the thermal conductivity practically remains constant either when it decreases the residual porosity (left side of Figure 6.15) or it increases the percentage of interstitials (right part of Figure 6.15). On the other side, when the processing time is doubled from 2 hours to 4 hours, the thermal conductivity of P/M titanium decreases with the increment of the relative density or the equivalent oxygen.

As it can be seen in Figure 6.15, the drop of the thermal conductivity appears when the equivalent oxygen content is higher than 0.45 wt.% indicating that below this percentage the benefits of the increment of the temperature, namely a higher relative density and a lower percentage of grain boundaries (grain growth), is predominant over the content of interstitial elements.

On the other side, when the $O_{Eq.}$ reaches approximately 0.45 wt.%, the amount of interstitials, which means, actually, lattice defects, is that high to hinder somehow the interaction of the particles responsible of the thermal conductivity (atoms, electrons, phonons, etc.) and to be predominant over the microstructural features leading to a decrement of the conductivity. Nonetheless, the thermal conductivity of P/M titanium is directly comparable or somewhat higher than the mean value of wrought titanium as shown in Table 6.1.

Table 6.1 – Comparison of thermal conductivity at room temperature values between wrought and P/M elemental titanium.

Elemental titanium (Grade 4)				
Wrought[8]		**P/M**		
k [W/m·ºC]	Chemical analysis [wt.%]	k [W/m·ºC]	Chemical analysis [wt.%]	Sintering conditions
17.30	O = 0.40 N = 0.05	17.87	O = 0.323 N = 0.020	1250ºC – 2h
		17.86	O = 0.327 N = 0.025	1300ºC – 2h
		17.89	O = 0.383 N = 0.024	1350ºC – 2h
		17.89	O = 0.370 N = 0.028	1250ºC – 4h
		17.40	O = 0.414 N = 0.053	1300ºC – 4h
		17.21	O = 0.413 N = 0.042	1350ºC – 4h

As it has been explained in Section 2.6.8, the specimens sintered at 1250ºC for 2 hours were also employed to evaluate the variation of the thermal conductivity with the temperature. In particular, the measurement was carried out increasing the temperature up to 300ºC and measuring the thermal conductivity every 50ºC.

Since the specific heat at constant pressure (C_p), which is used to calculate the thermal conductivity, as well as the thermal conductivity itself, greatly depends on the temperature, the thermal conductivity results obtained by "measurements" are compared with that of the "thermal conductivity calculated" (see Eq. 11 and 12 in Section 2.6.8)[8] and the value found in the literature[24] and they are presented in Figure 6.16.

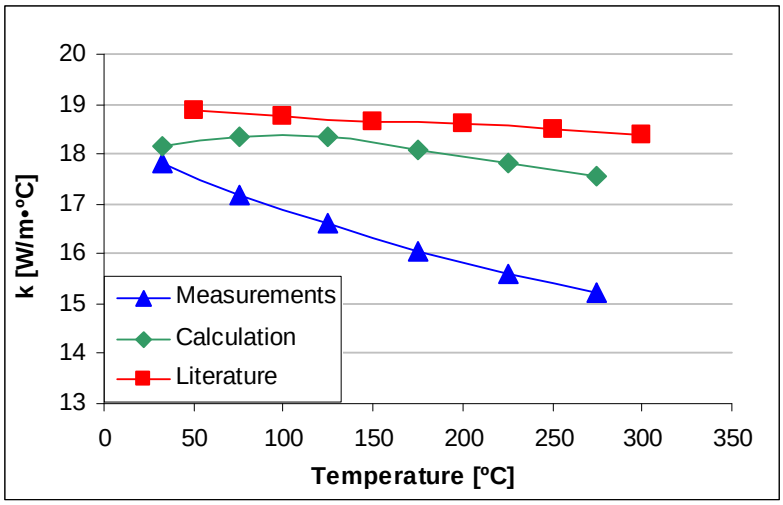

Figure 6.16 – Thermal conductivity as a function of temperature for elemental titanium specimens.

As it can be seen in Figure 6.16, the thermal conductivity obtained by the "measurements" decreases quite markedly when increases the temperature.

The same behaviour was found by Powell and Tye[24] on wrought titanium even if the drop is less important and the values somewhat higher ("literature"). This difference could be mainly due to the effect of the residual porosity.

When the conductivity is calculated considering the effect of the temperature on the specific heat ("calculation"), the thermal conductivity slightly increases up to 150ºC and then starts to decrease and the values are much similar to those found in the literature.

6.1.1.8 – Electrical Resistivity

The results of the electrical resistivity at room temperature calculated from the data of the electrical conductivity measured employing the van der Pauw's method[25, 26] (see Section 2.6.9) are presented in Figure 6.17.

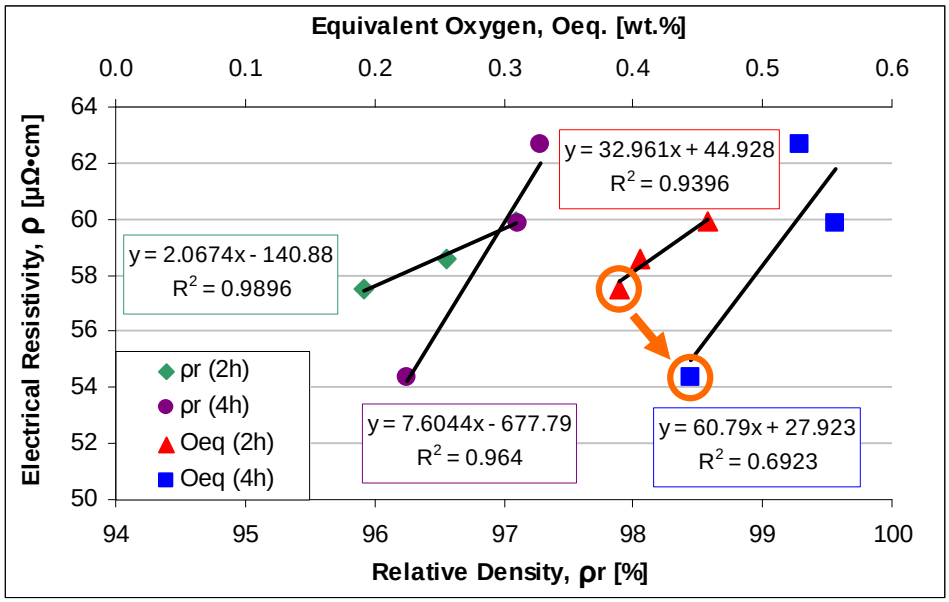

Figure 6.17 – Electrical resistivity at room temperature as a function of the relative density and equivalent oxygen content for elemental titanium specimens.

As it can be seen in Figure 6.17, the electrical resistivity at room temperature of elemental titanium obtained by the conventional P/M route increases either with the relative density or the equivalent oxygen content. However, the slope of the regression line is significantly different when considering the processing time as well as the scattering of the values, which is considerably higher for 4 hours.

The increment of the electrical resistivity is mainly due to the increasing of the interstitial elements dissolved inside the matrix whilst the grain growth induced by choosing a longer time provokes a drop of the resistivity most probably due to the lower quantity of grain boundaries.

This is clearly visible comparing the values of the specimens sintered at 1250ºC during 2 (▲) or 4 (■) hours, labelled in Figure 6.17 by circles, where the 4 hours components have higher equivalent oxygen but lower electrical resistivity due to the important grain growth induced by the doubling of the processing time (see Figure 6.13 a and b).

When compared to the wrought material, the electrical resistivity of P/M elemental titanium is similar, and the slight differences are, once again, explicable considering the amount of interstitial elements dissolved in the titanium and the presence of residual porosity as it can be seen in Table 6.2. The electrical resistivity measured on P/M specimens is lower than that of the wrought alloy when the amount of interstitials is lower and viceversa.

Table 6.2 – Comparison of electrical resistivity values between wrought and P/M elemental titanium.

Elemental titanium (Grade 4)				
Wrought[8]		**P/M**		
ρ [μΩ·cm]	Chemical analysis [wt.%]	ρ [μΩ·cm]	Chemical analysis [wt.%]	Sintering conditions
60.0	O = 0.40 N = 0.05	57.5	O = 0.323 N = 0.020	1250ºC – 2h
		58.6	O = 0.327 N = 0.025	1300ºC – 2h
		59.9	O = 0.383 N = 0.024	1350ºC – 2h
		54.3	O = 0.37 N = 0.028	1250ºC – 4h
		59.8	O = 0.414 N = 0.053	1300ºC – 4h
		62.7	O = 0.413 N = 0.042	1350ºC – 4h

6.1.2 – Hot Isostatic Pressing (HIP)

In this section the influence of introducing a secondary process of HIP on the final physical, chemical and mechanical properties of either rectangular shaped specimens or "dogbone" tensile samples is discussed.

Based on the relative density results of Figure 6.2 and knowing that a minimum of 92% of theoretical density is needed to obtain a residual porosity composed exclusively by closed porosity[27], a sintering temperature of 1250ºC–2h was chosen to sinter the components that would be subsequently processed by HIP. This processing condition should provide the required level of residual porosity and, simultaneously, limit the manufacturing costs.

As it was described in Chapter 2, four different HIP conditions changing one parameter (temperature, time or pressure) every time were studied using rectangular three–point bending test samples:

- ✓ **HIP–1**: T = 1000ºC, P = 100 MPa , t = 20 min — Reference conditions
- ✓ **HIP–2**: T = 1000ºC, P = 100 MPa, t = 2 h — To study the influence of time
- ✓ **HIP–3**: T = 850ºC, P = 100 MPa, t = 20 min — To study the influence of temperature
- ✓ **HIP–4**: T = 850ºC, P = 200 MPa, t = 20 min — To study the influence of pressure

Based on the results obtained on three–point bending specimens, especially referring to the relative density and the mechanical properties, tensile test samples sintered at 1250ºC during 2 hours were subjected to the HIP–2 cycle.

6.1.2.1 – Relative Density

The results of relative density compared to the value obtained for P&S specimens at 1250ºC–2h are presented in Figure 6.18.

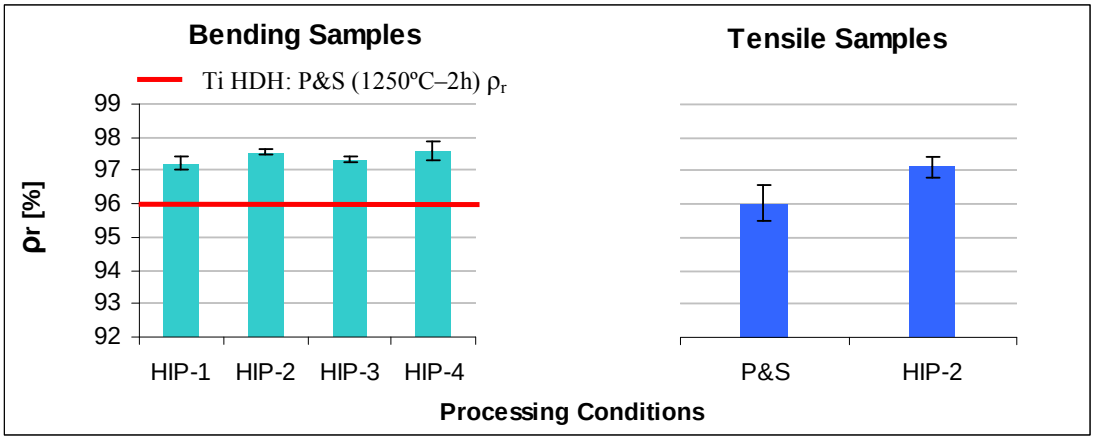

Figure 6.18 – Relative density as a function of the HIP cycle for elemental titanium specimens: bending (left) and tensile (right).

As it can be seen in Figure 6.18, HIP induces a slight increase in relative density, of approximately 1% to 2% compared to P&S components reaching values in between 97% and 98%, and there is not a significant influence of the parameters studied. Not fully dense material could be obtained most probably due to the fact that most of the residual porosity is concentrated on the surface of the specimens and it is, actually, open to the exterior[28].

Comparing the relative density of P&S and HIP–2 for tensile specimens (Figure 6.18–right), it can be seen that HIP leads to an increase in relative density of approximately 1% just like it was for rectangular samples and, once again, not fully dense material is obtained due to the open porosity present in the surface of the specimens.

6.1.2.2 – Chemical Analysis

The results of oxygen and nitrogen determination for bending and tensile specimens after HIP are presented in Figure 6.19 and in Figure 6.20, respectively.

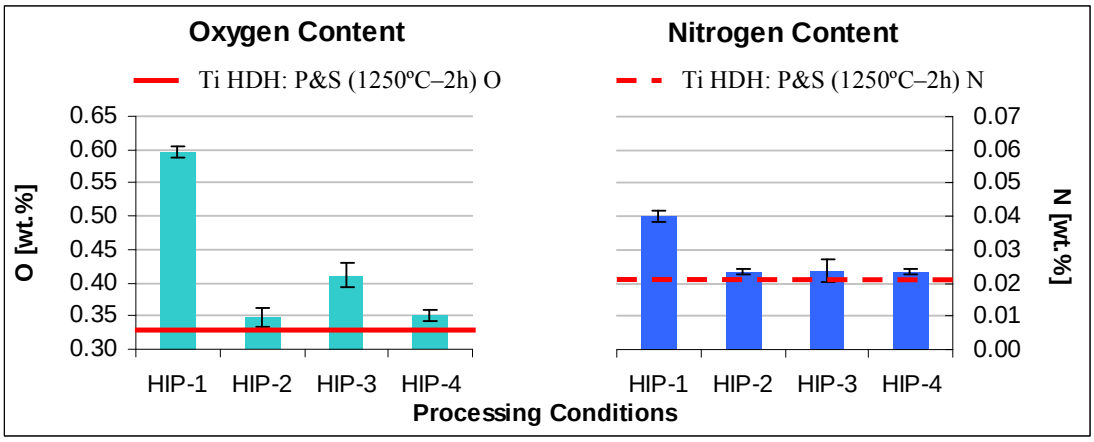

Figure 6.19 – Chemical analysis as a function of the HIP cycle for elemental titanium bending specimens: oxygen (left) and nitrogen (right).

Oxygen content (Figure 6.19–left) of HIPed components is always higher compared to the as–sintered specimens, thus, some contamination from the inert atmosphere occurred during processing. In particular, the samples HIPed under the HIP–1 conditions reach a 0.60 wt.% of oxygen, almost the double compared to the as–sintered parts.

On the other hand, nitrogen (Figure 6.19–right) is practically the same for the different hot isostatic pressed samples with the exception of the HIP–1 condition where there has been some nitrogen pick–up.

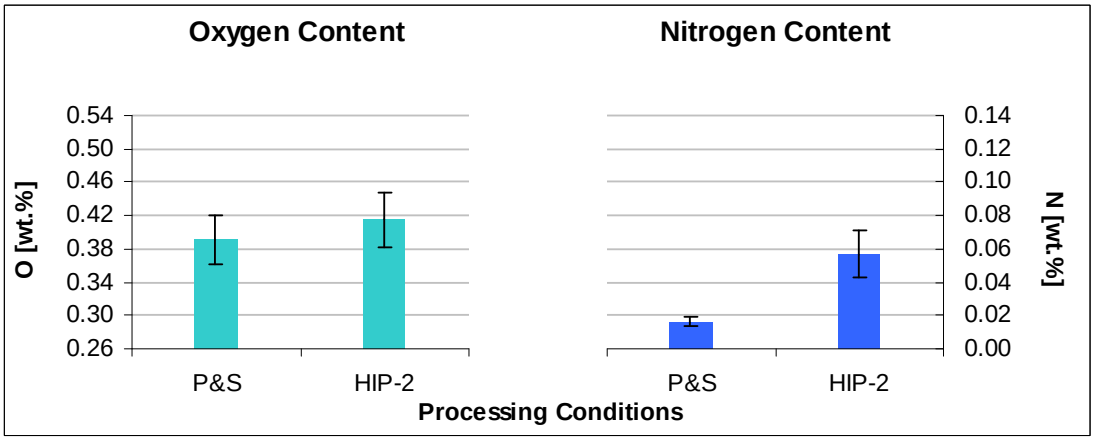

Figure 6.20 – Chemical analysis as a function of the HIP cycle for elemental titanium tensile specimens: oxygen (left) and nitrogen (right).

In the case of tensile specimens, as shown in Figure 6.20, there is oxygen and nitrogen pick–up from the HIP atmosphere and the final content results to be higher either compared to P&S tensile samples or to HIP–2 bending specimens.

6.1.2.3 – Hardness

The results of the Vickers hardness measurement carried out on HIPed components are shown in Figure 6.21.

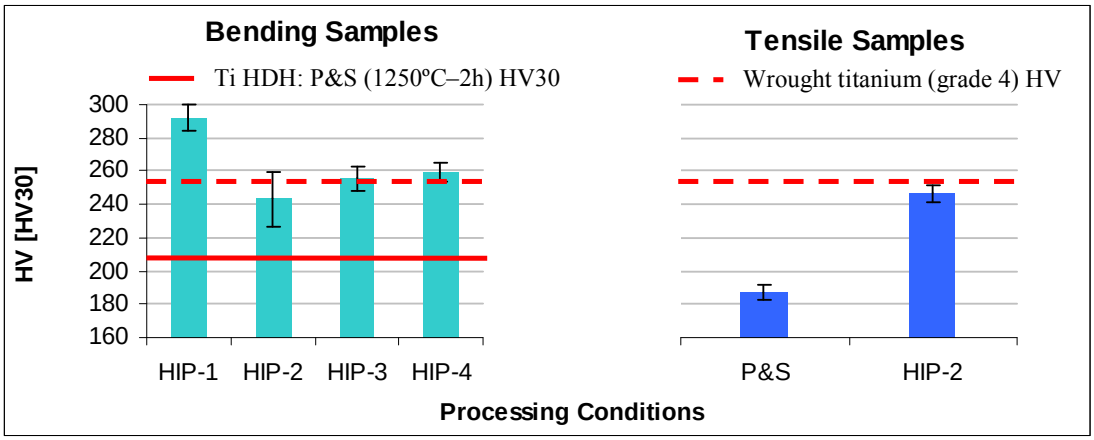

Figure 6.21 – Hardness as a function of the HIP cycle for elemental titanium specimens: bending (left) and tensile (right).

HIP seems to have a strong effect on the final hardness (Figure 6.21) due to the improvement of the final relative density, the increment of the interstitials, especially oxygen, and the microstructural changes.

In the case of HIP–2, HIP–3 and HIP–4 the increment of hardness is similar and the values are approximately 22% higher than the as–sintered material. On the other side, in the case of HIP–1, the increment is greater than 40% mainly due to the much higher oxygen and nitrogen content (Figure 6.19).

The hardness of tensile test specimens post–processed under the HIP–2 conditions (245 HV30) is equal to that of bending specimens but, in this case, the increment with respect to P&S is slightly higher due to the lower hardness found in P&S tensile components. Moreover, the HIP process permits to obtain hardness values similar to that of the wrought material independently of the type of specimens and processing conditions.

When the hardness mean values are represented versus the equivalent oxygen content (Figure 6.22), it can be noted that the data can be well fitted with a linear relationship.

Due to the low number of data available it can not be estimated the influence of the processing temperature being one of them higher (1000ºC) and the other lower (850ºC) than the beta transus of elemental titanium (882ºC). Anyway, it seems that, for a processing temperature of 850ºC, the effect of the interstitials is overcome by the microstructural change, such as grain growth for HIP–4, which will be described in Section 6.1.2.6.

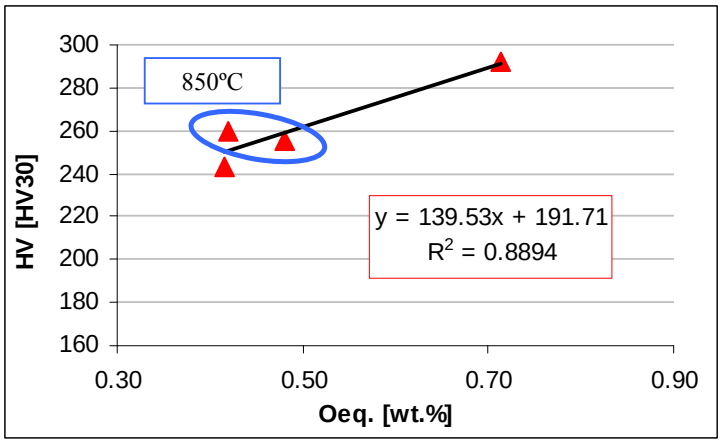

Figure 6.22 – Hardness as a function of equivalent oxygen content for elemental titanium HIPed bending specimens.

6.1.2.4 – Properties from Bending Test

A representative bending stress–strain curve for each one of the HIP conditions studied compared to that of the samples sintered at 1250ºC during 2 hours is shown in Figure 6.23.

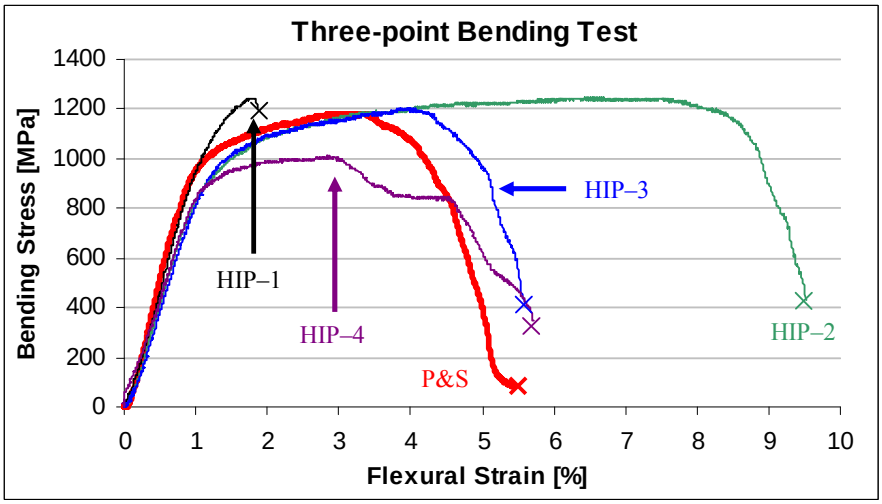

Figure 6.23 – Representative bending stress–strain curves for elemental titanium HIPed specimens.

The flexural stress–strain curve of HIPed samples (Figure 6.23) resembles that of pressing and sintering components where the stress decreases continuously after a plateau at the maximum strength. An exception to this general behaviour is the curve of HIP–1 where there is almost no plastic deformation due to the much higher oxygen and nitrogen content dissolved in these specimens.

Regarding the flexural modulus, even if there is some little variation between the single specimens the mean value obtained is 101 ± 7 GPa which is somewhat higher compared to the value of the as–sintered samples, which is 97 ± 7 GPa. The increment of the mean value of the flexural modulus is most probably due to the reduction of the residual porosity.

Maximum bending strength and flexural strain mean values with their relative standard deviation for each HIP experiment are displayed in Figure 6.24.

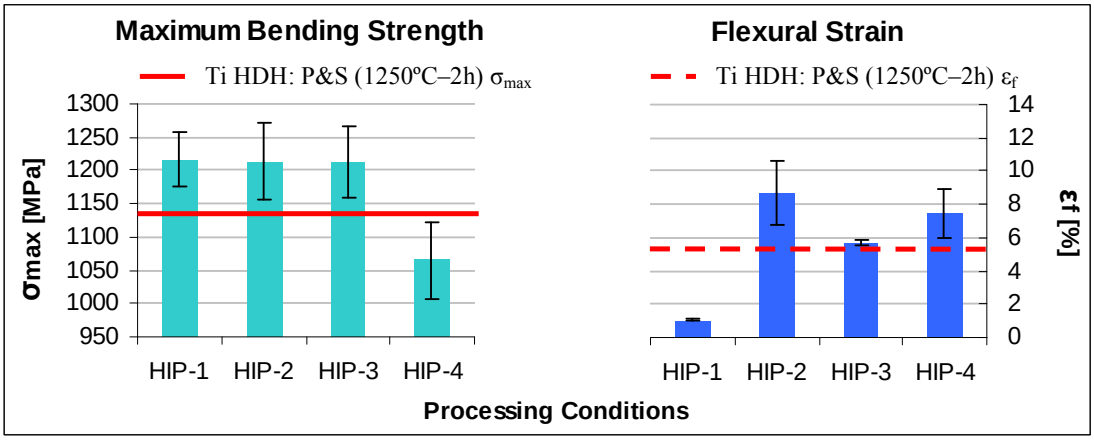

Figure 6.24 – Mechanical properties as a function of the HIP cycle for elemental titanium specimens: maximum bending strength (left) and flexural strain (right).

As it can be noticed in Figure 6.24, the maximum bending strength of HIPed samples is similar to that obtained on sintered samples (only 30 MPa higher) with the exception of HIP–4 which is lower. This is due to the significant grain growth provoked by the higher pressure as explained in Section 6.1.2.6.

Since the maximum bending strength values of HIP–1, HIP–2 and HIP–3 are, practically, identical but their chemical analysis significantly different, it seems that the maximum bending strength is not greatly dependent on the total amount of oxygen and nitrogen or their strengthening effect is balanced by the microstructural changes.

On the other side, flexural strain shows that a longer processing time or a higher pressure induces an increment in strain. The HIP–3 process, with low temperature, low pressure and short time does not change the flexural strain compared to P&S specimens.

Since the parameters employed are the same but the temperature is higher, the strain of HIP–1 should be higher than HIP–3; however, this property seems to be significantly lowered by the high oxygen and nitrogen percentage.

To study the effect of the interstitials, a correlation between the maximum bending strength and flexural strain mean values with the equivalent oxygen content are presented in Figure 6.25.

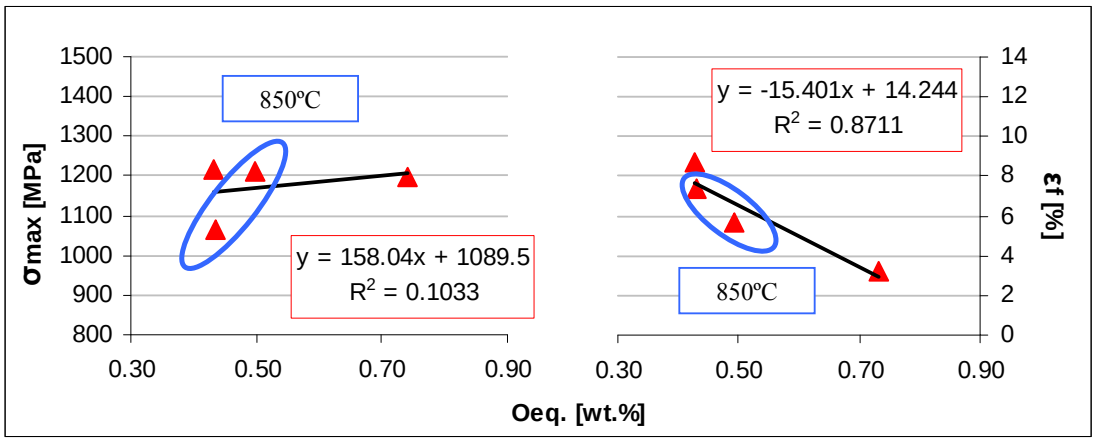

Figure 6.25 – Mechanical properties as a function of the equivalent oxygen content for elemental titanium HIPed bending specimens: maximum bending strength (left) and flexural strain (right).

As it can be seen in Figure 6.25, there is not a clear correlation between the maximum bending strength of HIP elemental titanium components and the equivalent oxygen content most probably due to the influence of the microstructural changes induced by the selection of the processing temperature below or above the beta transus which is described in Section 6.1.2.6.

The processing temperature of 850ºC seems to lead to an important increment of strength with the equivalent oxygen content whereas it remains almost constant for 1000ºC. This indicates a great influence from the microstructural changes induced by the selection of the HIP parameters.

Conversely to maximum bending strength, a quite good linear relationship could be found between the flexural strain and the content of interstitial elements where the higher their percentage the lower the deformation of the samples and the influence of the microstructural features seems to be much lower.

6.1.2.5 – Properties from Tensile Test

The comparison of the tensile stress–strain curve and the ultimate tensile strength and strain mean values between P&S and HIP–2 are displayed in Figure 6.26 and Figure 6.27, respectively.

As it can be seen in Figure 6.26, specimens subjected to HIP reach higher strength and lower strain values compared to P&S specimens but the shape of the tensile stress–strain is not affected by the post–process because composed by an elastic deformation followed by plastic yielding before fracture.

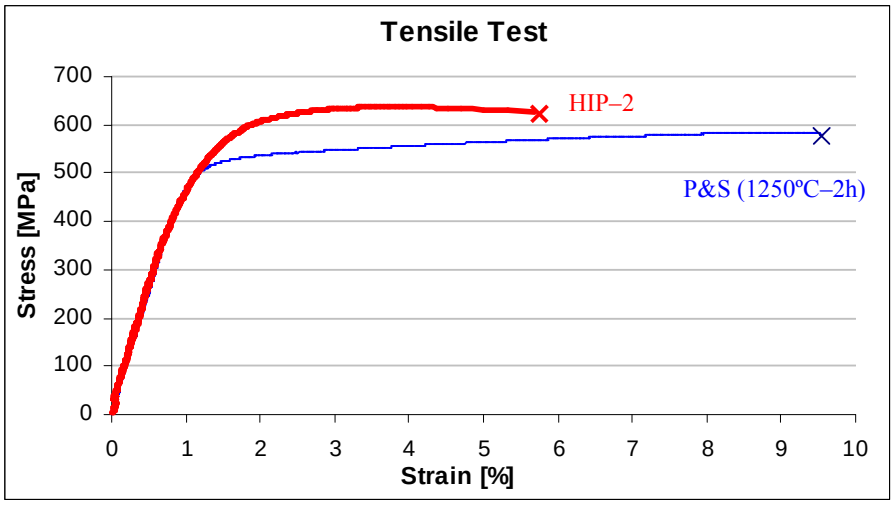

Figure 6.26 – Representative tensile stress–strain curves for elemental titanium P&S (1250ºC–2h) and HIPed specimens.

The dynamic Young's modulus measurements determined by long–wavelength method[8] indicate that the lowering of the residual porosity leads to an increment of the elastic modulus. In particular, the mean value obtained on HIPed specimens is 115 ± 3 GPa compared to 104 ± 9 GPa for sintered samples.

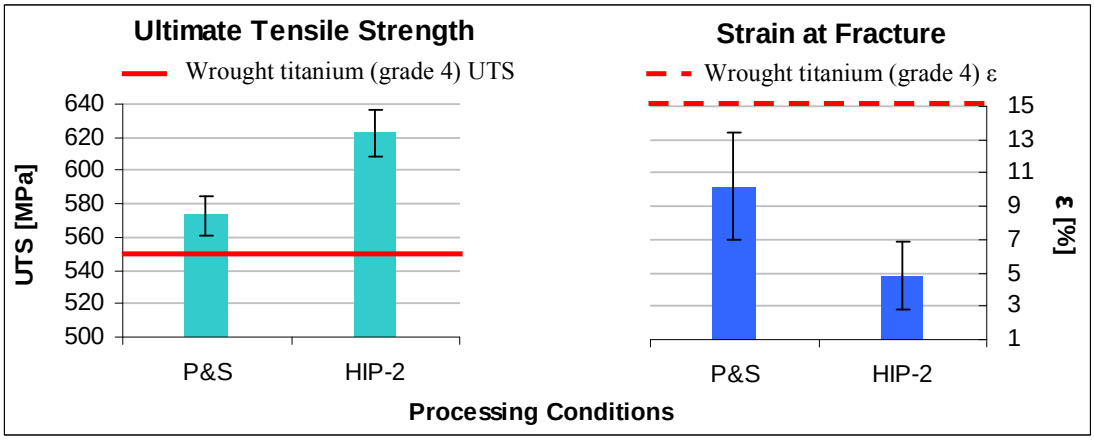

Figure 6.27 – Mechanical properties as a function of the processing method for elemental titanium specimens: ultimate tensile strength (left) and strain (right).

The ultimate tensile strength of HIPed components (Figure 6.27), whose mean value is 620 MPa, is higher either than P&S samples or wrought titanium grade 4 products. Thus, with the processing condition considered, the HIP step leads to an increase in strength in elemental titanium.

On the contrary, the strain of HIPed samples is approximately half of P&S specimens. This behaviour is most probably due to the combined effect of greater content of interstitials and microstructural changes (see Section 6.1.2.6).

6.1.2.6 – Microstructural Analysis

Microstructural features of elemental titanium components subjected to different HIP cycles analysed by optical microscopy are presented in Figure 6.28. The microstructural features were revealed by means of Kroll's reactant.

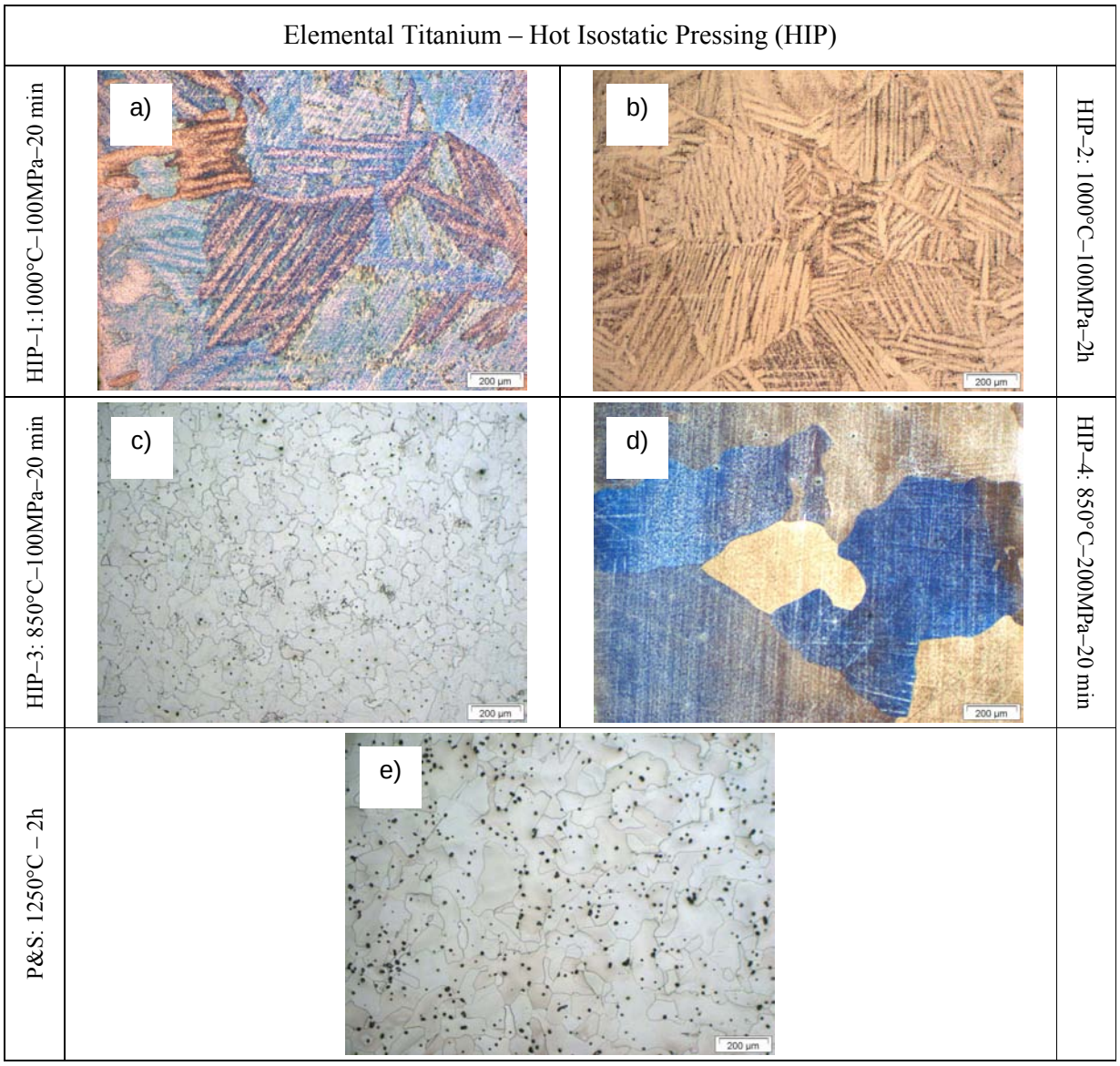

Figure 6.28 – Optical microscopy images for elemental titanium subjected to diverse HIP cycles: a) HIP–1, b) HIP–2, c) HIP–3 and d) HIP–4 and pressing and sintering: e) P&S 1250ºC–2h.

As it can be seen in Figure 6.28, HIP–1 leads to a microstructure composed by large alpha grains and numerous alpha platelets that have a distinctly cored appearance derived from the beta transformation and the level of impurities[29, 30].

This microstructure is the result of the cooling from 1000ºC where elemental titanium is completely composed by beta phase (B.C.C.), which is less dense than the alpha phase (H.C.P.), and the crossing of the beta transus with an applied external stress induced by the pressure, factors which induces mismatch plasticity[31].

Increasing the time up to 2 hours at the maximum temperature (HIP–2) induces the formation of a greater quantity of transformed beta or acicular alpha lowering the size of the alpha grains. The diminishing of the mean alpha grain size and the increment of the amount of the alpha platelets justify the higher flexural strain and similar maximum bending strength of samples processed under the HIP–2 conditions with respect to HIP–1 which could not be explain on the bases of the chemical analysis.

The HIP–3, where the specimens where processed in the alpha field, results in a microstructure composed of equiaxed alpha grains of similar size compared to the as–sintered samples (Figure 6.28–e), due to the refining effect of oxygen[5], but with lower amount of residual porosity, which clarifies why maximum bending strength is slightly higher but the flexural strain is quite the same of specimens sintered at 1250ºC–2h.

In the case of HIP–4 conditions, the doubling of the processing pressure in the alpha field provokes a significant increase in the size of the alpha grains that compose the final microstructure which explains the decrease of the maximum bending strength and the increment in flexural strain shown in Figure 6.24.

As in the case of P&S tensile specimens, a fractographic study of HIPed tensile samples was carried out and the micrographs of fracture surface are shown in Figure 6.29.

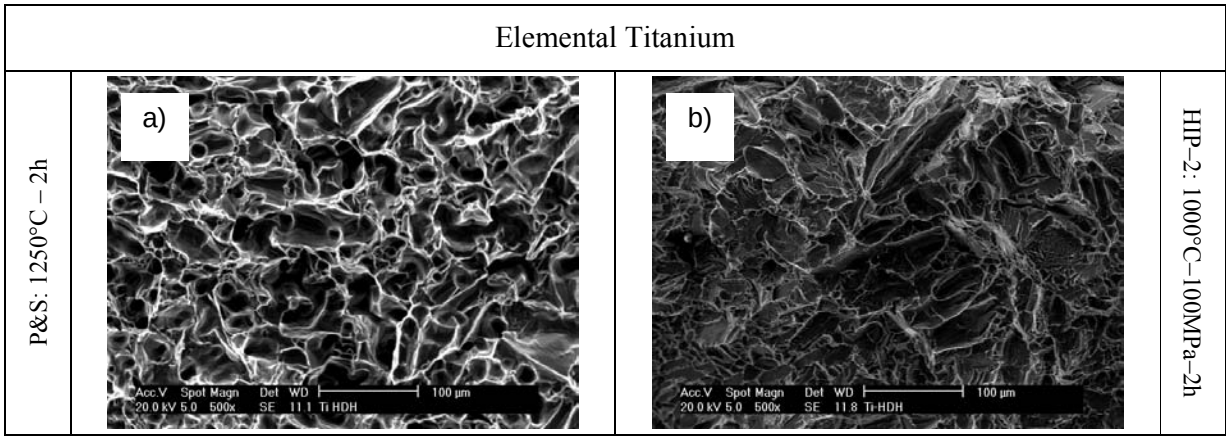

Figure 6.29 – Fracture surface from tensile test specimens for elemental titanium: a) P&S (1250ºC–2h) and b) HIP–2.

As it can be noted in Figure 6.29, the fracture surface of HIPed components is very different from that of P&S samples which is composed by equiaxed and well distributed dimples (Figure 6.29 a). In specimens subjected to HIP there are less visible uniform dimples, some conical dimples where the serpentine glide can be distinguished and many cleavage facets. This fractography completely agrees with the higher strength and lower ductility shown in Figure 6.27.

6.1.3 – Conventional Hot–pressing (HP)

As it has been described in the experimental procedure (Chapter 2), the preparation of the mould for the vacuum hot-pressing experiments can be summarised as follows:

- insert the lower graphite punch into the mould;
- line the inner of the graphite mould with the low reactivity graphite foil;
- place a graphite disc with the top face coated with a high temperature ceramic boron nitride (BN) spray which should prevent the reaction between titanium and the graphite tools and facilitate the mould release;
- pour and level the loose powder;
- place a graphite disc with the bottom face coated with the BN spray;
- cold uniaxially press the whole assemble at approximately 18 MPa.

These steps were repeated for each one of the compositions to be hot–pressed, since all the powders were processed at the same time. The amount of powder loaded for each material, approximately 75 g, gives as a result a disc of 65 mm in diameter and 5 mm in thickness.

During the hot–pressing cycle, the machine records the programmed temperature [ºC], the actual temperature [ºC] of the specimens by means of a thermocouple, the densification rate [mm/min], the pressure applied [kN] and the vacuum level [%]. An example of the graph recorded for a hot–pressing cycle carried out during the development of this thesis is shown in Figure 6.30 and it refers to samples sintered at 1100ºC during 1 hour at a pressure of 30 MPa.

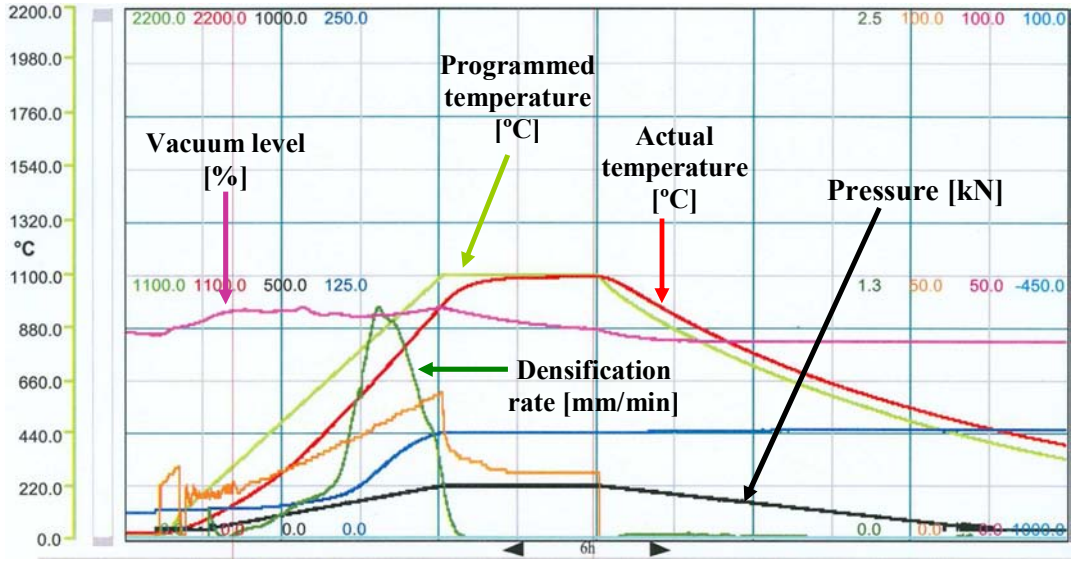

Figure 6.30 – Example of conventional hot–pressing cycle used to sintered elemental titanium and titanium alloy powders at 1100ºC.

Regarding the graphs recorded during the three conventional hot–pressing cycles studied (900ºC, 1100ºC and 1300ºC) such as the one shown in Figure 6.30, it should be mentioned that the actual temperature of the specimens reached the programmed temperature with some delay of approximately half an hour with the exception of the highest temperature, namely 1300ºC, where there is no delay.

This is the reason why the experiment at 1300ºC was stopped just after 30 minutes instead of one hour, in order to guarantee that the samples of the diverse hot–pressing cycles were dwell at the processing temperature during half an hour.

Concerning the densification rate, as it can be seen in Figure 6.30, the densification is already completed when the samples reach the processing temperature. The same behaviour was found at 1300ºC, while at 900ºC the densification ends approximately after 10 minutes at temperature. This is because at lower temperature lower energy is available for the diffusion processes which govern the densification of the powder.

6.1.3.1 – Relative Density

From the 65 mm disc obtained by HP, rectangular shaped specimens for the three–point bending test were cut and measured. The relative density results determined on these samples are displayed in Figure 6.31.

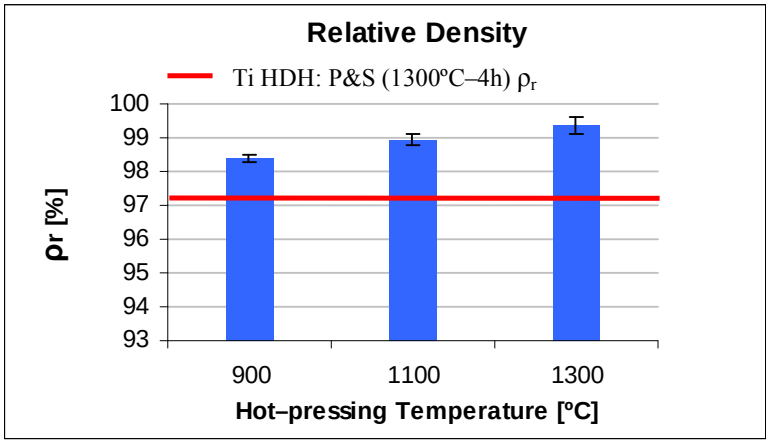

Figure 6.31 – Relative density as a function of the processing temperature for elemental titanium hot–pressed specimens.

Analysing the results of relative density shown in Figure 6.31, it can be seen that, as expected, this property increases with the processing temperature and, in this case, it increases constantly approximately 0.5% every 200ºC.

When compared to the best result obtained with the P&S route (1350ºC–4h), hot–pressing relative density values are always higher since they range between 98.3% and 99.4%.

It is clear that the simultaneous application of temperature and pressure during the sintering of the loose powder leads to higher densities than increasing the time at a given temperature (P&S).

6.1.3.2 – Chemical Analysis

In Chapter 2 (experimental procedure), it has been described that half of the three–point bending test samples cut from the original disc were grinded in order to remove the surface that was in contact with the boron nitride (BN) coating to determine the possible effect on the final composition.

The results of the chemical analysis, precisely oxygen, nitrogen and carbon (since the titanium powder was processed in a graphite die) are presented in Figure 6.32.

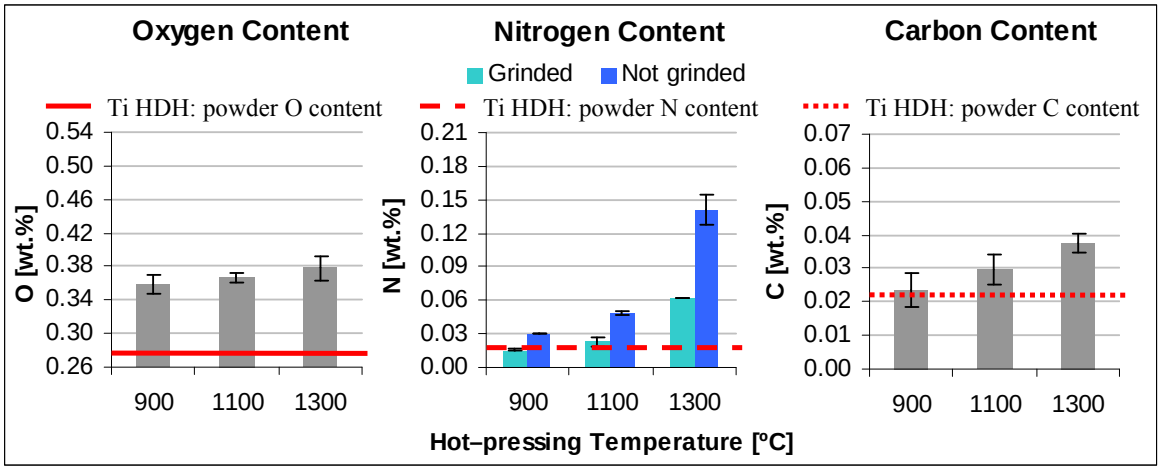

Figure 6.32 – Chemical analysis as a function of the processing temperature for elemental titanium hot–pressed specimens: oxygen (left), nitrogen (centre) and carbon (right).

Regarding the data shown in Figure 6.32, in the case of oxygen and carbon determination, no significant differences were found between grinded and not grinded specimens and, therefore, the data got from both types of samples were used in order to calculate the mean value and the relative standard deviation. Nevertheless, for nitrogen content, two values are presented for each temperature depending of the grinding step.

Oxygen content (Figure 6.32–left) increases with the processing temperature; even if these are higher compared to the powder content, the values obtained are similar to those of P&S specimens suggesting that oxygen pick–up derives from the oxygen adsorbed onto the particle surface or trapped between the powder particles.

Nitrogen percentage (Figure 6.32–centre) rises with the temperature with respect to the powder content independently of the grinding of the surface. Moreover, the nitrogen content of the not grinded specimens is always the double of the grinded samples or even greater. This indicates that there was some kind of interaction between the titanium powder and the BN coating used to facilitate mould release and to prevent reaction with the graphite disc.

On the other hand, as it can be seen on the right side of Figure 6.32, carbon content follows the same trend of the other two interstitial elements reaching a maximum content of 0.04 wt.%. Once again, this points out that the titanium powder reacted with the graphite mould and carbon diffuses through the titanium matrix.

Resuming, oxygen increases to values similar to those of pressing and sintering (Figure 6.3) even if the vacuum level is notably lower. Nitrogen seems to remain confined in the outer part of the specimens while in the centre its percentage is directly comparable with that of vacuum sintered samples (Figure 6.3). Finally, carbon, which has the lowest solubility in titanium[7], increases due to the contact with the graphite die or the carbon reach atmosphere generated by the graphite at high temperature[32].

To confirm the BN surface contamination of the hot–pressed elemental titanium specimens, SEM analysis, using backscattered electron, was carried out and the results are shown in Figure 6.33.

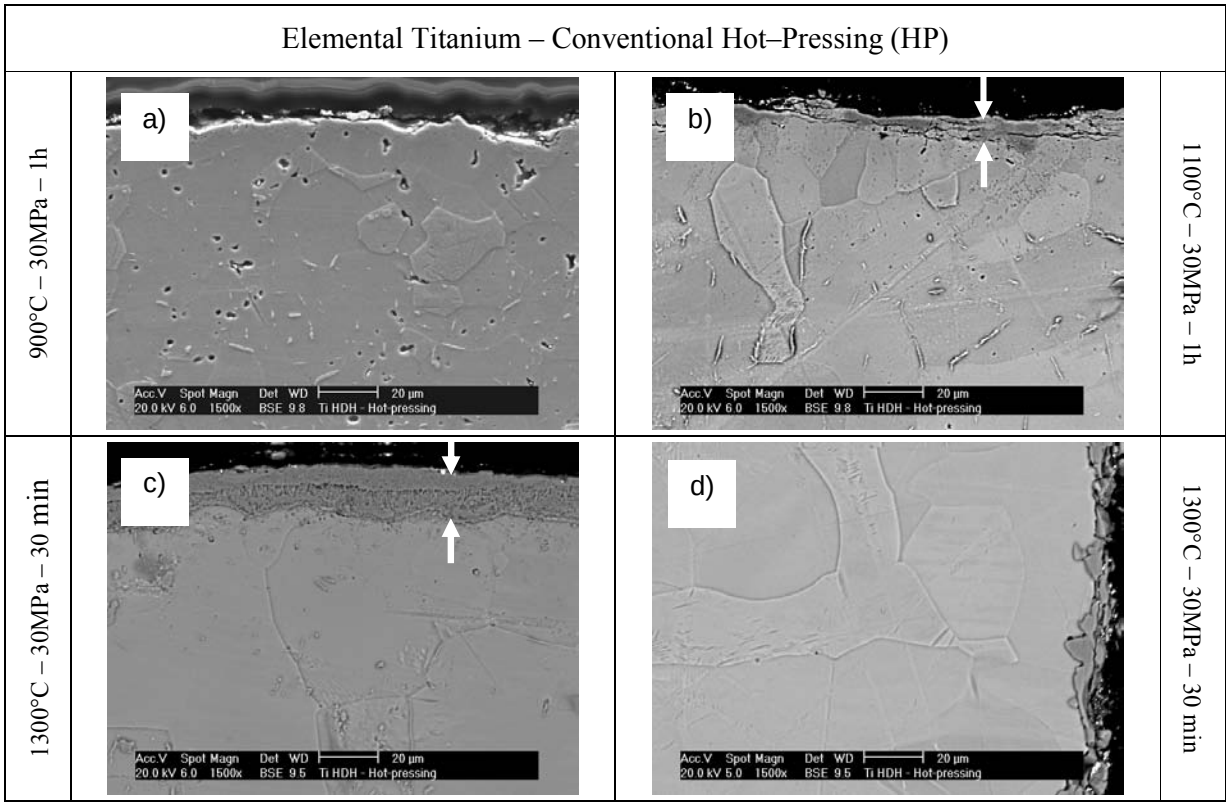

Figure 6.33 – SEM images of the surfaces of the specimens in contact with the BN coating: a) 900ºC, b) 1100ºC and c) 1300ºC, or the graphite mould d): 1300ºC.

As it was supposed on the bases of the chemical analysis results, elemental titanium powder reacts both with the BN coating and the graphite mould as BSE–SEM analysis results (Figure 6.33) reveal.

When considering the interaction of elemental titanium powder with BN, it can be seen that in samples processed at 900ºC there is no reaction layer most probably due to the relative low energy available for the decomposition of BN and the diffusion of boron and nitrogen through titanium (Figure 6.33 a).

At 1100ºC (Figure 6.33 b) an irregular dark layer variable between 5 μm and 10 μm is clearly visible and at 1300ºC this layer is already well–formed, relatively uniform and thicker (20 μm), see Figure 6.33 c). Moreover, the inner part of the reacted layer is porous and composed by columnar grains whereas the outer part is completely dense.

Energy dispersive X–ray analysis indicates that the interaction layer is composed by titanium and nitrogen (on average 6.5 wt.% equivalent to 19.5 at.%) but boron was not considered because the quantitative analysis of boron is virtually impossible using EDS analysis due to the relatively poor peak to background ratio of the boron peak.

About the interaction with the graphite die, either at 900ºC or 1100ºC there are small reacted zones but a layer could not be found as in the case of the samples processed at 1300ºC where it can be seen a non uniform layer of approximately 5–10 μm thick (Figure 6.33 d).

To better understand the nature of the reaction that goes on between the titanium powder and the BN coating, XRD analysis of the surface of the not–grinded hot–pressed samples was carried out and the results are presented in Figure 6.34.

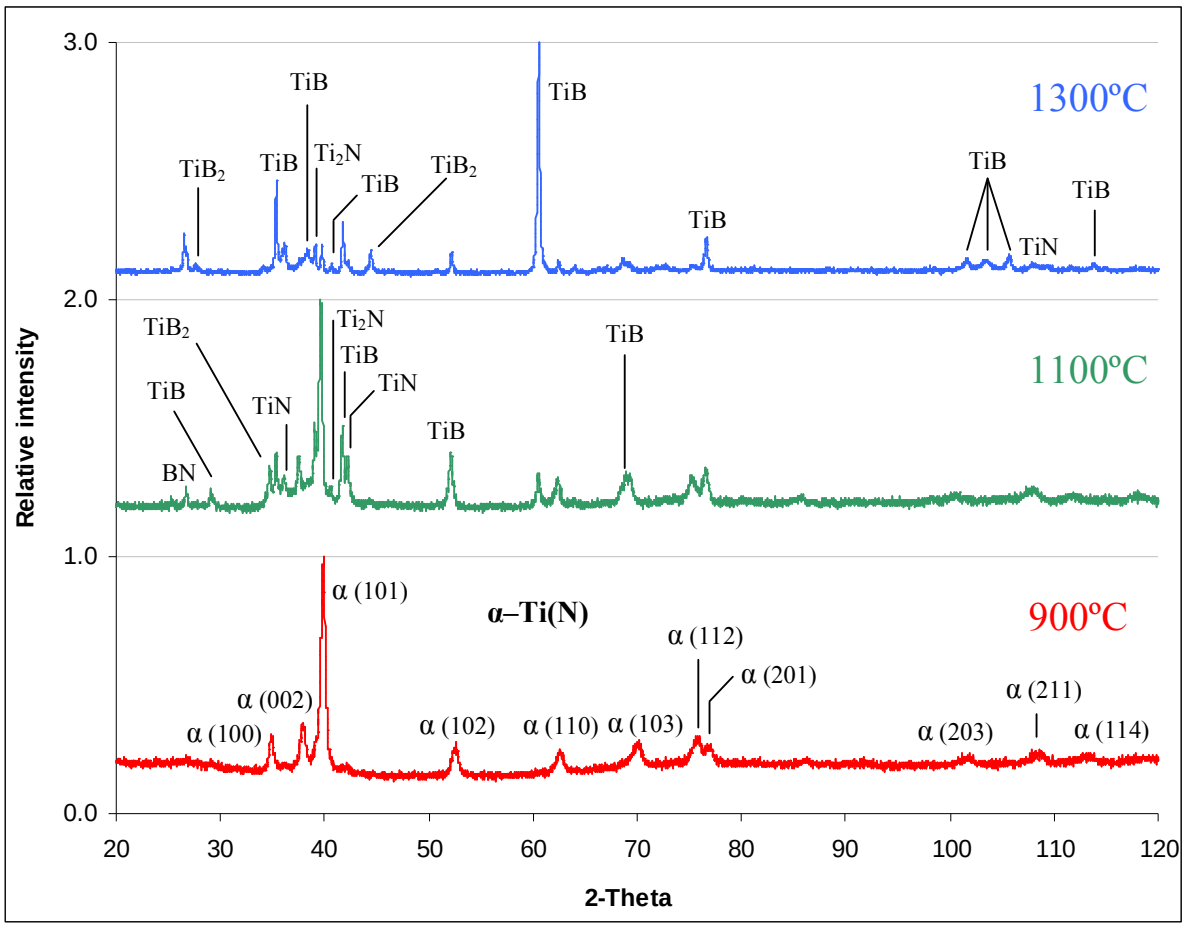

Figure 6.34 – XRD patterns of the surface of conventional hot–pressed elemental titanium specimens.

From XRD results (Figure 6.34) it can be stated that at 900°C the powder picks–up some nitrogen from the BN coating forming an interstitial solid solution of nitrogen in titanium α–Ti(N). Its peaks are slightly shifted from those of elemental alpha titanium which are marked in the XRD pattern of the powder sintered at 900ºC since it is well known that the increasing of the interstitial elements, such as nitrogen, in titanium induces an increment of both the "a" and "c" parameters of the hexagonal unit cell[33, 34].

When raising the temperature at 1100°C the amount of nitrogen increases diffusing inside the titanium matrix. This increment reflects in a slight displacement of the peaks of alpha titanium towards lower diffraction angles.

Moreover, the increment of nitrogen seems to be high enough to promote the formation of the stoichiometric compounds like Ti_2N and TiN. In the XRD pattern of the powder sintered at 1100ºC also boron, which was not detected at 900ºC, is moving toward the titanium powder forming the stable compound TiB and TiB_2.

The absence of boron or titanium boride at 900ºC is mainly due to the higher solubility of nitrogen in titanium with respect to that of boron being, in beta titanium, as high as 22 at.% and lower than 0.2 at.% for nitrogen and boron, respectively[35], even though of the greater diffusion coefficient of boron in titanium compared to nitrogen (for example at approximately 850ºC: $D_N = 1 \times 10^{-10}$ cm^2/sec[36] and $D_B = 2.16 \times 10^{-7}$ cm^2/sec[37]).

From the XRD of the specimens sintered at 1300°C, it seems that the higher temperature promotes the diffusion of nitrogen from the surface towards the titanium matrix since the relative intensity of the solid solution and TiN diminish. On the other side, boron content in the surface increases, allowing the formation of TiB as well as TiB_2, whose peaks' relative intensity increases.

It is worth mentioning that the abnormal high relative intensity of the TiB peak at 60.6º, which correspond to the (020) plane, is due to the preferred growth direction of TiB, which is [010][38].

These results are in agreement with the binary phase diagram[35] and ternary system (shown in Figure 35) where, according to the calculation of chemical equilibrium in the BN–Ti system[39] and studies about the reactions occurring at the BN–Ti interface[40, 41], diffusion of BN towards titanium leads to the formation of new phases, namely, TiB_2 (directly at the interface) and TiN (further from the interface towards the material) already at 950ºC.

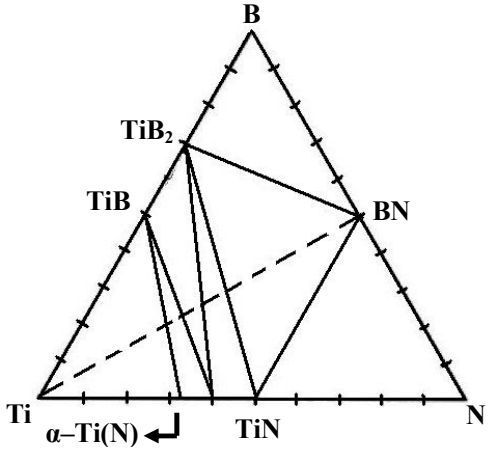

Figure 6.35 – 1090ºC isothermal section of the B–N–Ti ternary system[38, 42].

Moreover, Faran et al.[38] studied the interaction of BN sample immersed into loose titanium powder when subjected to an annealing treatment at 1000–1200ºC obtaining similar results. In particular, they found out that the reaction zone is constituted by Ti borides (TiB and TiB_2) and nitrides (TiN_{1-x} and TiN).

Other experimental results discussed by Tomashik[43] in a review of the B–N–Ti ternary system indicate that the TiN_{1-x} is a good diffusion barrier for boron at a temperature up to 1000ºC which helps to explain why boron was not detected in the specimens hot–pressed at 900ºC.

Other works have been done considering the hot–pressing technique to obtain porous titanium compacts[44] or composite materials[45] where a BN coating was used to avoid the reaction between graphite and the powder but none of them reports any kind of interaction.

6.1.3.3 – Hardness

Figure 6.36 shows the variation of the Vickers hardness with the hot–pressing temperature for elemental titanium specimens.

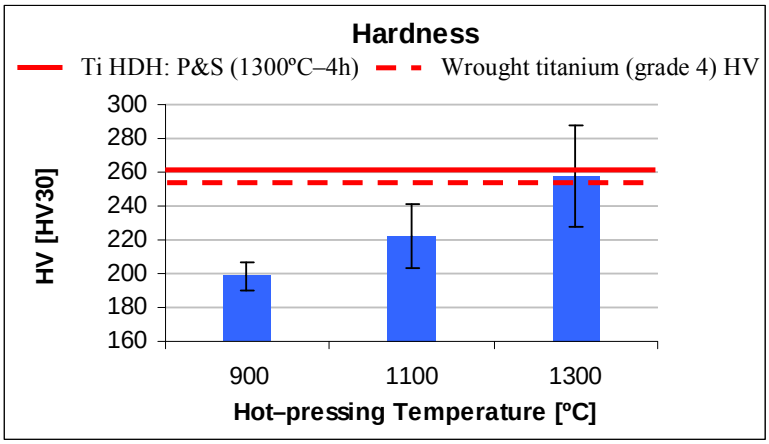

Figure 6.36 – Hardness as a function of the processing temperature for elemental titanium hot–pressed specimens.

Analysing Figure 6.36, it can be seen that hardness values of elemental titanium samples increases continuously with the sintering temperature, just like the relative density. Generally, the hardness values of the samples hot–pressed at 900ºC or 1100ºC are similar to those of P&S specimens sintered during 2 hours (Figure 6.5) whereas that of samples hot–pressed at 1300ºC resembles that of P&S at 1300ºC–4h or 1350ºC–4h.

Since nitrogen is almost equals for P&S and HP, this is mainly due to the balance of the level of relative density and the amount of oxygen dissolved.

6.1.3.4 – Properties from Bending Test

As it has been said, half of the three–point bending test samples were grinded and the other half were not to study the influence of the contamination of the surface. Therefore, two different stress–strain behaviours for each processing conditions were obtained and an example is displayed in Figure 6.37.

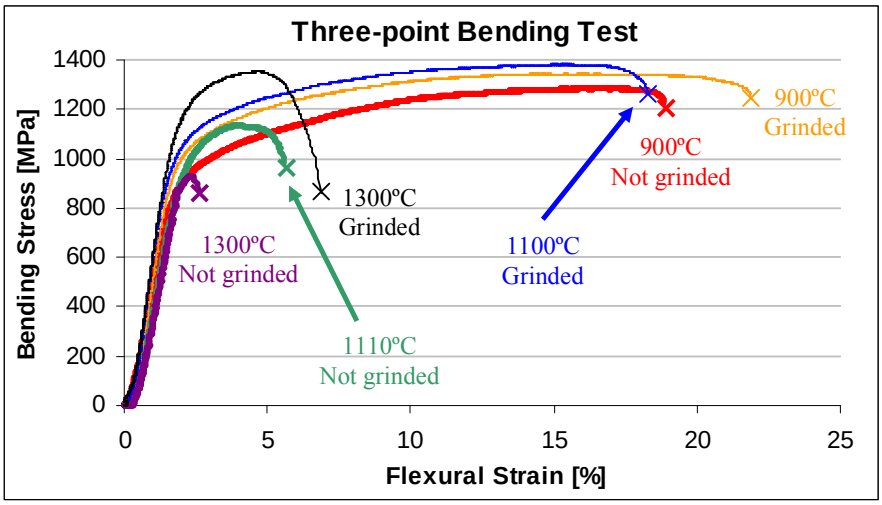

Figure 6.37 – Representative bending stress–strain curves for elemental titanium hot–pressed specimens.

Analysing the bending stress–strain curves represented in Figure 6.37, it can be seen that the removal of the outer surface changes the maximum strength and strain but does not change the shape of the stress–strain curves of the specimens hot–pressed at 900ºC or 1300ºC.

On the contrary, the grinding of the surface changes completely the bending behaviour of specimens sintered at 1100ºC, since for not grinded samples the curve looks like the ones of specimens processed at 1300ºC whereas the introduction of the grinding step makes the curve much more similar to that of sample hot–pressed at 900ºC and, therefore, with a much greater deformation and toughness.

This behaviour is most probably due to the thickness of the reacted layer and the diffusion of the interstitial elements inside the titanium matrix that increase with the temperature. In particular, at 900ºC there is only the formation of a solid solution of nitrogen in titanium which slightly brittle the material.

As explained in Section 6.1.3.2, at 1100ºC there is already an outer layer formed by nitrides and borides which significantly brittles the material and its removal makes it much more ductile. At 1300ºC, the removal of the outer layer is not that beneficial due to the higher percentage of contaminants dissolved.

Another information provided by the stress–strain curve is the flexural modulus which, in this case, seems to increase with the temperature and, thus, with the relative density, for grinded specimens.

The difference with the flexural modulus determined on pressed and sintered components is mainly due to the L/D ratio of the specimens tested since the decreasing L/D ratio produces a decrease in flexural modulus[16-18]. This is clearly visible in Figure 6.38 where the flexural modulus data of elemental titanium processed by diverse P/M techniques studied in this thesis are plotted versus the ratio between the span length (L) and the thickness (t) of the specimens.

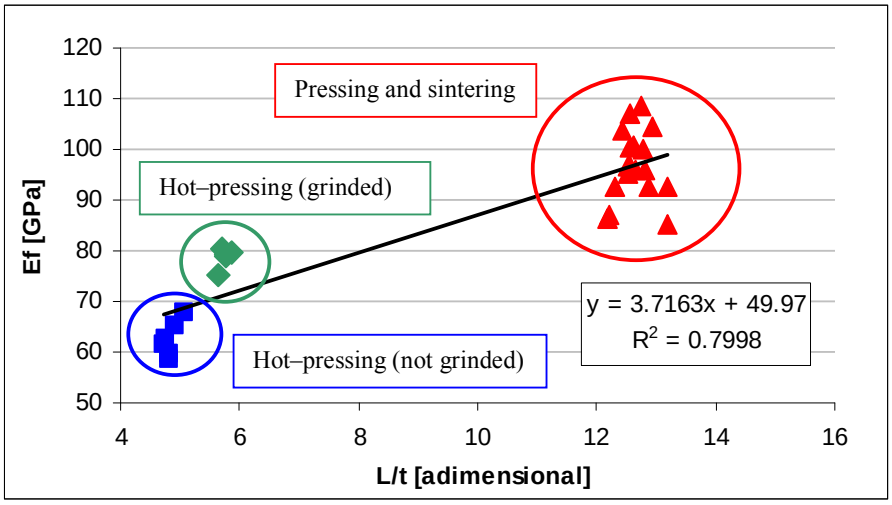

Figure 6.38 – Flexural modulus as a function of the L/t ratio for elemental titanium obtained by the diverse P/M methods studied.

As it can be seen in Figure 6.38, the flexural modulus of elemental titanium obtained either by pressing and sintering or hot–pressing is highly dependent on the length between supports (L) and thickness (t) ratio where a thicker specimen has a lower flexural modulus. This can be easily noticed comparing the values of the flexural modulus for the hot–pressed components where the removal of the outer layer induces an increment of approximately 10 GPa.

It is worth mentioning that the greater scattering of the not grinded specimens depends on the thickness of the reacted layer and that of P&S samples depends on the different levels of relative density obtained by employing different sintering parameters.

The mean values of maximum bending strength and flexural strain for grinded and not grinded specimens are represented in Figure 6.39 as a function of the processing temperature.

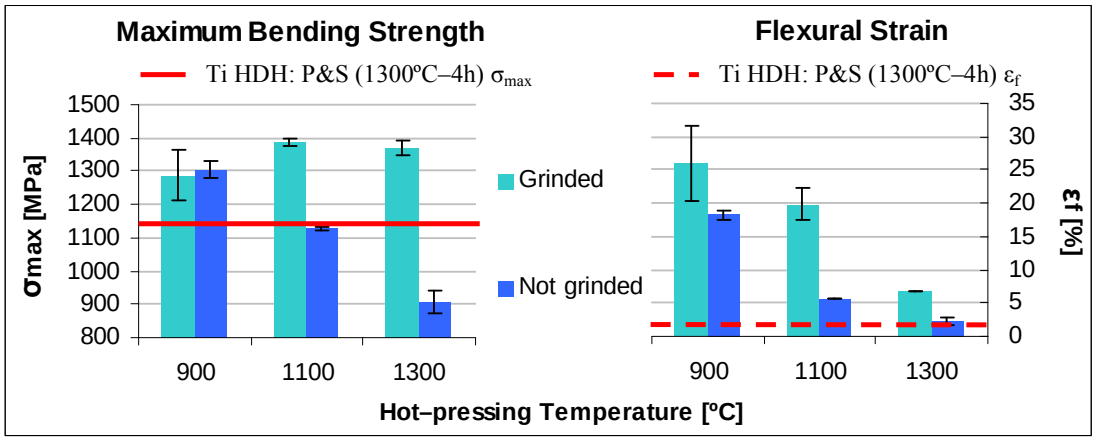

Figure 6.39 – Mechanical properties as a function of the processing temperature for elemental titanium hot–pressed specimens: maximum bending strength (left) and flexural strain (right).

As it can be seen in Figure 6.39–left, the maximum bending strength values for grinded samples increase slightly with the hot–pressing temperature or remain constant but they are always higher than the value of the P&S samples sintered at 1300ºC–4h.

This trend is in accordance with the relative density and the interstitials content of hot–pressed specimens. For the not grinded samples, the maximum bending strength significantly decrease with the temperature, which can be due to the reacted layer on the surface, whose thickness increases with the temperature, which brittles the material. Nonetheless, the maximum bending strength obtained at the lowest temperature matches with the flexural stress found by other authors in wrought titanium (1281 MPa)[13].

On the other hand, the flexural strain (Figure 6.39–right) decrease with the hot–pressing temperature for both grinded and not grinded samples even thought the strain for grinded specimens is significantly higher.

Compared to the flexural strain of P&S samples, the HP grinded specimens have higher strain, for the same processing temperature (1300ºC). Provided that the interstitials content is similar, the main influencing could be the lower porosity of hot–pressed samples but the microstructure would also have an influence on the mechanical behaviour and its study is presented in Section 6.1.3.5

6.1.3.5 – Microstructural Analysis

As for the other types of powder processing, the microstructure of hot–pressing specimens was analysed by SEM and LOM. The results by LOM on etched samples, which are representative, are shown in Figure 6.40.

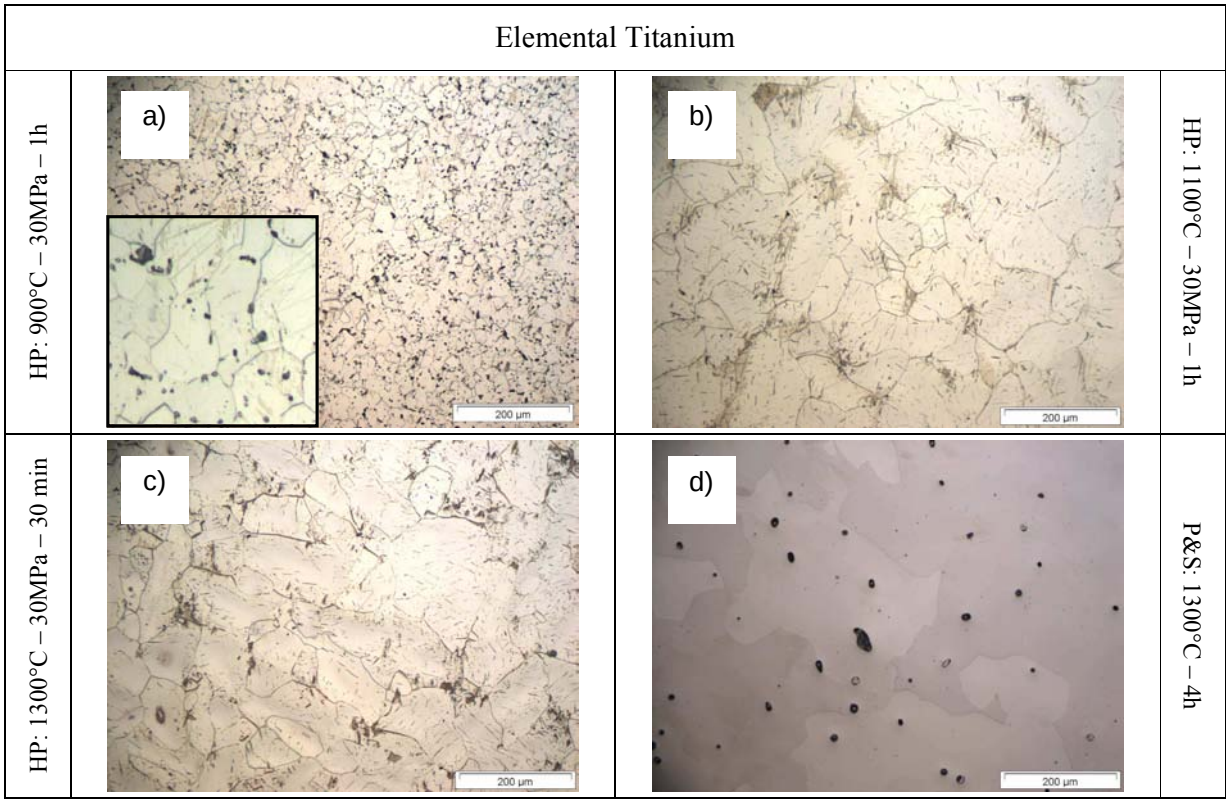

Figure 6.40 – Optical microscopy images for elemental titanium hot–pressed at: a) 900ºC, b) 1100ºC and c) 1300ºC, and d): P&S at 1300ºC–4h (reference).

As it can be seen in Figure 6.40, the microstructure of elemental titanium processed by means of hot–pressing is mainly composed by not equiaxed alpha grains and some transformed beta platelets[29]. The grain size grows with the processing temperature, especially when the temperature increases from 900ºC to 1100ºC. This is most probably due to the fact that 900ºC is very close to the beta transus and, thus, at the beginning, part of the thermal energy available is employed in the allotropic transformation.

Compared to pressing and sintering specimens, the grain size of the hot–pressed samples seems to be smaller, which justify the higher maximum bending strength obtained after the removal of the outer layer.

During the microstructural analysis it was also discovered that inside the alpha grains, as well as at the grain boundaries, there were needle–like grains or platelets with different size and orientation as it can be seen in Figure 6.41, which shows a magnification of the microstructure of specimens hot–pressed at 1100ºC and 1300ºC.

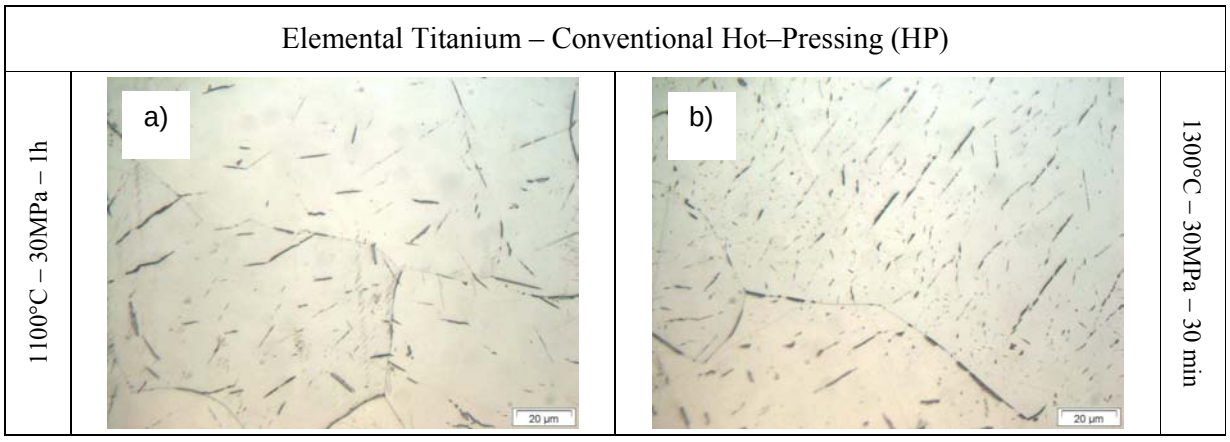

Figure 6.41 – Details of the needle–like grains or platelets found in elemental titanium hot–pressed specimens: a) 1100ºC and b) 1300ºC.

The needle–like grains shown in Figure 6.41 derive from the original beta phase present at 1100ºC or 1300ºC but they can not be due exclusively to the cooling of the samples since the cooling rate is not high enough to promote their formation.

Once checked by XRD analysis that these features are not either nitrides or borides derived by the diffusion of this interstitials towards the titanium matrix, they are most probably due to the mismatch plasticity induced by the phase transformation, where the beta lattice is less dense than the alpha one, under pressure. Therefore, they could be due to the mismatch plasticity provokes by the internal stress (β→α) and the external stress[46] (uniaxial pressure).

On the other hand, they could also be reorientation bands (RBs) where their appearance indicates a change in the deformation process of the material. In particular, the deformation changes from translational (laminar) plastic flow to a stage where the evolving rotational (turbulent) motion of large dislocations assemblies coexist with the remaining translational slip of individual dislocations[47]. This stage is dependent on the sample properties (geometry, structure state) and on the deformation conditions (temperature, rate of deformation and type of loading).

Anyhow, when elemental titanium is deformed at high temperature in the beta phase region, these RBs are called microband substructures since the large plastic deformation at high temperature can lead to the formation and movement of high density of dislocations more easily, which result in local rotational deformation of the substructural elements inside the grains[48].

Another interesting factor is the distribution of this structure of dislocations since the specimens hot–pressed at 1100ºC (Figure 6.41 a) are characterised by heterogeneous groups or bands whilst the microstructure of the samples sintered at 1300ºC (Figure 6.41 b) is characterised by a more homogeneous distribution of the dislocations throughout the grains.

This is because the increase in dislocation density (ρ) versus the applied strain (ε) is characterised by two linear regions, an initial region of high slope (Stage I) followed by a second region whose slope is an order of magnitude smaller (stage II), distinguishable by the homogeneity of the distribution of the dislocations within the grains[49].

Nevertheless, the size of the needle–like grains shown in Figure 6.41 reaches a maximum length of 15–20 μm, much longer than that found by Chu et al.[48] who studied the hot–pressing of elemental titanium applying a uniaxial pressure of 20 MPa. This makes more plausible to think that they are beta needles or a combination of both effects where, obviously, the very fines needles (1 μm in length) could be RBs.

6.1.4 – Inductive Hot–pressing (IHP)

In order to carry out the experiments, approximately 1.5 g of powder was loaded into a 10 mm diameter graphite mould to attain disc shaped samples of around 3.8 mm height. Before the hot–pressing step, the specimens were cold uniaxially consolidated by means of the two graphite punches in a manual press. During the study, the uniaxial pressure and the time were kept constant at 50 MPa and 15 minutes, respectively, whereas the temperature was changed (1100ºC and 1300ºC).

Figure 6.42 shows an example of the inductive hot–pressing cycle used for elemental titanium, where it can be noticed that the total processing time is approximately 40 minutes, much shorter than a conventional hot–pressing cycle of 6 hours or longer (Figure 6.30), thanks to the higher heating and cooling rate employable.

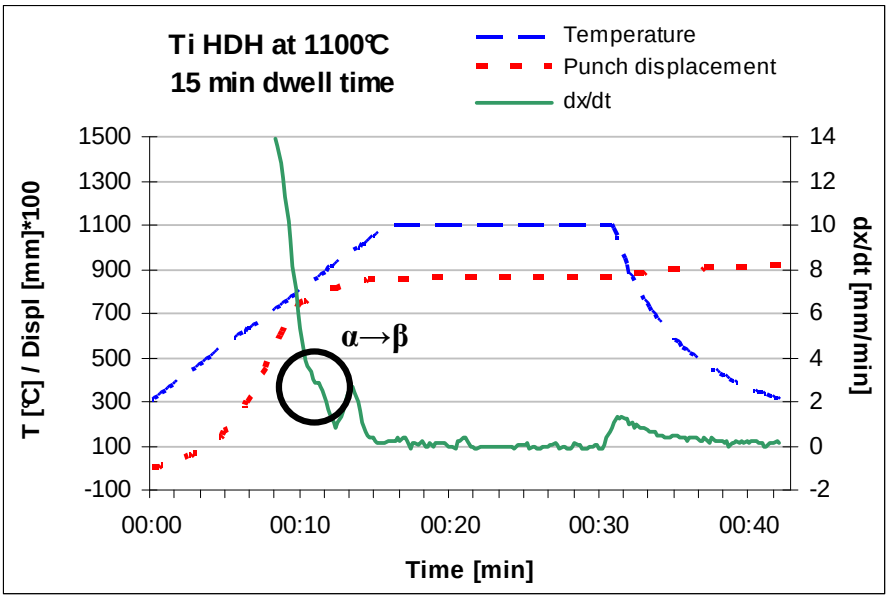

Figure 6.42 – Temperature, punch displacement and densification rate profiles recorded during the processing of elemental titanium by inductive hot–pressing at 1100ºC.

Analysing the densification rate (dx/dt) shown in Figure 6.42, it can be seen that the densification is, practically, completed when the maximum temperature is reached since the curve stabilises. The variation recorded just before the cooling of the specimens is associable to the shut–down of the current where the samples start to cool and shrink.

Moreover, it should be noticed that, during the heating step, at a temperature slightly lower than 900ºC a peak is formed which matches with the allotropic transformation (beta transus) from H.C.P. alpha to B.C.C. beta. Exactly the same behaviour was found when processing the elemental titanium powder at 1300ºC.

6.1.4.1 – Relative Density

As for conventional hot–pressing, before the characterisation, the specimens obtained were sandblasted to clean the surfaces which were in contact with the graphite mould and punches during consolidation. Moreover, due to the relatively small size of the specimens, only hardness measurements could be carried out to determine the influence of the processing parameters on the mechanical properties.

The results of the relative density measurements carried out on the elemental titanium hot–pressed specimens are presented in Figure 6.43.

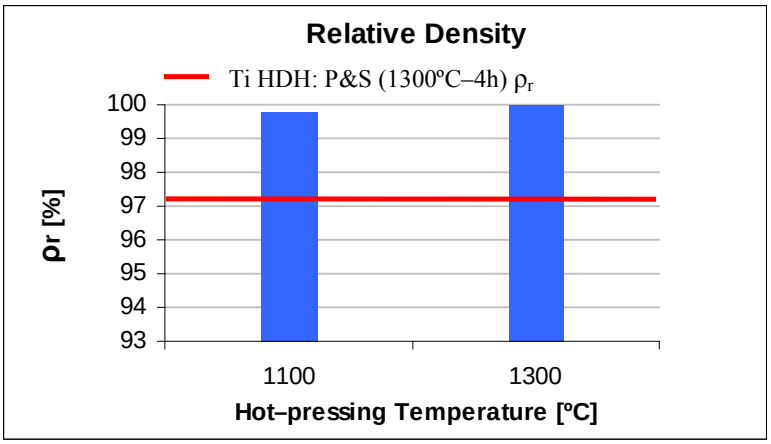

Figure 6.43 – Relative density as a function of the processing temperature for elemental titanium inductive hot–pressed specimens.

As it can be seen in Figure 6.43, inductive hot–pressing permits to obtain fully dense material at both temperatures considered in this study. Therefore, inductive hot–pressing results to be more advantageous in terms of final density either compared to P&S or conventional hot–pressing, reducing significantly the total processing time.

Similar results were obtained by Liu and Kao[50] using a process called "resistance sintering" or by Zadra et al.[51] when processing elemental titanium powders by means of spark plasma sintering, a consolidation technique very similar to inductive hot–pressing.

6.1.4.2 – Chemical Analysis

Chemical analysis, precisely oxygen, nitrogen and carbon determination results are shown in Figure 6.44.

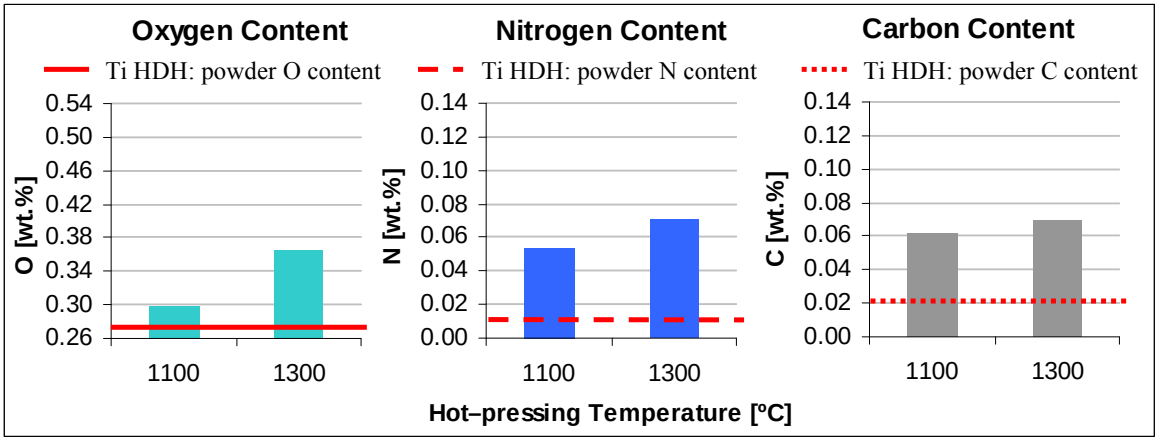

Figure 6.44 – Chemical analysis as a function of the processing temperature for elemental titanium inductive hot–pressed specimens: oxygen (left), nitrogen (centre) and carbon (right).

As it can be noted in Figure 6.44, there is some important contamination of the specimens with respect to the initial amount of each one of the chemical element considered. However, the values shown are directly comparable to the ones obtained for P&S and conventional hot–pressing confirming that the contamination derives from the elements adsorbed on the powder particles. More in detail, with respect to the specimens sintered at 1300ºC during 4 hours (O = 0.414 wt.% and N = 0.0535 wt.%), oxygen is lower and nitrogen just a little bit higher.

Compared to conventional hot–pressing, it seems that, in general, inductive hot–pressing leads to lower oxygen contamination, especially at low temperatures, at the same time that to a somewhat higher nitrogen and carbon percentage.

6.1.4.3 – Hardness

The variation of the Vickers hardness with the inductive hot–pressing temperature for elemental titanium is presented in Figure 6.45.

Hardness of inductive hot–pressed titanium components (Figure 6.45) increases with the processing temperature and the values obtained are very similar either to P&S specimens or to conventional hot–pressed samples processed at the same temperature even though of the longer sintering time.

The chemical analysis results match perfectly with the hardness values since the lower oxygen content effect is balanced by the higher nitrogen and carbon.

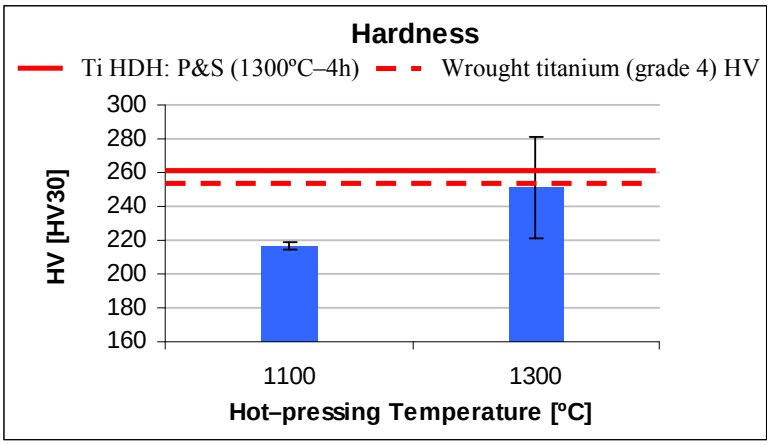

Figure 6.45 – Hardness as a function of the processing temperature for elemental titanium inductive hot–pressed specimens.

When considering hardness measurements and contaminants contents of conventional hot–pressed and inductive hot–pressed samples, due to the similar processing conditions and relative density values, a good correlation exist with a R^2 coefficient of 0.89 using the equation proposed by Okazaki and Conrad[49] to calculate the equivalent interstitial concentration or oxygen equivalent which influences the VHN.

6.1.4.4 – Microstructural Analysis

Microstructural analysis either by optical microscopy or by SEM of elemental titanium processed by inductive hot–pressing was performed and the results of LOM are presented in Figure 6.46.

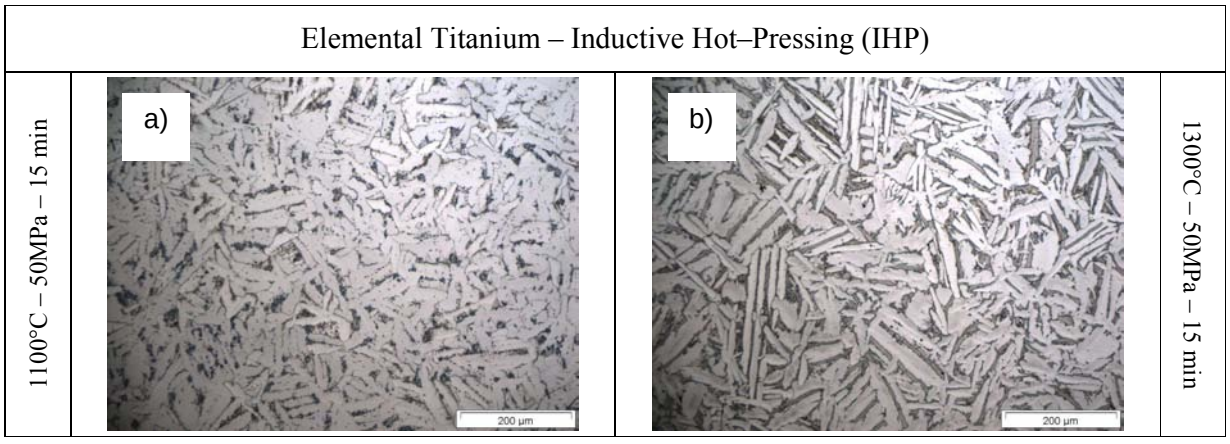

Figure 6.46 – Optical microscopy images for elemental titanium inductive hot–pressed at: a) 1100ºC and b) 1300ºC.

The microstructure of inductive hot–pressed elemental titanium specimens (Figure 6.46) is composed by alpha grains and alpha platelets with cored appearance, resulting in a microstructure of irregular and plate–like alpha grains[51], where the amount of this last in much higher in the samples processed at the 1300ºC.

Liu and Kao found a similar microstructure when processing elemental sponge titanium by resistance sintering. The microstructure is thus constituted by a dark phase, which is considered as secondary alpha (which was once melt during sintering and transformed back to α–phase during subsequent cooling) dispersed in a light matrix of primary α[50].

The greater amount of transformed beta or acicular alpha found in comparison to conventional hot–pressed components is manly due to the much faster cooling intrinsic of the inductive hot–pressing.

As in conventional hot–pressed samples, microband substructures generated by the formation and movement of high density of dislocations in the beta phase region were found. However, the microbands seem to be much more concentrated at the alpha grain boundaries and less in amount, most probably due to the faster cooling rate which favours the formation of transformed beta.

If the elemental titanium powder was processed at a temperature below the alpha to beta transformation temperature, the microstructure would have been composed by a homogeneous distribution of fine and equiaxed alpha grains as found in other studies[45, 51].

6.1.5 – P/M Techniques Comparison

In this section a comparison of the results obtained in terms of relative density, Vickers hardness, maximum bending strength and flexural strain for the different powder metallurgy methods for processing elemental titanium powder is presented.

It is worth mentioning that in the case of mechanical properties the comparison was done, where possible, between samples processed by diverse techniques and different parameters but having similar equivalent oxygen content.

The best relative density, intended as the highest value, for each technique considered and discussed in this chapter is presented in Figure 6.47.

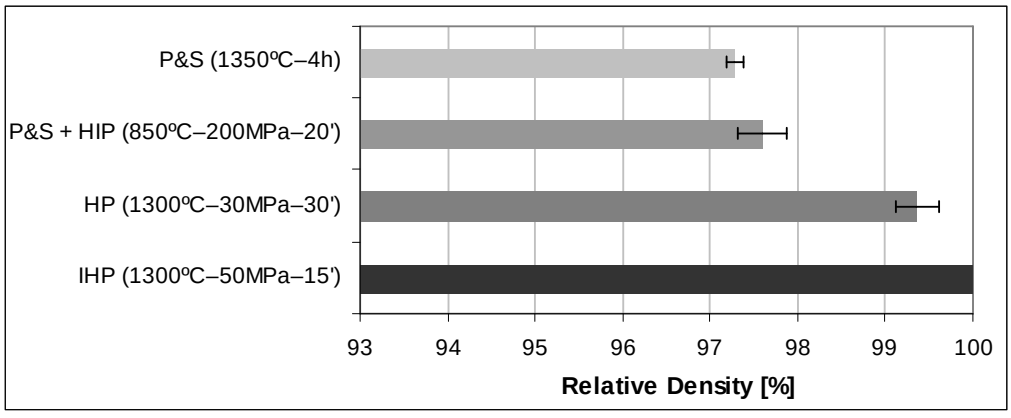

Figure 6.47 – Comparison of the highest relative density for elemental titanium obtained by different P/M techniques.

As it can be seen in Figure 6.47, samples processed by pressing and sintering reach relative densities of approximately 97% and the application of secondary processing by HIP only leads to a small decrease in residual porosity most probably due to the fact that the porosity in concentrated in the surface of the specimens[28].

The application of a uniaxial pressure during the sintering step (hot–pressing) permits to increase the final relative density where the higher the pressure the lower the residual porosity. In the case of inductive hot–pressing there is also a contribution of the external electric field on the densification behaviour of the powder. Nonetheless, employing hot–pressing method fully dense materials can be obtained.

The equivalent oxygen for the comparison of the Vickers hardness (Figure 6.48) for different P/M methods was calculated employing the formula proposed by Okazaki and Conrad[11] (see Eq. 14 in Section 2.7). The Vickers hardness data shown in Figure 6.48 refer to samples obtained by different P/M techniques but with equivalent oxygen content of approximately 0.45 wt.%.

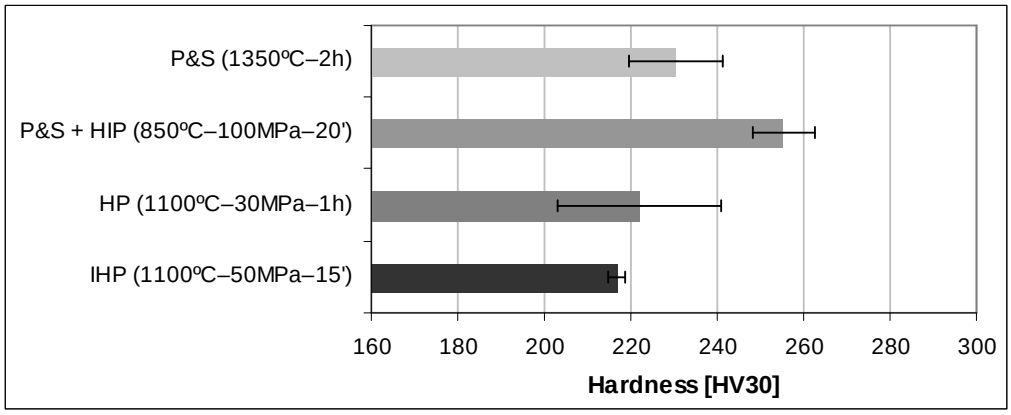

Figure 6.48 – Comparison of the hardness for elemental titanium obtained by different P/M techniques (equivalent oxygen content of approximately 0.45 wt.%).

Comparing the hardness of elemental titanium processed by diverse P/M routes and excluding the effect of chemical interstitials (Figure 6.48), it can be noticed that there is a strong influence from the consolidation approaches since these determine the final relative density and the microstructure constituents.

More in detail, P&S leads to a hardness of 235 HV30 and a subsequent HIP in the alpha phase region (850ºC) induces an increment in hardness due to the reduction of the residual porosity. On the other side, hot–pressing results in a higher relative density and lower hardness most probably due to the appearance of transformed beta as a microstructural constituent. This is further confirmed by the slightly lower hardness of inductive hot–pressed specimens where the amount of alpha platelets is higher provoked by the faster cooling with respect to conventional hot–pressing.

It has been shown that the final chemical analysis greatly influences the mechanical properties of titanium and titanium alloys, therefore, the equation suggested by Wood[19] (see Eq. 15 in Section 2.7) was used to compare the maximum bending strength obtained for diverse P/M techniques.

In particular, the data shown in Figure 6.49 correspond to specimens with an equivalent oxygen content of approximately 0.48 wt.%. It is worth remembering that no flexural properties could be determined in inductive hot–pressed materials due to the limited dimensions of the specimens.

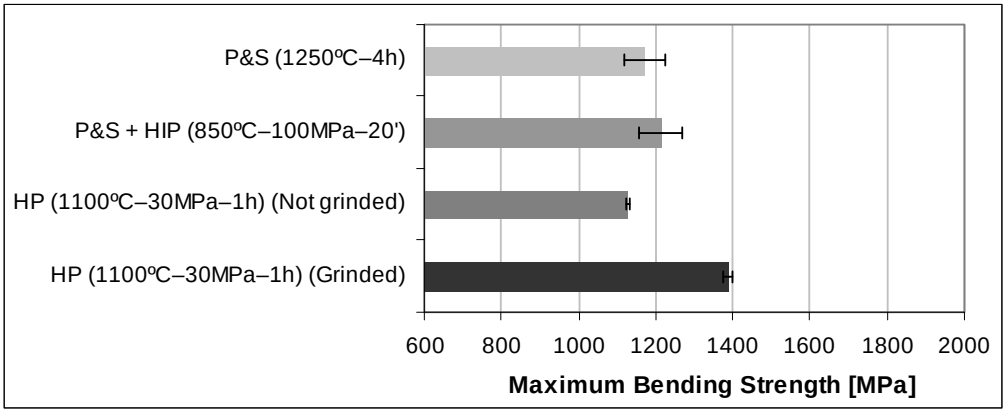

Figure 6.49 – Comparison of the maximum bending strength for elemental titanium obtained by different P/M techniques (equivalent oxygen content of approximately 0.48 wt.%).

As it can be seen in Figure 6.49, excluding the effect of the interstitial elements, the maximum bending strength slightly increases when elemental titanium is subjected to a secondary HIP process compared to P&S mainly due to the higher final relative density.

Hot–pressing allows reaching higher strength most probably thanks to the formation of a microstructure composed by alpha grains and beta platelets. Nevertheless, the contamination of the surface from the BN coating, which results in the formation of a reacted layer composed by titanium nitrides and borides decreases the maximum bending strength approximately 250 MPa.

Regarding the flexural strain, the equation found by Wood[19] (see Eq. 16 in Section 2.7) where nitrogen has approximately two times the effect of oxygen and carbon has half the effect of oxygen on the strain was used and the results are shown in Figure 6.50.

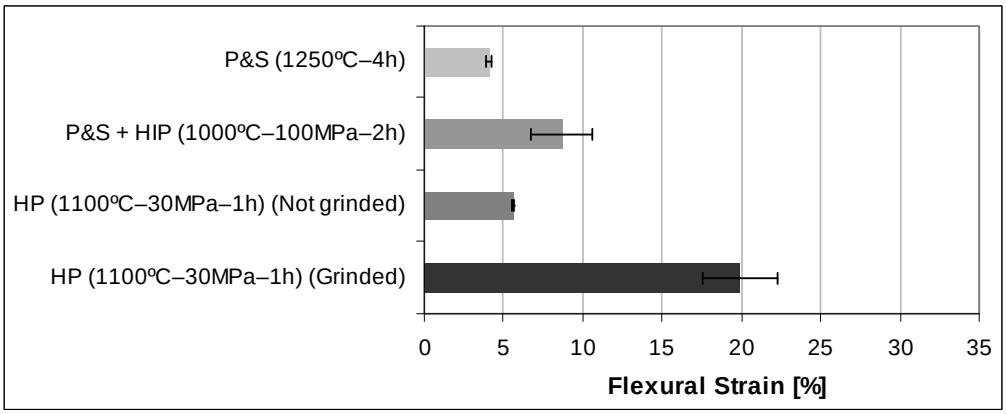

Figure 6.50 – Comparison of the flexural strain for elemental titanium obtained by different P/M techniques (equivalent oxygen content of approximately 0.45 wt.%).

Analysing the flexural strain data (Figure 6.50), it can be stated that, once more, the application of a post–processing by HIP or the employment of a uniaxial pressure increases the toughness of elemental titanium due to the lower residual porosity and the respective microstructural features.

It should be specified that the application of the pressure to loose powder seems to be much more effective. Nonetheless, a grinding step is needed after the consolidation to remove the reaction layer which brittles significantly the material.

6.1.6 – Partial Conclusions

Based on the results of the study of processing elemental titanium by different P/M techniques, it can be concluded that:

Uniaxial Pressing and Sintering (P&S): near–net shape titanium components with a final maximum relative density of approximately 97% can be obtained with the simplest P/M approach even if precautions should be taken during their design regarding the shrinkage induced by the sintering step that can be as high as 14.5% in volume.

The highest values for mechanical properties are maximum bending strength of 1200 MPa and flexural strain of 5% as well as UTS of 590 MPa and strain of 12% and hardness values comparable with wrought titanium grade 4 can be attained.

Care must be taken during the handling and the processing of the powder because oxygen or nitrogen pick–up can occurred resulting in a strengthening and lost of toughness of elemental titanium.

The final microstructure of P&S titanium is composed exclusively by alpha grains and their size increases either with the sintering temperature or the time where the time has the strongest effect.

The specimens submitted to tensile test show ductile fracture by microvoids coalescence known as dimple rupture mainly located at residual porosity sites.

Finally, slightly higher thermal conductivity at room temperature and equals electrical resistivity can be attained by processing elemental titanium by P&S in comparison to the conventional metallurgical route.

Hot Isostatic Pressing (HIP): applying a HIP cycle as secondary process to reduce the residual porosity leads to an increment of the final relative density even if it is not as effective as desired, most probably due to the open porosity typical of floating die P&S components.

Better mechanical properties can be obtained but care must be taken in the selection of the processing parameters since their combination can result in a great variety of microstructures. In particular, the application of a pressure of 200 MPa in the alpha phase region induces an abnormal alpha grain growth. However, annealing heat–treatments could be carried out to recover the initial microstructure composed by only alpha grains.

Conventional Hot–pressing (HP): the consolidation of the powder under the simultaneous application of temperature and pressure allows to reach always higher relative density compared to P&S even if the temperature is lower and the dwell time is shorter. Similar hardness can be attained using the same processing temperature but shorter time compared to P&S.

The utilisation of a graphite mould and a high stability BN coating to facilitate mould release and to prevent reactions could not avoid completely the interaction with elemental titanium. Therefore, elemental titanium components obtained by hot–pressing should be either milled or grinded in order to remove the surface reacted layer which is constituted by titanium nitrides and borides.

Finally, higher maximum bending strength (1400 MPa) and significantly greater flexural strain (26%) than P&S can be achieved due to the lower percentage of residual porosity and the formation of alpha platelets induced by the strain provoked by the application of a uniaxial pressure at high temperatures. Most probably, a microstructure composed by alpha grains could be obtained by annealing the components once consolidated.

Inductive Hot–pressing (IHP): the consolidation of the powder under simultaneous temperature and pressure by induction heating permits to attain fully dense material with hardness and chemical compositions similar to the previously described methods. Once again, contamination from the graphite mould could occur and machining by milling should be performed to remove the contaminated layer.

The total processing time results to be much shorter thanks to the higher heating and cooling rates employable. However, the faster cooling leads to the formation of a greater amount of transformed beta which influences the final mechanical properties.

6.2 – Ti–3Al–2.5V ALLOY

In this section are presented and discussed the results obtained from the processing and characterisation of the P/M Ti–3Al–2.5V alloy. It is worth remembering that Ti32–PA was obtained by the conventional blending of elemental titanium and a Ti–6Al–4V prealloyed powder whilst Ti32–MA by adding an Al:V master alloy to elemental titanium.

The properties attained for the different P/M processing methods are shown as a comparison between the two fabrication routes in order to identify advantages and disadvantages. Moreover, the final properties are compared to that of elemental titanium (Section 6.1) and to that of wrought Ti–3Al–2.5V since, as it has been said in Chapter 1, no studies about the P/M processing of the Ti–3Al–2.5V alloy were found.

6.2.1 – Uniaxial Pressing and Sintering (P&S)

6.2.1.1 – Relative Density

To better understand and explain the results of relative density obtained (Figure 6.51), it is interesting to know that the green density of Ti32–PA (69.00% ± 0.75%) results to be much lower compared to Ti32–MA (86.64% ± 0.24%), in agreement with the compressibility test results (see Section 3.2.5).

Consequently, the volume variation induced by the sintering step is much more pronounced for Ti32–PA that has a mean shrinkage of 25% where this value slightly increases with the increment of the temperature. Conversely, the time does not influence significantly the contraction of the components as much as the temperature does. Ti32–MA shows the same behaviour than Ti32–PA with processing time and temperature although the average shrinkage is about 11% due to the higher green density of the samples.

The densification of the samples increases with the temperature for both powders where the densification of Ti32–MA is always higher with respect to Ti32–PA. Therefore, since Ti32–PA starts from a lower green density and it has a smaller densification, Ti32–MA would reach higher final relative density (Figure 6.51).

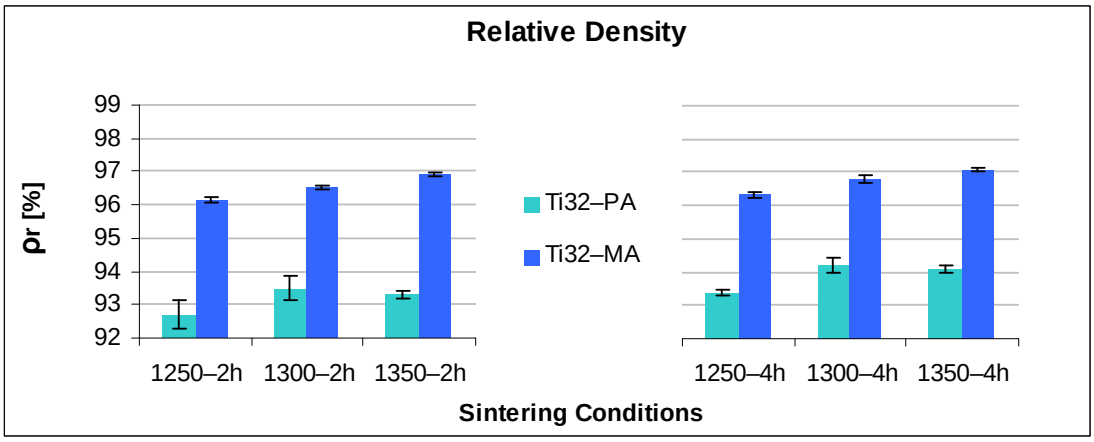

Figure 6.51 – Relative density as a function of the sintering conditions for Ti32–PA and Ti32–MA bending specimens.

As expected, the relative density (Figure 6.51) increases with the sintering temperature and it is a little bit higher for longer processing time. Furthermore, Ti32–MA reaches always higher relative density than Ti32–PA and similar to that of elemental titanium (Figure 6.2). The final lower relative density of Ti32–PA shown in Figure 6.51 compared to Ti32–MA is mainly due to the lower compaction pressure (300 MPa) applied to consolidate the specimens which results in a lower green density.

Based on these results, tensile test specimens were sintered studying only the influence of the sintering temperature since increasing the time to 4 hours does not lead to a significant increment in terms of relative density to justify the higher production costs.

Tensile test specimens with "dogbone" geometry were produced for both Ti32–PA and Ti32–MA using a pressure of 700 MPa reaching a green density of 82.86% ± 0.57% for Ti32–PA and 86.34% ± 0.39% for Ti32–MA. The green density obtained for Ti32–PA is much higher compared to that of bending specimens due to the difference in the applied pressure whereas the value for Ti32–MA coincides with that of bending samples. The results of the relative density of tensile test samples sintered materials are shown in Figure 6.52.

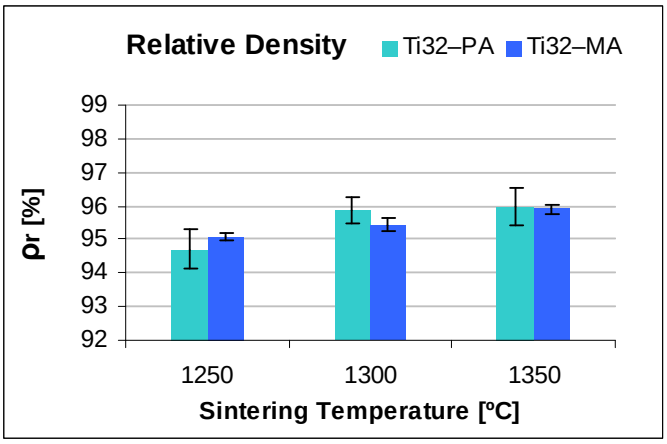

Figure 6.52 – Relative density as a function of the sintering temperature for Ti32–PA and Ti32–MA tensile specimens (sintering time: 2h).

As for the bending specimens, the relative density of the tensile samples (Figure 6.52) increases with the sintering temperature reaching comparable values on the case of Ti32–MA but somewhat lower than those shown in Figure 6.51.

When considering Ti32–PA, it should be noted that the final relative density of sintered tensile specimens is, on average, 2.5% higher compared to the rectangular samples due to the greater pressure used to press them. Therefore, the comparison of the relative density of samples produced from the two types of powder (PA and MA) does not indicate a better method because the values obtained for both alloys are very similar.

The values of relative density of the tensile test specimens made out of Ti–3Al–2.5V alloy shown in Figure 6.52 are, in general, 1–1.5% lower than the values obtained from elemental titanium powders (Figure 6.2–right) whilst the values for the three–point bending test of the Ti32–MA (Figure 6.51) are similar to that of elemental titanium (Figure 6.2–left).

6.2.1.2 – Chemical Analysis

Chemical analysis of the Ti–3Al–2.5V alloy processed by pressing and sintering was performed in three–point bending test specimens determining oxygen (Figure 6.53) and nitrogen (Figure 6.54) content as well as in tensile test samples (Figure 6.55) due to the great influence of these interstitials on the mechanical properties of titanium[5, 6].

Figure 6.53 shows the oxygen content of the sintered samples as a function of the sintering temperature and time for bending samples compared to the content of the starting powder.

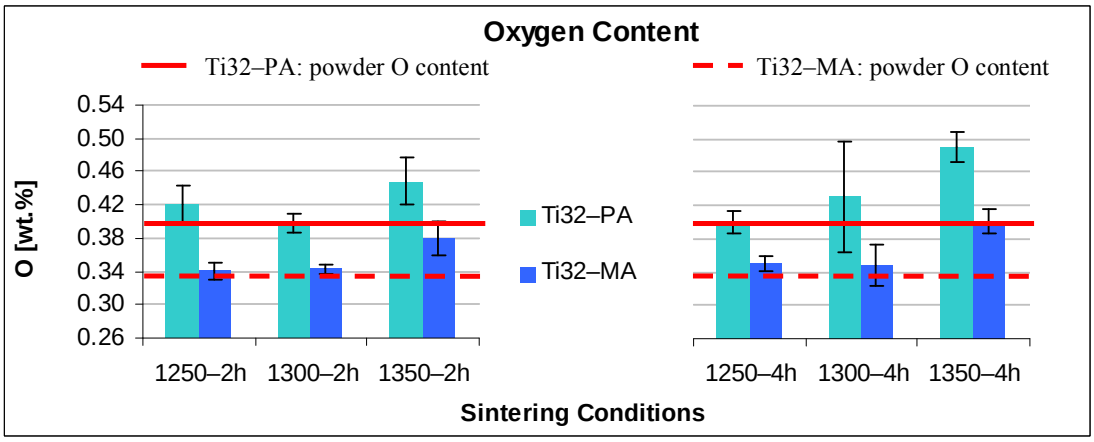

Figure 6.53 – Oxygen content as a function of the sintering conditions for Ti32–PA and Ti32–MA bending specimens.

As it can be seen in Figure 6.53, although there is not a clear correlation with the temperature or the time, it is possible to say that only for the highest sintering temperature the oxygen content of sintered samples is significantly higher than that of the starting powder. Moreover, Ti32–MA samples contain lower amount of oxygen than Ti32–PA samples also due to the lower oxygen content of the starting powder.

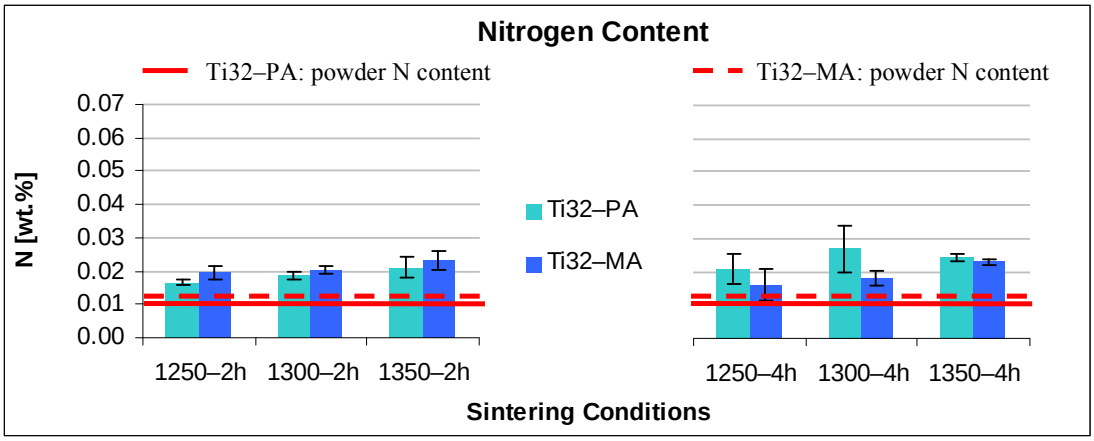

Figure 6.54 – Nitrogen content as a function of the sintering conditions for Ti32–PA and Ti32–MA bending specimens.

Regarding the nitrogen content, Figure 6.54 shows data for sintered specimens and starting powders. In this case, the nitrogen content of starting powders, as well as that of the sintered specimens, is quite similar and the difference between Ti32–PA and Ti32–MA is almost insignificant. Generally, the mean value of nitrogen content for all the sintering conditions, and independently of the powder production route, is about 0.02 wt.% which indicates that it increases compared to the starting powder. Nevertheless, this value is lower than the figure specified for this alloy produced by conventional metallurgy, which is equal to 0.03 wt.%[9].

The oxygen and nitrogen content determined on tensile test specimens is reported in Figure 6.55.

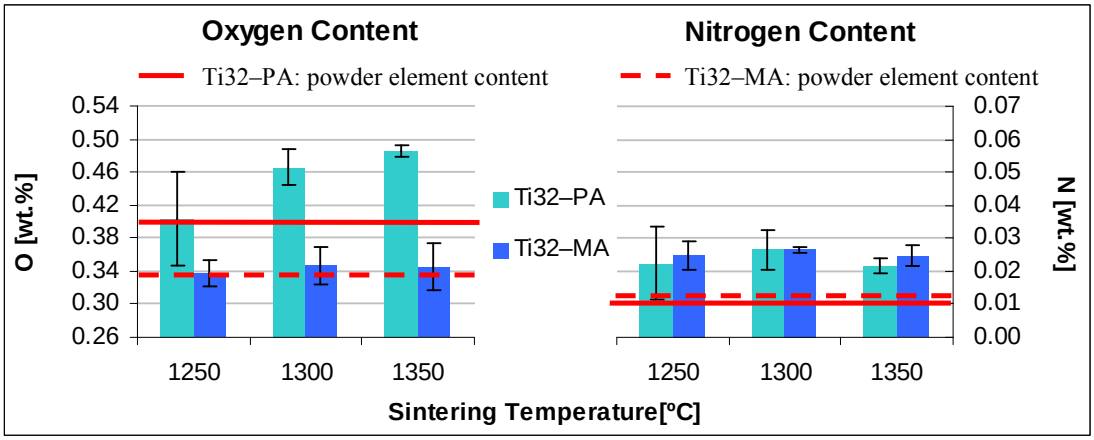

Figure 6.55 – Chemical analysis as a function of the sintering conditions for Ti32–PA and Ti32–MA tensile specimens: oxygen (left) and nitrogen (right).

As it can be seen in Figure 6.55, the oxygen content of the sintered specimens increases with the temperature for the Ti32–PA alloy whereas it remains approximately constant for the Ti32–MA. On the other side, there is always some nitrogen pick–up during sintering.

The chemical analysis results shown in Figure 6.55 are similar to those shown in Figure 6.53 and Figure 6.54 with the exception of the values of oxygen of tensile samples of the Ti32–PA alloy, which are a little bit higher. This difference could be due mainly to three factors: the handling of the powder, the level of vacuum, since the sintering step is normally carried out discontinuously (by batches), and the greater amount of powder used and, in turns, the greater amount of oxygen adsorbed into the surface of the powder particles, or a combination of their all.

6.2.1.3 – Hardness

The results of Vickers hardness (HV30) measured in the cross–section of the bending specimens are presented in Figure 6.56.

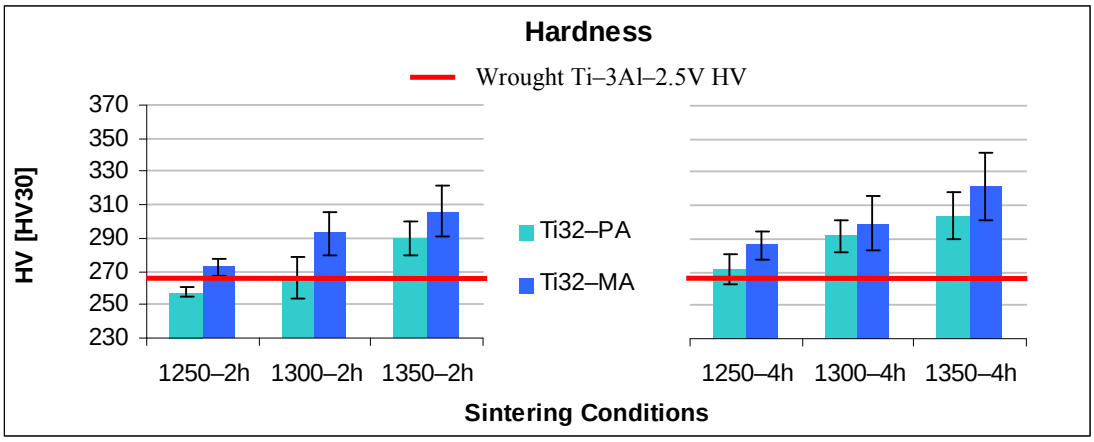

Figure 6.56 – Hardness as a function of the sintering conditions for Ti32–PA and Ti32–MA bending specimens.

Generally, the hardness of sintered Ti–3Al–2.5V titanium alloy (Figure 6.56) increases with the sintering temperature and time, as expected for powder metallurgy materials, due to the increment of the relative density or decrement of the residual porosity.

Moreover, the materials get harder for longer processing time where the doubling of the dwell time from 2 hours to 4 hours has the same effect, an increment of approximately 15 HV30, than increasing the sintering temperature in 50ºC. Normally, the values obtained for Ti32–MA are higher compared to Ti32–PA, which is in agreement with the density values (Figure 6.51).

The hardness of wrought Ti–3Al–2.5V ranges between 220 HV and 300 HV, depending on the heat treatment[8], with a common mean value of 267 HV[9]. Consequently, the behaviour of the P/M Ti–3Al–2.5V alloys studied, which equals or overcomes the hardness of wrought material despite of the residual porosity, could be due to the higher content of interstitial elements (Figure 6.53 and Figure 6.54).

Finally, no significant differences where found on the hardness measurement carried out on tensile test specimens compared to those shown in Figure 6.56 since they range between 280–310 HV30. In this case, the slightly lower relative density (Figure 6.52) is balanced by the higher amount of interstitials (Figure 6.55).

The variation of the Vickers hardness of the Ti–3Al–2.5V alloys produced by the two approaches (PA and MA) was analysed considering the equivalent oxygen content, obtained by means of the Okazaki and Conrad's equation[11].

The results are divided as a function of the sintering conditions (Figure 6.57), the P/M approach (Figure 6.58–left) and as general trend (Figure 6.58–right).

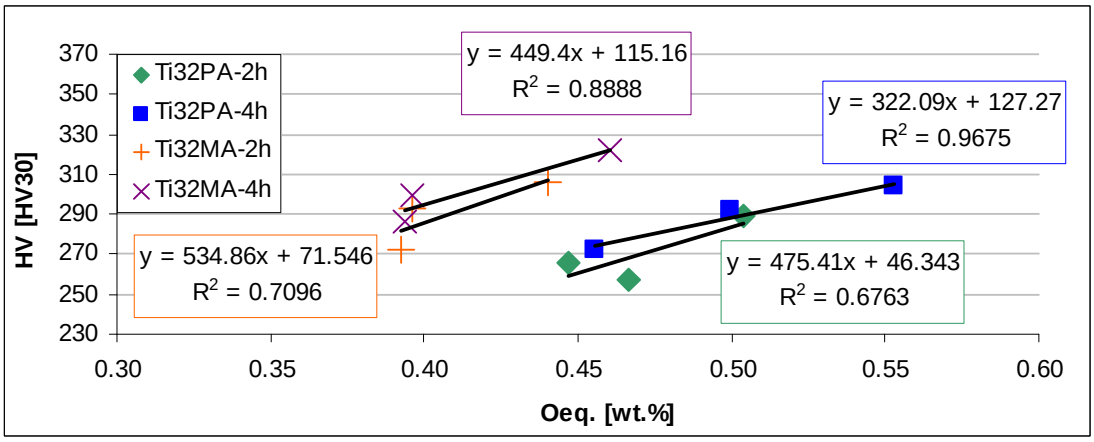

Figure 6.57 – Hardness as a function of equivalent oxygen content for Ti32–PA and Ti32–MA bending specimens: influence of temperature and time.

The analysis of the variation of the hardness of the Ti–3Al–2.5V titanium alloy considering the influence of the sintering temperature and time reveals that, as expected, this mechanical property increases with the increment of the amount of interstitial elements dissolved obtaining different relationships where the best one has a coefficient of determination R^2 as high as 0.96% (Figure 6.57). Moreover, it can be noticed that for a similar equivalent oxygen content (for example 0.45 wt.%) Ti32–MA is much harder than Ti32–PA or, to obtain similar hardness (for example 290 HV30), the Ti32–PA alloy needs a much higher equivalent oxygen content.

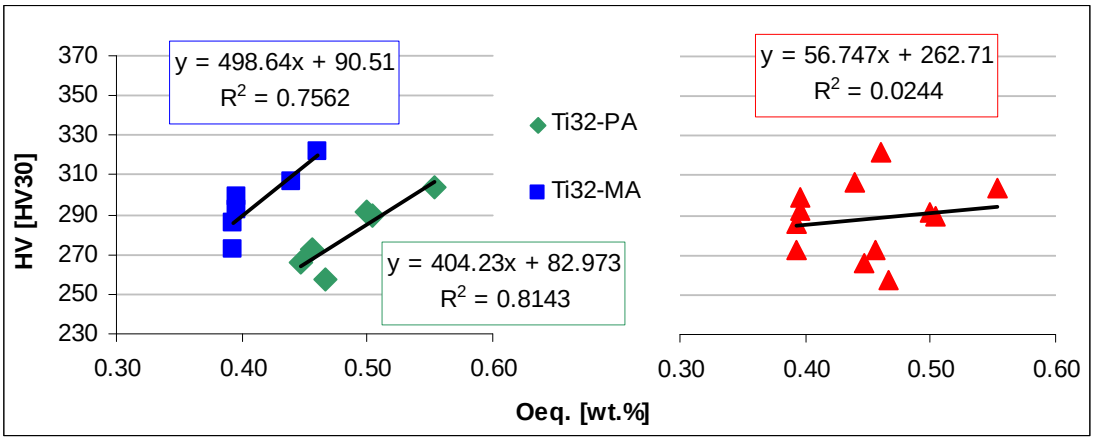

Figure 6.58 – Hardness as a function of equivalent oxygen content for Ti32–PA and Ti32–MA bending specimens: influence of the powder production route (left) and general trend (right).

This behaviour, which can also be seen in considering the data as a function of the P/M approach (Figure 6.58–left), is mainly due to the higher relative density of Ti32–MA bending samples than Ti32–PA but it is also influenced by the microstructural features.

Finally, when the data of the two alloys are analysed together in order to find out a general trend for the Ti–3Al–2.5V alloy no such a good correlation could be found, as shown in Figure 6.58–right due to the difference in terms of relative density.

6.2.1.4 – Properties from Bending Test

Examples of bending stress–strain curves obtained from the three–point bending tests for Ti32–PA and Ti32–MA samples divided for 2 hours and 4 hours of dwell time are shown in Figure 6.59 and Figure 6.60, respectively.

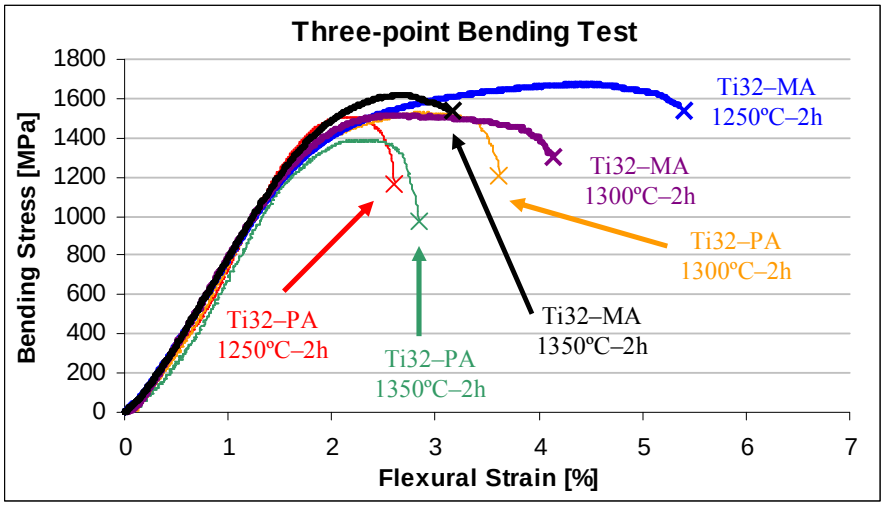

Figure 6.59 – Representative bending stress–strain curves for Ti32–PA and Ti32–MA specimens (sintering time: 2 h).

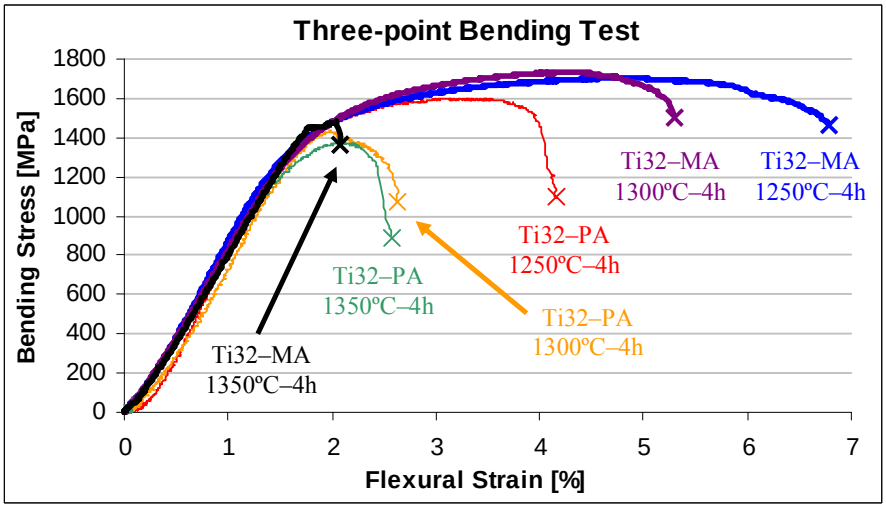

Figure 6.60 – Representative bending stress–strain curves for Ti32–PA and Ti32–MA specimens (sintering time: 4 h).

Analysing Figure 6.59 and Figure 6.60, it can be noted that, generally, the lower the processing temperature the higher the maximum strength and the greater the flexural strain with the only exception of the prealloyed powder sintered at 1250ºC for 2 hours. The mechanical behaviour of the two materials is very similar independently of the processing parameters since the material deforms elastically up to approximately 1200 MPa and then plastically.

The amount of plastic deformation is greatly influenced by the sintering condition but the materials do not fail catastrophically since the rupture strength is lower than the maximum bending strength, as it was for elemental titanium (Figure 6.7). From these curves, it is possible to obtain several important data such as the flexural modulus, the maximum bending strength and the flexural strain.

Regarding the flexural modulus, the mean values attained are 93 GPa ± 5 GPa for Ti32–PA and 101 GPa ± 6 GPa for Ti32–MA. The difference in terms of flexural modulus between Ti32–PA and Ti32–MA is mainly due to the greater percentage of residual porosity after sintering of Ti32–PA (Figure 6.51).

The value of flexural modulus of the Ti32–MA alloy, which can be compared to that of elemental titanium since the L/D ratio of the specimens is similar and both materials were pressed at 700 MPa, results to be a little bit higher, as it was expected, due to the presence of the alloying elements which makes the material more rigid.

The maximum bending strength and flexural strain mean values comparison between Ti32–PA and Ti32–MA sintered under the same range of temperatures and times is displayed in Figure 6.61 and Figure 6.64.

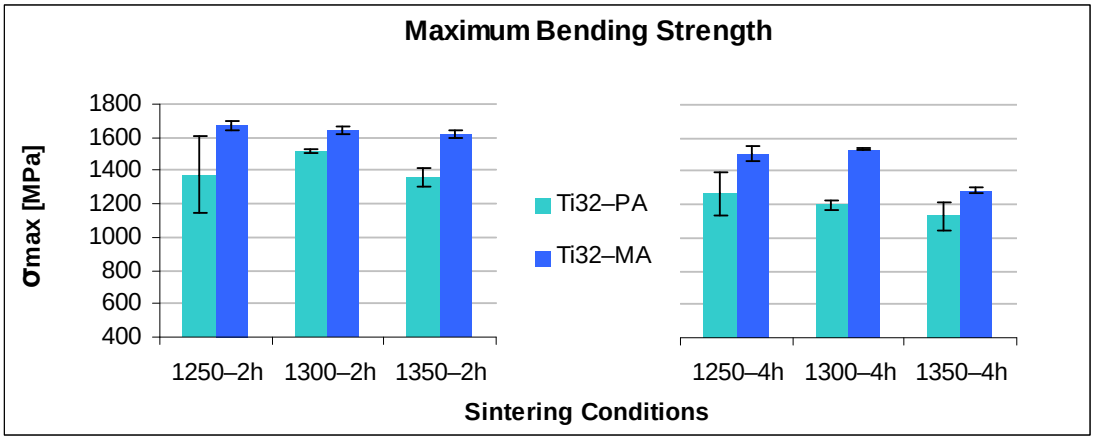

Figure 6.61 – Maximum bending strength as a function of the sintering conditions for Ti32–PA and Ti32–MA bending specimens.

As it can be seen in Figure 6.61, the maximum bending strength of Ti32–PA samples decreases with the sintering temperature and time. The only exception is 1250ºC–2h which has lower maximum bending strength but much higher standard deviation (1375 ± 235 MPa). Conversely, the maximum bending strength of Ti32–MA remains almost constant between 1250ºC and 1300ºC and then slightly decreases for both processing time.

In general, Ti32–MA reaches higher maximum bending strength with much lower variability compared to Ti32–PA in each one of the sintering condition studied. This is mainly due to the higher relative density and lower interstitials content of Ti32–MA compared to Ti32–PA but mitigated by the bigger grain size of the Ti32–MA alloy (see Section 6.2.1.6).

Generally, the maximum bending strength of P/M Ti–3Al–2.5V is, at least, 200 MPa higher with respect to the elemental titanium powder processed in the same range of temperatures and times (Figure 6.8–left).

To study the effect of interstitials, the variation of the maximum bending strength with the equivalent oxygen content (see Eq. 15 in Section 2.7, equation proposed by Wood)[19] was analysed. The results are presented for the diverse sintering conditions (Figure 6.62), for the P/M approach (Figure 6.63–left) and for the general trend (Figure 6.63–right).

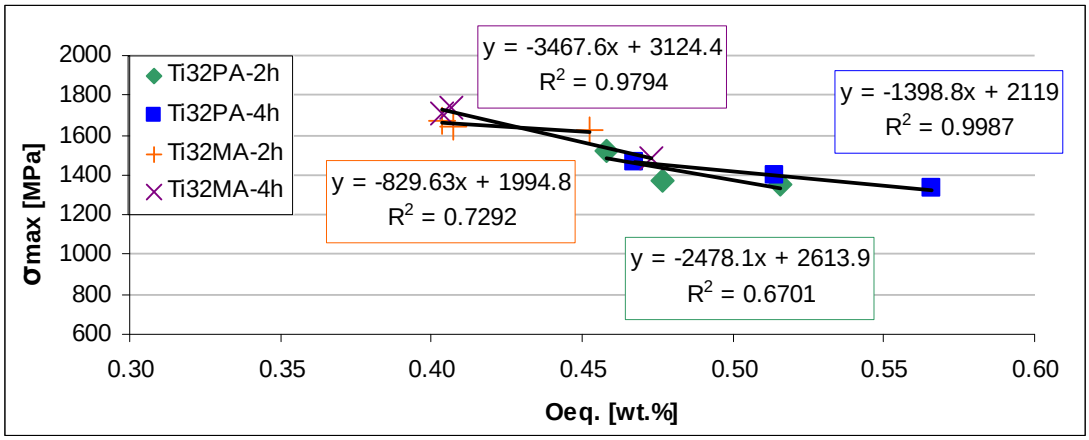

Figure 6.62 – Maximum bending strength as a function of the equivalent oxygen content for Ti32–PA and Ti32–MA bending specimens: influence of temperature and time.

As it can be seen in Figure 6.62, the maximum strength of the P/M Ti–3Al–2.5V determined by the three–point bending test decreases with the increment of the equivalent oxygen content and the data can be approximated by linear correlations with R^2 as high as 0.98%. Moreover, components sintered under different temperatures or times but with similar equivalent oxygen content show maximum bending strength values alike indicating a great influence of the total amount of interstitials on the maximum bending strength.

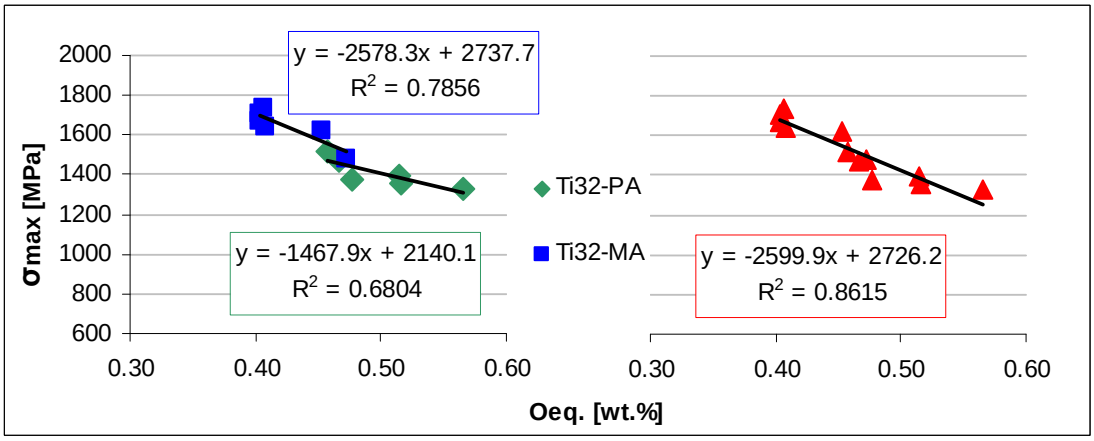

Figure 6.63 – Maximum bending strength as a function of the equivalent oxygen content for Ti32–PA and Ti32–MA bending specimens: influence of the powder production route (left) and general trend (right).

Considering the maximum bending strength data regarding each one of the P/M approaches (Figure 6.63–left), two very similar and overlapping decreasing trends are found which, therefore, allows to propose a linear decreasing general trend for the Ti–3Al–2.5V alloy with R^2 of 0.86 (Figure 6.63–right). This was not the case for hardness (Figure 6.58–right) where a general trend for the Ti–3Al–2.5V alloy could not be highlighted due to the greater influence of the residual porosity and microstructural features.

The flexural strain of P/M Ti–3Al–2.5V (Figure 6.64) decreases with the sintering temperature and it is lower for longer time (4 hours). Once again, Ti32–MA performs better than Ti32–PA since, normally, reaches higher flexural strain as it was for the maximum bending strength. Moreover, the differences in terms of flexural strain between the samples obtained by the two powder production route are more marked for a dwell time of 4 hours.

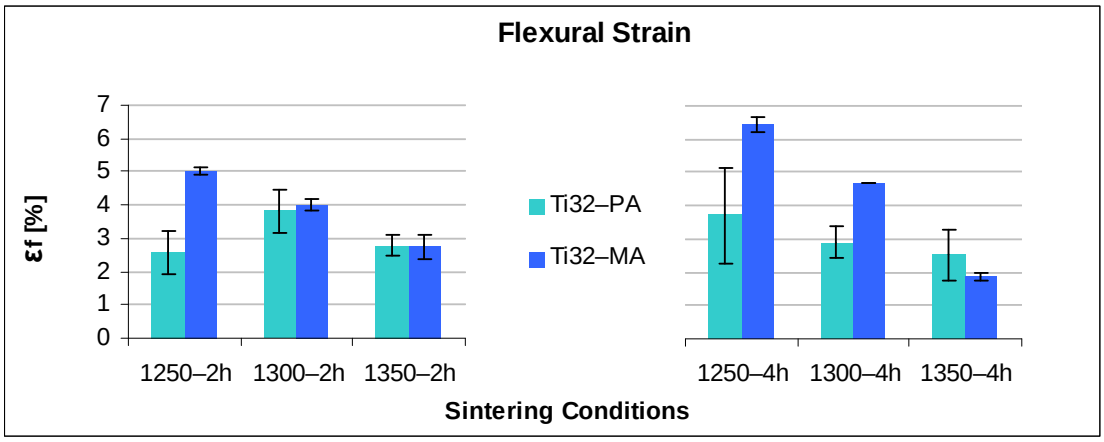

Figure 6.64 – Flexural strain as a function of the sintering conditions for Ti32–PA and Ti32–MA bending specimens.

The great difference in terms of flexural strain between the two powder production routes is mainly due to the difference of relative density achieved (Figure 6.51) because the residual porosity acts as crack initiation or stress concentration sites. Anyway, the higher oxygen content of Ti32–PA compared to that of Ti32–MA, as well as the coarser microstructural feature of Ti32–MA, contribute to increase the difference between the two materials.

Conversely to maximum bending strength, the flexural strain of P/M Ti–3Al–2.5V results to be lower compared to that of elemental titanium (Figure 6.8–right) which is quite reasonable due to the presence of the alloying elements.

Flexural strain data were analysed against the equivalent oxygen content determined by the equation proposed by Wood[19] (see Eq. 16 in Section 2.7) and the results are shown in Figure 6.65 for the two sintering times studied and in Figure 6.66 for both of the two powder preparation routes and as general behaviour.

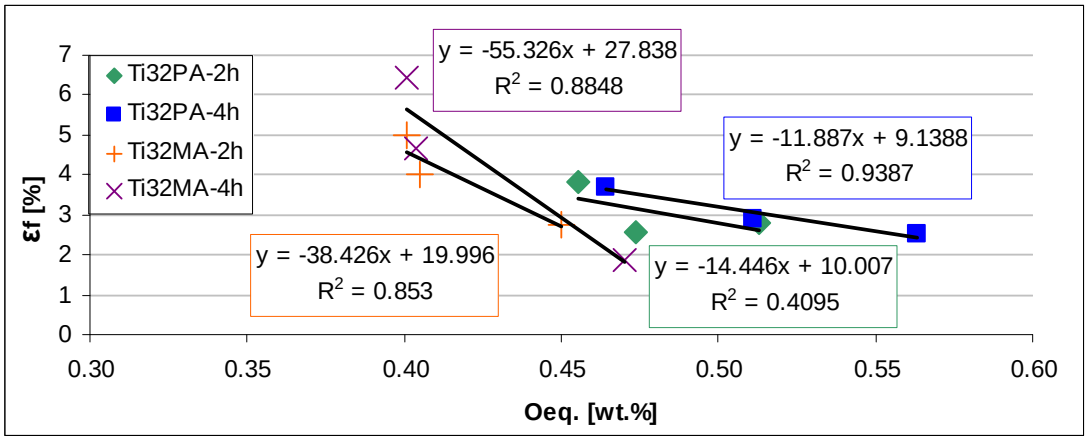

Figure 6.65 – Flexural strain as a function of the equivalent oxygen content for Ti32–PA and Ti32–MA bending specimens: influence of temperature and time.

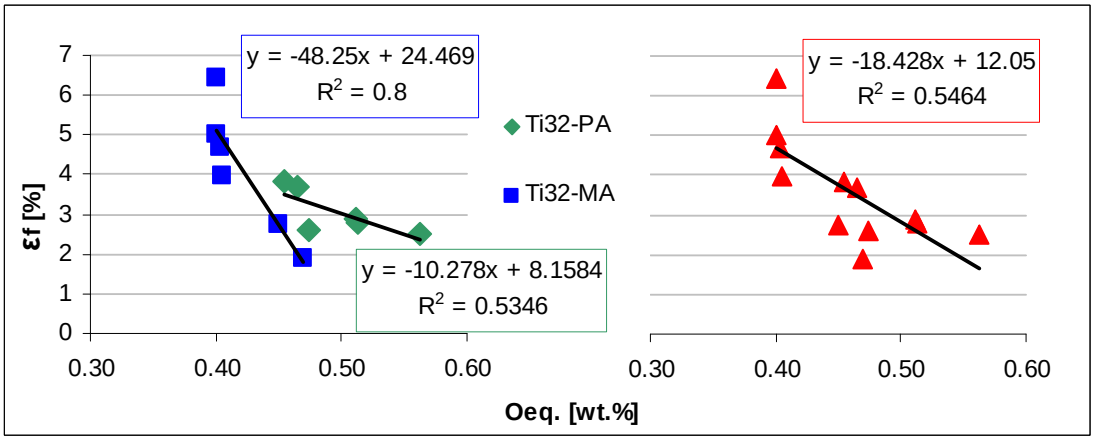

Figure 6.66 – Flexural strain as a function of the equivalent oxygen content for Ti32–PA and Ti32–MA bending specimens: influence of the powder production route (left) and general trend (right).

As it can be seen in Figure 6.65, the flexural strain of both Ti32–PA and Ti32–MA decreases with the increment of the equivalent oxygen content, which is normally higher for Ti32–PA.

When considering the data as a function of the powder production method (Figure 6.66–left), a clear decreasing linear trend of the flexural strain with the equivalent oxygen content is found. Furthermore, the slope of the regression line for Ti32–MA is greater than that of Ti32–PA indicating that Ti32–PA is less influenced by the content of interstitials. This way, the general trend of the flexural strain for the Ti–3Al–2.5V alloy (Figure 6.66–right) can be approximated with a decreasing linear regression line where the scattering of the data highlights the influenced from both the relative density and the microstructural features, which will be discussed in Section 6.2.1.6.

6.2.1.5 – Properties from Tensile Test

The typical tensile stress–strain curves obtained from the tensile tests for the Ti32–PA and Ti32–MA alloys are displayed in Figure 6.67.

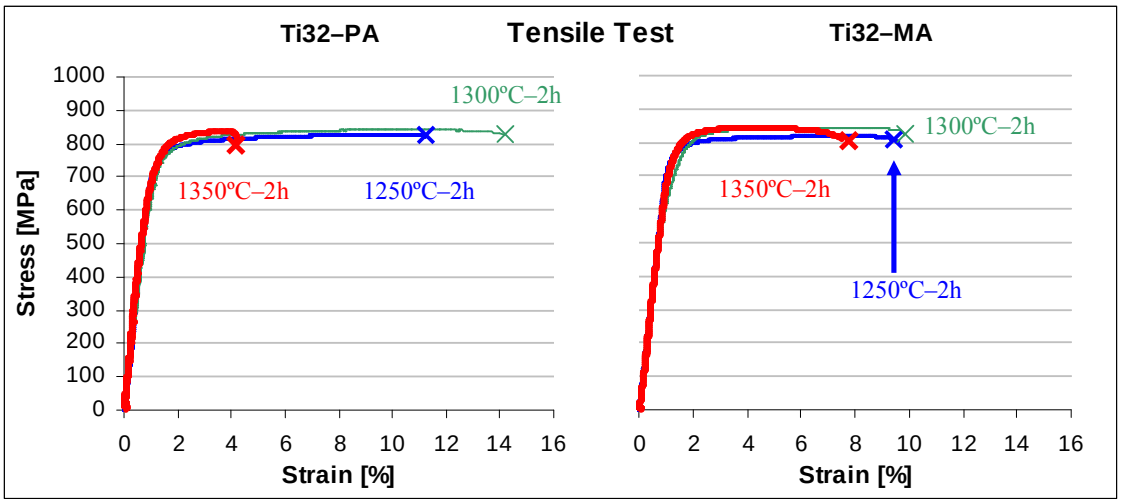

Figure 6.67 – Representative tensile stress–strain curves for Ti32–PA and Ti32–MA specimens.

As it can be seen in Figure 6.67, the shape of the tensile stress–strain curves of Ti32–PA and Ti32–MA samples, which are a representative example, are similar since the materials undergo an elastic deformation up to approximately 700 MPa and then start to deform plastically. From these stress–strain curves, the UTS, strain and Young modulus can be obtained where this last parameter seems to be similar for both alloys.

Nonetheless, dynamic elastic modulus measurements for Ti32–PA results in a Young modulus of 108 ± 6 GPa, which is in agreement with that of wrought Ti–3Al–2.5V (107 GPa[9]), whilst for Ti32–MA the value obtained (75 ± 35 GPa) is quite low most probably due to some experimental error as the great standard deviation demonstrates.

The UTS and strain mean values for the different sintering conditions employed to process the Ti32–PA and Ti32–MA alloys are shown in Figure 6.68.

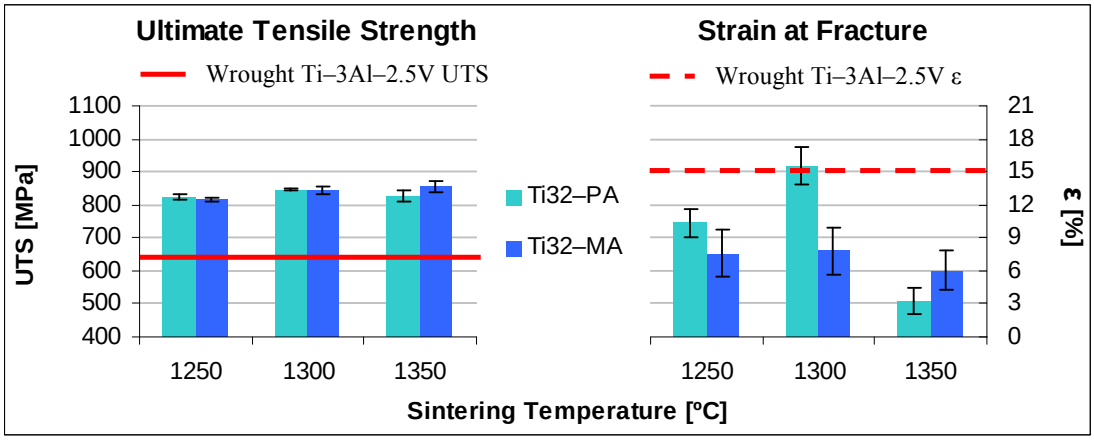

Figure 6.68 – Mechanical properties as a function of the sintering temperature for Ti32–PA and Ti32–MA specimens: ultimate tensile strength (left) and strain (right).

As expected, UTS mean values (Figure 6.68–left) are almost constant although a slight increment can be observed with the sintering temperature, specifically from 820 MPa (1250ºC–2h) to 850 MPa (1350ºC–2h). These values are most probably the balance between the decrement of the residual porosity, the increment of the interstitial elements and the grain growth induced by the sintering temperature.

The P/M alloys reach a significantly higher strength compared to wrought Ti–3Al–2.5V in the mill annealed state (UTS = 620 MPa) due to the higher oxygen percentage. However, the strength attained is similar to that of the wrought Ti–3Al–2.5V subjected to a combined process of cold–working and stress–relieve (C.W.S.R., UTS = 860 MPa), a typical industrial process applied for tubing[9].

On the other side, the strain of powder metallurgy Ti–3Al–2.5V increases from 1250ºC to 1300ºC and, then, it decreases being this behaviour more marked for Ti32–PA.

Conversely to UTS, the strain is somewhat lower compared to mill annealed wrought Ti–3Al–2.5V (15%), which is the typical behaviour of P/M materials due to the residual porosity. Nevertheless, the values obtained are directly comparable to that of C.W.S.R. Ti–3Al–2.5V (10%).

When compared to elemental titanium (Figure 6.12), P/M Ti–3Al–2.5V results to be stronger due to the effect of the alloying elements and the presence of the beta phase whilst the strain is not significantly affected.

6.2.1.6 – Microstructural Analysis

Microstructural characterisation by optical microscopy for samples sintered during 2 or 4 hours was performed on etched specimens and the results are presented in Figure 6.69 and Figure 6.70, respectively. Moreover, the scanning electron microscopy was used to carry out the fractographic study of the broken tensile test samples and the results are displayed in Figure 6.71.

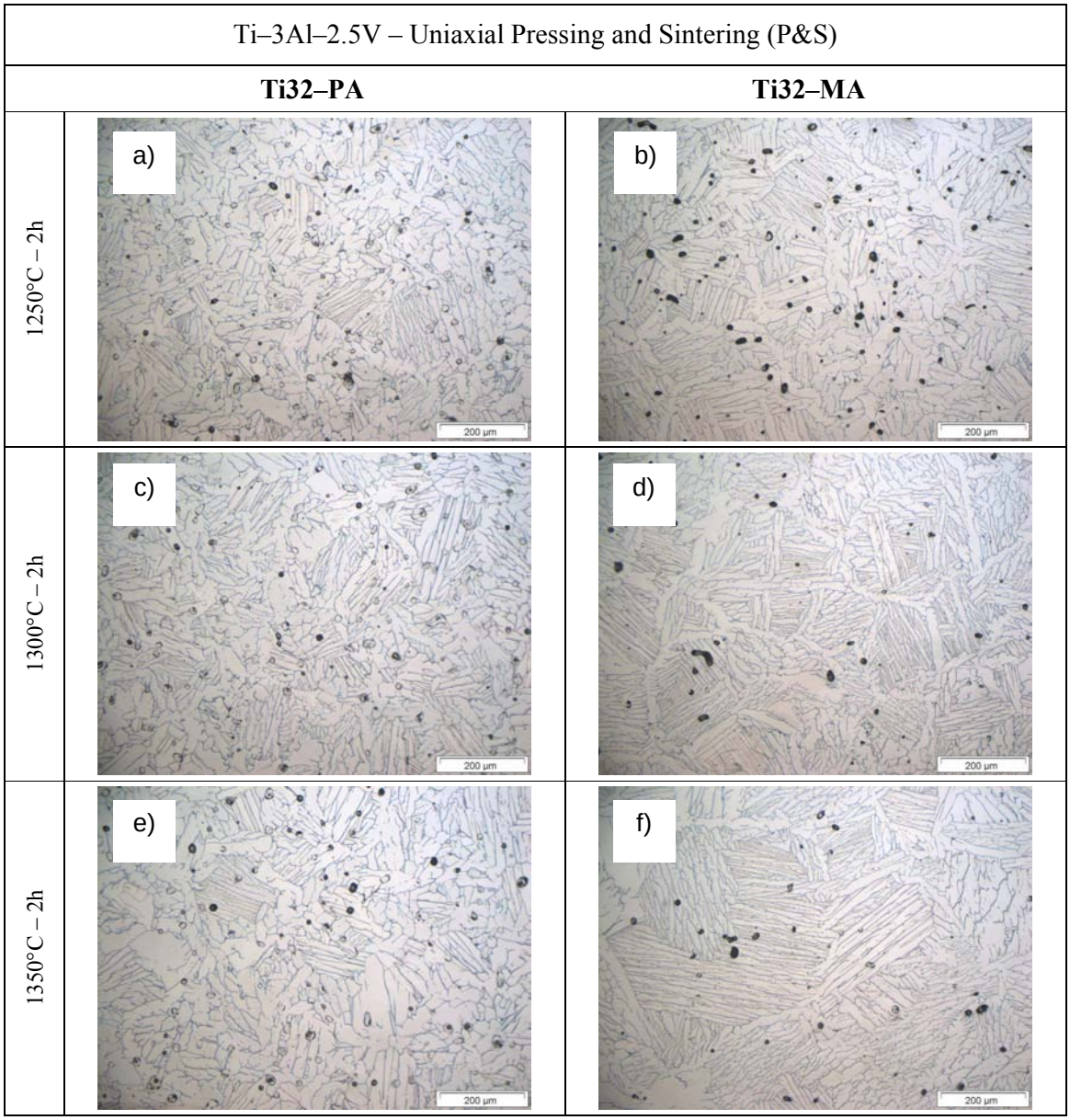

Figure 6.69 – Optical microscopy images for Ti32–PA and Ti32–MA sintered for 2 hours at: a) and b) 1250°C, c) and d) 1300°C and e) and f) 1350ºC.

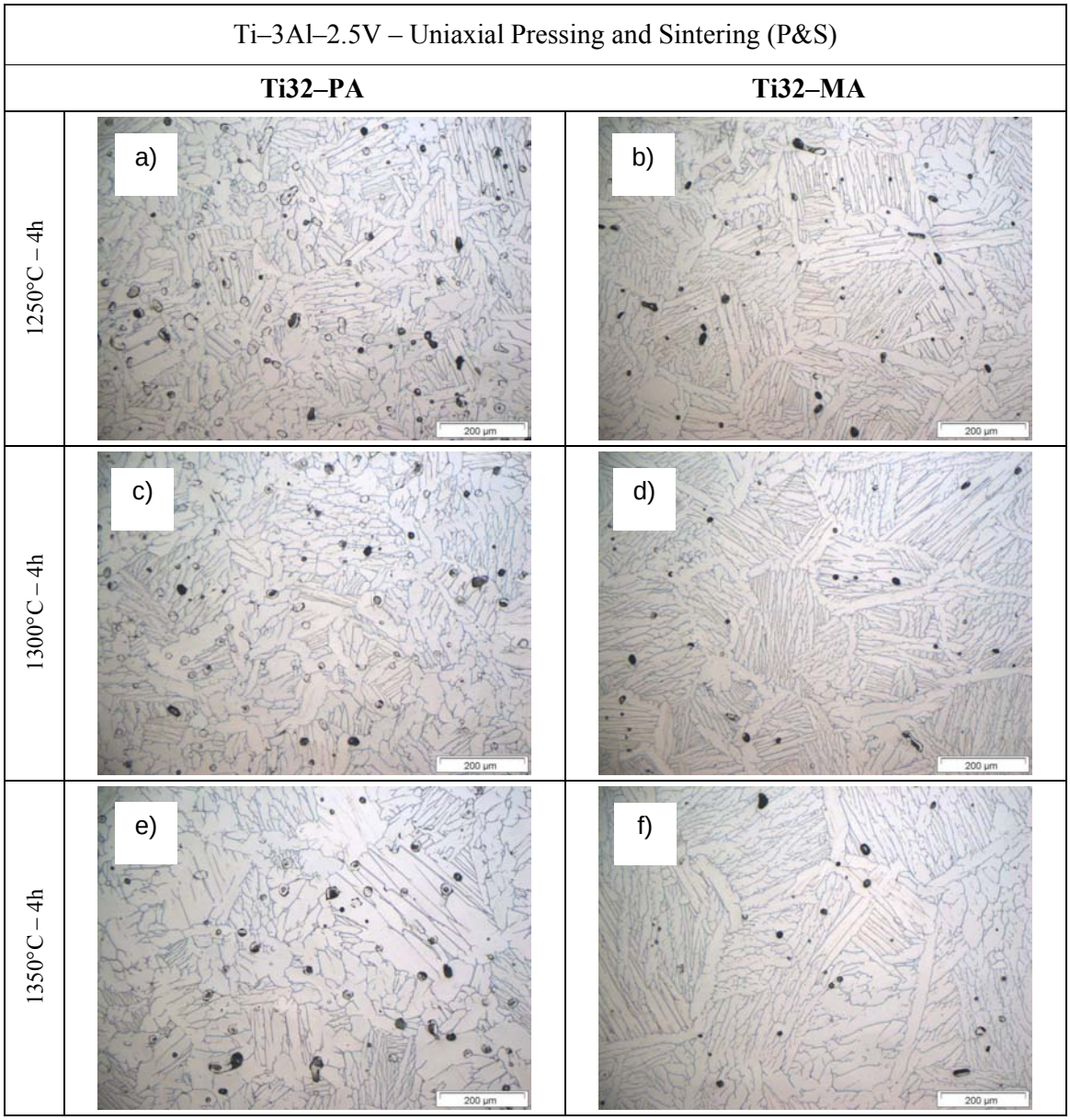

Figure 6.70 – Optical microscopy images for Ti32–PA and Ti32–MA sintered for 4 hours at: a) and b) 1250°C, c) and d) 1300°C and e) and f) 1350ºC.

Basically, the microstructure of P/M Ti–3Al–2.5V is composed by alpha grains and α + β lamellae. Furthermore, it seems that the mean α grain size grows with the temperature and the lamellae get thicker and longer, being this behaviour more pronounced for longer time (Figure 6.70 compared to Figure 6.69). Moreover, the basketweave colonies of Ti32–MA seem to be finer than those of Ti32–PA, which is especially visible at the highest sintering temperature studied (at 1350ºC–4h a more pronounced grain growth in the Ti32–PA generates an inhomogeneous grain size distribution).

On the other side, as expected, it can be seen that the total amount of residual porosity diminishes with the temperature and it is higher for Ti32–PA in agreement with the relative density data.

It is worth mentioning that the distribution of the alloying elements in the Ti32–MA was checked by SEM in BSE mode and EDS analysis. At the processing conditions studied, the distribution of the alloying elements is completely homogeneous in agreement with the results of the preliminary sinterability study (Chapter 5).

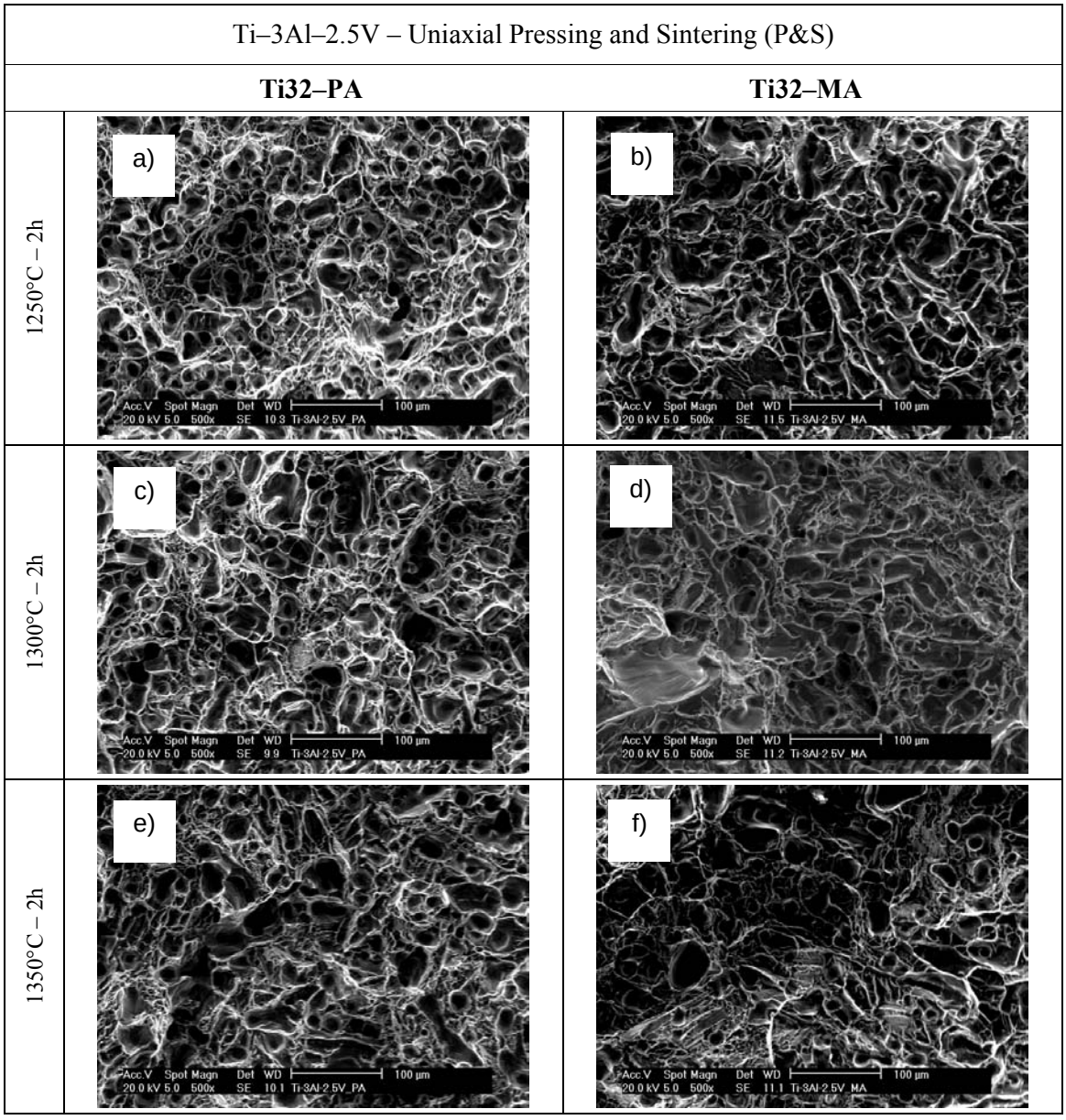

Figure 6.71 – Fracture surface from tensile test specimens for Ti32–PA and Ti32–MA sintered for 2 hours at: a) and b) 1250ºC, c) and d) 1300ºC and e) and f) 1350ºC.

Analysing the evolution of the fracture surface with the sintering temperature (Figure 6.71), it can be seen that there is not a great variation between them since the fracture surface is characterised by a distribution of non equiaxed dimples relatively uniform in size typical of ductile metals.

When comparing the powder production approach, it can be seen that Ti32–MA has a mixture of non equiaxed coarse and fine dimples and some small area of cleavage, especially at 1300°C, which could be due to the presence of some impurity from the master alloy. This is in agreement with the mechanical properties and, in particular, with the significantly lower strain of Ti32–MA with respect to Ti32–PA at 1300ºC–2h (Figure 6.68).

6.2.1.7 – Thermal Conductivity

As for P&S elemental titanium, the thermal conductivity at room temperature and the evolution of the thermal conductivity with the temperature up to 300ºC were measured for Ti32–PA and Ti32–MA alloys. The results of these characterisations are analysed considering the relative density obtained for each sintering condition and the equivalent oxygen content calculated by means of the formula proposed by Conrad[23] (see Eq. 17 in Section 2.7).

The data of the thermal conductivity at room temperature are presented in Figure 6.72 and Figure 6.73 for Ti32–PA and Ti32–MA, respectively.

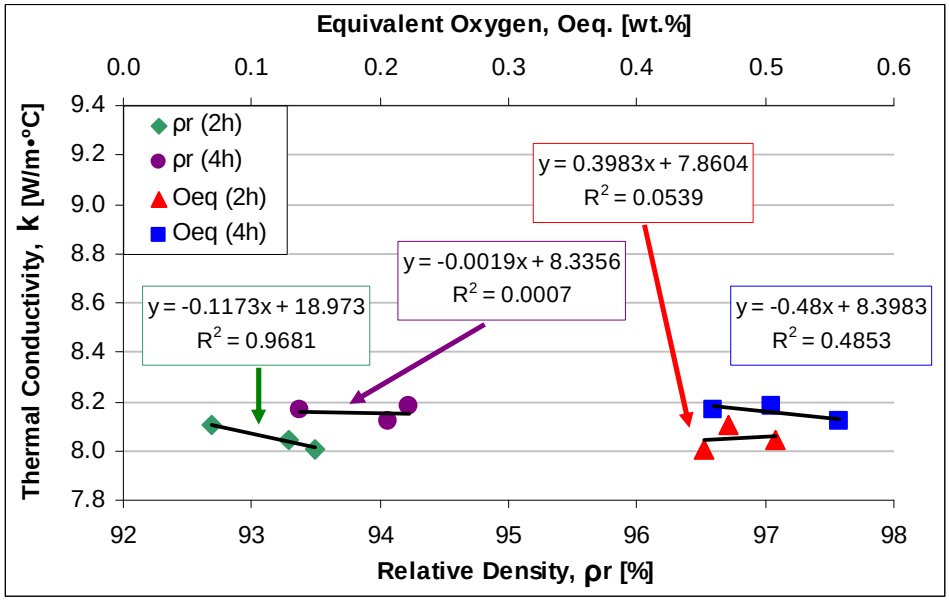

Figure 6.72 – Thermal conductivity at room temperature as a function of the relative density and equivalent oxygen content for Ti32–PA specimens.

As it can be seen in Figure 6.72, the thermal conductivity values for Ti32–PA lay between 8.0 W/m·ºC and 8.2 W/m·ºC and, consequently, the variation found is not that significant. This seems to indicate that the thermal conductivity at room temperature of Ti32–PA is not greatly influenced by the microstructural features and to the fact that the relative density is just a bit higher than 92%.

This limited variation could be the compromise between the relative density (or conversely the amount of residual porosity with different size and distribution), the characteristics of microconstituents (α and β) and the total content of interstitials that balance themselves.

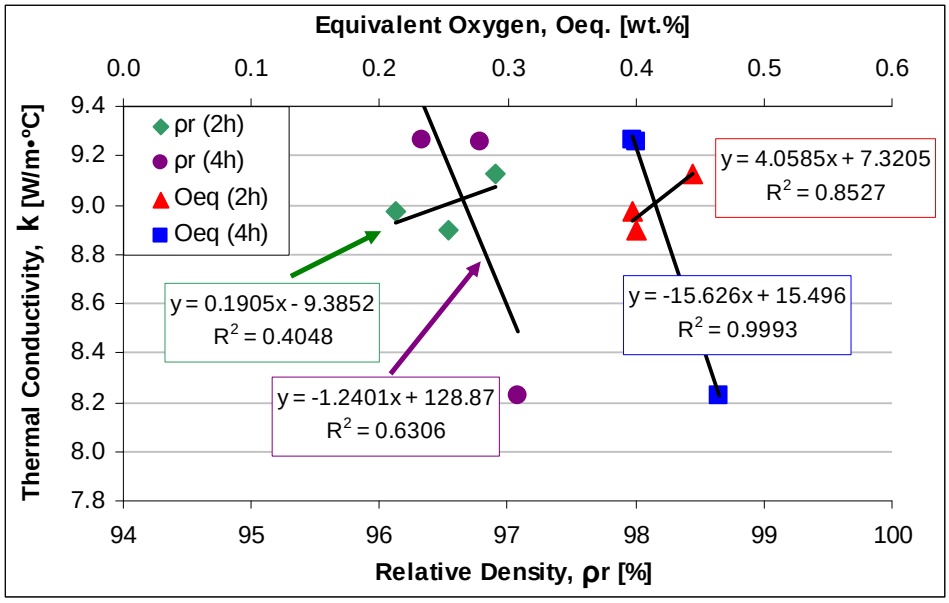

Figure 6.73 – Thermal conductivity at room temperature as a function of the relative density and equivalent oxygen content for Ti32–MA specimens.

In the case of the Ti32–MA alloy, the thermal conductivity at room temperature (Figure 6.73) increases with the increment of either the relative density or the equivalent oxygen content for 2 hours of processing time. This is most probably due that the effect of lowering the residual porosity and grain growth induced by the increment of the temperature overcomes the effect of the interstitial elements.

When considering the data for the components sintered at 4 hours, the thermal conductivity is almost constant but then drops suddenly. This drop coincides with the specimens sintered at 1350ºC and it is quite surely due to the greater $O_{Eq.}$ found in these samples and to the heterogeneous grain size distribution which characterise them, as visible in Figure 6.70 f). Apart from the value measured on the specimens sintered at 1350ºC–4h, the variation of the thermal conductivity at room temperature of Ti32–MA is limited, since the values range between 8.9 W/m·ºC and 9.3 W/m·ºC.

Comparing the powder production route, it can be seen that Ti32–MA has always a greater thermal conductivity than Ti32–PA. This can be explained on the bases of the greater relative density, lower equivalent oxygen content and bigger grain size of Ti32–MA with respect to Ti32–PA.

With respect to the conventional value of thermal conductivity indicated for this alloy, generally, k measured in products fabricated from Ti32–PA and Ti32–MA results to be directly comparable or somewhat higher, respectively, as it can be seen from the data reported in Table 6.3.

Table 6.3 – Comparison of thermal conductivity at room temperature values between wrought and P/M Ti–3Al–2.5V alloy.

Ti–3Al–2.5V						
Wrought[8]		**P/M**				
		Ti32–PA		**Ti32–MA**		
k [W/m·ºC]	Chemical analysis [wt.%]	k [W/m·ºC]	Chemical analysis [wt.%]	k [W/m·ºC]	Chemical analysis [wt.%]	Sintering conditions
8.30	O = 0.15 N = 0.03	8.10	O = 0.421 N = 0.017	8.97	O = 0.340 N = 0.020	1250ºC – 2h
		8.00	O = 0.397 N = 0.019	8.90	O = 0.343 N = 0.020	1300ºC – 2h
		8.04	O = 0.448 N = 0.021	9.13	O = 0.380 N = 0.023	1350ºC – 2h
		8.16	O = 0.401 N = 0.021	9.26	O = 0.350 N = 0.016	1250ºC – 4h
		8.18	O = 0.431 N = 0.027	9.25	O = 0.348 N = 0.018	1300ºC – 4h
		8.12	O = 0.490 N = 0.024	8.23	O = 0.401 N = 0.023	1350ºC – 4h

As it has been said, the variation of the thermal conductivity with the temperature was measured in Ti32–PA and Ti32–MA specimens sintered at 1250ºC for 2 hours. The results of this characterisation are presented in Figure 6.74 as a comparison between the "measurement" and "calculation" (see Eq. 11 and 12 in Section 2.6.8) values for Ti32–PA and Ti32–MA alloys and "literature"[8] for wrought alloy of the same composition.

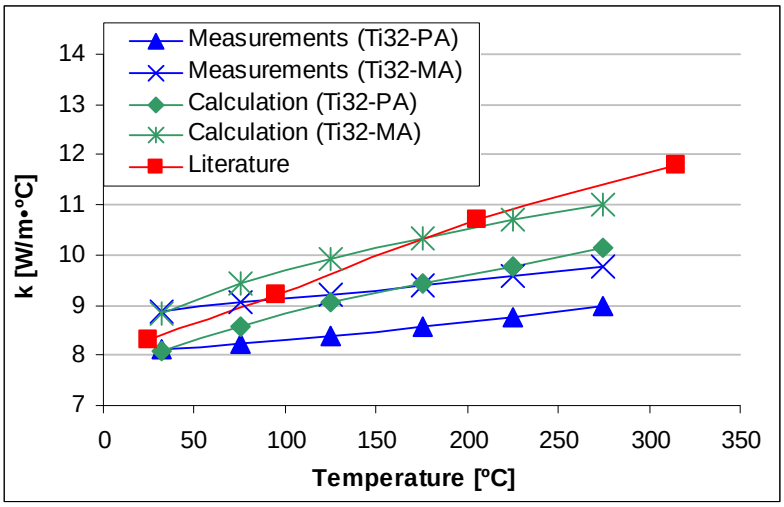

Figure 6.74 – Thermal conductivity as a function of temperature for Ti32–PA and Ti32–MA specimens.

As it can be seen in Figure 6.74, the thermal conductivity increases with the temperature but the measured and calculated values for each material increases with different slope, being higher the calculated than the measured.

Compared to the values found in the literature for the wrought alloys, Ti32–PA values either measured or calculated are always lower, whilst the measured values of Ti32–MA are higher up to 100ºC and the calculated ones up to 180ºC than the wrought alloy. Moreover, the ratio at which the thermal conductivity of the wrought alloys increases with the temperature is greater than the P&S products since the higher the temperature the bigger the relative effect of the porosity on this property.

6.2.1.8 – Electrical Resistivity

Electrical conductivity measurements by means of the van der Pauw technique[25, 26] were carried out on the sintered Ti32–PA and Ti32–MA specimens and the results, expressed in terms of electrical resistivity, are displayed in Figure 6.75 and Figure 6.76, respectively.

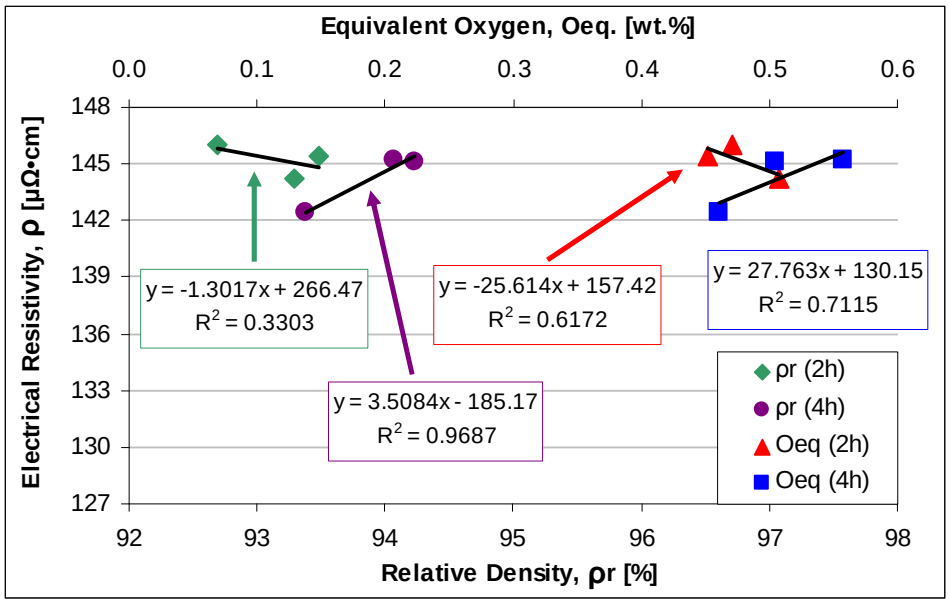

Figure 6.75 – Electrical resistivity at room temperature as a function of the relative density and equivalent oxygen content for Ti32–PA specimens.

Analysing the electrical resistivity data for the Ti32–PA alloy (Figure 6.75), it can be seen that this property decreases for 2 hours and increases for 4 hours of dwell time but this variation is not very important since the values range between 142 and 146 μΩ·cm. Therefore, it seems that neither the relative density nor the equivalent oxygen content have a significant influence on the electrical resistivity or relative density, interstitials and microstructural features balance themselves as in the case of the thermal conductivity.

Conversely to the Ti32–PA alloy, the trends of the electrical resistivity for the Ti32–MA alloy (Figure 6.76) always increases either for 2 or 4 hours for the relative density as well as for the equivalent oxygen content. Moreover, as in the case of the Ti32–MA alloy the variation of the resistivity with the different sintering conditions is not that significant. The only exceptions are the products sintered at 1350ºC–4h which have a higher resistivity, most probably due to the heterogeneous grain size distribution found in the components that also lowers the thermal conductivity (see Figure 6.73).

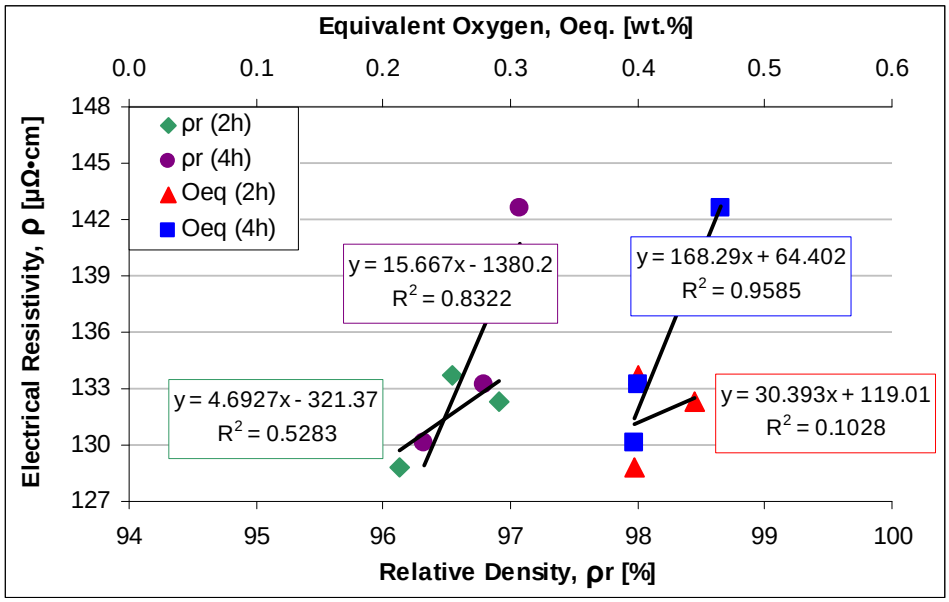

Figure 6.76 – Electrical resistivity at room temperature as a function of the relative density and equivalent oxygen content for Ti32–MA specimens.

Comparing the PA and MA materials, the specimens of Ti32–MA have lower electrical resistivity than Ti32–PA, which is equivalent to a higher electrical conductivity. This behaviour could have been expected due to the higher thermal conductivity found in the Ti32–MA alloy owed to the higher relative density of this material.

Table 6.4 – Comparison of electrical resistivity values between wrought and P/M Ti–3Al–2.5V alloy.

Ti–3Al–2.5V						
Wrought[8]		**P/M**				
		Ti32–PA		**Ti32–MA**		
ρ [μΩ·cm]	Chemical analysis [wt.%]	ρ [μΩ·cm]	Chemical analysis [wt.%]	ρ [μΩ·cm]	Chemical analysis [wt.%]	Sintering conditions
126.0	O = 0.15 N = 0.03	146.0	O = 0.421 N = 0.017	128.8	O = 0.340 N = 0.020	1250ºC – 2h
		145.4	O = 0.397 N = 0.019	133.7	O = 0.343 N = 0.020	1300ºC – 2h
		144.2	O = 0.448 N = 0.021	132.3	O = 0.380 N = 0.023	1350ºC – 2h
		142.4	O = 0.401 N = 0.021	130.1	O = 0.350 N = 0.016	1250ºC – 4h
		145.2	O = 0.431 N = 0.027	133.2	O = 0.348 N = 0.018	1300ºC – 4h
		145.2	O = 0.490 N = 0.024	142.6	O = 0.401 N = 0.023	1350ºC – 4h

In comparison to the value of electrical resistivity of the wrought alloys (see Table 6.4), the components obtained by the MA approach have very similar electrical resistivity even though of the higher amount of interstitials and the presence of the residual porosity while the products fabricated with the PA powder have higher resistivity most probably due to the lower relative density and to the slightly higher equivalent oxygen content with respect to Ti32–MA.

6.2.2 – Hot Isostatic Pressing (HIP)

As for elemental titanium, the influence of the post–processing by hot isostatic pressing on the final properties of sintered Ti–3Al–2.5V alloy specimens was studied and the results are discussed in this section.

It is worth remembering the processing conditions considered:

- ✓ **HIP–1**: T = 1000ºC, P = 100 MPa , t = 20 min — Reference conditions
- ✓ **HIP–2**: T = 1000ºC, P = 100 MPa, t = 2 h — To study the influence of time
- ✓ **HIP–3**: T = 850ºC, P = 100 MPa, t = 20 min — To study the influence of temperature
- ✓ **HIP–4**: T = 850ºC, P = 200 MPa, t = 20 min — To study the influence of pressure

6.2.2.1 – Relative Density

In order to carry out the HIP of the three–point bending test specimens, the powder was compacted into rectangular shaped samples using the optimum consolidation pressure (300 MPa for Ti32–PA and 700 MPa for Ti32–MA) and sintered at 1250°C for 2 hours.

The variation on the relative density of the HIPed samples on the three–point bending test and tensile test specimens are displayed in Figure 6.77.

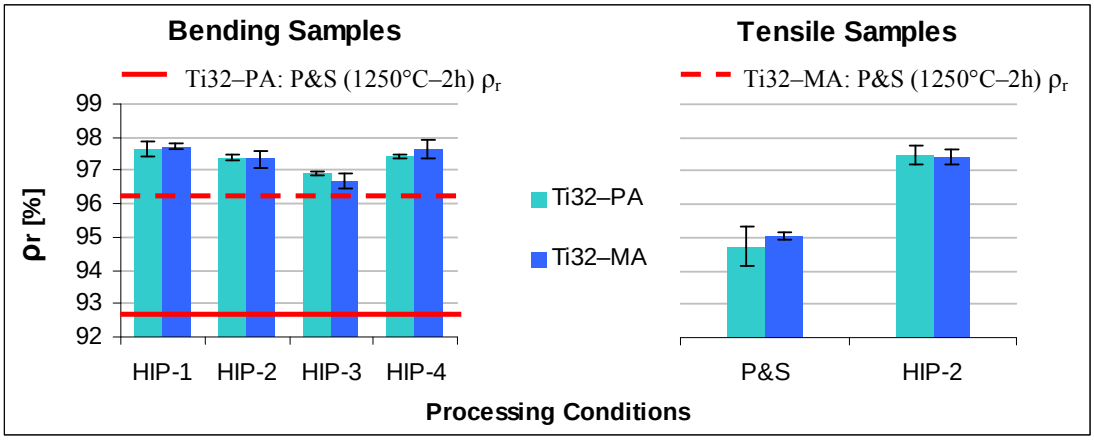

Figure 6.77 – Relative density as a function of the HIP cycle for Ti32–PA and Ti32–MA specimens: bending (left) and tensile (right).

As it can be seen in Figure 6.77, the introduction of a secondary processing of HIP induces, on average, an increment in terms of relative density of 4.5% and 1% for Ti32–PA and Ti32–MA with respect to P&S samples. It is important to remark that this difference is mainly due to the low relative density of Ti32–PA that is raised and levelled to that of Ti32–MA by means of the HIP process.

Comparing the diverse HIP cycles, it can be noticed that there are slight differences of ± 0.5–1% between them, where the lowest value corresponds to HIP–3 and that prolonging the time HIP–2 is not as effective as increasing the pressure HIP–4 since the relative density of HIP–2 samples is lower than that of HIP–1 samples and the relative density of HIP–4 specimens is higher than that of HIP–3 specimens.

Despite the difference in terms of relative density due to the compacting pressure or the geometry of the components, the final relative density obtained in tensile test samples (Figure 6.77–right) is similar to that of three–point bending test specimens. Furthermore, the values shown in Figure 6.77, which range between 97% and 98% are the same of elemental titanium (Figure 6.18) and not fully dense materials could be attained due to the open residual porosity concentrated on the surface of the specimens[28].

6.2.2.2 – Chemical Analysis

Oxygen and nitrogen mean values of the samples submitted to the various HIP cycles studied are shown in Figure 6.78 and Figure 6.79 for bending and tensile specimens, respectively.

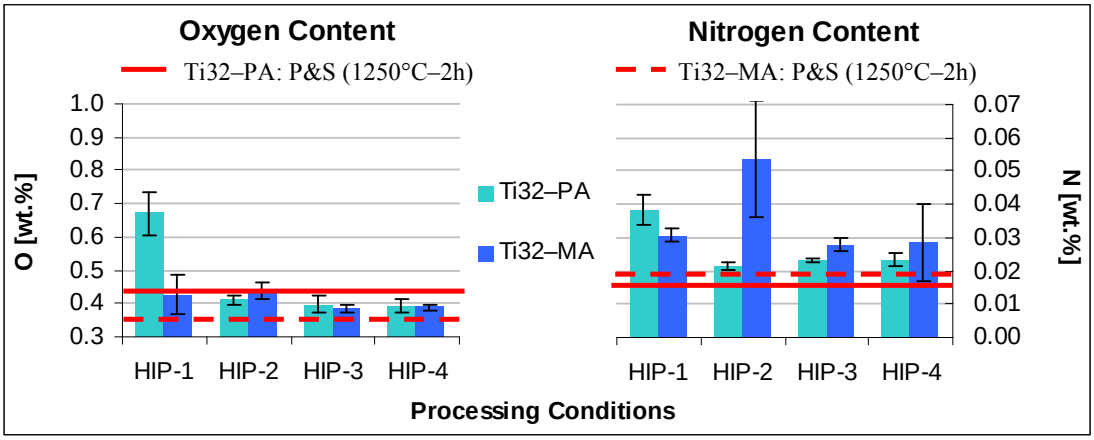

Figure 6.78 – Chemical analysis as a function of the HIP cycle for Ti32–PA and Ti32–MA bending specimens: oxygen (left) and nitrogen (right).

As it can be seen in Figure 6.78, oxygen content of the HIPed Ti32–PA samples is, practically, the same for all the processing cycles and similar to the content of the specimens as–sintered with the exception of the HIP–1 condition where the oxygen raises up to 0.67 wt.%. For Ti32–MA there is some oxygen pick-up compared to the sintered specimens and this increment is slightly lower for a lower processing temperature (HIP–3 and HIP–4).

On the other side, nitrogen content stays almost constant for both alloys indicating that there is always some contamination by the processing atmosphere which is very remarkable for Ti32–MA in the HIP–2 cycle.

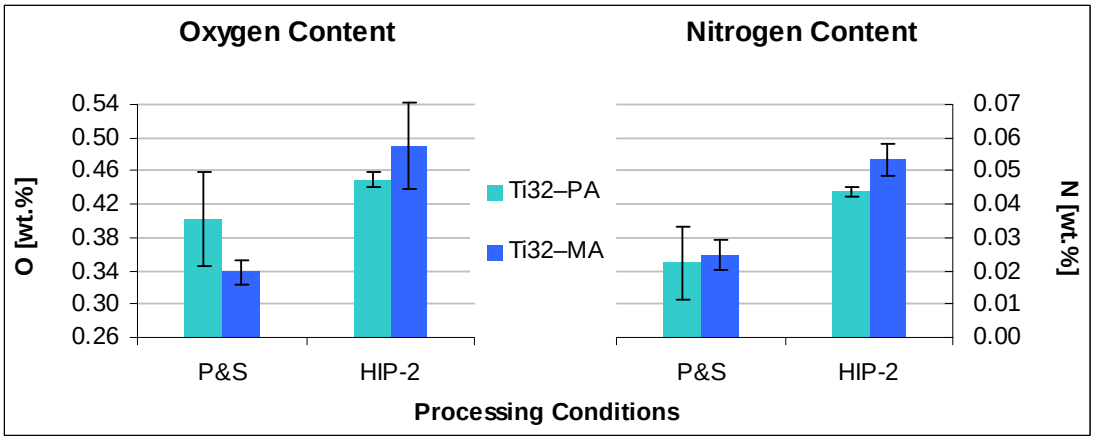

Figure 6.79 – Chemical analysis as a function of the HIP cycle for Ti32–PA and Ti32–MA tensile specimens: oxygen (left) and nitrogen (right).

As it can be seen in Figure 6.79, there is always some contamination during the processing of the tensile test samples by HIP where this contamination is more marked for Ti32–MA. The values shown in Figure 6.79 are similar to those of bending samples (Figure 6.78).

6.2.2.3 – Hardness

The variation on the hardness of P/M Ti–3Al–2.5V HIPed bending and tensile test specimens is displayed in Figure 6.80.

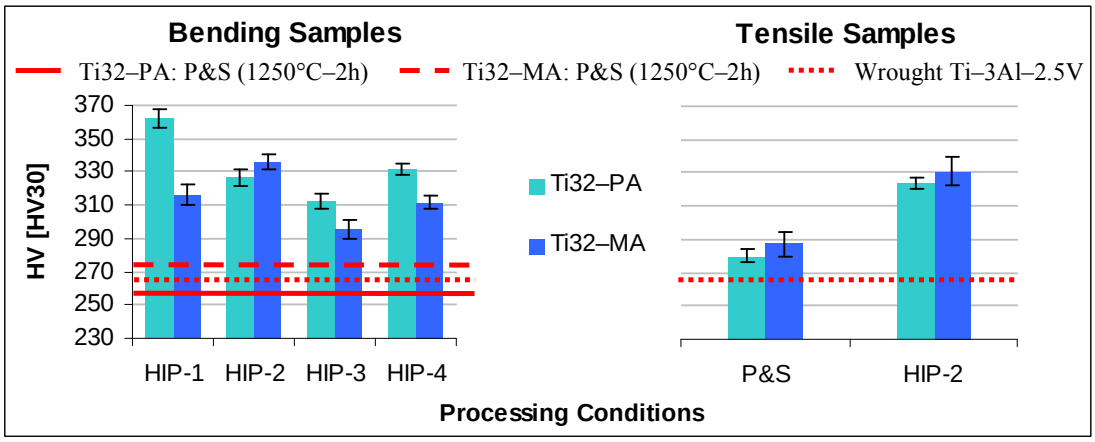

Figure 6.80 – Hardness as a function of the HIP cycle for Ti32–PA and Ti32–MA specimens: bending (left) and tensile (right).

Regarding the hardness (Figure 6.80), HIP leads to an increment in hardness compared to P&S. In particular, the increment is greater for Ti32–PA samples than for Ti32–MA. Moreover, the increment is more important for higher processing temperatures (HIP–1 and HIP–2) or, for the same temperature, higher pressure (HIP–4).

Comparing the powder production route, Ti32–PA results to be harder than Ti32–MA but, since the relative density is very similar, this is most probably correlated to the chemical analysis of each single material and processing condition as well as alpha mean grain size and relative amount of α + β lamellae, which will be discussed in Section 6.2.2.6.

Once again, in comparison to wrought Ti–3Al–2.5V, the hardness of HIPed samples is noticeably higher but this is most probably due to the greater content of contaminants which the starting powder already has.

Analysing the hardness in relation to the content of interstitials, it can be noticed that the high hardness value obtained for Ti32–PA in the HIP–1 conditions perfectly matches with the great amount of oxygen found in comparison to the other cycles. The same it can be stated for Ti32–MA where, this time, it is the nitrogen which has the greatest influence on the final hardness.

Nevertheless, to better understand the variation of the hardness of the HIPed components with the amount of interstitials, the equivalent oxygen content was calculated (see Eq. 14[11] in Section 2.7) and the result is shown in Figure 6.81.

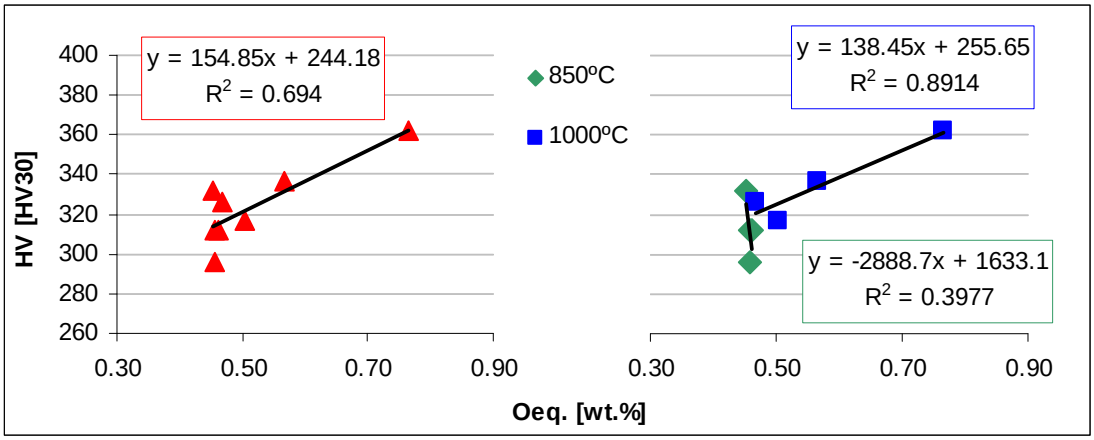

Figure 6.81 – Hardness as a function of equivalent oxygen content for Ti32–PA and Ti32–MA HIPed bending specimens: general trend (left) and influence of the HIP temperature (right).

As it can be seen in Figure 6.81, the hardness values of HIPed Ti32–PA and Ti32–MA alloys can be approximated by a linear regression with a coefficient of determination of about 0.7 indicating that, as expected, the higher the equivalent oxygen content, the harder the material. Nonetheless, it can also be noticed that there is an important scattering of the data which is most probably due differences in residual porosity and microstructural changes induced by the different processing condition.

Actually, when the data are subdivided as a function of the processing temperature (Figure 6.81–right), two different trends are found indicating a significant change in the microstructural features between using a HIP temperature in the β field (1000ºC) or in the α + β field (850ºC). Moreover, the influence of the processing temperature on the microstructure of HIPed P/M Ti–3Al–2.5V components and, therefore, on the final mechanical properties seems to be much more important for 850ºC because there is a scattering of approximately 40 HV30 for very similar equivalent oxygen content. This indicates that there is a key contribution both from the powder production route and the pressure applied during the hot isostatic pressing cycle.

6.2.2.4 – Properties from Bending Test

The bending stress–strain curves comparison for the diverse HIP cycles which were divided for the two P/M approaches is presented in Figure 6.82.

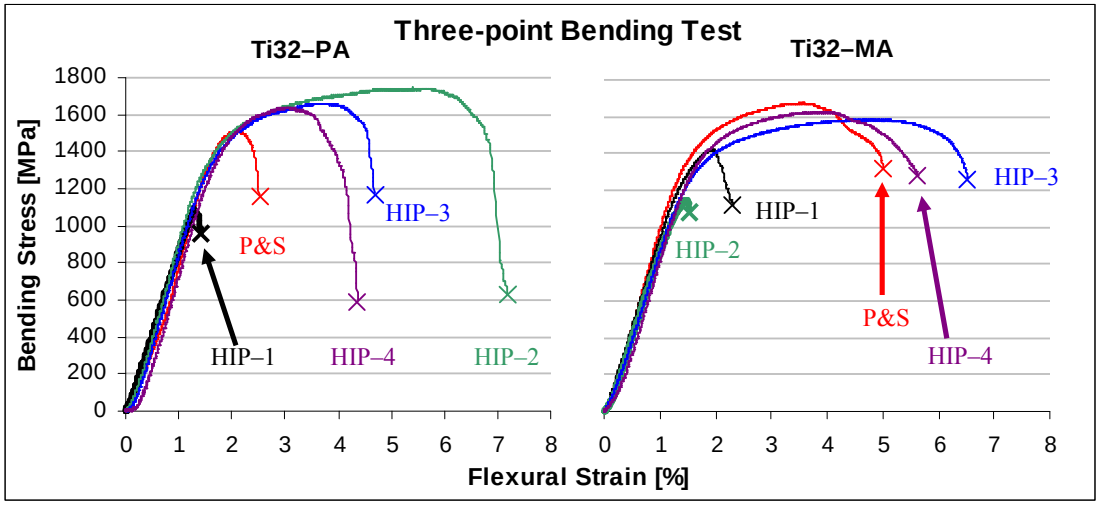

Figure 6.82 – Representative bending stress–strain curves for Ti32–PA and Ti32–MA HIPed specimens.

As it can be seen in Figure 6.82, the bending stress–strain curves of Ti–3Al–2.5V alloys follow the same trend of elemental titanium (Figure 6.23) since the transverse rupture strength is lower than the maximum bending strength. It is worth mentioning that HIP seems to change the fracture mode because the stress–strain curve is in this case composed by a linear elastic deformation followed by plastic yielding and by a more significant drop of the stress before fracture, making the failure less catastrophic.

The flexural modulus calculated from the stress–strain curves results to be slightly higher compared to the P&S components most probably due to the lower residual porosity and equals to 100 ± 9 GPa for Ti32–PA and to 108 ± 3 GPa for Ti32–MA.

Maximum bending strength and flexural strain mean values for Ti32–PA and Ti32–MA HIPed specimens are displayed in Figure 6.83.

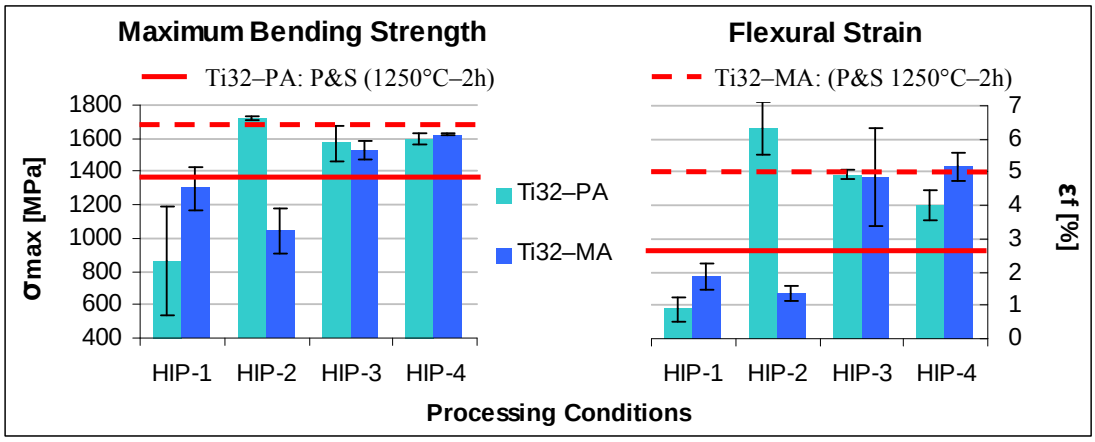

Figure 6.83 – Mechanical properties as a function of the HIP cycle for Ti32–PA and Ti32–MA specimens: maximum bending strength (left) and flexural strain (right).

The data shown in Figure 6.83 indicate that the processing of the samples by HIP in the α + β field (850ºC) permits to maintain or increase the bending properties of the Ti–3Al–2.5V alloy whereas a temperature in the β field (1000ºC) leads to a decrement the mechanical properties.

Compared to sintered materials, Ti32–PA specimens always reach higher mechanical properties with the exception of HIP–1 meanwhile in the case of Ti32–MA the maximum bending strength is always, at least, 50 MPa lower. Nevertheless, the flexural strain shows an important increment in the HIP–3 and HIP–4 conditions.

As for P&S specimens, the mechanical properties determined in the HIPed products by the three–point bending test were analysed on the bases of the equivalent oxygen content and the results are displayed in Figure 6.84 and Figure 6.85.

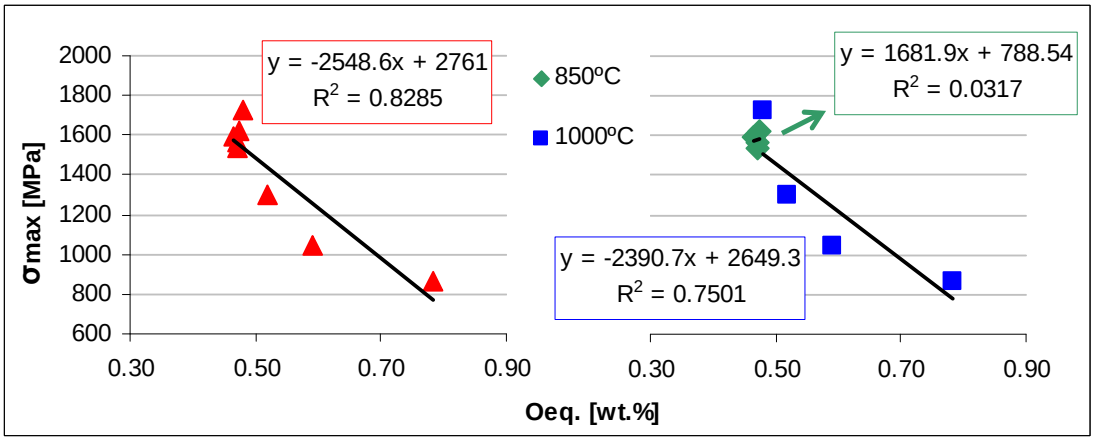

Figure 6.84 – Maximum bending strength as a function of equivalent oxygen content for Ti32–PA and Ti32–MA HIPed bending specimens: general trend (left) and influence of the HIP temperature (right).

As it can be seen in Figure 6.84, the maximum bending strength of HIP Ti–3Al–2.5V samples decreases when the percentage of interstitials increases. Moreover, a processing temperature below or above the beta transus affects importantly the strength. In particular, for the specimens HIPed at 850ºC a correlation with the equivalent oxygen content could not be found because the equivalent oxygen content of the specimens is very similar whilst for the specimens HIPed at 1000ºC the increment of the interstitials decreases the maximum strength.

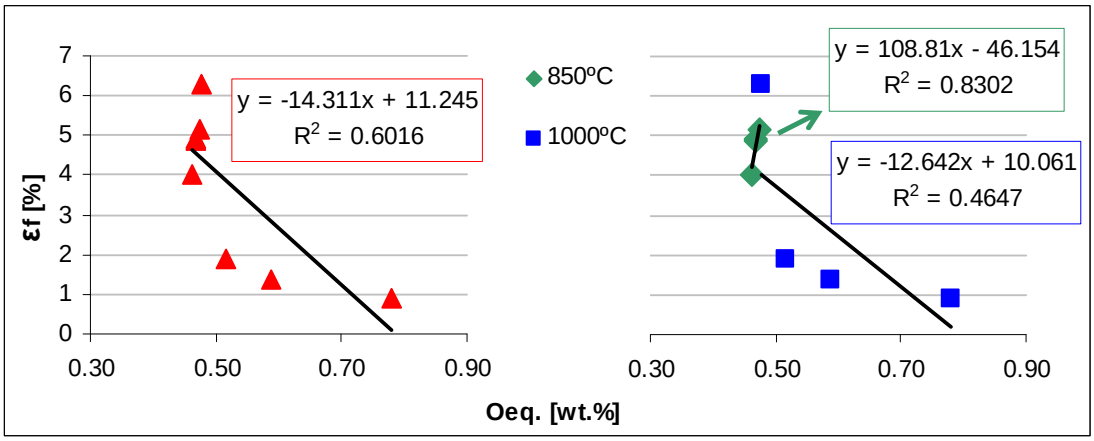

Figure 6.85 – Flexural strain as a function of equivalent oxygen content for Ti32–PA and Ti32–MA HIPed bending specimens: general trend (left) and influence of the HIP temperature (right).

As it can be seen in Figure 6.85, the flexural strain has the same trend of maximum bending strength but the scattering of the data is bigger. Once again, the flexural strain of the specimens HIPed at 850ºC does not seem to be greatly dependent on the amount of interstitials which is exactly the opposite for the samples HIPed at 1000ºC (Figure 6.85–right).

6.2.2.5 – Properties from Tensile Test

The tensile stress–strain curves of the HIPed tensile samples, in comparison to those of the sintered specimens, are reported in Figure 6.86.

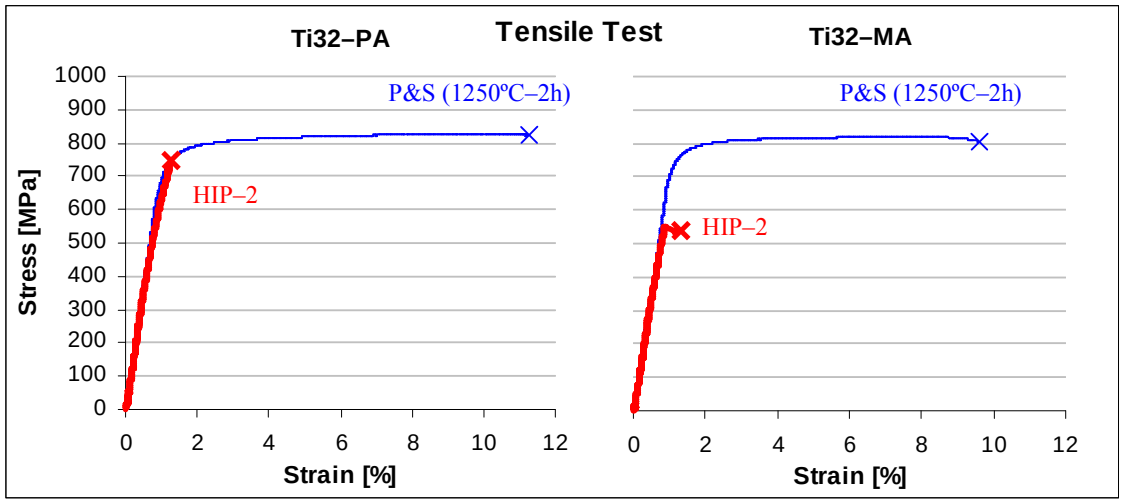

Figure 6.86 – Representative tensile stress–strain curves for Ti32–PA and Ti32–MA P&S (1250ºC–2h) and HIPed specimens.

As it can be seen in Figure 6.86, HIPed samples behave like the pressed and sintered ones in the elastic part of the tensile curve but the fracture occurs at lower stress and without any appreciable plastic deformation.

Dynamic Young modulus determined on HIPed sample is 112 ± 1 GPa and 116 ± 1 GPa for Ti32–PA and Ti32–MA respectively, similar to the value of the wrought Ti–3Al–2.5V. The slight increment of the Young's modulus after HIP compared to P&S could be mainly due to the reduction of the residual porosity.

Figure 6.87 shows the comparison of the ultimate tensile strength and strain mean values between P&S and HIPed samples for the two alloys considered.

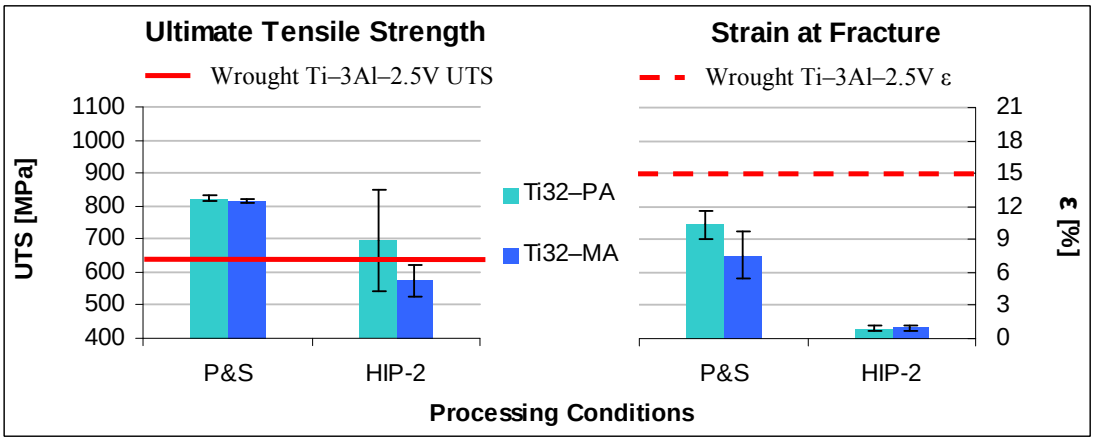

Figure 6.87 – Mechanical properties as a function of the processing method for Ti32–PA and Ti32–MA specimens: ultimate tensile strength (left) and strain (right).

The data shown in Figure 6.87 indicate that, on average, the HIP of the Ti–3Al–2.5V alloy leads to a reduction in terms of UTS compared to the P&S specimens obtaining strength values comparable to those of the wrought alloys in the annealed state. Nonetheless, the most important drop is in terms of strain which goes down to approximately 1% which is significantly lower either with respect to the wrought alloy or the P&S samples. This reduction of the mechanical properties is most probably due to the contamination of the specimens (Figure 6.79), the effect that these interstitials elements have on the microstructure and the microstructural changes induced by the HIP process.

6.2.2.6 – Microstructural Analysis

The results of the microstructural characterisation carried out by optical microscopy are presented in Figure 6.88. Besides, a fractographic study of HIPed tensile samples was carried out and the micrographs of the fracture surface are shown in Figure 6.89.

Comparing the microstructure obtained for HIP–1 conditions (Figure 6.88), it can be seen that Ti32–PA is composed by alpha grains and very fine α + β lamellae (dark zones) whilst Ti32–MA has a coarser microstructure of alpha grains and α + β lamellae although the percentage of alpha seems to be greater in Ti32–PA (Figure 6.88 a). The same differences on the microstructural features but somewhat attenuated can be noticed in HIP–2 where, in general, Ti32–MA has a coarser microstructure.

The changes between HIP–1 and HIP–2 can be attributed to the reduction of oxygen and the increment of nitrogen from HIP–1 to HIP–2 in Ti32–PA and Ti32–MA, respectively because oxygen refines the microstructure and nitrogen promotes the formation of needles of alpha titanium[5].

HIP–3 and HIP–4 microstructures are mainly composed by alpha grains since the processing temperature is in the α + β field but, once again, normally, the Ti32–MA grain size seems to be greater than Ti32–PA one.

Comparing the microstructures of HIPed and P&S (Figure 6.69), it can be noticed that the selection of a processing temperature of 850ºC, below the nominal beta transus for this alloy (935ºC[9]), leads to a microstructure similar to that obtained by furnace cooling in P&S samples (Figure 6.69 a and b), especially for Ti32–PA.

On the other hand, a post–processing by HIP at 1000ºC results in a coarsening of the alpha phase and a reduction of the relative amount of α + β lamellae obtaining a bimodal microstructure composed by primary alpha grains and fine α + β lamellae.

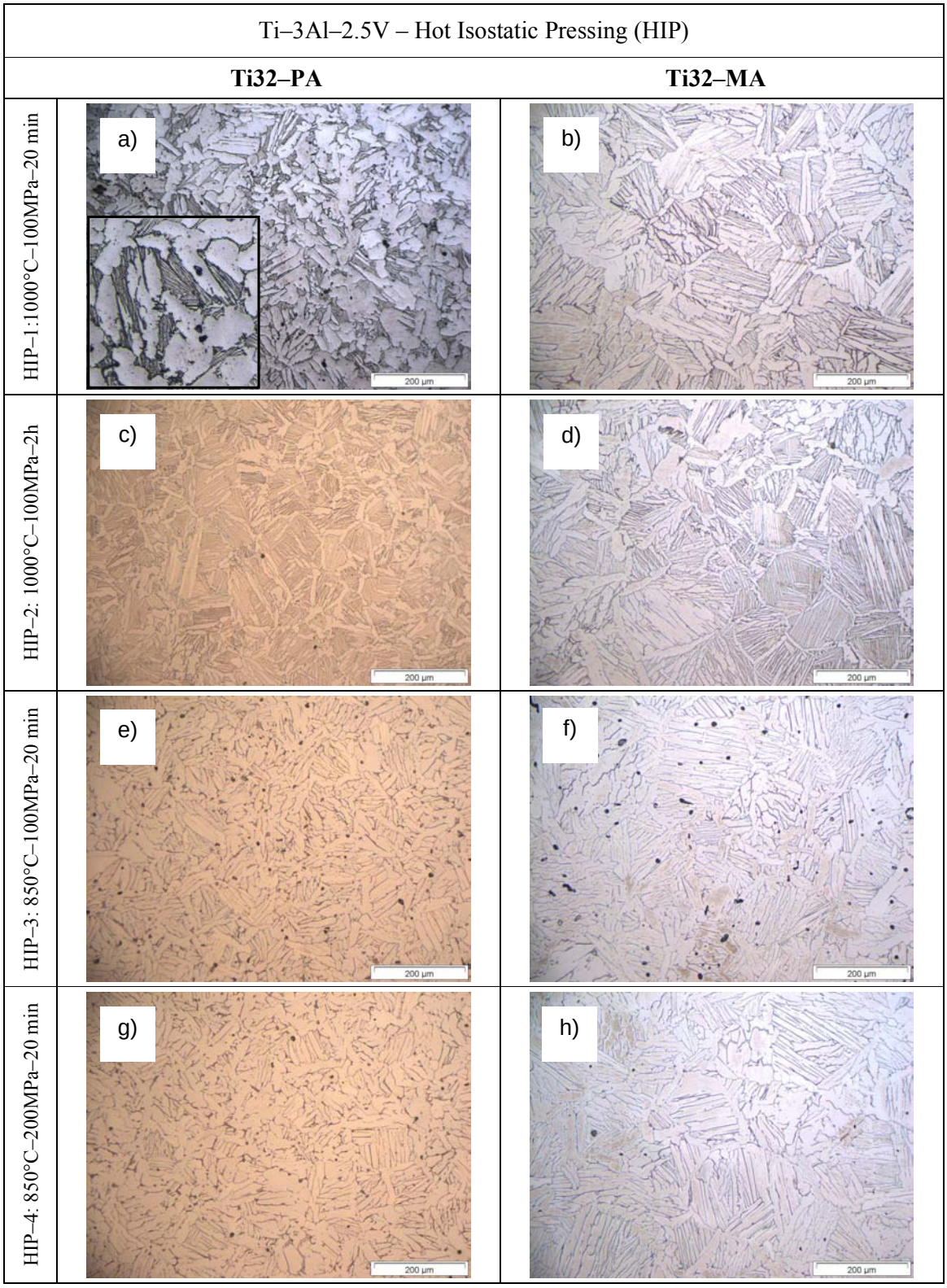

Figure 6.88 – Optical microscopy images for Ti32–PA and Ti32–MA subjected to diverse HIP cycles: a) and b) HIP–1, c) and d) HIP–2, e) and f) HIP–3 and g) and h) HIP–4.

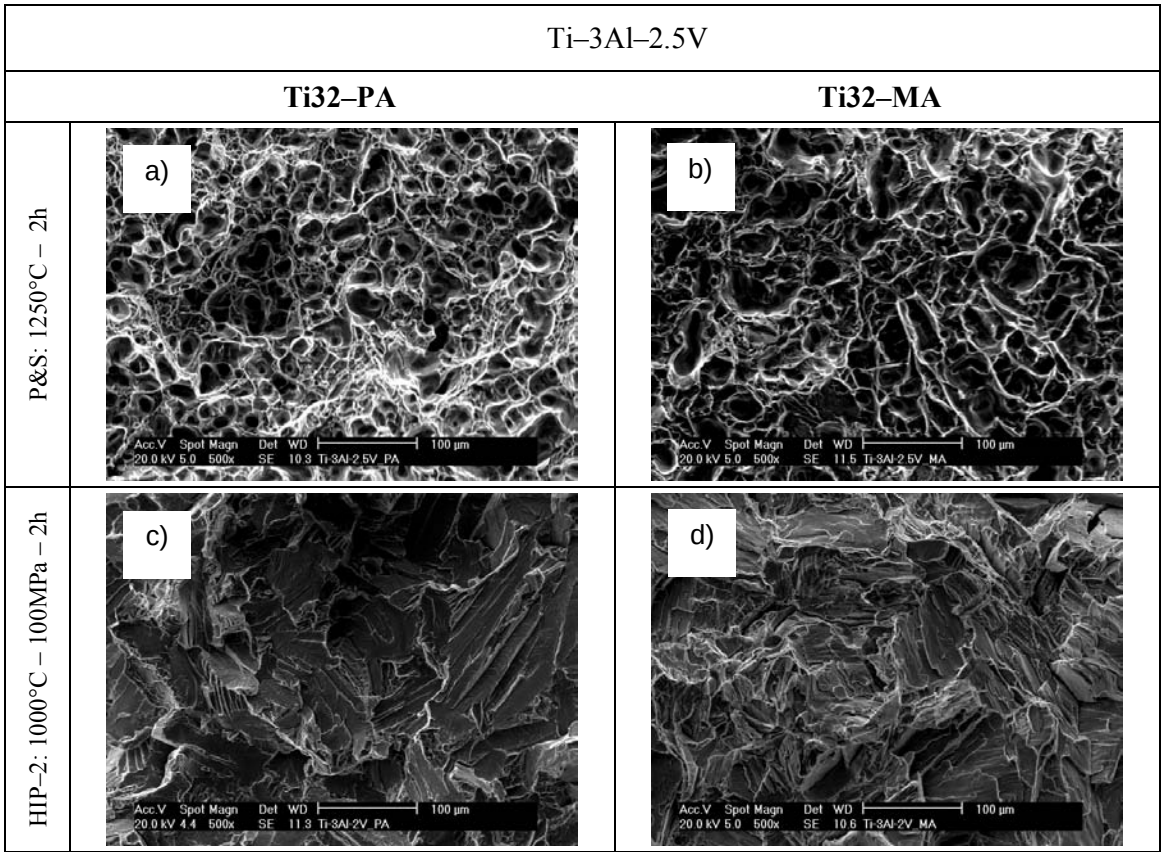

Figure 6.89 – Fracture surface from tensile test specimens for Ti32–PA and Ti32–MA: a) and b) P&S (1250ºC–2h) and c) and d) HIP–2.

As it was found in terms of microstructural features, the fracture surface of the HIPed samples is completely different from that of the P&S sample (Figure 6.89). In particular, the fracture mode is mainly brittle and, thus, characterised by various cleavage surfaces meanwhile the fracture of P&S samples is ductile and the surface composed by equiaxial dimples. This result justifies the very low strain obtained in the tensile test where the materials do not show any plastic deformation (Figure 6.87).

6.2.3 – Conventional Hot–pressing (HP)

As already mentioned in Section 6.1.3, during conventional hot–pressing the powders were loaded into a graphite mould and consolidated at three different temperatures applying a pressure of 30 MPa and an effective dwell time of 30 minutes. The results of their characterisations are discussed in this chapter.

6.2.3.1 – Relative Density

The results of relative density for Ti32–PA and Ti32–MA alloys obtained by conventional hot–pressing are presented in Figure 6.90

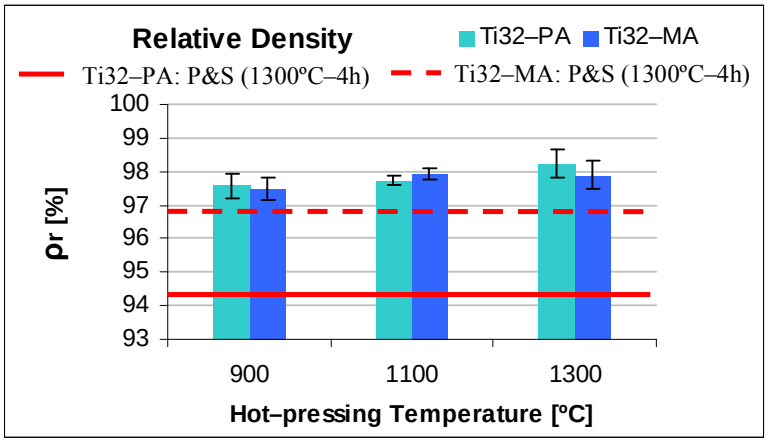

Figure 6.90 – Relative density as a function of the processing temperature for Ti32–PA and Ti32–MA hot–pressed specimens.

As it can be seen in Figure 6.90, the relative density of hot–pressed samples increases with the processing temperature, where the values range between 97% and 98%.

Compared to pressing and sintering samples, the consolidation of Ti32–MA by means of hot–pressing leads to a slightly higher relative density of approximately 1% reaching maximum values of 98%.

In the case of Ti32–PA, the difference is much greater due to the lower pressure used to compact the three–point bending test samples. Actually, when the Ti32–PA powder is pressed with the same pressure as Ti32–MA, there is almost no difference in final relative density, as it was demonstrated during the discussion of the tensile test samples results (Figure 6.52).

The relative density obtained by processing the Ti–3Al–2.5V alloy by conventional hot–pressing is somewhat lower (approximately 1%) than that of elemental titanium (Figure 6.31) most probably due to the fact that some of the thermal energy in invested in the diffusion of the alloying elements instead of in the densification of the material.

6.2.3.2 – Chemical Analysis

The results of the chemical analysis were subdivided between the elements that do not change significantly, oxygen and carbon, with the grinding process used to remove the surface of the specimens and the one that changes, nitrogen, and they are shown in Figure 6.91 and Figure 6.92.

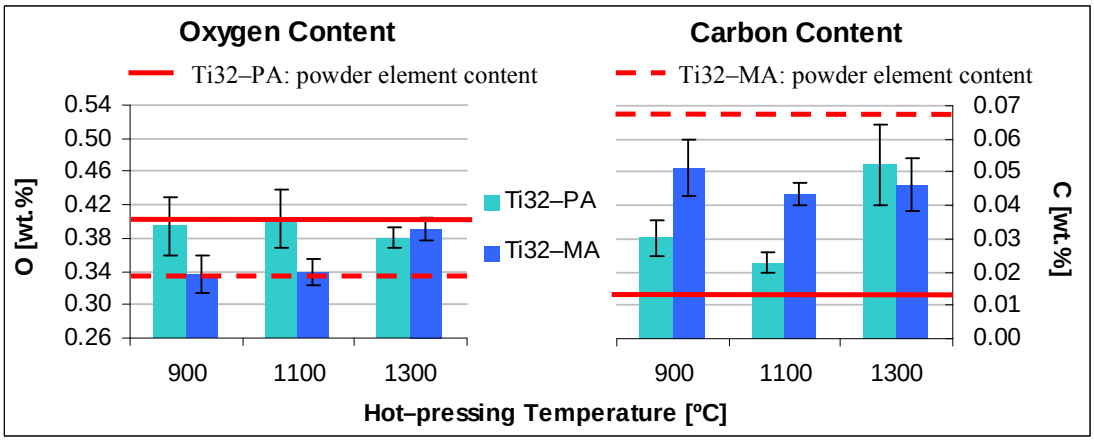

Figure 6.91 – Chemical analysis as a function of the processing temperature for Ti32–PA and Ti32–MA hot–pressed specimens: oxygen (left) and carbon (right).

Analysing the oxygen content shown in Figure 6.91–left, it can be noticed that there is no oxygen pick up with respect to the initial content of the powder with the exception of the Ti32–MA processed at the highest temperature considered (1300ºC). This indicates that the level of vacuum used to process the material is appropriate to consolidate the Ti–3Al–2.5V powders.

On the other side, the carbon percentage (Figure 6.91–right) increases independently of the temperature up to a maximum value of 0.05 wt.% most probably due to the interaction with the graphite mould.

It should be mentioned that the comparison with the initial carbon content of the Ti32–MA powder is not really reliable since this powder has some wax, added for the milling process, which burns and evaporates at 300ºC. Nevertheless, the final carbon content measured in the hot–pressed components is lower than the maximum of 0.08 wt.% specified for the Ti–3Al–2.5V alloy[9].

Results of nitrogen content are divided for the two materials (Ti32–PA and Ti32–MA) as a function of the grinding of the surface in contact with the BN coating, in order to determine the interaction of the materials with the coating, as it can be seen in Figure 6.92.

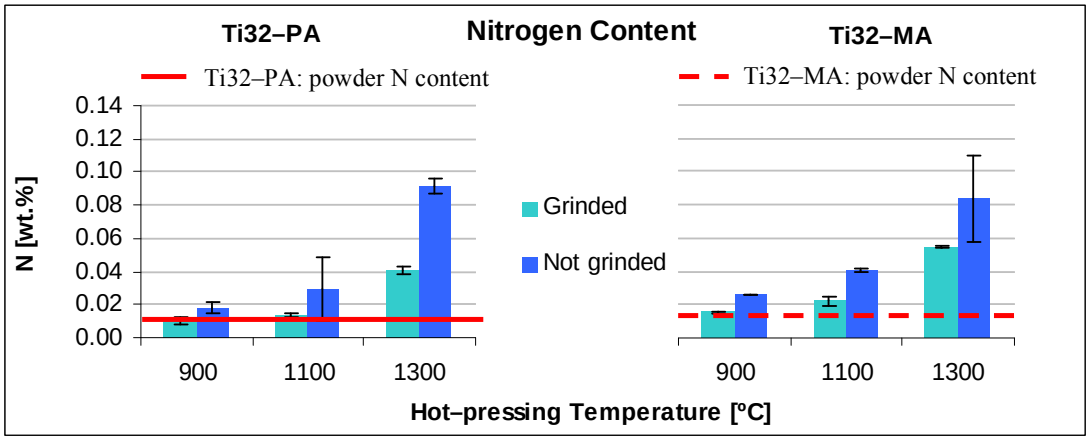

Figure 6.92 – Nitrogen content as a function of the processing temperature for Ti32–PA and Ti32–MA hot–pressed specimens.

Generally, the grinding of the surface, at least, halves the final nitrogen content, indicating that the interaction is strongly concentrated in the surface of the specimens even if there is some diffusion through the material. Moreover, the final percentage increases with the processing temperature due to the great amount of thermal energy which favours diffusion processes and, especially, of interstitial elements. However, for the grinded samples, it can be stated that there is nitrogen pick up only at the highest hot–pressing temperature (1300ºC).

SEM analysis as well as XRD analysis of the reacted layer were carried out in order to quantify the magnitude of the interaction but since there were not significant differences with the results shown for elemental titanium (see Figure 6.33 and Figure 6.34), the results of these characterisation are not reported.

6.2.3.3 – Hardness

The results of hardness measurements carried out on the cross–section of the specimens are displayed in Figure 6.93.

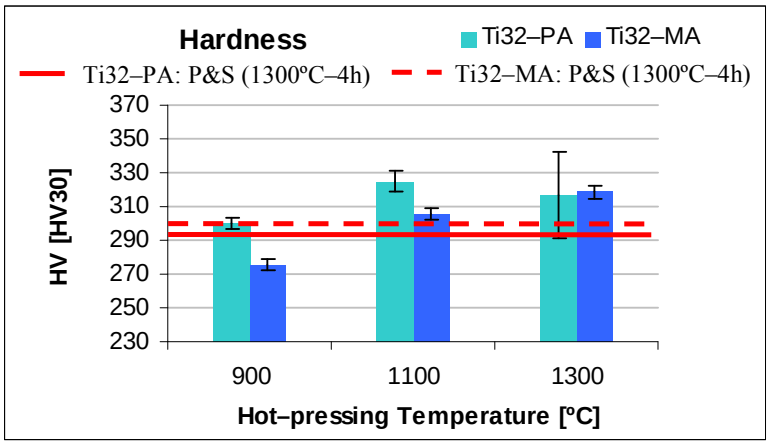

Figure 6.93 – Hardness as a function of the processing temperature for Ti32–PA and Ti32–MA hot–pressed specimens.

As it can be seen in Figure 6.93, the hardness of hot–pressed Ti32–PA and Ti32–MA specimens increases with the processing temperature with the exception of Ti32–PA processed at 1300ºC where the Vickers hardness is somewhat lower but with a much greater standard deviation.

Generally, the hardness of Ti–3Al–2.5V sintered by conventional hot–pressing is similar or somewhat higher than that of P&S sintered at 1300ºC during 4 hours due to the combine effect of interstitials and microstructural features.

Moreover, these two factors, and especially the chemical analysis, are responsible for the higher hardness in comparison to the wrought Ti–3Al–2.5V alloy, whose mean value is 267 HV[9].

6.2.3.4 – Properties from Bending Test

As explained, from hot–pressing were obtained discs of 65 mm from which rectangular samples for bending test were cut. The comparison of the bending stress–strain curves for Ti32–PA and Ti32–MA are subdivided considering the removal of the reacted layer and displayed in Figure 6.94 and Figure 6.95.

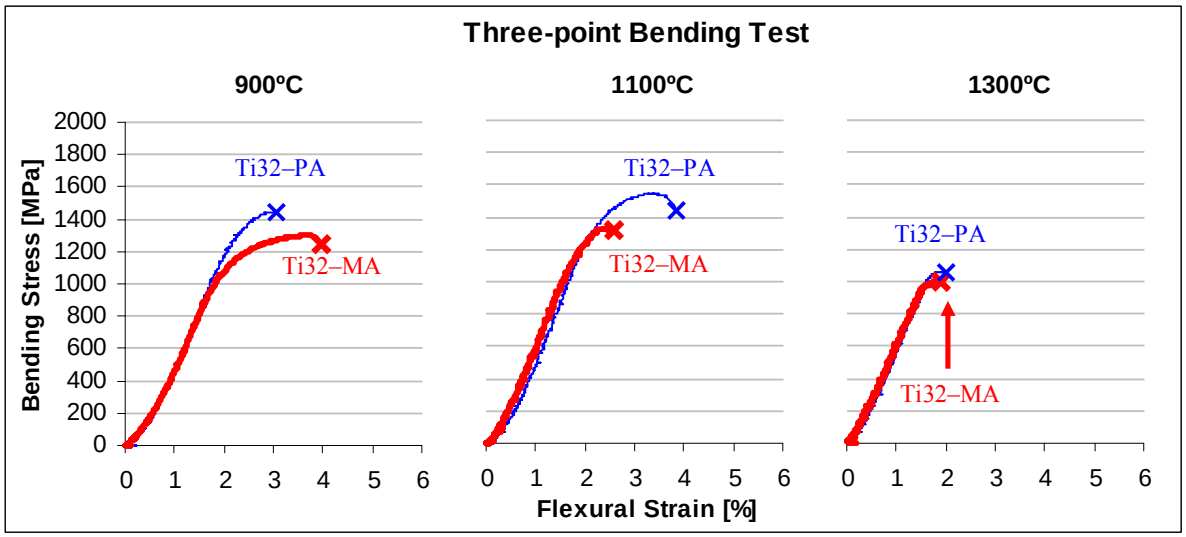

Figure 6.94 – Representative bending stress–strain curves for Ti32–PA and Ti32–MA hot–pressed specimens (without the removal of the outer surface).

The bending stress–strain behaviour of not grinded specimens made out of Ti32–PA and Ti32–MA alloys (Figure 6.94) are similar and resemble that of P&S specimens (Figure 6.59 and Figure 6.60) where the linear elastic deformation step is followed by a plastic deformation and a catastrophic failure without the stress drop which characterised the HIPed samples (Figure 6.82).

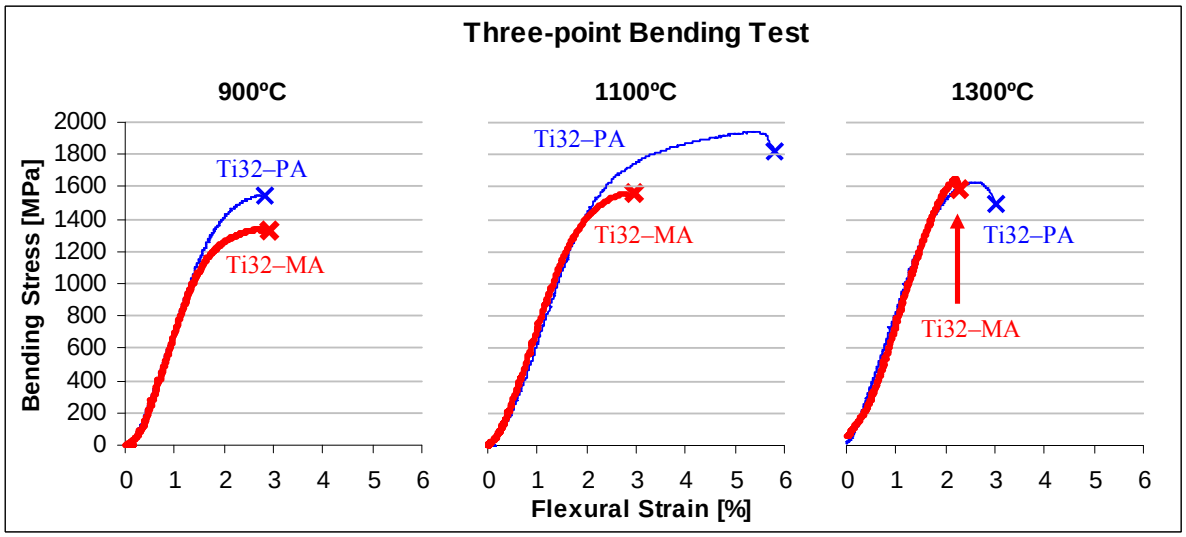

Figure 6.95 – Representative bending stress–strain curves for Ti32–PA and Ti32–MA hot–pressed specimens (after the removal of the outer surface).

The bending stress–strain curves of surface grinded samples (Figure 6.95) resemble very much the ones shown in Figure 6.94 but differences in terms of maximum bending strength and flexural strain can be noticed.

However, the two types of material have the same response to the loading in the elastic part of the curve since they overlap and the alloys fail after a small plastic yielding and strain hardening with the only exception of Ti32–PA sintered at 1100ºC, where the plastic deformation is significantly greater.

As explained for elemental titanium specimens, the flexural modulus determined by the three–point bending test is greatly influenced by the L/D ratio of the specimens since increasing the L/D ratio produces an increment in terms of flexural modulus[16-18]. The analysis of the variation of the flexural modulus measured either in P&S or hot–pressed Ti–3Al–2.5V samples with the L/t ratio is displayed in Figure 6.96.

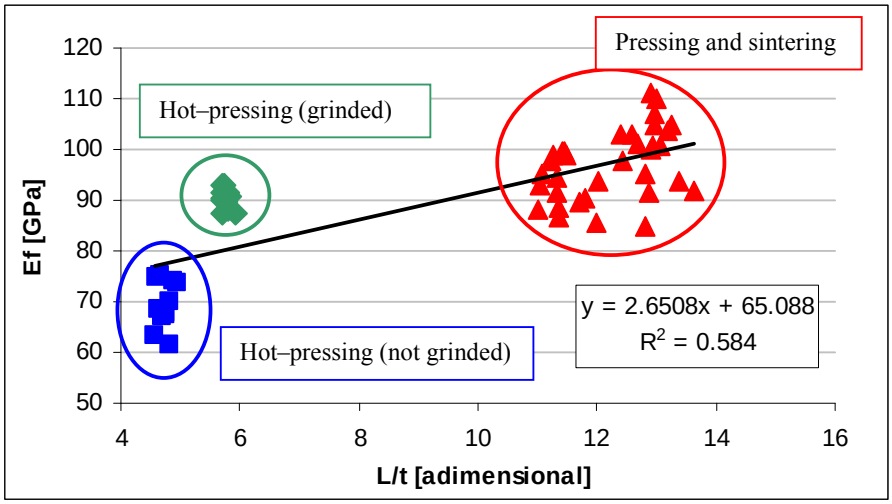

Figure 6.96 – Flexural modulus as a function of the L/t ratio for Ti32–PA and Ti32–MA obtained by the diverse P/M methods studied.

The data shown in Figure 6.96 indicate that, as expected, the flexural modulus of both Ti32–PA and Ti32–MA increases when the L/t ratio increases and, therefore, when the thickness of the specimens decreases, since during the development of this thesis the span length (L) was kept constant.

Considering the flexural modulus data for P&S samples, it can be noticed that they have a deviation of ± 15 GPa for a constant value of L/t which is then due to the different level of relative density attained using various combination of temperature and time as well as compacting pressure.

As it was for elemental titanium, the removal of the outer layer contaminated by nitrogen and boron of HP samples leads to an increment of 10 GPa, on average. Moreover, it can be noticed that the data for not grinded specimens have a much greater scattering compared to those of the grinded specimens, once again most probably due to the influence of the thickness of the reacted layer.

The comparison of the mean value of maximum bending strength and flexural strain for Ti32–PA and Ti32–MA are presented in Figure 6.97 and Figure 6.98.

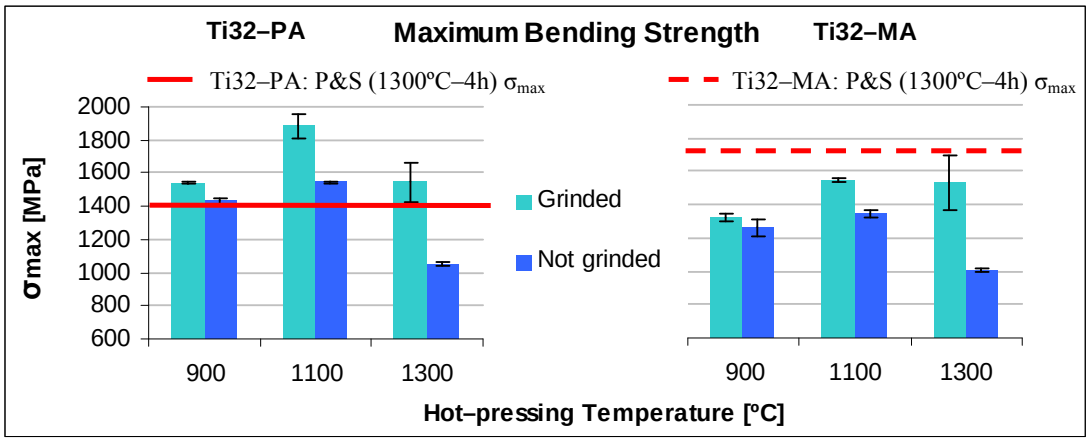

Figure 6.97 – Maximum bending strength as a function of the processing temperature for Ti32–PA and Ti32–MA hot–pressed specimens.

Analysing the mean values of maximum bending strength shown in Figure 6.97, it can be seen that the increment of the processing temperature from 900ºC to 1100ºC leads to an increment in strength but a further increase provokes a drop of this property. Furthermore, the Ti32–PA specimens reach higher maximum bending strength than Ti32–MA. This behaviour could be explained by the fact that the specimens hot–pressed at 1100ºC see the benefits of the decrement of the residual porosity and the homogenisation of the microstructure, which is not the case for samples processed at 900ºC as the microstructural analysis (Section 6.2.3.5) demonstrates whereas at 1300ºC the strength is affected by the grain growth induced by the higher processing temperature.

The removal of the reacted surface by grinding gets more important with the raising of the temperature for both materials because at 900ºC the difference of maximum bending strength between grinded and not grinded specimens of the same material is lower than 50 MPa and at 1300ºC is, approximately, 500 MPa.

Apart from the samples pressed at 1300ºC and tested without removing the surface, the maximum bending strength of Ti32–PA consolidated by hot–pressing is higher than that of the specimens obtained by P&S. This can be explain on the bases of the lower density of P&S Ti32–PA samples due to the lower compacting pressure used (300 MPa). As a consequence, Ti32–PA processed by hot–pressing reaches, in general, higher bending strength than P&S samples whereas the maximum values of bending strength of Ti32–MA are higher in samples processed by pressing and sintering in all the conditions.

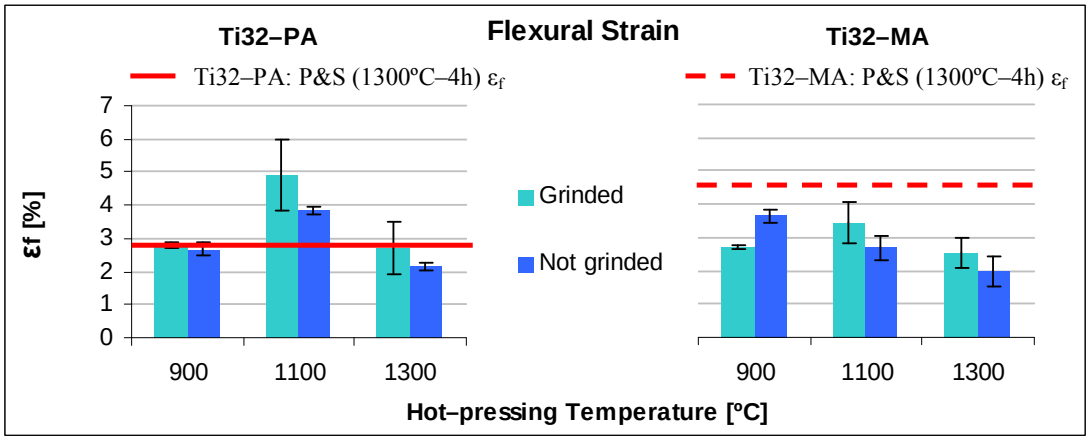

Figure 6.98 – Flexural strain as a function of the processing temperature for Ti32–PA and Ti32–MA hot–pressed specimens.

As it can be seen in Figure 6.98, normally, the flexural strain of hot–pressed Ti–3Al–2.5V follows the same trend as the maximum bending strength, therefore increasing from 900ºC to 1100ºC and then decreasing. The behaviour can be well explained on the bases of the chemical analysis results since the content of the elements with the strongest effect on ductility, oxygen and nitrogen[5, 6], does not increase significantly at 1100ºC but then it does for a processing temperature of 1300ºC. As for elemental titanium, the removal of the surface of the specimens leads to an improvement on ductility but it is not as important as for the maximum bending strength.

In comparison to P&S specimens sintered at 1300ºC during 4 hours, the processing of the Ti32–PA alloy by HP leads to an increment in ductility just in the case of the hot–pressing at 1100ºC whilst in the other cases the flexural strain is similar. On the other hand, the flexural strain of hot–pressed Ti32–MA is always lower than that of P&S samples.

6.2.3.5 – Microstructural Analysis

Ti32–PA specimens present higher mechanical properties compared to Ti32–MA, even though of the similar relative density. The reason of this behaviour should be found in microstructure and Figure 6.99 shows a representative micrograph for the two materials hot–pressed at 900ºC, 1100ºC and 1300ºC taken at the same magnification for comparison.

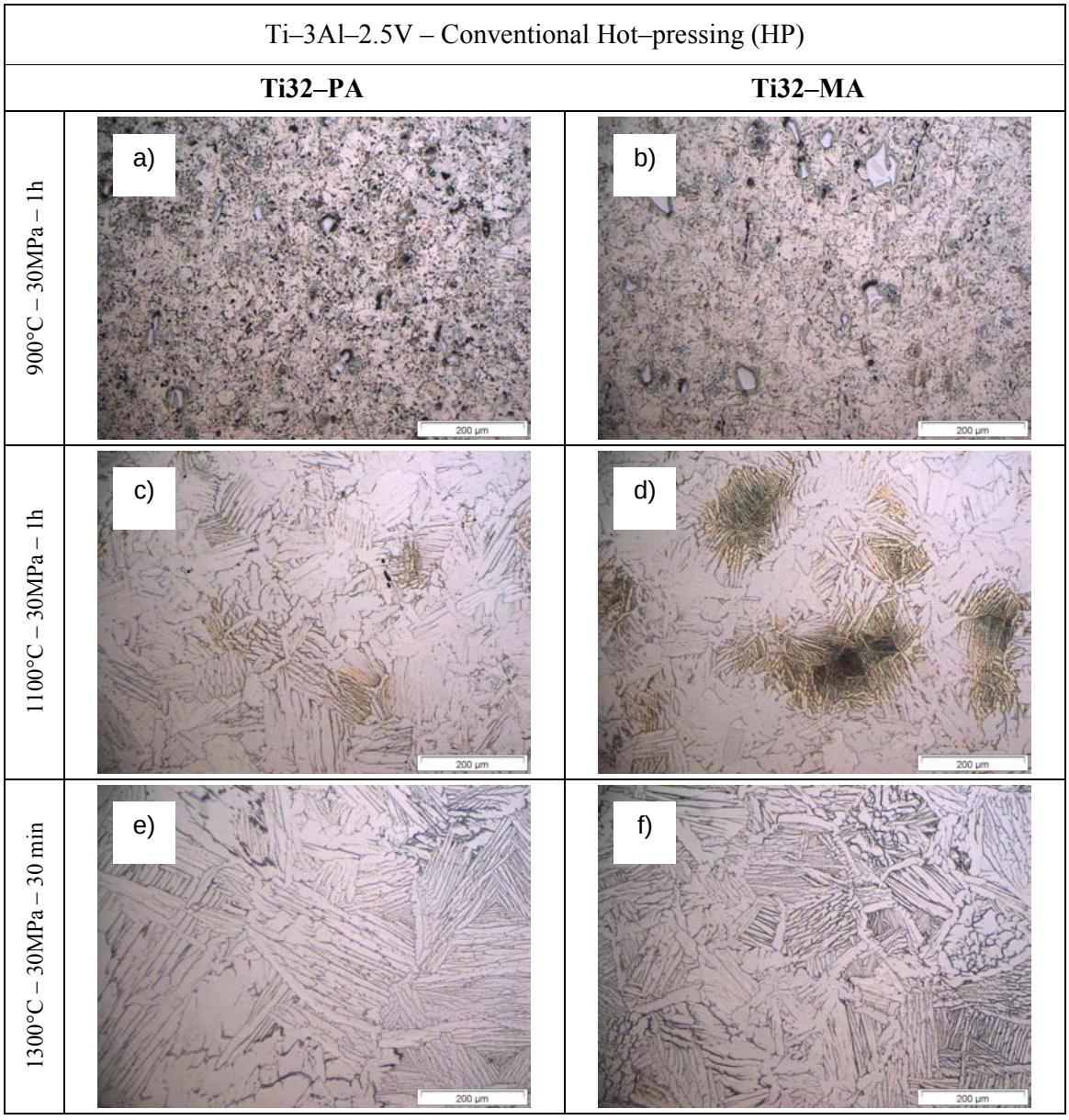

Figure 6.99 – Optical microscopy images for Ti32–PA and Ti32–MA hot–pressed at: a) and b) 900ºC, c) and d) 1100ºC and e) and f) 1300ºC.

The microstructure of Ti32–PA and Ti32–MA hot–pressed at 900ºC (Figure 6.99 a and b) is characterised by porosity and undissolved particles (titanium and master alloy) which confirms the results previously described. In this case, the microstructure is not fully developed and it is constituted by alpha phase because the processing temperature is below the nominal beta transus for the Ti–3Al–2.5V alloy, which is 935ºC[9].

The materials processed at 1100ºC are characterised by denser and more heterogeneous microstructure and no original undissolved particle can be found. The microconstituents are alpha grains and α + β lamellae being these last much finer for Ti32–MA but concentrated in some areas. This is most probably due to the fact that more thermal energy is invested to diffuse the elemental alloying elements of Ti32–MA and, consequently, less energy is available for the development of the stable microstructure at that temperature and for grain growth.

The main significant difference between the microstructure of the specimens hot–pressed at 1100ºC and 1300ºC is the grain growth induced by the higher processing temperature. The greater grain size helps to justify the decrease of the maximum bending strength of the samples processed at 1300ºC compared to those sintered at 1100ºC, which is more pronounced for Ti32–PA coinciding with a greater grain growth.

6.2.4 – Inductive Hot–pressing (IHP)

Both Ti32–PA and Ti32–MA were processed by inductive hot–pressing at two temperatures (1100°C and 1300°C) during 15 minutes and the results of their characterisation are discussed in this section.

Figure 6.100 shows the graph registered during the processing of the alloys at 1100°C where the profiles of the temperature, punch displacement and densification rate can be seen.

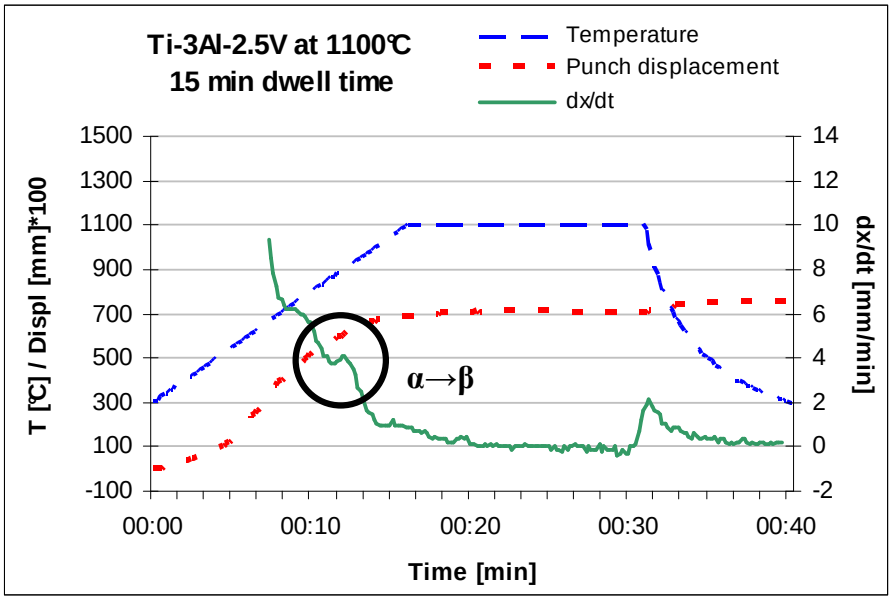

Figure 6.100 – Temperature, punch displacement and densification rate profiles recorded during the processing of the Ti–3Al–2.5V alloy by inductive hot–pressing at 1100ºC.

Analysing Figure 6.100, it can be noticed that the processing time is approximately 40 minutes, much shorter with respect to conventional hot–pressing (Figure 6.30) and that the densification (dx/dt) starts already during the heating of the powder and it is, almost, completed after 5 minutes of dwell time at the processing temperature. Moreover, the change from the alpha phase to the beta phase can be clearly identified in the densification rate profile at somewhat lower temperature than the beta transus of the alloy (935ºC) because this phase transformation corresponds to that of elemental titanium used to fabricate the Ti–3Al–2.5V powders.

6.2.4.1 – Relative Density

Once obtained, the specimens were taken out of the graphite mould and sandblasted to clean the surfaces. Subsequently, the specimens were cut in two halves to proceed with the characterisation. The results of relative density are presented in Figure 6.101.

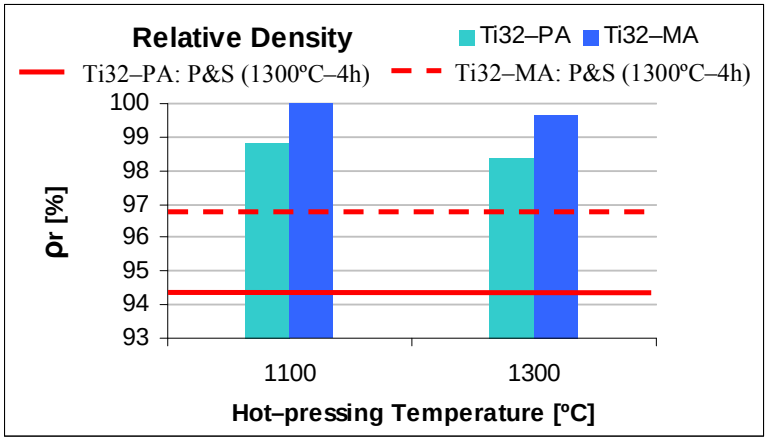

Figure 6.101 – Relative density as a function of the processing temperature for Ti32–PA and Ti32–MA inductive hot–pressed specimens.

As it can be seen in Figure 6.101, the processing of the Ti–3Al–2.5V alloy by means of inductive hot–pressing allows to attain fully dense materials, with 1% maximum of residual porosity. Only in the case of Ti32–PA hot–pressed at 1300°C, the final relative density is only slightly higher than 98% (Figure 6.101). Moreover, it can be noticed that employing inductive hot–pressing to process the Ti–3Al–2.5V alloy leads to an increment of relative density between 2.5% and 5% for Ti32–MA and Ti32–PA, respectively, with respect to P&S samples where the greater increment found in the Ti32–PA powder is, again, due to the low level of relative density obtained in P&S samples which were pressed at 300 MPa.

The microstructural analysis of the Ti32–PA alloy specimens processed by inductive hot–pressing reveals that the lower than expected relative density found when using a processing temperature of 1300ºC is due to an error during the preparation of the die for the consolidation which resulted in some graphite embedded into the surface of the component, as it can be seen in Figure 6.102.

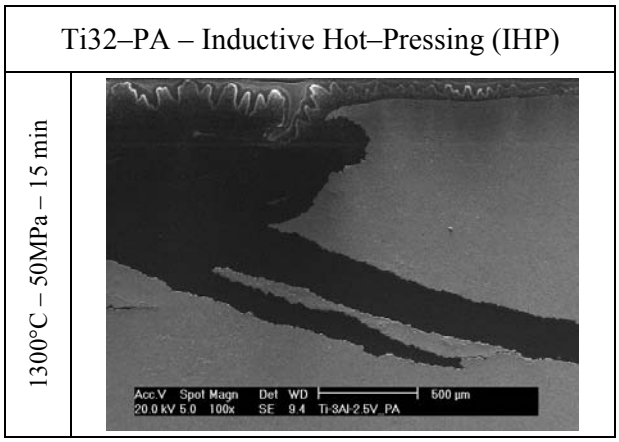

Figure 6.102 – Detail of the surface of the Ti32–PA specimen hot–pressed at 1300ºC.

As a consequence, avoiding this sort of contamination from the graphite mould, whose density is significantly lower than that of titanium, practically one hundred percent dense Ti–3Al–2.5V components can be fabricated.

6.2.4.2 – Chemical Analysis

The results of chemical analysis, precisely oxygen, nitrogen and carbon content, are shown in Figure 6.103.

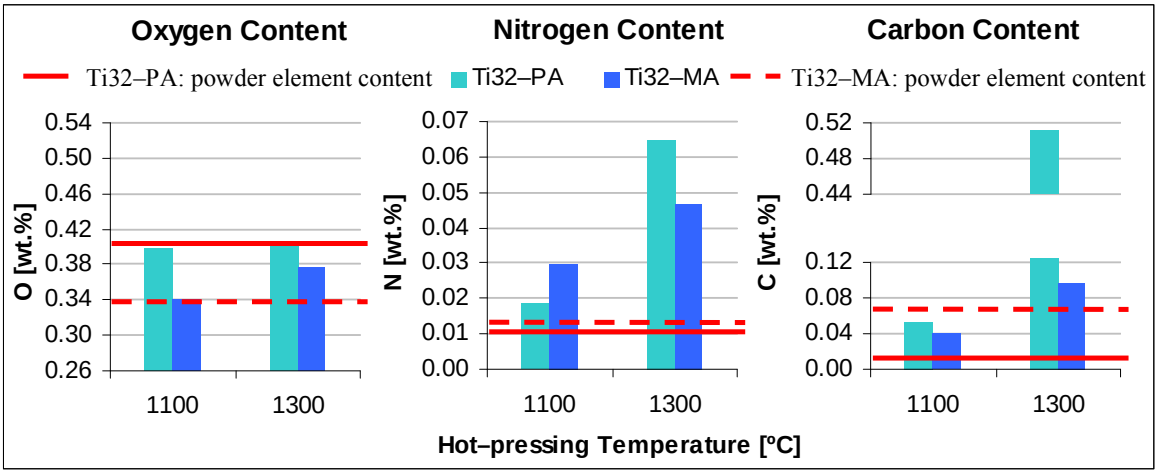

Figure 6.103 – Chemical analysis as a function of the processing temperature for Ti32–PA and Ti32–MA inductive hot–pressed specimens: oxygen (left), nitrogen (centre) and carbon (right).

Oxygen percentage of Ti32–PA and Ti32–MA powders consolidated by inductive hot–pressing (Figure 6.103) remains at the same level of the starting powder, indicating that there is no oxygen pick–up, with the exception of Ti32–MA at 1300°C. Compared to pressing and sintering components, the amount of oxygen is similar.

Concerning nitrogen, it can be seen that there is always some nitrogen contamination with respect to the powder, it increases with the temperature and it is more significant for Ti32–PA. Therefore, the final content is higher compared to P&S but similar to that of conventional hot–pressing.

Carbon percentage follows the same trend as nitrogen, it increases with the processing temperature and it is higher for Ti32–PA. However, it should be specified that the very high carbon percentage found in Ti32–PA at 1300°C is due to the presence of some part of the graphite disc that was used to separate the powders which was embedded in the sample as previously described (see Figure 6.102) and that could not be removed.

6.2.4.3 – Hardness

The variation of the Vickers hardness with the processing temperature for the Ti–3Al–2.5V alloy sintered by inductive hot–pressing is shown in Figure 6.104.

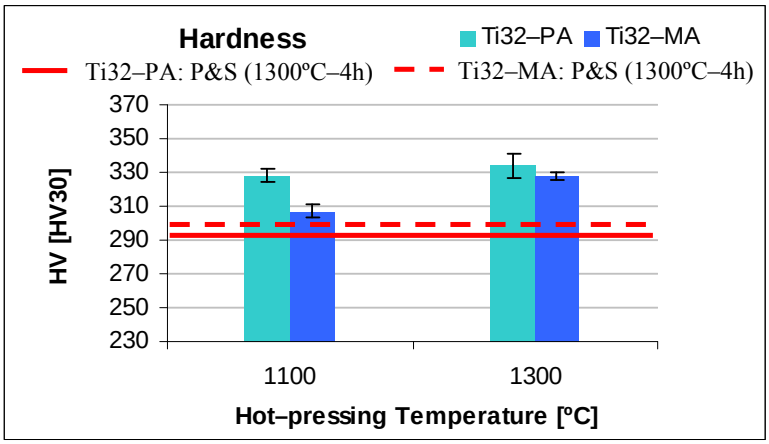

Figure 6.104 – Hardness as a function of the processing temperature for Ti32–PA and Ti32–MA inductive hot–pressed specimens.

The hardness of inductive hot–pressed Ti–3Al–2.5V specimens (Figure 6.104) increases with the processing temperature being this increment more important for Ti32–MA even though Ti32–PA is always somewhat harder than Ti32–MA.

The increment of the hardness with the temperature and the differences between the values found in the two alloys are mainly due to the total amount of interstitials dissolved and to the microstructural feature.

The hardness values shown in Figure 6.104 result to be higher in comparison to those of pressing and sintering samples but very similar to those of conventional hot–pressed components processed at the same temperature (Figure 6.93). Moreover, fully dense P/M Ti–3Al–2.5V results to be harder compared to the wrought alloy in the annealed state (267 HV) due to the greater amount of interstitials dissolved in the matrix and, most probably, to the differences in microstructure.

6.2.4.4 – Microstructural Analysis

The results of the microstructural analysis by optical microscopy are shown in Figure 6.105.

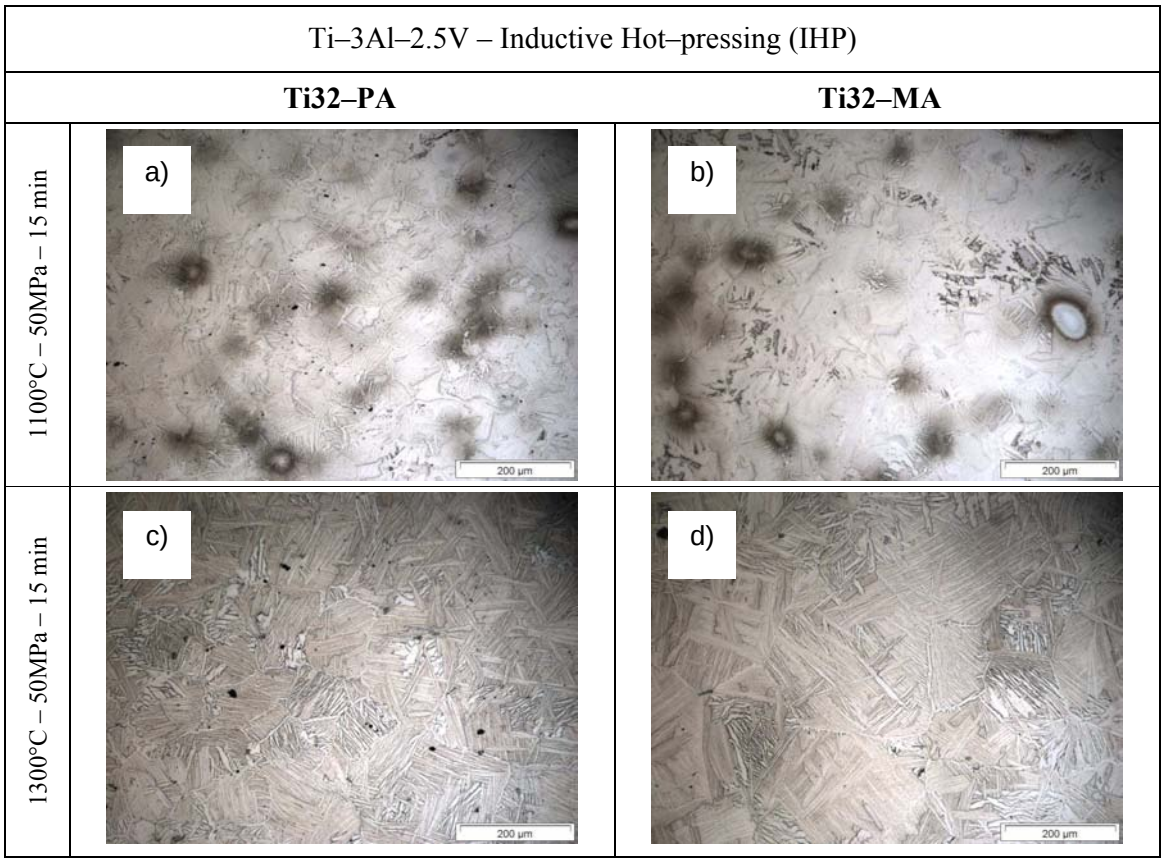

Figure 6.105 – Optical microscopy images for Ti32–PA and Ti32–MA inductive hot–pressed at: a) and b) 1100ºC and c) and d) 1300ºC.

As it can be seen in Figure 6.105, the lower processing temperature of 1100°C combined with the short processing time is not high enough the allow the formation of a homogeneous microstructure.

Due to the intrinsic differences of the two powder production routes, the microstructure of Ti32–MA results to be less uniform than that of Ti32–PA. Therefore, the basketweave microstructure is constituted by alpha grains, fine regions of α + β lamellae and undissolved master alloy particles.

On the other side, a higher processing temperature leads to a homogeneous microstructure for both kind of powders where the microconstituents of the Ti32–MA seems to be slightly coarser which justifies the lower hardness of Ti32–MA samples compared to Ti32–PA specimens.

6.2.5 – P/M Techniques Comparison

In this section the comparison of the best results obtained by producing the Ti–3Al–2.5V alloy by diverse conventional and advanced P/M techniques is discussed.

The highest values of relative density, equivalent to the lowest residual porosity, are compared in Figure 6.106.

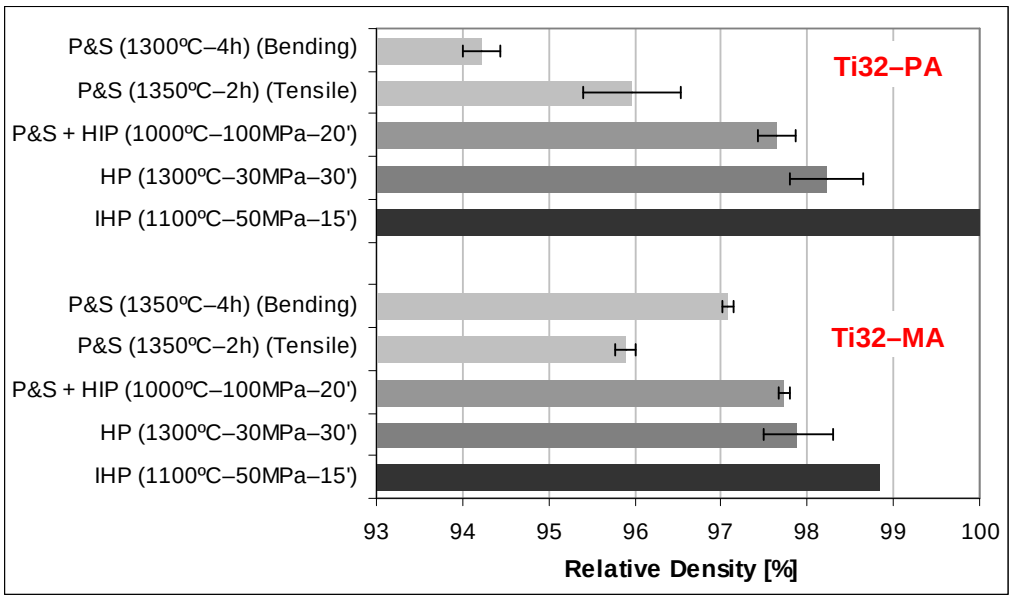

Figure 6.106 – Comparison of the highest relative density for Ti32–PA and Ti32–MA obtained by different P/M techniques.

Analysing the data shown in Figure 6.106, it can be seen that the HIP process leads to an increment of the relative density with respect to P&S materials but it does not allow to reach fully dense materials due to the open porosity present in the samples [28]. On the other side, the hot–pressing technique permits to obtain similar values to HIP with the conventional process and fully dense alloys with the inductive method.

Comparing the powder production route, it seems that the mixing of elemental titanium powder with a prealloyed Ti–6Al–4V powder (Ti32–PA) permits to reach slightly higher final relative density with respect to the master alloy addition approach (Ti32–MA) most probably because less thermal energy is invested in diffusion processes.

The only exception noticeable in Figure 6.106 is the relative density of P&S three–point bending test samples of Ti32–PA which is lower than Ti32–MA but this is due to the lower pressure employed during the compaction of the rectangular shaped specimens.

Based on the results of the tensile test samples, it would be expected that, if the three–point bending test specimens of Ti32–PA powder could have been pressed at 700 MPa, they would have reached, at least, the same relative density of their counterpart as in the case of tensile samples.

For Vickers hardness comparison, presented in Figure 6.107, the equivalent oxygen content of the samples was calculated using the formula proposed by Okazaki and Conrad (Eq. 14 in Section 2.7)[11] where the N:O ratio is equal to 1.96 and the C:O ratio is 0.52. In particular, the hardness data shown in Figure 6.107 corresponds to specimens which have an equivalent oxygen content of approximately 0.45 wt.%. This permits to analyse the comparison without the influence of the interstitial on hardness.

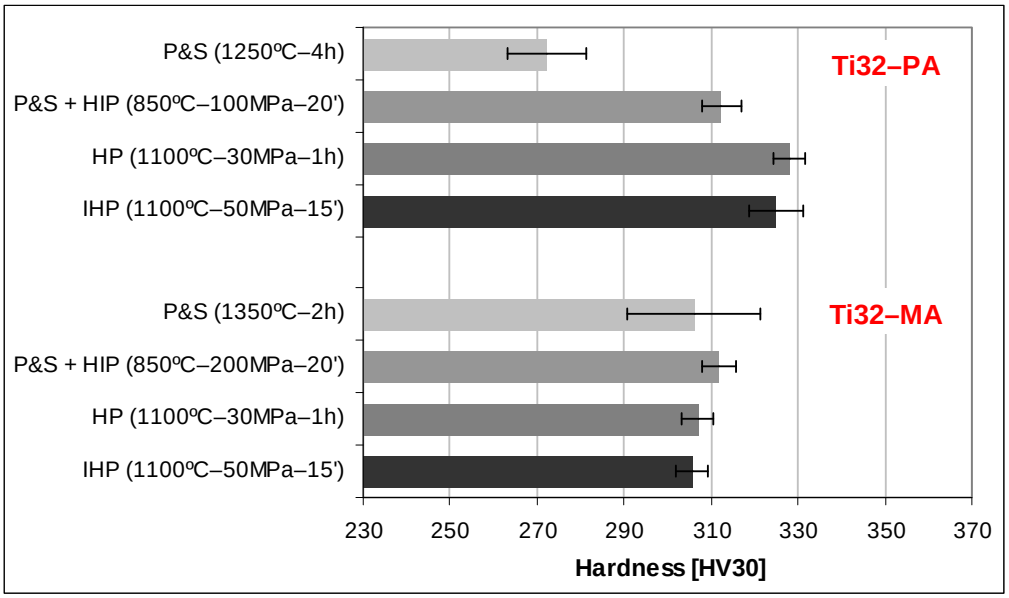

Figure 6.107 – Comparison of the hardness for Ti32–PA and Ti32–MA obtained by different P/M techniques (equivalent oxygen content of approximately 0.45 wt.%).

As it can be seen in Figure 6.107, the hardness of Ti32–PA follows the same trend of the relative density; therefore, it increases with the density where the lower hardness of P&S specimens is due to the lower relative density (approximately 93%).

On the other hand, the hardness of Ti32–MA seems to be more invariant and independent of the residual porosity but this is most probably due to the fact that the increment of the relative density in HIP and hot–pressing is balanced by the microstructural changes correlated.

Nonetheless, it should be specified that the equivalent oxygen percentage of the Ti32–MA processed by HP or IHP considered for the comparison is somewhat lower (0.42 wt.%) than 0.45 wt.%, which could justify the lower values respect to Ti32–PA processed under the same conditions.

Generally, on average, the hardness of Ti32–PA and Ti32–MA results to be 30–40 HV30 higher compared to the wrought alloy (267 HV for an equivalent oxygen content of 0.37 wt.%).

As in the case of elemental titanium, the comparison of the maximum bending strength is based on the calculation of the equivalent oxygen content by means of the linear correlation suggested by Wood (Eq. 15 in Section 2.7)[19] where the ratio for nitrogen and carbon to oxygen are 2.29 and 0.76, respectively. It is worth mentioning that the equivalent oxygen of the maximum bending strength data presented in Figure 6.108 is about 0.47 wt.%.

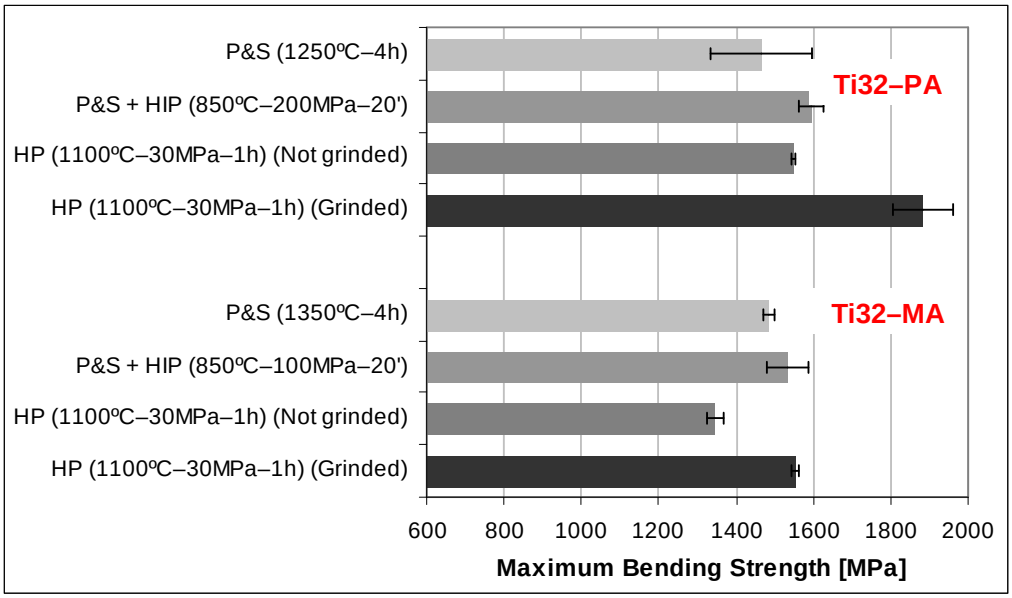

Figure 6.108 – Comparison of the maximum bending strength for Ti32–PA and Ti32–MA obtained by different P/M techniques (equivalent oxygen content of approximately 0.47 wt.%).

The data in Figure 6.108 show that the application of a post–processing of HIP leads to a slight increment of maximum bending strength most probably due to the reduction of the residual porosity.

The best performance is obtained in the hot–pressed components after the removal of the outer surface, once again due to the somewhat higher relative density and the finer α + β lamella found as features of the microstructure. The presence of the reacted surface in the conventional hot–pressed specimens entails an important drop of the strength either compared to the value attained with other processing techniques or to the value of the grinded samples.

Finally, the flexural strain values for Ti32–PA and Ti32–MA are compared in Figure 6.109 on the bases of an equivalent oxygen content of 0.47 wt.% (see Eq. 16, Wood[19]).

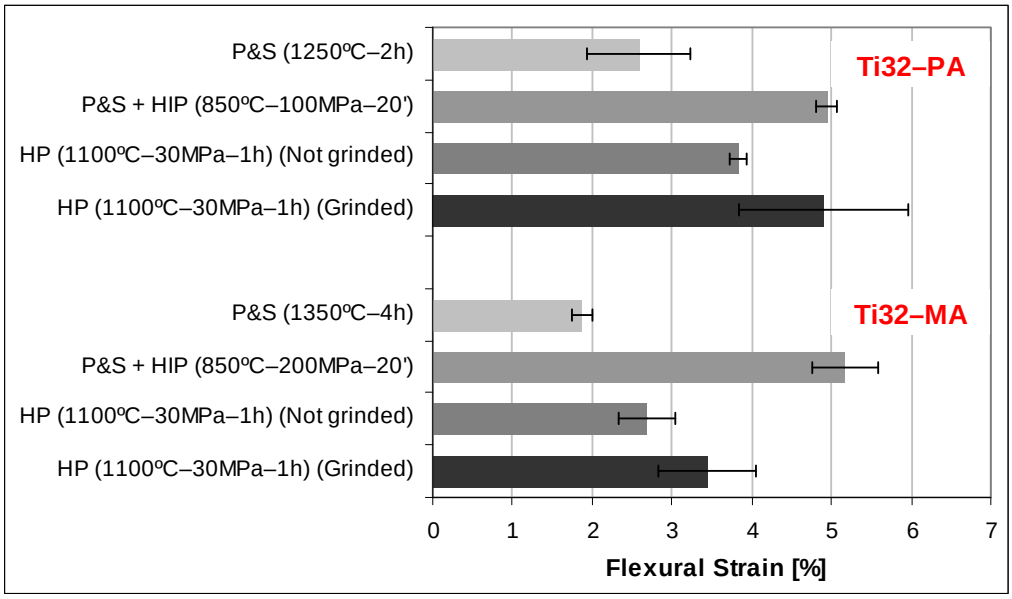

Figure 6.109 – Comparison of the flexural strain for Ti32–PA and Ti32–MA obtained by different P/M techniques (equivalent oxygen content of approximately 0.47 wt.%).

As it can be seen in Figure 6.109, the lowest values of flexural strain for Ti32–PA is obtained in the pressing and sintering approach due to the fact that these samples have quite low relative density of approximately 93%.

The processing of the Ti32–PA powder by means of conventional hot–pressing leads to an increment of the flexural stain, independently of the fragile surface layer formed during the interaction with the BN coating. When the outer layer is removed, the flexural strain of hot–pressed components increases significantly equalising the ductility of HIPed specimens, even if the values present greater standard deviation.

On the other hand, the flexural strain of Ti32–MA alloy increases with the pressure employed during the processing from the pressing and sintering (P&S) to hot–pressing and, then, HIP as post–processing. The removal of the reacted layer in the hot–pressed samples leads to an increment of the ductility of the Ti32–MA alloy.

Comparing the powder production route, it can be noticed that hot–pressed (not grinded) and HIPed flexural strain values for Ti32–PA and Ti32–MA are similar.

Concerning P&S samples, the lower ductility of Ti32–MA is most probably due to the microstructural features and, in particular, to the grain growth induced by a higher temperature and longer time. The lower flexural strain of Ti32–MA hot–pressed at 1100ºC and grinded can be due to the microstructural differences found and, especially, to the presence of thinner and more concentrated $\alpha + \beta$ lamellae of the Widmanstätten structure generated from a less homogeneous distribution of the alloying elements.

6.2.6 – Partial Conclusions

Based on the results of the study of processing of the Ti–3Al–2.5V alloy by different P/M techniques, it can be concluded that:

Uniaxial Pressing and Sintering (P&S): the processing of the Ti–3Al–2.5V alloy by means of pressing and sintering allows reaching final relative density as high as 97% with a mean shrinkage of the components of 4.5% during sintering. Nonetheless, it is important to remark that using a lower compacting pressure leads to lower relative density and a significant higher shrinkage during sintering.

The hardness of the uniaxial pressed samples increases with the sintering temperature and time reaching values comparable or somewhat higher with respect to the wrought materials most probably due to the higher percentage of interstitial elements. This higher content is either due to the greater amount already present in the starting powder as well as to the handling and sintering of the powders which provokes the diffusion of the elements adsorbed on the powder particles surface.

Mechanical properties obtained determined by bending tests decrease with the temperature and the time; however, minimum values of maximum bending strength of 1400 MPa and flexural strain of 2% were attained.

Regarding tensile properties, the UTS seems not to be really affected by the processing parameters studied and it results to be higher than the one of wrought material due to the total amount of interstitials dissolved.

On the other side, the ductility is much more influenced by the sintering process and the values are lower compared to the wrought alloy in the annealed state, which is the normal behaviour of P/M materials. Nevertheless, when sintering the Ti32–PA at 1300°C during 2 hours, a strain of 15%, the same of wrought Ti–3Al–2.5V, can be obtained.

The increment of the sintering temperature and time leads to alpha grain size growth and $\alpha + \beta$ lamellae thickening, which are the microconstituents.

The analysis of the fracture surfaces reveals that the fracture is mainly ductile and, therefore, the surface is composed by equiaxed dimples of different sizes.

Thermal conductivity at room temperature and electrical resistivity comparable to that of wrought Ti–3Al–2.5V are also reached.

Hot Isostatic Pressing (HIP): the post–processing by HIP of sintered components does not permit to obtain fully dense materials due to open porosity present in the specimen but it increases the relative density in approximately 1%. It is worth mentioning that the HIP can level the final density of components compacted at different pressures and, thus, having different sintered relative densities.

Generally, lowering the HIP temperature decreases the hardness whilst a longer dwell time as well as the increasing of the applied pressure makes the material harder.

Selecting a HIP temperature in the β field generally provokes a decrement of the strength, either maximum bending strength or UTS, and a significant drop of the ductility down to 1%. Furthermore, it changes the fracture mode from ductile to brittle and, therefore, by cleavage as the fractography analysis reveals. On the other side, the static mechanical properties (bending and tensile) remain, practically, constant by choosing a HIP temperature in the α + β field.

Conventional Hot–pressing (HP): the relative density of the specimens hot–pressed increases with the processing temperature reaching values similar to those of the samples post–processed by HIP.

The hardness of conventional hot–pressed components increases with the processing temperature and it is somewhat higher than in P&S samples due either to the higher relative density, the contamination of the specimens and the microstructure features.

About the contaminations from the processing, carbon pick–up along the thickness of the sample in contact with the graphite mould leads to an increment of the final content of this element up to 0.05 wt.%, equals to the limit specified for this alloy.

On the other hand, a strong reaction with the BN coating of the graphite disc placed in between the powders provokes a significant increment of the nitrogen percentage and the generation of a reaction layer, composed by titanium nitrides and borides, whose thickness increases with the temperature, reaching almost 25 μm at 1300°C.

The removal of the outer surface allows to increase the maximum bending strength from 50 to 500 MPa, depending on processing temperature, and the flexural strain about a 0.5% on average.

The microstructure analysis reveals that the lowest temperature considered, namely 900°C, is not high enough to guarantee the complete diffusion of the alloying elements and to obtain a homogeneous microstructure.

At higher temperature this problem is overcome and the microstructure constituents are α grains and Widmanstätten areas where these features are smaller and finer, respectively, in the Ti32–MA alloy since, most probably, more thermal energy is invested in the diffusion of the alloying elements.

Inductive Hot–pressing (IHP): when the hot–pressed components are compacted with the help of an inductive current, the total processing time is very much shorter and fully dense materials as hard as when heated in the conventional way can be attained.

Interstitial elements pick–up takes place during the processing, especially nitrogen and carbon that justifies the hardness.

The short dwell time at temperature, 15 minutes, and the fast cooling typical of this process does not permit the development of a homogenous microstructure at 1100°C, especially for Ti32–MA, and it affects the final morphology of the microconstituents. On the other hand, a processing temperature of 1300ºC leads to a homogeneous microstructure.

6.3 – Ti–6Al–4V ALLOY

In this chapter the results relative to the Ti–6Al–4V alloy either from a commercial prealloyed powder (Ti64–PA) or starting from an Al:V master alloy (Ti64–MA) are presented and discussed.

The analysis of the results will be done comparing the producing method in order to point out advantages and disadvantages of the two alloy fabrication approaches and, where possible, the results obtained by the characterisation of the materials studied will be compared with the properties attained by other authors.

6.3.1 – Uniaxial Pressing and Sintering (P&S)

6.3.1.1 – Relative Density

To better understand the behaviour of the alloys during sintering and the values of relative density, it is interesting to know the green density, the volume change and the densification.

More in detail, green density mean values are 72.13 ± 0.50% for Ti64–PA (pressed at 400 MPa) and 85.85 ± 0.22% for Ti64–MA (pressed at 700 MPa) due to the different compacting pressure whilst the volume variation induced by sintering increases either with the increment of the sintering temperature or time for both Ti64–PA and Ti64–MA. Moreover, Ti64–PA specimens obtained higher shrinkage than Ti64–MA samples, with mean values of 22% and 9% respectively, due to the lower green density.

The densification of the specimens increases with sintering temperature and time and, once again, the values obtained for prealloyed powder (74% on average) are much greater compared to master alloy addition powder (59% on average). This is another direct consequence of the compaction pressure which results in a lower green density and, theoretically, in a higher densification.

The relative density results of Ti64–PA and Ti64–MA for the diverse sintering conditions are presented in Figure 6.110.

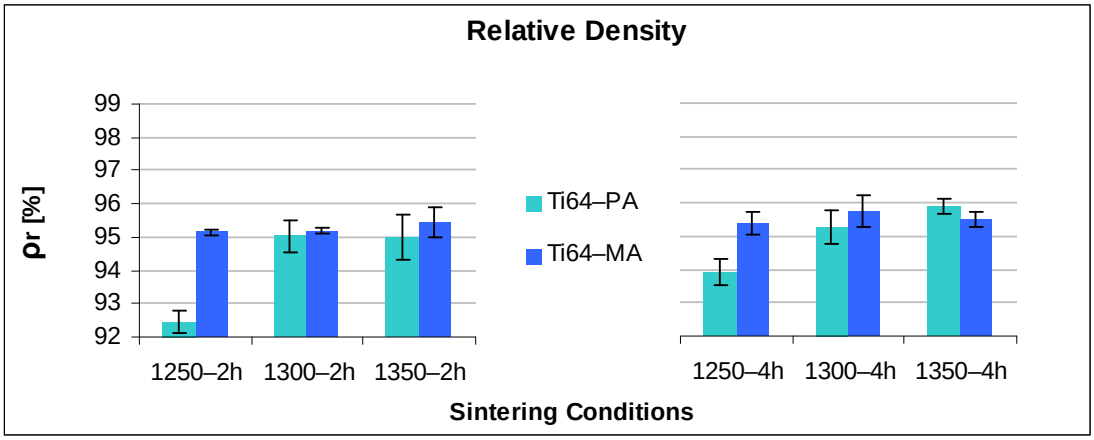

Figure 6.110 – Relative density as a function of the sintering conditions for Ti64–PA and Ti64–MA bending specimens.

The relative density of both Ti64–PA and Ti64–MA (Figure 6.110) increases with the sintering temperature and is always a little bit higher for longer processing time. Generally, specimens from Ti64–MA reach higher relative density than Ti64–PA with the exception of 1350°C–4h. Moreover, the difference between Ti64–PA and Ti64–MA is much more pronounced for the lowest temperature considered which can be correlated with the lower green density of the sample produced with Ti64–PA and the thermal energy available.

Apart from Ti64–PA sintered at 1250°C either 2 hours or 4 hours, relative density values for the Ti–6Al–4V alloy ranges between 95% and 96%, similar to that obtained by other authors using elemental titanium powders (sponge or HDH) blended with elemental powders[20, 52-54] or master alloys[3, 53, 55, 56].

As for the other materials, specimens with "dogbone" geometry for the tensile test were pressed and sintered at three temperatures during 2 hours because the sintering time of 4 hours leads only to a slight increment of relative density.

The green density of tensile test samples is 81.98% ± 0.49% for Ti64–PA and 86.56% ± 0.38% for Ti64–MA, respectively. These values are in agreement with the compressibility study and it is interesting to notice that when pressing the prealloyed powder at 700 MPa (tensile test specimens) instead of 400 MPa (three–point bending test samples) there is an increment of approximately 10% of green density which should lead to a lower shrinkage. Moreover, the mean green density values attained are similar to that of Ti32–PA and Ti32–MA (see Section 6.2.1.1).

The results of relative density for Ti64–PA and Ti64–MA with dogbone geometry for the three sintering conditions used are displayed in Figure 6.111.

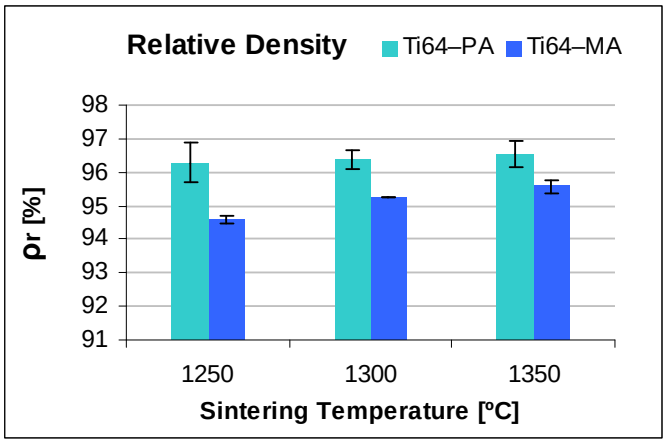

Figure 6.111 – Relative density as a function of the sintering temperature for Ti64–PA and Ti64–MA tensile specimens (sintering time: 2h).

As it can be seen in Figure 6.111, the relative density of both Ti–6Al–4V materials slightly increases with the sintering temperature. Moreover, the final relative density of the Ti64–PA alloy is, normally, at least, 1% higher than Ti64–MA, which starts from a higher green density but undergoes a much lower shrinkage.

This suggests that the greater amount of thermal energy spent for the diffusion of the alloying elements in the Ti64–MA powders limits somehow the densification and, thus, the final relative density obtained. Moreover, the densification of the Ti64–PA alloy is also favoured by the slightly lower powder particle size (Table 3.8).

Compared to three–point bending test samples (Figure 6.110), the relative density of Ti64–PA is higher in dogbones samples due to the difference in compacting pressure employed whilst for Ti64–MA is similar. Nonetheless, the relative density obtained with the Ti64–MA powder is somewhat lower than Ti32–MA and the relative density of Ti64–PA slightly higher than Ti32–PA (Figure 6.52), this is due to the relative amount of alloying elements that have to diffuse, which can be schematised as: Ti64–PA (prealloyed, almost no alloying elements diffusion) < Ti32–PA (homogenisation between Ti64–PA and elemental Ti) < Ti32–MA (homogenisation between elemental Ti and Al:V master alloy) < Ti64–MA (homogenisation between elemental Ti and a double quantity of Al:V master alloy compared to Ti32–MA).

Some authors suggest that the lower relative density obtainable with the Ti–6Al–4V alloy produced by the blending elemental approach using elemental powder in comparison to prealloyed powders is due to the reaction between aluminium and titanium ($Ti+Al \rightarrow TiAl_3$) which hinders consolidation[53, 57, 58].

6.3.1.2 – Chemical Analysis

The results of the chemical analysis carried out on the sintered materials are displayed in Figure 6.112 (oxygen) and Figure 6.113 (nitrogen) for bending samples and Figure 6.114 for tensile specimens, respectively.

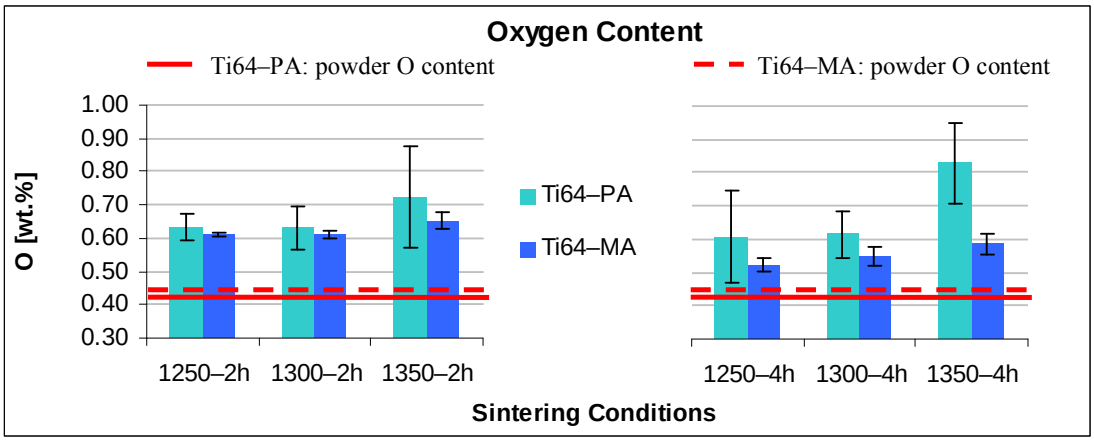

Figure 6.112 – Oxygen content as a function of the sintering conditions for Ti64–PA and Ti64–MA bending specimens.

The percentage of oxygen (Figure 6.112) found in the sintered specimens of Ti64–PA stays almost constant at 0.60 wt.% for 1250ºC and 1300ºC independently of the dwell time and it increases significantly to 0.75 wt.% or 0.83 wt.% at 1350°C for 2 hours or 4 hours of sintering time, respectively. On the other hand, the oxygen content of the Ti64–MA always increases with the sintering temperature with the exception of 1300°C–2h, which is equals to 1250ºC–2h, but reaching lower values compared to Ti64–PA, especially when the samples are sintered for 4 hours.

It is worth mentioning that there is always, at least, a 0.20 wt.% and a 0.12 wt.% oxygen pick–up for Ti64–PA and Ti64–MA, respectively, with respect to the initial content of the powder which will probably affect significantly the mechanical properties. This contamination could derive from the handling of the powder, the air trapped in the green specimens or the different surface area of the powders.

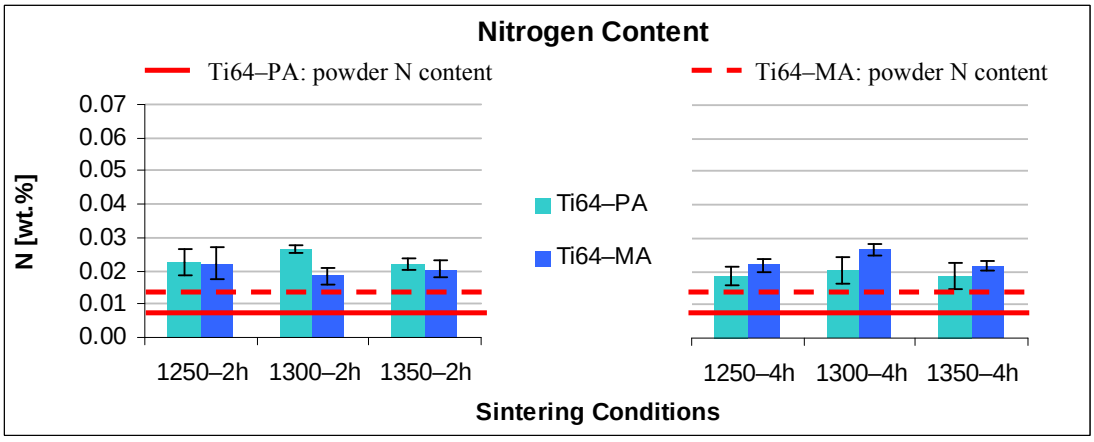

Figure 6.113 – Nitrogen content as a function of the sintering conditions for Ti64–PA and Ti64–MA bending specimens.

Concerning nitrogen content, as it can be noted in Figure 6.113, there is no that big variation of this interstitial element either with the temperature or the processing time since the values obtained are similar and around 0.02 wt.%.

Even if there has been some nitrogen pick–up with respect to the initial content of the powder, the final quantity of this element is well below the limit indicated by the international standards (0.05 wt.%).

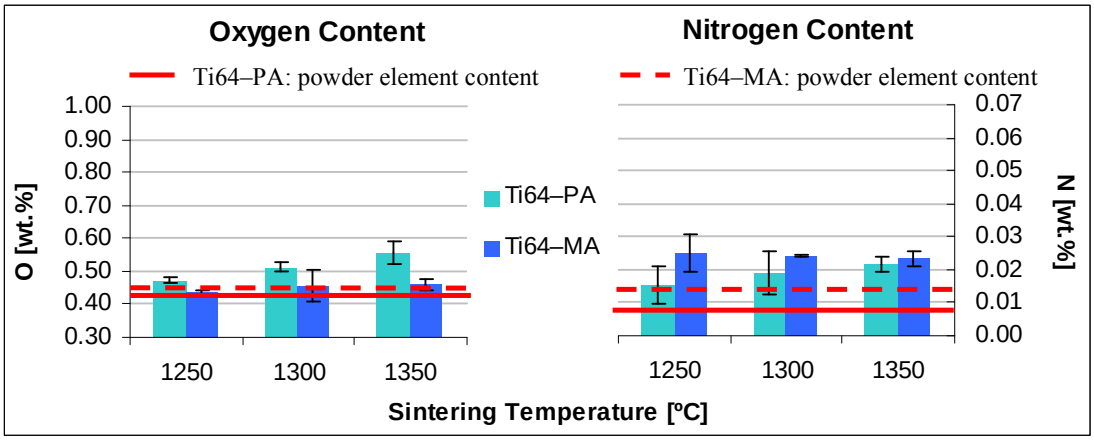

Figure 6.114 – Chemical analysis as a function of the sintering conditions for Ti64–PA and Ti64–MA tensile specimens: oxygen (left) and nitrogen (right).

In the case of the tensile samples, the data shown in Figure 6.114 indicate that there is either some oxygen or nitrogen pick–up with respect to the amount that characterised the starting powder, where the increment of oxygen is higher for Ti64–PA whereas the increment of nitrogen for Ti64–MA.

The difference of chemical analysis between the bending and the tensile test samples is mainly due to the combination of the handling of the powder and the level of vacuum, since the sintering step is normally carried out discontinuously (by batches).

6.3.1.3 – Hardness

The results of hardness measurements, represented as mean values plus standard deviation, for Ti64–PA and Ti64–MA bending samples are shown in Figure 6.115.

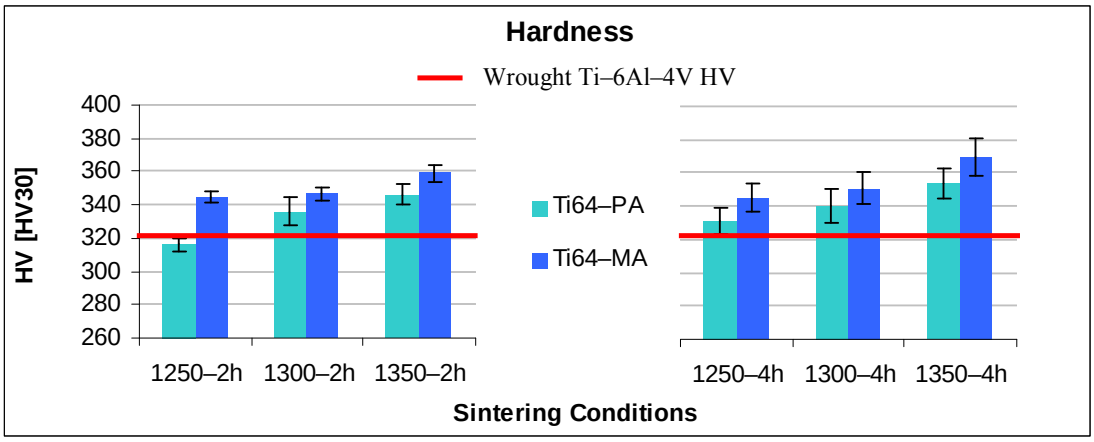

Figure 6.115 – Hardness as a function of the sintering conditions for Ti64–PA and Ti64–MA bending specimens.

As it can be seen in Figure 6.115, the hardness of P/M Ti–6Al–4V increases with the sintering temperature as well as with the time, reaching the maximum values at the higher temperature and for longer time.

As in the case of the relative density, Ti64–MA components reach higher values with respect to Ti64–PA which well correlates with the decrement of residual porosity induced by the sintering (Figure 6.110).

Compared to wrought alloy, both the powder metallurgy Ti–6Al–4V analysed are rather harder with the exception of the Ti64–PA sintered at 1250°C during 2 hours. This can be justified taking into account that the oxygen content of the starting powder is already higher with respect to the limit specified for the wrought alloy. Moreover, for Ti64–PA sintered at 1250ºC–2h accounts also the low relative density (92.5%).

In comparison to the hardness of the three–point bending test samples, the measurements carried out on tensile samples are somewhat lower (on average 35 HV30) and, since the relative density is similar, is most probably due to the lower amount of contaminants dissolved inside the matrix (Figure 6.114 compared to Figure 6.112 and Figure 6.113).

The variation of the hardness of P/M Ti–6Al–4V with the amount of interstitial elements was considered on the bases of the Okazaki and Conrad's[11] formula and the results are presented for each alloy as a function of the sintering conditions in Figure 6.116 and Figure 6.117.

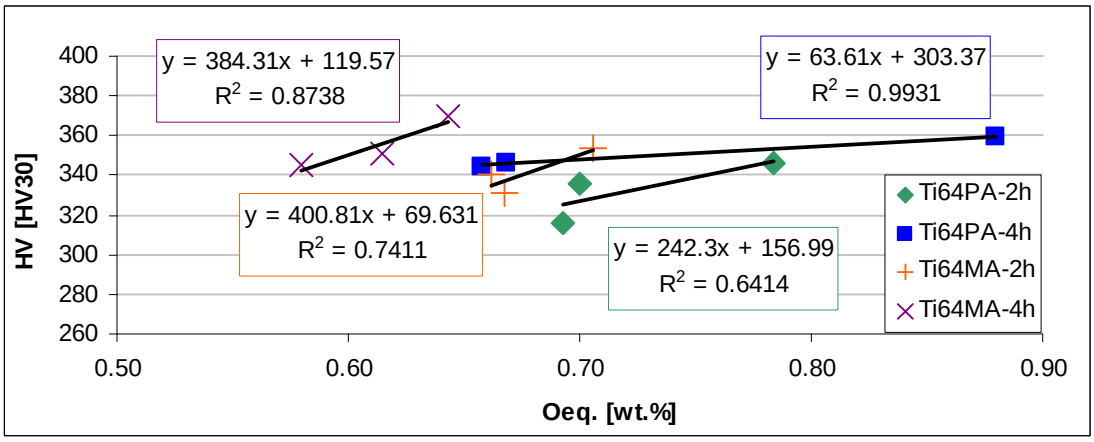

Figure 6.116 – Hardness as a function of equivalent oxygen content for Ti64–PA and Ti64–MA bending specimens: influence of temperature and time.

Data presented in Figure 6.116 are divided in relation to the sintering conditions and four correlations are found depending of the P/M approach and sintering time. All of them indicate that the hardness increases with the equivalent oxygen content showing linear correlations with different slopes.

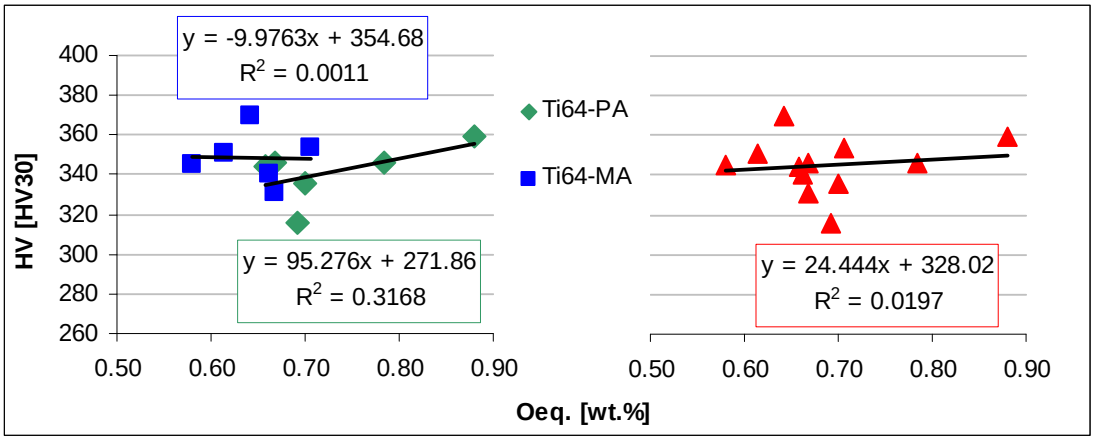

Figure 6.117 – Hardness as a function of equivalent oxygen content for Ti64–PA and Ti64–MA bending specimens: influence of the powder production route (left) and general trend (right).

However, considering the two P/M approaches (Figure 6.117–left), there are not correlations between the hardness and the equivalent oxygen content, particularly, for Ti64–MA. This could indicate a very strong effect of the microstructural features, such as mean alpha grain size, thickness of α + β lamellae and relative amount of these two microconstituents.

Since there is no correlation for each individual P/M approach, no general linear relationship could be found for the P/M Ti–6Al–4V (Figure 6.117–right) most probably due to the parameters already mentioned but with a much greater influence from the different level of relative density obtained on each type of powder.

6.3.1.4 – Properties from Bending Test

The bending stress–strain behaviour found for the P/M Ti–6Al–4V alloy submitted to bending tests is presented in Figure 6.118 and Figure 6.119 for 2 hours and for 4 hours of dwell time, respectively.

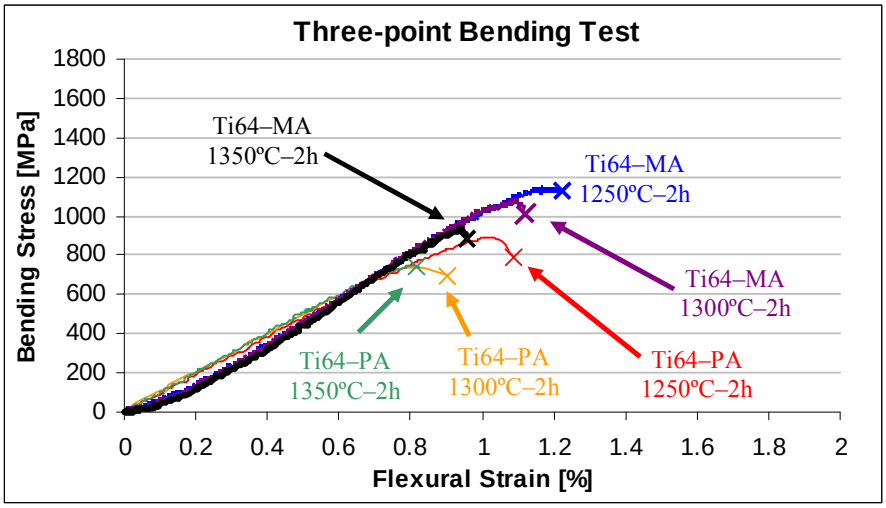

Figure 6.118 – Representative bending stress–strain curves for Ti64–PA and Ti64–MA specimens (sintering time: 2 h).

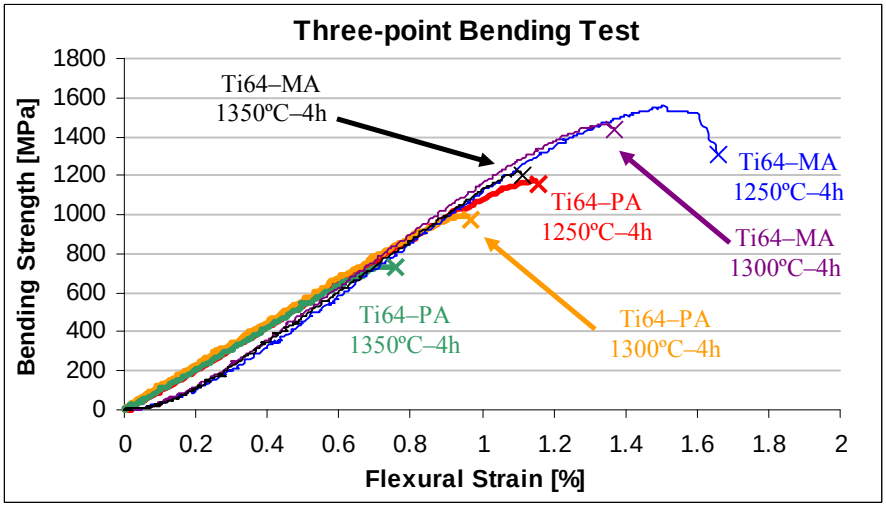

Figure 6.119 – Representative bending stress–strain curves for Ti64–PA and Ti64–MA specimens (sintering time: 4 h).

As it can be seen in Figure 6.118 and Figure 6.119, with some exceptions, such as the Ti64–MA sintered at 1250°C–4h, the material seems to behave elastically without important plastic yielding before fracture. Moreover, the Ti–6Al–4V alloy shows a more fragile behaviour compared to both elemental titanium and the Ti–3Al–2.5V alloy since the stress–strain curves show only a small plastic deformation. This is due to the higher amount of alloying elements and to the higher content of interstitials found in Ti64–PA and Ti64–MA specimens.

The mean values of the flexural modulus are 98 GPa ± 8 GPa for Ti64–PA and 104 GPa ± 5 GPa for Ti64–MA, respectively. Since the thickness of the specimens tested is very similar, the higher stiffness of Ti64–MA components is most probably due to the higher relative density attained through the P&S process.

The Ti–6Al–4V alloy, both Ti64–PA and Ti64–MA, produced by the conventional powder metallurgy method has, on average, slightly higher flexural modulus than elemental titanium and the Ti–3Al–2.5V alloy, due to the presence of the alloying elements which makes the material more rigid.

The comparison of the mean values of maximum bending strength and flexural strain between Ti64–PA and Ti64–MA are shown in Figure 6.120 and Figure 6.123, respectively.

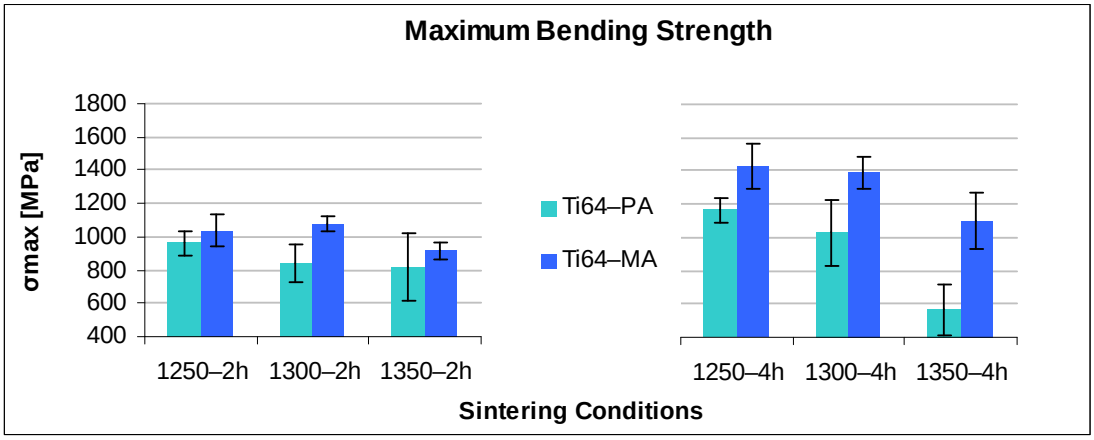

Figure 6.120 – Maximum bending strength as a function of the sintering conditions for Ti64–PA and Ti64–MA bending specimens.

As it can be seen in Figure 6.120, the general trend of the maximum bending strength is to decrease with the increment of the sintering temperature and Ti64–MA always reaches higher maximum bending strength with respect to Ti64–PA.

Regarding the time, normally, a longer processing time leads to a higher strength with the exception of the prealloyed powder sintered at 1350°C during for 4 hours which reaches the lowest value.

The behaviour described is due to the combined effect of the relative density (higher for Ti64–MA), the total amount of interstitials (somewhat higher for Ti64–PA) and the microstructural features, where Ti64–PA shows a finer microstructure as it will be discussed in Section 6.3.1.6.

In general, the maximum bending strength of Ti64–PA and Ti64–MA is lower than that of Ti32–PA, Ti32–MA and elemental titanium. This behaviour is the opposite to that of the UTS, which increases with the amount of alloying elements.

Even though of the high oxygen content, the maximum bending strength shown in Figure 6.120 is, on average, similar to the values found in the literature for wrought biomedical devices (903–1090 MPa)[59]. Therefore, avoiding oxygen and nitrogen contamination should lead to higher maximum bending strength values.

Equivalent oxygen content was calculated by means of Wood equation[19] in order to evaluate the influence of the interstitials on the maximum bending strength and the results are shown in Figure 6.121 and Figure 6.122 for sintering condition and P/M approach or general trend, respectively.

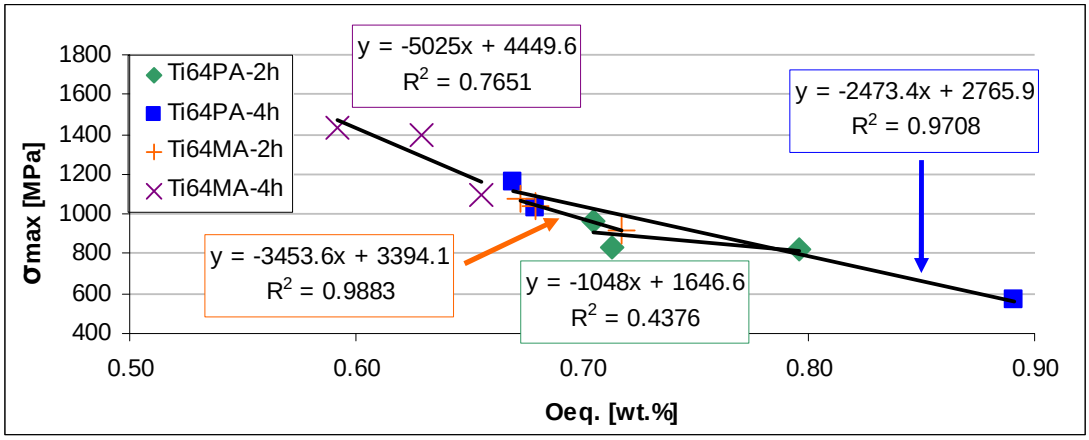

Figure 6.121 – Maximum bending strength as a function of the equivalent oxygen content for Ti64–PA and Ti64–MA bending specimens: influence of temperature and time.

The trends shown in Figure 6.121 present a general decreasing behaviour with good approximation with the exception of the Ti64–PA sintered during 2 hours, most probably because it is affected by the low relative density attained at 1250ºC in comparison to the other processing temperature.

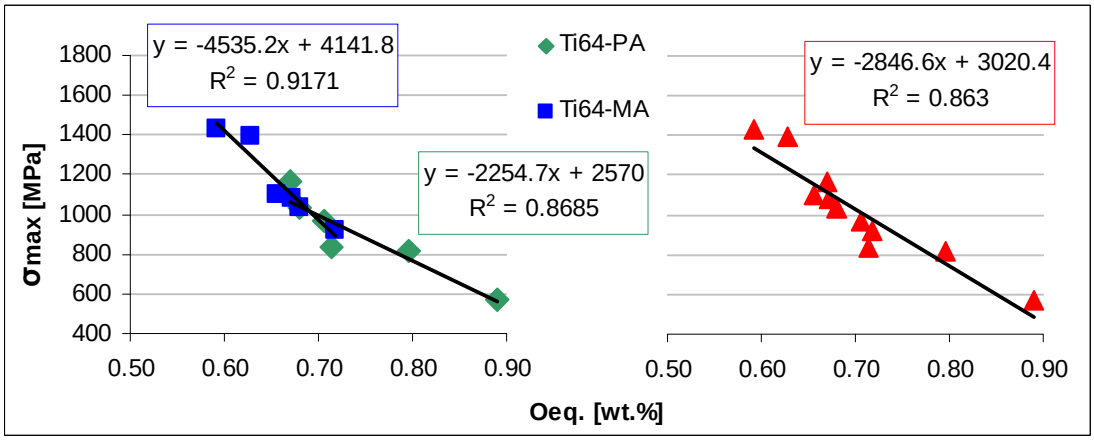

Figure 6.122 – Maximum bending strength as a function of the equivalent oxygen content for Ti64–PA and Ti64–MA bending specimens: influence of the powder production route (left) and general trend (right).

On the other side, the behaviour of the P/M Ti–6Al–4V subdivided on the bases of the P/M approach (Figure 6.122–left) is very similar and well correlated with the equivalent oxygen content. Finally, the general trend results in a quite good linear correlation (Figure 6.122–right) between the maximum bending strength and the amount of interstitials dissolved into the titanium matrix for the Ti–6Al–4V obtained by pressing and sintering. This indicates that the parameter with the strongest effect is on the maximum bending strength is the content of interstitials.

Similarly to the maximum bending strength, the flexural strain of both Ti64–PA and Ti64–MA (Figure 6.123) decreases with the processing temperature mainly for a sintering time of 4 h and Ti64–MA shows higher values than Ti64–PA.

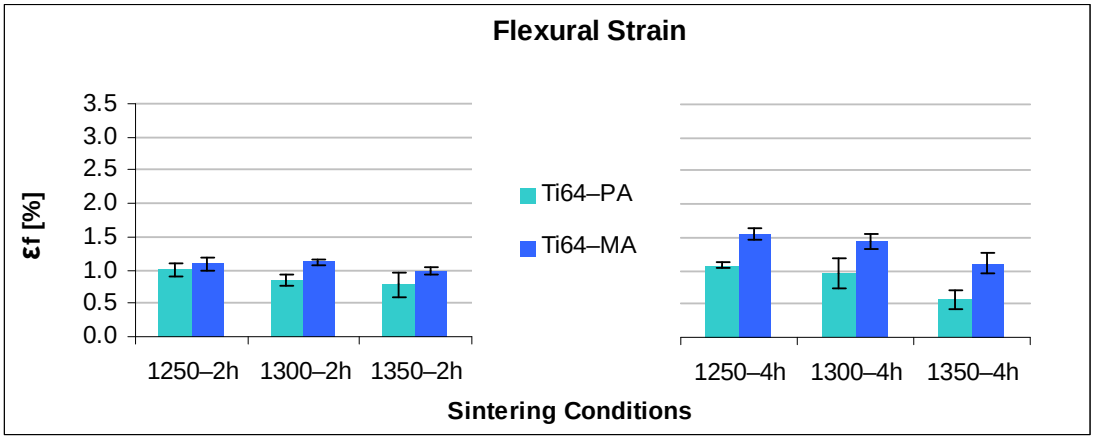

Figure 6.123 – Flexural strain as a function of the sintering conditions for Ti64–PA and Ti64–MA bending specimens.

This could explain on the bases of the higher relative density of Ti64–MA components, the higher content of interstitials dissolved and the finer microstructure of the Ti64–PA (see Section 6.3.1.6). The finer microstructure is due to the fact that the thermal energy available is mainly invested in the densification of the material instead of the diffusion of the alloying elements and grain growth.

Compared to elemental titanium and Ti–3Al–2.5V, the flexural strain of Ti–6Al–4V is, on average, 2.5% lower due to the effect of the alloying elements and the higher amount of interstitials.

The equation proposed by Wood[19] for evaluating the ductility of titanium was used to better understand the influence of the interstitials on the flexural strain and the results are presented in Figure 6.124 and Figure 6.125.

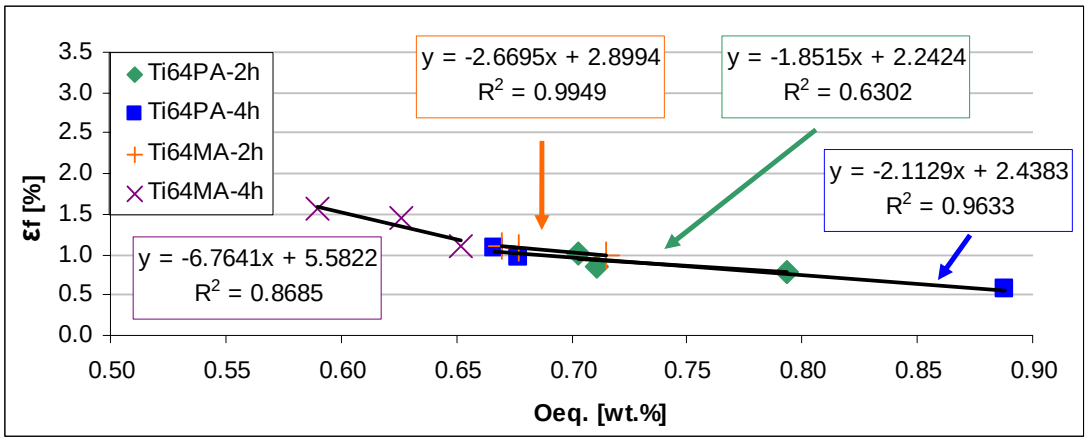

Figure 6.124 – Flexural strain as a function of the equivalent oxygen content for Ti64–PA and Ti64–MA bending specimens: influence of temperature and time.

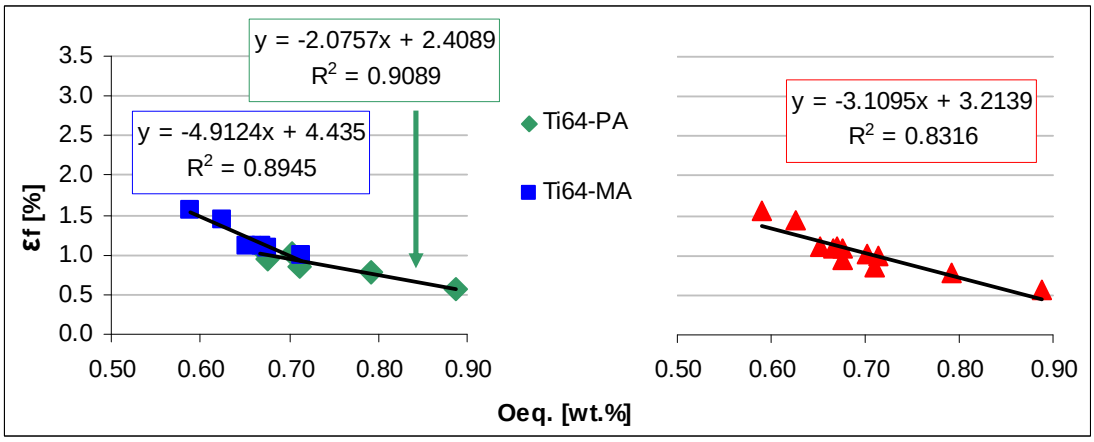

Figure 6.125 – Flexural strain as a function of the equivalent oxygen content for Ti64–PA and Ti64–MA bending specimens: influence of the powder production route (left) and general trend (right).

As it can be seen in Figure 6.124, when the ductility of P/M Ti–6Al–4V is analysed on the bases of the $O_{Eq.}$, good linear correlations are found between these two parameters indicating that the amount of interstitials dissolved into the titanium matrix has a very strong effect. This last effect seems to overcome the benefits of the reduction of the residual porosity and the alpha grain growth which, normally, increases the ductility.

Therefore, this leads to a decreasing trend for both Ti64–PA and Ti64–MA (Figure 6.125–left) and to a general trend of the ductility of P/M Ti–6Al–4V (Figure 6.125–right) where, once again, the most critical factor is the amount of interstitials dissolved by the material.

6.3.1.5 – Properties from Tensile Test

The typical tensile stress–strain behaviour found for Ti64–PA and Ti64–MA materials sintered in the range 1250–1350ºC is displayed in Figure 6.126.

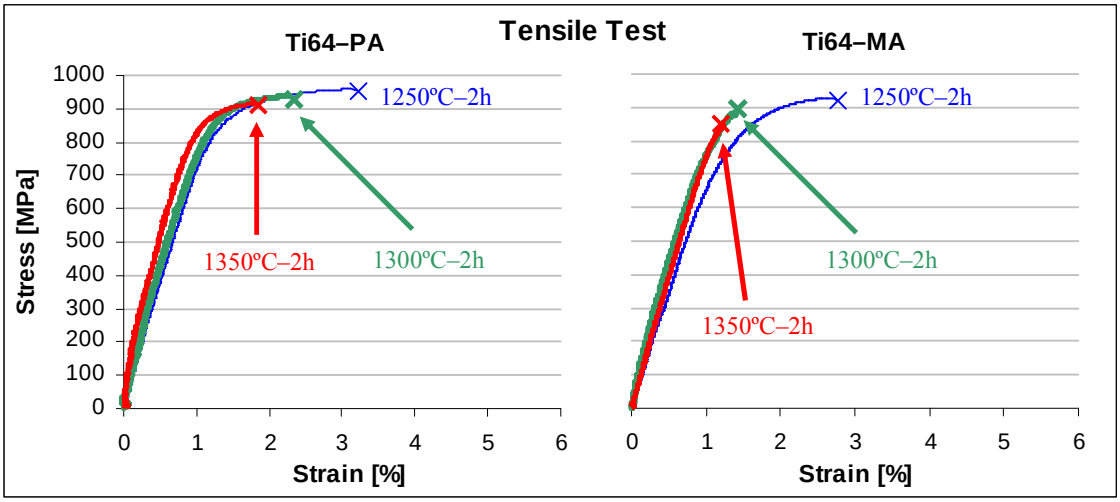

Figure 6.126 – Representative tensile stress–strain curves for Ti64–PA and Ti64–MA specimens.

As it can be seen in Figure 6.126, the typical tensile stress–strain curves for the Ti–6Al–4V processed by pressing and sintering are composed by an elastic part, up to approximately 800 MPa, and then some plastic deformation, which is limited to 3% as maximum.

Dynamic Young modulus for Ti64–PA and Ti64–MA specimens 111 ± 6 GPa and 110 ± 1 GPa, just slightly lower compared to the nominal value of 114 GPa of wrought Ti–6Al–4V [9].

The variation of the ultimate tensile strength and maximum strain with the sintering temperature and compared to the wrought alloy are shown in Figure 6.127.

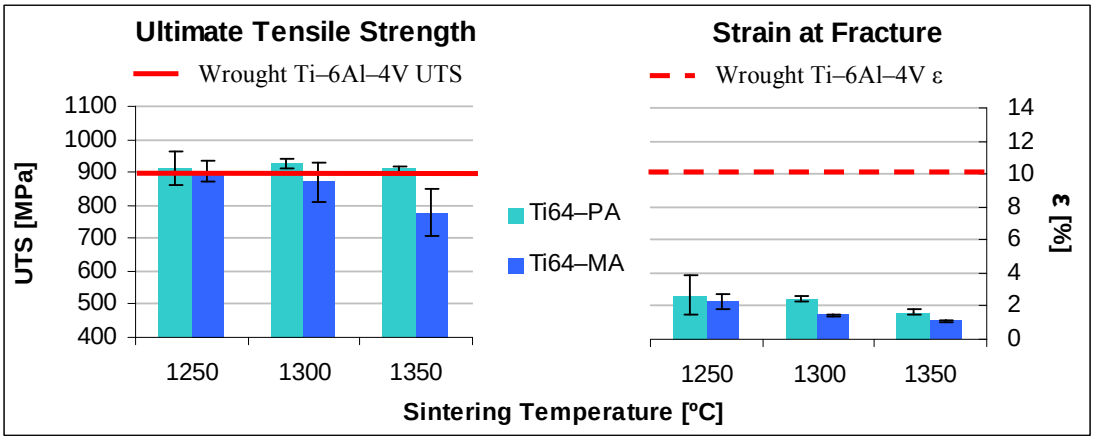

Figure 6.127 – Mechanical properties as a function of the sintering temperature for Ti64–PA and Ti64–MA specimens: ultimate tensile strength (left) and strain (right).

Analysing the data shown in Figure 6.127, it can be seen that the UTS of the Ti64–PA alloy stays practically constant with the increasing of the sintering temperature whereas that of Ti64–MA decreases from 900 MPa down to 780 MPa. This difference is most probably due to the combination of the lower residual porosity and higher oxygen content of Ti64–PA tensile samples compared to Ti64–MA specimens.

Moreover, it can be seen that, apart from the Ti64–MA powder sintered at 1350ºC, the UTS values obtained are similar to that of the wrought alloy (900 MPa) and similar to that obtained by other authors using titanium sponge fines (830–920 MPa)[53, 55, 60] or titanium hydride powders (970 MPa)[52].

On the other side, the strain of both kind of alloys (Figure 6.127) decreases with the temperature indicating that the effect of diminishing the residual porosity and grain growth (see Section 6.3.1.6) is overcame by the effect of the oxygen and nitrogen content, as it was for flexural strain. Moreover, the smaller deformation found for the Ti64–MA alloy is affected to the greater amount of residual porosity (Figure 6.111).

When compared to the wrought alloy, the strain values obtained in Ti–6Al–4V P/M components is lower due to the greater amount of interstitial elements and the residual porosity; by the way, the values are similar to that presented by other authors (between 1% and 6%)[3, 53, 55, 56].

6.3.1.6 – Microstructural Analysis

A microstructural analysis by optical microscopy was carried out to study the development of the microstructure and the evolution of the porosity and the results are displayed in Figure 6.128 and Figure 6.129.

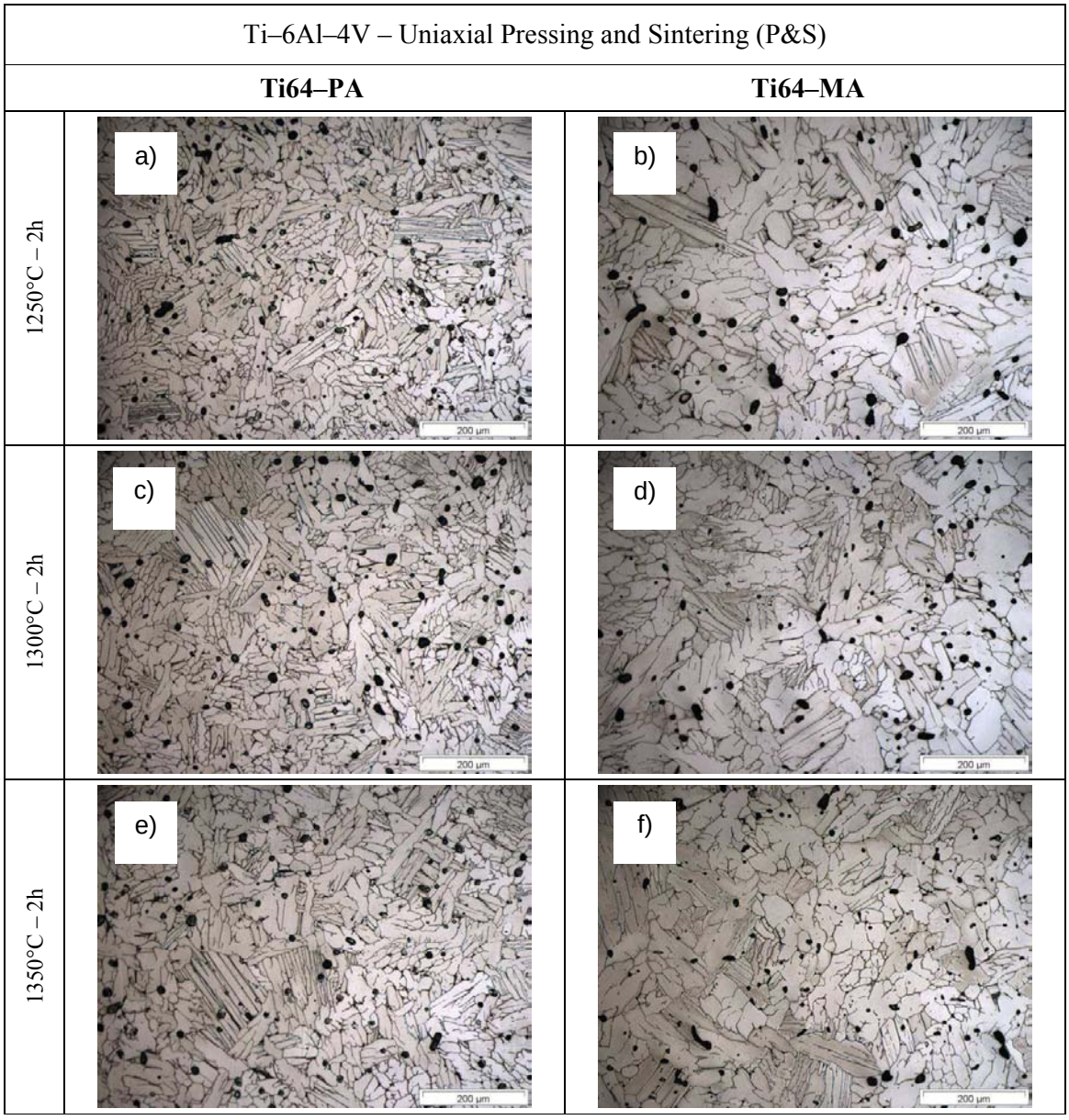

Figure 6.128 – Optical microscopy images for Ti64–PA and Ti64–MA sintered for 2 hours at: a) and b) 1250°C, c) and d) 1300°C and e) and f) 1350ºC.

The microstructure analysis by optical microscopy (Figure 6.128 and Figure 6.129) confirms that the microconstituents of the Ti–6Al–4V titanium alloy are alpha grains and α + β lamella typical of a slow cooling of a α + β titanium alloy from the beta field.

When comparing the powder production route, the microstructure components of the Ti64–PA are smaller than Ti64–MA. The reason for the finer microstructure of Ti64–PA could be the combination of smaller particle size of the starting powder and the greater thermal energy invested for the densification. The microstructural analysis is in agreement with the results of flexural strain (Figure 6.123).

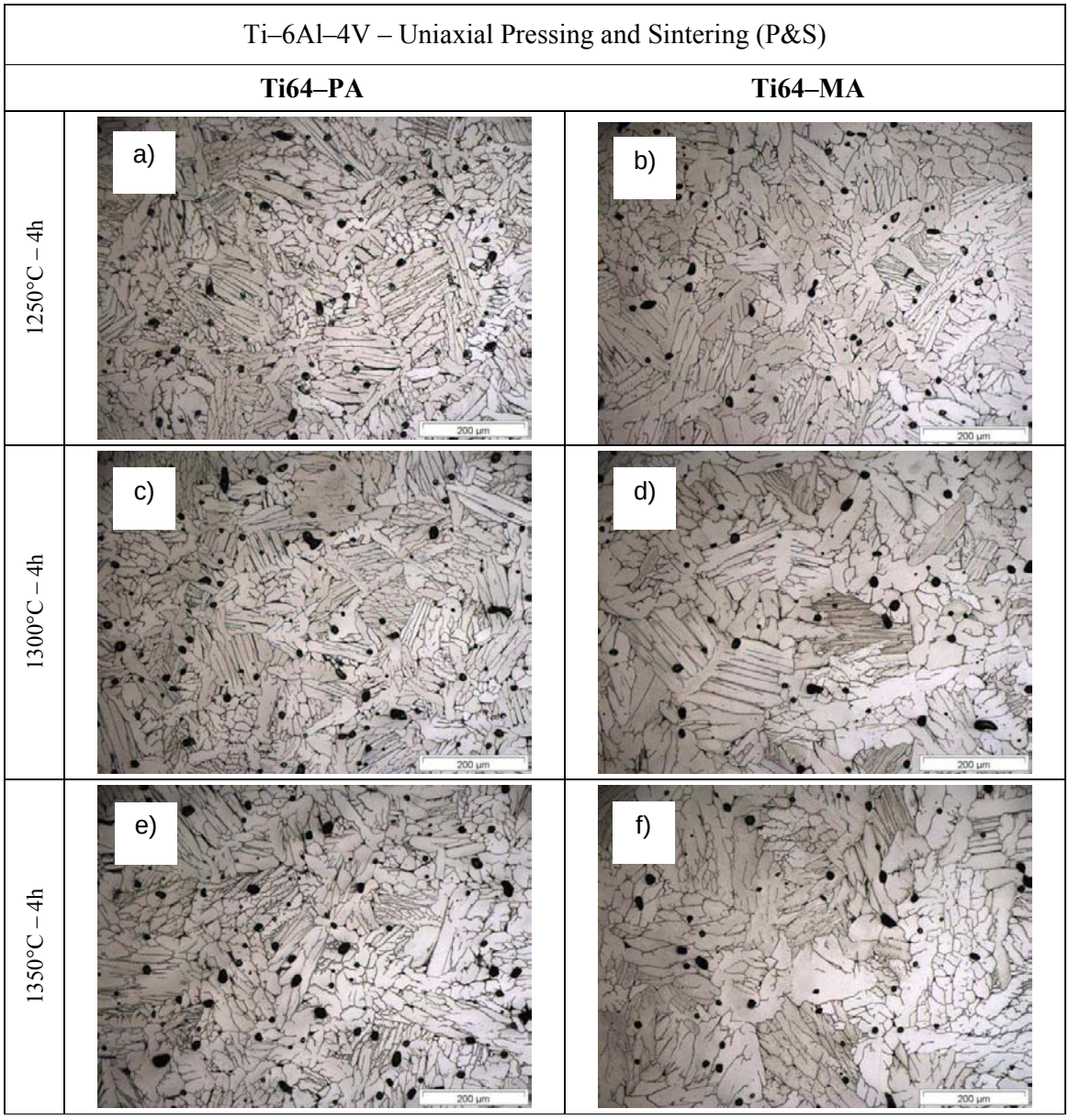

Figure 6.129 – Optical microscopy images for Ti64–PA and Ti64–MA sintered for 4 hours at: a) and b) 1250°C, c) and d) 1300°C and e) and f) 1350ºC.

As well as for the Ti–3Al–2.5V alloy, the microstructure is homogeneous without undissolved alloying element particles detected during the microstructure analysis by backscattered electrons or during energy dispersive spectroscopy analysis of the Ti64–MA, as the results discussed for the preliminary sinterability study (Chapter 5) indicate.

The fractographic analysis of the tensile test specimens by SEM was carried out and the results are presented in Figure 6.130.

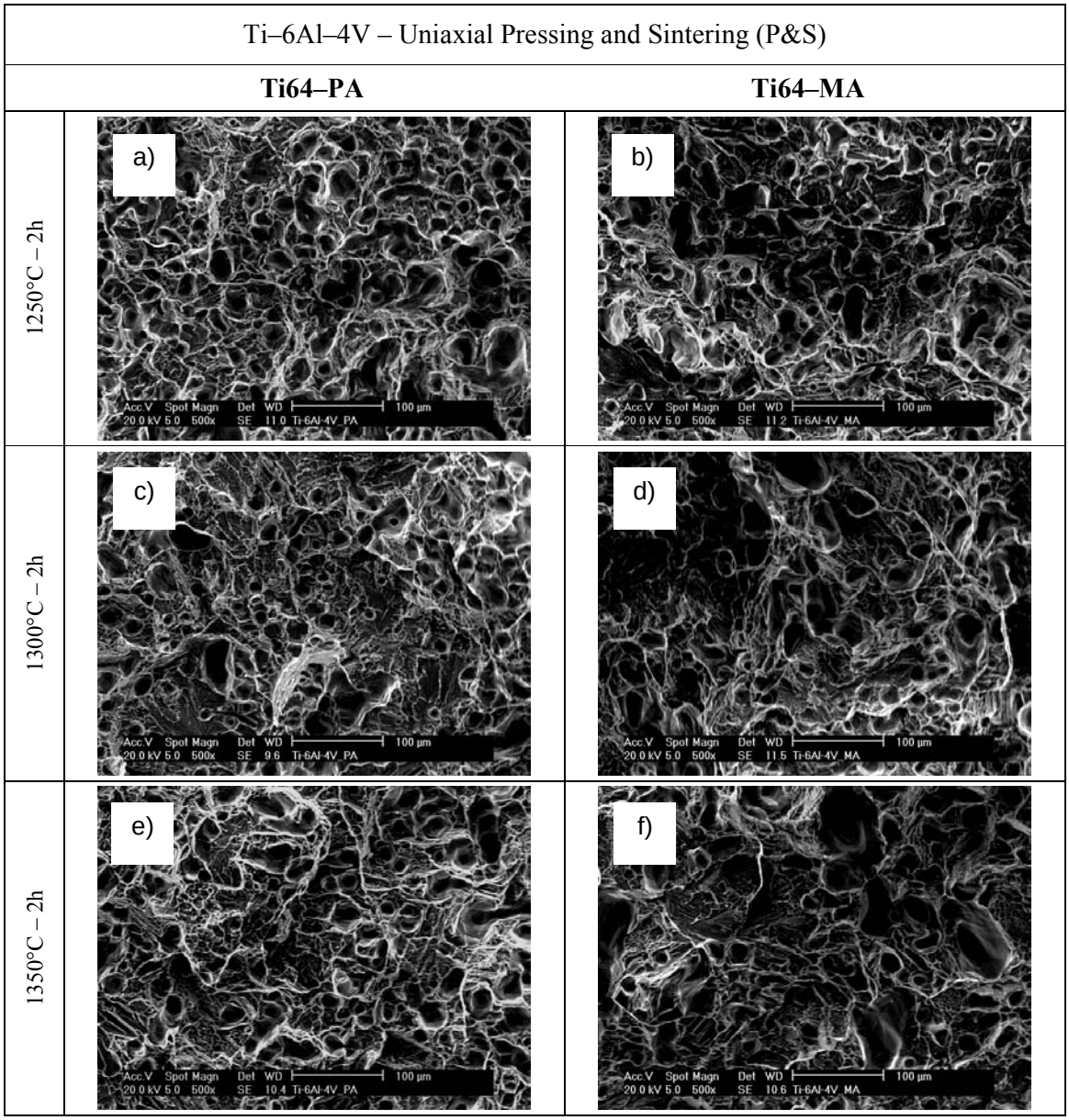

Figure 6.130 – Fracture surface from tensile test specimens for Ti64–PA and Ti64–MA sintered for 2 hours at: a) and b) 1250ºC, c) and d) 1300ºC and e) and f) 1350ºC.

From the analysis of the fracture surface (Figure 6.130), it can be seen that the materials present ductile fracture due to microvoid coalescence where the size of the dimples found in the Ti64–MA alloy seem to be larger than Ti64–PA.

This is most probably due to the larger size of the residual porosity of Ti64–MA which acts as few and widely spaced nucleation site, whilst in Ti64–PA the lower size and more uniformly distributed porosity leads to a more limited microvoid growth.

Nonetheless, this pore–assisted fracture is the typical behaviour of the Ti–6Al–4V titanium alloy obtained by the conventional powder metallurgy route and it is similar to those formed on ingot metallurgy processed materials[55].

6.3.1.7 – Thermal Conductivity

Specimens of Ti64–PA and Ti64–MA sintered under the conditions described before were prepared to measure thermal and electrical properties.

The results of the variation of the thermal conductivity at room temperature with the relative density and equivalent oxygen content were divided as a function of the alloy type, Ti64–PA and Ti64–MA (Figure 6.131 and Figure 6.132).

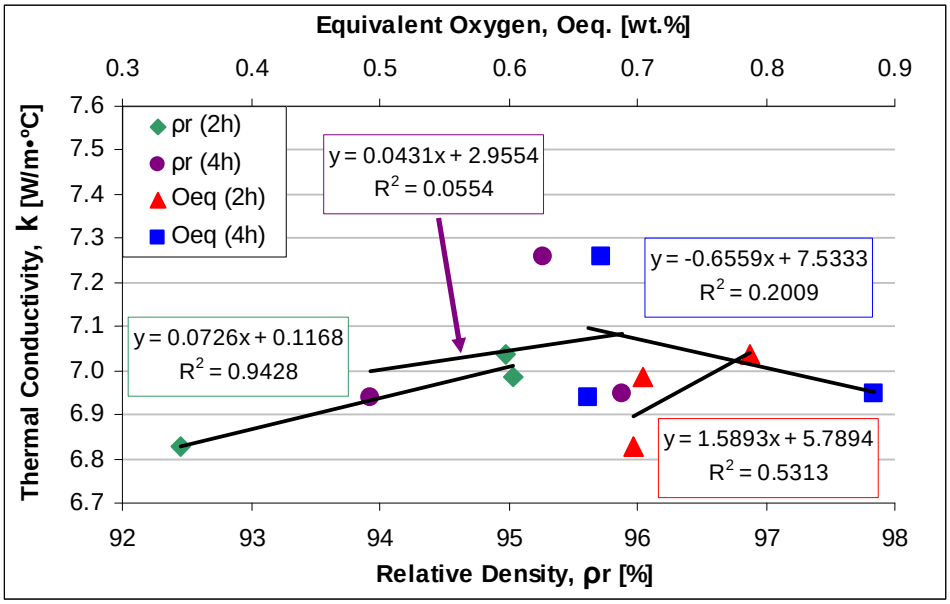

Figure 6.131 – Thermal conductivity at room temperature as a function of the relative density and equivalent oxygen content for Ti64–PA specimens.

There is no correlation between the thermal conductivity at room temperature and the relative density or the equivalent oxygen content for the Ti64–PA alloy (Figure 6.131). However, it seems that the increment of the relative density from 92% to values higher than 95% induces an increment of k most probably because with a 94% of relative density the pore structure is constituted by isolated pores whereas in the range of 86–94% there are still interconnected pores[3].

Conversely to Ti64–PA, the Ti64–MA alloy (Figure 6.132) is characterised by the increment of the thermal conductivity at room temperature both with the decreasing of the residual porosity and the increment of the equivalent oxygen content where the slope of the approximation line is significantly different for the two processing times (Figure 6.132). Therefore, it seems that a longer processing time, which induced some grain growth, leads to a smoother increment of the thermal conductivity both with the relative density and the equivalent oxygen content.

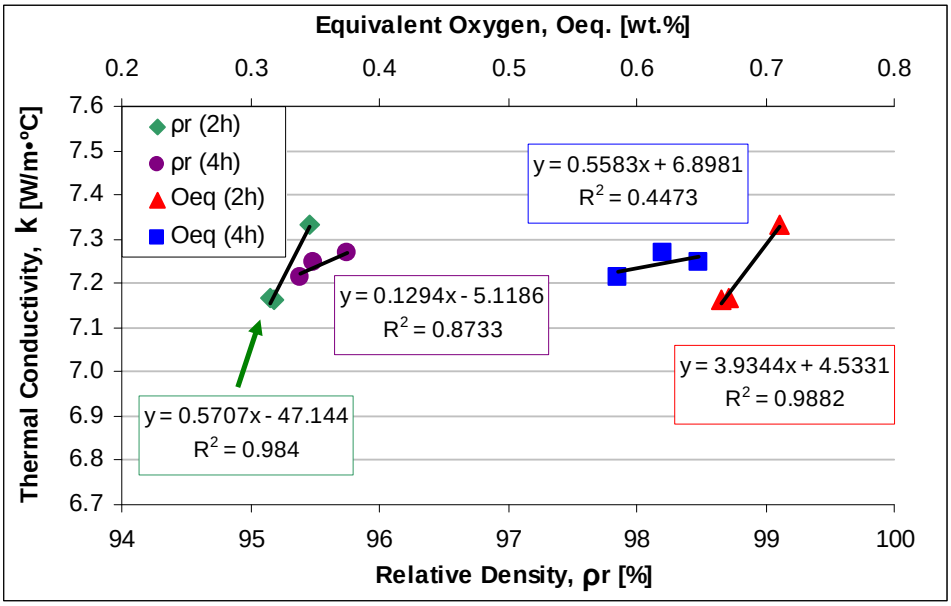

Figure 6.132 – Thermal conductivity at room temperature as a function of the relative density and equivalent oxygen content for Ti64–MA specimens.

No significant differences were found between the values of the two types of powders, as it was for the Ti32–PA and Ti32–MA, since with a relative density of 95%, a k of approximately 7 W/m·ºC is obtained in both materials (see Table 6.5).

Table 6.5 – Comparison of thermal conductivity at room temperature values between wrought and P/M Ti–6Al–4V alloy.

Ti–6Al–4V						
Wrought[8]		**P/M**				
		Ti64–PA		**Ti64–MA**		
k [W/m·ºC]	Chemical analysis [wt.%]	k [W/m·ºC]	Chemical analysis [wt.%]	k [W/m·ºC]	Chemical analysis [wt.%]	Sintering conditions
6.60	O = 0.20 N = 0.05	6.83	O = 0.634 N = 0.023	6.94	O = 0.609 N = 0.022	1250ºC – 2h
		6.99	O = 0.632 N = 0.027	7.26	O = 0.612 N = 0.018	1300ºC – 2h
		7.04	O = 0.725 N = 0.022	6.95	O = 0.652 N = 0.020	1350ºC – 2h
		7.17	O = 0.607 N = 0.019	7.21	O = 0.552 N = 0.022	1250ºC – 4h
		7.16	O = 0.604 N = 0.020	7.27	O = 0.547 N = 0.026	1300ºC – 4h
		7.33	O = 0.829 N = 0.019	7.25	O = 0.586 N = 0.022	1350ºC – 4h

Analysing the data shown in Table 6.5, it can be noticed that the thermal conductivity measured on pressing and sintering specimens is always higher than the nominal value of wrought Ti–6Al–4V, independently of the sintering conditions employed. It is remarkable that the highest values obtained for P&S components are similar to that of Ti–6Al–4V ELI, where the content of the interstitials is kept very low (O = 0.13 wt.% and N = 0.03 wt.%).

Bearing in mind the presence of the residual porosity and the higher content of interstitials of P&S specimens, it can be stated that the thermal conductivity is greatly influenced by the mean grain size which must be bigger in P/M samples than that of wrought Ti–6Al–4V in the annealed state.

Samples of Ti64–PA and Ti64–MA materials sintered at 1250ºC were also used to study the evolution of the thermal conductivity with the temperature, up to 300ºC. The values obtained from the "measurements" were compared to those "calculated" in order to consider the variation of the specific heat at constant pressure (C_p), see Eq. 12 (Section 2.6.8), and to those found in the literature. The comparison is displayed in Figure 6.133.

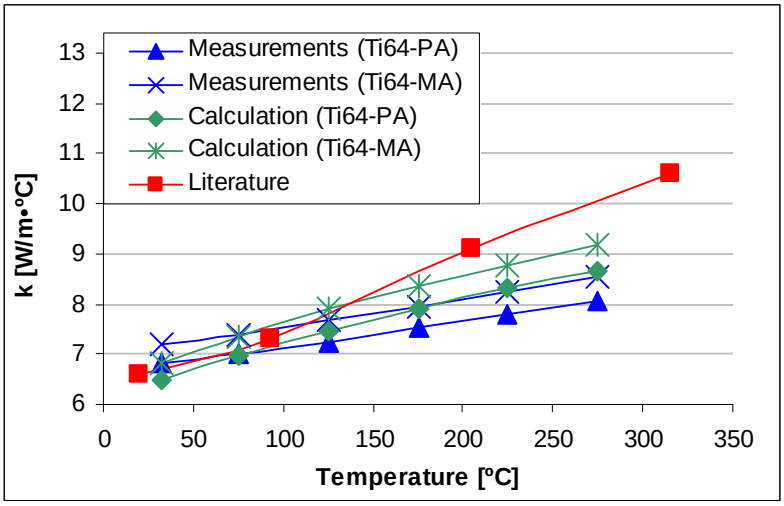

Figure 6.133 – Thermal conductivity as a function of temperature for Ti64–PA and Ti64–MA specimens.

As it can be seen in Figure 6.133, the thermal conductivity of pressing and sintering Ti–6Al–4V components increases with the testing temperature independently of the P/M approach. As expected, the values obtained after the calculation for considering the effect of C_p are somewhat higher than the values measured on the samples.

When compared to the wrought alloy data, powder metallurgy Ti–6Al–4V specimens have a lower thermal conductivity from approximately 150ºC, since the thermal conductivity of the wrought alloy increases with the temperature much faster than in P&S components most probably due to the greater influence of the residual porosity.

6.3.1.8 – Electrical Resistivity

The electrical conductivity and the electrical resistivity of the Ti64–PA and Ti64–MA samples produced by different sintering conditions were measured by means of the van der Pauw's method.

The trend of the electrical resistivity with the relative density and equivalent oxygen content is shown in Figure 6.134 and Figure 6.135 for Ti64–PA and Ti64–MA, respectively.

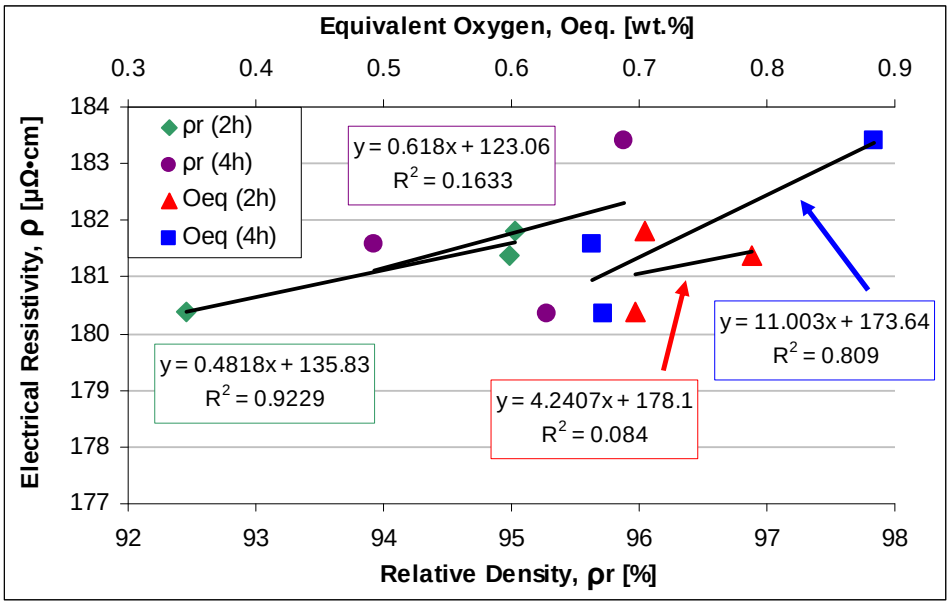

Figure 6.134 – Electrical resistivity at room temperature as a function of the relative density and equivalent oxygen content for Ti64–PA specimens.

The electrical resistivity data for the Ti64–PA alloy (Figure 6.134) indicate that this property increases with the relative density, which is not expected but could be due to the characteristics of the residual porosity, namely the mean size and the shape, since a more uniform distribution of small pores could hinder more the movement of the electrons than less pores of bigger size. On the other side, the electrical resistivity seems to increase with the amount of interstitial elements dissolved inside the matrix even though it can not be well represented by a linear relation due to the influence of other factors.

The electrical resistivity measured in Ti64–MA alloy specimens (Figure 6.135) has two opposite trends depending on the sintering time: it decreases for 2 hours of dwell time and it increases for 4 hours, with both the relative density and the equivalent oxygen content but the dispersion of the relatively limited.

Comparing the data of electrical resistivity of Ti64–PA and Ti64–MA, the former are slightly higher mainly due to the higher equivalent oxygen content.

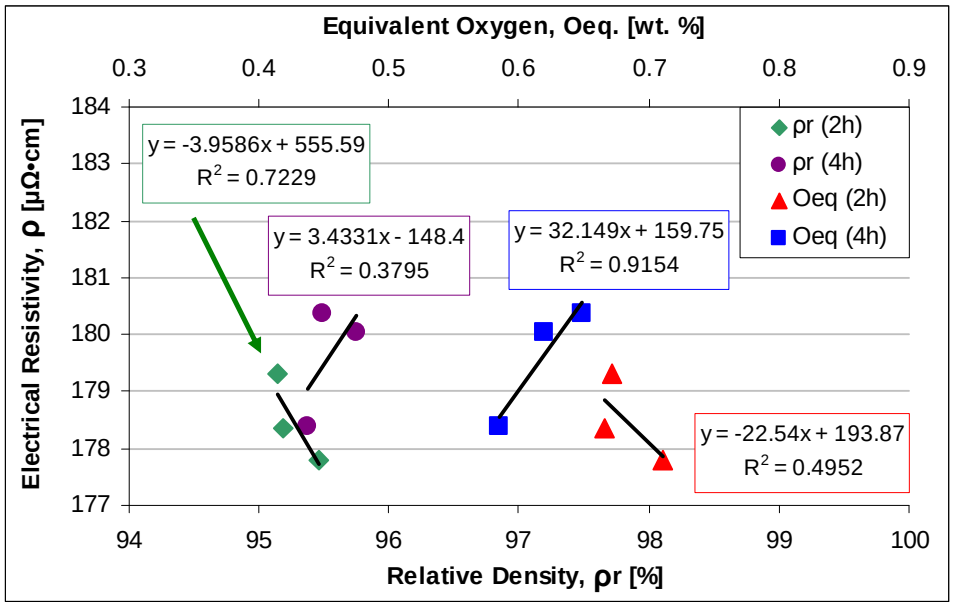

Figure 6.135 – Electrical resistivity at room temperature as a function of the relative density and equivalent oxygen content for Ti64–MA specimens.

The electrical resistivity of Ti64–PA and Ti64–MA is, generally, higher that that of the wrought alloy (Table 6.6) due to the amount of interstitials and the presence of the residual porosity.

Table 6.6 – Comparison of electrical resistivity values between wrought and P/M Ti–6Al–4V alloy.

Ti–6Al–4V						
Wrought[8]		**P/M**				
		Ti64–PA		**Ti64–MA**		
ρ [μΩ·cm]	Chemical analysis [wt.%]	ρ [μΩ·cm]	Chemical analysis [wt.%]	ρ [μΩ·cm]	Chemical analysis [wt.%]	Sintering conditions
171.0	O = 0.20 N = 0.05	180.4	O = 0.634 N = 0.023	179.3	O = 0.609 N = 0.022	1250ºC – 2h
		181.8	O = 0.632 N = 0.027	178.3	O = 0.612 N = 0.018	1300ºC – 2h
		181.4	O = 0.725 N = 0.022	177.3	O = 0.652 N = 0.020	1350ºC – 2h
		181.6	O = 0.607 N = 0.019	178.4	O = 0.552 N = 0.022	1250ºC – 4h
		180.4	O = 0.604 N = 0.020	180.0	O = 0.547 N = 0.026	1300ºC – 4h
		183.4	O = 0.829 N = 0.019	180.4	O = 0.586 N = 0.022	1350ºC – 4h

6.3.2 – Hot Isostatic Pressing (HIP)

This section deals with the results of the characterisation of Ti64–PA and Ti64–MA sintered at 1250ºC during 2 hours and post–processed by applying a HIP treatment.

The processing conditions considered during the HIP study are:

- ✓ **HIP–1**: T = 1000ºC, P = 100 MPa , t = 20 min — Reference conditions
- ✓ **HIP–2**: T = 1000ºC, P = 100 MPa, t = 2 h — To study the influence of time
- ✓ **HIP–3**: T = 850ºC, P = 100 MPa, t = 20 min — To study the influence of temperature
- ✓ **HIP–4**: T = 850ºC, P = 200 MPa, t = 20 min — To study the influence of pressure

As for the other titanium alloys studied, rectangular samples for bending tests were post–processed by the four HIP conditions whereas dogbone specimens for tensile test were submitted only to the HIP–2 condition. It should be remembered that all the samples were pressed at 700 MPa, with the exception of Ti64–PA rectangular samples (400 MPa), and sintered at 1250ºC during 2 hours.

6.3.2.1 – Relative Density

The variation of the relative density with the processing parameters as well as the comparison between Ti64–PA and Ti64–MA are displayed in Figure 6.136.

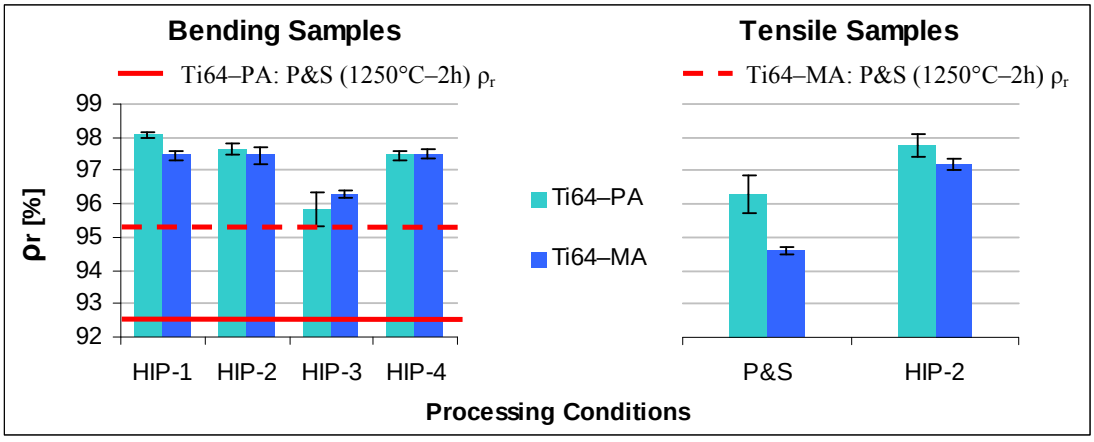

Figure 6.136 – Relative density as a function of the HIP cycle for Ti64–PA and Ti64–MA specimens: bending (left) and tensile (right).

As it can be seen in Figure 6.136, the application of a post–processing HIP cycle to sintered Ti–6Al–4V samples leads to an increment of the relative density of 1% minimum (HIP–3). On the other side, using a temperature of 1000ºC (HIP–1), a longer dwell time (HIP–2) or a higher pressure (HIP–4) induces a further increment of the relative density reaching values close to 98%. As already stated for elemental titanium and the Ti–3Al–2.5V alloy, no fully dense materials could be obtained by HIP most probably due to the presence of open porosity concentrated in the surface of the samples.

Comparing the P/M approach, the final relative density of bending samples (Figure 6.136 – right) reaches similar values for the two types of materials (PA and MA) but all the HIP cycles provoke higher densification in Ti64–PA than in Ti64–MA, as sintered relative density of Ti64–PA was lower. The same behaviour was observed during the comparison between Ti32–PA and Ti32–MA. Thus, HIP process can level the relative density of samples made from the two types of powders. This is confirmed when analysing the densification of "dogbone" specimens (Figure 6.136–right) where both materials processed with the same conditions reach values of relative density of 97–98% after HIP.

The majority of the researches carried out on HIP of the Ti–6Al–4V alloy were performed by consolidating spherical loose powder produced by different methods (such as PREP[61], KRZ[62] and gas atomisation[63]) or elemental titanium sponge fines blended with master alloy[64] obtaining, almost fully dense material (relative density higher than 99%) using different processing conditions (890–950ºC, 100–150 MPa and 1–4 h).

The master alloy addition approach has also been studied using the CHIP process (cold and hot isostatic pressing) attaining fully dense specimens due to uniform distribution of the green density of cold isostatically pressed samples[65].

Minabe et al.[66] developed a pressure assisted sintering processed called sinter–HIP where after 90 minutes at sintering temperature under vacuum, an argon gas pressure of 98 MPa is applied to increase the density. In particular, the authors report that sinter–HIPed materials have a relative density similar to that shown in Figure 6.136 but with problems in terms of homogenisation of the alloying elements[66].

6.3.2.2 – Chemical Analysis

Chemical analyses of the HIPed Ti64–PA and Ti64–MA specimens were carried out and the results are shown in Figure 6.137 and Figure 6.138 for bending samples and tensile specimens, respectively.

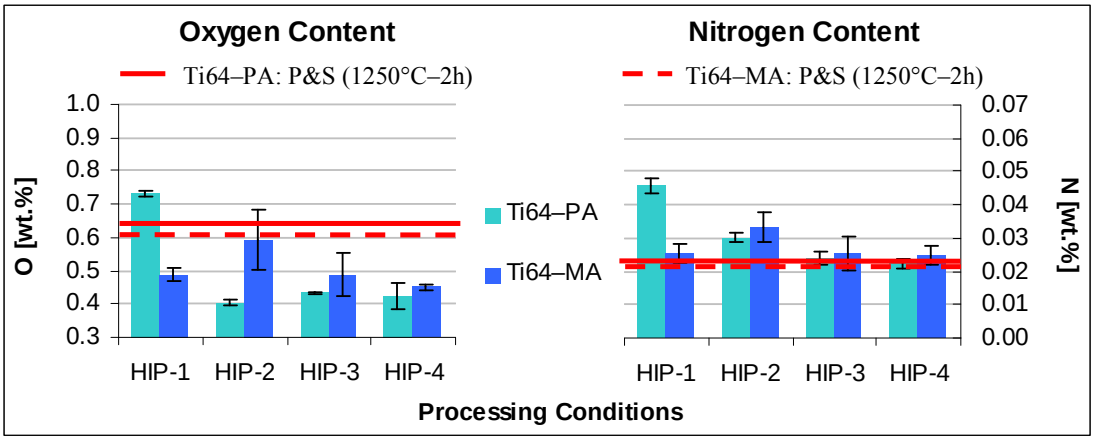

Figure 6.137 – Chemical analysis as a function of the HIP cycle for Ti64–PA and Ti64–MA bending specimens: oxygen (left) and nitrogen (right).

As it can be seen in Figure 6.137–left, oxygen stays approximately constant at 0.42 wt.% for the Ti64–PA alloy with the exception of the specimens HIP–1. In the case of the Ti64–MA alloy, oxygen increases for longer processing time whereas the decreasing of the processing temperature (HIP–3 and HIP–4) or the increment of the applied pressure (HIP–4) does not change significantly the final oxygen percentage. What is remarkable is that the final oxygen percentage of HIPed components is lower compared to the respective P&S samples confirming that the high oxygen found in the P&S specimens (Figure 6.112) is due to some punctual contamination of the samples.

On the other hand, nitrogen follows the same trend as oxygen since its values are almost constant for all the HIP conditions with the exception of HIP–2 (longer time) where there is a slight increment up to 0.03 wt.% and the Ti64–PA samples post–processed in the HIP–1 conditions (0.046 wt.%). The rest of the samples present the same value than sintered specimens.

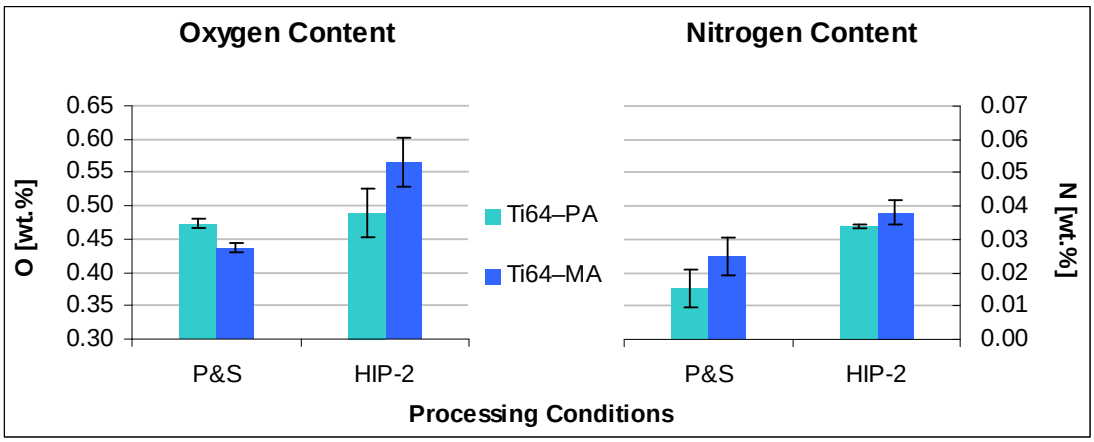

Figure 6.138 – Chemical analysis as a function of the HIP cycle for Ti64–PA and Ti64–MA tensile specimens: oxygen (left) and nitrogen (right).

With respect to tensile samples, the chemical analysis results shown in Figure 6.138 indicate that during the HIP cycles there was some contamination by oxygen and nitrogen. The elements pick–up is more pronounced for Ti64–MA, especially for oxygen content, since the final amount is approximately 0.10 wt.% higher than Ti64–PA. Generally, the results of the chemical analysis shown in Figure 6.138 are comparable to those of bending samples.

6.3.2.3 – Hardness

The results of hardness compared to the respective values obtained in pressing and sintering samples are displayed in Figure 6.139.

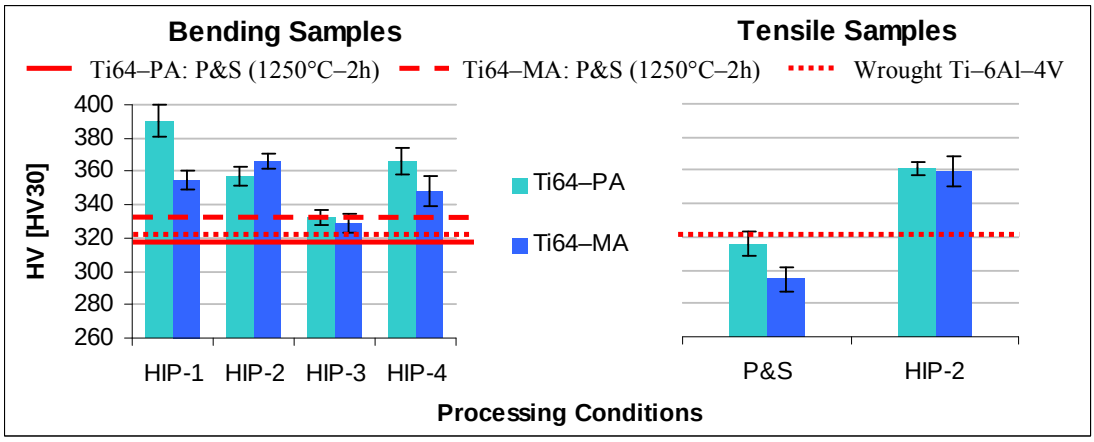

Figure 6.139 – Hardness as a function of the HIP cycle for Ti64–PA and Ti64–MA specimens: bending (left) and tensile (right).

Hardness mean values (Figure 6.139) seem to follow the same trend of the relative density, since the lowest values were obtained for the HIP–3, and these values result to be higher than the respective sintered materials. This behaviour is due to the increment of relative density, the amount of interstitials dissolved and the microstructural changes induced by each specific HIP cycle, which will be discussed in Section 6.3.2.6.

In general, the hardness of HIPed Ti–6Al–4V is greater than the nominal value of the wrought alloy most probably due to the microstructural changes induced by the HIP cycle and the greater amount of the interstitial elements, since oxygen and nitrogen are limited to 0.20 wt.% and 0.05 wt.%, respectively, in the wrought material.

The variation of the hardness of the Ti64–PA and Ti64–MA alloys with the equivalent oxygen content calculated using the equation proposed by Okazaki and Conrad[11] is presented in Figure 6.140.

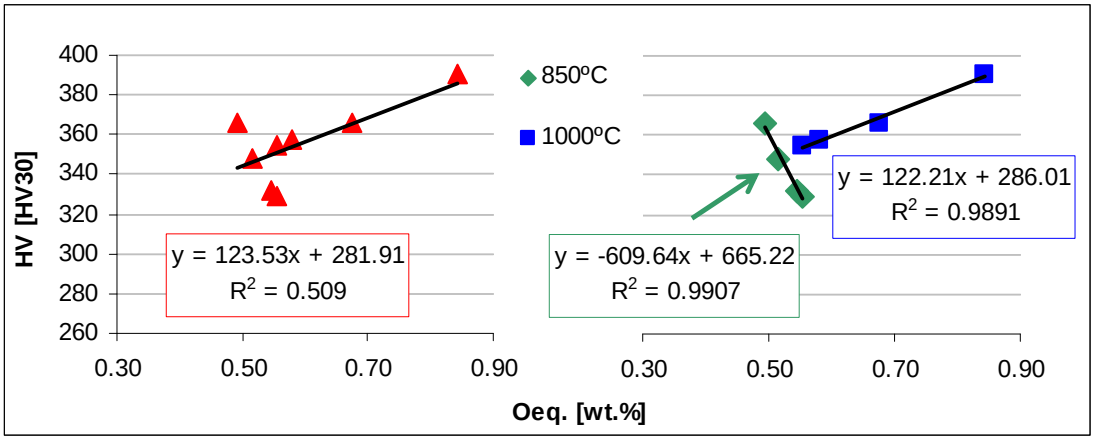

Figure 6.140 – Hardness as a function of equivalent oxygen content for Ti64–PA and Ti64–MA HIPed bending specimens: general trend (left) and influence of the HIP temperature (right).

As it can be seen in Figure 6.140, the hardness of the P/M Ti–6Al–4V alloy post–processed by HIP increases with the amount of interstitials and it can be represented by a linear approximation obtaining a coefficient of determination R^2 of 0.51. This poor correlation can be due to the differences of relative density but it is much more influenced by the microstructural features. Actually, the data shown in Figure 6.140 can be subdivided considering the processing temperature, being 850ºC below the beta transus for this alloy, and 1000ºC already in the β field, being the nominal beta transus 996ºC.

When the data are grouped as indicated and as shown in Figure 6.140–right, two opposite trends are found: the one corresponding to 1000ºC increases with the equivalent oxygen content, which is the expected; the other for 850ºC decreases with the increment of the total amount of interstitial elements, most probably due to the growth of the alpha grains.

As already evinced from the analysis of the correlation between hardness and equivalent oxygen content for P&S specimens, the higher the amount of alloying elements the worse this correlation. This is, further, confirmed by comparing the coefficient of determination of the linear correlation of HIPed Ti–6Al–4V (Figure 6.140 – R^2 = 0.51) with Ti–3Al–2.5V (Figure 6.81 – R^2 = 0.69) and elemental titanium (Figure 6.22 – R^2 = 0.89) indicating a more powerful effect of the microstructural features.

6.3.2.4 – Properties from Bending Test

Representative bending stress–strain curves obtained by three–point bending tests of HIP Ti64–PA and Ti64–MA materials are displayed in Figure 6.141.

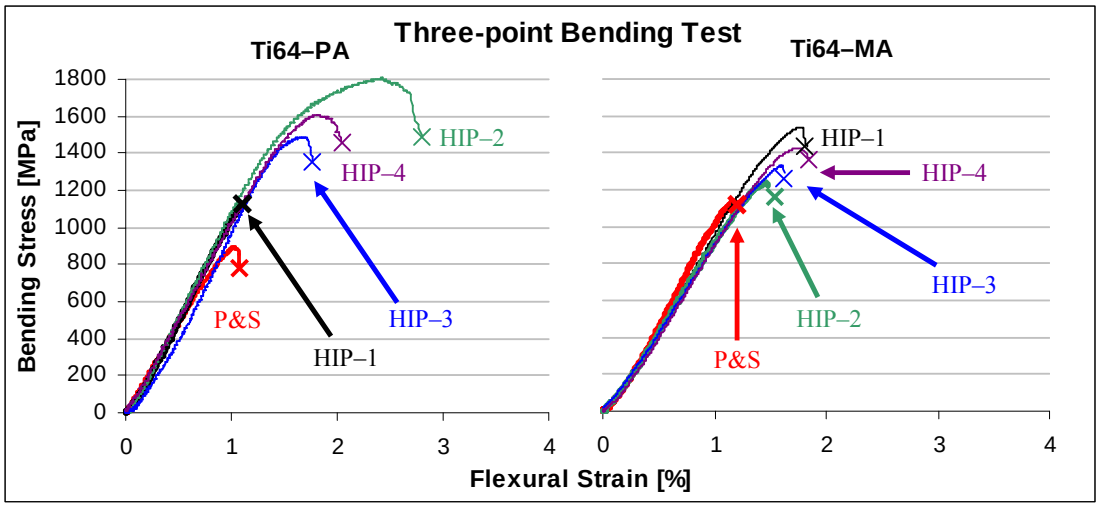

Figure 6.141 – Representative bending stress–strain curves for Ti64–PA and Ti64–MA HIPed specimens.

In the case of the Ti–6Al–4V alloy, the HIP cycle induces some small change in the stress–strain behaviour (Figure 6.141) with respect to P&S, leading to some plastic deformation before fracture, especially for the prealloyed powder, which does not occur in the case of P&S specimens (Figure 6.118 and Figure 6.119). From these curves are obtained the flexural modulus, the maximum bending strength and the flexural strain.

From the linear region of the curves, the values of the flexural modulus were obtained and the mean values were calculated attaining 106 ± 6 GPa and to 109 ± 6 GPa for Ti64–PA and Ti64–MA, respectively. Since the dimension of the specimens and, thus, the L/t ratio of the HIPed specimens is practically the same of that of P&S samples, the flexural modulus values can be compared indicating that the higher relative density achieved after the HIP process makes the material a little bit stiffer as found for the other materials studied in this thesis. This increment is, obviously, greater for the Ti64–PA alloy (from 98 MPa to 106 MPa) due to the higher improvement obtained in terms of relative density compared to Ti64–MA (from 104 MPa to 109 MPa).

The maximum bending strength and flexural strain of HIPed specimens are shown in Figure 6.142 and compared to the values of the as–sintered materials.

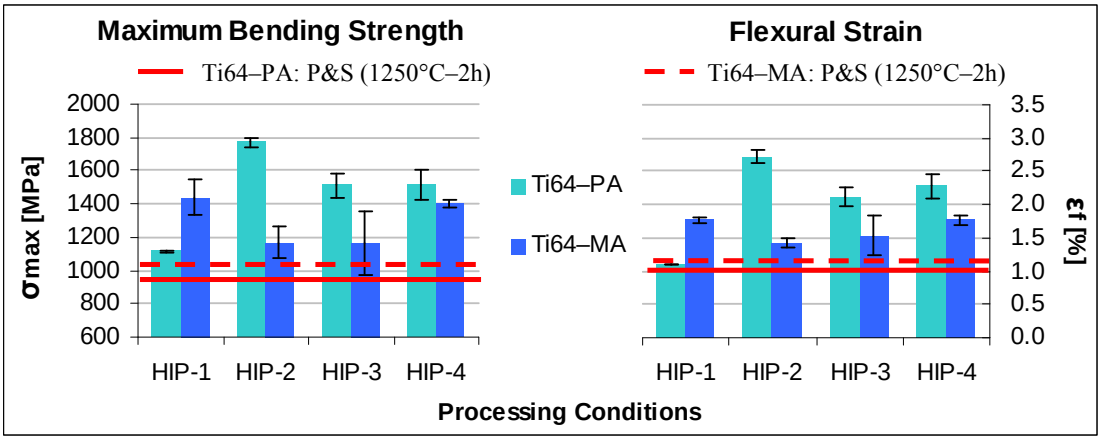

Figure 6.142 – Mechanical properties as a function of the HIP cycle for Ti64–PA and Ti64–MA specimens: maximum bending strength (left) and flexural strain (right).

Generally, the post–processing by HIP of the Ti–6Al–4V alloy permits to increase both the strength and the flexural strain with respect to the P&S specimens (Figure 6.142). More in detail, for the Ti64–PA alloy, HIP–1 presents the lowest strength, which is, however, 100 MPa higher than that of P&S; HIP–2 permits to reach a maximum bending strength of 1800 MPa and HIP–3 and HIP–4 have the same effect obtaining an intermediate value (1500 MPa) between the previous two conditions. The same trend can be used to describe the behaviour of the flexural strain even if the ductility of HIP–3 is somewhat lower than that of HIP–4.

On the other side, the Ti64–MA alloy reaches values of maximum bending strength of 1400 MPa when processed by using HIP–1 or HIP–4 conditions and 1160 MPa for HIP–2 or HIP–3. Once again, the flexural strain has the same tendency of the maximum bending strength. This behaviour is again due to the combined effect of level of relative density, amount of interstitials dissolved, which greatly varies from one HIP cycle to another, and the microstructural features (see Section 6.3.2.6).

Comparing the powder production route, it can be seen that Ti64–PA reaches higher maximum bending strength and flexural strain due to the lower oxygen content. The only exceptions are the components processed using the HIP–1 conditions which have higher oxygen and nitrogen content (Figure 6.137).

The variation of the mechanical properties with the equivalent oxygen content determined using the equation proposed by Wood[19] is presented in Figure 6.143 and Figure 6.144 for maximum bending strength and flexural strain, respectively.

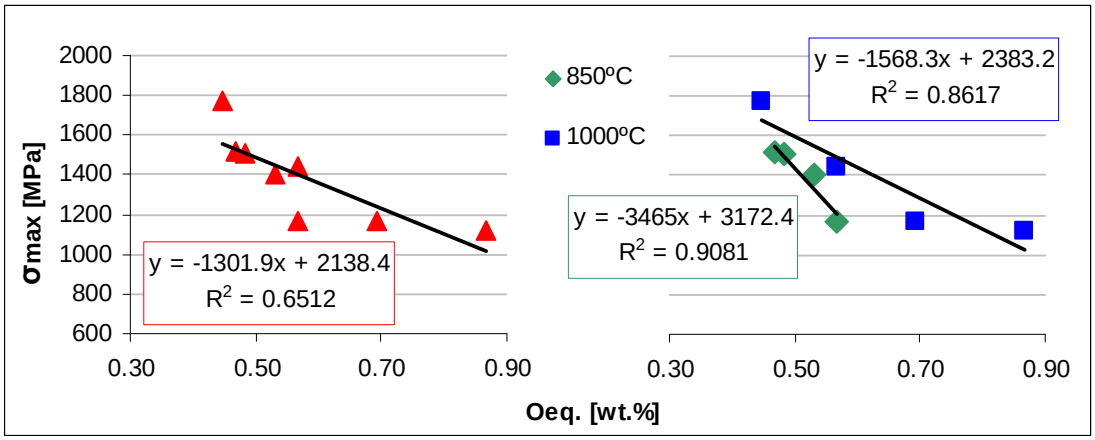

Figure 6.143 – Maximum bending strength as a function of equivalent oxygen content for Ti64–PA and Ti64–MA HIPed bending specimens: general trend (left) and influence of the HIP temperature (right).

As it can be seen in Figure 6.143, the maximum bending strength decreases with the increment of the equivalent oxygen content. When the data are separated considering the processing temperature (Figure 6.143–right) it results that, for a processing temperature below the beta transus (850ºC), the decrement of the maximum bending strength is more pronounced than for a temperature just above the beta transus (1000ºC) possible due to the relative microstructural changes (Section 6.3.2.6).

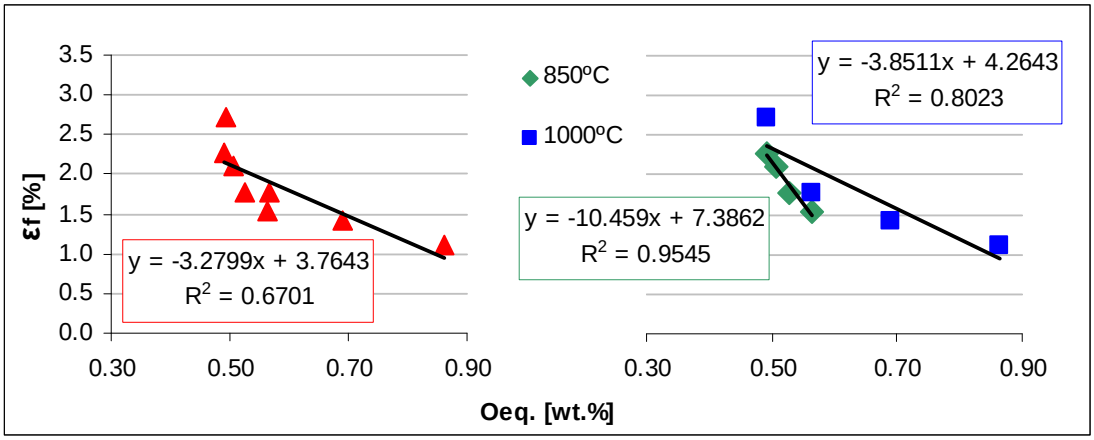

Figure 6.144 – Flexural strain as a function of equivalent oxygen content for Ti64–PA and Ti64–MA HIPed bending specimens: general trend (left) and influence of the HIP temperature (right).

The tendency of the flexural strain versus the equivalent oxygen content (Figure 6.144) is similar to that shown in Figure 6.143 for the maximum bending strength, since the ductility decreases with the increment of the interstitials dissolved. Once again, the processing temperature of 850ºC leads to a faster decrement of the flexural strain with the equivalent oxygen content.

6.3.2.5 – Properties from Tensile Test

The typical behaviour under tensile load of the Ti–6Al–4V samples post–processed by HIP is compared with that of the P&S components in Figure 6.145 whilst the mean values of ultimate tensile strength and strain are shown in Figure 6.146.

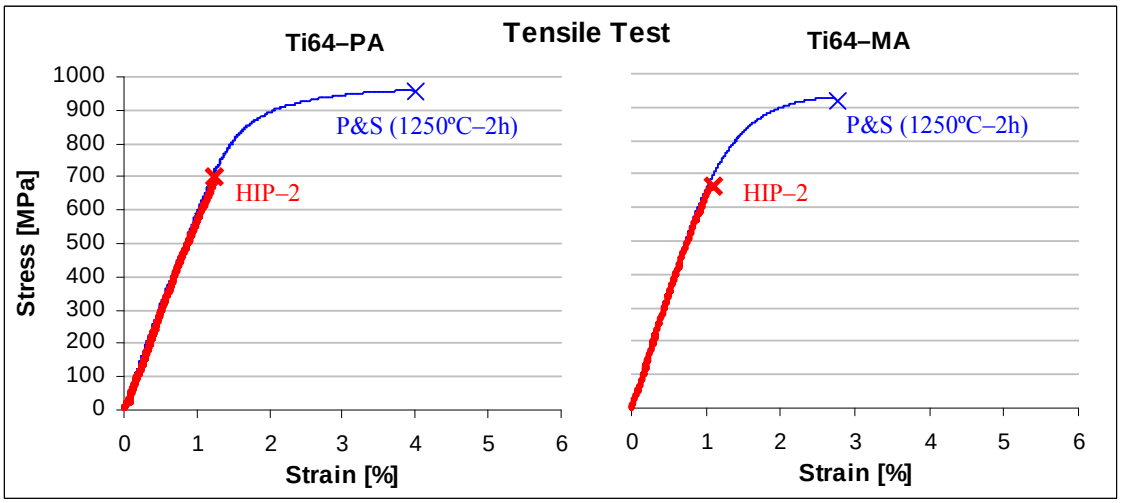

Figure 6.145 – Representative tensile stress–strain curves for Ti64–PA and Ti64–MA P&S (1250ºC–2h) and HIPed specimens.

As already found for both elemental titanium and the Ti–3Al–2.5V alloy, the post–processing of the P/M Ti–6Al–4V specimens in the β field leads to a practically elastic behaviour of the material reaching lower strength and strain compared to the starting sintered material and inhibiting the plastic deformation of the alloy (Figure 6.145). This is most probably due to the microstructural changes induced by the HIP cycle employed.

The values of dynamic Young's modulus obtained are 117 ± 3 GPa for Ti64–PA and 120 ± 1 GPa for Ti64–MA, which are very similar to the conventional value of 114 GPa indicated for the wrought Ti–6Al–4V alloy in the annealed state. The values found confirm that the reduction of the residual porosity provokes an increment of the stiffness of the material which, in this case, is more pronounced for the Ti64–MA alloy (P&S: 110 GPa) due to the lower relative density of the P&S tensile samples (Figure 6.136) compared to Ti64–PA (P&S: 111GPa).

As already expected on the bases of the stress–strain curves, the ultimate tensile strength of the P/M Ti–6Al–4V subjected to a HIP cycle at 1000ºC during 2 hours (Figure 6.146) is, approximately, 250 MPa lower than that of P&S samples reaching a maximum strength of 670 MPa for Ti64–PA and 640 MPa for Ti64–MA. A similar decrement is obtained in terms of strain which drops down to 1%. This behaviour is due to the contamination of the specimens and the microstructural change induced by the processing temperature of 1000ºC in the β field, which is discussed in Section 6.3.2.6.

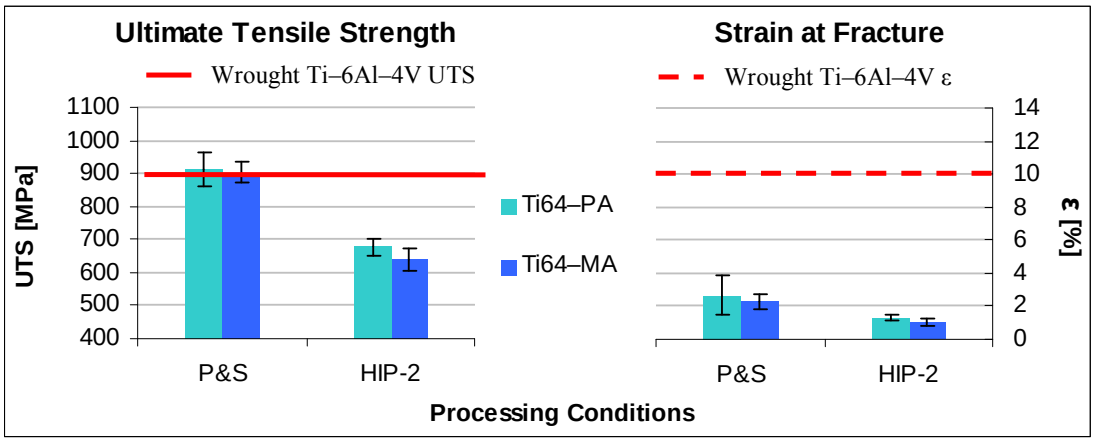

Figure 6.146 – Mechanical properties as a function of the processing method for Ti64–PA and Ti64–MA specimens: ultimate tensile strength (left) and strain (right).

Similar mechanical properties after HIP were obtained in the Ti32–PA and Ti32–MA alloys (Figure 6.87) which also have very similar final interstitials content (Figure 6.79) to that of Ti64–PA and Ti64–MA. No terms of comparison could be found in the literature since the data available refer to HIP cycle carried out between 890ºC and 960ºC, 100–150 MPa, 1–4 h and, therefore, all of them with a processing temperature located in the α + β field, below the beta transus.

In all the cases, the ultimate tensile strength ranges between 911 MPa and 1040 MPa and the strain between 10 % and 17%[61-65, 67]. The only exception is the work of Minabe et al. where the sinter–HIPed specimens were processed at 1250ºC (98 MPa approximately 4 hours) obtaining good mechanical properties (UTS = 911 MPa and strain = 9%) due to the very low oxygen content (0.10 wt.%) but without any discussion about the effect of the microstructural features on the final properties[66].

6.3.2.6 – Microstructural Analysis

The microstructure of the Ti64–PA and Ti64–MA specimens subjected to different HIP cycles was analysed by optical microscopy and the micrographs are shown in Figure 6.147.

The analysis of the microstructure of the P/M Ti–6Al–4V alloy HIPed at 1000ºC during 20 minutes (Figure 6.147 a and b) reveals that the microconstituents are alpha grains and α + β lamellae looking much more similar to a bimodal microstructure instead of a than a lamellar structure obtained by slow cooling from the β field. Moreover, Ti64–PA is characterised by regions of α + β lamella finer compared to those of Ti64–MA.

The prolongation of the processing time to 2 hours (Figure 6.147 c and d) induces the formation of a significant greater number of regions of α + β lamellae making the microstructure of the Ti64–PA alloy resembling a bimodal microstructure composed by primary alpha and transformed beta (acicular α) as for HIP–1 samples. On the other side, Ti64–MA microstructure does not seem to be refined because is characterised by big regions of alpha grains. These differences are most probably due to the relative percentages of oxygen and nitrogen dissolved inside the titanium matrix because, oxygen refines the microstructure and nitrogen promotes the formation of needles of alpha titanium[5].

When considering the 850ºC processing temperature (Figure 6.147 e and f), the microconstituents are still alpha grains and α + β lamella but the small regions of very fine lamellae do not appear. Furthermore, Ti64–PA is characterised by a greater amount of residual porosity than that of Ti64–MA.

Conversely to elemental titanium, where the increment of the applied pressure results into an abnormal grain growth (Figure 6.28 d), no such kind of effect can be observed in Ti64–PA and Ti64–MA specimens HIPed at 200 MPa (Figure 6.147 g and h), therefore, the microstructure is similar to that of HIP–3 samples.

The comparison of the microstructure of Ti64–PA and Ti64–MA processed at 850ºC indicates that the PA material has a somewhat bigger alpha mean grain size with respect to MA, which contributes to the higher flexural strain found in the Ti64–PA components.

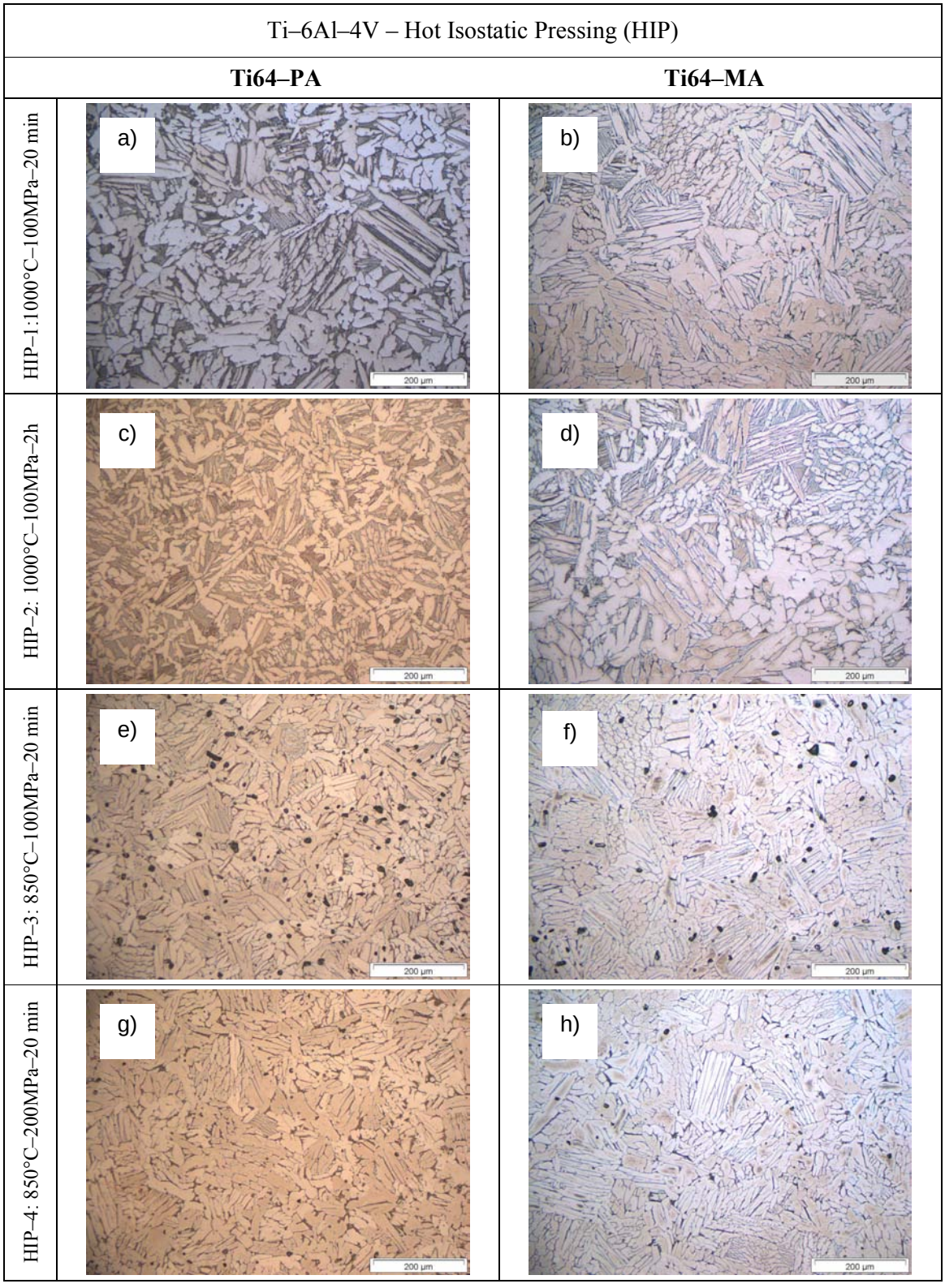

Figure 6.147 – Optical microscopy images for Ti64–PA and Ti64–MA subjected to diverse HIP cycles: a) and b) HIP–1, c) and d) HIP–2, e) and f) HIP–3 and g) and h) HIP–4.

The results of the fractographic study of HIPed tensile samples made out of Ti64–PA and Ti64–MA are shown in Figure 6.148.

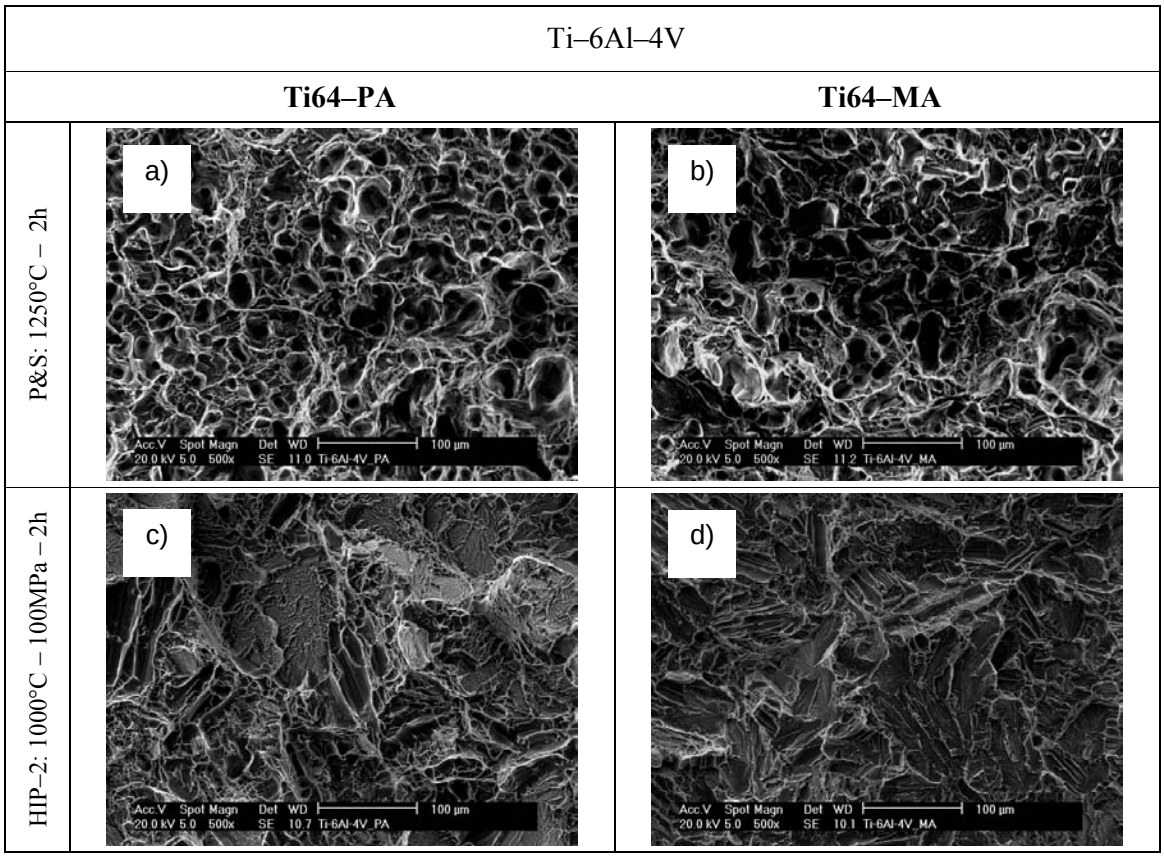

Figure 6.148 – Fracture surface from tensile test specimens for Ti64–PA and Ti64–MA: a) and b) P&S (1250ºC–2h) and c) and d) HIP–2.

From the comparison of the fracture surface between the P&S and HIP specimens (Figure 6.148), it is clear that the post–processing of the Ti–6Al–4V changes the fracture mode from ductile, due to microvoids coalescence (P&S) to mainly brittle and, thus, with a fracture surface characterised by cleavage facets. This leads the material to fracture without any plastic deformation in accordance with the results of the tensile properties.

6.3.3 – Conventional Hot–pressing (HP)

This section deals with the results of the processing and characterisation of the Ti64–PA and Ti64–MA alloys by means of conventional hot–pressing.

6.3.3.1 – Relative Density

The results of the variation of the relative density of Ti64–PA and Ti64–MA with the sintering temperature are presented in Figure 6.149.

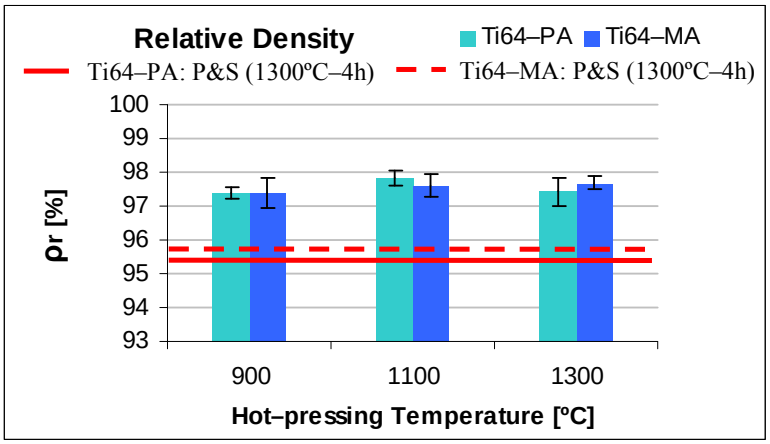

Figure 6.149 – Relative density as a function of the processing temperature for Ti64–PA and Ti64–MA hot–pressed specimens.

The final relative density of Ti64–PA and Ti64–MA (Figure 6.149) does not seem to be greatly influenced by the hot–pressing temperature employed, since the values are all within the 97–98% range. These values are, on average, 2% higher than the values obtained with the P&S route employing the same processing temperature of 1300ºC, but for 4 hours of dwell time, either for Ti64–PA and Ti64–MA.

Moreover, the relative density attained when processing the Ti–6Al–4V alloy is very similar to that of hot–pressed Ti–3Al–2.5V (Figure 6.90) and slightly lower than elemental titanium (Figure 6.31).

Similar results were obtained by other authors when processing the Ti–6Al–4V starting from spherical powder (REP)[68, 69], hydride powder[68, 69] or spherical powder, whose manufacturing route is not specified[70].

6.3.3.2 – Chemical Analysis

As for the other materials, the results of the chemical analysis carried out on Ti64–PA and Ti64–MA hot–pressed specimens were divided as a function of the removing of the outer surface when this step results to be significant. Therefore, in the case of oxygen and carbon content where the difference between grinded and not grinded samples is not important, a single value for each material and processing condition was considered and the results are shown in Figure 6.150.

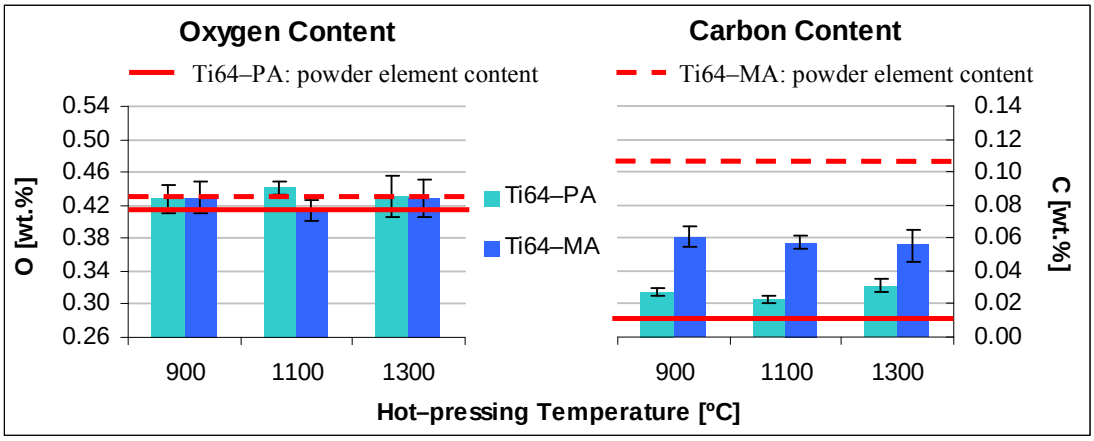

Figure 6.150 – Chemical analysis as a function of the processing temperature for Ti64–PA and Ti64–MA hot–pressed specimens: oxygen (left) and carbon (right).

As it can be seen in Figure 6.150, oxygen content remains constant with the increasing of the processing temperature and there is few oxygen pick–up with respect to the initial content of the starting powder for both Ti64–PA and the maximum oxygen content is always approximately 0.42 wt.%.

Concerning carbon content, this seems to remain constant at 0.03 wt.% for Ti64–PA and 0.06 wt.% for Ti64–MA independently of the temperature used. When compared to the initial amount of carbon dissolved in the powder, it can be seen that some carbon diffuses through the material in the case of Ti64–PA whilst it decreases for Ti64–MA.

This last phenomenon is due to the manufacturing process of the Ti64–MA powder whose master alloy was milled using a wax as process control agent. Then, it can be supposed that the wax is eliminated during the heating up of the powder but not as efficiently as in the P&S samples sintered under high vacuum, since in those specimens a lower carbon percentage was measured. Nevertheless, the carbon contents shown in Figure 6.150 are lower than the limit specified for this element in the Ti–6Al–4V alloy, which is equal to 0.08 wt.%.

About nitrogen content measurements, the results were divided as a function of the removal of the outer layer and they are displayed in Figure 6.151.

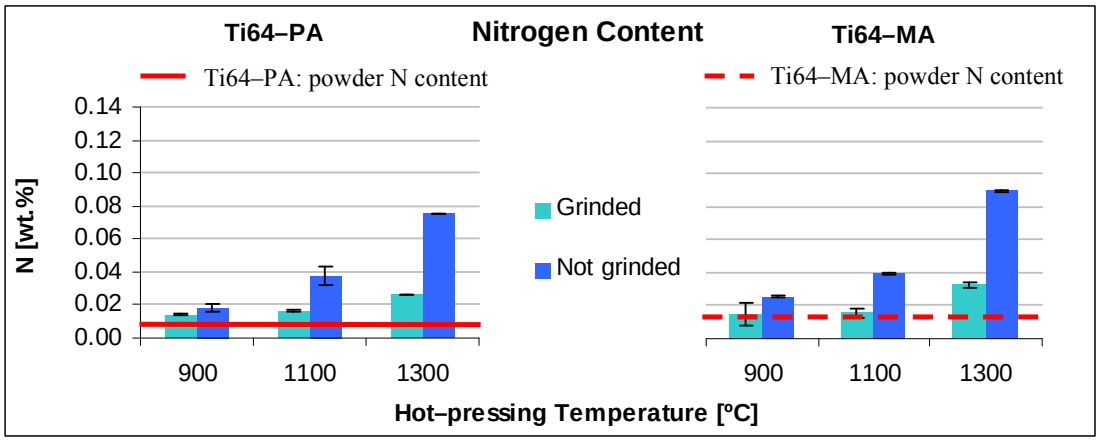

Figure 6.151 – Nitrogen content as a function of the processing temperature for Ti64–PA and Ti64–MA hot–pressed specimens.

Analysing the data shown in Figure 6.151, it can be noticed that there is always some nitrogen pick–up and nitrogen content increases with the hot–pressing temperature. Moreover, the increment is much more important for the highest temperature (1300ºC) reaching approximately 0.08 wt.%. On the other side, the nitrogen content results to increase with respect to the percentage found in the starting powder indicating that nitrogen diffuses through the titanium matrix. Besides, the removal of the surface of the specimens, at least, halves the final nitrogen content.

The chemical analysis and, in particular, the nitrogen content reveals that there was some interaction between the processed powder and the BN coating used to cover the graphite mould. Thus, the surface of the specimens was analysed by means of SEM in backscattering mode and by XRD as for the other materials. The results of the characterisation performed on the Ti–6Al–4V specimens are not reported because not significant differences with the results shown for elemental titanium (Figure 6.33 and Figure 6.34) were found. This is because the alloying elements (vanadium and aluminium) do not react with the BN coating as it was already found for the Ti–3Al–2.5V alloy (see Section 6.2.3.2).

6.3.3.3 – Hardness

The variation of the hardness measured on the cross–section of the specimens with the hot–pressing temperature is shown in Figure 6.152.

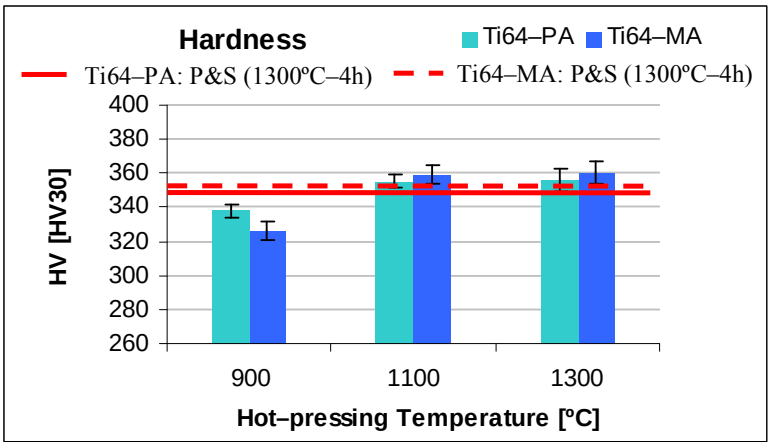

Figure 6.152 – Hardness as a function of the processing temperature for Ti64–PA and Ti64–MA hot–pressed specimens.

The hardness of the hot–pressed samples (Figure 6.152) increases approximately 20–30 HV30 when the temperature is increased from 900ºC to 1100ºC but then it stays almost constant with the processing temperature. The values obtained are similar for Ti64–PA and Ti64–MA and just slightly higher than those of P&S specimens.

Considering that hot–pressed Ti–6Al–4V specimens have lower oxygen, higher relative density (roughly 2%) and similar hardness (350 HV30) than P&S ones, there must be some influence from the microstructural features such as the relative percentage of α and β phase and mean alpha grain size (see Section 6.3.3.5).

The higher hardness compared to the nominal value of the Ti–6Al–4V in the annealed state (321 HV) is mainly due to the higher oxygen content of the hot–pressed specimens.

6.3.3.4 – Properties from Bending Test

The comparison of the typical bending stress–strain behaviour between grinded and not grinded Ti–6Al–4V specimens determined by three–point bending tests is presented in Figure 6.153 and Figure 6.154.

As it can be seen in Figure 6.153, both Ti64–PA and Ti64–MA materials reach the maximum load practically without an appreciable plastic deformation before fracture. The stress–strain behaviour of the Ti64–PA and Ti64–MA alloys is very similar between them and to that of P&S specimens indicating that hot–pressing is not able to change the stress–strain behaviour of the Ti–6Al–4V alloy which, actually, also happened for Ti32–PA (Figure 6.94).

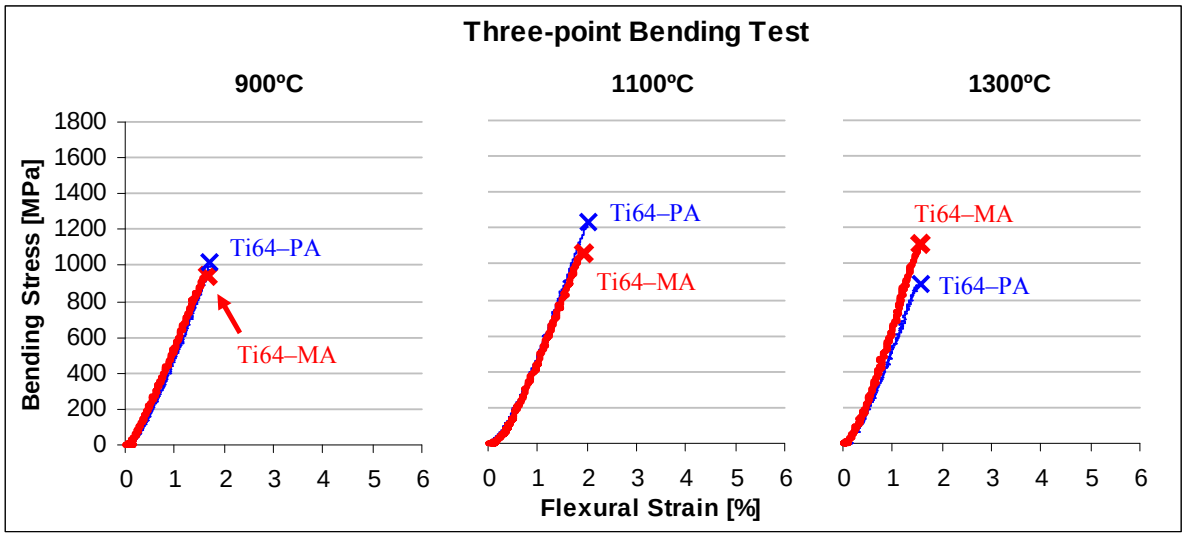

Figure 6.153 – Representative bending stress–strain curves for Ti64–PA and Ti64–MA hot–pressed specimens (without the removal of the outer surface).

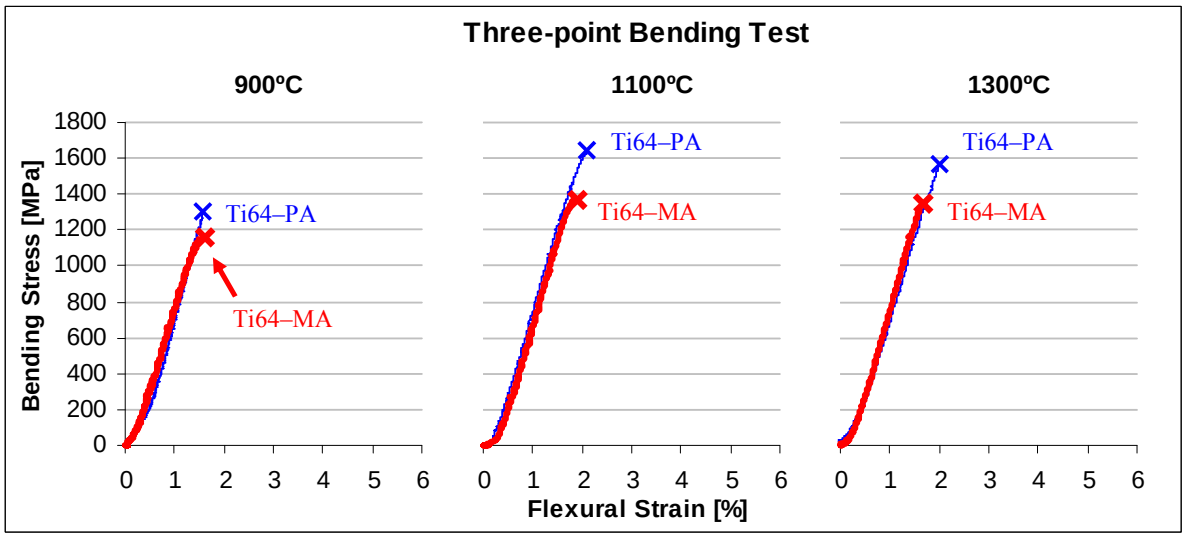

Figure 6.154 – Representative bending stress–strain curves for Ti64–PA and Ti64–MA hot–pressed specimens (after the removal of the outer surface).

Analysing the graphs of Figure 6.154, it can be seen that the main effect of the removal of the outer layer is to induce an increment of the maximum bending strength but without a significant improvement of the ductility and without changing the shape of the stress–strain curves.

Elastic modulus values as determined on the bases of the slope of the elastic portion of the stress–strain curves of hot–pressed Ti–6Al–4V specimens give as result 80 ± 13 GPa for Ti64–PA and to 82 ± 14 GPa for Ti64–MA. The effect of the L/t ratio on the flexural modulus of three–point bending test specimens considering P&S and hot–pressed samples is shown in Figure 6.155.

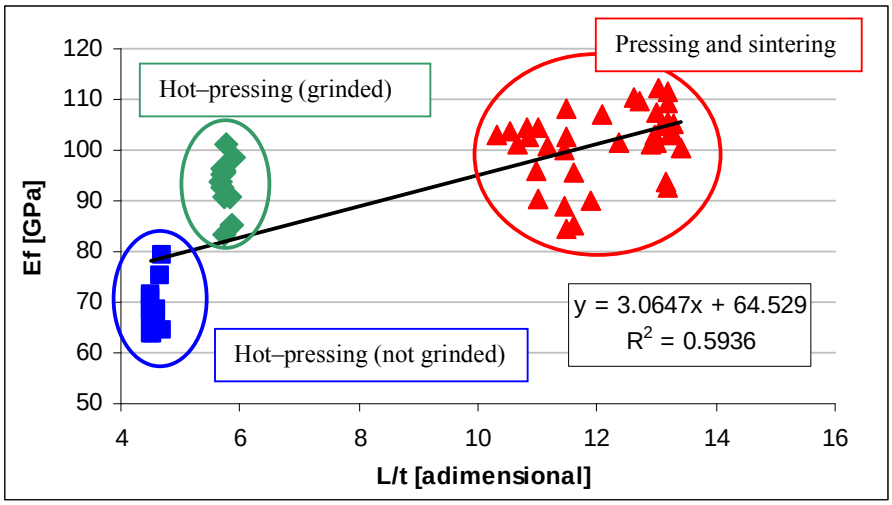

Figure 6.155 – Flexural modulus as a function of the L/t ratio for Ti64–PA and Ti64–MA obtained by the diverse P/M methods studied.

As expected, the flexural modulus of hot–pressed specimens (Figure 6.155) is lower than that of pressing and sintering samples due to the L/D effect; decreasing of the L/D ratio produces a decrement in flexural modulus[16-18]. Since L was kept constant during the development of this thesis, the thicker the components, the lower the flexural modulus.

The comparison of the maximum bending strength and flexural strain between Ti64–PA and Ti64–MA is displayed in Figure 6.156 and Figure 6.157.

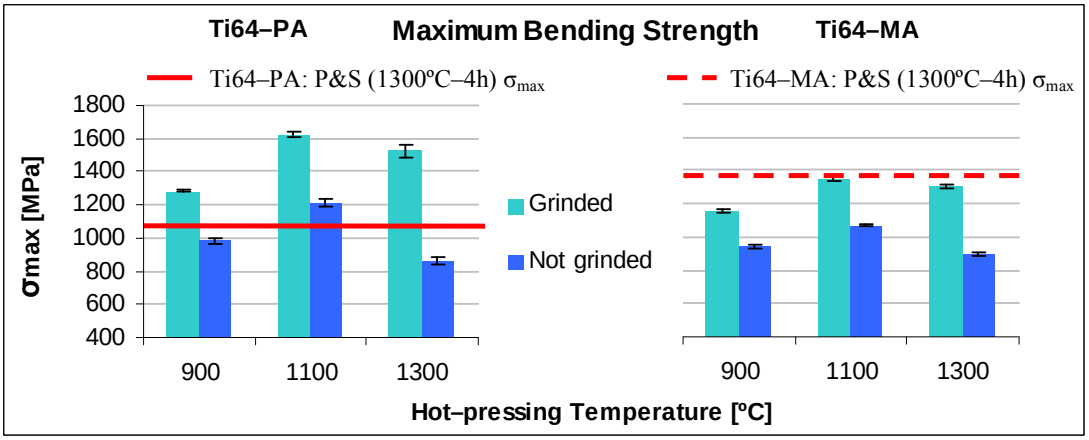

Figure 6.156 – Maximum bending strength as a function of the processing temperature for Ti64–PA and Ti64–MA hot–pressed specimens.

As it can be seen in Figure 6.156, the maximum bending strength of both Ti64–PA and Ti64–MA increases when raising the processing temperature from 900ºC to 1100ºC but then it slightly decreases when processing the materials at 1300ºC.

The description of the variation of the maximum bending strength with the processing temperature can be applied either to grinded and not grinded specimens. However, it is clear that the removal of the surface contaminated by nitrogen and boron, where titanium nitrides and borides where detected, leads to a significant improvement of the strength ranging from 200 MPa in the case of the Ti64–MA processed at 900ºC to 660 MPa for the Ti64–PA alloy sintered at 1300ºC. It is also clear that the difference between grinded and not grinded samples gets higher with the processing temperature since the higher thermal energy permits a faster diffusion of nitrogen and boron towards titanium giving as a result the formation of a thicker layer which makes the material more brittle.

Generally, Ti64–PA reaches higher strength than the Ti64–MA either before or after the grinding process with the only exception of the not grinded specimens processed at 900ºC and 1300ºC, whose maximum strength is similar. Since the final relative density obtained is almost equals in Ti64–PA and Ti64–MA, the higher strength of Ti64–PA alloy is most probably due to the somewhat lower contamination by interstitials and differences in microstructural features.

When compared to the pressing and sintering route, the components obtained by conventional hot–pressing have two opposite behaviour since the Ti64–PA alloy reaches higher or comparable maximum bending strength, especially after the removal of the surface layer, whereas the Ti64–MA alloy reaches similar or lower bending strength than P&S samples. As it was for the Ti–3Al–2.5V alloy, this trend can be explained remembering the compacting pressure used to manufacture the P&S three–point bending test samples made out of the Ti64–PA powder which was limited to 400 MPa, instead of the 700 MPa used for the Ti64–MA powder, resulting in a lower relative density.

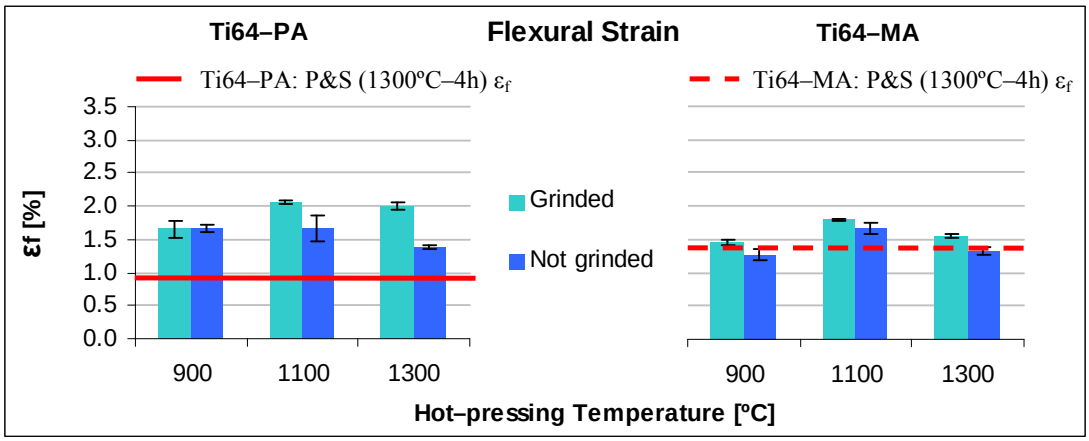

Figure 6.157 – Flexural strain as a function of the processing temperature for Ti64–PA and Ti64–MA hot–pressed specimens.

As it can be seen in Figure 6.157, the trend of the flexural strain with the temperature is exactly the same as that of the maximum bending strength since it increases from 900ºC to 1100ºC, but then it decreases. This is due to the combination of the small changes of relative density, percentage of interstitials and microstructural features for the three processing temperatures (see Section 6.3.3.5).

Once again, this behaviour is applicable to both grinded and not grinded specimens and the removal of the outer layer leads to an improvement of the ductility of the materials since in some cases the not grinded samples show a slightly higher flexural strain due to the elimination of the brittle layer composed by titanium nitrides and borides.

Comparing the two powder production approaches, it can be seen that the Ti64–PA is more ductile than Ti64–MA which could be due to the slightly lower percentage of nitrogen and carbon but also to the microstructural features.

Compared to P&S samples, HP specimens present higher flexural strain especially in the case of Ti64–PA were values are almost the double for HP. In general, the higher ductility of the hot–pressed components is due to the higher relative density and to the lower total amount of interstitial elements, especially in terms of oxygen content which results to be the element with the strongest influence on ductility.

6.3.3.5 – Microstructural Analysis

The results of the microstructural analysis done by means of optical microscopy on polished and etched specimens of Ti64–PA and Ti64–MA obtained by conventional hot–pressing are presented in Figure 6.158.

The micrograph of the specimens hot–pressed at 900ºC (Figure 6.158 a and b) indicates that this temperature is not high enough to guarantee the complete homogenisation of the microstructure, especially in the case of the master alloy addition powder, since some small particles of the master alloy are still visible. Moreover, the residual porosity can be clearly distinguished.

When the materials are processed at 1100ºC, a great difference between the microstructure of the PA and MA powders is visible. Ti64–PA microstructure (Figure 6.158 c) is composed by approximately the same amount of alpha grains and $\alpha + \beta$ lamellae uniformly distributed throughout the microstructure whereas Ti64–MA alloy (Figure 6.158 d) is characterised by a greater percentage of alpha grains and small and concentrated Widmanstätten areas most probably located near former master alloy particles and, therefore, near zones where locally the percentage of alloying elements is higher. This explains the higher bending properties, especially the strength, of Ti64–PA compared to Ti64–MA.

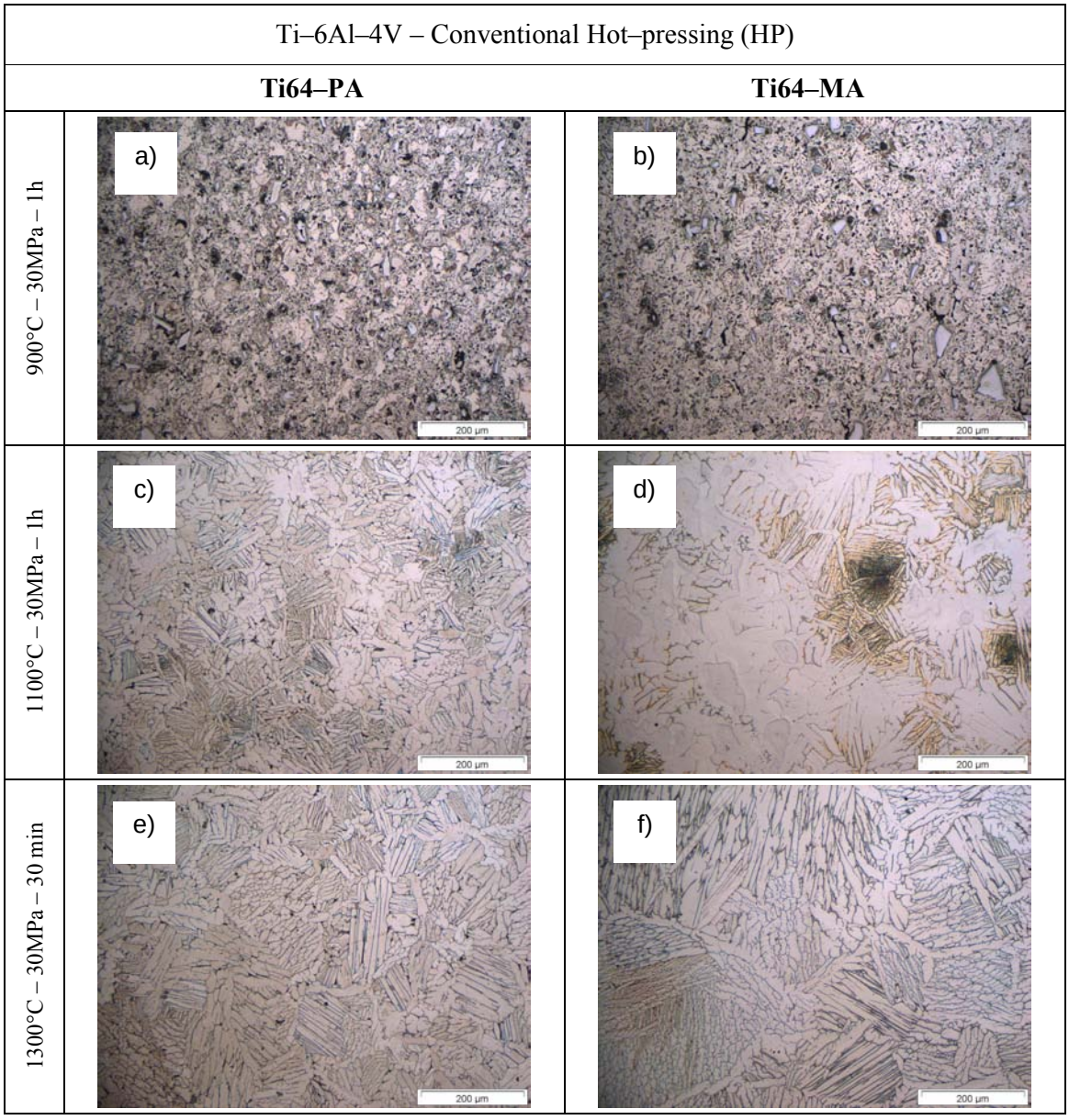

Figure 6.158 – Optical microscopy images for Ti64–PA and Ti64–MA hot–pressed at: a) and b) 900ºC, c) and d) 1100ºC and e) and f) 1300ºC.

At the highest temperature considered (1300ºC), the microstructure of both Ti64–PA and Ti64–MA (Figure 6.158 e and f) is homogeneous and composed by alpha grains and α + β lamellae. Nonetheless, Ti64–PA is characterised by a very uniform microstructure whilst Ti64–MA by large α grains and long lamellae resulting in a less homogeneous grain size distribution which could justify the lower ductility of the alloy compared to Ti64–PA.

Finally, from microstructural analysis it seems that the percentage of residual porosity is lower than the expected from the relative density data (Figure 6.149) since very small and isolated pores can be seen in all the micrographs.

6.3.4 – Inductive Hot–pressing (IHP)

Figure 6.159 shows an example of the graph recorded during the inductive hot–pressing of the Ti64–PA and Ti64–MA powders at 1300ºC where it can be noticed that the total processing time is about 50 minutes, much shorter compared to conventional hot–pressing (6–8 hours).

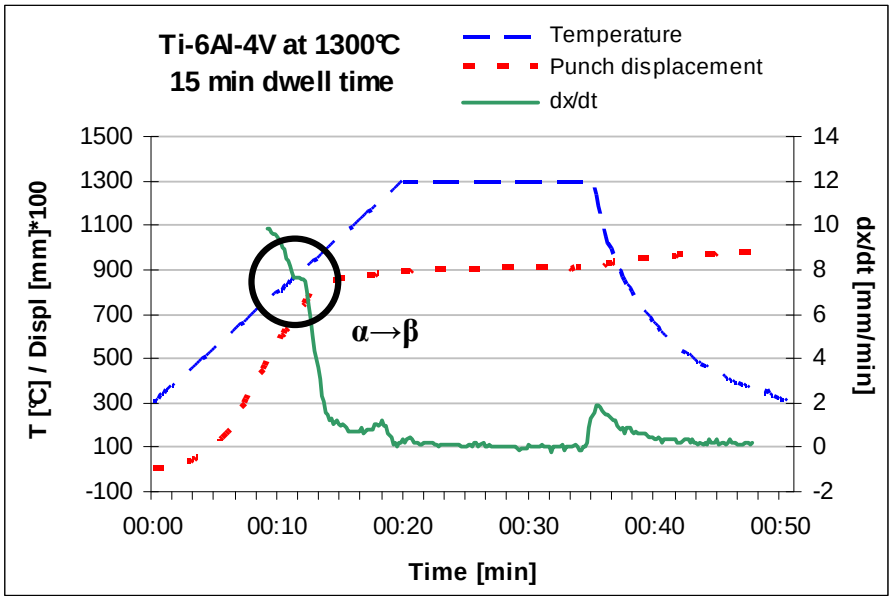

Figure 6.159 – Temperature, punch displacement and densification rate profiles recorded during the processing of the Ti–6Al–4V alloy by inductive hot–pressing at 1300ºC.

Moreover, the dx/dt trend indicates that the densification is practically completed when reaching the maximum temperature and the alpha to beta transformation is displaced towards a lower temperature compared to the conventional value for this alloy due to the presence of elemental titanium.

6.3.4.1 – Relative Density

The hot–pressed specimens were removed from the graphite mould and sandblasted in order to clean the surfaces before to proceed with their characterisation. The comparison of the results of relative density between the Ti64–PA and Ti64–MA are displayed in Figure 6.160.

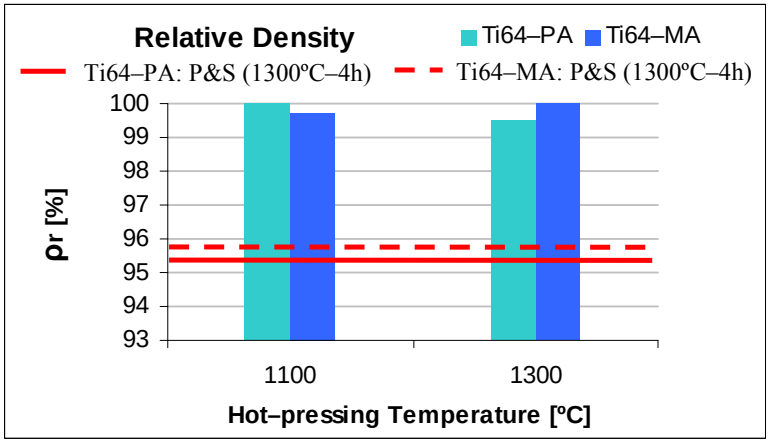

Figure 6.160 – Relative density as a function of the processing temperature for Ti64–PA and Ti64–MA inductive hot–pressed specimens.

As it can be seen in Figure 6.160, fully dense materials can be obtained by inductive hot–pressing (IHP) for both PA and MA alloys. Again, as for the other materials, there is a difference of approximately 4–5% in terms of relative density between the P&S and IHP Ti–6Al–4V specimens.

Almost fully dense materials were obtained when processing the Ti–6Al–4V alloy using spark sintering[71], induction hot–pressing[72] or spark plasma sintering[73], where these processes are field assisted sintering techniques[74] similar to inductive hot–pressing.

6.3.4.2 – Chemical Analysis

The results of the chemical analysis to determine the content of interstitials (oxygen, nitrogen and carbon content) of inductive hot–pressed Ti–6Al–4V specimens are shown in Figure 6.161.

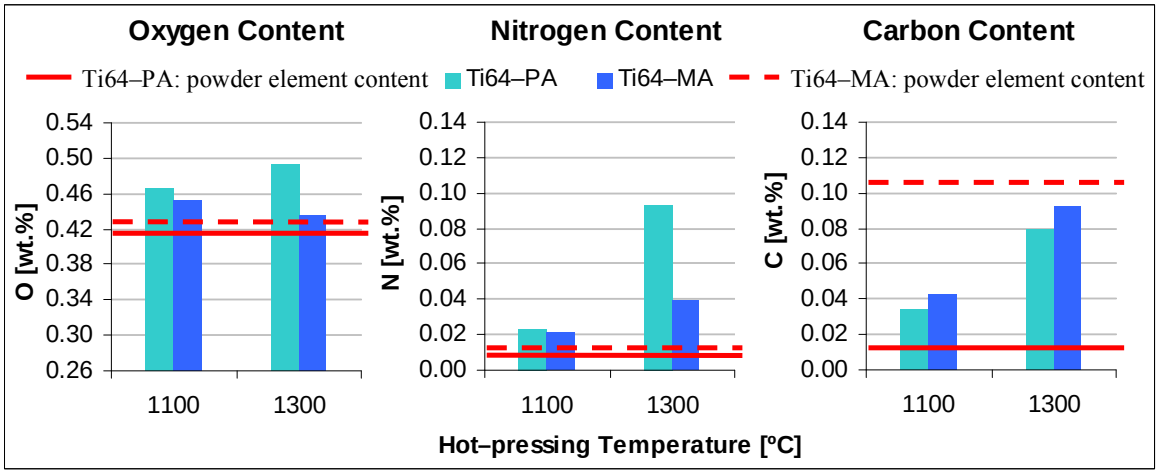

Figure 6.161 – Chemical analysis as a function of the processing temperature for Ti64–PA and Ti64–MA inductive hot–pressed specimens: oxygen (left), nitrogen (centre) and carbon (right).

As it can be seen in Figure 6.161, there is some oxygen pick–up during the processing of the Ti–6Al–4V powders by inductive hot–pressing being this phenomenon more pronounced in Ti64–PA. The values obtained are similar to that of conventional hot–pressed samples and approximately 0.15 wt.% lower than P&S components (Figure 6.112).

Nitrogen content increases with the hot–pressing temperature from 0.02 wt.% for specimens processed at 1100ºC to 0.093 wt.% and 0.04 wt.% at 1300ºC for Ti64–PA and Ti64–MA, respectively.

Finally, the amount of carbon dissolved in the matrix increases with the temperature and it is always higher with respect to the content of the powders. This indicates that there is some carbon pick–up from the graphite mould.

In the case of the Ti64–MA powder, whose carbon content is always greater than Ti64–PA, there should be also a contribution from the wax used for the milling of the master alloy, which can not be completely eliminated due to the fast heating rate employed during the inductive hot–pressing cycles.

6.3.4.3 – Hardness

The comparison of the results of Vickers hardness between Ti64–PA and Ti64–MA powder are displayed in Figure 6.162.

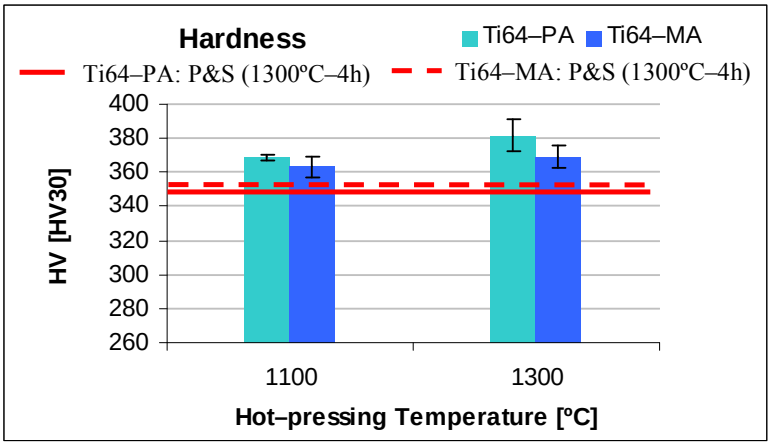

Figure 6.162 – Hardness as a function of the processing temperature for Ti64–PA and Ti64–MA inductive hot–pressed specimens.

Concerning the hardness obtained in IHP Ti–6Al–4V samples (Figure 6.162), it can be seen that there is a slight increase when the processing temperature is higher, especially for the Ti64–PA powder, and it is due to some interstitials pick–up since the difference in terms of relative density does not justify completely this increment.

In comparison to the respective P&S specimens sintered at 1300ºC during 4 hours, the IHP specimens have a slightly higher hardness which is due to the higher relative density, which was approximately 4% (Figure 6.160). Furthermore, the hardness values shown in Figure 6.162 are similar to those of the conventional hot–pressed (Figure 6.152) and higher compared to the value of the wrought alloy (321 HV) due to the higher amount of interstitials dissolved by Ti64–PA and Ti64–MA.

6.3.4.4 – Microstructural Analysis

The analysis of the microstructural features and the surface of the inductive hot–pressed specimens were carried out by means of optical microscopy and the micrographs are presented in Figure 6.163.

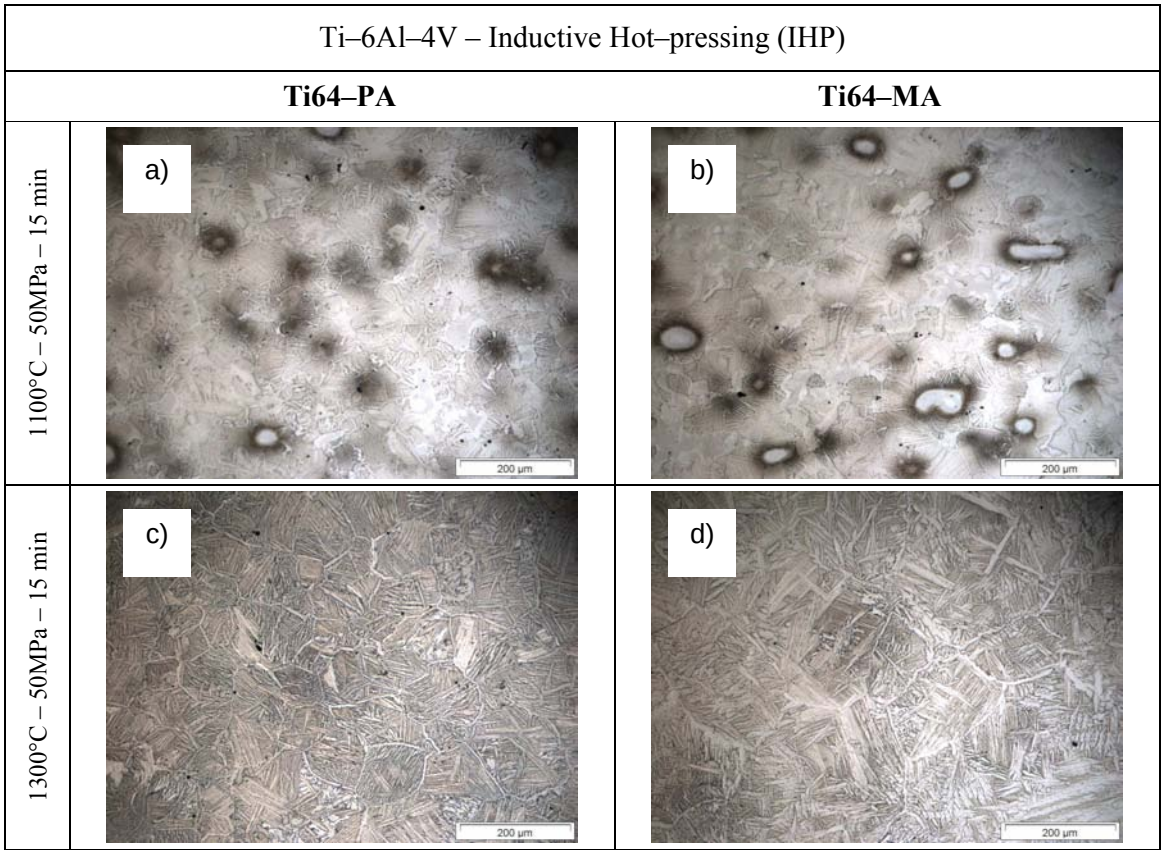

Figure 6.163 – Optical microscopy images for Ti64–PA and Ti64–MA inductive hot–pressed at: a) and b) 1100ºC and c) and d) 1300ºC.

The microstructure of Ti–6Al–4V processed by IHP at 1100ºC (Figure 6.163 a and b) is not fully developed showing undissolved particles in both Ti64–PA and Ti64–MA. This processing temperature is not high enough to guarantee the complete diffusion of the alloying elements and, therefore, the obtaining of a homogeneous microstructure.

It is worth mentioning that Ti64–PA should not have problems concerning the diffusion of the alloying elements since it is a prealloyed powder; however, as it was found during the XRD analysis of the starting powder (see Figure 5.10) some Al:V compound was added by the supplier to adjust to final composition during the production of the powder.

The raising of the processing temperature to 1300ºC permits to obtain fully homogeneous microstructure (Figure 6.163 c and d), where the alpha phase assumes the acicular morphology (Widmanstätten type alpha–beta structure) typical of the alloy when is processed over the β transus[71, 73]. Therefore, the final microconstituents are alpha phase grain boundaries, acicular alpha and α + β lamella but without any traces of undiffused particles.

Comparing the two P/M approaches, it seems that the microconstituents of Ti64–MA alloy are somewhat coarser that those of Ti64–PA due to the bigger particle size of the starting powder.

Generally, the microstructure of inductive hot–pressed Ti–6Al–4V components is much finer with respect to that obtained by other manufacturing routes such as P&S (Figure 6.128 and Figure 6.129) and HP (Figure 6.158) due to the faster cooling rate employed.

6.3.5 – P/M Techniques Comparison

This section deals with the comparison of the physical and mechanical properties of the Ti–6Al–4V prealloyed and master alloy addition powders processed by the P/M techniques described previously.

It is worth mentioning that for the relative density the highest values obtained in each case will be considered whereas for mechanical properties, where possible, a common or similar equivalent oxygen content was used as comparing factor.

The highest values of relative density for the Ti–6Al–4V are displayed in Figure 6.164.

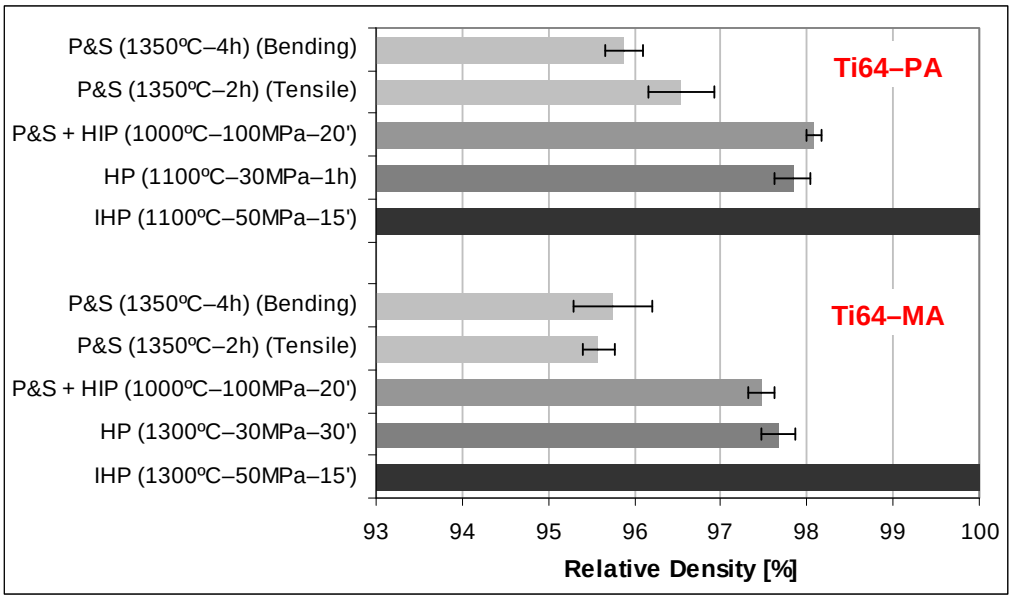

Figure 6.164 – Comparison of the highest relative density for Ti64–PA and Ti64–MA obtained by different P/M techniques.

From the data shown in Figure 6.164, it can be seen that the conventional P/M route of pressing and sintering permits to obtain values of relative density as high as 96%.

The application of a post–processing step by HIP reduces the percentage of residual porosity in approximately 2% but it does not permit to obtain fully dense materials due to the open porosity.

Similar results to HIP in terms of relative density (almost 98%) can be obtained by processing the Ti–6Al–4V powder by conventional hot–pressing due to the simultaneous application of a uniaxial pressure during sintering.

Finally, fully dense materials can be easily obtained by inductive hot–pressing where the benefit of the densification under a uniaxial pressure is enhanced by the inductive current. Furthermore, it can be noticed that, apart from the inductive hot–pressing process, Ti64–MA reaches slightly lower final relative density than Ti64–PA.

The comparison of the Vickers hardness obtained in the diverse P/M techniques is based on the equivalent oxygen content (Okazaki and Conrad equation[11]) and the results for specimens having an equivalent oxygen content of 0.54 wt.% are presented in Figure 6.165.

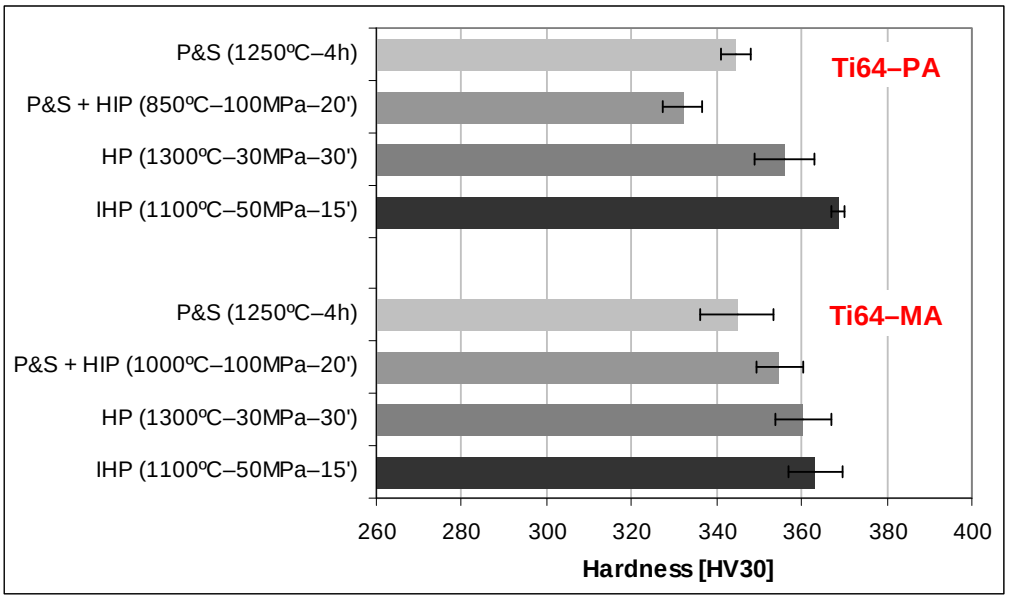

Figure 6.165 – Comparison of the hardness for Ti64–PA and Ti64–MA obtained by different P/M techniques (equivalent oxygen content of approximately 0.54 wt.%).

From the data shown in Figure 6.165, it can be seen that the hardness of the P/M Ti–6Al–4V alloy follows the same trend of the relative density, which is the normal behaviour for P/M materials.

The similar hardness obtained in P&S Ti64–PA and Ti64–MA sintered at 1250ºC–4h (Figure 6.165) is due to the compromise between higher amount of interstitials and finer microstructure of Ti64–PA and higher relative density of Ti64–MA. About this, it is worth mentioning that the lowest equivalent oxygen content found for P&S specimens is higher than the mean values used for the comparison (0.54 wt.%), being 0.66 wt.% and 0.58 wt.% for Ti64–PA and Ti64–MA, respectively.

The application of a post–processing by HIP can either induce a decrement (Ti64–PA) or an increment (Ti64–MA) in terms of hardness depending on the temperature selected. More in detail, a temperature located in the α + β field (see Ti64–PA value) leads to a microstructure characterised by fine regions of α + β lamella, such as the one obtainable by a furnace cooling. On the other side, a temperature just above the beta transus of this alloy (see Ti64–MA value) provokes the growth of the alpha mean grain size at the expenses of the α + β lamellae which gets thinner and lower in relative percentage obtaining a bimodal microstructure.

The processing of the Ti–6Al–4V alloy by hot–pressing, regardless of the way the heat is supplied, results in a higher final hardness compared to both P&S and HIPed specimens. In particular, comparing the values of HIP with that of hot–pressing (HP and IHP) which have similar relative density and equivalent oxygen content, the higher hardness is due to the microstructural features such as alpha mean grain size, acicular alpha as well as α + β lamellae morphology and relative percentage.

In general, the hardness of P/M Ti–6Al–4V is higher than the nominal value of the wrought material in the annealed state (321 HV with a maximum equivalent oxygen content of 0.37 wt.%) due to the balance between the effect of the residual porosity, chemical analysis and microstructural features characteristic of the processing technique and parameters studied.

The variation of the maximum bending strength determined on Ti64–PA and Ti64–MA samples has been analysed considering the equivalent oxygen content based on the formula proposed by Wood (Eq. 15 in Section 2.7)[19] and the results for samples with 0.57 wt.% of equivalent oxygen content are shown in Figure 6.166.

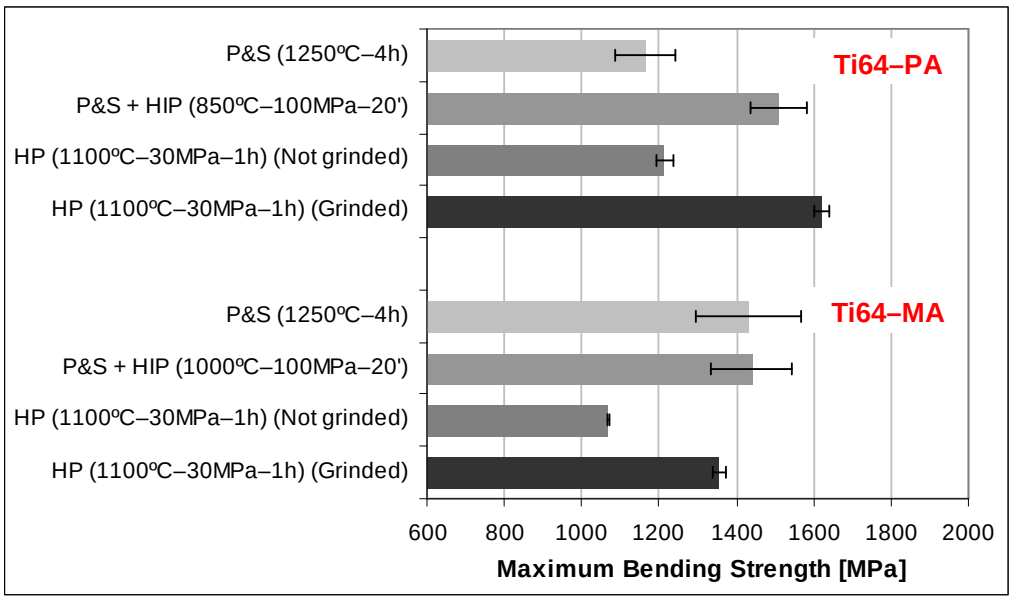

Figure 6.166 – Comparison of the maximum bending strength for Ti64–PA and Ti64–MA obtained by different P/M techniques (equivalent oxygen content of approximately 0.57 wt.%).

The data shown in Figure 6.166 indicate that the compacting pressure has a significant effect on the maximum strength since P&S Ti64–PA (pressed at 400 MPa) has a maximum bending strength 200 MPa lower than Ti64–MA (pressed at 700 MPa).

Once again, the HIP process can lead to an improvement or can maintain the maximum strength depending on the processing temperature, below the beta transus (850ºC) or above (1000ºC). This is due to the microstructural changes induced by each specific processing condition.

The conventional hot–pressing process permits to obtain maximum bending strength values slightly lower compared to the of P&S and HIPed samples due to the effect of the morphology of the acicular alpha and α + β lamella. Once again, the removal of the reacted layer composed by titanium nitride and borides, which brittles the material, leads to an important improvement of the maximum strength in spite of the effect of the other factors.

Equivalent oxygen content for the evaluation of the flexural strain was obtained on the bases of the equation found by Wood[19] and the results for specimens with an equivalent oxygen content of 0.50 wt.% are displayed in Figure 6.167.

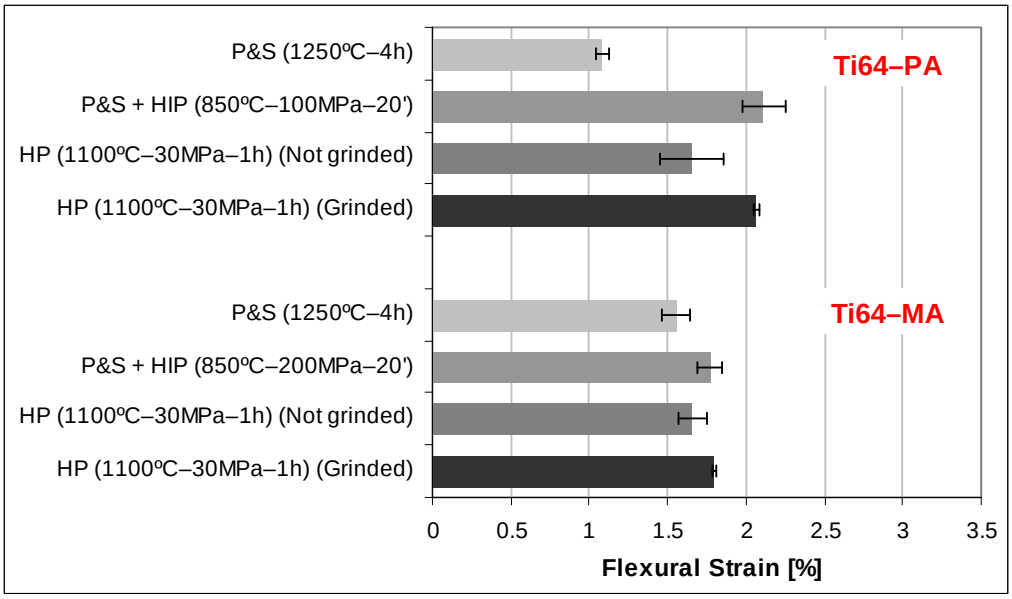

Figure 6.167 – Comparison of the flexural strain for Ti64–PA and Ti64–MA obtained by different P/M techniques (equivalent oxygen content of approximately 0.50 wt.%).

As it can be seen in Figure 6.167, the flexural strain is greatly influenced by the final relative density of P&S specimens and, thus, from the compacting pressure, as it was for the maximum bending strength.

The HIP process in the α + β field (850ºC) leads to an improvement of the ductility of the material which increases with the lowering of the residual porosity (Ti64–PA compared to Ti64–MA) and due to the alpha mean grain size growth which can be somewhat affected by the increasing of the processing pressure.

Conventional hot–pressing permits to obtain higher flexural strain than P&S and similar to HIP where the slightly grater relative density seems to balance the changes in microstructural features.

The presence of the brittle layer due to the interaction with the boron nitride coating used during the sintering of the material reduces the flexural strain of approximately 0.5 %.

6.3.6 – Partial Conclusions

Based on the results of the study of processing of the Ti–6Al–4V alloy by different P/M techniques, it can be concluded that:

Uniaxial Pressing and Sintering (P&S): the employment of the conventional powder metallurgy route for processing the Ti–6Al–4V alloy, generally, permits to obtain a relative density between 95% and 96% when using a sintering temperature between 1250ºC and 1350ºC and a dwell time of 2 or 4 hours.

The content of interstitials results to be a very critical factor since their percentage and, in particular, that of oxygen can rise importantly being detrimental for the mechanical properties. More in detail, the hardness of P&S Ti–6Al–4V is, commonly, 25 HV30 higher compared to that of the wrought alloy in the annealed stated.

When subjected to a bending load the material deforms elastically and it fails catastrophically with a very limited plastic yielding with the exception of some particular case such as Ti64–MA sintered at 1250ºC during 4 hours. Moreover, the increment of the interstitials, which normally leads to an increment of both the hardness and the ultimate tensile strength, leads to a decrement of the maximum bending strength. Nevertheless, maximum bending strength values similar to that of biomedical implants are obtained.

Ultimate tensile strength equals to that of wrought Ti–6Al–4V can be easily obtained but the strain is lower due to presence of the residual porosity. Actually, fractography analysis indicates that P/M Ti–6Al–4V fails in a ductile way by a pore–assisted mechanism such as microvoid coalescence.

The microstructure of the sintered specimens is composed by homogeneously distributed alpha grains and relatively small $\alpha + \beta$ lamellae which is the typical microstructure expected for this alloy.

Finally, the combination of residual porosity, microstructural features and amount of interstitial elements of the P&S specimens permits to obtain thermal conductivity, both at room temperature or up to 300ºC, and electrical resistivity comparable to that of the wrought alloy.

Hot Isostatic Pressing (HIP): the application of a post–processing by HIP to sintered specimens leads to an increment of relative density variable between 1% and 5% depending on the processing parameters employed. It is worth mentioning that in this case not fully dense materials could be obtained due to the open porosity.

The bending stress–strain behaviour of the P&S Ti–6Al–4V alloy can be improved by HIP, attaining a material with a higher plastic deformation before fracture. The changes of maximum bending strength or UTS mean values, as well as ductility, greatly depend on the combination of the level of relative density, percentage of contaminants and microstructural features. This is due to the fact that a HIP process carried out in the $\alpha + \beta$ field (850ºC) induces an increment of the amount of alpha phase reducing the relative amount of $\alpha + \beta$ lamellae.

On the other side, a processing temperature of 1000ºC, which is located just above the beta transus, in the beta field, provokes the formation of transformed beta zones characterised by fine regions of α + β lamellae. There is also a contribution from the powder production route where the master alloy addition powder seems to have slightly coarser microconstituents.

Conventional Hot–pressing (HP): the processing of Ti64–PA and Ti64–MA powders by conventional hot–pressing allows to obtain relative density comparable to that of HIPed samples (approximately 98%) regardless of the powder production route.

There is a strong interaction between the processed powder and the BN coating used to avoid the interaction with the graphite die which leads to the formation of a reaction layer on the sample surface, formed by titanium nitrides and borides, that gets thicker with the increment of the processing temperature.

The removal of the reacted layer increases the maximum bending strength from 200 MPa to 660 MPa depending on the processing parameters and the mean values are, normally, similar to those of pressing and sintering samples.

The processing temperature of 900ºC does not guarantee the formation of homogeneous microstructures since undissolved particles can be identified whereas at higher processing temperatures (1100ºC and 1300ºC) the microconstituents are alpha grains and α + β lamellae typical of a slow cooling of this alloy.

Inductive Hot–pressing (IHP): when the heating of the specimens during hot–pressing is supplied by an induction current, fully dense materials can be obtained with very short processing time for the two processing temperatures studied. However, to permit the complete diffusion of the alloying elements and to reach a homogeneous microstructure, the processing temperature of 1300ºC must be employed.

The final amount of interstitials dissolved in inductive hot–pressed Ti64–PA and Ti64–MA specimens is similar to that of HP samples and the hardness of IHP results to be slightly higher than that of HP, most probably due the appearance of acicular alpha in the microstructure due to the fast cooling characteristic of this manufacturing method.

6.4 – Ti–6Al–7Nb ALLOY

This section deals with the discussion of the results obtained through the processing by different P/M techniques and the characterisation of the biomedical Ti–6Al–7Nb alloy produced by master alloy addition.

6.4.1 – Uniaxial Pressing and Sintering (P&S)

6.4.1.1 – Relative Density

As for the other materials studied, it is interesting to know some physical parameters such as the green density (85.98% ± 1.18%), the shrinkage, which increases with the temperature and it is greater for longer sintering times ranging from 8% to 10.5%, and the densification of the samples (60–74%) to better understand the behaviour of the alloy.

The variation of the relative density with the sintering conditions (temperature and time) is presented in Figure 6.168.

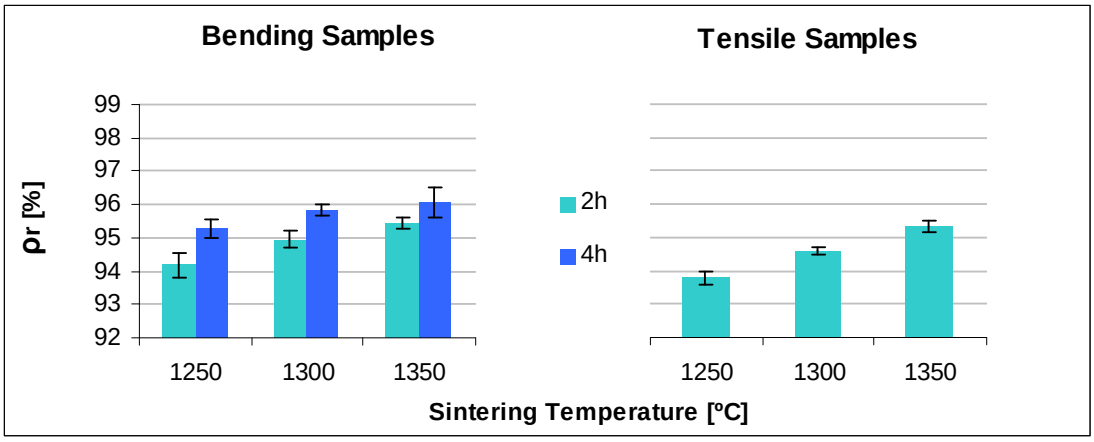

Figure 6.168 – Relative density as a function of the sintering temperature and time for Ti–6Al–7Nb specimens: bending (left) and tensile (right).

As it can be seen in Figure 6.168, the relative density of the Ti–6Al–7Nb alloy increases with the sintering temperature for both processing times ranging from 94% to 96% where the increment seems to be slightly higher from 1250ºC to 1300ºC than from 1300ºC to 1350ºC.

On the other side, the final relative density of the tensile test specimens (Figure 6.168–right) increases with the sintering temperature and the values are similar to those of the three–point bending test samples.

In general, the values obtained for both bending and tensile samples resemble those of the other materials pressed at 700 MPa and, in particular, those of Ti64–MA (Figure 6.110). As for this last alloy, the densification of Ti67–MA could have been limited by the formation of the titanium aluminade ($TiAl_3$)[53, 57, 58] which is possible due to the presence of some elemental aluminium in the starting powder even though this phase was not detected during the XRD analysis of sintered samples (Figure 5.14).

6.4.1.2 – Chemical Analysis

The results of the chemical analysis (oxygen and nitrogen) carried out on the sintered samples is displayed in Figure 6.169 and Figure 6.170 for bending and tensile specimens, respectively.

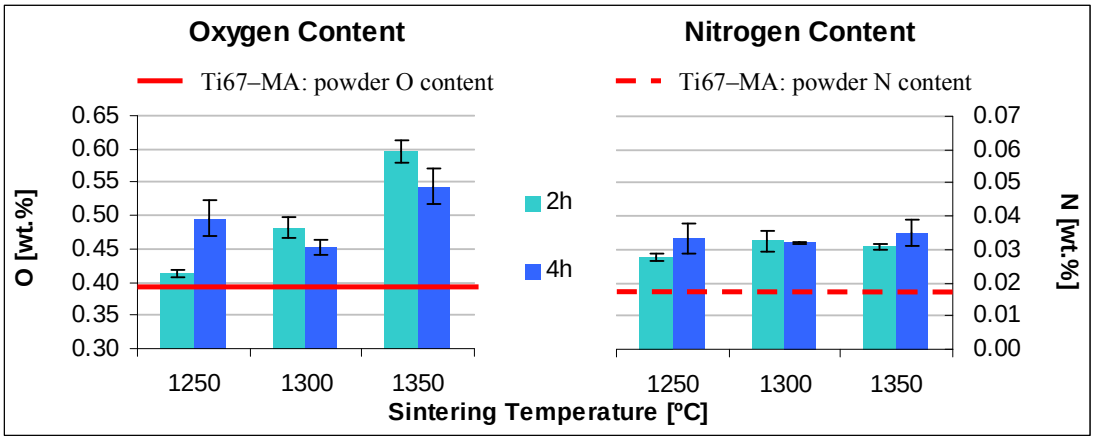

Figure 6.169 – Chemical analysis as a function of the sintering temperature and time for Ti–6Al–7Nb bending specimens: oxygen (left) and nitrogen (right).

As it can be seen in Figure 6.169, oxygen content increases with the sintering temperature whereas nitrogen content stays approximately constant. In all the cases oxygen and nitrogen content of sintered samples is higher than that of the powder, once again due to the handling of the powder and the elements adsorbed onto the surface of the powder particles.

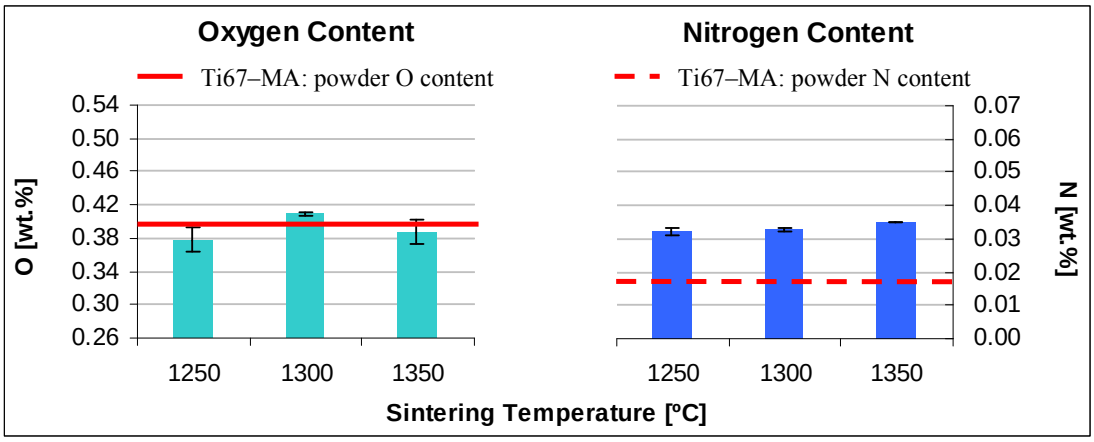

Figure 6.170 – Chemical analysis as a function of the sintering temperature and time for Ti–6Al–7Nb alloy tensile specimens: oxygen (left) and nitrogen (right).

The chemical analysis data shown in Figure 6.170 reveals that tensile samples have lower final oxygen and very similar nitrogen content, both practically constant with the sintering temperature, with respect to the bending specimens. Compared to the initial amount of these elements present in the starting powder, it can be seen that there is just very small nitrogen pick–up.

6.4.1.3 – Hardness

Figure 6.171 shows the results of the hardness measurements carried out on Ti67–MA specimens sintered under different sintering conditions.

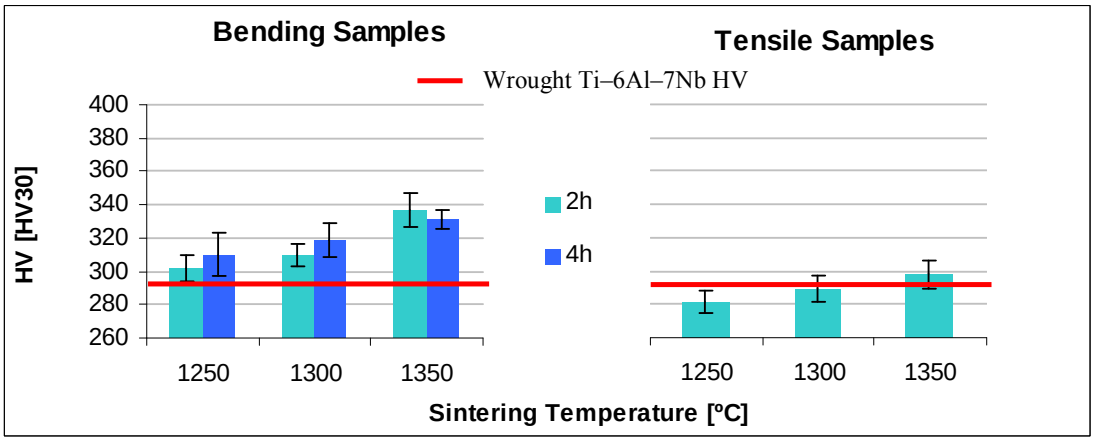

Figure 6.171 – Hardness as a function of the sintering temperature and time for Ti–6Al–7Nb specimens: bending (left) and tensile (right).

The hardness of Ti67–MA (Figure 6.171) increases with the processing temperature and it is slightly higher for longer dwell time with the exception of 1350°C–4h which is lower than 1350°C–2h.

On the other side, the hardness of tensile specimens increases with the sintering temperature and it is, normally, 20 HV30 lower than the rectangular bending samples. The trend found and the differences between the two types of specimens are mainly due to the lower amount of interstitials, specially, oxygen in tensile samples.

The values of hardness obtained on bending samples are in between the hardness specified for medical devices (290 HV)[59] and that specified for the wrought alloy by Semlitsch et al. (350 HV)[75].

Figure 6.172 shows the correlation between Vickers hardness and equivalent oxygen content calculated by Okazaki and Conrad's relationship[11] (Eq. 14 in Section 2.7).

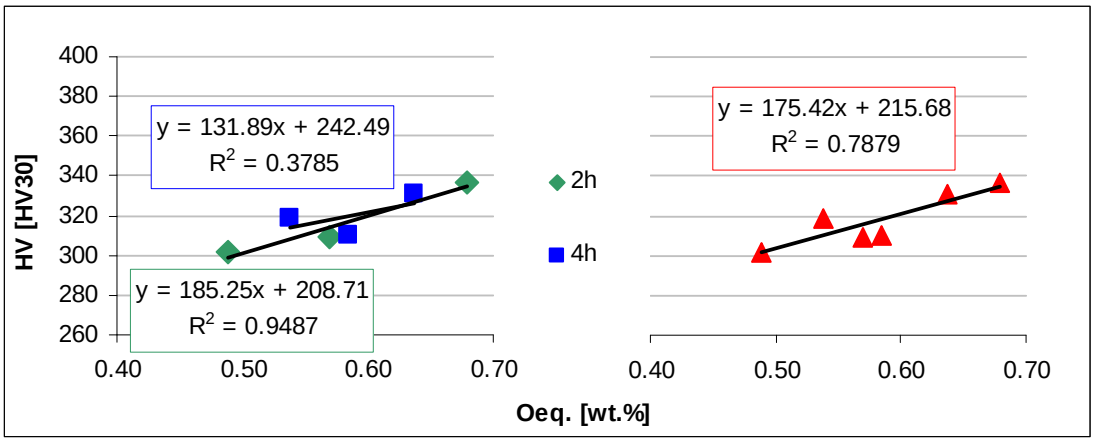

Figure 6.172 – Hardness as a function of equivalent oxygen content for Ti–6Al–7Nb bending specimens: for diverse sintering times (left) and general trend (right).

The Vickers hardness versus equivalent oxygen content analysis for the Ti–6Al–7Nb alloy obtained by pressing and sintering (Figure 6.172) confirms that the hardness of this alloy increases with the increment of the interstitial elements dissolved inside the matrix, being the linear correlation better for specimens sintered for 2 hours.

6.4.1.4 – Properties from Bending Test

A representative example of the bending stress–strain curves for each one of the processing condition studied, obtained by the three–point bending test, is presented in Figure 6.173.

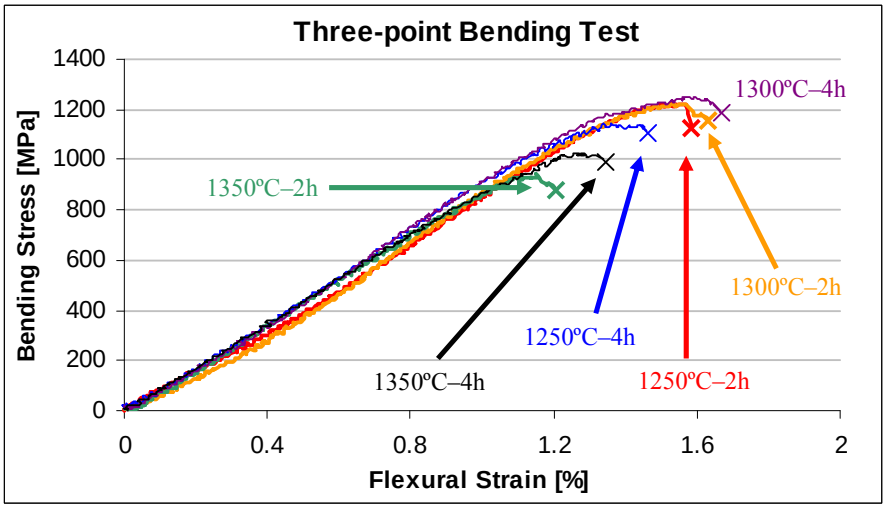

Figure 6.173 – Representative bending stress–strain curves for Ti–6Al–7Nb specimens.

The bending stress–strain curves shown in Figure 6.173 indicate that the material shows predominantly an elastic behaviour with a very little plastic deformation before rupture, like the other α + β titanium alloy studied (Ti–6Al–4V).

The mean flexural modulus measured on the curves results to be 97 GPa with a standard deviation of ± 6 GPa very similar to that found for the Ti–6Al–4V alloy.

The maximum bending strength and flexural strain variation for the various sintering temperatures and times is presented in Figure 6.174.

As it can be seen in Figure 6.174, the maximum bending strength decreases with the sintering temperature for 2 hours of sintering, whilst it increases from 1250ºC to 1300ºC and then decreases, for 4 hours.

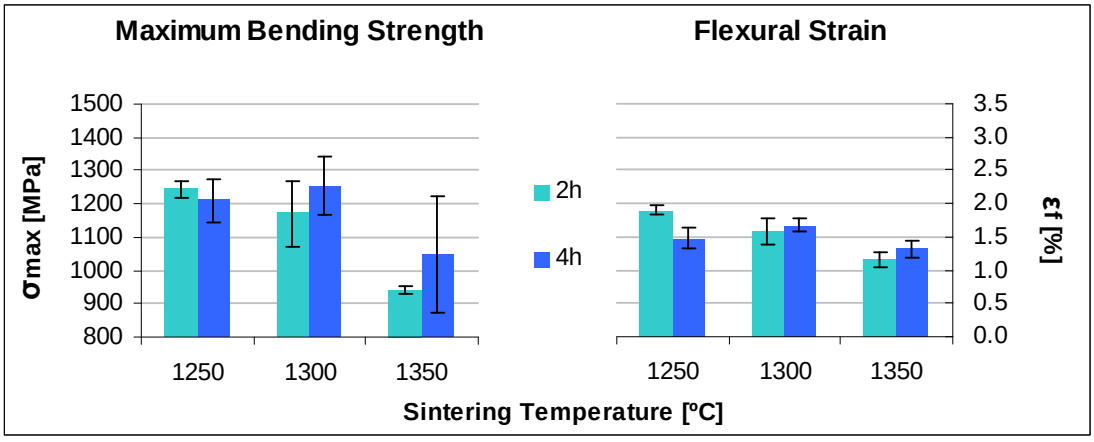

Figure 6.174 – Mechanical properties as a function of the sintering temperature and time for Ti–6Al–7Nb specimens: maximum bending strength (left) and flexural strain (right).

This general trend is affected by the content of interstitials and, therefore, the maximum bending strength of 1300°C and 1350°C–4h is higher than that of 1300°C and 1350°C–2h because these last ones have higher oxygen content and, as shown for the other alloys, the higher the equivalent oxygen content, the lower the maximum bending strength. Furthermore, the values obtained are, at least comparable, or higher than that found in the literature, precisely 990 MPa, obtained in wrought Ti–6Al–7Nb biomedical devices[59].

The same statements can be applied to the flexural strain since it decreases from 2% to 1.2% with the sintering temperature (for 2h) and it slightly increases to 1.7% and then decreases to 1.3% for 4 h showing a strong dependence on oxygen content.

The relationship between maximum bending strength and flexural strain with the amount of interstitials can be better studied through the correlation with the equivalent oxygen content, as shown in Figure 6.175 and Figure 6.176, respectively.

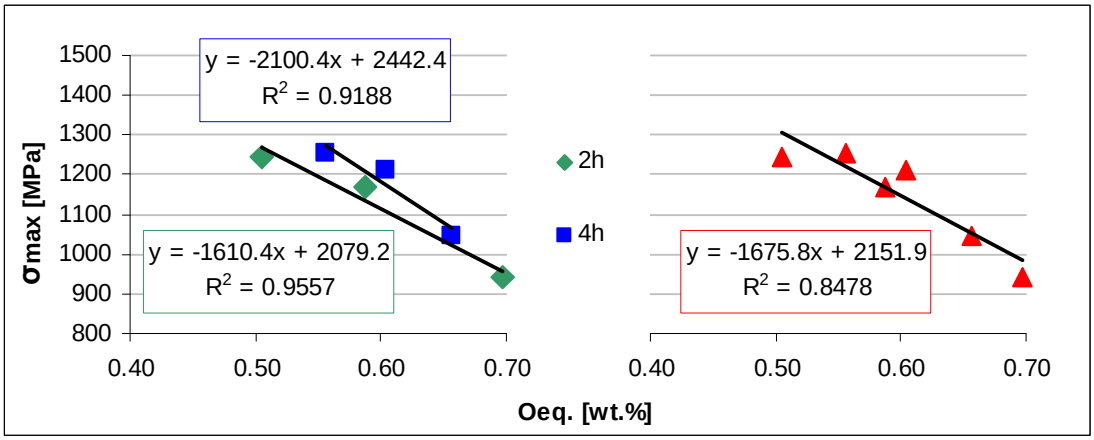

Figure 6.175 – Maximum bending strength as a function of the equivalent oxygen content for Ti–6Al–7Nb bending specimens: for diverse sintering times (left) and general trend (right).

As it can be seen in Figure 6.175, there is a very strong correlation between the maximum bending strength and the equivalent oxygen content, where the maximum bending strength decreases with the increment of the interstitial elements, even though the strengthening effect of oxygen and nitrogen[5, 6], as it was for the other materials.

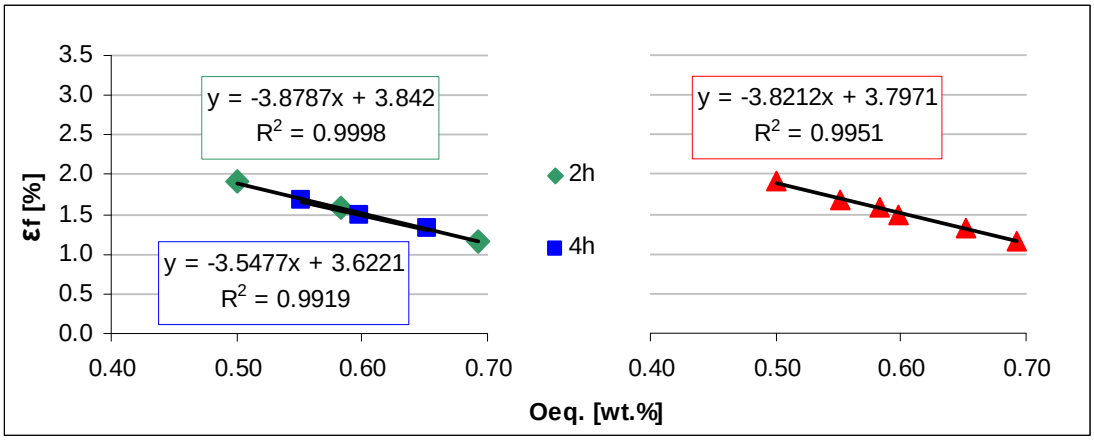

Figure 6.176 – Flexural strain as a function of the equivalent oxygen content for Ti–6Al–7Nb bending specimens: for diverse sintering times (left) and general trend (right).

An even stronger linear correlation could be found between the amount of interstitial elements dissolved into the Ti–6Al–7Nb matrix and its flexural strain since the R^2 coefficient is close to 1 as shown in Figure 6.176. As expected, the higher the contamination of the specimens the lower the ductility of the material since either oxygen or nitrogen brittles titanium alloys[5-7].

6.4.1.5 – Properties from Tensile Test

Representative examples of tensile stress–strain curves showing the behaviour of the Ti–6Al–7Nb alloy submitted to tensile test are displayed in Figure 6.177.

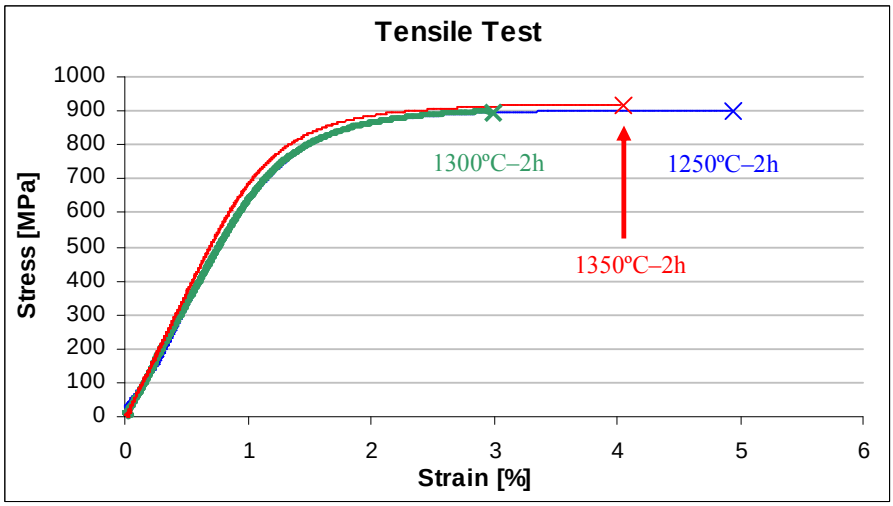

Figure 6.177 – Representative tensile stress–strain curves for Ti–6Al–7Nb specimens.

The tensile stress–strain curves of the Ti–6Al–7Nb alloy (Figure 6.177) sintered in the 1250–1350ºC range for 2 hours are all composed by an elastic deformation followed by plastic deformation until fracture.

Dynamic Young modulus measured on these specimens is equal to 101 ± 25 GPa, which is very similar to the nominal value of 105 GPa[9]. The high standard deviation is due to some abnormal data which could have been affected by the residual stress of some samples.

The mean values of the ultimate tensile strength (UTS) and strain obtained from the tensile testing of the Ti–6Al–7Nb alloy are shown in Figure 6.178.

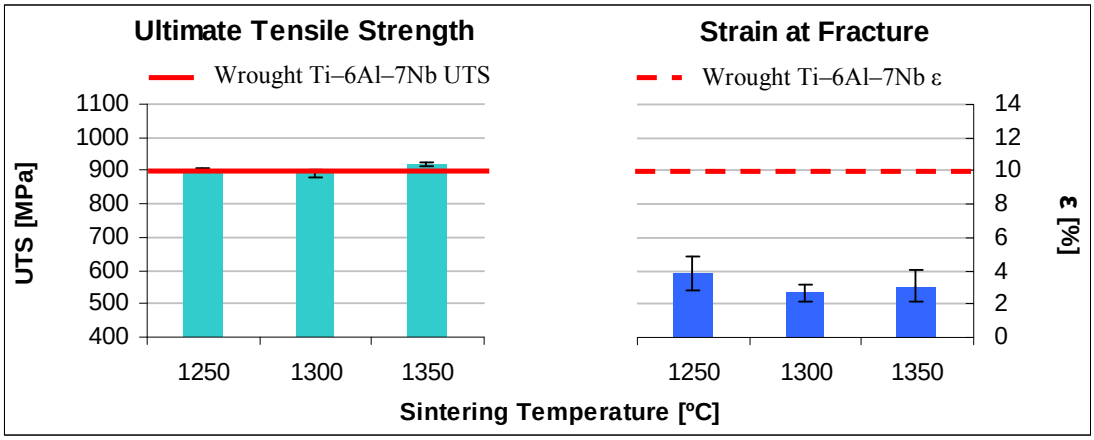

Figure 6.178 – Mechanical properties as a function of the sintering temperature and time for Ti–6Al–7Nb specimens: ultimate tensile strength (left) and strain (right).

As it can be seen in Figure 6.178, the UTS remains constant at around 900 MPa with the sintering temperature with very low standard deviation. This indicates that the strengthening effect of the interstitials and the benefit of the higher relative density could be balanced by the grain growth.

Furthermore, the UTS of Ti67–MA is similar to that of the wrought alloy (900 MPa) or that obtained by Itoh et al.[76] (approximately 850 MPa) when processing by metal injection moulding a spherical elemental titanium powder mixed with an Al:Nb master alloy (sintering range similar to that shown in Figure 6.178).

On the other hand, the ductility of the Ti–6Al–7Nb alloy decreases with the increment of the sintering temperature even thought the samples processed at 1300ºC has somewhat lower strain than those sintered at 1350ºC. In this case, it seems that the content of interstitials has a stronger effect.

As expected, the strain of the P/M Ti–6Al–7Nb is lower with respect to the wrought alloy due to the residual porosity and the high oxygen percentage. Nonetheless, similar results in terms of strain were obtained when casting the Ti–6Al–7Nb alloy in a silica–based mould (1–3 %)[77].

6.4.1.6 – Microstructural Analysis

Images of the Ti–6Al–7Nb alloy sintered under different conditions taken by optical microscopy are shown in Figure 6.179.

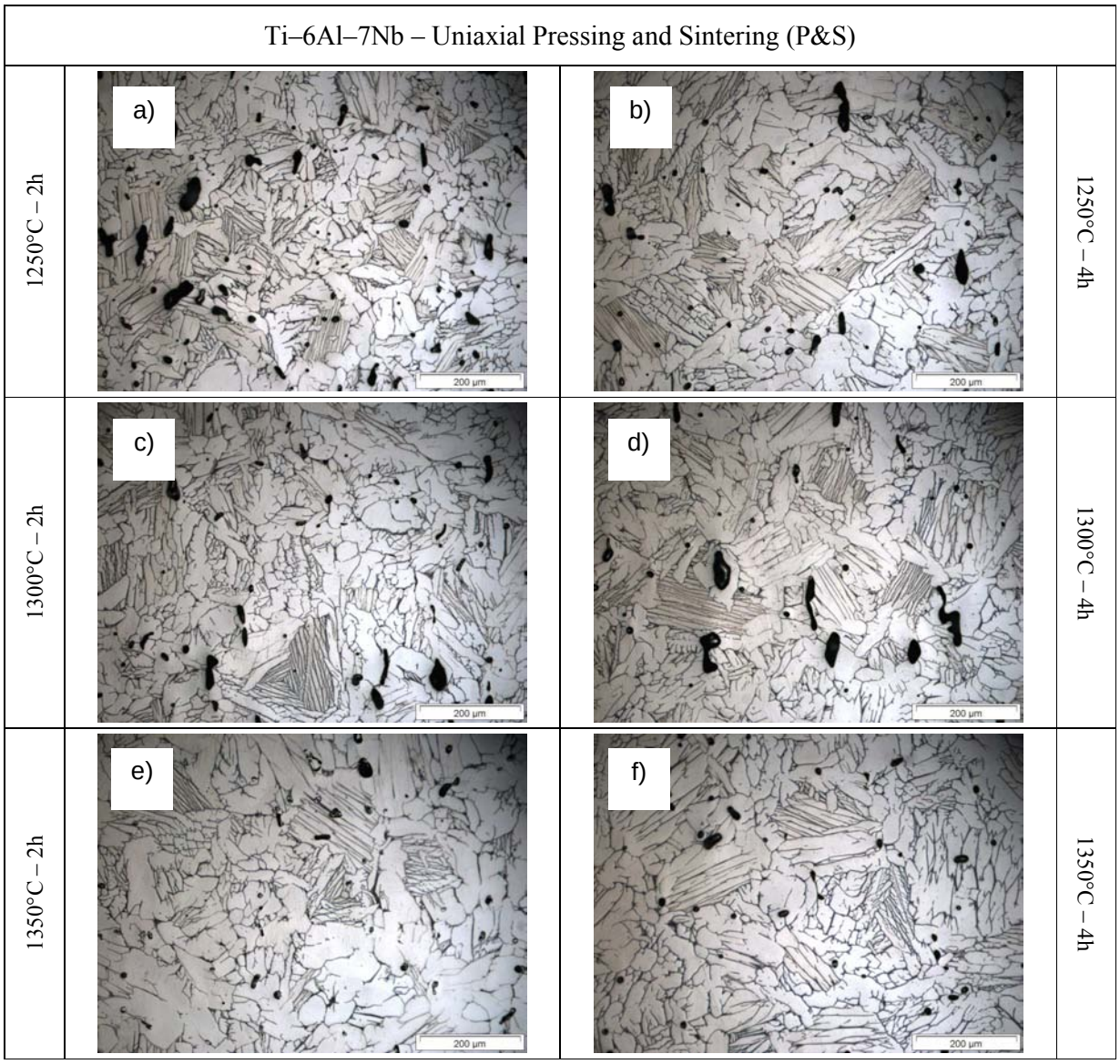

Figure 6.179 – Optical microscopy images for Ti–6Al–7Nb sintered at: a) 1250°C–2h, b) 1250°C–4h, c) 1300°C–2h d) 1300°C–4h, e) 1350°C–2h and f) 1350°C–4h.

Microstructural analysis (Figure 6.179) indicates that the residual porosity diminishes with the increment of the sintering temperature and time, corresponding to a higher relative density, and gets more spherical in shape.

The microstructural constituents of the Ti–6Al–7Nb alloy are elongated alpha grains, whose size increases significantly with the processing temperature, and very fine α + β lamellae distributed throughout the microstructure. Furthermore, the alpha mean grain size of the Ti–6Al–7Nb alloy processed by P&S seems to be coarser than the one obtained in the Ti–6Al–4V alloy, both Ti64–PA and Ti64–MA (Figure 6.128 and Figure 6.129).

As in the case of the other titanium alloys studied in this thesis, a fractographic study of the tensile specimens was carried out and the results are shown Figure 6.180.

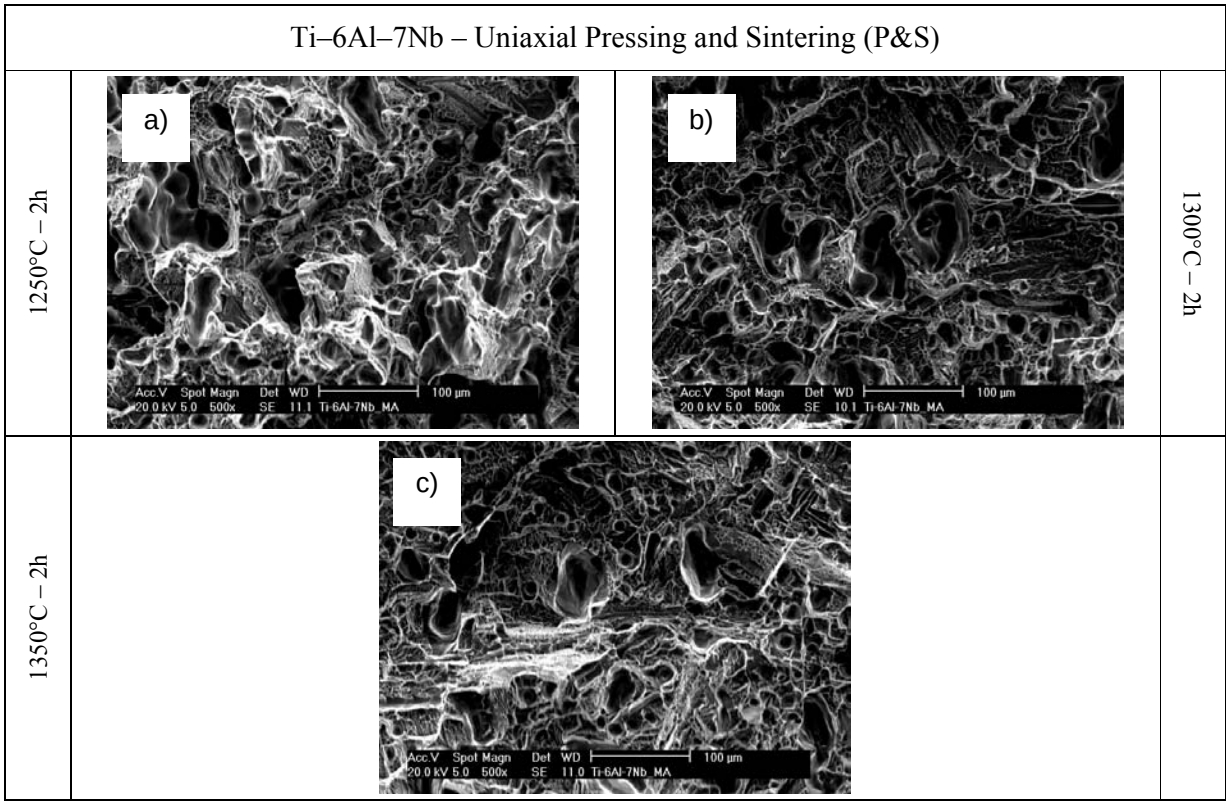

Figure 6.180 – Fracture surface from tensile test specimens for Ti–6Al–7Nb sintered for 2 hours at: a) 1250ºC, b) 1300ºC and c) 1350ºC.

The fractography study (Figure 6.180) reveals that the materials fail in a ductile way as the fracture surface is composed by dimples. From the shape of these conical dimples it seems that they were generated from the residual porosity (pore–assisted fracture). During the analysis, no cleavage zones could be found in the fracture surfaces.

6.4.1.7 – Thermal Conductivity

Thermal properties such as the thermal conductivity at room temperature as well as the variation of this property with the temperature up to 300ºC were also determined in the pressed and sintered specimens obtained from the Ti–6Al–7Nb alloy.

The results of these characterisations are presented as a function either of the relative density or the equivalent oxygen content, calculated on the basis of the equation proposed by Conrad[23], and divided by the processing time.

Thermal conductivity at room temperature data, obtained by infrared measurements, are shown in Figure 6.181.

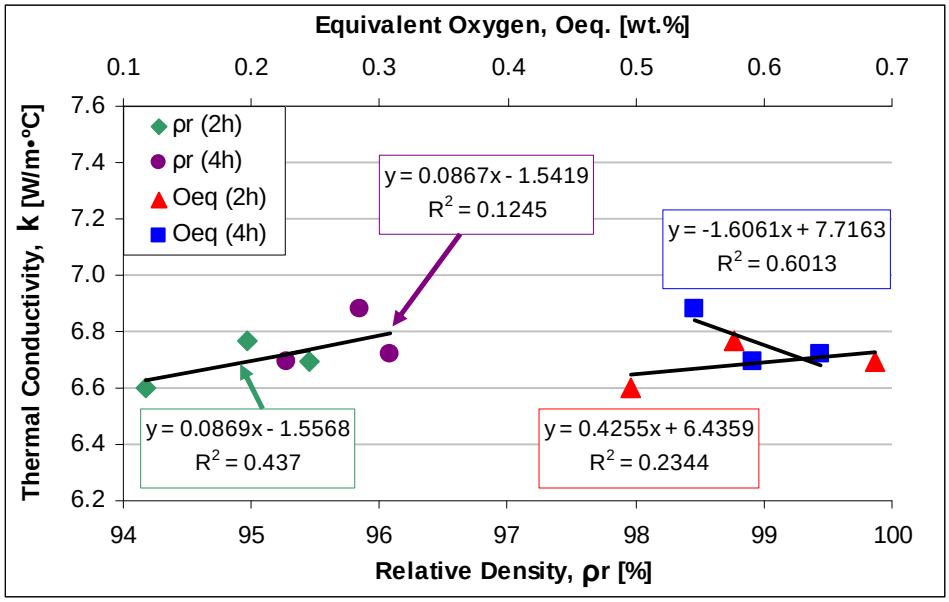

Figure 6.181 – Thermal conductivity at room temperature as a function of the relative density and equivalent oxygen content for Ti–6Al–7Nb specimens.

Analysing the thermal conductivity at room temperature of the Ti–6Al–7Nb alloy (Figure 6.181), it can be noticed that this property increases with the relative density (left side).

When considering the trend of the thermal conductivity versus the equivalent oxygen content (right side) two diverse behaviours are found: k increases with the equivalent oxygen content for 2 hours sintering whereas it decreases for 4 hours. It is worth mentioning that excluding the thermal conductivity of the components sintered at 1250ºC during 2 hours which have an equivalent oxygen content somewhat lower than 0.50 wt.%, the thermal conductivity decreases with the amount of interstitial elements dissolved into the matrix.

In comparison to the wrought Ti–6Al–7Nb alloy obtained by the conventional route (see Table 6.7), Ti67–MA specimens have slightly lower but comparable thermal conductivity value. The lower values are most probably due to the combination of various parameters such as the presence of residual porosity, the content of interstitials and the microstructural features.

Table 6.7 – Comparison of thermal conductivity at room temperature values between wrought and P/M Ti–6Al–7Nb alloy.

Ti–6Al–7Nb				
Wrought[8]		**P/M**		
k [W/m·ºC]	Chemical analysis [wt.%]	k [W/m·ºC]	Chemical analysis [wt.%]	Sintering conditions
7.0	O = 0.20 N = 0.05	6.60	O = 0.412 N = 0.028	1250ºC – 2h
		6.77	O = 0.482 N = 0.033	1300ºC – 2h
		6.69	O = 0.596 N = 0.031	1350ºC – 2h
		6.69	O = 0.496 N = 0.033	1250ºC – 4h
		6.88	O = 0.453 N = 0.032	1300ºC – 4h
		6.72	O = 0.544 N = 0.035	1350ºC – 4h

The samples sintered at 1250ºC during 2 hours were also employed to determine the variation of the thermal conductivity with the temperature. The trend of the data obtained by the IR "measurements" are compared in Figure 6.182 with that of the thermal conductivity "calculated" in order to consider the effect of the temperature on the specific heat and that found in the literature[59].

It is worth remembering that the Ti–6Al–7Nb alloy was developed specifically to produce femoral components for hip prostheses[8, 59, 78] and, therefore, no thermal conductivity data versus the temperature are available in the literature. For comparison, the equation for the C_p of alpha titanium (Section 2.6.8) seems to be a good approximation for $\alpha + \beta$ titanium alloys and it was used to calculate the data shown in Figure 6.182.

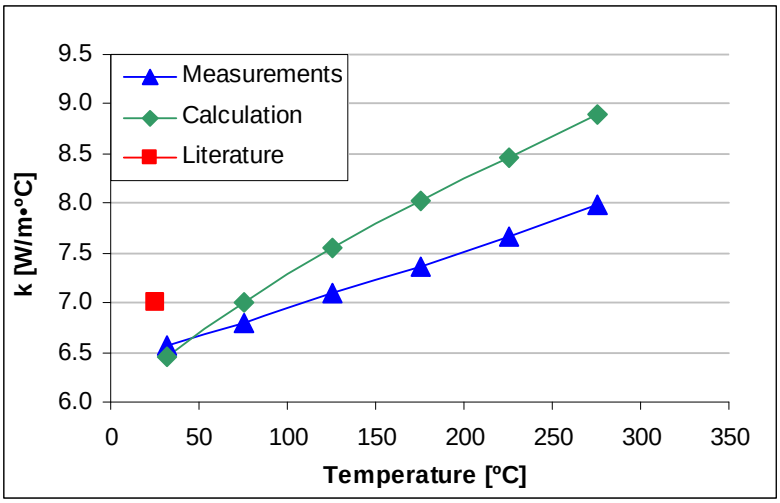

Figure 6.182 – Thermal conductivity as a function of temperature for Ti–6Al–7Nb specimens.

The infrared measurements of the thermal conductivity (Figure 6.182) indicates that this property increases with the temperature from approximately 6.6 W/m·ºC at room temperature to 8.0 W/m·ºC at 300ºC. This increment is mainly due to the thermal energy supplied to the system, which results in a higher mobility (longer mean free path) of electrons and phonons through the material in this range of temperature.

When considering the effect of the temperature on the specific heat (calculation), the same trend is obtained but the discrepancy between the measured and calculated values gets more and more evident as at 300ºC the difference is already of almost 1 W/m·ºC.

As it has been said, there are not values available in the literature for the comparison with the wrought alloys. Based on the results shown and on the data available for the α + β Ti–6Al–4V alloy (Figure 6.133), a similar trend but with slightly higher values, due to the lack of residual porosity, is expected for the wrought Ti–6Al–7Nb alloy.

6.4.1.8 – Electrical Resistivity

Like for the other materials, the electrical resistivity was measured by means of the van der Pauw method[25, 26] (see Section 2.6.9) and the results are presented in Figure 6.183 versus either the relative density or the equivalent oxygen content.

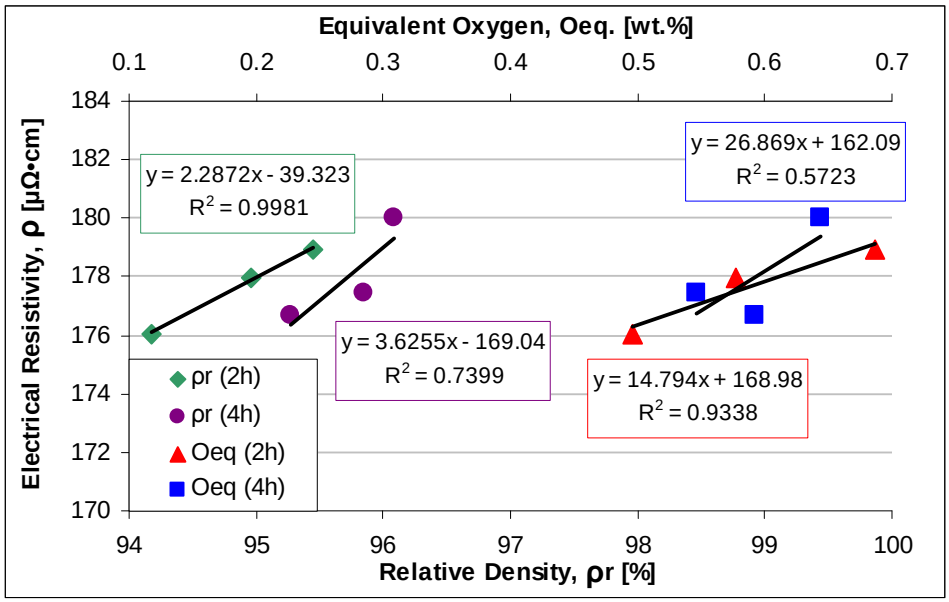

Figure 6.183 – Electrical resistivity at room temperature as a function of the relative density and equivalent oxygen content for Ti–6Al–7Nb specimens.

The analysis of the data shown in Figure 6.183 indicates that the increment of both the relative density and the equivalent oxygen content leads to a higher resistivity, which can be well estimated by a linear regression.

When comparing the data divided by the sintering time, it can be noticed that a longer processing time leads to a steeper linear regression with a greater scattering of the values most probably due to the stronger influence on the microstructural features such as grain growth or pore coarsening.

As it can be seen in Table 6.8, the electrical resistivity of Ti67–MA components is, on average, approximately 20 μΩ·cm higher compared to that of the wrought alloy due to the residual porosity and the greater amount of dissolved interstitials which obstruct the movement of the electrons.

Table 6.8 – Comparison of electrical resistivity values between wrought and P/M Ti–6Al–7Nb alloy.

Ti–6Al–7Nb				
Wrought[8]		**P/M**		
ρ [μΩ·cm]	Chemical analysis [wt.%]	ρ [μΩ·cm]	Chemical analysis [wt.%]	Sintering conditions
158.0	O = 0.20 N = 0.05	176.1	O = 0.412 N = 0.028	1250ºC – 2h
		178.0	O = 0.482 N = 0.033	1300ºC – 2h
		179.0	O = 0.596 N = 0.031	1350ºC – 2h
		176.7	O = 0.496 N = 0.033	1250ºC – 4h
		177.5	O = 0.453 N = 0.032	1300ºC – 4h
		180.0	O = 0.544 N = 0.035	1350ºC – 4h

6.4.2 – Hot Isostatic Pressing (HIP)

The HIP cycles used to study the influence of the processing parameters on the physical and mechanical properties of the three–point bending test specimens are the same as for the other titanium alloys:

- ✓ **HIP–1**: T = 1000ºC, P = 100 MPa , t = 20 min — Reference conditions
- ✓ **HIP–2**: T = 1000ºC, P = 100 MPa, t = 2 h — To study the influence of time
- ✓ **HIP–3**: T = 850ºC, P = 100 MPa, t = 20 min — To study the influence of temperature
- ✓ **HIP–4**: T = 850ºC, P = 200 MPa, t = 20 min — To study the influence of pressure

It is worth mentioning that, opposite to the other materials studied, the processing of the Ti–6Al–7Nb alloy at 1000°C means that this alloy is still in the α + β field just below its beta transus (1010ºC).

6.4.2.1 – Relative Density

The results of the relative density measured on HIPed components are displayed in Figure 6.184.

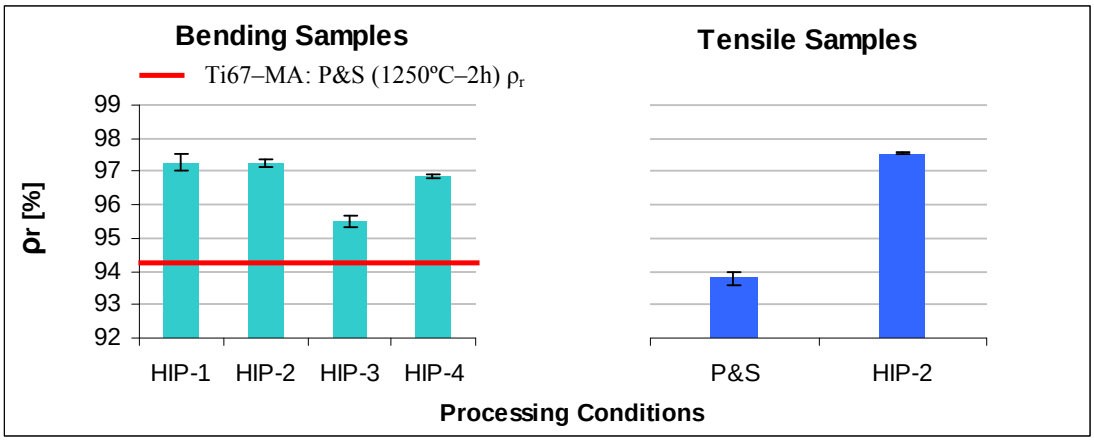

Figure 6.184 – Relative density as a function of the HIP cycle for Ti–6Al–7Nb specimens: bending (left) and tensile (right).

As it can be seen in Figure 6.184, the post–processing of the P&S Ti–6Al–7Nb specimens by HIP always leads to an increment of the final relative density at around 97% with the exception of (HIP–3). This behaviour was already found in the other titanium alloys studied.

Compared to the P&S samples, the HIP process always induces a minimum increment of relative density of 1.3% that can be, then, increased up to 3% reaching a final relative density of approximately 97%.

As for the three–point bending test samples, the application of a HIP process to tensile test specimens (Figure 6.184–right) leads to an increment of relative density up to 97.5%.

Once again, not fully dense materials are obtained after HIP due to the open porosity left in the specimens. The values of relative density shown in Figure 6.184 are similar to those of the Ti–6Al–4V alloy (Figure 6.136).

6.4.2.2 – Chemical Analysis

As for the other materials, oxygen and nitrogen content of the specimens post–processed by HIP was measured in order to point out possible variations with respect to as–sintered material and the results are reported in Figure 6.185 and Figure 6.186.

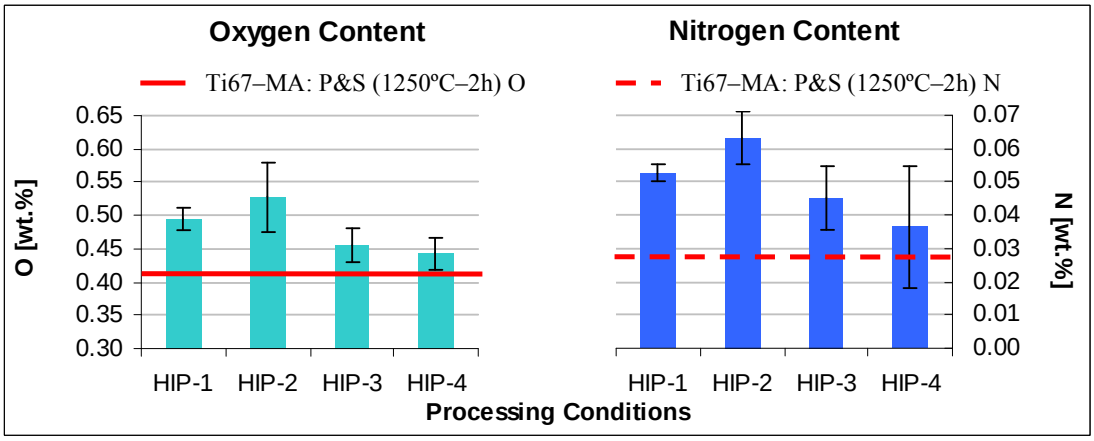

Figure 6.185 – Chemical analysis as a function of the HIP cycle for Ti–6Al–7Nb bending specimens: oxygen (left) and nitrogen (right).

As it can be seen in Figure 6.185, oxygen and nitrogen content of the Ti–6Al–7Nb three–point bending test samples follows the same pattern; their percentage increases with the processing time (HIP–1 and HIP–2) and it is lower for a lower processing temperature (HIP–3 and HIP–4).

In comparison to the amount of these elements in the pressed and sintered specimens, there is always some contamination which varies from 0.03% to 0.11% for oxygen and from 0.009% to 0.035% for nitrogen.

Once gain, this contamination derives from the atmosphere (Ar) used during HIP and it changes from one condition or material to the other also due to the fact that the HIP cycles studied are carried out by batches.

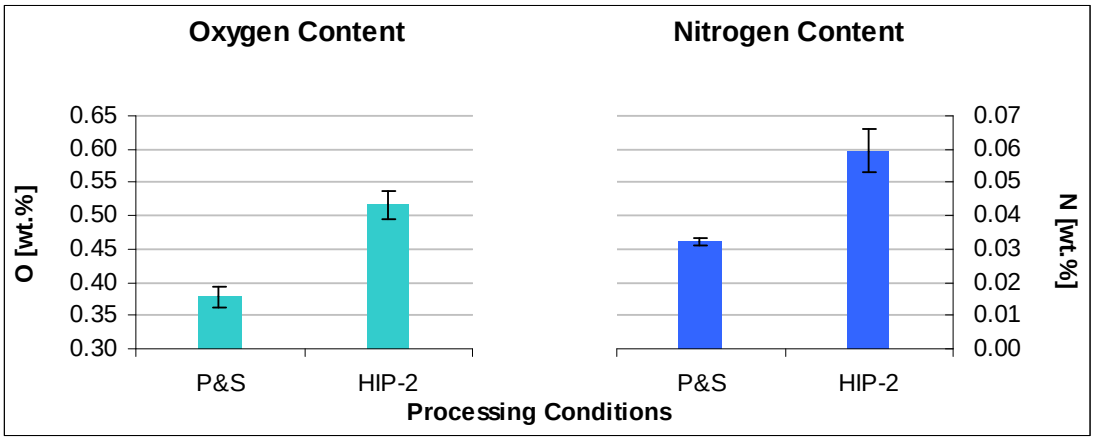

Figure 6.186 – Chemical analysis as a function of the HIP cycle for Ti–6Al–7Nb alloy tensile specimens: oxygen (left) and nitrogen (right).

Regarding the tensile specimens (Figure 6.186), it can be seen that there is a significant contamination from the HIP atmosphere either in terms of oxygen and nitrogen. Nevertheless, the final values are similar to those obtained in bending samples.

6.4.2.3 – Hardness

The results of hardness determined on the Ti–6Al–7Nb HIPed samples are reported in Figure 6.187.

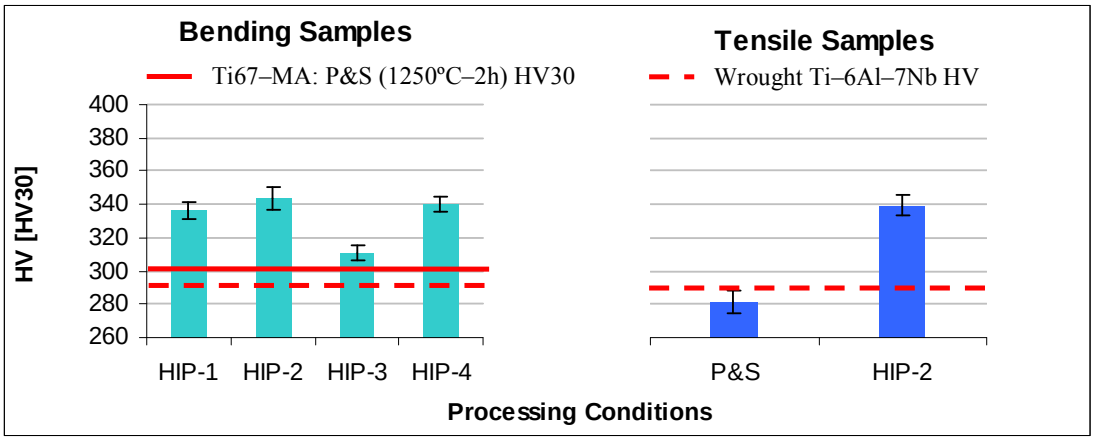

Figure 6.187 – Hardness as a function of the HIP cycle for Ti–6Al–7Nb specimens: bending (left) and tensile (right).

The hardness of the HIPed Ti–6Al–7Nb components follows the same trend of the relative density, indicating that these two properties are related, and it is, generally, higher with respect to the P&S samples. Apart from the HIP–3 cycle, the hardness of HIPed components is approximately 340 HV30 for both bending and tensile samples which is similar to the value specified by Semlitsch et al. (350 HV)[75].

Vickers hardness mean values versus equivalent oxygen content calculated by Okazaki and Conrad's[11] equation (see Eq. 14 in Section 2.7) is shown in Figure 6.188.

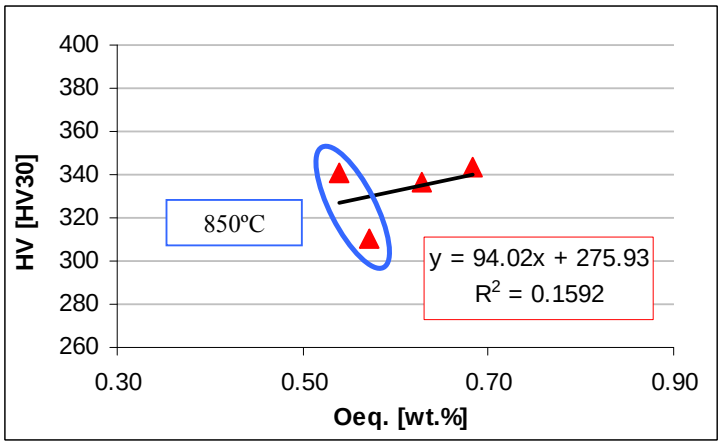

Figure 6.188 – Hardness as a function of equivalent oxygen content for Ti–6Al–7Nb HIPed bending specimens.

Conversely to the other materials processed by HIP studied in this thesis, the hardness of the Ti–6Al–7Nb specimens does not follow a linear relationship since the coefficient of determination R^2 is quite low (Figure 6.188). This is due to the strong effect of the processing temperature on the microstructural features (see Section 6.4.2.6) because analysing the two data available for 850ºC it seems that the hardness decreases with the increment of the equivalent oxygen content.

6.4.2.4 – Properties from Bending Test

The representative bending stress–strain behaviour of the Ti–6Al–7Nb HIPed samples tested by means of the three–point bending tests is shown in Figure 6.189.

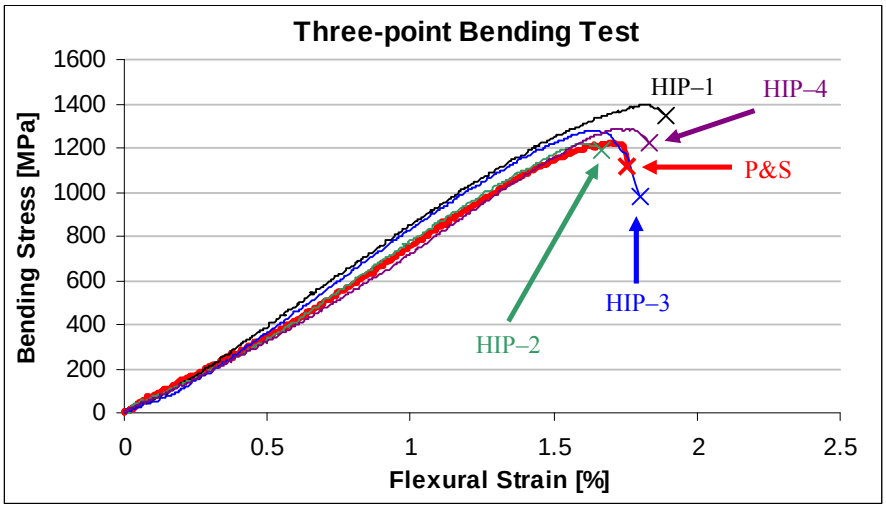

Figure 6.189 – Representative bending stress–strain curves for Ti–6Al–7Nb HIPed specimens.

The flexural stress–strain curves of the Ti–6Al–7Nb HIPed components (Figure 6.189) present an elastic part followed by a small plastic deformation as it was for P&S specimens (Figure 6.173).

The Young modulus mean value calculated for the HIPed samples, 102 ± 8 GPa, is slightly higher with respect to P&S (97 ± 6 GPa) which is most probably due to the lower residual porosity since HIPed specimens have the same dimensions of P&S samples and, therefore, the effect of the L/t ratio can be excluded.

From the three–point bending tests, the maximum bending strength and the maximum flexural strain mean values were obtained and the results are presented in Figure 6.190.

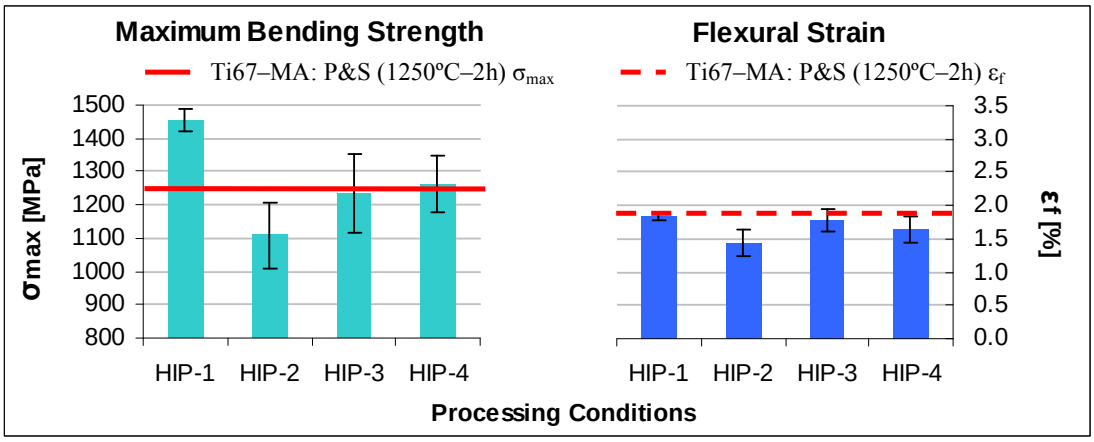

Figure 6.190 – Mechanical properties as a function of the HIP cycle for Ti–6Al–7Nb specimens: maximum bending strength (left) and flexural strain (right).

Theoretically, the higher relative density obtained after the HIP process should lead to a higher maximum bending strength compared to P&S samples; by the way, as it can be seen in Figure 6.190, this happens only for HIP–1 specimens. In particular, the maximum bending strength of HIP–2 samples seems to be significantly lowered by the higher amount of interstitial (Figure 6.185).

On the other hand, when the material is processed at 850ºC there is no improvement most probably because the benefits of a higher relative density are balanced by the microstructural changes induced by a HIP with a temperature in the lower part of the α + β filed (see Section 6.4.2.6).

On the other side, it seems that the HIP process does not lead to any improvement in flexural strain since the values shown in Figure 6.190 are equals or lower than those of as–sintered material.

The analysis of the variation of the mechanical properties determined by means of the three–point bending test with the equivalent oxygen content is presented in Figure 6.191.

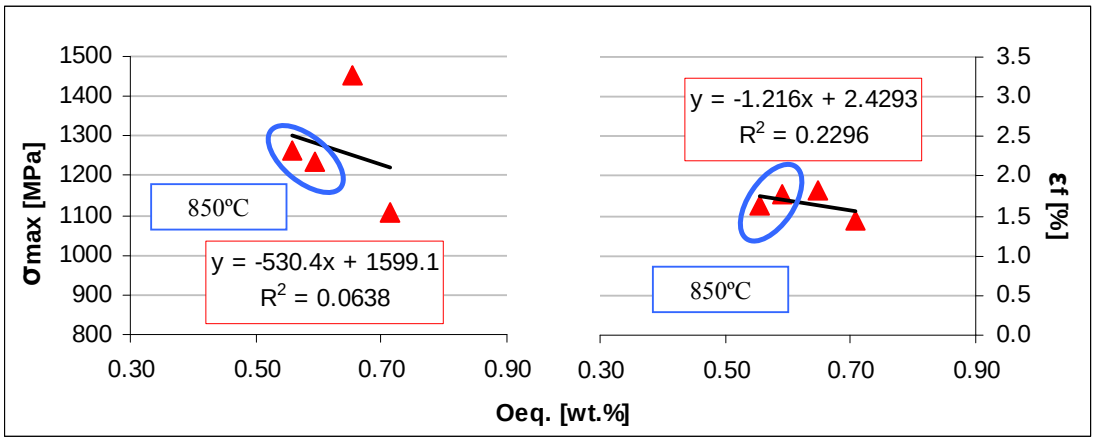

Figure 6.191 – Mechanical properties as a function of the equivalent oxygen content for Ti–6Al–7Nb HIPed bending specimens: maximum bending strength (left) and flexural strain (right).

The low values of R^2 of Figure 6.191 indicates that the mechanical properties of HIPed Ti–6Al–7Nb components are much more influenced from other aspects such as the microstructural features and, therefore, from the selection of the processing temperature, time or pressure than from the amount of elements dissolved inside the matrix.

6.4.2.5 – Properties from Tensile Test

Figure 6.192 shows the stress–strain curves of P&S and HIP samples to compare the tensile behaviour.

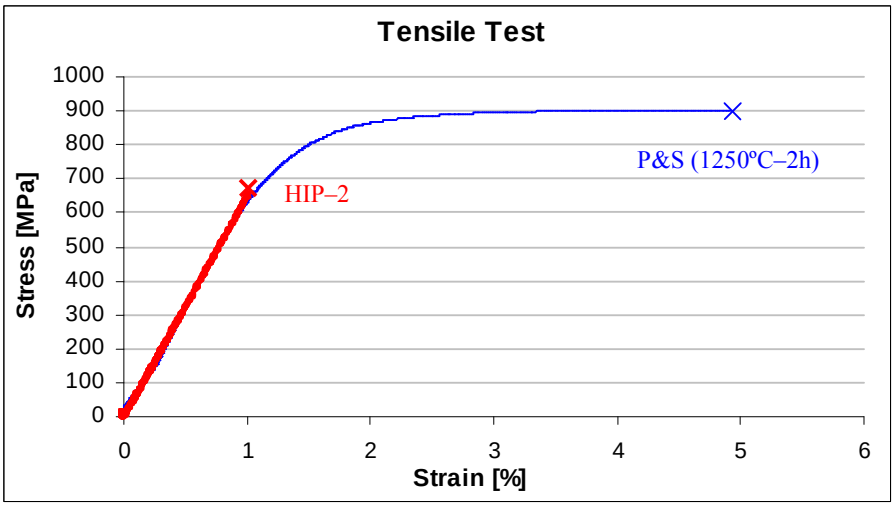

Figure 6.192 – Representative tensile stress–strain curves for Ti–6Al–7Nb P&S (1250ºC–2h) and HIPed specimens.

The tensile stress–strain curves shown in Figure 6.192 indicate that the material deforms elastically without any appreciable plastic yielding before breaking at approximately 700 MPa exactly when it should start to deform plastically as the P&S curve used for comparison reveals. This change in deformation behaviour is most probably a consequence of the higher amount of interstitials determined by the chemical analysis (Figure 6.186) and the changes in terms of microstructural features induced by the HIP process at 1000°C.

The value of Young modulus determined by measuring the speed of the sound through the material, known as dynamic Young modulus, is 115 ± 3 GPa. It can be noticed that the reduction of the residual porosity induced by the HIP process leads to an increment of the dynamic Young modulus compared to that of P&S samples (101 ± 25 GPa).

The ultimate tensile strength and strain mean values determined on the Ti–6Al–7Nb HIPed components compared to the value obtained in the P&S samples and to the value of the wrought alloy are presented in Figure 6.193.

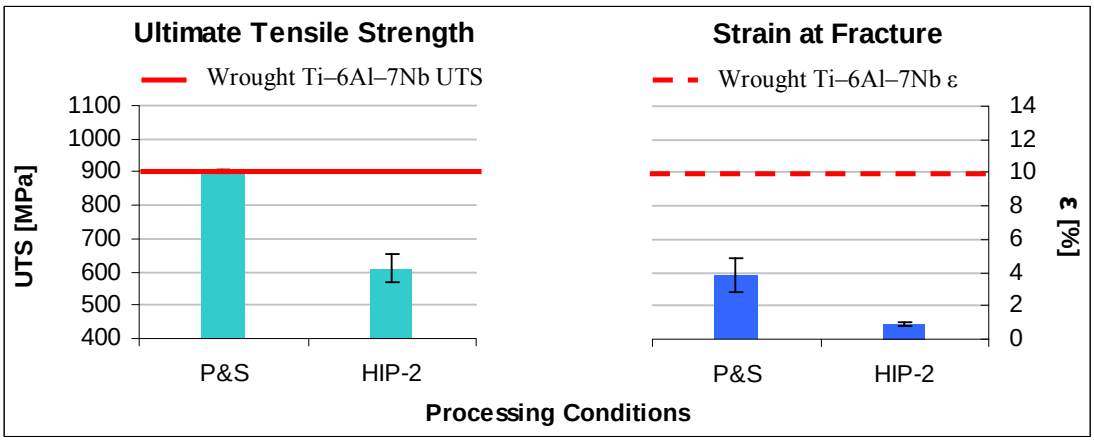

Figure 6.193 – Mechanical properties as a function of the processing method for Ti–6Al–7Nb specimens: ultimate tensile strength (left) and strain (right).

As it can be seen in Figure 6.193, either the UTS or the strain of the HIPed samples drop significantly with respect to the properties determined on the pressed and sintered specimens. This is again most probably due to the higher level of contamination of HIP samples and the changes of the microstructure. A similar behaviour was found in the other α + β titanium alloy, the Ti–6Al–4V (Figure 6.146), whose values of UTS and strain are comparable.

6.4.2.6 – Microstructural Analysis

The results of the microstructural analysis by optical microscopy are shown in Figure 6.194 and the results of the fractographic study in Figure 6.195.

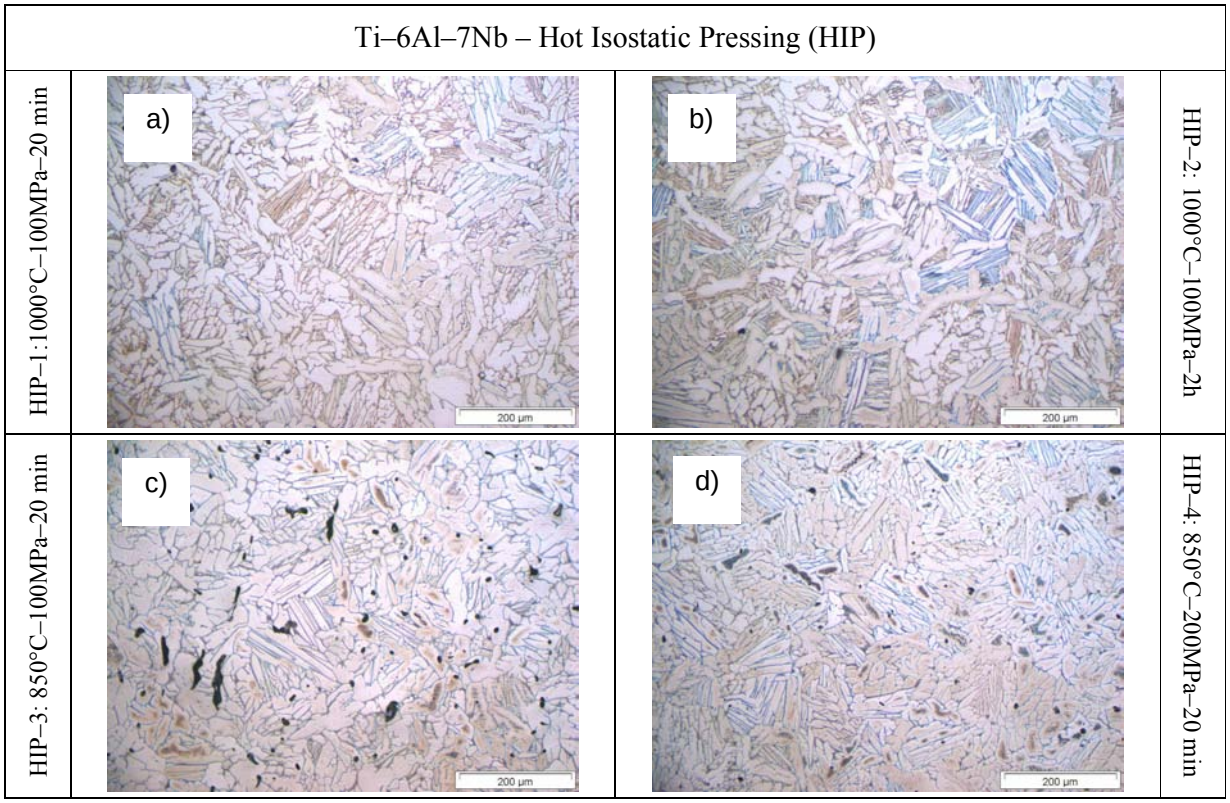

Figure 6.194 – Optical microscopy images for Ti–6Al–7Nb subjected to diverse HIP cycles: a) HIP–1, b) HIP–2, c) HIP–3 and d) HIP–4.

As it can be seen in Figure 6.194 a) and b), a processing temperature of 1000ºC, near the beta transus, leads to a microstructure constituted by primary alpha grains and areas of fine α + β lamellae (transformed beta). This microstructure resembles a bimodal microstructure normally attained by heat treatment, such as air cooling from high temperatures in the α + β region[22], instead of a slow–cooled microstructure. The presence of some acicular alpha in conjunction with the higher percentage of contaminants found for HIP–2 condition explain the lower tensile properties of these specimens (Figure 6.193).

In the case of HIP–3 and HIP–4 (processed at 850ºC) the microstructure is significantly different with respect to the other processing conditions since it is far below the beta transus and, consequently, composed primarily by alpha grains and the increment of the applied pressure seems to refine the microstructure. This could explain the slightly higher maximum bending strength and somewhat lower flexural strain of HIP–4 samples compared to HIP–3 ones, which, besides, have higher percentage of residual porosity.

Comparing the microstructure of the Ti–6Al–7Nb alloy obtained by uniaxial pressing and sintering (Figure 6.179 a) with that of the same alloy post–processed by HIP, it can be noticed that the microstructure of samples HIPed at 850ºC is similar to P&S ones, although both alpha grain size and α + β lamellae seem to be finer. The main changes are observed for samples processed at 1000ºC.

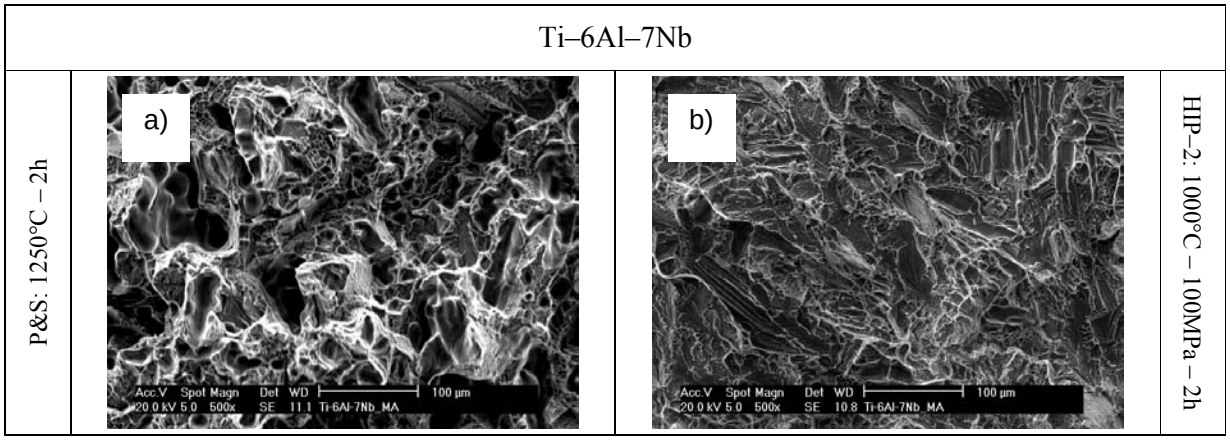

Figure 6.195 – Fracture surface from tensile test specimens for Ti–6Al–7Nb: a) P&S (1250ºC–2h) and b) HIP–2.

The fractographic characterisation of the fracture surface (Figure 6.195) confirms that the alloy breaks in a much more fragile way compared to P&S specimens since many cleavages zones could be identified altogether with much finer dimples. This explains why the HIPed material does not deform plastically under a uniaxial load and it is most probably due either to the great amount of interstitial elements or the higher cooling rate of the HIP process compared to P&S and the correlated microstructural changes induced.

6.4.3 – Conventional Hot–pressing (HP)

As for the other titanium alloy considered in this thesis, the production of the Ti–6Al–7Nb alloy fabricated by conventional hot–pressing was considered and the results are presented and discussed in this section.

6.4.3.1 – Relative Density

Once obtained, the components were sandblasted in order to remove any eventual residue from the BN coated graphite disc and characterised. The results of the relative density and are shown in Figure 6.196.

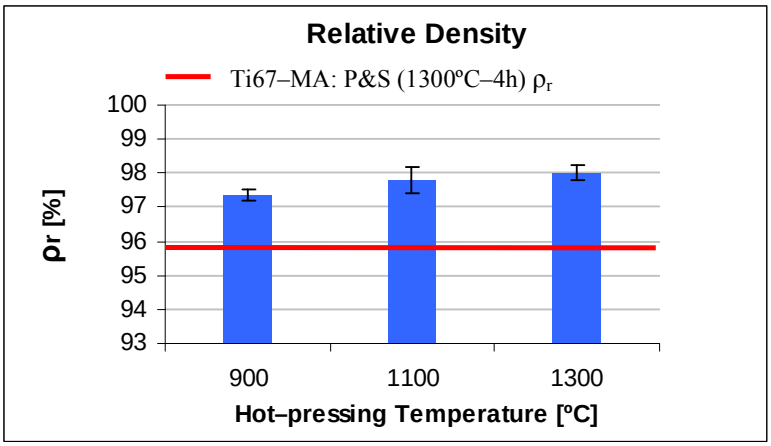

Figure 6.196 – Relative density as a function of the processing temperature for Ti–6Al–7Nb hot–pressed specimens.

The relative density of the hot–pressed components (Figure 6.196) increases with the processing temperature and it is higher than that of P&S specimens.

These results are similar to those found for the Ti–6Al–4V alloy (Figure 6.149) and to that of Henriques et al. (98% at 1300ºC)[79] considering the blending elemental approach but starting from elemental powders instead of a master alloy.

6.4.3.2 – Chemical Analysis

The results of the chemical analysis (Figure 6.197) are subdivided between grinded and not grinded specimens only in the case of nitrogen content because only for this element a significant difference was found.

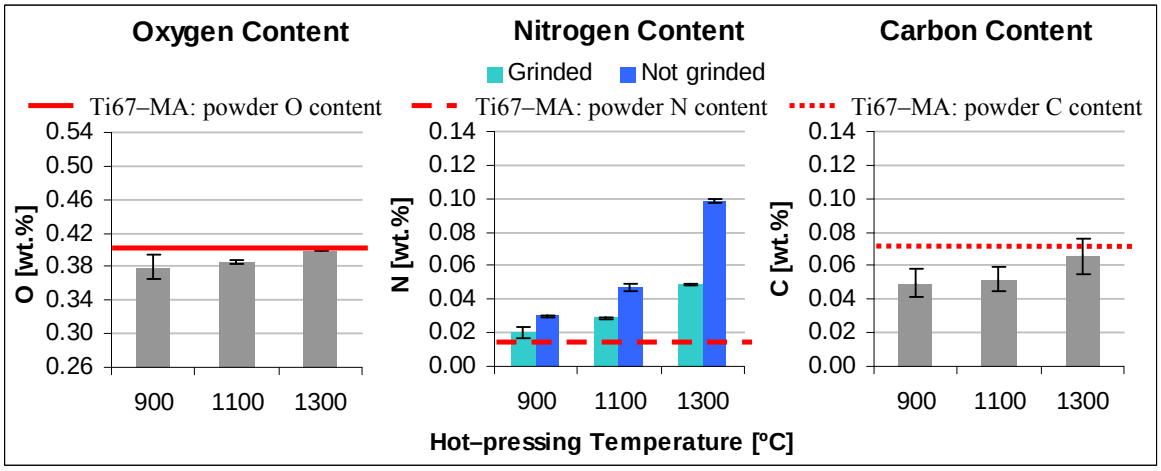

Figure 6.197 – Chemical analysis as a function of the processing temperature for Ti–6Al–7Nb hot–pressed specimens: oxygen (left), nitrogen (centre) and carbon (right).

As it can be seen in the left part of Figure 6.197, the final oxygen content of the conventionally hot–pressed samples slightly increases with the temperature but it is very similar to the amount of the starting powder indicating that, practically, there is no oxygen contamination.

On the other side, there is always some nitrogen pick–up with respect to the powder content, which is mainly concentrated on the outer surface, and can be assumed from the comparison of the nitrogen content between grinded and not grinded specimens.

For carbon, its content increases with the temperature most probably due to some interaction with the graphite mould and it results to be lower than the initial amount of the powder. It should be kept in mind that the high value of the powder is due to the wax used to mill the master alloy employed to produce the Ti–6Al–7Nb alloy.

The magnitude of the interaction of the Ti–6Al–7Nb powder with the BN coating of the graphite disc was analysed by means of SEM using the BSE mode and XRD. As for the other titanium alloys, no important differences were found compared to elemental titanium (Figure 6.33 and Figure 6.34) due to the higher affinity of titanium, compared to niobium and aluminium, for nitrogen and boron.

6.4.3.3 – Hardness

Figure 6.198 shows the variation of the hardness with the hot–pressing temperature for the Ti–6Al–7Nb alloy.

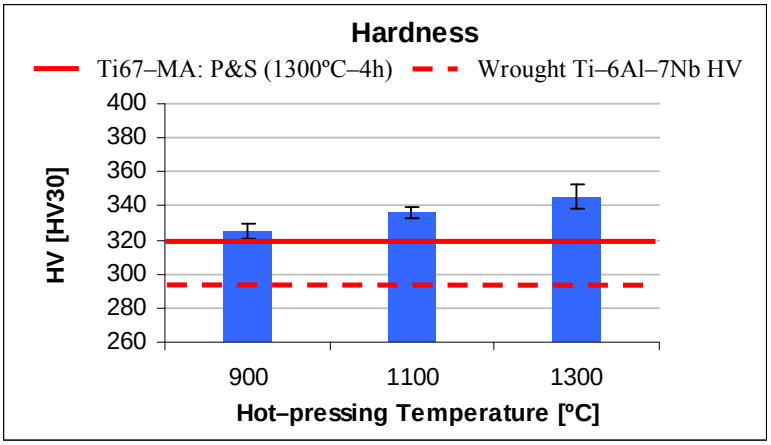

Figure 6.198 – Hardness as a function of the processing temperature for Ti–6Al–7Nb hot–pressed specimens.

Concerning the hardness of the material (Figure 6.198), the alloy gets harder when increasing the temperature, and thus with the relative density, ranging from 325 HV30 to 354 HV30. In comparison to P&S samples, the hot–pressed components always reach, at least, the same hardness which is mainly due to the greater relative density.

The hardness values found are comparable to that of the wrought alloy (which ranges from 290HV to 350 HV)[75] and that found by other authors when using vacuum hot–pressing (350 HV)[80].

6.4.3.4 – Properties from Bending Test

The representative bending stress–strain curves of the Ti–6Al–7Nb conventionally hot–pressed components obtained during the three–point bending test is presented in Figure 6.199.

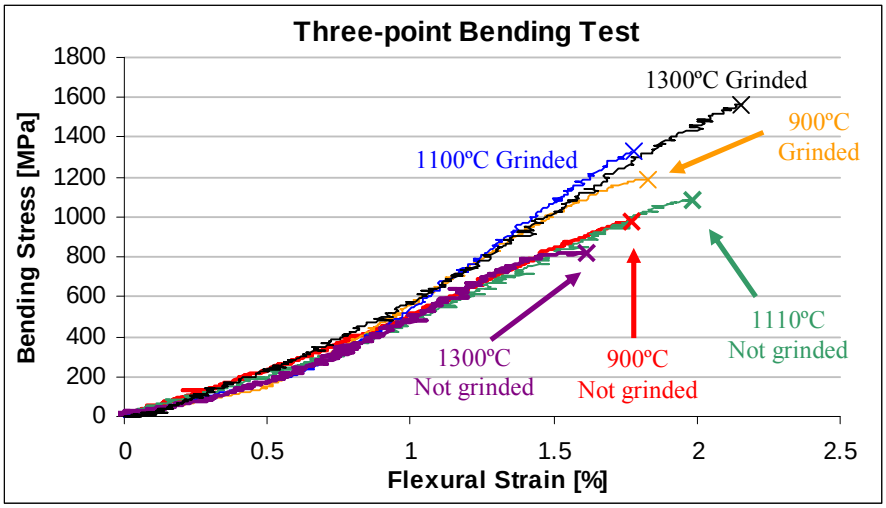

Figure 6.199 – Representative bending stress–strain curves for Ti–6Al–7Nb hot–pressed specimens.

From the curves shown in Figure 6.199, it can be stated that the material presents an elastic behaviour up to fracture, without plastic deformation.

The flexural modulus determined from the bending stress–strain curves of the hot–pressed components is equals to 78 ± 12 GPa. Once again, the great difference in flexural modulus compared to P&S specimens is mainly due to geometric factors and precisely to the L/D ratio[16-18] or, in this case, to the ratio between the span length (L) and the thickness (t) of the specimens, as shown in Figure 6.200.

Analysing the data presented in Figure 6.200, it can be seen that the flexural modulus of P/M Ti–6Al–7Nb is not only influenced by geometric factors, even if these play the most important role. The scattering of the flexural modulus of P&S specimens is mainly due to the residual porosity while the value determined in hot–pressed samples is affected by the reacted surface layer.

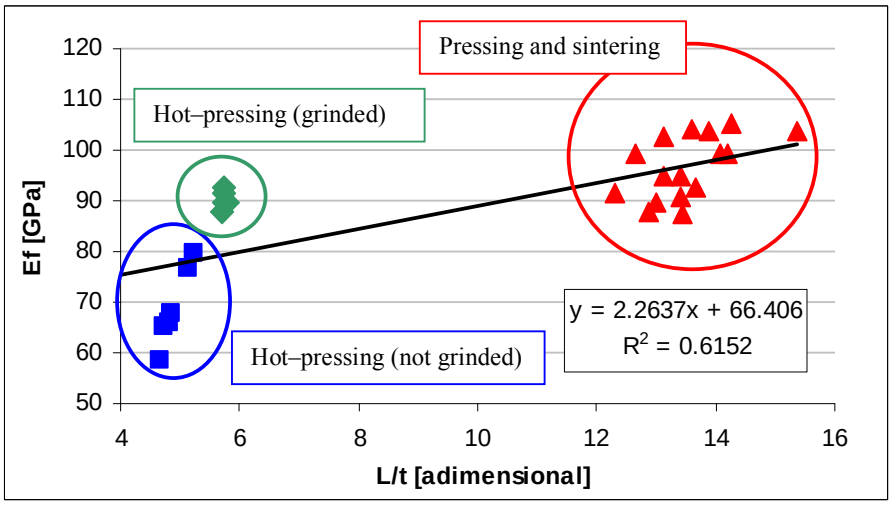

Figure 6.200 – Flexural modulus as a function of the L/t ratio for Ti–6Al–7Nb obtained by the diverse P/M methods studied.

The maximum bending strength and the flexural strain mean values for the various hot–pressing conditions, and differentiated between grinded and not grinded, are reported in Figure 6.201.

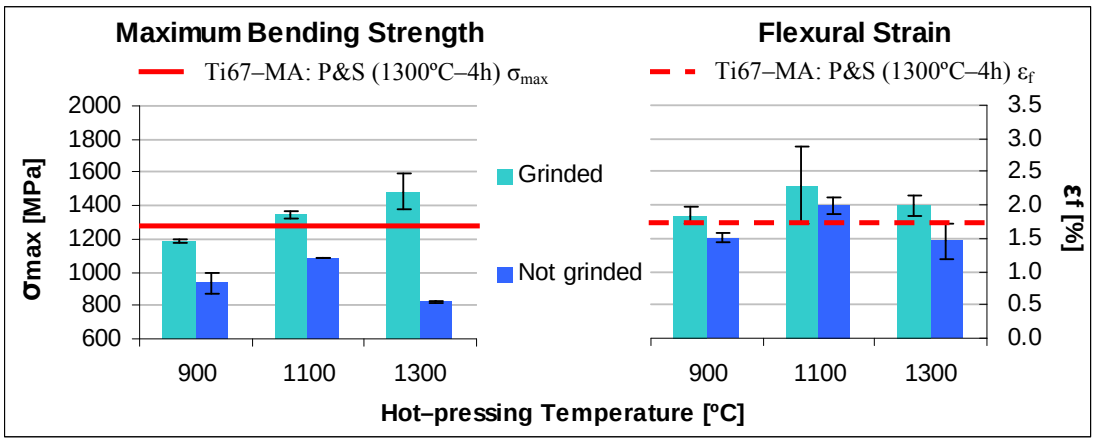

Figure 6.201 – Mechanical properties as a function of the processing temperature for Ti–6Al–7Nb hot–pressed specimens: maximum bending strength (left) and flexural strain (right).

The analysis of the maximum bending strength (Figure 6.201–left) indicates that this property increases with the processing temperature when the outer layer is removed whereas it increases from 900ºC to 1100ºC and then decreases for not grinded samples. On the other hand, the flexural strain increases from 900ºC to 1100ºC and it decreases when further increases the hot–pressing temperature for both grinded and not grinded samples (Figure 6.201–right).

In general, the grinding of the surface leads to an important improvement of the maximum bending strength (from 250 MPa to 660 MPa higher) and an increment of the flexural strain between 0.3% and 0.5%. Exactly the same behaviour with similar values in terms of maximum bending strength and flexural strain improvement was found for the α + β Ti–6Al–4V alloy (Figure 6.156 and Figure 6.157).

In general, with respect to P&S, the hot–pressed samples present higher maximum strength exclusively when the outer surface is removed whereas the flexural strain is similar, independently of the outer layer.

6.4.3.5 – Microstructural Analysis

Figure 6.202 shows the results of the microstructural characterisation carried out at the optical microscopy as well as micrographs of the P&S samples processed at 1300°C during 4 hours for comparison.

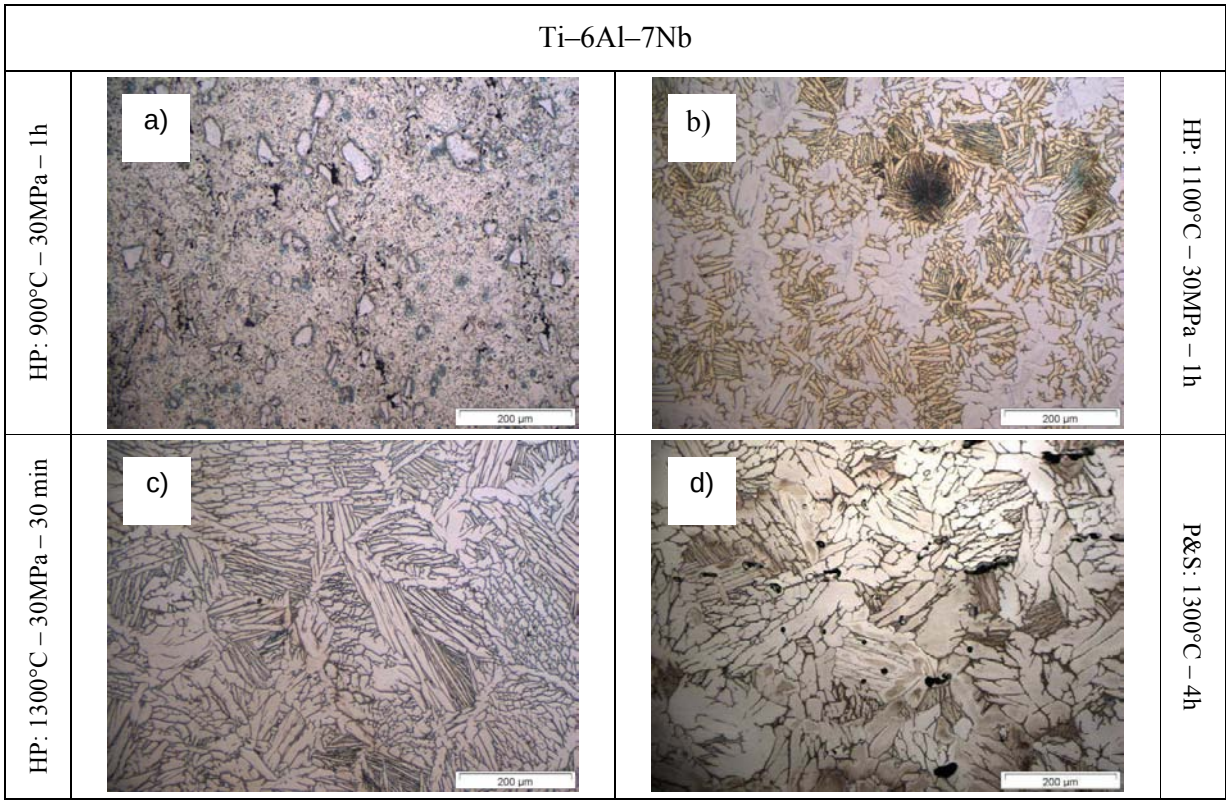

Figure 6.202 – Optical microscopy images for Ti–6Al–7Nb hot–pressed at: a) 900ºC, b) 1100ºC and c) 1300ºC, and d): P&S at 1300ºC–4h (reference).

The microstructure of the samples hot–pressed at 900ºC (Figure 6.202 a) is composed mainly by alpha grains and undissolved powder particles (master alloy) since this temperature is far below the nominal beta transus and it is not high enough to promote the complete diffusion of the alloying elements and to reach a homogeneous microstructure.

When the processing temperature is set at 1100°C, not undissolved particles could be identified and the microstructure is composed of approximately equal amount of large, irregular, elongated and interconnected alpha grains and Widmanstätten areas of very fine α + β lamellae. It seems that this temperature is not high enough to promote the complete homogenisation of the microstructure.

At 1300°C, the typical alpha grains plus α + β lamellae microstructure is well formed and it seems to be composed by finer features than P&S samples, most probably due to the shorter processing time at temperature (Figure 6.202 d).

6.4.4 – Inductive Hot–pressing (IHP)

The Ti–6Al–7Nb alloy was processed by means of inductive hot–pressing and the graph concerning the monitoring of the processing parameters, precisely temperature, punch displacement and densification rate, registered during the sintering of the Ti–6Al–7Nb at 1300°C is reported in Figure 6.203.

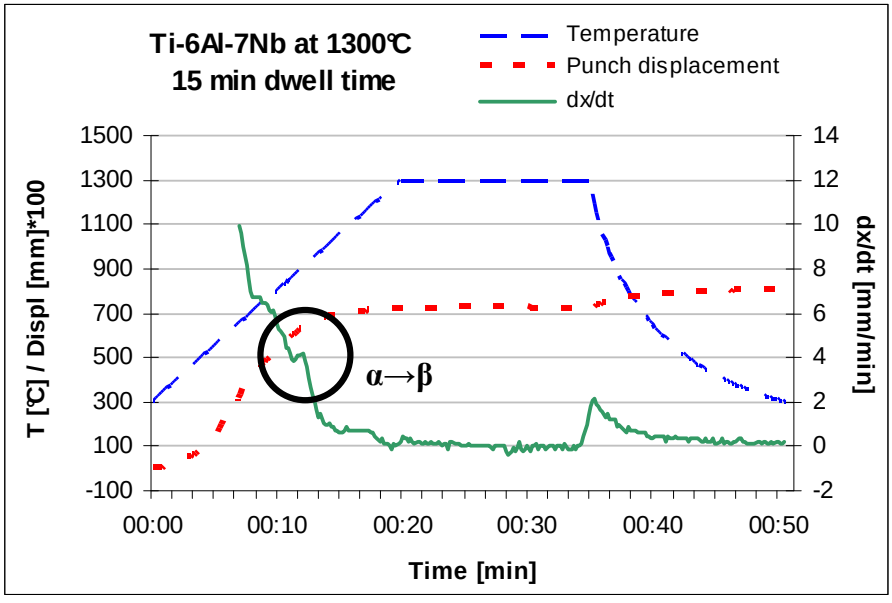

Figure 6.203 – Temperature, punch displacement and densification rate profiles recorded during the processing of the Ti–6Al–7Nb alloy by inductive hot–pressing at 1300°C.

Analysing the graph which monitored the processing parameters (Figure 6.203), it can be seen that the densification of the powder (dx/dt) is, basically, completed few minutes after reached the processing temperature, which is the same behaviour found in the other titanium alloys. Moreover, around 900°C, the crossing of the beta transus and the corresponding phase transformation of elemental titanium can be identified.

6.4.4.1 – Relative Density

Once cleaned by sandblasting, the components were cut and analysed. The results of the relative density are presented in Figure 6.204.

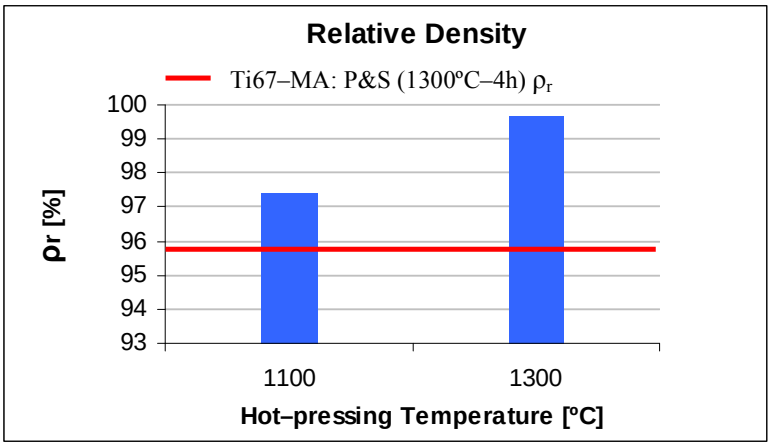

Figure 6.204 – Relative density as a function of the processing temperature for Ti–6Al–7Nb inductive hot–pressed specimens.

As it can be seen in Figure 6.204, the processing of the biomedical Ti–6Al–7Nb alloy by inductive hot–pressing permits to reach fully dense material employing a temperature of 1300°C. At 1100°C the relative density is greater than 97%, which is approximately 1.5% higher than that of P&S specimens sintered at 1300°C during 4 hours.

The relative density value obtained with the Ti–6Al–7Nb alloy processed at 1100ºC is the lowest of all the materials considered in this thesis when processed by IHP and it is not due to the intrinsic behaviour of the alloy but to an erroneous preparation of the graphite matrix which led to the embedding of some graphite into the surface of the specimens, which could not be removed, as Figure 6.205 demonstrates.

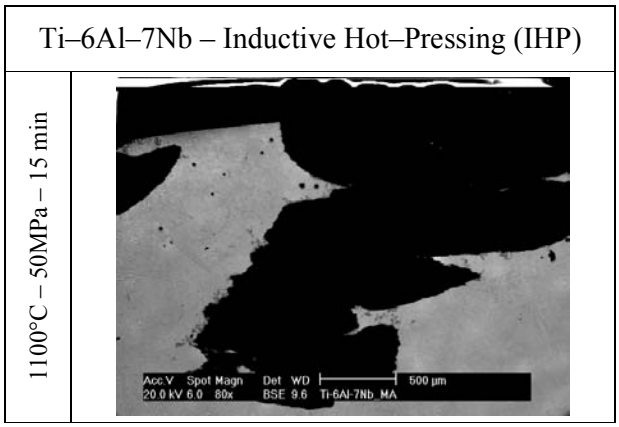

Figure 6.205 – Detail of the surface of the Ti–6Al–7Nb specimen hot–pressed at 1100ºC.

6.4.4.2 – Chemical Analysis

The results of the chemical analysis, precisely oxygen, nitrogen and carbon content, are presented in Figure 6.206.

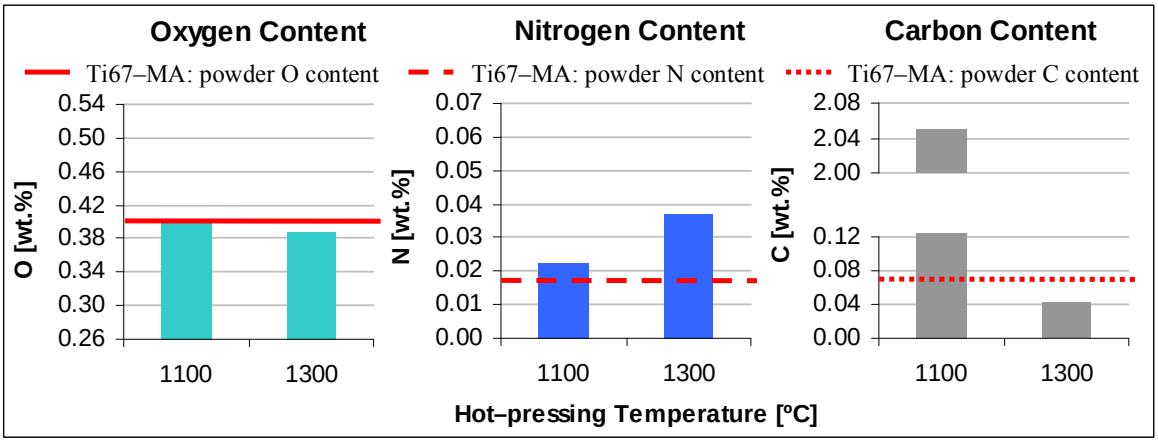

Figure 6.206 – Chemical analysis as a function of the processing temperature for Ti–6Al–7Nb inductive hot–pressed specimens: oxygen (left), nitrogen (centre) and carbon (right).

The chemical analysis (Figure 6.206) reveals that the oxygen content of the samples processed at 1100°C is slightly higher compared to 1300°C and to the initial powder content, indicating that there is no oxygen pick–up.

For nitrogen the behaviour is the opposite since the percentage of this element increases with the processing temperature and, therefore, it is at 1300°C where its content is higher. This indicates that there is always nitrogen pick–up from the environment even if the final values are lower than the specified for this alloy.

Carbon content is approximately 0.40 wt:% either due to some contamination from the graphite mould or the incomplete elimination of the wax used to produce the master alloy. It is worth mentioning that the very high value found for the components hot–pressed at 1100ºC is due to the fact that part of the graphite disc used to separate the different powders processed was embedded inside the material and could not be completely removed (Figure 6.205).

6.4.4.3 – Hardness

The Vickers hardness variation with the inductive hot–pressing temperature for the Ti–6Al–7Nb alloy is presented in Figure 6.207.

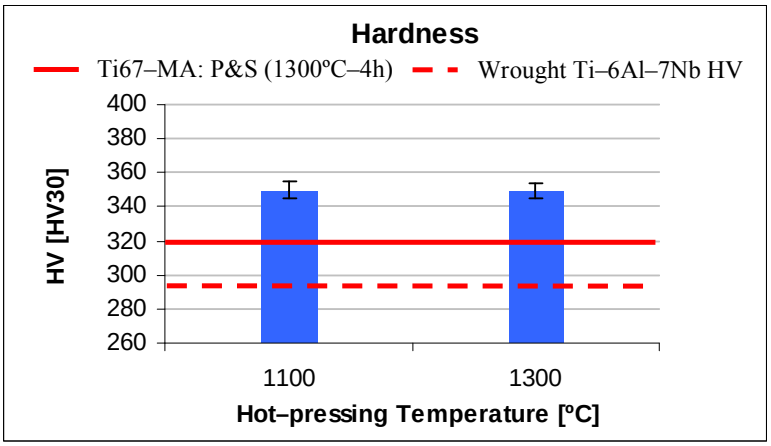

Figure 6.207 – Hardness as a function of the processing temperature for Ti–6Al–7Nb inductive hot–pressed specimens.

The hardness of the inductive hot–pressed Ti–6Al–7Nb samples (Figure 6.207) remains constant even if the relative density, apparently, increases, suggesting that the actual relative density of the specimens processed at 1100ºC is higher than the value shown in Figure 6.204.

The values obtained, approximately 350 HV30, are higher compared to the P&S components, most probably due to the lower amount of residual porosity, but comparable to those of the conventional hot–pressed specimens and the value specified by the researchers that developed this alloy (350 HV)[75].

6.4.4.4 – Microstructural Analysis

Figure 6.208 shows the results of the microstructural characterisation carried out by optical microscopy of the inductive hot–pressed samples of the Ti–6Al–7Nb alloy.

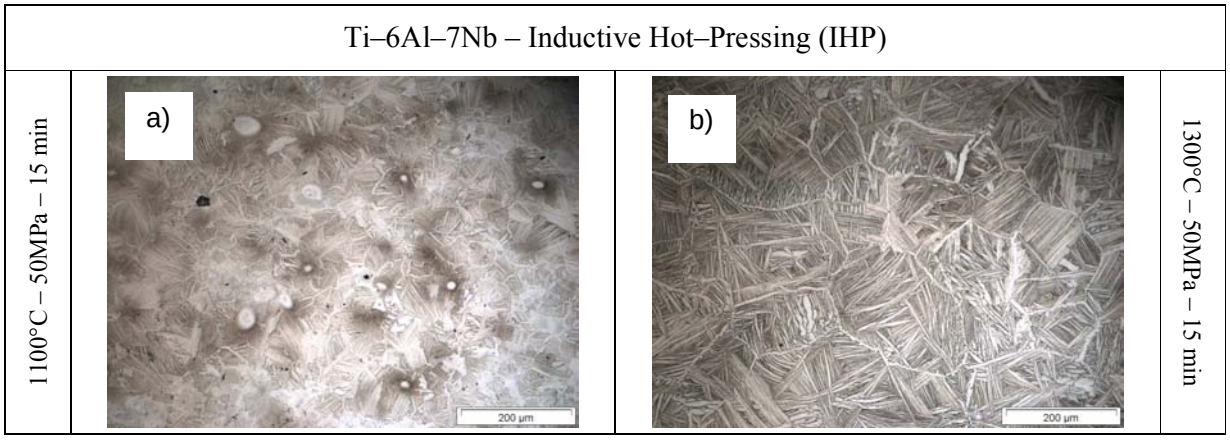

Figure 6.208 – Optical microscopy images for Ti–6Al–7Nb inductive hot–pressed at: a) 1100ºC and b) 1300ºC.

As it can be seen in Figure 6.208, the microstructural constituents of the Ti–6Al–7Nb alloy hot–pressed at 1100°C are some alpha grains and α + β lamellae even if some undissolved master alloy particles are still visible and the microstructure is not fully developed.

When the processing temperature is raised to 1300°C, the microstructure is still composed by α grains as well as some acicular alpha, due to the fast cooling rate, and α + β lamellae resulting in the typical basketweave microstructure.

6.4.5 – P/M Techniques Comparison

In this section the properties (relative density and mechanical properties like hardness, maximum bending strength and strain) of the Ti–6Al–7Nb alloy processed by various P/M techniques are compared, where possible, on the bases of the equivalent oxygen content.

In the case of the relative density, whose results are displayed in Figure 6.209, the highest value obtained is considered.

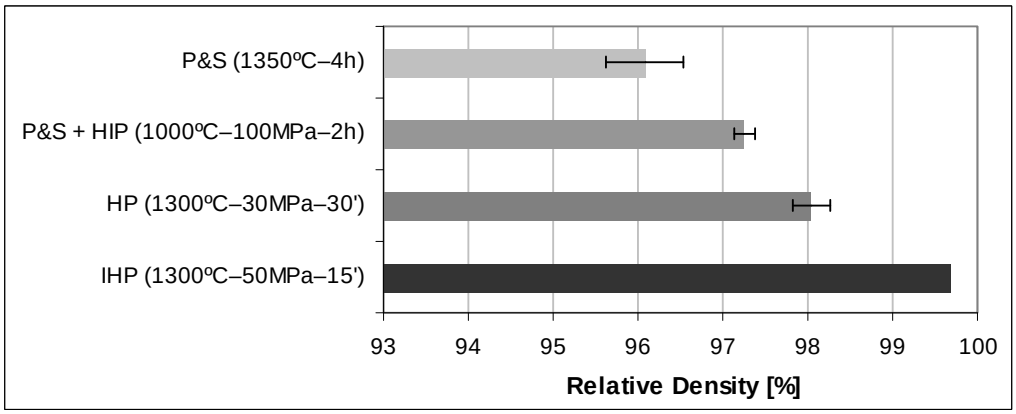

Figure 6.209 – Comparison of the highest relative density for Ti–6Al–7Nb obtained by different P/M techniques.

As it can be seen in Figure 6.209, the highest relative density obtained by P&S is approximately 96% and the application of a post–processing by HIP leads only to an improvement of 2% due to the superficial porosity that could not be sealed.

Higher relative density can be reached by applying a uniaxial pressure simultaneously with a thermal cycle, that are HP and IHP results. In particular, the inductive heating results to be much faster and permits to reach, practically, fully dense material.

As for the other titanium alloys considered in this thesis, the comparison of the Vickers hardness values for the different P/M methods has been done using the formula proposed by Okazaki and Conrad[49] and the results, whose equivalent oxygen content is approximately 0.49 wt.%, are reported in Figure 6.210.

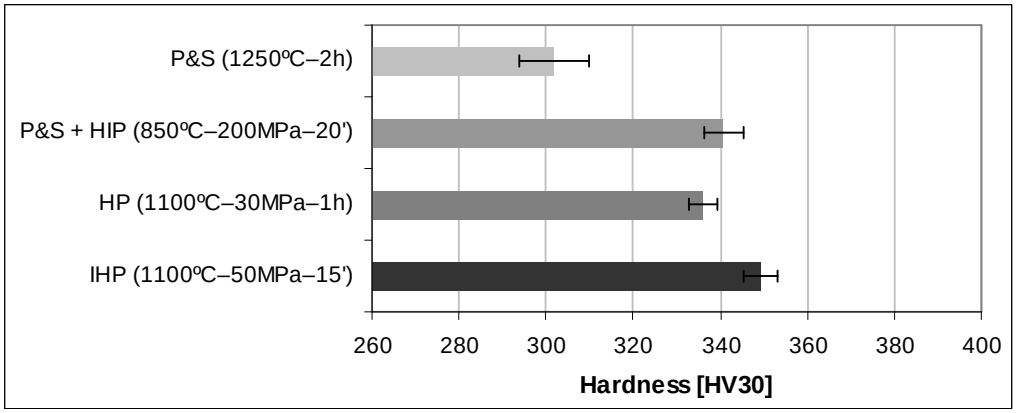

Figure 6.210 – Comparison of the hardness for Ti–6Al–7Nb obtained by different P/M techniques (equivalent oxygen content of approximately 0.49 wt.%).

As it can be seen in Figure 6.210, when the effect of the contaminants is excluded, the hardness of the material increases with the increment of relative density from 300 to 335 HV30 when the relative density increases from 94.2% (P&S) to 97.8% (HP).

The only exception on this trend is the hardness of the HIPed samples but, here, there is a quite important effect from the contaminants since the lowest equivalent oxygen found was 0.54 wt.%, which brings the hardness to 340 HV30.

The equation proposed by Wood[19] for the calculation of the variation of the UTS with the equivalent oxygen percentage was used to compare the maximum bending strength obtained in P&S, HIP and conventionally hot–pressed components with and without the removal of the outer surface contaminated by BN. An equivalent oxygen content of 0.51 wt.%, common to the diverse methods with the exception of HIP (0.56 wt.%), was determined and the comparison of the maximum bending strength values is presented in Figure 6.211.

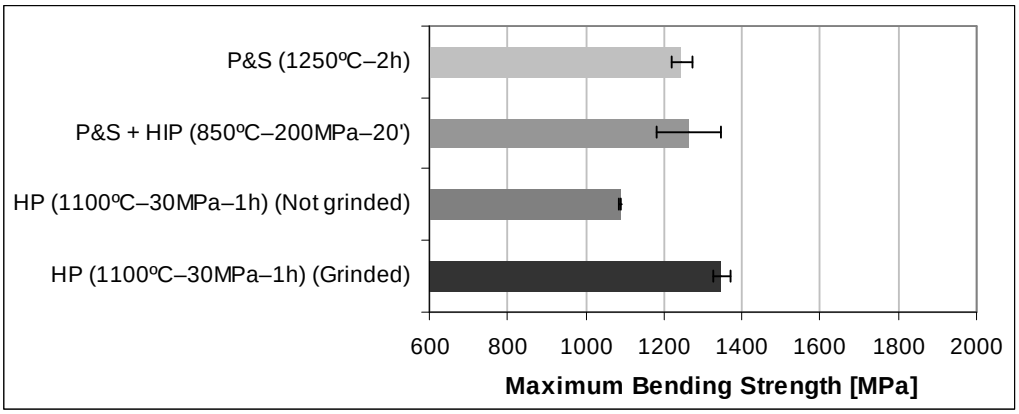

Figure 6.211 – Comparison of the maximum bending strength for Ti–6Al–7Nb obtained by different P/M techniques (equivalent oxygen content of approximately 0.51 wt.%).

Analysing Figure 6.211, it can be seen that the increment of the relative density leads to an increment of maximum bending strength, since the maximum bending strength of HIPed components is higher than that of P&S.

In the case of conventional hot–pressed samples, to reach higher maximum bending strength than P&S it is mandatory to remove the contaminated layer composed by titanium nitrides and borides.

Regarding the flexural strain determined by the three–point bending test, the formula proposed by Wood[19] to estimate the effect of the equivalent oxygen content on the reduction area parameter (R.A.) was considered, and the results are shown in Figure 6.212. It is worth mentioning that the equivalent oxygen content of the samples whose flexural data are shown in Figure 6.212 is approximately 0.55 wt.%.

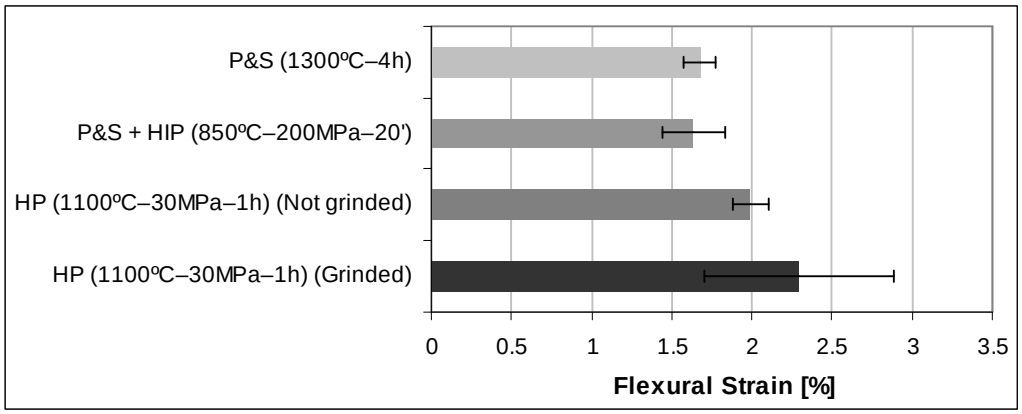

Figure 6.212 – Comparison of the flexural strain for Ti–6Al–7Nb obtained by different P/M techniques (equivalent oxygen content of approximately 0.55 wt.%).

As it can be seen in Figure 6.212, the maximum flexural strain increases with the increment of the relative density but the variation is quite limited. It is worth mentioning that the lower deformation of the HIPed components is also affected by a slightly higher $O_{eq.}$ which is equals to 0.58 wt.%, whilst the removal of the outer layer in hot–pressed samples is beneficial to increase the ductility.

6.4.6 – Partial Conclusions

Based on the results of the study of processing of the Ti–6Al–7Nb alloy by different P/M techniques, it can be concluded that:

Uniaxial Pressing and Sintering (P&S): the sintering of Ti–6Al–7Nb components obtained by uniaxial pressing and sintering leads to a shrinkage which increases with the processing temperature and it is higher for longer dwell times ranging from 8.5% to 10.5%.

Exactly the same trend was found for the densification, which increases from 60% to 74%, and the relative density, which ranges from 94 to 96%, a quite common value for titanium alloys processed by conventional P/M. As general behaviour, the contamination of the components increases with the sintering temperature.

Microstructural analysis indicates that the microconstituents are alpha grains, whose mean size increases with temperature and time, and α + β lamellae whereas fractography points out that the material fails in a ductile way when subjected to a uniaxial tensile load.

Finally, somewhat lower thermal conductivity at room temperature and slightly higher electrical resistivity compared to the wrought alloy are obtained with the processing parameters studied.

Hot Isostatic Pressing (HIP): the post–processing of the sintered components does not permit to obtain fully dense materials due to the open porosity present in the sintered specimens but the relative density can be increased from 94% to 97%.

About mechanical properties of HIP specimens, generally, the hardness is higher, bending properties similar and the tensile properties lower compared to the as–sintered material.

As it is well known, the microstructure of α + β titanium alloys is strongly dependent on the heat treatment, thus, the selection of the HIP process leads to different microstructure as a function of the processing temperature. In particular, a processing temperature of 1000ºC, in the upper part of the α + β field, near the β transus, results in a bimodal microstructure whereas a processing temperature of 850ºC in a lamellar structure similar to that of P&S but somewhat finer.

Conventional Hot–pressing (HP): the processing of the Ti–6Al–7Nb alloy by conventional hot–pressing leads to an increment of the relative density of 2% compared to P&S, reaching similar hardness values.

The contamination of the components by the graphite mould and the BN coating used to separate the material is an issue which gets more important when the processing temperature is increased.

Selecting a temperature of 900°C, undissolved master alloy particles are still visible and the contamination is primary due to some nitrogen diffusion towards the titanium matrix.

When the temperature is raised the alloying elements complete their diffusion but a more serious contamination, which results in the formation of titanium nitrides and borides, occurs which has a significant influence on the mechanical properties.

The removal of the outer reacted layer permits to obtain maximum bending strength and flexural strain values similar or higher than those of P&S.

The relatively short processing time generates, normally, a microstructure composed by alpha grains and Widmanstätten areas or lamellae finer than those found in P&S components, with the exception of the samples processed at 900°C, where the microconstituents are alpha grains and undissolved master alloy particles.

Inductive Hot–pressing (IHP): by means of the inductive hot–pressing method, fully dense material with similar hardness and level of contamination than pressed and sintered components can be produced. Precautions against contamination from the graphite tools should be taken in order to avoid the machining of the surface.

The very short dwell time at temperature, 15 minutes, and the fast cooling rate intrinsic to the field assisted sintering technology leads to a much finer microstructure either compared to P&S or conventional hot–pressing, but could leave not completely dissolved master alloy particles at low processing temperature.

6.5 – REFERENCES

[1] F. H. Froes, et al., "Cost–effective Synthesis of Ti–6Al–4V Alloy Components via the Blended Elemental P/M Approach" in *Symposium on TMS Symposium on High Performance Metallic Materials for Cost Sensitive Applications*, Seattle, WA, 2002

[2] W. Wei, et al., "Effect of Fe Addition on Sintering Behaviour of Titanium Powder", *Powder Metallurgy,* vol. 46, pp. 246-250, 2003

[3] G. Friedman and R. Regn, "Titanium PM Gyro Components", *Metal Powders Report,* pp. 273-281, 1984

[4] H. El Kadiri, et al., "Development of a Ti-based Alloy: Design and Experiment", *JOM,* vol. 61, pp. 60-66, 2009

[5] R. I. Jaffee and I. E. Campbell, "The Effect of Oxygen, Nitrogen and Hydrogen on Iodide Refined Titanium", *Transactions of the American Institute of Mining and Metallurgical Engineers,* vol. 185, pp. 646-654, 1949

[6] R. I. Jaffee, et al., "Alloys of Titanium with Carbon, Oxygen and Nitrogen", *Transactions of the American Institute of Mining and Metallurgical Engineers,* vol. 188, pp. 1261-1266, 1950

[7] W. L. Finlay and J. A. Snyder, "Effects of Three Interstitial Solutes (Nitrogen, Oxygen and Carbon) on the Mechanical Properties of High-purity Alpha Titanium", *Journal of Metals* vol. 188, pp. 277-286, 1950

[8] R. Boyer, et al., "Materials Properties Handbook: Titanium Alloys", 2nd ed, ASM-International, Ed. Ohio, USA, 1998

[9] RMI, "Titanium Company: Titanium Alloy Guide", *available at: http://rtiintl.s3.amazonaws.com/RTI-Reports/tiguideWeb.pdf,* 2000

[10] G. Lütjering and J. C. Williams, *Titanium: Engineering Materials and Processes*, 1st ed. Manchester, UK, Springer, pp. 1-356, 2003

[11] K. Okazaki and H. Conrad, *Trans. TIM,* vol. 14, pp. 364-367, 1973

[12] ASTM E 855, "Standard Test Method for Bending Test of Metallic Flat Materials for Spring Applications Involving Static Loading", 2000

[13] G. Plotino, et al., "Flexural Properties of Endodontic Posts and Human Root Dentin", *Dental Materials,* vol. 23, pp. 1129-1135, 2007

[14] M. P. Walker, et al., "Mechanical Properties and Surface Characterization of Beta Titanium and Stainless Steel Orthodontic Wire Following Topical Fluoride Treatment", *Angle Orthodontist,* vol. 77, pp. 342-348, 2007

[15] J. J. Xu, et al., "Mechanical Properties of Titanium Hydride", *Journal of Alloys and Compounds,* vol. 436, pp. 82-85, 2007

[16] R. A. Rodford, et al., "Variation of Young's Modulus with the Test Specimen's Aspect Ratio", *Biomaterials,* vol. 14, pp. 781-786, 1993

[17] P. Alander, et al., "The Span Length and Cross-sectional Design Affect Values of Strength", *Dental Materials,* vol. 21, pp. 347-353, 2005

[18] D. A. Stewardson, et al., "The Flexural Properties of Endodontic Post Materials", *Dental Materials,* vol. 26, pp. 730-736, 2010

[19] R. A. Wood, "The Effect of Interstitials on the Mechanical Properties of Titanium and its Alloys" in *Titanium Metallurgy Course* New York University, 1965

[20] O. M. Ivasishin, et al., "Cost-effective Blended Elemental Powder Metallurgy of Titanium Alloys for Transportation Application", in *Development in Light Metals*, vol. 188, pp. 55-62, 2000

[21] I. J. Polmear, *Light Alloys. From Traditional Alloys to Nanocrystals*, 4th ed, Butterworth-Heinemann, UK, pp. 299-365, 2006
[22] V. A. Joshi, *Titanium Alloys: An Atlas of Structures and Fracture Features*, Taylor & Francis, pp. 1-15, 2006
[23] H. Conrad, "The Rate Controlling Mechanism during Yielding and Flow of α-titanium at Temperatures below 0.4 TM", *Acta Metallurgica,* vol. 14, pp. 1631-1633, 1966
[24] R. W. Powell and R. P. Tye, "The Thermal and Electrical Conductivity of Titanium and its Alloys", *Journal of the Less Common Metals,* vol. 3, pp. 226-233, 1961
[25] L. J. van der Pauw, "A Method of Measuring Specific Resistivity and Hall Effect of Discs of Arbitrary Shape", *Philips Research Reports,* vol. 13, pp. 1-9, 1958
[26] L. J. van der Pauw, "A Method of Measuring Specific Resistivity and Hall Effect on Lamellae of Arbitrary Shape", *Philips Technical Review,* vol. 20, pp. 220-224, 1958
[27] R. M. German, *Powder Metallurgy Science*, 2nd Edition ed. Princeton, USA, MPIF - Metal Powder Industries Federation, pp. 191-340, 1994
[28] P. G. Esteban, "Diseño y Procesado por vía Pulvimetalúrgica Convencional de Aleaciones de Ti de Bajo Coste" in *Tesis Doctoral*, Universidad Carlos III de Madrid, 2009
[29] C. G. Goetzel and V. S. de Marchi, "Electrically Activated Pressure Sintering (Spark Sintering) of Titanium Powders", *Modern Developments in Powder Metallurgy,* vol. 3, pp. 80-87, 1971
[30] C. G. Goetzel and V. S. de Marchi, "Electrically Activated Pressure Sintering (Spark Sintering) of Titanium Powders", *Modern Developments in Powder Metallurgy,* vol. 3, pp. 134-136, 1971
[31] B. Ye, et al., "Enhanced Densification of Ti-6Al-4V Powders by Transformation-mismatch Plasticity", *Acta Materialia,* vol. 58, pp. 3851-3859, 2010
[32] A. Bose and W. B. Eisen, *Hot Consolidation of Powders & Particulates*. Princeton, USA, Metal Powder Industries Federation, pp. 1-88, 2003
[33] R. I. Jaffee, "The Physical Metallurgy of Titanium Alloys", *Progress in Metal Physics,* vol. 7, pp. 65-163, 1958
[34] H. Sibum, et al., *Titanium, Titanium Alloys, and Titanium Compounds*, 2002
[35] J. L. Murray, *Phase Diagrams of Binary Titanium Alloys*, 1st ed, ASM International, pp. 1-345, 1987
[36] Y. S. Matychak, et al., "Thermodiffusion Saturation of α-Titanium with Nitrogen from a Rarefied Atmosphere", *Materials Science,* vol. 45, pp. 72-83, 2009
[37] S. V. Divinski, et al., "Tracer diffusion of boron in [alpha]-Ti and [gamma]-TiAl", *Intermetallics,* vol. 16, pp. 148-155, 2008
[38] E. Faran, et al., "Experimental Study of the Reaction Zone at Boron Nitride Ceramic-Ti Metal Interface", *Materials Science and Engineering A,* vol. 288, pp. 66-74, 2000
[39] E. Benko, "Calculations of Chemical Equilibria in BN-Ti System" in *Powder Metallurgy World Congress*, Paris, pp. 14-72, 1994
[40] E. Benko, "Wettability Studies of Cubic Boron Nitride by Silver-titanium", *Ceramics International,* vol. 21, pp. 303-307, 1995
[41] E. Benko, "Chemical Reactions Occurring at a BN-AgTi Interface", *Ceramics International,* vol. 22, pp. 219-222, 1996

[42] E. Faran, et al., "Coating of BN via Solid State Reaction with Ti Powder", *Materials Letters,* vol. 43, pp. 192-196, 2000
[43] V. Tomashik, "Boron–Nitrogen–Titanium", *available at: http://www.springermaterials.com/pdfs/10.1007/978-3-642-02700-0_7.pdf,* 2010
[44] I.-H. Oh, et al., "Mechanical Properties of Porous Titanium Compacts Prepared by Powder Sintering", *Scripta Materialia,* vol. 49, pp. 1197-1202, 2003
[45] I. Montealegre Meléndez, et al., "Consolidation of Titanium Matrix Composites to Maximum Density by Different Hot Pressing Techniques", *Materials Science and Engineering: A,* vol. 527, pp. 4466-4473, 2010
[46] D. C. Dunand and C. M. Bedell, "Transformation-mismatch Superplasticity in Reinforced and Unreinforced Titanium", *Acta Materialia,* vol. 44, pp. 1063-1076, 1996
[47] V. A. Moskalenko and A. R. Smirnov, "Temperature Effect on Formation of Reorientation Bands in [alpha]-Ti", *Materials Science and Engineering A,* vol. 246, pp. 282-288, 1998
[48] C. L. Chu, et al., "Microband Substructure in Pure Titanium Fabricated by Powder Metallurgical Process with Hot Pressing at 1100° under a Pressure of 20 MPa", *Journal of Materials Science Letters,* vol. 20, pp. 1869-1872, 2001
[49] H. Conrad, "Effect of Interstitial Solutes on the Strength and Ductility of Titanium", *Progress in Materials Science,* vol. 26, pp. 123-404, 1981
[50] C. H. Liu and P. W. kao, "Microstructure and Mechanical Properties of Resistance Sintered Titanium", *Scripta Metallurgica et Materialia,* vol. 24, pp. 2279-2284 1990
[51] M. Zadra, et al., "Microstructure and Mechanical Properties of CP-titanium Produced by Spark Plasma Sintering", *Powder Metallurgy,* vol. 51, pp. 59-65, 2008
[52] O. M. Ivasishin, et al., "High Integrity, Low Cost Titanium Powder Metallurgy Components", *High-performance Metallic Materials for Cost Sensitive Applications, Proceedings,* pp. 117-128, 2002
[53] O. M. Ivasishin, "Cost-effective Manufacturing of Titanium Parts with Powder Metallurgy Approach", *Materials Forum* vol. 29, pp. 1-8, 2005
[54] V. A. R. Henriques, et al., "Production of Titanium Alloys for Advanced Aerospace Systems by Powder Metallurgy", *Materials Research,* vol. 8, pp. 443-446, 2005
[55] J. E. Smugeresky and D. B. Dawson, "New Titanium Alloys for Blended Elemental Powder Processing", *Powder Technology,* vol. 30, pp. 87-94, 1981
[56] O. M. Ivasishin, et al., "Synthesis of Alloy Ti-6Al-4V with Low Residual Porosity by a Powder Metallurgy Method", *Powder Metallurgy and Metal Ceramics,* vol. 41, pp. 382-390, 2002
[57] V. S. Moxson, et al., "Production and Applications of Low Cost Titanium Powder Products", *International Journal of Powder Metallurgy,* vol. 34, pp. 45-53, 1998
[58] O. M. Ivasishin, et al., "Titanium Powder Metallurgy for Automotive Components", *Materials Technology,* vol. 17, pp. 20-25, 2002
[59] ASM International, *Materials and Coatings for Medical Devices: Cardiovascular*. Ohio, USA, ASM International, pp. 151-186, 2009
[60] D. Eylon, et al., "Status of Titanium Powder Metallurgy" in *Industrial Applications of Titanium and Zirconium: 3rd Conference*, pp. 48-65, 1984

[61] J. P. Herteman, et al., "Mechanical-properties of Advanced Titanium Powder-metallurgy Compacts", *Powder Metallurgy International,* vol. 17, pp. 116-119, 1985
[62] R. Mohs and H. Sibum, "Powder Metallurgical Production of Titanium Alloy Ti6Al4V Parts", *Powder Metallurgy International,* vol. 16, pp. 163-166, 1984
[63] L. Wang, et al., "Properties and Forming Process of Prealloyed Powder Metallurgy Ti-6Al-4V Alloy", *Trans. Non Ferrous Met. Soc. China,* vol. 17, pp. s639-s643, 2007
[64] D. Eylon, et al., "Property Improvement of Low Chlorine Titanium Alloy Blended Elemental Powder Compacts by Microstructure Modification", *Progress in Powder Metallurgy,* vol. 42, pp. 625-634, 1986
[65] M. Frary, et al., "Microstructure and Mechanical Properties of Ti/W and Ti-6Al-4V/W Composites Fabricated by Powder-metallurgy", *Materials Science and Engineering A,* vol. 344, pp. 103-112, 2003
[66] M. Minabe and H. Endoh, "Development of High Density Sintered Titanium Alloys using a Sinter-HIP Process", *Metal Powders Report,* pp. 673-682, 1990
[67] R. W. Broomfield, et al., "Application of Advanced Powder Process Technology to Titanium Aeroengine Components", *Powder Metallurgy,* vol. 28, pp. 27-34, 1985
[68] R. K. Malik, "Vacuum Hot Pressing of Titanium Alloy Powders", *Progress in Powder Metallurgy,* vol. 31, pp. 277-288, 1975
[69] W. H. Kao and L. M. Orsborn, "Consolidation Characteristics of Rotating Electrode and Hydride Titanium Powders", *Powder Metallurgy of Titanium Alloys,* pp. 163-173, 1980
[70] L. J. Huang, et al., "In situ TiBw/Ti-6Al-4V Composites with Novel Reinforcement Architecture Fabricated by Reaction Hot Pressing", *Scripta Materialia,* vol. 60, pp. 996-999, 2009
[71] C. G. Goetzel and V. S. de Marchi, "Electrically Activated Pressure Sintering (Spark Sintering) of Titanium-aluminium-vanadium Alloy Powders", *Modern Developments in Powder Metallurgy,* vol. 4, pp. 127-150, 1971
[72] R. K. Malik, "Hot Pressing of Titanium Aerospace Components", *The International Journal of Powder Metallurgy & Powder Technology,* vol. 10, pp. 115-129, 1974
[73] A. Molinari and M. Zadra, "Influence of the Sintering Temperature on Microstructure and Tensile Properties of Ti6Al4V Produced by Spark Plasma Sintering" in *EUROPM 2009*, Copenhagen - Denmark, pp. 267-272, 2009
[74] J. R. Groza and A. Zavaliangos, "Sintering Activation by External Electrical Field", *Materials Science and Engineering A,* vol. 287, pp. 171-177, 2000
[75] M. Semlitsch, et al., "Fifteen Years Experience with Ti-6AI-7Nb Alloy for Joint Replacements" in *Titanium '95: Science and Technology*, Birmingham - UK, pp. 1742-1759, 1995
[76] Y. Itoh, et al., "Fabrication of Ti-6Al-7Nb Alloys by Metal Injection Molding", *Materials Science Forum,* vol. Progress in Powder Metallurgy, Pts 1 and 2, pp. 357-360, 2007
[77] E. Kobayashi, et al., "Mechanical Properties and Corrosion Resistance of Ti-6Al-7Nb Alloy Dental Castings", *Journal of Materials Science: Materials in Medicine,* vol. 9, pp. 567-574, 1998

[78] M. Semlitsch, et al., "Titanium-aluminium-niobium Alloy Development for Biocompatible, High Strength Surgical Implants", *Biomedizinische Technik/Biomedical Engineering,* vol. 30, pp. 334–339, 1985

[79] V. A. R. Henriques, et al., "Microstructural Evolution during Hot Pressing of the Blended Elemental Ti-6%Al-7%Nb Alloy", *Materials Science and Engineering A,* vol. 347, pp. 315-324, 2003

[80] V. A. R. Henriques, et al., "Production of Titanium Alloys for Medical Implants by Powder Metallurgy", *Key Engineering Materials* vol. Advanced Powder Technology II pp. 443-448, 2001

CHAPTER 7

GENERAL CONCLUSIONS

This thesis deals with the production of elemental titanium (grade 4), near–α (Ti–3Al–2.5V) and α + β (Ti–6Al–4V and Ti–6Al–7Nb) titanium alloys by the two classical P/M approaches of prealloying (PA) and blending elemental (BE). In particular, for BE, the master alloy addition (MA) approach using irregular hydride–dehydride (HDH) was considered.

Moreover, the processing by the conventional P/M route of pressing and sintering (P&S) as well as by advanced techniques such as hot–pressing (HP) or hot isostatic pressing (HIP) of the previously mentioned materials was studied.

The analysis of the powder features of both purchased and produced powders by means of particle size distribution by laser diffraction, apparent density, flow rate, compressibility test, green strength, dilatometric analysis and differential thermal analysis permitted to define the processing parameters to study, such as the sintering temperature range.

On the bases of the analysis of the final physical properties (densification behaviour and relative density), chemical analysis (percentage of interstitials such as oxygen, nitrogen and carbon), mechanical characterisation by means of both three–point bending test (maximum bending strength, flexural strain and flexural modulus) and tensile test (ultimate tensile strength, strain and Young modulus) as well as Vickers hardness measurements, X–ray analysis and microstructural characterisation, the following conclusions, divided for the processing method studied, can be evinced:

Uniaxial Pressing and Sintering (P&S)

- Elemental titanium, PA and MA powders are suitable for the conventional pressing and sintering route where, normally, the master alloy addition powders have better compressibility.

- The relative density of the materials studied increases when the sintering temperature is ranged between 900ºC and 1400ºC, reaching maximum values of 95% to 97% depending on the material and the compaction pressure.

- Mechanical properties, both under bending or tensile loads are equivalent to that of the respective wrought alloy although the ductility is, generally, lower due to the presence of the residual porosity. Nevertheless, values of elongation of 12% in elemental titanium and 15% in the Ti–3Al–2.5V alloy were obtained. The materials fail in a ductile way, by a pore–assisted mechanism such as microvoid coalescence, when subjected to a uniaxial load.

- The microstructure of the sintered specimens is constituted by homogeneously distributed α grains for elemental titanium, and α grains and α + β lamellae for the near–α and α + β alloys. Generally, the microconstituents seem to be slightly coarser for MA alloys.

- The increment of the sintering time does not seem to be as effective as the increment of the sintering temperature to attain higher relative density. Furthermore, a longer processing time can lead to an important change of the mechanical properties either due to the interstitials pick–up, which normally increases with both the temperature and the time, or the grain growth (α mean grain size and thickening of the α + β lamellae).

- Values of thermal conductivity at room temperature and electrical resistivity are comparable to those of the respective wrought materials regardless the residual porosity and, normally, higher amount of interstitial elements.

Hot Isostatic Pressing (HIP):

- The application of a post–processing by HIP to sintered specimens leads to an increment of relative density and levels the final density of components compacted at different pressure and, thus, having a diverse relative percentage of residual porosity. Not fully dense materials are obtained due to the open porosity present on the specimens.

- Similar or higher mechanical properties than as–sintered materials can be obtained depending on the combination of processing parameters. Nevertheless, a processing temperature above the beta transus changes the tensile fracture mode from ductile to brittle.

- For elemental titanium, HIP processing in the beta phase region (1000ºC) leads to the formation of α platelets and a high processing pressure (200 MPa) in the alpha phase region (850ºC) induces an abnormal grain growth.

- For titanium alloys, the selection of a processing temperature above or near the beta transus leads to a microstructure composed by a higher percentage of primary α than as–sintered materials and transformed beta (bimodal microstructure). On the other side, a processing temperature in the α + β field leads to a microstructure similar to that of P&S components but slightly finer.

- Independently of the type of alloy and of the processing parameters employed, the components obtained by MA alloys seem to have a coarser microstructure.

Hot–pressing (HP):

- The consolidation of the powder under a simultaneous application of temperature and pressure allows reaching higher relative density than P&S, reaching values of 98%.

- Elemental titanium and titanium alloy powders react with the processing tools and, in particular, with the BN coating applied to the graphite discs used to avoid the interaction with carbon and facilitate the release of the components. The interaction does not seem to be influenced by the composition of the alloy since the reacted layer is constituted by titanium nitrides and borides and, therefore, is titanium which reacts with the BN coating.

- Comparable or improved bending properties with respect to the pressing and sintering route are, generally, obtained for all the materials processed. The mechanical properties can be improved by the mechanical removing of the reacted layer.

- The microconstituents of elemental titanium processed by means of hot–pressing are non–equiaxed α grains and transformed β platelets, whilst the microstructure of the titanium alloys, generally finer than that of pressing and sintering components, is constituted by α grains and Widmanstätten areas.

- Conversely to the P&S route or the post–processing by HIP, smaller α grains and finer α + β zones are achieved with MA powders compared to PA.

Inductive Hot–pressing (IHP):

- The IHP technique permits to obtain fully dense elemental titanium and titanium alloys.

- Similar mechanical properties (hardness) and chemical composition to those of other powder metallurgy routes are normally obtained.

- The fast cooling of the IHP method leads to a microstructure composed by α grains and α platelets, resulting in a highly heterogeneous microstructure of irregular and plate–like grains for elemental titanium and to a basketweave microstructure in titanium alloys.

- The very short dwell time at temperature, 15 minutes, and the fast cooling rate, intrinsic to the field assisted sintering technology, leads to a much finer microstructure, either compared to P&S or conventional hot–pressing.

CHAPTER 8

SUGGESTIONS FOR FURTHER WORK

Based on the results exposed throughout this doctoral thesis and keeping in mind the main objective of obtaining high relative density materials with properties comparable to the respective wrought alloys, the following ideas for further works can be suggested:

- ✓ **Study of fatigue and creep properties** since these are critical properties for the application of titanium alloys in many industries such as the aerospace or the automotive;

- ✓ **Determination of the mechanical properties** considered during the development of this thesis, both bending and tensile, **at high temperature** to study the possibility to employ these materials at temperatures up to 500ºC;

- ✓ **Measurement of the corrosion resistance in different corrosion media** since these properties could be affected by the presence of the residual porosity, especially if this is located in the surface of the components;

- ✓ **Study of the heat–treatments normally applied in the industry**, especially for the $\alpha + \beta$ alloys, with the aim to identify eventual significant differences in the behaviour of the PM materials compared to the wrought alloys and to modify the final mechanical properties for a specific application;

- ✓ **Determination of the biocompatibility of the PM alloys** by means of in–vitro analysis by immersion in simulated body fluid since, practically, all the materials studied can be used to produce biomedical products;

- ✓ **Study of the behaviour of the new metallic powders produced by the latest reduction processes**, such as the ITP/Armstrong or the FFC/Cambridge, during its shaping by PM techniques which could lead to the substitution of the hydride–dehydride (HDH) elemental titanium powder. Since the ITP/Armstrong process can also produce titanium alloys, the behaviour of these prealloyed powders could also be studied;

- ✓ **Processing of the alloys developed during this thesis by means of other advanced P/M techniques** like metal injection moulding (MIM), extrusion or sinter–forging.